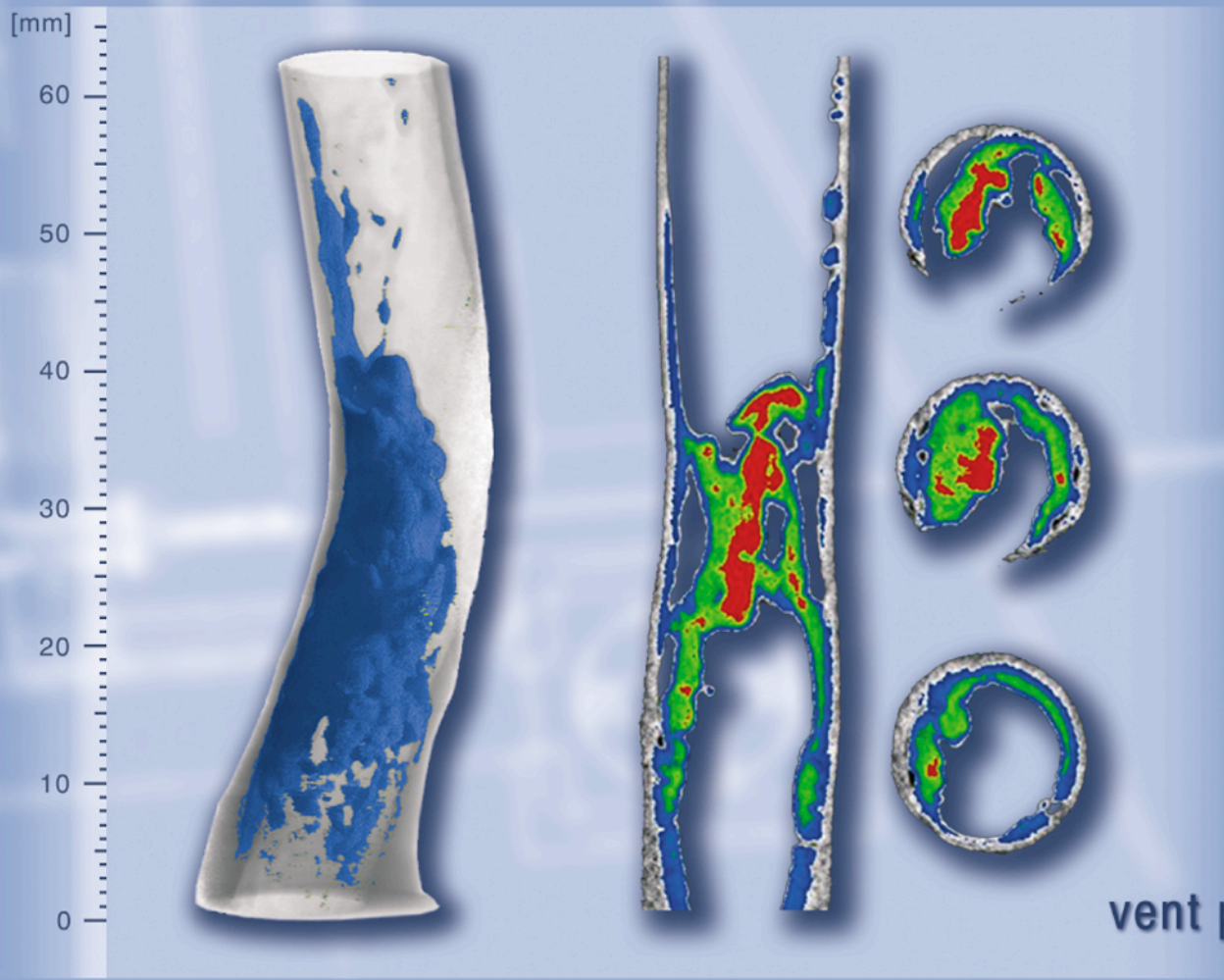
Hahn-Meitner-Institut Berlin
in der Helmholtz-Gemeinschaft

Berlin Neutron Scattering Center



BENSC EXPERIMENTAL REPORTS 2004

BENSC
EXPERIMENTAL REPORTS
2004

edited by

Y. Kirschbaum, A. Brandt,
M. Tovar, D. Bischoff and R. Michaelsen

Berlin Neutron Scattering Center
Hahn-Meitner-Institut Berlin
in der Helmholtz Gemeinschaft

April 2005

Berichte des Hahn-Meitner-Instituts Berlin

HMI - B 601

ISSN 0936 - 0891

Cover pictures: Applications of modern Neutron Tomography

Front page:

Two-dimensional cuts through a vent pipe of an aircraft engine, calculated from neutron tomography data, were imaged. The investigations were initiated by a request from British aviation industry as well as the British Air Accident Investigation Branch. Aim of the experiments was to get a deeper insight view on the oil and fuel sedimentation process inside the vent pipe without destroying the sample.

The different colours in the pictures correspond to different densities of the sediments. Using these information in combination with information about the structure and the volume fraction of the sediments (also determinable by neutron tomography), the history of the sedimentation process can be reconstructed. For more detailed information please see experimental report PHY-04-1075-LT (page 171).

Back page:

Two further fields of application of neutron tomography are geology and archaeology.

On the upper left of the back a neutron tomography image of a granite which underwent a hydrothermal alteration is presented (the picture below shows the sample on the CONRAD instrument, where the experiment was carried out). The alteration is indicated by the high volume fraction of the mineral Kaolinit (orange coloured), a typical product of the reaction of the feldspar of the granite with hot water. These neutron tomography results are a valuable contribution in solving the formation process of geological samples. More information is given in report MAT-04-1083 (page 169).

Neutron tomography serves also as a first choice tool to investigate delicate samples non-destructively. It allows the scientists to visualize archaeological samples, elucidate their inner structure and look for sample details like inscriptions or engravings. On the right hand of the back a neutron tomography image of an ancient glass, approximately I-II century A.D. stemming from excavations in Altino near Venice, Italy, is presented. Void structures in the inner of the sample can be seen as light areas due to their different absorption behaviour (voids are marked by arrows, areas of high absorption resulting from soil in inclusions and on the surface are coloured red). The size and the distribution of the voids could be determined quantitatively and gives the archaeologists substantial hints in revealing details of the glass production process in the antique. For further details please see report EF V7 (page 170).

The cover was designed by *screenworks*, Leibnizstraße 59, 10629 Berlin, www.screenworks.de

---

Editorial:

The *Berlin Neutron Scattering Center* (BENSC) is a department of *the Hahn-Meitner-Institut Berlin* GmbH. BENSC develops and runs the Neutron Scattering Instruments at the Berlin Research Reactor BER II and is responsible for the service to external users.
The *Hahn-Meitner-Institut Berlin in der Helmholtz-Gemeinschaft* (HMI) is a national research institution financed by the Federal Republic of Germany and the City State of Berlin.

Address:

Berlin Neutron Scattering Center
BENSC
The Scientific Secretary
Dr. Rainer Michaelsen
Hahn-Meitner-Institut
in der Helmholtz-Gemeinschaft
Glienicker Strasse 100
D – 14109 Berlin

Phone: +49-30-8062 3043, -2304

FAX: +49-30-8062 2523

Email: bensc@hmi.de

Net: http://www.hmi.de/bensc

CONTENTS

Introduction	**IV**
List of BENSC Instruments	**VI**
How to apply for BENSC Beam Time	**X**
Acknowledgement for Support by the European Commission	**XI**
List of Contributed Reports	**XIII**

Part I: EXPERIMENTAL REPORTS 2004

Magnetism		**1**
Magnetic Structure and Phase Transitions	1	
Magnetic Thin Films	65	
Structure		**69**
Chemical Structure	69	
Structural Excitations	86	
Soft Matter		**93**
Biology		**124**
Material Science and Industrial Applications		**145**
Development of Instruments and Methods		**178**
Fundamental Physics and Others		**192**

Part II: LIST OF BENSC PUBLICATIONS

Theses	**210**
Papers 2004 (and Supplement 2003, 2002)	**211**
Conference Contributions and Seminar Talks	**224**
Contributions to the BENSC Users' Meeting 2004	**235**

AUTHOR INDEX **239**

Introduction

The present volume of 207 BENSC Experimental Reports - 162 from external users and 45 from BENSC staff members - gives an overview of the experimental work carried out at BENSC during the year 2004. The number of reports is only slightly lower than 2003 - in spite of the three months shutdown of the research reactor BER2 at the end of the year, required for the replacement of the cold neutron guide 4 in connection with the BENSC upgrade project *Neutron Guide Hall II*.

BENSC User Service

BENSC is open to the national and international user community, whereby about 70% of the beam time is available to external users; 20% for long term collaborating groups from German universities and other research institutions and 50% for peer reviewed short term projects.

Updated and detailed descriptions of all essential BENSC neutron scattering instruments are available on the BENSC webpage.

http://www.hmi.de/bensc/instrumentation

A colour printed version (brochure HMI-B 577 [March 2001]) is available on request.

BENSC puts special emphasis on sample environment under extreme conditions: high magnetic fields, high pressure, high, low and ultra low temperatures. The sample environment group has published a detailed technical handbook on BENSC sample environment. The handbook is being updated continuously and available on the internet under

http://www.hmi.de/bensc/sample-env/home.html

Scientific Selection Panel

The short-term project beam time allocations for the scheduled instruments are established on a semi-annual basis in collaboration with a scientific selection panel, the 'user committee'. The 2004 beam time quota for short-term projects of the external user groups were allocated at two user committee sessions in November 2003 and May 2004. Twelve external and two in-house committee members were involved:

External members:

Dr. M. Enderle
ILL Grenoble, France

Dr. Bela Farago
ILL Grenoble, France

Prof. Dr. M. Lerch
Techn. Univ. Berlin, Germany

Prof. Dr. M. Loewenhaupt
Techn. Univ. Dresden, Germany

Prof. Dr. J. Lu
UMIST, Manchester, U.K.

Dr. R. May
ILL Grenoble, France

Prof. Dr. K. McEwen
University College of London, U.K.

Dr. L. Pintschovius
FZ Karlsruhe, Germany / LLB Saclay, France

Prof. Dr. G. Renger
Techn. Univ. Berlin, Germany

Prof. Dr. D.K. Ross
Salford University, Greater Manchester, U.K.

Prof. Dr. V. Sechovsky
Charles Univ. Prague, Czech Republic

Prof. Dr. J. Texeira
CEA/CNRS/LLB Saclay, France

Internal members:

Prof. Dr. F. Mezei,
HMI Berlin

Dr. H.A. Graf
HMI Berlin

Support for European Access to BENSC from the European Commission

Right from the start of the BENSC user operation in 1993, the access of European research groups to BENSC was generously supported by the European Community under framework programmes FP3, FP4, and FP5 of the European Commission - with values of the BENSC access grants increasing from contract to contract.

The EU support is available for research groups from European Member States as well as for groups from the Associated States. Within the four years of the FP5 contract period under the ***Access to Research Infrastructures*** action of the ***Improving Human Potential Programme (IHP)***, formally ending in February 2004, BENSC delivered an annual mean of roughly 550 instrument days to the European research groups,

distributed to ~80 different projects/year with a total of ~175 visits/year. As listed on page XI, an important proportion of the contributions in this volume report on EU supported experiments.

The share of these EU supported BENSC users in the number of BENSC publications in high-ranking journals is superproportionally high.

The successful European Access to BENSC actions are now continued under the 6th EU Framework Programme (FP6), however, with a slightly modified contractual situation: BENSC is now a partner in the ***Integrated Infrastructure Initiative for Neutron Scattering and Muon Spectroscopy (NMI3).*** NMI3 brings together 23 partners from 14 countries, including 11 research infrastructures, together with other interested organisations. The most important branch of NMI3 includes 12 different Access Activities offering European users approximately 5000 beam days of access to 150 instruments at different facilities with support for travel and subsistence. Under NMI3, BENSC will serve for a minimum access of 1040 instrument days, distributed over four years.

In the first year under NMI3 (reactor operation period Jan.-Sept. 2004), BENSC delivered already 480 instrument days for European users. A total of 117 individual users from 55 groups from 14 countries were involved, the majority of these EU supported users, i.e. 72 individual researchers, were new users.

Deutsche Neutronenstreutagung 2004

The impact of BENSC on the national neutron user community was shown at the *Deutsche Neutronenstreutagung 2004, Dresden, 1 - 4 September 2004.* At this conference, a third of all contributions reported on results of experiments at BENSC: 34% of the talks and 32% of the posters. The majority of these BENSC contributions were presented by external users. For three specific scientific fields, *Magnetism* (clearly magnetism!), *Biological Systems*, and *Materials* the BENSC partition scored the 50% level.

New Neutron Guide Hall

The construction of the new neutron guide hall progressed in big steps. The ceremony of laying of the foundation stone of the building was held on 8 December 2003, and due to the relatively mild winter 2003/2004, progress was very quick and at the end of the year the new hall was completed. Some pictures of the progress are displayed on the following pages.

It is intended that the wide-angle spin-echo instrument V5 will move from the old hall to the new hall. V5 will profit from the replacement of the old neutron guide by a new ballistic guide with multispectral neutron beam injection.

Further planned and fully financed instruments in the new hall are

VSANS High resolution SANS, equipped with a novel focusing technique

EXED Extreme Environment Diffractometer, equipped with TOF-monochromatisation.

The experiment site for EXED is additionally provided for the project of a 25T high field magnet, and will be suited as well for potential projects with even higher steady magnetic fields.

Progress of HMI instruments at BESSY

To promote complementary use of neutrons and synchrotron radiation, HMI has initiated an upgrade project for the synchrotron source BESSY including the development and installation of two new insertion devices.

The HMI UE46 undulator provides polarized soft X-rays with, by orders of magnitude, worldwide highest brightness and flux density. The undulator is operational since 2002, with full user service at the PGM beamline for magnetic nanostructures and magnetic films. The delivery of the high field magnet for the reflectometry option is now expected for 2005.

The second insertion device, a 7T-wiggler, went operational in late summer 2004. The wiggler provides X-rays for two beam lines:

a) White beam for the materials science diffractometer EDDI (Residual Stress and Texture Analysis) for an energy range exceeding 100 keV.
b) Monochromatic beam for resonant magnetic scattering and high-resolution diffraction (MagS).

The user service at the Wiggler beam lines will start in April 2005.



Rainer Michaelsen

List of BENSC Instruments

Instruments in the Experiment Hall (Thermal Neutrons)

March 2005

No.	Instrument	ext.	Tube	Instrument Staff	ext.	Room
E 1	Thermal 3-Axis Spectrometer with Polarization Analysis	3101	D 1N	Hans A.Graf Vadim Sikolenko	2778 2847	LS 335 LR 141
E 2	Flat-Cone- and Powder Diffractometer (E2a: Neutron Photography)	3102	R 1	Univ. Tübingen: Jens-Uwe Hoffmann (Uni Tüb) Hans-Peter Nabein (co-op Uni Tüb)	 2185 2708	 A 241 A 239
E 3	Residual Stress Analysis and Texture Diffractometer	3103	T 2	Rainer Schneider Tobias Poeste (co-op TU Berlin) Robert Wimpory	3096 3237 3098	A 132 A 131 A 133
E 4	2-Axis Diffractometer (E4a: Test Device)	3104	R 2	Karel Prokes N.N.	2804	LR 138
E 5	4-Circle Diffractometer	3104	R 3	Manfred Reehuis (co-op MPI-FKF Stuttg.)	2692	A 343
E 6	Focusing Single Crystal Diffractometer	3105	T 4	Norbert Stüßer N.N.	3171	LR 142
E 7	Residual Stress Analysis Diffractometer	3107	D 1S	Rainer Schneider Florian Henkel	3096 3098	A 132 A 133
E 9	Fine Resolution Powder Diffractometer (FIREPOD)	3106	T5	Dimitri Argyriou N.N. Michael Tovar	3016 2768	LR 137 LR 144
E 10	^{3}He-Diffractometer (HELINE)		D 1S	Konrad Siemensmeyer	2757	LS 132

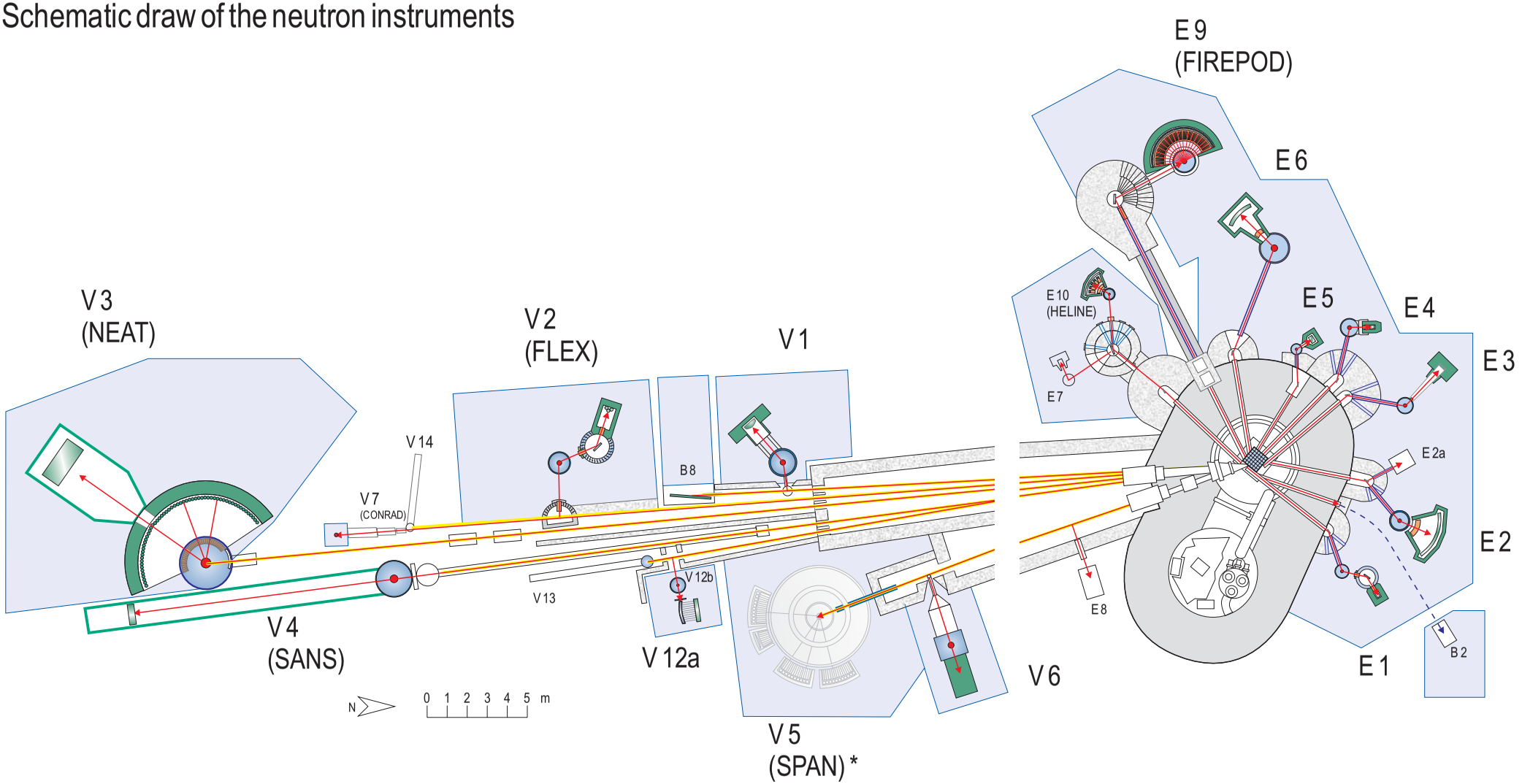
Instruments in the Cold Neutron Guide Hall

No.	Instrument	ext.	Tube	Instrument Staff	ext.	Room
V 1	Membrane Diffractometer	3121	NL 1A	Thomas Hauß (co-op TU Darmstadt) Silvia Dante	2071 2071	LS 333 LS 333
V 2	3-Axis Spectrometer for Cold Neutrons (FLEX)	3122	NL 1B	N.N. Habicht (co-op TU Darmstadt) Oleg Sobolev	 2807 3067	 A 333 A 331
V 3	Time-of-Flight Spectrometer (NEAT)	3123	NL 2^o	Margarita Russina Jörg Pieper Alexandra Buchsteiner	3159 3073 3179	A 351 A 348 A 349
V 4	Small Angle Scattering Instrument (SANS)	3124	NL 3A	Albrecht Wiedenmann Uwe Keiderling Elvira Garcia-Matres Jörg Haug André Heinemann	2283 2339 3240 2339 2769	LR 211 LR 209 LR 208 LR 209 LR 208
V 5	Spin-Echo Spectrometer with Time of Flight Option (SPAN) *(under re-construction)*	3125	NL 4B	Catherine Pappas Carlos Fehr	2046 3072	A 346 A 344
V 6	Reflectometer *(under re-construction)*	2806	NL 4B	Roland Steitz Sebastian Schemmel (co-op TU Berlin) Elena Maltsieva	2149 2924 3077	A 221 A 226 A 223
V 7	Cold n Tomography (CONRAD)		NL 1B$_u$	Nikolay Kardjilov Andre Hilger	2298 2490	A 317 A 316
B 8	n-Autoradiography	3121	NL 1A	Birgit Schröder-Smeibidl Lee-Ann Mertens	2337 2292	GE 145 V 122
V 12a	Double-Crystal Diffractometer (Tomography)	3131	NL 3B	Wolfgang Treimer (TFH Berlin) Markus Strobl (TFH Berlin)	2221 2490	A 319 A 316
V 12 b	Double-Crystal Diffractometer (Tomography)	3131	NL 3B	Wolfgang Treimer (TFH Berlin) Markus Strobl (TFH Berlin)	2221 2490	A 319 A 316
V 13	Fundamental Physics		NL 3B	Margarita Russina	3159	A 351
V 14	Mirror Test Device		NL 1B^o	Thomas Krist	2045	A 233
V 15	EXED *(under construction)*		NL 4A	Judith Peters	3068	A 336
V 16	VSANS *(under construction)*		NL 4C	Daniel Clemens	2280	V 131

Sample Environment		Michael Meissner Peter Smeibidl Sebastian Gerischer Klaus Kiefer	2204 3080 3133 3141	LS 131 LR 147 LS 113 LS 130

BENSC Neutron Scattering Center

Schematic draw of the neutron instruments



*V5 has moved to the recently opened neutron guide hall II

Progress of the new Neutron Guide Hall II



Cornerstone ceremony, December 9th, 2003
Prof. Dr. M. Steiner (on the left)
and the architect B. Tibes (on the right)



Topping-out ceremony

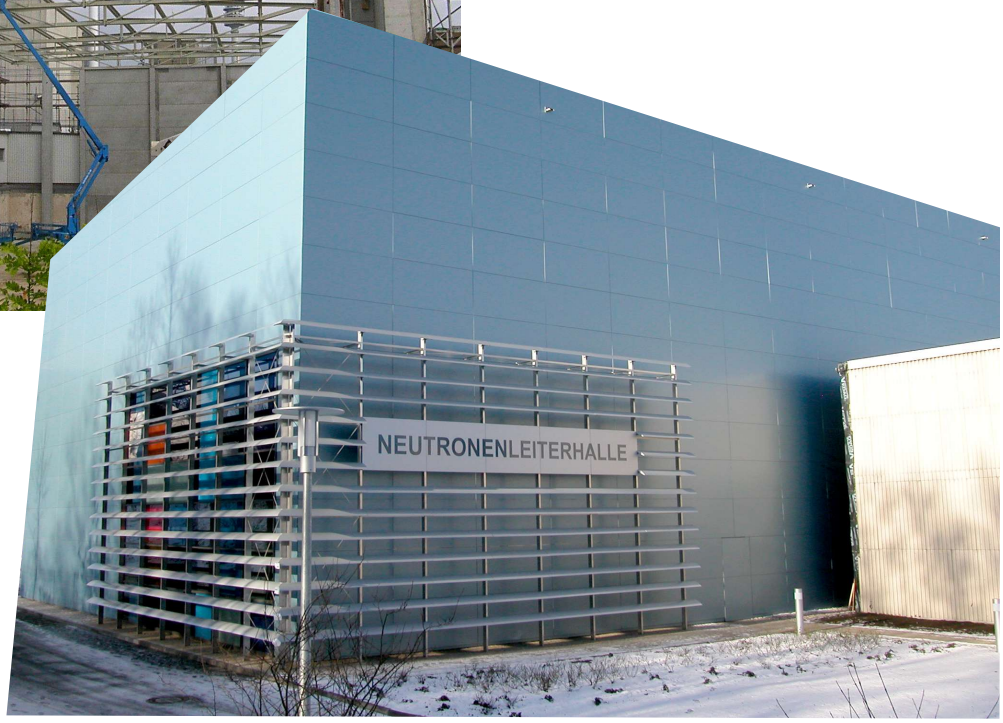
June 30th, 2004





Under construction

Summer 2004



Neutron Guide Hall II

Completed December 2004



January 2005

How to Apply for BENSC Beam Time

BENSC is open to both the national and the international user community with up to 70% of the beam time available to external users. The main portion of this beam time is foreseen for short term research proposals. Applications for short term beam time will be examined by a scientific selection committee twice each year,

deadlines for submission of proposals are 15 March and 15 September.

Requests for urgent experiments (Directors's discretionary time) and for industrial use may be submitted at any time.

Applications for BENSC beam time should be made **electronically**. The BENSC **ONLINE PROPOSAL SUBMISSION (OPS)** system is available in the internet via

http://www.hmi.de/bensc/user-info/user-info_en.html

Further information on BENSC instrumentation can be obtained from the internet via

http://www.hmi.de/bensc/instrumentation/instrumentation_en.html

The latest four-colour printed version of the instrumentation brochure (HMI-B 577) is on the market since March 2001 and available on request**:**

BENSC-HMI
Office of the Scientific Secretary
Glienicker Str. 100
D - 14109 Berlin (Wannsee)
Germany
Phone +49 - 30 - 8062 2304
Fax: +49 - 30 - 8062 2523
Email: **bensc@hmi.de**

The BENSC Experimental Reports are intended as interim summaries. In view of the short time available between the termination of certain experiments and the deadline for this report, the results presented here have to be considered as very preliminary. The inclusion of reports in this volume does not constitute a publication in the usual sense. Final results will be submitted for publication in regular scientific journals.

Acknowledgement for Support by the European Commission

The access of BENSC users from European Community Member States and Associated States to BENSC has been substantially supported by the European Community under the Framework Programmes FP5 and FP6.

FP5: Access to Research Infrastructure Action of the Improving Human Potential Programme (IHP), second BENSC contract, effective 11/2001 - 02/2004, with contract number ***HPRI-CT-2001-00138.***

FP6: BENSC is a partner in the EU supported network of European neutron facilities – the **Neutron and Muon Integrated Infrastructure Initiative (NMI3)**, an action within the EU FP6 activity 'Structuring the European Research Area: Research Infrastructures'. NMI3 brings together 23 partners from 14 countries, including 11 research infrastructures.
The BENSC Access contract under NMI3 is effective for 4 years, from 01/2004 until 12/2007, the relevant EU contract number (NMI3) for acknowledgements is ***RII3-CT-2003-505925***

Results of EU supported groups are contained in 65 reports of this volume.

IHP-nº	p.	authors	affiliation
556	130	Steriotis et al.	NCSR Demokritos, GR
557	90	Steriotis et al.	NCSR Demokritos, GR
559	154	Ramsay et al.	Univ. Montpellier, F
566	107	Magazu et al.	Univ. Messina, I

NMI3-nº	p.	authors	affiliation
1003	144	Toca Herrera et al.	BOKU Wien, A
1004	65	Meerschaut et al.	KU Leuven, B
1005	66	Temst et al.	KU Leuven, B
1007	156	Strunz et al.	ASCR NPI Rez, CZ
1008	13	Janousova et al.	CU Prague, CZ
1009	14	Prchal et al.	DES, CU Prague, CZ
1010	6	Svoboda et al.	CU Prague, CZ
1011	34	Pissas et al.	NCSR Demokritos, GR
1012	140	Steriotis et al.	NCSR Demokritos, GR
1013	132	Appavou et al.	CEA-LLB Saclay, F
1014	133	Longeville et al.	CEA-LLB Saclay, F
1016	99	El Harrak et al.	CEA-LLB Saclay, F
1017	54	Brulet et al.	CEA-CNRS, F
1018	101	Cousin et al.	CNRS-LLB Saclay, F
1019	102	Sarazin et al.	ICS Strasbourg, F
1020	116	Delajon et al.	Univ. Strasbourg, F
1021	56	Baglioni et al.	Univ. Firenze, I
1022	141	Berti et al.	Univ. Firenze, I
1023	96	Triolo, A. et al.	CNR IPCF Messina, I
1024	106	Triolo, A. et al.	CNR IPCF Messina, I
1025	147	Wimpory et al.	JRC-IE Petten, NL
1026	24	Gondek et al.	JU Krakow, PL
1027	25	Wawrzynska et al.	JU Krakow, PL
1028	32	Wolska et al.	AMU Poznan, PL
1029	95	Czarneck et al.	AMU Poznan, PL
1030	71	Borowiec et al.	PAS IP Warsaw, PL
1031	196	Tripadus et al.	IFIN-HH Bucharest, RO
1032	103	Cosgrove et al.	Univ. Bristol, UK
1033	104	Dreiss et al.	Univ. Bristol, UK
1034	22	Bull et al.	RAL ISIS, UK
1035	128	Bradshaw et al.	Univ. Edinburgh, UK
1036	115	Bowers et al.	Univ. Exeter, UK
1038	148	Edwards et al.	Open Univ., UK
1039	149	Edwards et al.	Open Univ., UK
1040	152	Georgiev et al.	Univ. Salford, UK
1041	174	Bastürk et al.	ATI, Wien, A
1042	203	Trinker et al.	ATI Wien, A
1042	204	Trinker et al.	ATI Wien, A
1045	67	Popova et al.	KU Leuven, B
1046	50	Mesot et al.	PSI & ETHZ, CH
1047	15	Kamarad et al.	ASCR IP Prague, PL
1050	157	Strunz et al.	ASCR NPI Rez, CZ
1053	58	Herrero-Albillos et al.	Univ. Zaragoza, E
1054	37	Mergia et al.	NCSR Demokritos, GR
1057	51	Enderle et al.	ILL, Grenoble, F
1059	100	Carrot et al.	CNRS-LLB Saclay, F
1061	175	Fiori et al.	Univ. Ancona, I
1063	126	Baldelli Bombelli et al.	Univ. Firenze, I
1067	176	Triolo, R. et al.	Univ. Palermo, I
1068	166	Kardjilov et al.	HMI Berlin, D
1069	135	De Francesco et al.	Univ. Perugia, I
1070	188	Iolin et al.	IPE, Riga, LV
1071	127	Bouwstra et al.	Univ. Leiden, NL
1073	33	Wolska et al.	AMU Poznan, PL
1074	35	Regulski et al.	Univ. Warsaw, PL
1075	36	Szymczak et al.	PAS IP Warsaw, PL
1076	159	Zrnik et al.	TU Kosice, SK
1078	105	Richardson et al.	Univ. Bristol, UK
1079	129	Bradshaw et al.	Univ. Edinburgh, UK
1080	9	Coldea et al.	Univ. Oxford, UK
1082	68	Mergia et al.	NCSR Demokritos, GR

Notice:

The quality of figures in the electronic versions, CD and WEB (http://www.hmi.de/bensc) – especially in colour presentation – is remarkably higher than in print version

List of Contributed Experimental Reports

Magnetic Structure and Phase Transitions

PAGE	TITLE	TEAM			PROPOSAL
1	***A magnetic field effect on spin density wave in $Pr_{0.88}LaCe_{0.12}CuO_4$***	P. Dai[1] H.J. Kang[1] H.A. Mook[2] Y. Ando[3] D. Argyriou[4]	[1]Univ. Tennessee, USA [2]ORNL, USA [3]CRI of EPI, JP [4]HMI Berlin	E4	**PHY-01-1465 DT**
2	***An in-plane magnetic field effect on superconductor $Pr_{0.88}LaCe_{0.12}CuO_4$***	P. Dai[1] H.J. Kang[1] H.A. Mook[2] Y. Ando[3] D. Argyriou[4]	[1]Univ. Tennessee, USA [2]ORNL, USA [3]CRI of EPI, JP [4]HMI Berlin	E1	**PHY-01-1465 DT**
3	***Magnetic excitations in nanocrystalline Tb***	O. Moze[1] J. Klenke[2]	[1]Univ. Modena [2]HMI Berlin	E1	**PHY-02-0420**
4	***Magnetic and structural disorder in single crystalline UPt_2Si_2***	S. Süllow[1] J. Klenke[2] R. Feyerherm[2]	[1]TU Braunschweig [2]HMI Berlin	E1	**PHY-02-0426 02-0445**
5	***Study of the magnetic spiral in $CsCuCl_3$ under pressure***	N. Stüßer[1] R. Sadykov[2]	[1]HMI Berlin [2]RAS, RU	E1 E6	**EF**
6	***Magnetic structure of $Tb_{0.5}Y_{0.5}Cu_2$ single crystal***	P. Svoboda	CU Prague, CZ	E2	**PHY-01-1439**
7	***Antiferromagnetic order in $CeIn_{3-x}Sn_x$***	O.Stockert[1] J. Arndt[2]	[1]MPI CPfS Dresden [2]TU Dresden	E2	**PHY-01-1546**
8	***Magnetic order in the high field phase of $CeCu_2Si_2$***	E. Faulhaber[1] O. Stockert[2] J.-U. Hoffmann[3]	[1]TU Dresden [2]MPI CPfS Dresden [3]HMI Berlin	E2	**PHY-01-1547**
9	***Field dependence of magnetic order in a 2D frustrated quantum magnet***	R. Coldea[1] D.A. Tennant[2] J.-U. Hoffmann[3] P. Smeibidl[3]	[1]Univ. Oxford, UK [2]Univ. St. Andrews, UK [3]HMI Berlin	E2	**PHY-01-1554**
10	***Diffuse neutron scattering in single crystalline $TbCu_2$***	S. Raasch[1,3] A. Kreyßig[1] M. Loewenhaupt[1] M. Rotter[2]	[1]TU Dresden [2]Univ. Wien, A [3]HMI Berlin	E2	**PHY-01-1446**
11	***Switching of the crystallographic structure of a $Tb_{0.5}Dy_{0.5}Cu_2$ single crystal***	S. Raasch[1,2] M. Frontzek[1] A. Kreyßig[1]	[1]TU Dresden [2]HMI Berlin	E2	**PHY-01-1445**
12	***Crystallographic superstructure in R_2PdSi_3 (R = Tb, Ho, Er) compounds***	M. Frontzek[1] A. Kreyßig[1] S. Raasch[1,2] T. Lonkai[2]	[1]TU Dresden [2]HMI Berlin	E2	**PHY-01-1548**
13	***Magnetic ground state of NdPtSn***	B. Janousova[1] V. Sikolenko[2] K. Prokes[2]	[1]CU Prague, CZ [2]HMI Berlin	E4	**PHY-01-1463**
14	***Field-induced changes in magnetic structure of DyNiAl***	J. Prchal[1] K. Prokes[2] P. Javorský[1]	[1]DES, CU Prague, CZ [2]HMI Berlin	E4	**PHY-01-1464**
15	***Magnetic structures of Y_2Fe_{17} under high pressure***	J. Kamarád[1] O. Prokhnenko[1] K. Prokes[2] V. Sikolenko[2]	[1]ASCR IP Prague, CZ [2]HMI Berlin	E4	**PHY-01-1580**
16	***Non-magnetic impurity effect on domain-growth in $Co_{1-x}Mg_xNb_2O_6$ (x = 0.0,0.005)***	S. Mitsuda[1] T. Nakajima[1] Y. Inomoto[1] V. Sikolenko[2] K. Prokes[2] S. Kausche[2]	[1]Tokyo US, JP [2]HMI Berlin	E4	**PHY-01-1582**

List of Contributed Experimental Reports

PAGE	TITLE	TEAM			PROPOSAL
17	***On the mechanism for magnetic detwinning of La_2CuO_4***	B. Keimer[1] U. Ulrich[1] K. Prokes[2]	[1]MPI FKF Stuttgart [2]HMI Berlin	E4	**PHY-01-1583-DT**
18	***Crystal and magnetic structure of $La_{2-x}Sr_xCuO_4$ with x = 0.01 and x = 0.03***	B. Keimer[1] C. Ulrich[1] G. Blumberg[2] Y. Ando[3] M. Reehuis[1,4]	[1]MPI Stuttgart [2]Bell Labs, NJ, USA [3]CRI of EPI, JP [4]HMI Berlin	E5	**EF**
19	***Crystal and magnetic structure of $LaTiO_3$***	C. Ulrich[1] B. Keimer[1] M. Reehuis[1,2] J. Hemberger[3]	[1]MPI Stuttgart [2]HMI Berlin [3]Univ. Augsburg, EKM	E5	**PHY-01-1481**
20	***Magnetic ordering in $DyVO_3$***	C. Ulrich[1] B. Keimer[1] M. Reehuis[1,2]	[1]MPI Stuttgart [2]HMI Berlin	E5	**PHY-01-1482**
21	***Magnetic and structural disorder in single crystalline UPt_2Si_2***	S. Süllow[1] J. Kreitlow[1] A. Loose[2] R. Feyerherm[2]	[1]TU Braunschweig [2]HMI Berlin	E5	**PHY-01-1480 01-1592**
22	***Influence of hydrostatic pressure on the antiferromagnetic background of $La_{2-x}Sr_xCuO_4$***	M. Bull[1] C. Panagopoulos[2] B. Lake[3] C. Frost[1]	[1]RAL ISIS, UK [2]Univ. Cambridge, UK [3]Univ. Oxford, UK	E6	**PHY-01-1466**
23	***Neutron diffraction measurement on ferrofluids***	M. Hofmann E. Steichele	TU München	E6	**PHY-01-1471**
24	***Neutron diffraction studies of RPdIn (R = Nd, Ho, Er) compounds***	L. Gondek[1] S. Baran[1] J. Hernandez-Velasco[2]	[1]JU Krakow, PL [2]HMI Berlin	E6	**PHY-01-1474**
25	***Magnetic structures of $R_3Ag_4Sn_4$ (R = Pr, Nd) and $Nd_3Cu_4Ge_4$***	E. Wawrzynska[1] J. Hernandez-Velasco[2] B. Penc[1] A. Szytula[1] K. Tomala[1]	[1]JU Krakow, PL [2]HMI Berlin	E6	**PHY-01-1475**
26	***Neutron Diffraction Study of RCu_xGe_2 (R = Ho, Er) and RCo_xSn_2 (R = Tb, Er, Ho) compounds***	E. Wawrzynska[1] J. Hernandez-Velasco[2] N. Stüßer[2] S. Baran[1] B. Penc[1] A. Szytula[1] A. Gil[3] D. Kaczorowski[4] A. Zygmunt[4]	[1]JU Krakow, PL [2]HMI Berlin [3]Univ. Czestochowa, PL [4]Univ. Wroclaw, PL	E6	**PHY-01-1589**
27	***The magnetic structure determination of the compound $Na_{12}Co_7O_{14}$***	M. Sofin O. Leynaud M. Jansen	MPI FKF Stuttgart	E6 E9	**CHE-01-1567**
28	***Low temperature magnetic behaviour of $CeNi_{0.6}Cu_{0.4}$***	N. Marcano[1] J.C. Gómez Sal[1] J. Hernandes-Velasco[2]	[1]CITIMAC, U.C, E [2]HMI Berlin	E6	**EF**
29	***Unusual magnetic behaviour in Sr_2PrO_4***	J. Hernandez-Velasco	HMI Berlin	E6 E9	**EF**
30	***Magnetization steps and phase separation in CMR systems $Pr_{0.5}Ca_{0.5}Mn_{1-x}M_xO_3$ (M = Cr, Ni, Ti; x ≤ 0.03)***	J.L. Garcia-Munoz[1] N. Bellido[1] C. Frontera[1] J. Hernandes-Velasco[2]	[1]CSIC, Barcelona, E [2]HMI Berlin	E6	**EF**
31	***Canted magnetic structure of $Fe(N_3)_2(bpy\text{-}d8)$***	R. Feyerherm M. Stüßer D. Többens	HMI Berlin	E6 E9	**EF**

List of Contributed Experimental Reports

PAGE	TITLE	TEAM			PROPOSAL
32	***Structural and magnetic studies of spinel oxides. Part 1. Iron substituted lithium-manganese oxides***	E. Wolska[1] J. Darul[1] P. Piszora[1] W. Nowicki[1] M. Tovar[2]	[1]AMU Poznan, PL [2]HMI Berlin	E9	**CHE-01-1456**
33	***Structural and magnetic studies of spinel oxides. Part 2. Effect of Li for Mn substitution on the $LiMn_2O_4$ structure***	E. Wolska[1] J. Darul[1] W. Nowicki[1] M. Tovar[2]	[1]AMU Poznan, PL [2]HMI Berlin	E9	**CHE-01-1570**
34	***Crystal and magnetic structure of $La_{1-x}Ca_xMnO_3$ for 0.1<x<0.2***	M. Pissas D. Stamopoulos	IMS, NCSR Demokritos, GR	E6 E9	**PHY-01-1454** **01-1472**
35	***Spin lattice coupling in β-MnO_2***	M. Regulski[1] W. Slawinski[1] D. Többens[2]	[1]Univ. Warsaw, PL [2]HMI Berlin	E9	**PHY-01-1571**
36	***Spin-state transition in $Nd_{1-x}Ba_xCoO_3$ system***	A.P. Sazonov[1] I.O. Troyanchuk[1] V. Sikolenko[2] H. Szymczak[3]	[1]ISSSP NAS Minsk, BY [2]HMI Berlin [3]PAS IP Warsaw, PL	E9	**PHY-01-1572**
37	***Neutron diffraction measurements of rare earth-Fe-Co-V intermetallic compounds***	K. Mergia[1] M. Gjoka[1] S. Messoloras[1] D. Többens[2]	[1]NCSR Demokritos, GR [2]HMI Berlin	E9	**PHY-01-1581**
38	***Crystal structure and magnetic ordering in Fe-doped In_2S_3***	A. Krimmel[1] D. Többens[2]	[1]Univ. Augsburg [2]HMI Berlin	E9	**MAT-01-1447**
39	***Variable temperature PND of $Na_{0.73}CoO_2$***	D. Argyriou N. Aliouane C. Milne	HMI Berlin	E9	**EF**
40	***Structure of hydrated Na_xCoO_2***	D. Argyriou N. Aliouane C. Milne	HMI Berlin	E9	**EF**
41	***Crystal structure of superconducting $Na_xCoO_2{\cdot}yD_2O$***	D. Argyriou N. Aliouane C. Milne	HMI Berlin	E9	**EF**
42	***Magnetic transitions in $TbMnO_3$ part 1***	D. Argyriou N. Aliouane C. Milne	HMI Berlin	E9	**EF**
43	***Magnetic transitions in $TbMnO_3$ part 2***	D. Argyriou N. Aliouane C. Milne	HMI Berlin	E2	**EF**
44	***Field induced magnetic transitions in $TbMnO_3$***	D. Argyriou N. Aliouane C. Milne	HMI Berlin	E4	**EF**
45	***Field-induced transition between magnetically disordered and ordered phases in underdoped $La_{2-x}Sr_xCuO_4$***	B. Khaykovich[1] S. Wakimoto[2] R.J. Birgeneau[2] M.A. Kastner[1] Y.S. Lee[1] K. Yamada[3]	[1]MIT Cambridge, USA [2]Univ. Toronto, CDN [3]Tohoku Univ., JP	V2	**PHY-02-0404** **02-0406**
46	***Dynamics of bond-alternating quantum S=1 chains in the high-field state***	A. Zheludev[1] L.-P. Regnault[2] M. Hagiwara[3] P. Vorderwisch[4]	[1]ORNL, USA [2]CEA, Grenoble, F [3]RIKEN, JP [4]HMI Berlin	V2	**PHY-02-0408** **02-0433**
47	***Magnetic instability in $Ca_{1.5}Sr_{0.5}RuO_4$***	P. Steffens[1] M. Braden[1] K. Habicht[2]	[1]Uni Köln [2]HMI Berlin	V2	**PHY-02-0430**
48	***Spin dynamics in the S=1/2 quantum spin system NH_4CuCl_3***	Ch. Rüegg[1,2] M. Allan[1] M. Oettli[1,2]	[1]ETHZ, CH [2]PSI Villigen, CH	V2	**PHY-02-0431**

List of Contributed Experimental Reports

PAGE	TITLE	TEAM			PROPOSAL
49	***Effect of a magnetic field on the spin gap in superconducting $Nd_{1.85}Ce_{0.15}CuO_{4+\delta}$***	P. Mang	Stanford Univ., US	V2	**PHY-02-0432**
50	***Field-induced static vs dynamic magnetism in underdoped LSCO***	J. Mesot R. Gilardi H.M. Roennow	LNS, PSI & ETH, CH	V2	**PHY-02-0451**
51	***Magnon linewidth studied by resonant spin-echo***	M. Enderle[1] S. Klimko[1] K. Habicht[2] P. Smeibidl[2]	[1]ILL, Grenoble, F [2]HMI Berlin	V2	**PHY-02-0453**
52	***Magnetic-field dependence of martensitic transformation temperatures in Ni_2MnGa***	S.M. Shapiro[1] P. Vorderwisch[2] P. Smeibidl[2]	[1]Brookhaven Nat. Lab., USA [2]HMI Berlin	V2	**PHY-02-0458**
53	***Pressure dependence of the magnetic phase diagram in MnSi***	L. Pintschovius[1] D. Reznik[2] C. Pfleiderer[2]	[1]FZ Karlsruhe [2]Univ. Karlsruhe	V4	**PHY-04-0938**
54	***SANS study of the magnetic phase separation in $Pr_{0.66}Ca_{0.33}MnO_3$***	A. Brûlet[1] D. Saurel[1,2] C. Martin[2] Ch. Simon[2]	[1]CEA-CNRS, F [2]CRISMAT, F	V4	**PHY-04-0941**
56	***SANSPOL Investigation of highly concentrated surfactant stabilized magnetic nanoparticles dispersions***	P. Baglioni[1] M. Bonini[1] F. Betti[1] A. Wiedenmann[2]	[1]Univ. Firenze, I [2]HMI Berlin	V4	**CHE-04-0945**
57	***Clustering in magnetic bulk metallic glasses***	R.A. Robinson[1] E.P. Gilbert[1] R. Woodward[2] D. Yu[1]	[1]ANSTO, AU [2]Univ. of Western AU	V4	**PHY-04-0954**
58	***Searching for ferromagnetic clusters in paramagnetic phase***	J. Herrero-Albillos[1] J. Campo[2] V. Garcia[1] M. Luis[1] F. Bartolome[2]	[1]Univ. Zaragoza, E [2]CSIC, Univ. Zaragoza, E	V4	**PHY-04-1020**
59	***SANS studies of Nd Fe Co Al alloy in the melt***	O. Perroud E. Garcia-Matres A. Wiedenmann	HMI Berlin	V4	**EF**
60	***10T high magnetic field studies of $Nd_{60}Fe_{20}Co_{10}Al_{10}$ alloys by SANSPOL***	E. Garcia-Matres A. Wiedenmann O. Perroud	HMI Berlin	V4	**EF**
61	***Field variation technique and Langevin behaviour of Co-ferrofluids***	A. Wiedenmann A. Heinemann	HMI Berlin	V4	**EF**
62	***Low dimensional magnetic correlations in R_2BaMO_5 (R=Y, Ho; M=Co, Ni) studied by SANS***	J. Hernández-Velasco E. Garcia-Matres	HMI Berlin	V4	**EF**
63	***Dynamics of spin freezing in the re-entrant spin glass FeNiMn. II***	V. Wagner[1] J. Hesse[2] C. Pappas[3] J. Klenke[3]	[1]PTP Braunschweig [2]TU Braunschweig [3]HMI Berlin	V5	**PHY-03-0300**
64	***ToF analysis of the transverse magnetic fluctuations in $Mn_{0.9}Cu_{0.1}$***	T. Hicks S. Harker	Monash Univ., AU	V5	**PHY-03-0333**

Magnetic Thin Films

65	***Field-induced twisted state in Fe/Cr multilayers***	J. Meersschaut C. L'abbé F. Almeida	KU Leuven, B	V6	**PHY-04-0972**
66	***Polarized neutron reflectivity on exchange bias nanostructures***	K. Temst[1] O. Popova[1] H. Loosvelt[1] M. Gierlings[2]	[1]KU Leuven, B [2]HMI Berlin	V6	**PHY-04-0973**

List of Contributed Experimental Reports

PAGE	TITLE	TEAM			PROPOSAL
67	***Polarized neutron reflectivity on exchange bias pattern structures***	O. Popova[1] M. Gierlings[2]	[1]KU Leuven, B [2]HMI Berlin	V6	**PHY-04-1054**
68	***Polarised neutron reflectivity measurements on Cr/Gd multilayers***	K. Mergia[1] S. Messoloras[1] T. Baczewski[2]	[1]NCSR Demokritos, GR [2]PAS, PL	V6	**PHY-04-1056**

Chemical Structure

69	***Diffuse scattering of cation-doped zirconia-oxyinitrides***	I. Kaiser-Bischoff[1] J.-U. Hoffmann[2]	[1]LMU München [2]HMI Berlin / Uni Tübingen	E2	**CHE-01-1440**
70	***Neutron diffraction on amorphous silicon sesquioxide (Si_2O_3)***	A. Hohl[1] T. Lonkai[2]	[1]TU Darmstadt [2]Uni Tübingen	E2	**CHE-01-1561**
71	***Structural and magnetic phase transitions of potassium-holmium double tungstates***	M.T. Borowiec[1] K. Prokes[2] V. Sikolenko[2]	[1]PAS IP Warsaw, PL [2]HMI Berlin	E4	**PHY-01-1441**
72	***Critical fluctuations in orientational glass $(NH_4I)_x(KI)_{1-x}$***	M. Ohl[1] M. Reehuis[2]	[1]FZ Jülich [2]HMI Berlin / MPI Stuttgart	E5	**PHY-01-1377**
73	***The ordering of ammonium in ferroelectric phase II of β-$LiNH_4SO_4$***	L.S. Smirnov[1] A. Loose[2]	[1]ITEP, Moscow, RU [2]HMI Berlin	E5	**PHY-01-1483**
74	***Exact determination of the deuteron positions of $ND_4(ND_3)_3Cl$***	Th. Roßmeier	Uni Regensburg	E5	**CHE-01-1484**
75	***Hydrogen compounds and intermetallic phases***	G. Auffermann[1] W. Bronger[2] N. Stüßer[3]	[1]MPI CPfS Dresden [2]RWTH Aachen [3]HMI Berlin	E6	**CHE-01-1467**
76	***Metal – Nitride – Hydrides***	G. Auffermann[1] R. Kniep[1] R. Chemnitzer[1] D. Többens[2]	[1]MPI CPfS Dresden [2]HMI Berlin	E9	**CHE-01-1450** **01-1562**
77	***Oxygen/Nitrogen order in doped tantalum oxynitride compounds***	H. Schilling[1] M. Lerch[1] M. Tovar[2]	[1]TU Berlin [2]HMI Berlin	E9	**CHE-01-1448**
78	***Structure and anion ordering in $BaPbO_{3-\delta}$***	S. Schorr[1] A. Franz[1] M. Tovar[2]	[1]Univ. Leipzig, IMKM [2]HMI Berlin	E9	**PHY-01-1452**
79	***Structure and cation ordering in the solid solution system $BaPbO_3$- $BaSnO_3$***	A. Franz[1] S. Schorr[1] M. Tovar[2]	[1]Univ. Leipzig, IMKM [2]HMI Berlin	E9	**PHY-01-1563**
80	***Structure investigation of the Kesterite-Stannite Series, Cu_2FeSnS_4 – Cu_2ZnSnS_4***	S. Schorr[1] M. Tovar[2]	[1]Univ. Leipzig, IMKM [2]HMI Berlin	E9	**PHY-01-1565**
81	***Phase diagram of $Sr_xBa_{1-x}TiO_3$ solid solutions***	A. Naberezhnov[1] E. Smirnova[1] M. Tovar[2]	[1]PTI St. Petersbg., RU [2]HMI Berlin	E9	**PHY-01-1575**
82	***Crystal structure and vacancies order in chalcopyrite related semiconductors CuX_nY_m(X=In, Ga; Y=S, Se; n=1, 3, 5; m= 2, 5, 8)***	D. Fuertes-Marrón J. Hernández-Velasco	HMI Berlin	E9	**EF**
83	***Study of paramagnetic crystals of family $A_2CuCl_4{\cdot}2H_2O$ (A = NH_4, K, Rb) – A combination of quasielastic neutron scattering with broadband dielectric spectroscopy***	A. Buchsteiner[1] M. Slaboszewska[2] A. Mickiewicz[2]	[1]HMI Berlin [2]Univ. Poznan, PL	V3	**EF**
84	***Surfactant aggregate structure in SBA-15 silica nanopores***	G.H. Findenegg[1] T. Shin[1] U. Keiderling[2]	[1]TU Berlin [2]HMI Berlin	V4	**CHE-04-0935**
85	***Surfactant aggregate structure in SBA-15 silica nanopores***	G.H. Findenegg[1] T. Shin[1] U. Keiderling[2]	[1]TU Berlin [2]HMI Berlin	V4	**CHE-04-1011**

List of Contributed Experimental Reports

PAGE	TITLE	TEAM			PROPOSAL
Structural Excitations					
86	***NRSE investigation of phonon lifetimes in the conventional superconductor Nb***	K. Habicht[1,2] F. Mezei[1] T. Keller[3] B. Keimer[3] S. Bayrakci[3]	[1]HMI Berlin [2]TU Darmstadt [3]MPI FKF Stuttgart	V2	**PHY-02-0438**
87	***Phonon dispersion in the martensitic phase of ferromagnetic Ni_2MnGa***	P. Vorderwisch[1] S.M. Shapiro[2]	[1]HMI Berlin [2]Brookhaven Nat. Lab., USA	V2	**PHY-02-0440**
88	***Triple axis study of the intrinsic of phonons in i-AlPdMn***	R.A. Brand[1] K. Habicht[2] T. Keller[3]	[1]Uni Duisburg [2]HMI Berlin [3]MPI Stuttgart	V2	**PHY-02-0372**
89	***Study of the aromatic H-bond in NH_4- and ND_4-tetraphenylborate***	N. Jalarvo[1] A. Desmedt[2] R. Lechner[1] F. Mezei[1]	[1]HMI Berlin [2]Univ. Bordeaux I, F	V3	**EF**
90	***SANS structural characterisation of pillared layered catalysts***	T.A. Steriotis[1] A. de Stefanis[2] G. Charalambopoulou[1] U. Keiderling[3]	[1]NCSR Demokritos, GR [2]CNR ISMN Rome, I [3]HMI Berlin	V4	**CHE-04-0876**
91	***Slow dynamics of Co_2RuO_4***	G.E. Granroth D.L. Abernathy G. Ehlers S.E. Nagler	ORNL/SNS, USA	V5	**PHY-03-0332**
92	***Phason dynamics in the icosahedral quasicrystal i-AlCuFe***	R.A. Brand[1] C. Pappas[2] C. Fehr[2]	[1]Uni Duisburg-Essen [2]HMI Berlin	V5	**PHY-03-0363**
Soft Matter					
93	***Investigation of DaPP static structure factor temperature evolution***	F. Mezei[1] O. Russina[1] J.-U. Hoffmann[1] T. Lonkai[2]	[1]HMI Berlin [2]Uni Tübingen	E2	**EF**
94	***Water mobility in graphite oxide***	A. Lerf[1] A. Buchsteiner[2]	[1]BAW Garching [2]HMI Berlin	V3	**PHY-03-0318**
95	***The study of changes in pyridinium cation dynamics in (bis)thiuorea pyridinium bromide inclusion compound***	P. Czarnecki[1] A. Marczak[1] A. Buchsteiner[2]	[1]AMU Poznan, PL [2]HMI Berlin	V3	**PHY-03-0323**
96	***Ordering upon melting: the effect of the fast dynamics on the order***	A. Triolo[1] O. Russina[2] F. Mezei[2] M. Russina[2]	[1]CNR IPCF Messina, I [2]HMI Berlin	V3	**PHY-03-0322**
97	***On the nature of the fast process in B_2O_3***	A. Triolo[1] O. Russina[2] F. Mezei[2] M. Russina[2]	[1]CNR IPCF Messina, I [2]HMI Berlin	V3	**PHY-03-0360**
98	***Diffusive relaxation processes in liquid ethylene glycol***	O. Sobolev[1] A. Novikov[2] J. Pieper[1]	[1]HMI Berlin [2]IPPE, Obninsk, RU	V3	**PHY-03-0336 EF**
99	***Controlled grafting from nano-silica beads***	A. El Harrak F. Boue J. Jestin G. Carrot J. Oberdisse	CEA-LLB Saclay, F	V4	**PHY-04-0940**

List of Contributed Experimental Reports

PAGE	TITLE	TEAM			PROPOSAL
100	***Controlled grafting from nano silica beads***	G. Carrot J. Jestin F. Boué	CNRS-LLB Saclay, F	V4	**PHY-04-1021**
101	***Tuning the hydrophobic interaction to act on the capacity of a polyelectrolyte to unfold a protein***	F. Cousin[1] J, Gummel[1] F. Boue[1] J. Haug[2]	[1]CNRS-LLB Saclay, F [2]HMI Berlin	V4	**OTH-04-0942**
102	***Huge polymer build with recognition groups directed hydrogen bonds self-assembly***	D. Sarazin[1] J.M. Guenet[1] A. Brandt[2] J.M. Lehn[3]	[1]ICS Strasbourg, F [2]HMI Berlin [3]ISIS Strasbourg, F	V4	**CHE-04-0943**
103	***The effect of particulate addition on surfactant stabilised emulsions***	T. Cosgrove[1] C.P. Chan[1] C. Dreiss[1] D. Clemens[2]	[1]Univ. Bristol, UK [2]HMI Berlin	V4	**CHE-04-0949**
104	***Silicate-based nanoparticles and their interactions with PDMS melts and solutions***	C. Dreiss T. Cosgrove C. Chan	Univ. Bristol, UK	V4	**CHE-04-0952**
105	***Surface effects from doping liquid crystals***	R. Richardson[1] Y. Gyn[2] J. Lau[2] U. Keiderling[3]	[1]Univ. Bristol, UK [2]ILL Grenoble, F [3]HMI Berlin	V4 V6	**PHY-04-1035** **04-1058**
106	***Nanoscale dynamics of a strong glass former across its glass transition***	A. Triolo[1] O. Russina[2] F. Mezei[2] C. Pappas[2] C. Fehr[2]	[1]CNR IPCF Messina, I [2]HMI Berlin	V5	**PHY-03-0334**
107	***Characterization of trehalose aqueous solutions by neutron spin echo as a function of temperature and concentration***	S. Magazù F. Migliardo	Univ. Messina, I	V5	**PHY-03-0302**
108	***Biocomposite planar polyelectrolyte multilayers as a tool to understand different DNA transport systems***	S. Gromelski[1] R. Krastev[1,2,3]	[1]MPI-KGF Golm [2]HMI Berlin [3]TU Berlin	V6	**BIO-04-1002 LT**
109	***Adsorption of B18 peptide on hydrophilic charged surfaces***	S. Rocha[1] R. Krastev[1,2,3] G. Brezesinski[1]	[1]MPI-KGF Golm [2]HMI Berlin [3]TU Berlin	V6	**CHE-04-0907 LT**
110	***Adsorption of amyloid beta (1-40) peptide on hydrophilic positively charged polymer***	S. Rocha[1] R. Krastev[1,2,3] G. Brezesinski[1]	[1]MPI-KGF Golm [2]HMI Berlin [3]TU Berlin	V6	**CHE-04-0907 LT**
111	***PEO-PPO-PEO triblock copolymers at the polymer/water Interface, part II***	R. Sedev[1] R. Steitz[2,4,5] G.H. Findenegg[2] M. Izerrouken[3]	[1]Univ. South Australia, AU [2]TU Berlin [3]CRND, Algeria [4]HMI Berlin [5]MPI-KGF Golm	V6	**CHE-04-0913**
112	***How bound is bound water in swollen polyelectrolyte multilayers?***	J.E. Wong[1] R. v. Klitzing[1] S. Schemmel[1] R. Steitz[1,2,3]	[1]TU Berlin [2]HMI Berlin [3]MPI-KGF Golm	V6	**PHY-04-0888** **04-0964**
113	***Density depletion at the interface between hydrophobic surfaces and water***	M. Grunze[1] M. Maccarini[1] R. Steitz[2,3,4]	[1]RKU Heidelberg [2]HMI Berlin [3]TU Berlin [4]MPI-KGF Golm	V6	**CHE-04-0895** **04-0966**
114	***Chemical switching of model cell membrane - Substrate interactions with weak polyelectrolytes***	M. Tanaka[1] F. Rehfeldt[1] E. Schneck[1] K. Seidel[1] R. Steitz[2,3,4]	[1]TU München [2]HMI Berlin [3]MPI-KGF Golm [4]TU Berlin	V6	**PHY-04-0968**

List of Contributed Experimental Reports

PAGE	TITLE	TEAM			PROPOSAL
115	***Critical and multilayer adsorption from alkane + perfluoroalkane mixtures***	J. Bowers[1] A. Zarbakhsh[2] J.R.P. Webster[3] I.A. McLure[4]	[1]Univ. Exeter,UK [2]Univ. London, UK [3]ISIS Chilton, UK [4]Univ. Sheffield, UK	V6	**PHY-04-0977**
116	***Hydration of lipid layers on polyelectrolyte multilayer support***	C. Delajon[1] R. Krastev[2,3,4]	[1]Univ. +ISIS, Strasbourg, F [2]MPI-KGF Golm [3]HMI Berlin [4]TU Berlin	V6	**CHE-04-0976**
117	***Soft supported lipid layers for adsorption studies of Aβ(25-35)***	S. Dante[1,3] Th. Hauß[2,3] R. Steitz[3,4,5] S. Schemmel[4]	[1]TU Darmstadt [2]Univ. Düsseldorf [3]HMI Berlin [4]TU Berlin [5]MPI-KGF Golm	V6	**BIO-04-0997 LT**
118	***Temperature dependent water depletion at the hydrophobic solid/liquid interface***	R. Steitz[1,2,3] G.H. Findenegg[1] S. Schemmel[1]	[1]TU Berlin [2]HMI Berlin [3]MPI-KGF Golm	V6	**CHE-04-0998 LT**
119	***Influence of the confinement on the amount of D_2O absorbed in polyelectrolyte films***	R. Krastev[1,2,3] N.C. Mishra[1]	[1]MPI-KGF Golm [2]HMI Berlin [3]TU Berlin	V6	**CHE-04-1004**
120	***Internal order of polyelectrolyte multilayers***	C.A. Helm M. Gopinadhan H. Ahrens J.-U. Günther	EMAU Greifswald	V6	**PHY-04-1049**
121	***Novel lipopolymer supported lipid bilayers***	P. Theato[1] R. Krastev[2,3,4]	[1]Univ. Mainz [2]MPI-KGF Golm [3]HMI Berlin [4]TU Berlin	V6	**CHE-04-1051**
122	***Neutron reflectivity and calcium-induced modification of a phospholipid/polymer layer***	M.H. Ropers[1] R. Krastev[2,3,4]	[1]INRA Nantes, F [2]MPI-KGF Golm [3]HMI Berlin [4]TU Berlin	V6	**PHY-04-1070 LT**
123	***Pretreatment dependent water depletion at a hydrophobic solid/liquid interface***	R. Steitz[1,2,3] G.H. Findenegg[1] S. Schemmel[1]	[1]TU Berlin [2]HMI Berlin [3]MPI-KGF Golm	V6	**PHY-04-1072 LT**

Biology

124	***Thermal expansion and electroweak interaction in the amino acid L-alanine***	H.N. Bordallo[1] M. Barthès[2] F. Denoyer[3] C. Fehr[1] D.N. Argyriou[1]	[1]HMI Berlin [2]Univ. Montpellier II, F [3]Univ. Paris XI, F	E9	**EF**
125	***Interaction of NK-2 with POPC***	R. Willumeit F. Förster S. Linser	GKSS Geesthacht	V1	**BIO-01-1488**
126	***A neutron diffraction study on nucleolipid membranes***	F. Baldelli Bombelli P. Baglioni S. Milani	Univ. Firenze, I	V1	**BIO-01-1600**
127	***Skin lipid organisation***	J. Bouwstra[1] G. Gooris[1] G. Charalambopoulou[2] T.A. Steriotis[2] Th. Hauß[3,4]	[1]Univ. Leiden, NL [2]NCSR Demokritos, GR [3]HMI Berlin [4]Univ. Düsseldorf	V1	**BIO-01-1601**
128	***Fusion peptides and the inverted hexagonal phase in phospholipids***	J. Bradshaw[1] K. Balali-Mood[1] Th. Hauß[2,3]	[1]Univ. Edinburgh, UK [2]HMI Berlin [3]Univ. Düsseldorf	V1	**BIO-01-1386 01-1487**
129	***Interaction of Alzheimer's β-amyloid (1-42) peptide with cholesterol-containing membranes***	J. Bradshaw R. Ashley K. Balali-Mood	Univ. Edinburgh, UK	V1	**BIO-01-1602**

List of Contributed Experimental Reports

PAGE	TITLE	TEAM			PROPOSAL
130	***Transport properties of hydrated stratum corneum***	T.A. Steriotis[1] G. Charalambopoulou[1] J. Pieper[2]	[1]NCSR Demokritos, GR [2]HMI Berlin	V3	**BIO-03-0288**
131	***Elastic resolution spectroscopy of protein solutions, stability of lactalbumin***	W. Doster[1] A. Buchsteiner[2]	[1]TU München [2]HMI Berlin	V3	**BIO-03-0317**
132	***Study of the influence of the pressure on the structure and dynamics of BPTI***	M.-S. Appavou[1] M.-C. Bellissent-Funel[1] B. Annighöfer[1] J. Pieper[2] A. Buchsteiner[2]	[1]CEA-LLB Saclay, F [2]HMI Berlin	V3	**BIO-03-0319**
133	***Dynamics of immobilized myoglobin the folding/unfolding transition***	S. Longeville[1] A. Haouz[2] J. Pieper[3]	[1]CEA-LLB, F [2]Institut Pasteur, Paris, F [3]HMI Berlin	V3	**BIO-03-0320**
134	***Using QUENS to explore the dynamics of serine proteases***	A. Zychlinsky[1] M. Ingersoll[1] H.N. Bordallo[2] T. Hauß[2,3] E. Garcia-Matres[2]	[1]MPI IB Berlin [2]HMI Berlin [3]Univ. Düsseldorf	V3	**BIO-03-0355**
135	***Picosecond internal dynamics of lysozyme embedded in a glucose matrix as affected by thermal unfolding***	A. de Francesco[1] A. Paciaroni[1] J. Pieper[2]	[1]Univ. Perugia, I [2]HMI Berlin	V3	**BIO-03-0359**
136	***Protein dynamics in the monomeric light-harvesting complex II of green plants***	J. Pieper[1] R.E. Lechner[1] K.-D. Irrgang[2] M. Rätsep[3]	[1]HMI Berlin [2]TU Berlin [3]FI Tartu, EE	V3	**EF**
137	***Structural organization of photo system II membranes of green plants***	J. Pieper[1] A. Buchsteiner[1] R.E. Lechner[1] Th. Hauß[1,3] M. Weß[2] G. Renger[2]	[1]HMI Berlin [2]TU Berlin [3]Univ. Düsseldorf	V3	**EF**
138	***Light-induced protein dynamics in bacteriorhodopsin***	J. Pieper[1] A. Buchsteiner[1] R.E. Lechner[1] Th. Hauß[1,2] N. Dencher[3]	[1]HMI Berlin [2]Univ. Düsseldorf [3]TU Darmstadt	V3	**EF**
139	***Dynamical transition in the amino acid L-alanine***	H.N. Bordallo[1] M. Barthès[2] F. Denoyer[3] C. Fehr[1] J. Pieper[1] A. Buchsteiner[1]	[1]HMI Berlin [2]Univ. Montpellier II, F [3]Univ. Paris XI, F	V3	**EF**
140	***Supramolecular organisation in gene delivery complexes***	T.A. Steriotis[1] G. Charalambopoulou[1] Th. Hauß[2,3] U. Keiderling[2]	[1]NCSR Demokritos, GR [2]HMI Berlin [3]Univ. Düsseldorf	V4	**BIO-04-0944**
141	***Reverse phases of phosphatidylnucleosides***	D. Berti F. Baldelli Bombelli F. Betti P. Baglioni	Univ. Firenze, I	V4	**BIO-04-0946**
142	***A SANS study of the porosity of biogenic silica from the fustules of diatom species***	C. Garvey[1] J. Ferris[1] J. Haug[2]	[1]ANSTO, AU [2]HMI Berlin	V4	**BIO-04-0953**
143	***A USANS study of the porosity of cultured diatoms***	C. Garvey[1] J. Ferris[1] M. Strobl[2,3]	[1]ANSTO, Australia [2]HMI Berlin [3]TFH Berlin	V12a	**BIO-04-0961**
144	***Adsorption of S-protein on polyelectrolyte multilayers***	J.L. Toca Herrera[1] R. Krastev[2,3,4]	[1]BOKU, Wien, A [2]MPI-KGF Golm [3]HMI Berlin [4]TU Berlin	V6	**BIO-04-0971**

List of Contributed Experimental Reports

PAGE	TITLE	TEAM			PROPOSAL
Material Science and Industrial Applications					
145	***Thermal stability and effect of the external magnetic field on 7M modulated structure in non-stoichiometric Ni-Mn-Ga ferromagnetic martensite***	N. Glavatska[1] I. Glavatskyy[1] J.-U. Hoffmann[2]	[1]NAS IMP Kiev, UA [2]HMI Berlin	E2	**MAT-01-1444**
146	***Residual stresses in ball bearing rings, -comparison of Neutron and X-ray diffraction measurements***	T. Hirsch[1] A. da S. Rocha[1] S. Poeste[2,3] R. Schneider[2]	[1]Univ. Bremen, IWT [2]HMI Berlin [3]TU Berlin	E3	**MAT-01-1391 01-1491**
147	***The impact of grain size on residual stress measurement in welded components***	R.C Wimpory[1,2] C. Ohms[1]	[1]JRC-IE Petten, NL [2]HMI Berlin	E3	**MAT-01-1493**
148	***Effect of fatigue crack propagation on residual stresses in a 2024 aluminium weld coupon***	L. Edwards[1] S. Pratihar[1] J.M.L. Tan[1] T. Poeste[2,3] R. Schneider[2] F. Henkel[2]	[1]Open Univ., UK [2]HMI Berlin [3]TU Berlin	E3	**MAT-01-1495**
149	***Residual stress relaxation in fatigued cold-expanded holes***	L. Edwards[1] S. Pratihar[1] J.M.L. Tan[1] T. Poeste[2,3] R. Schneider[2] F. Henkel[2]	[1]Open Univ., UK [2]HMI Berlin [3]TU Berlin	E3	**MAT-01-1496**
150	***Stress gradients below the surface of a model rocket nozzle***	M. Hofmann[1] T. Poeste[2,3] R. Schneider[3]	[1]TU München, FMR II [2]TU Berlin [3]HMI Berlin	E3	**MAT-01-1635**
151	***Study of the R-phase structure in NiTi shape memory alloys***	W. Schmahl[1] J. Khalil-Allafi[2]	[1]RU Bochum [2]Sahand Univ, Tabriz, IR	E9	**MAT-01-1449**
152	***Neutron powder diffraction line broadening and corrosion products of an electrochemically cycled $LaMMNi_{3.55}Co_{0.75}Mn_{0.4}Al_{0.3}$ battery electrode material***	P.A. Georgiev[1] M. Tovar[2] D.L. Ross[1]	[1]Univ. Salford, UK [2]HMI Berlin	E9	**MAT-01-1458**
153	***Phase analysis of Ni-Fe-base superalloys***	R. Gilles[1] M. Hölzel[1,2] D. Mukherji[3] D. del Genovese[4] P. Strunz[5] D. Többens[6]	[1]TU München [2]TU Damstadt [3]ETH Zürich, CH [4]IWF TU Braunschweig [5]PSI Villigen, CH [6]HMI Berlin	E9	**MAT-01-1453 01-1566**
154	***Mechanism of formation and structure of zeolite LTA colloids***	J.D.F. Ramsay[1] J.M. Condre[1] T.A. Steriotis[2] U. Keiderling[3]	[1]Univ. Montpellier II, F [2]NCSR Demokritos, GR [3]HMI Berlin	V4	**MAT-04-0873**
155	***Synergism effects between Ni and Cu on the radiation susceptibility of RPV model alloys***	A. Ulbricht[1] U. Keiderling[2]	[1]FZ Rossendorf [2]HMI Berlin	V4	**MAT-04-0937**
156	***Solution treatment of the single-crystal Ni-base superalloy Re_{81}***	P. Strunz[1] D. Mukherji[2] J. Rösler[3] R. Gilles[4]	[1]ASCR NPI Rez, CZ [2]ETH Zürich, CH [3]TU Braunschweig [3]TU München	V4	**MAT-04-0955**
157	***Solution treatment of the single-crystal Ni-base superalloy CMSX4***	P. Strunz[1] D. Mukherji[2] J. Rösler[3] R. Gilles[4]	[1]ASCR NPI Rez, CZ [2]ETH Zürich, CH [3]TU Braunschweig [4]TU Darmstadt	V4	**MAT-04-1018**

List of Contributed Experimental Reports

PAGE	TITLE	TEAM			PROPOSAL
158	***Investigation of the microstructure of ferrofluids using small angle neutron scattering***	S. Odenbach[1] L. Pop[1] O. Brunke[1] H. Engler[1] M. Kammel[2]	[1]Uni Bremen [2]HMI Berlin	V4	**MAT-04-1012**
159	***In-situ SANS study of microstructure homogenization in wrought nickel-base superalloy***	J. Zrnik[1] P. Strunz[2] P. Hornák[1] U. Keiderling[3]	[1]TU Kosice, SK [2]ASCR NPI Rez, CZ [3]HMI Berlin	V4	**MAT-04-1031**
160	***SANSPOL structure studies of cobalt - ferrofluids***	M. Kammel A. Wiedenmann A. Heinemann	HMI Berlin	V4	**EF**
161	***Crystallization behaviour of amorphous $Al_{94-x}Ni_6La_x$ (x=4-7) alloys***	J. Haug M. Wollgarten K.L. Sahoo	HMI Berlin	V4	**EF**
162	***Low temperature behaviour of ordering phenomena in ferrofluids***	A. Wiedenmann A. Heinemann	HMI Berlin	V4	**EF**
163	***Field dependence of ordering phenomena in ferrofluids***	A. Wiedenmann A. Heinemann	HMI Berlin	V4	**EF**
164	***Time dependence of field induced ordering in concentrated ferrofluids studied by SANS***	A. Wiedenmann U. Keiderling J. Haug	HMI Berlin	V4	**EF**
165	***SANS with polarisation analysis on ferrofluids using ^{3}He filter***	A. Wiedenmann[1] A. Rupp[1] W. Heil[2]	[1]HMI Berlin [2]Univ. Mainz	V4	**EF**
166	***Neutron tomography on white and polychromic marbles of archaeological interest***	N. Kardjilov[1] R. Triolo[2] A. Hilger[1] I. Manke[1]	[1]HMI Berlin [2]Univ. di Palermo, I	V7	**MAT-04-1062**
167	***Real-time imaging of diffusion processes in liquid metals***	A. Griesche N. Kardjilov A. Hilger	HMI Berlin	V7	**MAT-04-1080 EF**
168	***Investigation of the discharge process in a LiI-battery***	I. Manke N. Kardjilov A. Hilger	HMI Berlin	V7	**MAT-04-1081**
169	***Investigation of geological samples (granite)***	I. Manke J. Tiedemann N. Kardjilov A. Hilger	HMI Berlin	V7	**MAT-04-1083**
170	***Neutron tomography of archaeological glass samples***	F. Rustichelli[1] F. Fiori[1] N. Kardjilov[2] A. Hilger[2]	[1]Univ. Ancona, I [2]HMI Berlin	V7	**EF**
171	***Neutron tomography of aviation engine vent pipes***	C. Lewis[1] T. Cable[1] M. Strobl[2,3] A. Hilger[3] N. Kardjilov[3] W. Treimer[2,3]	[1]AAIB, UK [2]TFH Berlin [3]HMI Berlin	E8	**PHY-04-1074 LT**
172	***Tomographies of industrially manufactured silver rings***	F. Rustichelli[1] M. Strobl[2,3] N. Kardjilov[3]	[1]Univ. Ancona, I [2]TFH Berlin [3]HMI Berlin	E8	**PHY-04-1074 LT**
173	***Investigation of polymer electrolyte membrane fuel cell (PEMFC) water household***	I. Manke[1] J. Scholta[3] M. Strobl[1,2] A. Hilger[1] N. Kardjilov[1]	[1]HMI Berlin [2]TFH Berlin [3]ZSW Ulm	E8	**MAT-04-1085 EF**

List of Contributed Experimental Reports

PAGE	TITLE	TEAM			PROPOSAL
174	***Imaging of fibre reinforced low absorbing materials***	M. Bastürk[1] H. Rauch[1] M. Strobl[2,3] A. Hilger[3] N. Kardjilov[3]	[1]ATI Wien, A [2]TFH Berlin [3]HMI Berlin	V12a E8 V7	**MAT-04-1040**
175	***SANS investigation of microstructural features influencing crack growth in aluminium alloys***	F. Fiori[1] A. Manescu[1] V. Calbucci[1] M. Strobl[2,3]	[1]Univ. Ancona, I [2]HMI Berlin [3]TFH Berlin	V12a	**MAT-04-1042**
176	***Mesoscopic structure of marbles***	R. Triolo[1] F. Lo Celso[1] I. Ruffo[2] M. Strobl[3,4]	[1]Univ. Palermo, I [2]Univ. Mursia, I [3]TFH Berlin [4]HMI Berlin	V12a	**OTH-04-1043**
177	***Test and application of refraction and USANS contrast tomography***	M. Strobl[1,2] W. Treimer[1,2] A. Hilger[2] N. Kardjilov[2]	[1]TFH Berlin [2]HMI Berlin	V12a	**PHY-04-1074 04-1075 LT**

Development of Instruments and Methods

178	***Influence of external magnetic fields on ^{3}He filter cells made out of quartz glass***	V. Hutanu A. Rupp J. Klenke	HMI Berlin	E1	**EF**
179	***Phase contrast radiography with monochromatic neutrons***	M. Strobl[1,2]	[1]TFH Berlin [2]HMI Berlin	E8	**PHY-04-1074 LT**
180	***Manipulation of the spin-fan in NRSE***	K. Habicht	HMI Berlin	V2	**PHY-02-0388**
181	***Time-resolved SANS listmode data: generation with detector control program "Mesydaq" and treatment with "BerSANS-PC" data processing software***	U. Keiderling A. Wiedenmann J. Haug	HMI Berlin	V4	**EF**
182	***TOF-SANS on V4 after changing the detector readout system***	J. Haug U. Keiderling A. Wiedenmann	HMI Berlin	V4	**EF**
183	***Spin echo scattering angle measurement (SESAME)***	R. Pynn[1] M. Fitzsimmons[1] H. Fritzsche[2] J. Major[3]	[1]LANL, USA [2]NRC Chalk River, CA [3]MPI MF Stuttgart	V6	**MAT-04-0978**
184	***Tests of a fast speed camera for real-time imaging***	N. Kardjilov[1] A. Hilger[1] J. Brunner[2]	[1]HMI Berlin [2]TU München	V7	**MAT-04-1079 EF**
185	***Testing a crystal for tomographic applications***	W. Treimer[1,2] M. Strobl[1,2]	[1]TFH Berlin [2]HMI Berlin	E8	**PHY-04-1078 LT**
186	***Synchrotron tomography study on disc chopper coatings***	J. Peters A. Haibel A. Rack	HMI Berlin	BESSY	**EF**
187	***Divergence investigations for 3D refraction contrast tomography***	M. Strobl[1,2] W. Treimer[1,2]	[1]TFH Berlin [2]HMI Berlin	V12a	**PHY-04-1074 LT**
188	***Inelastic neutron scattering by ultrasound. Research by Bonse-Hart diffractometer***	E. Iolin[1] M. Strobl[2,3] W. Treimer[2,3] L. Rusevich[1] P. Mikula[4]	[1]IPE, Riga, LV [2]HMI Berlin [3]TFH Berlin [4]NPI, Prague, CZ	V12b	**PHY-04-1044**

PAGE	TITLE	TEAM			PROPOSAL
189	***Test of a radial cavity neutron spin analyser***	P. Falus[1] G. Felcher[1] A. Vorobiev[2] Th. Krist[3]	[1]ANL Argonne, USA [2]MPI-MF Stuttgart [3]HMI Berlin	V14	**PHY-04-1084 EF**
190	***Polarising bender used in transmission***	Th. Krist	HMI Berlin	V14	**EF**
191	***Recent performance studies of the instrument EXED***	J. Peters K. Lieutenant F. Mezei	HMI Berlin	EXED	**EF**

Fundamental Physics and Others

192	***Study of PNR in relaxor ferroelectrics $PbMg_{1/3}Nb_{2/3}O_3$ by quasielastic neutron scattering***	A. Naberezhnov[1] J. Klenke[2] S. Vakhrushev[1]	[1]PTI St. Petersbg., RU [2]HMI Berlin	E1	**PHY-02-0428**
193	***Melting-freezing phase transition in nanostructured mercury***	A. Naberezhnov[1] J.-U. Hoffmann[2] M. Tovar[2]	[1]PTI St. Petersbg., RU [2]HMI Berlin	E2	**PHY-01-1443**
194	***Neutron tomography of geological samples***	M. Strobl[1,2] J. Walter[3]	[1]TFH Berlin [2]HMI Berlin [3]FZ Jülich / GZG	E8	**PHY-04-1074 LT**
195	***Investigation of the low energy vibrational density of states in $Fe_{0.3}Y_{0.7}$ and $Fe_{1-x}Sn_x$ (x=0.3, 0.4 and 0.5) ribbons***	W. Keune[1] B. Sahoo[1] V. Kuncser[2] J. Pieper[3]	[1]Uni Duisburg-Essen [2]NIPM Bucharest, RO [3]HMI Berlin	V3	**PHY-03-0316**
196	***Molecular dynamics in triclycine sulphate by cold neutron spectroscopy***	V. Tripadus[1] A. Radulescu[2] J. Pieper[3] A. Buchsteiner[3]	[1]IFIN-HH Bucharest, RO [2]FZ Jülich [3]HMI Berlin	V3	**PHY-03-0326**
197	***SANS studies on undercooled metals***	O. Perroud A. Wiedenmann	HMI Berlin	V4	**EF**
198	***Search for partially ordered structures in very high concentrated Fe_3O_4 based magnetic liquids***	A. Wiedenmann A. Heinemann M. Kammel	HMI Berlin	V4	**EF**
199	***Coherence investigations with Si phase gratings***	W. Treimer[1,2] M. Strobl[1,2]	[1]TFH Berlin [2]HMI Berlin	V12a	**PHY-04-1077 LT**
200	***Refraction versus USANS by nearly perfect Si crystal surfaces***	W. Treimer[1,2] A. Qissabi[1] M. Strobl[1,2] A. Hilger[2]	[1]TFH Berlin [2]HMI Berlin	V12b	**PHY-04-1078 LT**
201	***Refraction versus USANS from different prepared perfect Si surfaces***	W. Treimer[1,2] A. Qissabi[1] M. Strobl[1,2] A. Hilger[2]	[1]TFH Berlin [2]HMI Berlin	V12b	**PHY-04-1078 LT**
202	***Investigations of neutron scattering by surface effects of perfect Si plates***	W. Treimer[1,2] A. Qissabi[1] M. Strobl[1,2] A. Hilger[2]	[1]TFH Berlin [2]HMI Berlin	V12b	**PHY-04-1078 LT**
203	***USANS with large area Si phase gratings***	M. Trinker[1] E. Jericha[1] M. Strobl[2,3] A. Hilger[2] W. Treimer[2,3]	[1]ATI Wien, A [2]TFH Berlin [3]HMI Berlin	V12a	**PHY-04-1041**
204	***USANS with large area Si phase gratings, part II***	M. Trinker[1] E. Jericha[1] M. Strobl[2,3] A. Hilger[3] W. Treimer[2,3]	[1]ATI Wien, A [2]TFH Berlin [3]HMI Berlin	V12b	**PHY-04-1041**

List of Contributed Experimental Reports

PAGE	TITLE	TEAM			PROPOSAL
205	***Search for scission neutrons using angular correlations in fission of U-235***	G.V. Danilyan[1] V.S. Pavlov[1] I. Karpikhin[1] V.A. Krakhotin[1] A.V. Fedorov[1] E. Brakhman[1] R. Golub[2] E. Korobkina[2] Th. Wilpert[2]	[1]ITEP Moscow, RU [2]HMI Berlin	V13	**PHY-05-007**
206	***Autoradiographs of the painting "The Old Man with the Cane and the Plume Cap" unknown artist, copy of Rembrandt, 82,5 x 102 cm^2***	C. Laurenze-Landsberg[1] C. Schmidt[1] L.A. Mertens[2] B. Schröder-Smeibidl[2]	[1]Gemäldegalerie Berlin [2]HMI Berlin	B8	**EF**
207	***Autoradiographs of the painting "The Hermit" unknown artist, 46,6 x 63,3 cm^2***	C. Laurenze-Landsberg[1] C. Schmidt[1] L.A. Mertens[2] B. Schröder-Smeibidl[2]	[1]Gemäldegalerie Berlin [2]HMI Berlin	B8	**EF**
208	***Autoradiographs of the painting "The Baptism of a Child" Jan Steen, 85 x 100 cm^2, Cat No. 795D***	C. Laurenze-Landsberg[1] C. Schmidt[1] L.A. Mertens[2] B. Schröder-Smeibidl[2]	[1]Gemäldegalerie Berlin [2]HMI Berlin	B8	**EF**

BENSC	**EXPERIMENTAL REPORT** **A magnetic field effect on spin density wave in $Pr_{0.88}LaCe_{0.12}CuO_4$**	Proposal N° PHY-01-1465DT Instrument **E4** Local Contact Dimitri Argyriou
Principal Proposer: Experimental Team:	Pengcheng Dai, University of Tennessee, USA Dimitri Argyriou, HMI, H. J. Kang, University H. A. Mook, Oak Ridge National Lab, USA Yoich Ando, Central Research Institute of Electric Power Industry, Japan	Date(s) of Experiment Feb/2004

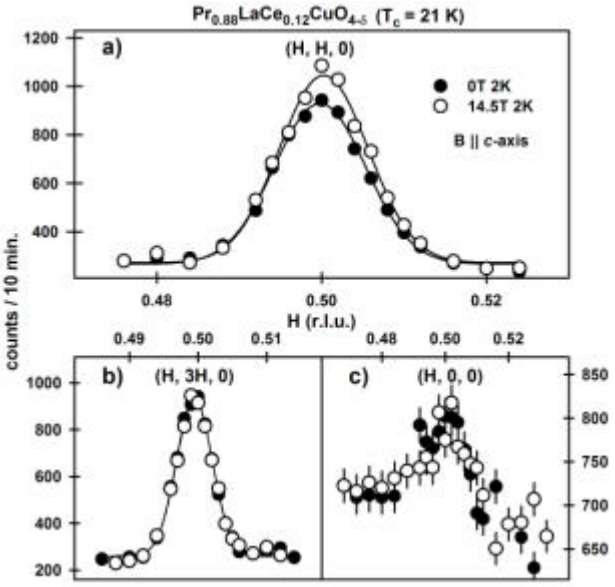
Date of Report: 9/10/04

The coexistence and competition of magnetism and superconductivity is one of the most important problems to be answered in understanding the mechanism of the high-transition-temperature superconductors. Several experimental results in hole-doped cuprates show that the antiferromagnetic order coexists with superconductivity. The antiferromagnetism has two-dimensional characteristic. It has long-range order in CuO_2 plane and short-range correlation between CuO_2 layers.

The antiferromagnetism has been predicted as a competing order in underdoped superconductors by theories [1,2]. The field-induced antiferromagnetism has been observed below transition temperature in hole-doped $La_{2-x}Sr_xCuO_4$ [3], and La_2CuO_{4+y} [4] in underdoped regime. This indicates that the antiferromagnetism competes with superconductivity. Our goal is to search similar results in electron-doped superconductors to see if this is universal phenomenon in high temperature cuprates.

The field-induced antiferromagnetism has also been observed in electron-doped superconductor $Nd_{1.85}Ce_{0.15}CuO_4$ [5]. However, it is difficult to separate the field-induced effect of Cu^{2+} in NCCO from that of Nd^{3+} in impurity phase $(NdCe)_2O_3$ which is induced from annealing process and lattice matched with NCCO [6]. Therefore, it is necessary to study electron-doped superconductors where the impurity phase has a nonmagnetic ground state. $Pr_{0.88}LaCe_{0.12}CuO_{4-d}$ is perfect for this purpose, since Pr^{3+} in impurity $(PrLaCe)_2O_3$ has nonmagnetic ground state.

After we found commensurate spin density wave in electron-doped PLCCO similar to that in LSCO, we performed field-induced effect experiment using 14.5T vertical magnet. The *c*-axis aligned magnetic field on PLCCO induces the antiferromagnetic order at (0.5, 0.5, 0) position (Fig. **a**). Meanwhile the magnetic field has no effect on residual antiferromagnetic position (0.5, 1.5, 0) (Fig. **b**). The H scan at (0.5, 0, 0) coming from impurity peak $(1, 1, 0)_c$ shows no field-induced effect (Fig. **c**).



Our experiment shows that an applied magnetic field in electron-doped superconductors, as well as hole-doped one can enhance the spin density wave order. The coexistence and competition of spin density wave and superconductivity is common nature regardless of electron or hole doping.

[1] Shou-Cheng Zhang, Science 275, 1089 (1997)
[2] D. Arovas *et al.* Phys. Rev. Lett. 79, 2871 (1997)
[3] B. Lake *et al.* Nature 415, 299 (2002)
[4] B. Khaykovich *et al.* Phys. Rev. B 66, 014528 (2002)
[5] H. J. Kang *et al.* Nature 423, 522 (2003)
[6] P. K. Mang *et al.* Nature 426, 139 (2003)

	EXPERIMENTAL REPORT **An in-plane magnetic field effect on superconductor $Pr_{0.88}LaCe_{0.12}CuO_4$**	Proposal N° PHY-01-1465 DT Instrument **E1** Local Contact Dimitri Argyriou
Principal Proposer: Experimental Team:	Pengcheng Dai, University of Tennessee, USA Dimitri Argyriou, HMI Berlin H. J. Kang, University of Tennessee, USA H. A. Mook, Oak Ridge National Lab, USA Yoich Ando, Central Research Institute of Electric Power Industry, Japan	Date(s) of Experiment July 2004

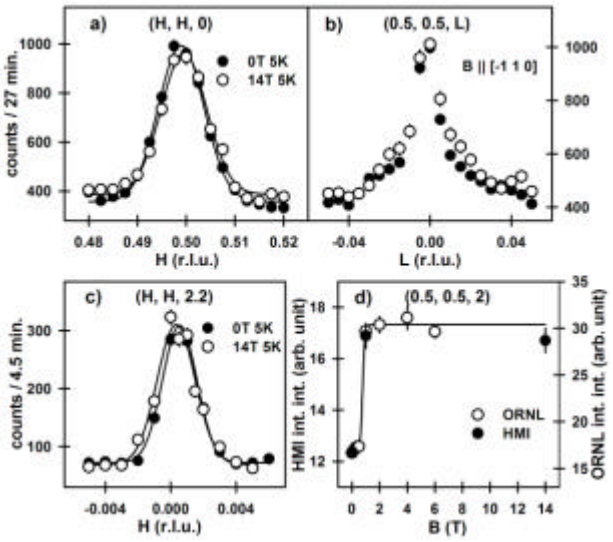
Date of Report: 9/10/04

It is believed that the magnetism has a key role in the mechanism of high-transition-temperature superconductors. As a result, many experiments have explored the effects of a magnetic field to determine what is competing with superconductivity, since the magnetic field is an excellent knob to control the strength of magnetism and superconductivity without changing the samples.

Several experiments on hole-doped cuprates show that the two-dimensional spin density wave coexists with superconductivity and it can be enhanced by a *c*-axis aligned magnetic field below T_c [1,2]. Since a similar field applied in the CuO_2 plane has little effect on superconductivity and spin density wave in LSCO [3], these results suggest that the antiferromagnetism competes with superconductivity.

We also find that the two-dimensional spin density wave coexists with superconductivity in electron-doped superconductor $Pr_{0.88}LaCe_{0.12}CuO_4$ [4] and it is enhanced by a *c*-axis aligned magnetic field [5]. Our first goal is to study the in-plane field effect to confirm that the field-induced antiferromagnetism by a *c*-axis aligned magnetic field is related to the suppression of superconductivity. Since the layered high-transition-temperature cuprates are highly anisotropic at zero field, the magnetic field perpendicular to CuO_2 plane can give much stronger effect than the one parallel to the plane. Second, we study the field effect on the impurity phase. Last, we check whether a high magnetic field induces magnetic moment at Pr^{3+}.

We aligned the crystal in (HHL) scattering plane and applied a magnetic field along [-110] direction using a vertical magnet. Figure **a** and **b** are the scans in-plane and out of plane direction, respectively. Both scans show no field-induced effect by the in-plane field. The scan at impurity position shows no field effect, either (Fig. **c**). Figure **d** shows the integrated intensity of (0.5, 0.5, 2) as a function of a field. The high field data are combined with low field data. The 1T of magnetic field B || [-110] induces the first order spin-flop transition in superconducting PLCCO sample. After spin-flop transition, the intensity is independent of a field. This indicates that the magnetic field does not induce moment at Pr^{3+} ions up to 14T.



The anisotropy of a magnetic field effect on spin density wave in electron-doped PLCCO indicates that the enhancement of antiferromagnetism is related to the suppression of superconductivity. This phenomenon is a common feature in high temperature cuprates, both hole and electron doping.

[1] B. Lake *et al.* Nature 415, 299 (2002)
[2] B. Khaykovich *et al.* Phys. Rev. B 66, 014528 (2002)
[3] B. Lake *et al.* unpublished
[4] Pengcheng Dai *et al.* submitted to Phys. Rev. Lett. (2004)
[5] H. J. Kang *et al.* unpublished

	EXPERIMENTAL REPORT **Magnetic Excitations in nanocrystalline Tb**	Proposal N° **PHY-02-420** Instrument **E1** Local Contact J. Klenke
Principal Proposer: Experimental Team:	O. Moze, Physics Dept, Modena Uni, Italy O. Moze J. Klenke, HMI	Date(s) of Experiment 14-22 Dec (2003)

Date of Report: 1 March 2004

The magnetic microstructure of a nanocrystalline hard magnet, Tb has recently been investigated for the first time by SANS (Weissműller et al, Phys. Rev. B **69**, 054402 [2004]). Two important parameters used in modelling the magnetic behaviour in this material, and indeed in understanding the nature of the large magnetic anisotropy in nanocrystalline Tb are the spin-wave stiffness constant D and the spin-wave gap Δ, which reflects dipolar and, most interestingly, anisotropy contributions. Estimates for nanocrystalline Tb of D are 150 meVÅ^2 and approximately 1.5 meV for Δ at 5 K.

We have recently attempted to measure the spin wave excitations in a rather small sample of nano Tb (dimensions of 0.4 x 8 x 8 mm^3) with a grain size of 9 nm. Elastic scans were performed above and below the ordering temperature of 224 K around the (100), (002) and (101) reciprocal lattice points of the nano Tb grains. The elastic scan at 300 K is displayed in Fig. 1 whilst an identical scan at 50 K is displayed in Fig. 2. The magnetic ordering within the Tb nano grains is evident in the increased intensity and sharpening up of the (100), (002) and (101) peaks. An incident energy of 14.7 meV was used to perform constant - q scans (at q = 0.1 and q = 0.2) with energy transfers of up to 8 meV at 50 K.

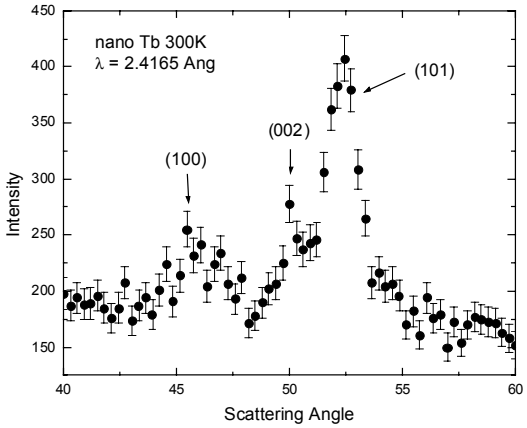


Fig. 1 Elastic scan for nano Tb at 300 K

No inelastic scattering was observable, even for relatively long counting times. This has to be attributed to the small amount of nano Tb available for this present experiment.

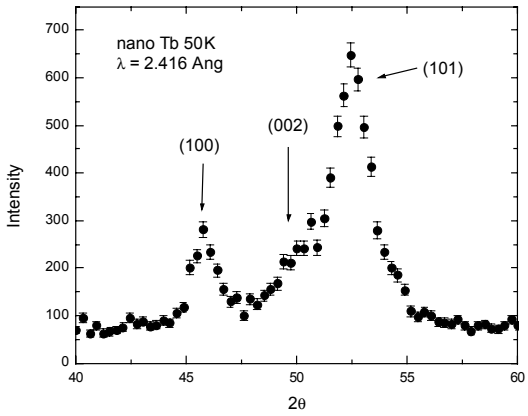


Fig. 2 Elastic scan for nano Tb at 50 K.

Efforts are presently underway to produce significantly more amounts of nanocrystalline Tb. It is envisaged that availability of more material will allow for a successful determination of the parameters D and Δ which control respectively the exchange and extremely high magnetic anisotropy energy terms in a prototypical nanocrystalline hard magnet such as Tb.

BENSC	**EXPERIMENTAL REPORT** **Magnetic and structural disorder in single crystalline UPt_2Si_2**	Proposal N° PHY-02-0426 PHY-02-0445 Instrument E1 Local Contact J. Klenke
Principal Proposer: Experimental Team:	S. Süllow, TU Braunschweig S. Süllow, TU Braunschweig J. Klenke, R. Feyerherm, HMI Berlin	Date(s) of Experiment 20.04.2004 – 27.04.2004 13.07.2004 – 18.07.2004

Date of Report: 04/01/2005

Recently, we have presented direct evidence for the presence of crystallographic disorder in a single crystalline, stoichiometric correlated electron material, UPt_2Si_2 [1]. The material crystallizes in the *P4/nmm* symmetry, while disorder is present in form of random static displacement of the Pt(2) and Si(2) atoms from their nominal high symmetry positions. We thus have a random bond disordered compound, that is, the U ions, which carry a magnetic moment, occupy a translationally invariant lattice, while the non-magnetic ligands are moderately disordered. The material undergoes an antiferromagnetically ordering transition (***k*** = [0 0 1]) at T_N ~ 32K [2,3]. In this situation we carried out a neutron diffraction study on the magnetically ordered state, in order to a.) directly establish the antiferromagnetic order and to b.) probe the effect of the crystallographic disorder on the magnetic properties.

Experiments have been performed on a crystal in as-grown form and after annealing it at 900˚C for 1 week. We have used the 3-axis spectrometer E1 of the BENSC, at temperatures 1.6 to 50K in zero applied field. Overall, we find for both the as-cast and annealed sample magnetic Bragg intensity at low temperatures. The temperature dependence and size of the intensity is in good agreement with previous work, and verifies the expected AFM ordering along ***k*** = [0 0 1], with a moment of $\mu_{ord} = 1.7\mu_B$ at lowest temperatures [3]. In Fig. 1 we depict the temperature dependence of the (1 0 0) reflection for as-grown and annealed sample. From a parameterization of the data close to the antiferromagnetic transition we obtain for the as-grown and annealed sample critical temperatures of $T_{N,ag}$=32.1K and $T_{N,ann}$=32.4K. The annealing thus slightly increases T_N, as expected.

Surprisingly, there is remaining and substantial Bragg intensity quite far above T_N. In view of susceptibility and specific heat data we attribute this intensity to magnetic clusters forming in the paramagnetic phase. Likely, these clusters correspond to better ordered regions in the crystals, and thus are the result of the crystallographic disorder. This notion is verified by a detailed study of the temperature dependence of the width of the (1 0 0) peak (Fig. 2). Here, we find that above T_N the Bragg starts to become not resolution limited, indicating that the intensity stems from small ordered regions within the crystals.

[1] S. Süllow, J. Kreitlow, A. Loose, R. Feyerherm, BENSC experimental report 2004.
[2] A. Otop et al., J. Appl. Phys. **95** (2004) 6702.
[3] R.A. Steeman et al., J. Phys.: Condens Matter **2** (1990) 4059

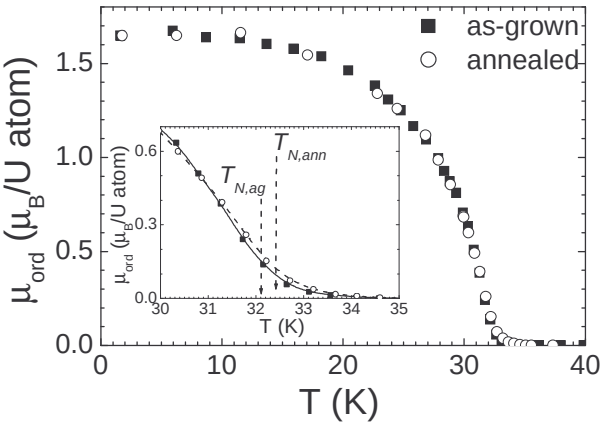


Fig. 1: The Bragg peak intensity of the (1 0 0) peak for as-grown and annealed UPt_2Si_2.

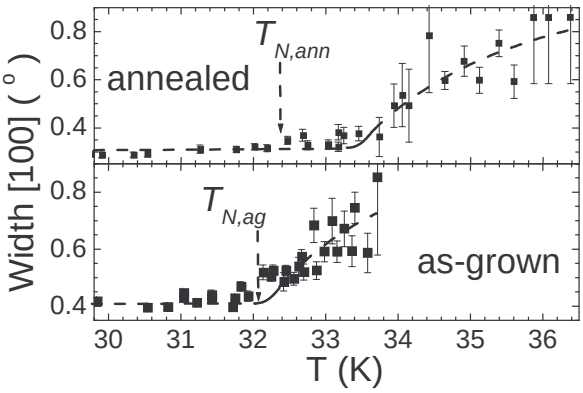


Fig. 2: The T dependence of the (1 0 0) Bragg peak width for as-grown and annealed UPt_2Si_2

	EXPERIMENTAL REPORT **Study of the magnetic spiral in $CsCuCl_3$ under pressure**	Proposal N° EF Instrument **E1&E6** Local Contact J. Klenke
Principal Proposer: Experimental Team:	Norbert Stüßer, HMI Berlin Ravil Sadykov, Inst. for High Pressure Physics, RAS Russia Norbert Stüßer Ravil Sadykov	Date(s) of Experiment E1: 24.5.-6.6.+15.6.-20.6. E6: 31.3.-4.4. 2004

Date of Report: 14.12.04

$CsCuCl_3$ belongs to the family of frustrated magnetic systems with a triangular lattice of antiferromagnetically coupled $S = 1/2$ spins of Cu^{2+}-ion in the *ab*-plane ("120° structure"); the dominating magnetic interaction along the *c*-axis is ferromagnetic and there is an additional antisymmetric interaction favouring a state with adjacent spins perpendicular to each other. The competition of both leads to an incommensurate long wavelength magnetic spiral along *c*. The magnetic structure forming below 10.6 K has a propagation vector (1/3 1/3 0.085). In the past $CsCuCl_3$ was investigated intensively in particular because quantum fluctuations lead to its rich phase diagram. Here we will present first results on the pressure dependence of the magnetic structure. Our experiments at the instruments E1 and E6 at the HMI show that the application of a hydrostatic pressure up to 13 kbar affects significantly the turning angles of spins along *c*. At 2 K the turning angle between adjacent spins along *c* changes from 5.1° at zero pressure to more than 7° at 13 kbar. This indicates that the structure under pressure has changed in a way which increases the relative strength of the antisymmetric exchange with respect to the ferromagnetic coupling. A thorough study of the crystal structure under pressure at low temperatures is needed in the future to get a clearer understanding of this behaviour. These measurements were done using CuBe-cells applying pressures up to a maximum of 8 kbar and NiCrAl-cells with pressures up to 13 kbar. The cells were loaded with a single crystal of $CsCuCl_3$. A mixture of fluorinert FC70 and FC77 was used as transmitting medium. Beside studying in particular $CsCuCl_3$ these measurements were done to get more experience to the different types of cells available for single crystal measurements. In the figures 1 and 2 below we show the shift in the magnetic satellite peak at (1/3 1/3 l) measured in a CuBe-cell at E1 and the shift in l with pressure as obtained from an experiment at E6 using a NiCrAl cell. The latter was additionally loaded with NaCl single crystal to determine the pressure. No NaCl crystal was loaded in the E1 experiments using the CuBe-cell. A maximum pressure of about 8 kbar, however, can be estimated by a comparison of the observed shift in l with the E6 data. All data collections were done at 2K and the quoted pressures were all determined at 2K. The pressure in the cells at room temperature was higher and reduces with falling temperature. In addition part of the applied pressure is transferred to "friction".

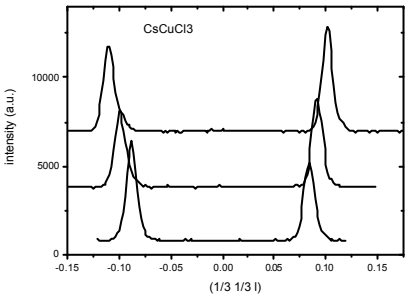


fig.1: magnetic satellite peaks measured at E1 at different pressures in a CuBe-cell.

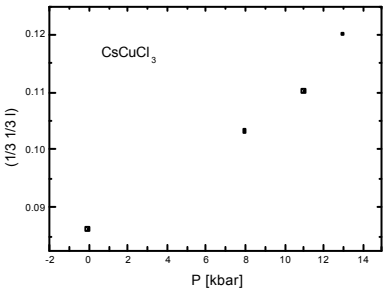


fig.2: shift in l of satellite reflection (1/3 1/3 l) as a function of pressure using a NiCrAl-cell.

	EXPERIMENTAL REPORT **Magnetic structure of $Tb_{0.5}Y_{0.5}Cu_2$ single crystal**	Proposal N° PHY-01-1439 Instrument **E2** Local Contact J.-U. Hoffmann
Principal Proposer: Experimental Team:	Svoboda Pavel, Charles Univ. Prague	Date(s) of Experiment 16.6. – 21.6. 2004

Date of Report: 20.12.2004

The Ising - axis conversion is an irreversible metamagnetic transition observed in the orthorhombic antiferromagnets RCu_2 (R = lanthanide) in high magnetic fields applied along the hard axis of magnetization. This transition in fields parallel to the crystallographic c – axis is connected with the conversion of the magnetic Ising axis from the orthorhombic a – to the c – direction for R = Ce, Pr, Tb and Dy. Such conversion manifests itself as a metamagnetic transition observed on the hard axis of magnetization when increasing magnetic field. When decreasing the field, the magnetization follows different curve, similar to the easy-axis magnetization. The axis conversion process is not limited to the ordered region only and occurs also in the paramagnetic range. The temperature dependence of the critical field of conversion frequently exhibits a minimum above the ordering temperature. Due to that, this process is not connected with the ordered magnetic moment and is usually described as the reorientation of the quadrupolar moment [1]. To further investigate the influence of a competition between the magnetic and the quadrupolar interactions a Y-diluted system is studied.

Several high-quality single crystalline ingots of the $(Tb_{0.5}Y_{0.5})Cu_2$ intermetallic compound were grown by the Czochralski pulling technique in the tetra-arc furnace of the Tohoku University. The melt of pure constituents (Tb - 3N, Y - 3N and Cu - 5N purity) was kept under Ar protective atmosphere and the pulling speed of the ingot was about 1 ~ cm/h. The quality of the single crystal of the grown ingot was checked by the Laue method. The powder X-ray analysis of the pulverized piece of each ingot did not reveal any foreign phase, preferential occupation or formation of the super-structure within the sensitivity of the method. Several well-defined samples (about 2 cmm size) were then cut-out of the ingots for the specific heat, magnetization, neutron diffraction and axis-conversion experiments.

The neutron diffraction experiment has been performed in the *a*-*c* and *a*-*b* scattering planes, respectively, in the temperature range 2 – 50 K.

As expected, the dilution of the Tb sublattice leads to weakening of the magnetic exchange which is documented by the lowering of the Néel temperature from T_N = 54 K in pure $TbCu_2$ [eg. 2] to T_N = 30 K in $(Tb_{0.5}Y_{0.5})Cu_2$. The neutron diffraction experiment has confirmed that the magnetic ordering is not a step-like transition as in pure compounds but is smeared through the range of about 5 K. In the same time, extremely sharp reflection of both nuclear and magnetic origin has been observed. This points to the clustering of Tb and Y ions in the crystal structure where clusters of different Tb concentration exhibit different ordering temperature and the observed transition forms an envelope on top of the individual transitions in clusters.

The observed magnetic structure is the same as is the ground state of the pure $TbCu_2$, i.e. collinear structure of Tb moments aligned along the *a*-axis with $\boldsymbol{q}$ = (2/3 1 0) propagation. Contrary to the pure compound, no incommensurate magnetic phase has been observed in the ordered region.

References:

[1] A. Lindbaum et al., J. Phys.: Condens. Mater. 12 (2000) 3219-3228

[2] M. Doerr et al., Physica B 284-288 (2000) 1331-1332

BENSC	**EXPERIMENTAL REPORT** **Antiferromagnetic order in $CeIn_{3-x}Sn_x$**	Proposal N° PHY-01-1546 Instrument **E2** Local Contact Jens-Uwe Hoffmann
Principal Proposer: O. Stockert, Max Planck Institute CPfS Dresden Experimental Team: J. Arndt, IFP, TU Dresden		Date(s) of Experiment 16.9. – 23.9.2004

Date of Report 6.1.2005

Quantum phase transitions (QPT), i.e. phase transitions occuring at $T = 0$, are of fundamental interest due to their accompanying fluctuations which result in anomalous behavior of the thermodynamic and transport properties at low temperatures. The correlated electron system $CeIn_{3-x}Sn_x$ can be tuned via Sn alloying from antiferromagnetically ordered $CeIn_3$ to mixed valent, nonmagnetic $CeSn_3$. It is of particular interest because the system crystallizes in the cubic Cu_3Au structure in the whole alloying range. Therefore fluctuations with reduced dimensionality as observed in other systems, can be ruled out as origin of the unusual low temperature behavior in $CeIn_{3-x}Sn_x$. Pure $CeIn_3$ orders antiferromagnetically below $T_N = 10.2\,K$ in a simple antiferromagnetic structure with a propagation vector $\tau = (1/2\ 1/2\ 1/2)$ and an ordered moment $\mu \approx 0.65\,\mu_B$ [1]. Upon Sn doping the transition in $CeIn_{3-x}Sn_x$ is continuously suppressed with a critical Sn concentration $x_c \approx 0.7$ where $T = 0$. In an intermediate concentration range $0.3 \leqslant x < 0.5$ a second transition occurs within the ordered state. Although the thermodynamic and transport properties of $CeIn_{3-x}Sn_x$ have been widely studied at high T in the past [2], only very recently the low-temperature properties have been investigated [3, 4].

The origin of the QPT in $CeIn_{3-x}Sn_x$ has not yet been identified. Therefore the aim of the present experiment was to shed light on to the nature of this magnetic-nonmagnetic transition. Information about the QPT can not only be obtained by measuring the critical spin fluctuations, but also from the ordered regime. In particular, theory predicts the variation of the Néel temperature T_N or the ordered moment μ with concentration x close to the QPT. Previous neutron diffraction on $CeIn_{3-x}Sn_x$ with $x = 0.3$ and 0.4 using the single detector instruments D15 and D23 at the ILL failed in observing any magnetic intensity along high symmetry directions [5]. Therefore we used for the experiment the flat-cone diffractometer E2 to be able to record intensity maps of reciprocal space. A $CeIn_{2.6}Sn_{0.4}$ single crystal was mounted on a ^{3}He stick with the $[110]-[001]$ plane as primary scattering plane. The measurements were performed with a neutron wavelength $\lambda = 1.2\,Å$ at temperatures 450 mK up to 4 K. Intensity maps were recorded from the 0th up to 0.5th layer at lowest temperature $T = 450\,mK$, at 2.25 K, i.e. in the intermediate phase and above T_N.

Our measurements confirm the cubic crystal structure at lowest temperature. However, despite long counting times and a careful examination of the data no traces of additional magnetic intensity have been found. One might speculate that $CeIn_{3-x}Sn_x$ in the vicinity to the QPT does not show long-range magnetic order, but exhibits only short-range magnetic correlations. Our findings are in line with results obtained previously at the ILL on different crystals with comparable Sn doping [5].

[1] J. M. Lawrence, S. M. Shapiro, Phys. Rev. B **22**, 4379 (1980); A. Benoit et al., Solid State Commun. **34**, 293 (1980).

[2] R. A. Elenbaas et al., J. Magn. Magn. Mater. **15–18**, 979 (1980); W. H. Dijkman et al., J. Magn. Magn. Mater. **15–18**, 970 (1980); J. M. Lawrence, Phys. Rev. B **20**, 3770 (1979).

[3] P. Pedrazzini et al., Physica B **312–313**, 406 (2002).

[4] J. Custers et al., Acta Phys. Pol. B **34**, 379 (2003); J. Custers, PhD thesis, Dresden (2004).

[5] W. Knafo et al., unpublished results; O. Stockert et al., unpublished results.

BENSC	**EXPERIMENTAL REPORT** **Magnetic order in the high field phase of $CeCu_2Si_2$**	Proposal N° PHY-01-1547 Instrument **E2** Local Contact Jens-Uwe Hoffmann
Principal Proposer: Experimental Team:	Enrico Faulhaber, TU Dresden Enrico Faulhaber, TU Dresden Oliver Stockert, MPI-CPfS Dresden Jens-Uwe Hoffmann, HMI Berlin	Date(s) of Experiment 8. 09. - 16. 09. 2004

Date of Report 06. 01. 2005

The tetragonal compound $CeCu_2Si_2$ shows quite unusual low-temperature properties. Depending on the growing conditions, the system can exhibit superconductivity, antiferromagnetic order, or both (called A/S-type). In a previous key experiment the magnetically ordered ground state (called A-phase) was found to be incommensurate antiferromagnetism determined by the nesting of the Fermi surface. Macroscopic measurements [2] show, that a magnetic high field phase, called B-phase, exists, and suggests that this phase is of antiferromagnetic origin. Due to the crystallographic anisotropy the required magnetic field for the transition into the B-phase is lowest for a field direction parallel to the crystallographic c axis. To search for possible magnetic satellite reflections, intensity maps of a reciprocal unit cell are highly desired.

The experiment was performed on the flat-cone diffractometer E2 using the VM4 cryomagnet and a dilution stick to reach the required temperatures. Unfortunately, the maximum magnetic field of the VM4 during the experiment ($\approx 4.3\,\mathrm{T}$) was considerable smaller than the stated value at the time of proposal writing ($\approx 5.5\,\mathrm{T}$). Since the critical field to reach the B-phase was determined [2] to be just below the maximum field of the VM4 cryomagnet, the experiment was expected to be difficult. The incident wavelength was $\lambda = 2.39$ Å. We used a single crystal of A/S-type $CeCu_2Si_2$ ($m \approx 680\,\mathrm{mg}$) mounted on a copper pin with the c axis parallel to the magnetic field. This setup allowed us to directly access the (H K 0) reciprocal plane. To access planes in the reciprocal space with a different c^* component, the flat-cone technique was applied. First we verified the known propagation vector in the A-phase at $T = 50\,\mathrm{mK}$ in an overcritical field of $B = 2\,\mathrm{T}$ to suppress superconductivity. Then, starting from $B = 2\,\mathrm{T}$ we observe a decay of magnetic intensity (shown in figure 1)

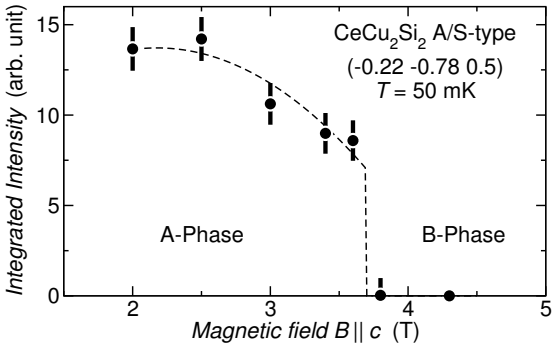


Figure 1: Integrated intensity of the (-0.22 -0.78 0.5) magnetic satellite reflection vs. applied magnetic field. The dashed line is a guide to the eye.

with increasing magnetic field. The sharp drop of magnetic intensity around $B = 3.7\,\mathrm{T}$ suggests a first order transition out of the A-phase. At highest field $B = 4.3\,\mathrm{T}$ we collected intensity maps in the reciprocal space every $0.1 \cdot c^*$, taking reciprocal maps (H K 0), (H K 0.1) etc. No significant magnetic intensity has been observed in these maps, even after some possible satellites were checked with increased statistics. Our findings might be due to different reasons: First, we don't know whether we reached the B-phase, because Tayama et al. [2] found a phase transition of unknown origin around $B \approx 3.1\,\mathrm{T}$ and the phase transition into the B-phase around $B \approx 4.1\,\mathrm{T}$. Second, it might be that the origin of the B-phase is no long-range antiferromagnetism, but rather short-range magnetic correlations, to whom we were not sensitive in this experiment. Also it might be that the magnetic intensity in the investigated reciprocal space volume is rather small due to the structure factor.

[1] O. Stockert *et al.*, *Phys. Rev. Lett.* **92** (2004) 136401

[2] T. Tayama *et al.*, *Phys. Rev.* **B67** (2003) 214504

BENSC	**EXPERIMENTAL REPORT** **Field dependence of magnetic order in a 2D frustrated quantum magnet**	Proposal N° PHY-01-1554 Instrument E2 Local Contact J-U.Hoffmann
Principal Proposer: Experimental Team	R. Coldea[1] R. Coldea[1], D.A. Tennant[2], J-U.Hoffmann[3], P. Smeibidl[3] [1]Oxford University, UK, [2]St.Andrews University, UK, [3]HMI Berlin	Date(s) of Experiment 26 July -1 August 2004 Date of report: 7 Jan 2005

The main motivation behind this project was to use magnetic fields to tune quantum fluctuations in a two-dimensional frustrated quantum magnet and to observe microscopically the evolution of the ground-state order. Experiments were made on Cs_2CuCl_4, a spin-1/2 antiferromagnet on an anisotropic triangular lattice, a system of topical interest as the first realization of a 2D magnet with spin-1/2 spinon excitations. In zero field the base-temperature ground state is an incommensurate spiral stabilized by the frustrated couplings, however this order is suppressed by relatively low in-plane fields (2.1T) and the main objective of the E2 experiment was to determine the nature of the ground state (magnetically ordered or spin-liquid) in the intermediate-field region up to ferromagnetic saturation (8T). This required diffraction measurements that probed the whole 3D Brillouin zone, only possible with the E2 instrument in flat-cone geometry combined with the large-vertical-opening-angle VM-4 magnet.

The magnetic diffraction pattern as a function of applied field was measured in a 3.7 g single crystal of Cs_2CuCl_4 mounted in the (*hk*) horizontal plane. Magnetic fields up to 4T were applied along the *c*-axis and a dilution fridge insert with a base temperature of 50 mK provided the cooling. The diffraction pattern was measured in the (*h*,*k*,*l*) layers for *l*=0, ½ and 1. The incident neutron energy on E2 was 14.3 meV (30' collimation) and the scattered beam was detected in the 80°-wide 400-channel multidetector bank. Counting times for an (Ω,2Θ) map of one magnetic reflection were between 0.5-1.5 hours. Typical scans are shown in Fig. 1. Complete data sets of magnetic reflections were collected at zero field in the incommensurate spiral phase, at 1.8 T in the incommensurate elliptical phase and at 2.5 T and 4 T in the commensurate AF and AF' phases respectively, see Fig 2(a).

Interestingly, whereas at low field the magnetic structure is an incommensurate spiral with an ordering wavevector along the **b*** axis, **Q**=(0,½+ε,0), above 2.1 T it becomes commensurate with the ordering wavevector on the Brillouin zone boundary $\mathbf{Q}_{AF}$=(0,½,½), see Fig. 2(b). Preliminary analysis suggests that the structure is based on spins ordered antiferromagnetically along *b* and antiferromagnetically or ferromagnetically along the other two triangular-lattice directions in the (*bc*) plane as indicated in Fig 2(c). A second transition occurs near 3.5 T manifested in a change in the relative magnetic peak intensities, but the ordering wavevector remains unchanged, this is probably due to a change of phase between the relative orientations of the spins between weakly-coupled (*bc*) layers. A full analysis of the data to determine the magnetic structures is currently in progress.

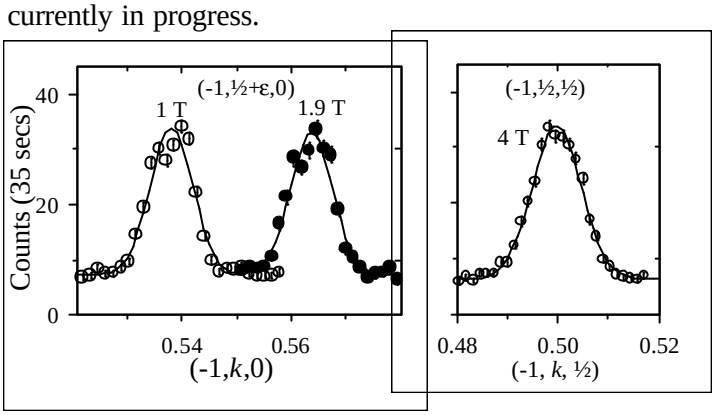


Fig. 1. Scans through magnetic Bragg peaks at *B*=1, 1.9 and 4 T.

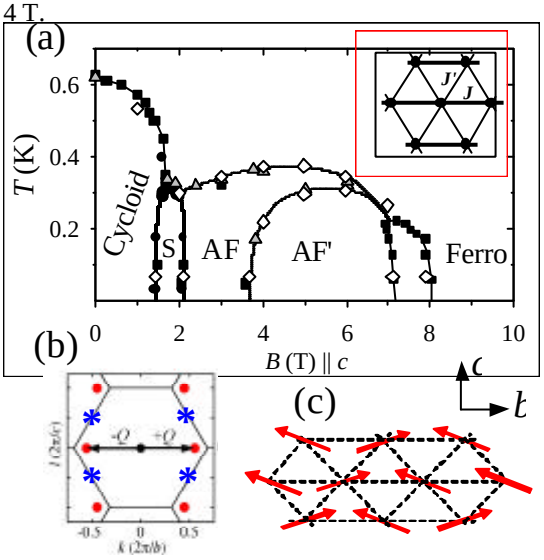


Fig.2. (a) Magnetic phase diagram in field along *c*. The present experiments showed that the intermediate-field region (AF and AF') which dominates most of the phase diagram has commensurate antiferromagnetic order. (b) Brillouin zone showing the incommensurate ordering wavevector **Q** (solid circles) in the spiral, elliptical and fan phases, and the commensurate $\mathbf{Q}_{AF}$ (stars) of the commensurate phases AF and AF'. (c) Proposed magnetic structure in the AF phase.

BENSC	**EXPERIMENTAL REPORT** **Diffuse neutron scattering in single crystalline $TbCu_2$**	Proposal N° PHY-01-1446 Instrument **E2** Local Contact Jens-Uwe Hoffmann
Principal Proposer: Experimental Team:	Raasch, Sebastian; TU Dresden Kreyssig, Andreas; TU Dresden Loewenhaupt, Michael; TU Dresden Rotter, Martin; University Vienna	Date(s) of Experiment 09.02.2004 – 15.02.2004

Date of Report: 18.03.2004

$TbCu_2$ is part of the orthorhombic RCu_2 (R = Rare Earth) family. With the exception of $LaCu_2$ all RCu_2 compounds crystallise in the $CeCu_2$ structure (*Imma*, #74), which is close to the hexagonal structure [Ref. 1]. Below $T_N = 54$ K $TbCu_2$ passes a magnetic phase transition from the paramagnetic state into an antiferromagnetic state. At $T = 40$ K another phase transition happens, where the spin alignment changes from incommensurate to commensurate.

Paramagnetic diffuse scattering contains valuable information about the magnetic structure. Magnetic short range order appears as diffuse scattered spots. Though in the paramagnetic state, one can observe competing ordering mechanisms. We wanted to get detailed quantitative information about the anisotropy of the exchange interaction and the direction of the magnetic moments.

Diffuse scattering has been done at $TbCu_2$ in the paramagnetic state at 55 K. The measurements were performed at the instrument E2 with ? = 2.396 ? and with a collimation of 30 minutes. Different reciprocal planes were examined: (*h k* 0), (*h* 0 *l*), (0 *k l*) and (1/3 *k l*). A typical measuring time for one plane was 12 hours. To prevent lambda half scattering, a 10 cm graphite filter was installed. The (*h* 0 *l*) plane has been measured again with a magnetic field of 4 T applied to the *b* direction.

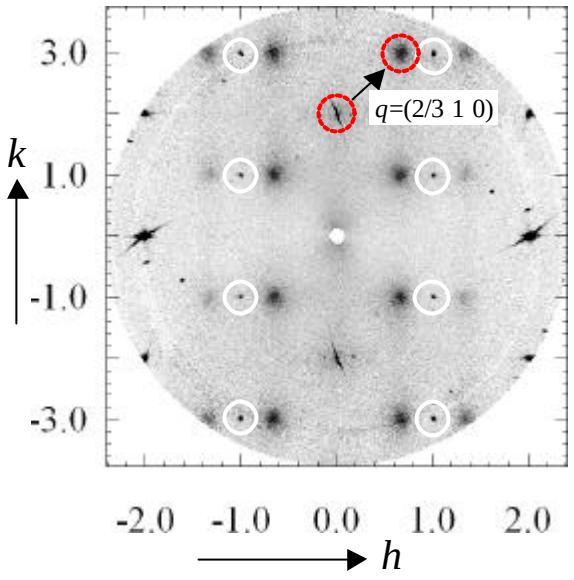


Figure 1: (*h k* 0) plane of $TbCu_2$ slightly above T_N. Forbidden reflections are marked with white circles.

Two groups of diffuse spots were found. The first one corresponds to the position were antiferromagnetic satellites appear below T_N. The associated propagation vector is q = (2/3 1 0). This feature is shown in figure 1. The origin of the second kind of diffuse scattering (no figure) is not yet understood. The spots are situated close to each existing (0 *k l*) reflection, shifted in *c* direction. This feature still exists below T_N and disappears smoothly at about 30 to 20 K. Further diffuse fine structure is visible. First data analysis with TVtueb confirms the possibility to deduce magnetic exchange parameters from the diffuse data. A significant higher statistic is necessary to take full advantage of this technique.

The behaviour of both groups of diffuse scattering has been observed at magnetic fields. Therefore the respective scattering angles were adjusted and the field was stepped up to 4 tesla along the b direction. No changes in their intensities (figure 2), shapes or positions were seen.

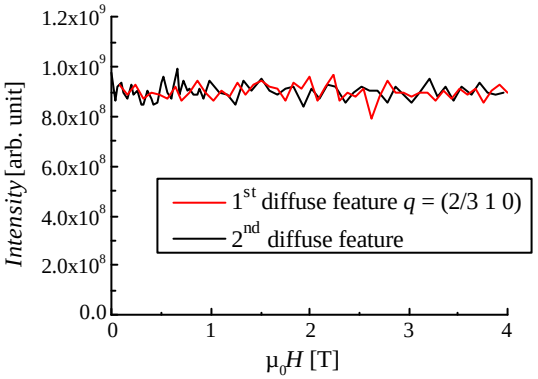


Figure 2: Intensity of both kinds of diffuse scattering in magnetic field.

In figure 1 another remarkable feature appears. Reflections with odd *h* and *k* values which are forbidden in the assumed space group *Imma* are visible. (marked with white circles). Further x-ray and neutron scattering experiments are proposed to find out the origin of those reflections. Two possibilities are in discussion. The first one is the Renninger effect (or "Umweganregung"). The second possibility assumes a small displacement of the atoms which is not yet considered in the space group Imma. The correct space group has to be found.

References:

[1] Astrid Schneidewind, Dissertation *Analyse magnetischer Strukturen an Seltenerd-Cu2-Verbindungen mittels magnetischer Röntgen- und Neutronenbeugung* TU Dresden (2002)

[2] Y. Hashimoto, H. Fujii, H. Fujiwara and T. Okamoto, *J.Phys.Soc.Jap.* **47** (1979) 67

	EXPERIMENTAL REPORT **Switching of the crystallographic structure of a $Tb_{0.5}Dy_{0.5}Cu_2$ single crystal**	Proposal N° PHY-01-1445 Instrument E2 Local Contact Jens-Uwe Hoffmann
Principal Proposer: Experimental Team:	S. Raasch; HMI-Berlin + TU Dresden S. Raasch; HMI-Berlin + TU Dresden M. Frontzek, A. Kreyssig; TU Dresden, IFP J.-U. Hoffmann, HMI Berlin	Date(s) of Experiment 19.03.2004-09.04.2004

Date of Report: 05.01.2005

$Tb_{0.5}Dy_{0.5}Cu_2$ belongs to the group of RCu_2 (R = rare earth) compounds where a structural conversion has been observed. This conversion can be effected by applying an external field. With the exception of $LaCu_2$ all RCu_2 compounds crystallise in the $CeCu_2$ structure (*Imma*, #74) which is a distorted hexagonal structure [1]. The antiferromagnetic ordering temperature of $Tb_{0.5}Dy_{0.5}Cu_2$ is T_N = 38 K. In [2] we already verified the twin-domain model, whereupon the crystal converts into two crystallographic twin-domains (TDs) if a magnetic field is applied along the magnetic hard c axis. The new TDs (twin-domains) are rotated about the b axis by plus/minus 60° with respect to the virgin structure. Because the crystal structure is pseudo hexagonal only slight atom rearrangements occur due to the conversion. The applied field direction (parallel c) is exactly between two *pseudo hexagonal directions* corresponding to the easy axes of the new TDs. Therefore both new TDs were populated by about 50 %.
In the actual experiment we wanted to investigate, whether one certain TD can be populated by almost 100 % by applying the magnetic field along the easy axis of the corresponding TD.

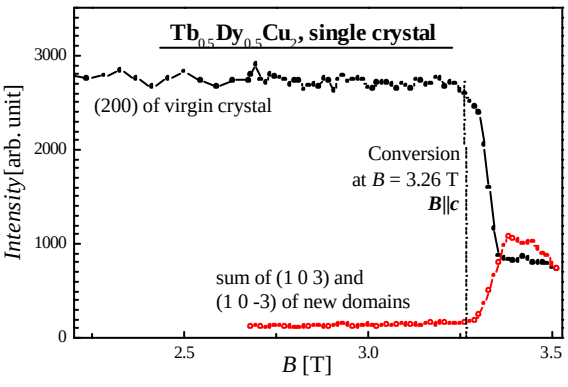


Figure 1: Integrated intensity of a virgin reflection (filled circles) and the sum of two converted reflections (open circles) during the structural conversion with $B \| c$. The background has not been subtracted.

At the beginning of the actual experiment the previous experiment has been repeated. To ensure the comparability and expressiveness of measured data we have chosen the same course of actions for all conversions consisting of seven steps. If possible for each step three scattering planes have been recorded: (h k 0), (h k ½) and (h k 1).

Step	1	2	3	**4 = conv.**	5	6	7
H[T]	0	0	2	next tab.	$>H_{conv}$	0	0
T[K]	55	29	29	29	29	29	55

For $B \| c$ we know from magnetization measurements the temperature with lowest conversion field is $T_{conv} \sim$ 29 K. Figure 1 shows measured intensities during the conversion with the field parallel to the c axis.
At the E2 the magnetic field is always parallel to the cryostat axis. Therefore a new virgin crystal had been oriented such, that after the conversion the converted crystal's scattering planes could be measured. As expected, before conversion no reflections corresponding to converted TDs could be measured. After the conversion, we have seen reflections belonging to only one TD. Reflections of the original crystal structure almost disappear (< 10 %).
Next, we reoriented the crystal at room temperature to perform a back conversion by applying the field along the virgin easy axis (effective crystal rotation by 60°). After the back conversion the virgin TD has been strongly repopulated (> 70 %).
As the temperature with lowest conversion field for the "60° conversion" is not known we used $T_{conv}(B \| c)$ = 29 K. The conversion fields H_{conv} were as follows (chronologic):

two TD conv.	$\pi(B, a) = 90°(B \| c)$	**3.26 T**
single TD conv.	$\pi(B, a) = 60°$	**2.95 T**
back conversion	$\pi(B, a) = 90°(B \| c)$	**2.26 T**

Our experiment showed that applying a magnetic field along the easy axis of one of the three possible TDs this TD can be selectively populated. This is a strong support for the TD model for RCu_2 compounds.

[1] Astrid Schneidewind, PhD-Thesis *Analyse magnetischer Strukturen an Seltenerd-Cu2-Verbindungen mittels magnetischer Röntgen- und Neutronenbeugung* TU Dresden (2002)
[2] Martin Rotter, Matthias Doerr, Michael Loewenhaupt, Pavel Svoboda, Jana Vejpravova *Axis Conversion Effect in $DyCu_2$* BENSC Report **PHY-01-1330** (2002)

BENSC	**EXPERIMENTAL REPORT** **Crystallographic superstructure of R_2PdSi_3 (R = Tb, Ho, Er, Tm) compounds**	Proposal N° PHY-01-1548 Instrument **E2** Local Contact Thomas Lonkai
Principal Proposer: Experimental Team:	M. Frontzek, A. Kreyssig, IFP, TU Dresden S. Raasch, IFP, TU Dresden u. BENSC T. Lonkai, BENSC	Date(s) of Experiment 29.06.04 - 04.07.04

Date of Report: 23.12.04

In previous neutron diffraction experiments on E2 concerning the magnetic structure of Tb_2PdSi_3 we observed a crystallographic superstructure which has not yet been reported for any member of the isostructual series of R_2PdSi_3 [1]. The superstructure is described by a propagation vector (1/2, 1/2, 1/8) with reflections of equal intensity on positions 2/8 and 3/8 in L (Fig. 1 top). In the recent experiment we investigated two questions whether other members of the R_2PdSi_3 also show this superstructure, and if we can influence the superstructure through annealing. For this purpose we measured full (*HHL*) planes with high statistic at room temperature on the diffractometer E2 on as-grown R_2PdSi_3 (R = Ho, Er, Tm) single crystals and on two different annealed (at 900°C for 100 hours and at 1200°C for 35 hours respectively) Tb_2PdSi_3 single crystals. In addition, we performed full scans of the (*H*0*L*) and (*HK*0) plane on the Ho_2PdSi_3 and Er_2PdSi_3 single crystals in order to compare this data with previous data for the Tb_2PdSi_3 single crystal.

As one result we found in all investigated single crystals a crystallographic superstructure describeable with the propagation vector of (1/2, 1/2, 1/8). For the Er_2PdSi_3 compound we found the identical superstructure compared to the one found in the Tb_2PdSi_3 compound. Interestingly, the Ho_2PdSi_3 and Tm_2PdSi_3 compound showed a slightly different structure yielding reflections at 1/8, 2/8 and 3/8 in L with different intensities (see Fig. 1).

Of major importance is that these slightly different structures could be transferred into each other through annealing as the measurement of the 900°C annealed Tb_2PdSi_3 crystal showed. The resulting superstructure is the same as for the Ho_2PdSi_3 and Tm_2PdSi_3 compound, respectively. The 1200°C annealed Tb_2PdSi_3 single crystal had unfortunately become partly polycrystalline through the annealing treatment. However, we could prove the remaining of the superstructure also in this crystal.

Since we had the opportunity to use the standard orange cryostat for two days during the experiment, we tried to evaluate if the changed superstructure in the 900°C annealed Tb_2PdSi_3 has an impact of the magnetic structure. As a preliminary result the long-range antiferromagnetic order we found in the as-grown crystal [1] seems not modified with the restriction that a detailed analysis is in progress.

A strong modification in the diffraction pattern of the magnetic intensity due to the short-range antiferromagnetic order [2] was observed. On some positions where diffuse magnetic intensity was found in the as-grown crystal we observed magnetic Bragg reflections which originate from a long-ranged antiferromagnetic order with a second propagation vector.

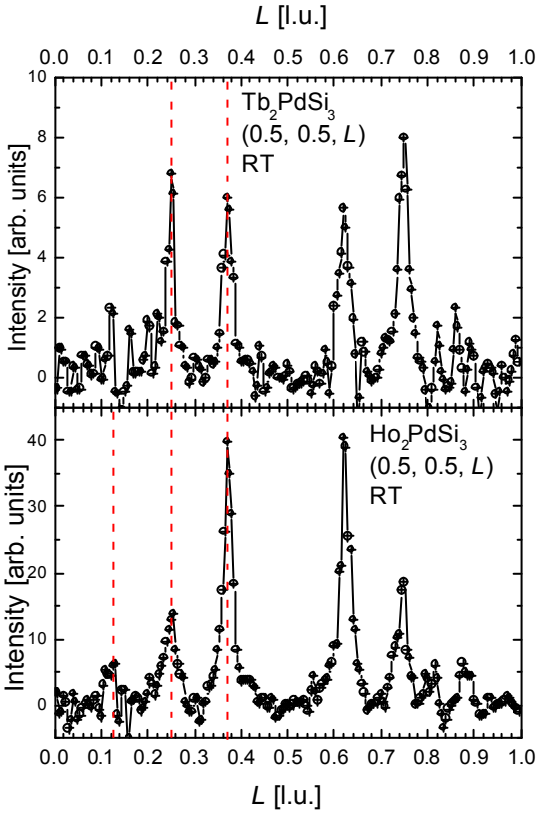


Fig. 1: Section along (0.5, 0.5, L) for Tb_2PdSi_3 (top) and Ho_2PdSi_3 (bottom). The positions 1/8, 2/8, 3/8 are marked.

[1] Experimental report PHY-01-1093
[2] Experimental report PHY-01-1175

	EXPERIMENTAL REPORT **Magnetic ground state of NdPtSn**	Proposal N° PHY-01-1463 Instrument **E4** Local Contact Vadim Sikolenko
Principal Proposer: Experimental Team:	Blanka Janousova, DES, Charles University Vadim Sikolenko, HMI Karel Prokes, HMI	Date(s) of Experiment 08-15/01/2004

Date of Report: 20.12.2004

The magnetic ground state of NdPtSn has been studied to provide comparison for the Kondo antiferromagnet CePtSn. In this compound the subtle interplay between single-ion crystal-field and RKKY interactions leads to AF ordering with magnetic propagation $\boldsymbol{q}_1$ = (0.160, 0.558, 0.130) at $T_M < T < T_N$ and $\boldsymbol{q}_2$ = (0, 0.513, 0) below T_M with T_N = 2.4 K and T_M = 1.9 K as suggested by the previous neutron Laue diffraction experiment on Vivaldi.

Our single-crystal diffraction data suggest that the AF ground state phase characterized by $\boldsymbol{q}_2$ is suppressed by application of magnetic field along the *c*-axis of the crystal (see Fig.1).

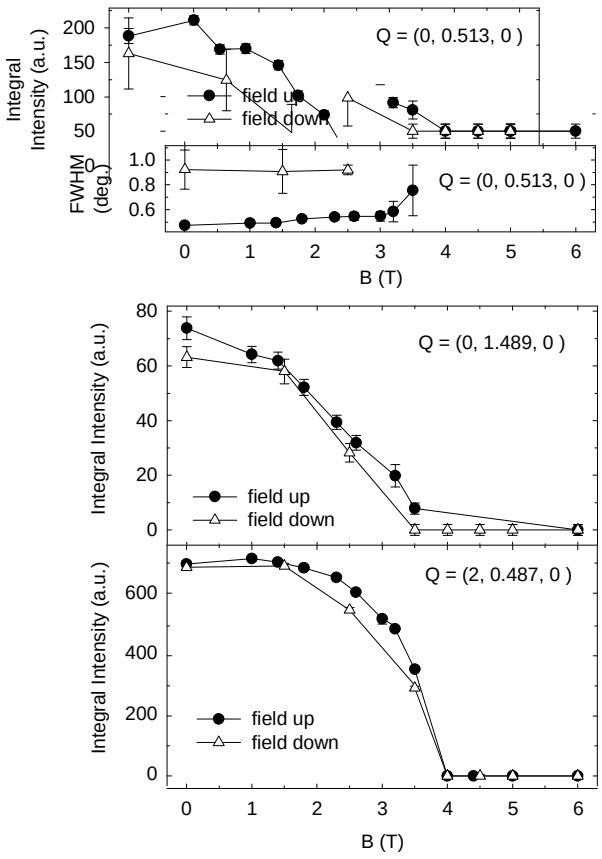


Fig.1
Neutron diffraction intensity in reflections corresponding to the magnetic propagation vector $\boldsymbol{q}_2$. Data taken at T = 0.5 K, B || c-axis.

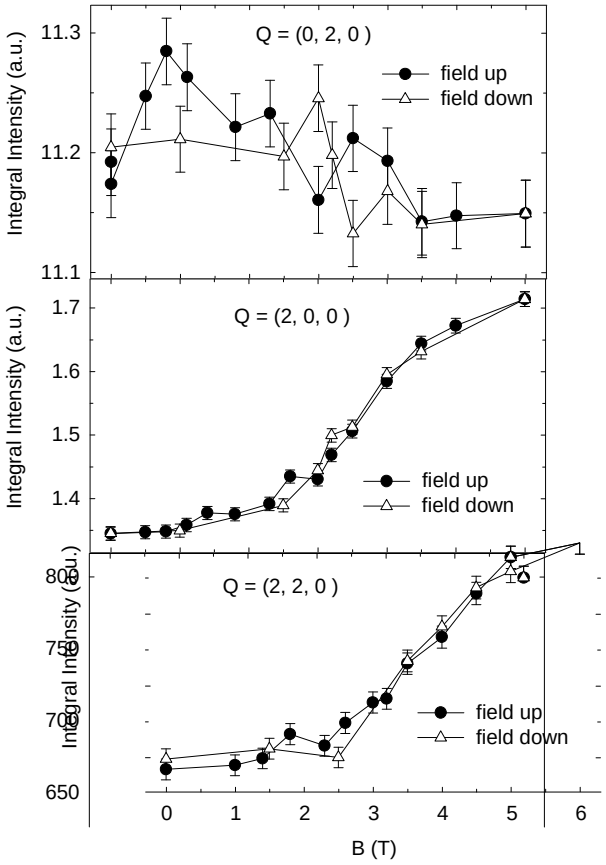


Fig.2
Neutron diffraction intensity in several nuclear reflections. Data taken at T = 0.5 K, B || c-axis.

When the magnetic field is applied along the *c*-axis, the magnetic intensity moves to the position of nuclear peaks (see Fig. 2) suggesting a field-forced ferromagnetic phase to appear above the metamagnetic transition reported from the bulk magnetic measurements [1]. The preliminary analysis of the data suggests the reorientation of magnetic moments along the applied field. The full analysis must be done for both the Vivaldi and E4 data together.

[1] B. Janousova et al., Physica B **329** (2003) 671

	EXPERIMENTAL REPORT **Field-induced changes in magnetic structure of DyNiAl**	Proposal N° PHY-01-1464 Instrument **E4** Local Contact **Karel Prokeš**
Principal Proposer: Experimental Team:	Jirí Prchal, Department of Electronic Structures, Charles University, Prague Jirí Prchal, DES, Charles University, Prague Karel Prokeš, HMI Berlin Pavel Javorský, DES, Charles University, Prague	Date(s) of Experiment 15.-24.1.2004

Date of Report: 02.03.2005

DyNiAl belongs to a large group of *RTX* compounds crystallizing in the ZrNiAl-type hexagonal structure, (s.g. P-62m). It orders ferromagnetically at $T_C = 31$ K with the magnetic moment oriented along the *c*-axis and it undergoes an order-order transition below $T_1 = 15$ K where an antiferromagnetic component described by $k = (0.5\ 0\ 0.5)$ appears within the basal plane [1,2]. Our studies on the single crystal showed a strong anisotropy within the basal plane [3]. There are two field-induced magnetic transitions in the compound when applying field along the *a*-axis (B||*a*) and along the *b*-axis (B||*b*) at 2 K [3]. In both cases, the first one occurs around 1.5T. In the B||*a* arrangement the higher transition field is 11-13 T. We have already performed neutron diffraction experiment on E4 with B||*b* arrangement (experimental report 12.1.2004).

In this study we performed the experiment in the B||*a* configuration with fields up to 14.5 T. The field dependencies of intensities of selected reflections (Fig.1) show two field-induced transitions – around 1.5-2T and 11-13T at the lowest temperature. At 18K, the "12 T" transition disappears and only gradual increase of the intensities is observed. This is in agreement with the ferromagnetic ordering in this temperature region. Although the geometry of the magnet restricted us to measure only few reflections of the (hhl) type, and (especially the (0.5 0 0.5)-type reflections were shielded by the coils), we still could refine the magnitude and the direction of the ferromagnetic component in higher fields (Fig.2). The magnitude of the F component in the lowest temperature 1.8 K (m(0T)=7.0(9)μ_B; m(14.5T) = 6.7(1.0)μ_B) is lower than the expected free-ion value of 10μ_B what corresponds to presence of AF component. Our refined value in zero field is in agreement with results obtained on the same crystal from larger number of reflections (experiment in ILL) $m^F(0T)^{ILL} = 7.1(3)\mu_B$. Surprisingly, the orientation of the F component in fields above 13 T are not yet fully oriented along the applied magnetic field – the angle with the field is approximately 40degrees.

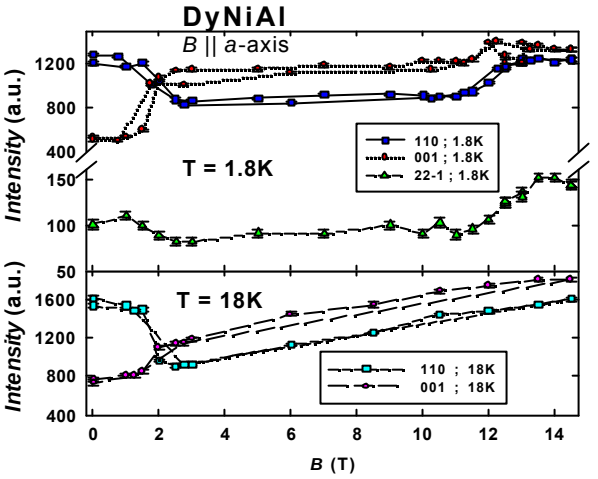


Fig. 1: The field dependence of selected ferromagnetic reflections in DyNiAl measured with magnetic field applied along a-axis in temperatures 1.8 K and 18 K.

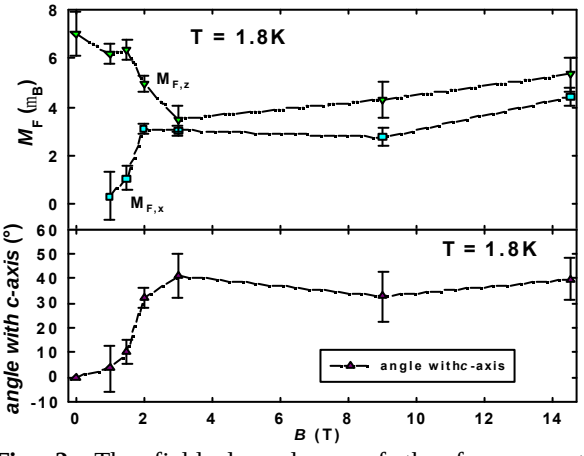


Fig. 2: The field dependence of the ferromagnetic moment components $M_{F,x}$, $M_{F,z}$ in DyNiAl. The angle between the resulting moment direction and *c*-axis is calculated.

References

[1] G. Ehlers, H. Maletta, Z. Phys. B 101 (1996) 317.
[2] P. Javorský et al., Physica B 234-236 (1997) 665.
[3] A.V. Andreev, N.V. Mushnikov, T. Goto, J. Prchal, Physica B 346–347 (2004) 201.

	EXPERIMENTAL REPORT **Magnetic structures of Y_2Fe_{17} under high pressure**	Proposal N° PHY-01-1580 Instrument **E4** Local Contact: K. Proke
Principal Proposer: Experimental Team:	J. Kamarád, Institute of Physics, Prague O. Prokhnenko, Institute of Physics, Prague K. Prokeš, Hahn-Meitner-Institut, Berlin V. Sikolenko, Hahn-Meitner-Institut, Berlin	Date(s) of Experiment 22. 6. - 4. 7. 2004

Date of Report: 31. 8. 2004

The ferromagnetic Y_2Fe_{17} compound was often used as a model of a ferromagnetic behaviour of the Fe-sublattice in the R_2Fe_{17} intermetallics. Recently, metamagnetic transition has been observed in Y_2Fe_{17} under high pressure at wide temperature range [1]. Using the neutron 2-axis (E4) diffractometer and the VM2 cryo-magnet, we tried to find the new magnetic structures that are induced in Y_2Fe_{17} by high hydrostatic pressures up to 1 GPa at temperatures from 5 K to 300 K and fields up to 6.5 T. By analogy of the magnetic behaviour of Y_2Fe_{17} with one of Lu_2Fe_{17} compound [2], we expected a presence of the helimagnetic structure in Y_2Fe_{17} under pressure. The Y_2Fe_{17} single crystal ($P6_3/mmc$) was oriented in high pressure CuBe cell with *a*-axis || *H* || axis of neutron diffractometer and with beam in the crystal *bc*-plane. A cryo-furnace OF-x was used for referential experiments with paramagnetic Y_2Fe_{17} at 400 K and zero pressure.

The presence of a non-collinear magnetic arrangement in Y_2Fe_{17} was clearly proved under high pressure above 0.7 GPa. For the first time, the satellites (000)+, (011)±, (002)± (004)± and (030)± with propagation vector $(00t_z)$ were observed in Y_2Fe_{17} by *l*-scans in reciprocal space under pressures 1.05 GPa and 0.85 GPa.

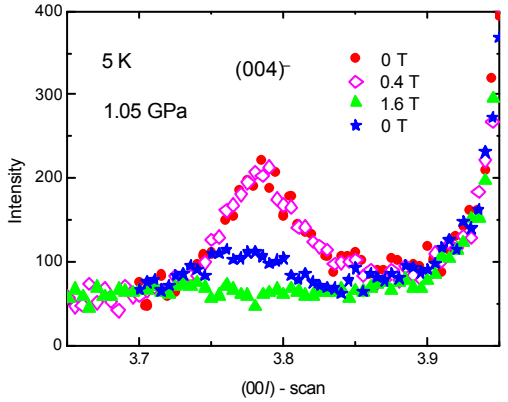


Fig.1: $(004)^-$ satellite at 5 K under pressure 1.05 GPa at different magnetic fields

The ferromagnetic ground state in Y_2Fe_{17} was completely suppressed by pressures above 1 GPa, see Fig.1, and restored (with a field hysteresis) by external field in accordance with the magnetic measurements. The observed complex temperature dependence of t_z indicates a presence of two structures in Y_2Fe_{17} at pressure 1.05 GPa, (LTP) at low and (HTP) at high temperatures, see Fig.2 [3]. The enhanced nuclear intensities of LTP indicate a commensurate (ferro- or antiferro-) component. HTP looks like the simple incommensurate spiral.

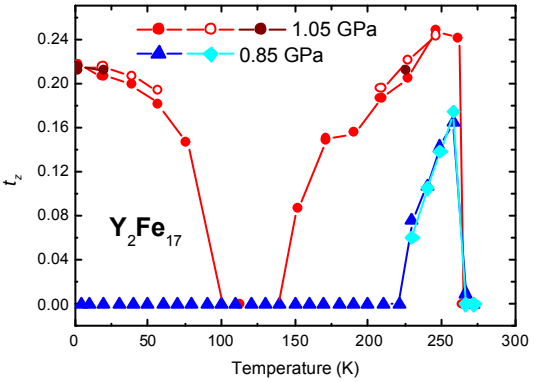


Fig.2: Temperature dependence of t_z under pressures 1.05 GPa and 0.85 GPa.

A similar complex temperature behaviour of t_z was found even in Lu_2Fe_{17}, Ce_2Fe_{17} and in Y_2Fe_{17} at higher pressures, where no ferro-phase is in between LTP and HTP. This verifies our hypothesis of a general similarity of the magnetic structures in R_2Fe_{17} (*R* = Y, Lu, Ce) under pressure. Using ω-scans, a large set of diffraction lines and their satellites was collected at the pressures 1.05 GPa and 0.85 GPa at four temperatures from 5 K up to 400 K in fields up to 6.5 T. The collected data will be used to a more detailed description of the pressure induced magnetic structures in the near future.

[1] Z.Arnold et al., High Pressure Res. **23** (2003) 165
[2] O. Prokhnenko et al., J.Magn.Magn.Mats. **258** (2003) 564
[3] O. Prokhnenko et al., Phys.Rev.Lett. - submitted

	EXPERIMENTAL REPORT **Non-magnetic impurity effect on domain growth in $Co_{1-x}Mg_xNb_2O_6$ (x=0.0,0.005)**	Proposal N° PHY-01-1582 Instrument **E4** Local Contact K.Prokes & V.Sikolenko
Principal Proposer: Experimental Team:	S.Mitsuda, Tokyo Univ. of Science T. Nakajima,Y.Inomoto, S. Mitsuda; Tokyo Univ. of Sci. V. Sikolenko, K. Prokes, S. Kausche; HMI Berlin	Date(s) of Experiment 19.8.2004 – 29.8.2004

Date of Report: Jan. 2005

Geometrically frustrated isosceles triangular Ising antiferromagnet $CoNb_2O_6$ shows slow domain growth kinetics in the four-fold degenerate antiferromagetic(AF) phase below T_{N2}~1.95K[1,2]. In previous experiments at HMI (2003)[3], We have found that the time evolution of average domain size along a axis $x(t)$ can be fitted to power law $x(t)=x_0+C(T)t^n$ with exponent n~0.2 over wide temperature range in AF phase. As shown in Fig.1 (a), strongly temperature dependent pre-factor $C(T)$ shows *'Arrhenius law'*-like behaviour expressed by $C(T)=C_0 exp(-\Delta E/k_BT)$, suggesting some kind of activation energy ΔE that is related to local barriers in the growth kinetics. Introducing temperature dependent time–scale $t(T) \mu C(T)^{-1/n}$, as shown in Fig.1(b), all time evolution data $x(t)$ measured at different temperatures can be scaled as $x(t) - x_0 \mu (t / t(T))^n$. Note that in the analysis, we fixed exponent n to 0.2 whose temperature invariance has been well confirmed by ac-susceptibility measurements [2].

In present experiments, to investigate how a small amount of non-magnetic impurity modifies the domain growth kinetics specific to an isosceles-triangular geometry of frustrated spins, we chose $Co_{1-x}Mg_xNb_2O_6$ x=0.005 sample [4] with lower transition temperature of T'_{N2} ~1.65K than T_{N2} below which AF ordering is realized. Performing the measurements as was in [3], we found that the power law with growth exponent n~0.2 is held over wide temperature range in AF phase, as shown in Fig.1(b), being consistent with the results of ac-susceptibility measurements for the x=0.005 sample.

As is seen in Fig.1(c), suppression of time evolution of $x(t)$ due to a small amount of non-magnetic impurity occurs: $x(t)$ of the x=0.005 sample is smaller than that of the x=0.00 sample at the same temperature. This can be interpreted as domain wall pinning effect: the A/D-type domain wall motion[3] that is dominated by the stochastic reversal of free magnetic chains due to the isosceles triangular lattice geometry of $CoNb_2O_6$, is easily disturbed by non-magnetic impurity.

Although *'Arrhenius law'* for the pre-factor $C(T)$ of the x=0.005 sample is also held as is seen in Fig.1(a), reduction in the activation energy $\Delta E/k_B$ from ~*10 K* to~*7 K* due to non-magnetic impurity occurs. Suppose that ΔE is related to the energy required to reverse a ferromagnetic 1D chain along c axis, we can explain the reduction in ΔE because the effective length of the chain is reduced by non-magnetic impurity. We need to clarify the physical meaning of ΔE.

It should be noted that recently introduced He^3 refrigerator with VM-3 cryomagnet was invaluable in present experiments to provide access to the temperature region of T=1.0 K~2.0 K.

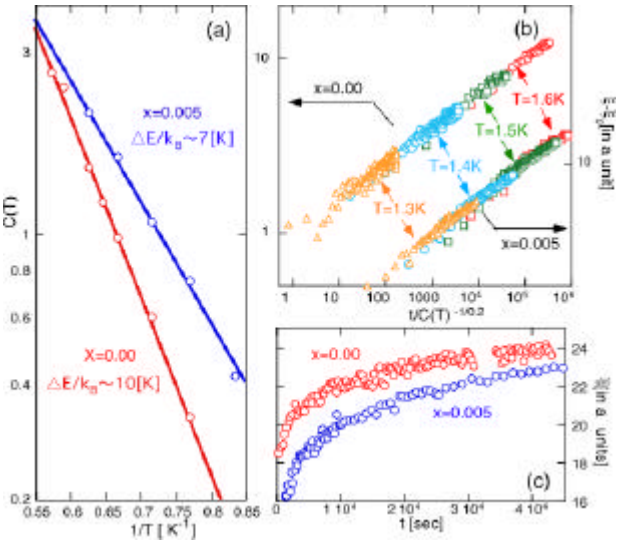


Fig.1 (a) Semi-log plot of the temperature dependence of $C(T)$, (b) Log-log plot of $x(t)- x_0$ vs. $t/C(T)^{-1/n}$ at several temperatures, (c) $x(t)$ at T=1.5 K, for the samples with x=0.00 and 0.005.

[1] S.Kobayashi, S.Mitsuda, T.Jogetsu, J.Miyamoto, and H.Katagiri, Phys.Rev. B **60**, R9908 (1999).

[2] S.Kobayashi, K.Okano, T.Jogetsu, J.Miyamoto, and S.Mitsuda, Phy.Rev. B **69**, 144430 (2004).

[3] S.Mitsuda, Y.Inomoto, K.Prokes, BENSC Experimental report 2003, PHY-01-1128 (2003).

[4] S. Mitsuda, H. Okano, S. Kobayashi and K. Prokes; J. Magn. & Magn. Mater. 272-276, Suppl. 1,(2004) E993

	EXPERIMENTAL REPORT On the mechanism for magnetic detwinning of La_2CuO_4	Proposal N° PHY-01-1583 DT Instrument **E4** Local Contact K. Prokes
Principal Proposer: Experimental Team:	B. Keimer, Max-Planck-Institut FKF, Stuttgart C. Ulrich, Max-Planck-Institut FKF, Stuttgart K. Prokes, Hahn-Meitner-Institut, Berlin	Date(s) of Experiment 16.6. – 21.6.2004

Date of Report: 18.1. 2005

We present elastic neutron scattering data on detwinned La_2CuO_4 (T_N = 313.8 K) under high magnetic fields of up to 14.5 T. In a striking set of experiments, Lavrov and coworkes [1] had demonstrated that single crystals of undoped and lightly doped $La_{2-x}Sr_xCuO_4$, the progenitor of the most extensively investigated high-temperature superconductor, can be detwinned by applying an high external magnetic field alone. Neutron diffraction data taken in previous HMI experiments in zero field indicate that the lattice structure of untwinned $La_{2-x}Sr_xCuO_4$ single crystals is substantially different from that previously observed in twined samples. We have measured the structural and magnetic superstructure reflections of untwinned La_2CuO_4 in order to uncover the microscopic origin of the intriguing magnetic-field-induced detwinning phenomena.

Elastic neutron scattering experiments at high magnetic fields up to 14.5 T were carried out at the two-axis diffractometer E4 at the Hahn-Meitner-Institut in Berlin.

For a magnetic field applied within the ab-plane, the intensity of the Bragg reflections (010) and (100) decreases with increasing magnetic field (see fig. 1). The (011) and (101) reflections on the other side increase with increasing magnetic field. Also the intensity of the reflections (103) and (013) increase with magnetic field, whereas the reflections (102) and (012) decrease. The Bragg peaks of the orthorhombic space group *Bmab*, in particular (h0l) with h,l = even, do not show any effect under high magnetic fields.

An extrapolation of the (010) Bragg peak intensities yields that the magnetic Bragg reflection (100) and (010) would disappear at a value of 12.3 T at room temperature.

Unfortunately we were not able to reach higher magnetic fields than 12.0 T at T = 300 K. Therefore we were not able to determine, whether this phase transition is related to the magnetic field induced detwinning of La_2CuO_4 observed by A.N. Lavrov et al. [1] in a magnetic field of 14 T.

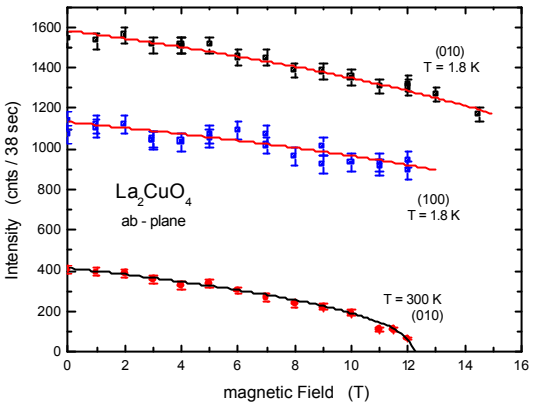


Fig 1: Magnetic field dependence of the (010) and (100) Bragg reflections of La_2CuO_4 for a magnetic field within the ab-plane.

At zero field the spins are antiferromagnetically ordered within the ab-plane. They are pointing predominantly along the a-axis but a weak additional canting towards the b-direction was observed [2]. We have measured the magnetic field dependence of the (100) and (210) magnetic Bragg reflections of La_2CuO_4 for a magnetic field applied parallel to the c-axis. At a magnetic field of H_c = 11.5 T the intensity of the (100) reflection decreases spontaneously whereas the (210) reflection increases. The field width of this transition is about 3 T. A hysteresis was observed when the magnetic field was reduced. As M.A. Kastner et al. [3] pointed out, this transition can be assigned to a transition from canted antiferromagnetism where the spins are within the ab-plane to ferromagnetic ordering. They have observed the transition at a critical field of 4.8 T on a sample with a reduced T_N of 230 K.

References:

[1] A.N. Lavrov, S. Komiya, and Y. Ando, Nature **418**, 385 (2002).

[2] M.A. Kastner et al., Phys. Rev. B **38**, 6636 (1988).

BENSC	**EXPERIMENTAL REPORT** **Crystal and magnetic structure of $La_{2-x}Sr_xCuO_4$ with $x = 0.01$ and $x = 0.03$**	Proposal N° **EF** Instrument **E5** Local Contact M. Reehuis
Principal Proposer: Experimental Team:	B. Keimer, C. Ulrich, MPI Stuttgart G. Blumberg, Bell Labs, Murray Hill, NJ Y. Ando, CRIEPI, Komae, Tokyo M. Reehuis, MPI Stuttgart, HMI Berlin	Date(s) of Experiment 15.06. – 04.07.04

Date of Report: 05.01. 2005

$La_{2-x}Sr_xCuO_4$ is the simplest high temperature superconductor and has served as a model system for numerous theories of high temperature superconductivity. A detailed microscopic picture of the evolution of the structural and magnetic properties as a function of doping has been derived from neutron data [1]. Almost all prior work has been carried out on twinned crystals. The properties of our untwinned samples were found to be substantially different. This lead us to a fundamental reinvestigation of the structural and magnetic properties. Recently, we have started to investigate the structural and magnetic properties of La_2CuO_4 and $La_{1.99}Sr_{0.01}CuO_4$ [2].

In this report we present the results of the structure refinements of $La_{1.97}Sr_{0.03}CuO_4$. Neutron diffraction data of this compound have been collected on the four-circle diffractometer E5 at 295 K using the neutron wavelength λ = 0.884 Å (copper). For the experiment we used an untwinned crystal with the dimensions 1.6 × 2.1 × 2.6 mm^3. With a total of 1024 reflections (481 unique) the crystal structure of $La_{1.97}Sr_{0.03}CuO_4$ could be refined in the orthorhombic space group *Bmab*. Here the La(Sr)-atoms are on the Wyckoff position 4*f*, the Cu-atoms on 4*a*, the O1-atoms on 8*e* and the O2-atoms on 8*f,* respectively. The refinement resulted in the residual $R(F)$ = 0.020 and the atomic parameters given in Table 1. All these values are similar to those obtained earlier for La_2CuO_4 and $La_{1.99}Sr_{0.01}CuO_4$ [2].

In order to investigate the magnetic order of $La_{1.99}Sr_{0.01}CuO_4$ and $La_{1.97}Sr_{0.03}CuO_4$ we used the longer neutron wavelength λ = 2.38 Å (PG). Due to the magnetic ordering of the copper sublattice magnetic intensity appeared spontaneously on the positions of the reflections 100 and 010 at the Néel temperature T_N = 243(2) K (Fig. 1). This temperature is lying much lower than that of the pure compound La_2CuO_4 T_N = 320(2) K. On the other hand no magnetic order has been found for $La_{1.97}Sr_{0.03}CuO_4$. From the refinement of the magnetic structure of $La_{1.99}Sr_{0.01}CuO_4$ we deduced the magnetic moments m_x = 0.192(29) m_B and m_y = 0.302(14) m_B. The spin sequences for the Cu-atoms on the Wyckoff position 4*a* (0,0,0; 0,½,½; ½,0,½; ½,½,0) are + – + – along *x* and + + – – along *y*, respectively. In contrast, for La_2CuO_4 the moments were found to be aligned only parallel to y. For this compound the total experimental moment m_{exp} = 0.427(8) m_B is considerably larger that of $La_{1.99}Sr_{0.01}CuO_4$ m_{exp} = 0.358(19) m_B.

Table 1. Results of the structure refinements of $La_{1.97}Sr_{0.03}CuO_4$ at 295 K.

a = 5.3407(6) Å, *b* = 5.3734(5) Å, *c* = 13.1206(13) Å

Bmab	*x*	*y*	*z*	*Pop*
La	0	–0.00552(4)	0.36128(2)	0.9972(14)
Cu	0	0	0	1.002(2)
O1	¼	¼	–0.00598(4)	1.004(2)
O2	0	0.03410(10)	0.18339(4)	1.000(2)

	U_{11}	U_{22}	U_{33}	U_{12}	U_{23}
La	0.56(2)	0.58(1)	0.35(1)	0	–0.04(1)
Cu	0.28(2)	0.32(1)	0.78(2)	0	0.01(1)
O1	0.51(2)	0.55(1)	1.46(2)	–0.23(2)	0
O2	2.28(3)	1.69(2)	0.61(2)	0	0.04(1)

The thermal parameters U_{ij} (given in 100 $Å^2$) are in the form $\exp[-2\pi^2(U_{11}\, h^2a^{*2} + \ldots 2U_{13}\, hla^*c^*)]$. For symmetry reasons the values U_{13} are equal to zero in this structure.

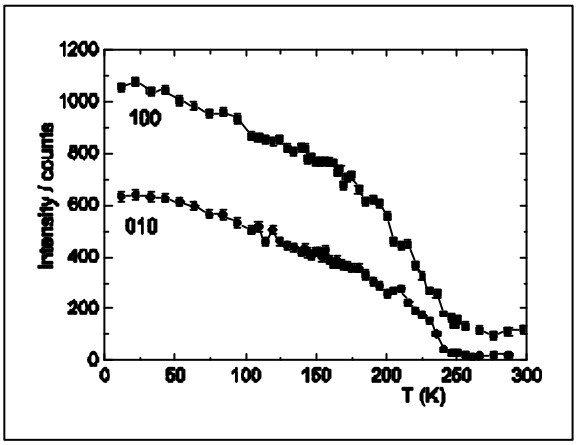


Fig. 1. Temperature dependence of the Bragg reflections 100, 010 of $La_{1.99}Cu_{0.01}O_4$.

[1] For a review, see M.A. Kastner, R.J. Birgeneau, G. Shirane, Y. Endoh, Rev. Mod. Phys. **70** (1998) 897.

[2] B. Keimer, G. Blumberg, Y. Ando, M. Reehuis, BENSC Experimental Report 2003, p. 32 and 33.

	EXPERIMENTAL REPORT **Crystal and magnetic structure of $LaTiO_3$**	Proposal N° **PHY-01-1481** Instrument **E5** Local Contact M. Reehuis
Principal Proposer:	C. Ulrich, B. Keimer, MPI Stuttgart M. Reehuis, MPI Stuttgart, HMI Berlin J. Hemberger, EKM, Institut für Physik, Universität Augsburg	Date(s) of Experiment 07.01. – 25.01.04
Experimental Team:	M Reehuis and C. Ulrich	

Date of Report: 04.01. 2005

$LaTiO_3$ is known as a Mott insulator which orders antiferromagnetically at T_N = 146 K. In order to understand the structural and magnetic properties we reinvestigated the crystal structure of $LaTiO_3$ at 295 K. Single-crystal data have been collected on the instrument E5 using the neutron wavelength λ = 0.89 Å (Cu-monochromator). For the data collection of $LaTiO_3$ a small single-domain cylindrical crystal with the dimensions *d* = 4.0 mm and *h* = 0.7 mm was available. A total of 1047 observations has been averaged to 476 independent data. As found recently for $YTiO_3$ [1] the atomic parameters of $LaTiO_3$ could be successfully refined in the orthorhombic space group *Pbnm* (No. 62, standard setting *Pnma*) (Table1 and 2). Here the atoms La and O1 are located on the Wyckoff position 4*c*: *x*, *y*, ¼, the O2-atoms on 8*d*: *x*, *y*, z. For the titanium atom only the anisotropic thermal parameters were refined, since this atom is on the position 4*b* (0, 0, ½). The refinement of a total of 29 parameters resulted in a residual of *R*(*F*) = 0.064.

For the investigation of the magnetic structure of $LaTiO_3$ the measurements were carried out using a PG-monochromator selecting the longer neutron wavelength λ = 2.38 Å. The presence of magnetic contributions could be established from the temperature dependence of primitive Bragg reflections at smaller angles of 2*q*. Below 145 K a spontaneous increase of magnetic intensity could be observed for the weak (in *Pbnm* allowed) reflection 101 and on the position of the forbidden one 011. This indicates a magnetic order of the Ti moments of a *G*-type, where the atoms (Ti1: ½, 0, 0; Ti2: ½, 0, ½; Ti3: 0, ½, 0; Ti4: 0, ½, ½) form the spin sequence + – – +. The moment direction here can be determined from the ratio of the magnetic intensities of 101 and 011: I(101)/I(011) ≈ 1/3 with m || *x*, I(101)/I(011) ≈ 3/1 with m || *y* and I(101)/I(011) ≈ 1/1 with m || *z*. We finally found a value of 0.54 suggesting an alignment preferably along the *x*-direction. Due to the absence of the reflections 100, 010 and 001 a magnetic order of an *A*- and/or *C*-type can be excluded. Also a ferromagnetic contribution could not be detected at the positions of nuclear Bragg peaks. But due to the fact that the nuclear reflections are relatively strong the presence of a *very weak* ferromagnetism can not be excluded.

Table 1. Positional parameters and occupancies of $LaTiO_3$ at 295 K.

a = 5.6264(18) Å, *b* = 5.6175(12) Å, *c* = 7.9198(19) Å

Pbnm	*x*	*Y*	*z*	*pop*
La	0.9935(2)	0.0449(3)	¼	0.996(4)
Ti	0	0	½	1.002(10)
O1	0.0813(3)	0.4909(4)	¼	1.000(6)
O2	0.7100(2)	0.2938(2)	0.04226(16)	1.002(4)

Table 2. Anisotropic thermal parameters of $LaTiO_3$ at 295 K (in 100 $Å^2$).

	U_{11}	U_{22}	U_{33}	U_{12}	U_{13}	U_{23}
La	0.48(4)	1.50(5	1.12(5)	–0.00(5)	0	0
Ti	0.32(9)	0.82(9)	0.84(9)	0.39(9)	–0.09(8)	0.04(8)
O1	0.71(7)	1.46(8)	1.00(6)	–0.21(6	0	0
O2	0.59(4)	1.10(5)	1.41(5)	–0.17(4)	0.14(4)	–0.18(5)

A *G*-type ordering along *x* could also be observed for $YTiO_3$ [2]. But here the moment value $m_{exp,x}$ = 0.082(12) m_B is very weak. In contrast to $LaTiO_3$ an additional weak component of an *A*-type [$m_{exp,y}$ = 0.047(13) m_B] and a strong ferromagnetic one [$m_{exp,z}$ = 0.544(13) m_B] was found along *y* and *z*, respectively. Despite of the different orientations of the Ti moments in both compounds the total magnetic moment m_{exp} = 0.553(11) m_B for $YTiO_3$ is very similar to the value m_{exp} = 0.53(3) m_B for $LaTiO_3$.

[1] J. Peters, W. Jauch, M. Reehuis, C. Ulrich, B. Keimer, BENSC Experimental Report 2003, p.244.

[2] C. Ulrich, G. Khaliullin, S. Okamoto, M. Reehuis, A. Ivanov, H. He, Y. Taguchi, Y. Tokura, B. Keimer, Phys. Rev. Letters **89** (2002) 167202.

	EXPERIMENTAL REPORT **Magnetic ordering in $DyVO_3$**	Proposal N° **PHY-01-1482** Instrument **E5** Local Contact M. Reehuis
Principal Proposer: Experimental Team:	C. Ulrich, B. Keimer, MPI Stuttgart M. Reehuis, MPI Stuttgart, HMI Berlin C. Ulrich, MPI Stuttgart	Date(s) of Experiment 09.08. – 29.08.04

Date of Report: 05.01. 2005

Vanadates with the formula RVO_3 (R = Y or rare earth element) exhibit many exciting properties which can be related to orbital or spin rearrangements. Recently we were able to explain the unusual properties of YVO_3 by novel orbital fluctuations [1]. This compound exhibits two different magnetic phase transitions at 75 K and 117 K, and a structural one at 200 K. In contrast, for $TbVO_3$ only one magnetic phase transition could be observed at 118 K; another structural one appears at 191 K [2, 3]. In fact, a second magnetic phase transition could be observed for the vanadates with smaller R^{3+}-ions (R^{3+} = Dy^{3+} – Lu^{3+}) [2].

A single crystal of $DyVO_3$ with the dimensions 3 × 3 × 3 mm^3 was grown by the floating zone technique [2]. Data were collected on the four-circle diffractometer E5 using the neutron wavelength l = 0.89 Å (copper). In order to investigate the magnetic order of the V- and Dy-atoms we measured the temperature dependence of the intensity of some prominent reflections. In Fig. 1 it can be seen for the reflection 100 that magnetic intensity spontaneously increases at the Néel temperature T_N = 141(2) K. This satisfies the reflection condition for a C-type ordering of the V-moments as given in Table 1.

Table 1. Spin sequences of the V- and Dy-moments along the x- and y-axis.

Dy	x	V	y
x, y, ¼	+	½ , 0, 0	+
–x, –y, ¾	+	½ , 0, ½	+
½ – x, ½ + y, ¼	–	0, ½ , 0	–
½ + x, ½ – y, ¾	–	0, ½ , ½	–

The absence of the reflections 010 and 001 suggests a moment direction parallel to the b-axis with a moment value m_{exp} = 1.37(9)? m_B at 90 K. Below this temperature the magnetic intensity of the 100 is continuously decreasing, while it is increasing for the 102. This can be ascribed to an induced C-type ordering of the dysprosium moments through the magnetically ordered vanadium sublattice, reaching at 10 K a moment value of about 0.8 m_B. A second magnetic phase transition for could not be observed. This is in contrast to the results of specific heat measurements as reported only recently [2]. A continuous increasing could also observed for the reflection 002. This suggests an additional induced ferromagnetic component of dysprosium parallel to the a-axis.

For the reflection 202 a minimum could be observed at about 170 K, whereas the 022 does not show any anomaly. This indicates the structural phase transition from the orthorhombic in to the monoclinic phase, where the atoms seem to shift in particular directions.

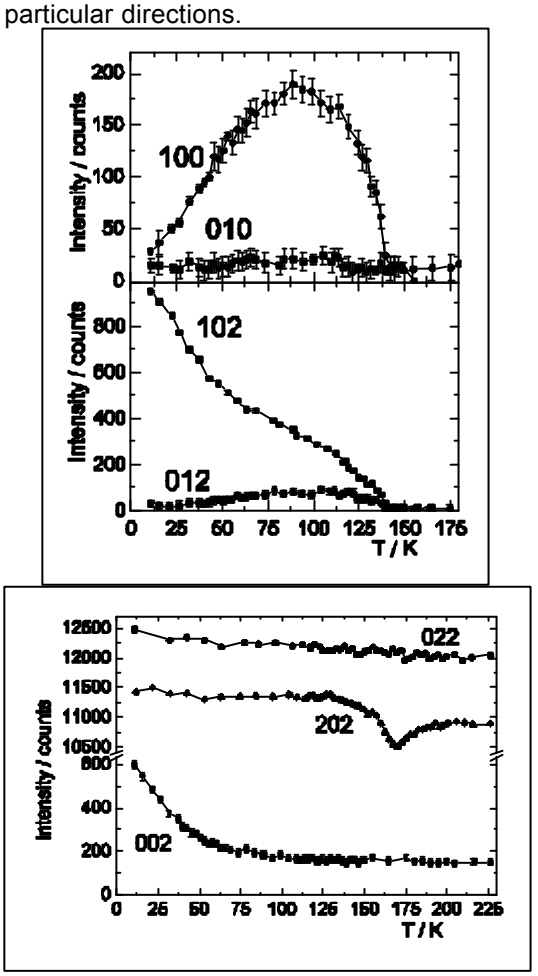


Fig. 1. Temperature dependence of the integrated intensities of some magnetic Bragg reflections.

[1] C. Ulrich, G. Khaliullin, J. Sirker, M. Reehuis, M. Ohl, S. Miyasaka, Y. Tokura, B. Keimer, Phys. Rev. Lett. **91**, 257202 (2003).

[2] S. Miyasaka, Y. Okimoto, M. Iwama, and Y. Tokura, Phys. Rev. B **68**, 100406(R) (2003).

[3] M. Reehuis, C. Ulrich, P. Pattison, B. Ouladdiaf, S. Miyasaka, Y. Tokura, B. Keimer, to be published.

BENSC	**EXPERIMENTAL REPORT** **Magnetic and structural disorder in single crystalline UPt_2Si_2**	Proposal N° PHY-01-1480 PHY-01-1592 Instrument E5 Local Contact M. Reehuis
Principal Proposer: Experimental Team:	S. Süllow, TU Braunschweig S. Süllow, J. Kreitlow, TU Braunschweig A. Loose, R. Feyerherm, HMI Berlin	Date(s) of Experiment 29.03.2004 – 08.04.2004 19.07.2004 – 29.07.2004

Date of Report: 04/01/2005

Recently, we have presented evidence for the presence of crystallographic disorder in a single crystalline, stoichiometric correlated electron material, UPt_2Si_2 [1]. First structural refinements indicated that at 300K the system crystallizes in the $CaBe_2Ge_2$-structure [2]. The effective mass m^* is moderately enhanced with a Sommerfeld coefficient to the specific heat of $\gamma = 32\mathrm{mJ/molK}^2$. The material undergoes an antiferromagnetically (AFM) ordering transition ($\boldsymbol{k}$ = [0 0 1]) at T_N = 32K, with weakly screened moments of $\mu_{ord} = 1.7\mu_B$. Furthermore, a recent thermodynamic investigation revealed a 1st order phase transition at ~305K, which apparently coincides with a lattice distortion [3]. The details of the distortion have not yet been fully resolved, but its existence points towards a structural instability, which might be the cause for the anomalous, disorder affected bulk properties. Therefore, with the bright elemental contrast between U, Pt and Si in a neutron scattering experiment the goal of our study was to directly establish the presence of disorder in a single-crystalline as-grown specimen UPt_2Si_2, and to study the effect of an annealing treatment on the structural properties of the compound. For this we have carried out a detailed structural analysis using neutron diffraction of a sample UPt_2Si_2 in as-grown and annealed (900°C for 1 week) form.

The experiments have been carried out on the 4-Circle Diffractometer E5 of the BENSC. In order to reduce thermal effects on the obtained spectra the study has been performed at a low temperature of 50K, stabilized by means of a standard flux-flow cryostat. In total, about 500 peaks have been measured, 200 of which are inequivalent. Based on this set of data we have performed a full refinement for the as-grown and the annealed crystal. The basic structure of UPt_2Si_2 is verified as the P4/nmm symmetry of the $CaBe_2Ge_2$-lattice, with lattice parameters of a = 4.1857Å and c = 9.6301Å in as-grown and annealed state. From our data there is no evidence for site exchange disorder in the compound.

On the other hand, the full refinement yields a clear signature of crystallographic disorder in UPt_2Si_2, that is in the thermal displacement parameters U_{11}/U_{22}. In the Tables 1 and 2 we summarize the fit parameters for the as-grown and the annealed sample. For both samples we find anomalously large values U_{11}/U_{22} for the Pt(2) and Si(2) site. Since the experiment has been carried out at a low temperature, the large values U_{11}/U_{22} cannot be temperature induced, and thus reflect a static and random displacement of the two ions from their high symmetry positions. It is thus for the first time that for a heavy fermion related material structural disorder has been directly measured by means of a structure determination technique.

	x	y	z	U11	U22	U33
U	¼	¼	0.7484(2)	0.45(4)	0.45(4)	0.08(4)
Pt(1)	¼	¼	0.3785(2)	0.10(3)	0.10(3)	0.28(4)
Pt(2)	¾	¼	0	**1.86(5)**	**1.86(5)**	0.14(4)
Si(1)	¾	¼	½	0.10(6)	0.10(6)	0.18(7)
Si(2)	¼	¼	0.1330(3)	**0.94(8)**	**0.94(8)**	0.29(8)

Table 1: Refinement parameters for as-grown single crystalline UPt_2Si_2.

	x	y	z	U11	U22	U33
U	¼	¼	0.7480(2)	0.66(5)	0.66(5)	0.26(7)
Pt(1)	¼	¼	0.3787(2)	0.25(5)	0.25(5)	0.39(6)
Pt(2)	¾	¼	0	**1.98(6)**	**1.98(6)**	0.30(5)
Si(1)	¾	¼	½	0.16(7)	0.16(7)	0.38(9)
Si(2)	¼	¼	0.1340(4)	**1.27(10)**	**1.27(10)**	0.42(12)

Table 2: Refinement parameters for annealed single crystalline UPt_2Si_2.

[1] A. Otop, F.J. Litterst, R.W.A. Hendrikx, J.A. Mydosh, S. Süllow, J. Appl. Phys. **95** (2004) 6702.

[2] R.A. Steeman, E. Frikkee, S.A.M. Mentink, A.A. Menovsky, G.J. Nieuwenhuys, J.A. Mydosh, J. Phys.: Condens Matter **2** (1990) 4059.

[3] H. Amitsuka, private communication (2003)

BENSC	**EXPERIMENTAL REPORT** **Influence of hydrostatic pressure on the antiferromagnetism of $La_{2-x}Sr_xCuO_4$**	Proposal N° PHY-01-1466 Instrument **E6** Local Contact J. Hernandez-Velasco N. Stüßer
Principal Proposer: Experimental Team:	Dr Martyn Bull ISIS Pulsed Neutron and Muon Source, UK Dr Christos Panagopoulos University of Cambridge, UK Dr Bella Lake, University of Oxford, UK Dr Christopher Frost ISIS Pulsed Neutron and Muon Source, UK	Date(s) of Experiment 4th February 2004 – 16th February 2004

Date of Report: 9th February, 2005

The interplay between magnetic fluctuations and superconductivity is a central, though poorly understood, feature in the physics of high-Tc superconductors (HTS). muSR and thermodynamic studies indicate the importance of competition between low-energy spin correlations and superconductivity, and an intimate relation of the former to the anomalous normal state properties in under doped HTS. In addition, neutron, muSR and NMR studies suggest the presence of spin-charge stripes in HTS. It is claimed by some that stripes drive superconductivity although our recent muSR studies suggest a competition between the two.
In this experiment we sought to clarify this important issue by performing neutron scattering experiments where instead of tuning the magnetic ground state by chemical doping we use pressure since the exchange energy, J, varies strongly with lattice parameter.
LSCO (x = 0.11) was selected for this study because it does not exhibit a pressure-induced transfer of charge to the CuO_2 layers such as is seen in other common HTS materials. This allows for a clean experiment carried out at a fixed doping state where only the magnitude of J is modified.
For comparison, we also selected a LSCO sample with x=0.03 in the glassy region where no superconductivty occurs. This sample is known to have an order magnitude larger magnetic moment, and would prove useful as a comparison.
For this experiment, we used samples with dimensions 4mm x 4mm x 4mm in order to be accommodated in the bore of a Cu/Be pressure cell.
The reduction in sample size and weak incommensurate signal led us to choose an instrument with high flux and good signal to noise. Instrument E6 was selected because the criteria were met in the instrument description on the BENSC webpages. The wide angular coverage of the detector bank seemed ideal for rapid realignment of the sample after pressurisation, and for locating incommensurate peak position changes as a function of pressure.
Our experience of this instrument during our time at HMI was *highly unsatisfactory* since the signal to noise of the instrument was appalling.

We began our experiment with the x=0.11 sample without pressure cell in order to calibrate the incommensurate peak size and position on this particular instrument. Whilst we were able to measure structural peaks satisfactorily, the noise and high background in the detector prevented us measuring any incommensurate magnetic signal despite collecting significant statistics over a number of days.
We then changed to the x=0.03 sample, where we were able to detect magnetic peaks at low temperature. One test in a pressure cell, allowed us to confirm that these peaks could be made to vanish with pressure.
However, since we were unable to measure the order magnitude smaller signal in x=0.11 sample without the pressure cell, we were unable to carry out the main part of our proposal.
We would like to thank Jorge Hernandez-Velasco for his substantial help in trying to make the experiment work.

Response to Experimental Report PHY-01-1466

By Norbert Stüßer

It is always difficult to clarify criticsm on an experiment performed about 1 year ago. Especially it is difficult for me since I was not really involved in the experiment itself. The critiscm adresses firstly the webpages which promise a high flux of neutrons at the sample position and secondly the present background during that time. The high flux is specified in the webpages with $5 \cdot 10^6$ n/cm^{2}s without any collimations. This will be of course reduced by using collimations in the instrument. This quantitative specification allows estimating the flux under the special conditions under which this experiment was performed. More difficult is to adress the criticism on the high background since this is determined by the sample, its environment and the instrument itself. Routine calibration measurements carried out before and after this experiment indicated no unusual background. In experiments with pressure cells the background is normally dominated by the scattering of the pressure cell. In case the background of the instrument itself was comparable to the background produced by the cell something was totally wrong. Unfortunately, it is now hard to clarify the origin for an unusual high background.

	EXPERIMENTAL REPORT **Neutron Diffraction Measurement on Ferrofluids**	Proposal N° PHY-01-1471 Instrument **E6** Local Contact N. Stüsser
Principal Proposer: Experimental Team:	M. Hofmann, FRM-II, TU München E. Steichele, TU München M. Hofmann	Date(s) of Experiment 5.-8.4.2004

Date of Report: 10.2.2005

Ferrofluids are suspensions of nanoparticles of ferro- or ferrimagnetic materials in carrier liquids like water or toluene etc.. The suspensions are stabilized by a „surfactant“ of chain molecules. Apart from technical and medical applications these materials have found a wide scientific interest as both magnetism and hydrodynamics play an important role in their physical behaviour. Due to the large magnetic moments of the nanoparticles (super-paramagnetism) many properties can be changed by relatively low magnetic fields. One of the outstanding effects is the magneto-viscosity: the viscosity of the ferrofluid depends on the angle between the shear forces (vorticity) and the magnetic field direction. The effect, known since 1968, is strong in hard magnetic materials and weak in soft magnetic materials and is explained by a microscopic model, in which the free rotation of the particles is hindered thus causing rotational viscosity. According to this model a stationary orientation of the nanoparticles can be expected, depending on the balance between magnetic and frictional moments. The change of orientation as function of magnetic field and shear forces should be visible like a texture in a polycrystalline diffraction experiment.

For the experiments at E6 a ferrofluid based on „Fomblin“, which is a perfluorinated polyether, was used. The ferrimagnetic core of the particles was cobalt ferrite ($CoFe_2O_4$) which is a magnetic hard material. Magnetic fields less than 0.1 Tesla did not show any effects on the diffraction patterns. However, the magnetization curves of the ferrofluid showed temperature dependant effects only at higher fields of about 1 –2 Tesla. The diffraction data showed the same trend for the main ferrimagnetic reflections (111) and (400) as depicted in figure 1. Due to the low concentration of magnetic particles (about 5 vol-%) the signal to noise ratio was quite poor (figure 2). Nevertheless it was possible to refine basic structural and magnetic parameters of the $CoFe_2O_4$ nanomaterial yielding a volume weighted particle size of about ~ 20(5) nm. The results prove that we can discern structural details of the ferrofluid using diffraction methods and the next step will be to check the magneto-viscosity provided a suitable sample cell, which allows simultaneously applying a magnetic field while stirring or moving the ferrofluid, will become available.

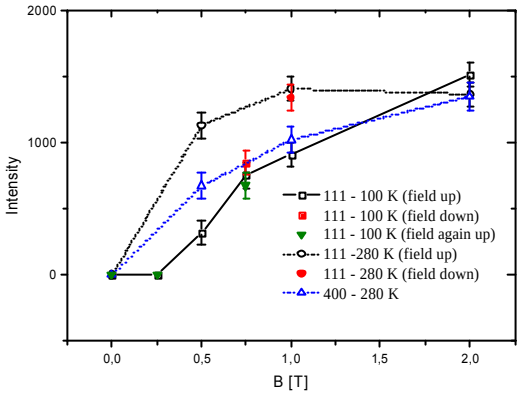


Figure 1 Magnetic intensities of several reflections as a function of magnetic field and temperature.

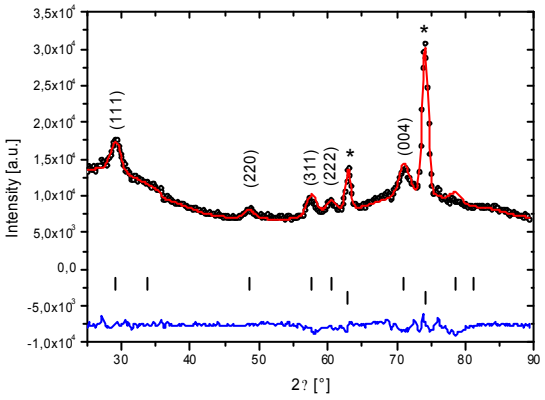


Figure 2 Rietveld refinement fit of Fomblin based $CoFe_2O_4$-Ferrofluid at T = 280 K and B = 0 T. The reflections marked with (*) are from the Al sample container.

	EXPERIMENTAL REPORT **Neutron diffraction studies of RPdIn (R – Nd, Ho, Er) compounds.**	Proposal N° PHY-01-1474 Instrument **E6** Local Contact Dr J. Hernandez-Velasco
Principal Proposer:	Dr Lukasz Gondek, Division of Physics, Agricultural University of Cracow, Mickiewicza 21, 31-120 Krakow, Poland	Date(s) of Experiment
Experimental Team:	Dr L. Gondek Dr S. Baran, Institute of Physics, Jagiellonian University, Reymonta 4, 30-059 Krakow, Poland Dr J. Hernandez-Velasco, BENSC, HMI, Glienicker Str. 100, D-14 109 Berlin	29 Apr – 03 May 2004

Date of Report: 25 Nov 2004

Structural and magnetic properties of the ternary intermetallic compounds RPdIn (R=Nd, Ho, Er) with hexagonal ZrNiAl-type structure are reported [1]. Magnetic phase transitions were studied by means of neutron powder diffraction experiments. Neutron diffraction measurements indicate ferromagnetic ordering for all investigated RPdIn compounds with transitions temperatures of 30 K (R=Nd), 22 K (R=Ho) and 11 K (R=Er). For NdPdIn compound a change of the direction of the Nd magnetic moments from the basal plane to the direction of the c-axis was observed. For both HoPdIn and ErPdIn rare earth magnetic moments are parallel to the c-axis. Observed magnetic moments at 1.5 K are as follow: 1.8 μ_B for NdPdIn, 8.1 μ_B for HoPdIn and 6.6 μ_B for ErPdIn.

The observed magnetic moments are reduced in comparison to the free ion values as well as to the effective values obtained from paramagnetic Curie-Weiss behaviour. On the other hand values of Nd, Ho and Er magnetic moments observed in neutron diffraction experiment are close to saturation magnetic moment estimated from magnetization curves collected at 4.2 K.

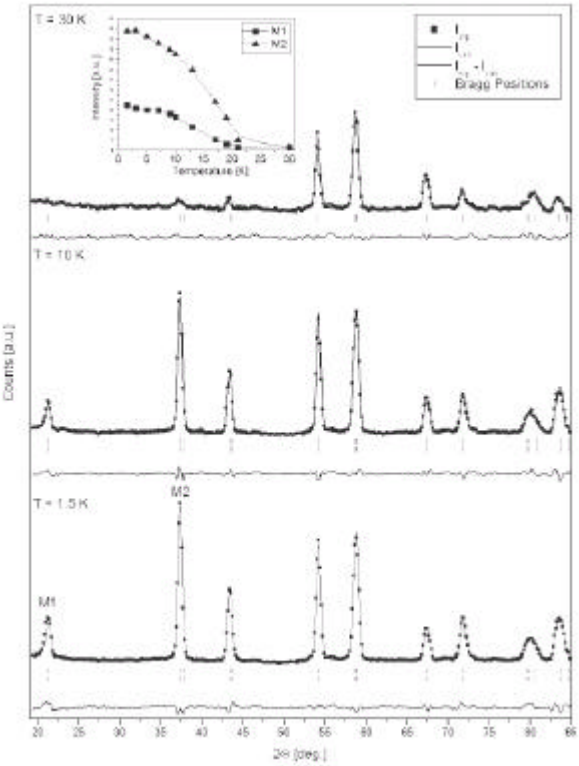


Fig. 1 Neutron diffraction patterns of HoPdIn compound at temperatures of 30 K, 10 K and 1.5 K.

REFERENCE:

[1] L. Gondek, S. Baran, A. Szytula, D. Kaczorowski, J. Hernandez-Velasco,
J. Magn. Magn. Mater. 285/1-2 pp 272-278

	EXPERIMENTAL REPORT **Magnetic structures of $R_3Ag_4Sn_4$ (R=Pr, Nd) and $Nd_3Cu_4Ge_4$**	Proposal N° PHY-01-1475 Instrument E6 Local Contact Dr N. Stüßer
Principal Proposer:	E. Wawrzynska, M. Smoluchowski Institute of Physics, Jagiellonian University, Reymonta 4, 30-059 Kraków, Poland	Date(s) of Experiment
Experimental Team:	J. Hernández-Velasco, BENSC, Hahn-Meitner Institut, Glienicker Straße 100, D-14109 Berlin-Wannsee, Germany B. Penc, A. Szytula, K. Tomala, M. Smoluchowski Institute of Physics, Jagiellonian University, Reymonta 4, 30-059 Kraków, Poland	16.02.2004-19.02.2004 20.05.2004-24.05.2004

Date of Report: 13.12.2004

Polycrystalline samples of $R_3Ag_4Sn_4$ (R=Pr, Nd) and $Nd_3Cu_4Ge_4$ intermetallics were studied with magnetometric, x-ray and neutron diffraction methods. All of them crystallize in the orthorhombic $Gd_3Cu_4Ge_4$-type structure (Immm space group), in which the rare earth atoms occupy two inequivalent 2d and 4e crystallographic positions, and order antiferromagnetically below their Néel temperatures of 12 K in the case of $Pr_3Ag_4Sn_4$, 5 K in the case of $Nd_3Ag_4Sn_4$ and 4.5 K in the case of $Nd_3Cu_4Ge_4$. All of the investigated compounds have collinear magnetic structures at low temperatures. In the case of $Pr_3Ag_4Sn_4$ an additional phase transition to a non-collinear structure is observed. The magnetic structures were studied with the support of group theoretical considerations. Table 1 presents a summary concerning the determined magnetic structures, which are described in detail in [1].

Table 1. Summary of the determined magnetic structures of $R_3Ag_4Sn_4$ (R = Pr, Nd) and $Nd_3Cu_4Ge_4$.

compound	T [K]	propaga-tion vector	4e sites	2d sites
$Pr_3Ag_4Sn_4$	1.5 – 9	**k**=(1,1,1)	2.83(6) μ_B + + – – ‖ a	3.2(1) μ_B – + ‖ a
	9 – 12	**k**=(0, ?,0)	2.4(2) μ_B + + – – ‖ a	2.8(4) μ_B – + ‖ a
$Nd_3Ag_4Sn_4$	1.5 – 5	**k**=(1,1, 1)	2.29(8) μ_B a-b plane	1.3(1) μ_B + – ‖ a
$Nd_3Cu_4Ge_4$	1.5 – 4.5	**k**=(1,1,1)	1.75(5) μ_B + + – – ‖ c	not ordered

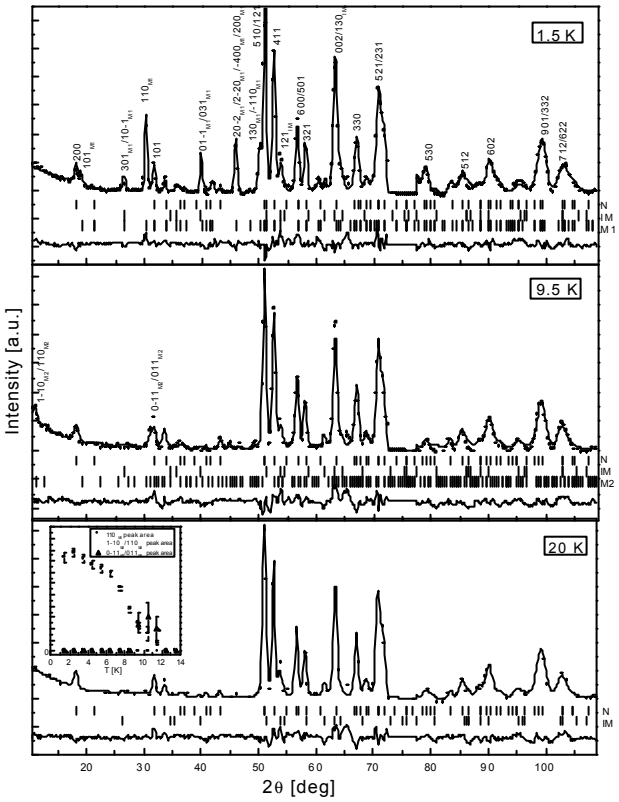


Fig 1. Neutron diffraction patterns of $Pr_3Ag_4Sn_4$ collected at 1.5, 9.5 and 20 K. The circles represent the experimental points, the solid lines are the calculated profiles for the model crystal and magnetic structures described in the text and the differences between the observed and calculated intensities (at the bottom of each diagram). The vertical bars indicate the Bragg peaks of nuclear (N for $Pr_3Ag_4Sn_4$ and IM for the $PrAg_2$ impurity phase) and magnetic (M1 and M2 for the phases connected with two propagation vectors) origin. The region around about 76° was excluded due to cryostat reflection. The inset shows the temperature dependence of the magnetic peak intensities.

References

[1] E. Wawrzynska, J. Hernández-Velasco, B. Penc, A. Szytula, K. Tomala, J. Phys.: Condens. Matter 16 (2004) 7535.

	EXPERIMENTAL REPORT Neutron Diffraction Study of RCu_xGe_2 (R = Ho, Er) and RCo_xSn_2 (R = Tb, Er, Ho) compounds	Proposal N° PHY-01-1589 Instrument E6 Local Contact Dr N. Stüßer
Principal Proposer:	E. Wawrzynska, M. Smoluchowski Institute of Physics, Jagiellonian University, Reymonta 4, 30-059 Kraków, Poland	Date(s) of Experiment
Experimental Team:	J. Hernández-Velasco, N. Stüßer, BENSC, Hahn-Meitner Institut, Glienicker Straße 100, D-14109 Berlin-Wannsee, S. Baran, B. Penc, A. Szytula, M. Smoluchowski Institute of Physics, Jagiellonian University, Reymonta 4, 30-059 Kraków, Poland A. Gil, Department of Mathematics and Natural Sciences Pedagogical University, Armii Krajowej 13/15, 42-800 Czestochowa, Poland D. Kaczorowski, A. Zygmunt, W. Trzebiatowski Institute of Low Temperature and Structure Research, Okólna 2, 50-950 Wroclaw, Poland	22.09.2004-26.09.2004

Date of Report: 04.02.2005

Polycrystalline samples of the RCu_xGe_2 (R = Ho, Er) and RCo_xSn_2 (R = Tb, Er, Ho) intermetallics were studied with magnetometric, x-ray and neutron diffraction methods. All of them crystallize in the orthorhombic $CeNiSi_2$-type structure (Cmcm space group), in which the rare earth atoms occupy the 4c crystallographic positions, and order antiferromagnetically below their Néel temperatures of 8.0 K in the case of $HoCu_{0.33}Ge_2$, 4.5 K in the case of $ErCu_{0.25}Ge_2$, 18.8 K in the case of $TbCo_{0.25}Sn_2$, 4.7 K in the case of $ErCo_{0.24}Sn_2$ and 5.6 K in the case of $HoCo_{0.23}Sn_2$.

Table 1. Summary of the determined magnetic structures of RCu_xGe_2 (R = Ho, Er) and RCo_xSn_2 (R = Tb, Er, Ho).

compound	T [K]	propagation vector	magnetic moment arrangement
$HoCu_{0.33}Ge_2$	1.5 – 8.0	**k**=(0,0,0)	8.18(21) μ_B + – + – || c
$ErCu_{0.25}Ge_2$	1.5 – 4.5	**k**=(0,0,0)	7.89(15) μ_B + – + – || a
$TbCo_{0.25}Sn_2$	1.5 – 18.8	**k**=(0,0,½)	7.14(8) μ_B + – – + a-c plane
$ErCo_{0.24}Sn_2$	1.5 – 4.7	**k**=(0,0,½)	6.15(13) μ_B + + – – || a
$HoCo_{0.23}Sn_2$	1.5 – 5.6	**k**=(½,½,0)	6.79(23) μ_B +– – + a-c plane

The compounds investigated have different magnetic orderings at low temperatures. Table 1 presents a summary concerning the determined parameters of the magnetic structures, which are described in detail in [1-3]. All structures were found to be commensurate to the crystal structure.

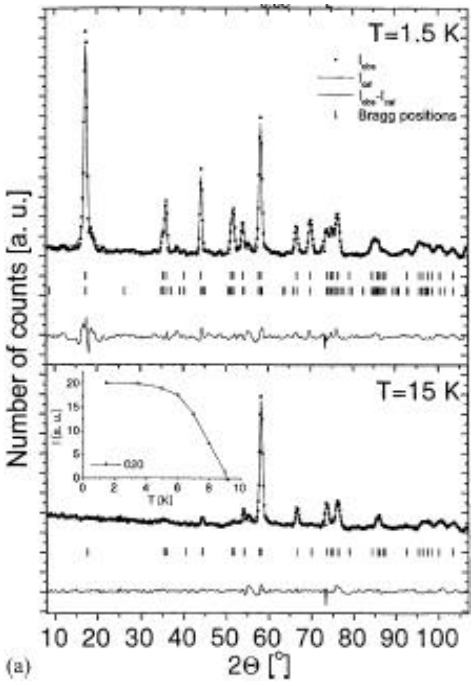


Fig 1. Neutron diffraction patterns of $HoCu_{0.33}Ge_2$ collected at 1.5 and 15 K. The squares represent experimental points, the solid curves are the calculated profiles for the crystal and magnetic structure and the differences between the observed and calculated intensities are plotted at the bottom of each diagram. The vertical bars indicate the Bragg peaks of nuclear and magnetic origin. The inset shows the temperature dependence of the 020 magnetic peak intensity.

References

[1] A. Gil et al., J. Alloys Comp. 365 (2004) 31.
[2] B. Penc et al., J. Alloys Comp. 375 (2004) L1.
[3] A. Gil et al., J. Alloys Comp. 384 (2004) L4.

BENSC	**EXPERIMENTAL REPORT** **The magnetic structure determination of the compound $Na_{12}Co_7O_{14}$**	Proposal N° CHE-01-1567 Instrument **E6/E9** Local Contact J. Hernandez-Velasco
Principal Proposer: Experimental Team:	Dr. Mikhail Sofin, Max Planck Institut für Festkörperforschung, Stuttgart Dr. Olivier Leynaud, ibid. Pr. Dr. Martin Jansen, ibid.	Date(s) of Experiment 12-14 July 2004 on E6 14-16 July 2004 on E9

Date of Report: 10 February 2005

The compound $Na_{12}Co_7O_{14}$ is one of the last member in the Na-Co-O system, recently synthesised in our laboratory. This system is interesting especially considering some recent discoveries on physical properties like thermoelectric and superconductive properties.

It crystallises in the space group C *1 2/c 1* (n°15), with cell parameters a = 20.52 Å, b = 8.05 Å, c = 11.35 Å and β = 95.3°. The structure is quite complex, and three different Co atom environments are observed.
Incertitude about the Co ratio of the compound was however observed during the refinement, the site occupancy factor for the third Co atom being close to 0.6 and we wondered about the presence of a superstructure (e.g. with a ratio of 0.5).

This compound presents a long range order at about 20 K that we thought being antiferromagnetic. The gap between Zero Field Cooled (ZFC) and Field Cooled (FC) measurements below T_K (see figure), is indicative of a spin freezing. Another interesting fact is the highly negative value of the Curie paramagnetic temperature showing that the Curie-Weiss law is probably not applicable on these data.

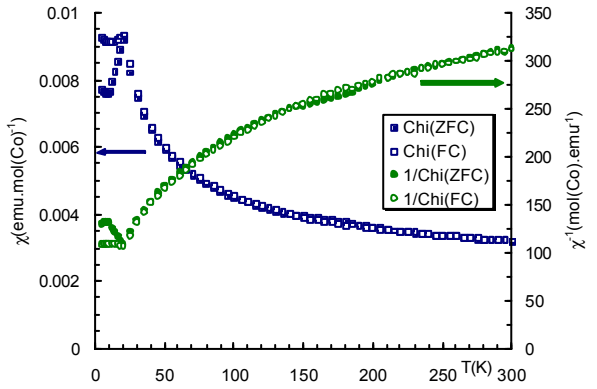


Figure: Magnetic susceptibility and its inverse with ZFC and FC modes for $Na_{12}Co_7O_{14}$.

Magnetic frustrations have already been attributed to similar cases, and we hoped that the solving of the magnetic structure could have help us to establish and explain such phenomena.

The experiments were carried only on the E9 instrument, E6 being disabled following severe technical problems on the station. We decided to perform two experiments, one at low temperature and one at ambient temperature in order to obtain the magnetic structure of this compound, and to obtain sufficient information about nuclear structure.

On the nuclear structure, the single crystal data were confirmed by neutron powder diffraction. We have been unable so far to obtain any reliable data tending to prove if the content of the compound is more likely $Na_6Co_{3.6}O_7$ than $Na_6Co_{3.5}O_7$, the refinement of the occupation factor being in the same order inside the estimated square deviation. However, not any supplementary peak being related to a superstructure has been found, confirming the statistical distribution observed for one of the Co atoms.

No difference was observed between high and low temperature patterns. Two main hypotheses can be proposed. First we are in presence of a magnetic frustration, and in this case the remaining moment can be very small and cannot be detected with the low flux available on the E9 instrument. Second, the very negative value for theta could also be indicative of spin glass behaviour, which is intrinsically non periodic and therefore with no diffraction pattern.

Supplementary magnetic measurements, especially with AC susceptibility would probably be able to help us in the determination between these two cases.

	EXPERIMENTAL REPORT **Low temperature magnetic behaviour of $CeNi_{0.6}Cu_{0.4}$**	Proposal N° EF Instrument **E6** Local Contact J. Hernández-Velasco
Principal Proposer: Experimental Team:	N. Marcano, J. C. Gómez Sal, CITIMAC, U.C J. Hernández-Velasco, BENSC-HMI Berlin. *current address:* F.CC.Químicas Univ.Complutense Madrid	Date(s) of Experiment 1.6.-3.6.2004

Date of Report: 15.2.2005

In the $CeNi_{1-x}Cu_x$ system, depending on *x*, the compounds could crystallise in the FeB-type orthorhombic structure, or in the CrB-type, the change takes place around *x*=0.15. A brief summary of the complex magnetic behaviour of this series can be condensed in the sketch picture displayed in Fig. 1. The magnetic interactions are modified by substitution of Cu by Ni, then decreasing the number of conduction electrons, and a change from antiferromagnetism to ferromagnetism appears as in other similar $RNi_{1-x}Cu_x$ series. The magnetic structures of these compounds present an interesting evolution from a pure antiferromagnetic structure for CeCu with **k**=[1/2,0,0], and the moments lying in the ***ac*** plane, to a ferromagnetic one for $CeNi_{0.4}Cu_{0.6}$ with a Ce magnetic moment $\mu=0.6\mu_B$ in the ***b*** axis. This magnetic moment value is strongly reduced with respect to that of the free ion, due to the increasing Kondo effect, related to the decreasing cell volume. The Kondo T have been determined from quasielastic neutron scattering.

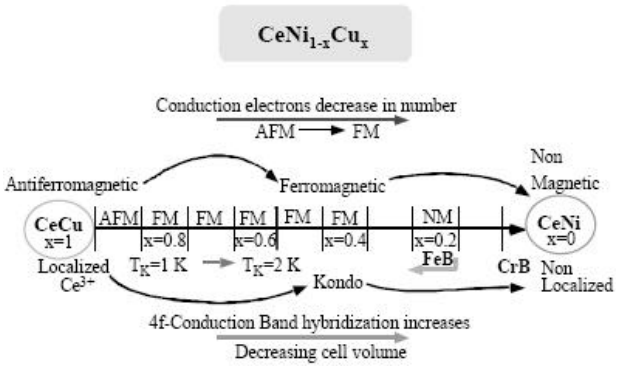


Figure 1.- Schematic magnetic properties of $CeNi_{1-x}Cu_x$ [1].

This work has been carried out to complete the magnetic phase diagram of the $CeNi_{1-x}Cu_x$ series [2], where the poor Cu compounds *x*=0.5 show very low T_C and spin-glass behaviour at higher temperatures.

An experimental disadvantage in addition to the low magnetic ordering temperature in $CeNi_{0.6}Cu_{0.4}$, is the rather low value of the magnetic moment in the ordered state, which is around our detection limit for a powder. In this sense, the experiment was performed collecting patterns during long counting time to obtain enough statistics. The sample was kept in an orange cryostat using a dilution stick device.
We have shown before an increase of certain reflections under applied magnetic field, pointing to a ferromagnetic structure, however the straightforward determination of the ground state, *i.e.* at H=0, was not completed. In the present case we got the qualitative proof of the expected behaviour, see Fig 2.

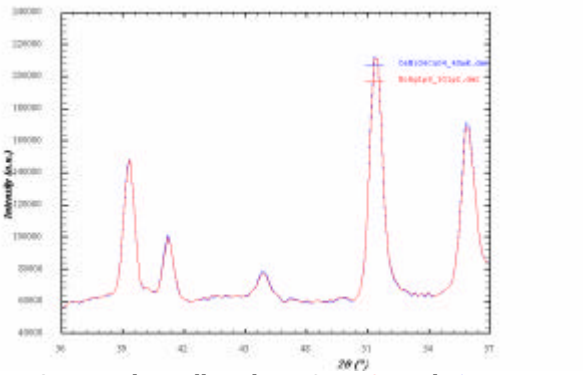


Figure 2.- NPD data collected on E6 at **1.6K** and **40 mK**.

The intensity of the reflection (111) is 6.5% larger at the low T, being the standard deviation of the measurement below the difference in the I profile between both T. A rough estimation is possible considering $<\mu>\sim\propto (I_{111Mag})^{1/2}$ and taking the previous knowledge on $CeNi_{0.5}Cu_{0.5}$ ($\mu\sim0.5\mu_B$), where I_{111} was 20.9% larger at 43mK than at 5K and scaling to this phase supposing equal structure factors in both cases for $I_{111Nuclear}$. In such a way $\mu\sim0.28\ \mu_B$ for $CeNi_{0.6}Cu_{0.4}$.

[1] J.C. Gómez Sal et al. *J. Magn. Magn. Mat*. **242**, 125 (2002).
[2] N. Marcano, *Ph.D. Thesis*, Univ. Cantabria, 2004.

BENSC	**EXPERIMENTAL REPORT** **Unusual Magnetic behaviour in Sr_2PrO_4**	Proposal N° EF Instrument **E6/E9** Local Contact J. Hernández-Velasco
Principal Proposer: Experimental Team:	J. Hernández-Velasco, BENSC-HMI Berlin. *current address:* F.CC.Químicas Univ.Complutense Madrid	Date(s) of Experiment E9: 2.12.03 E6: 2/3.2.04

Date of Report: 15.2.2005

We have recently succeed in the chemical preparation of highly pure Sr_2PrO_4, an orthorhombic oxide which presents a 1D-framework of edge sharing [PrO_6] octahedra forming chains along the crystallographic ***c***-axis. These infinite chains are far from each other and only connected through non magnetic [SrO_6] trigonal prisms. Magnetic susceptibility measurements using a SQUID magnetometer in the temperature range from RT down to 1.7K show a net maximum at 3.2 K, see Fig. 1.

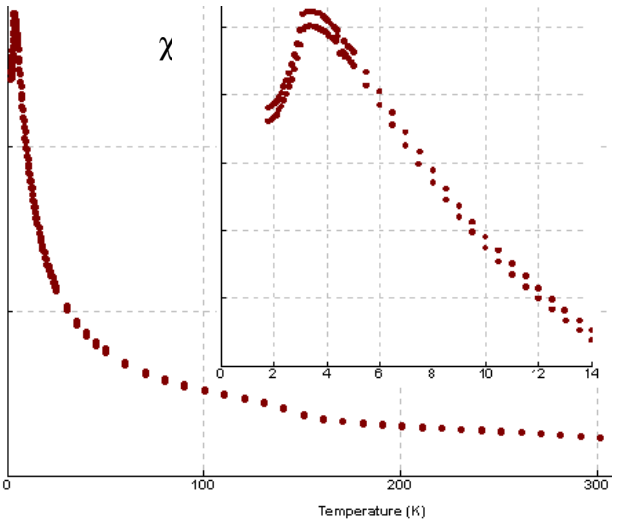


Figure 1.- Temperature dependence of Magnetic susceptibility measured at applied magnetic field *H*=500Oe. Low T range is shown in the inset, both for ZFC (bottom) and FC (top curve).

Neutron diffraction experiments using both E6 and E9 collecting patterns at temperatures below and above that of the χ maximum do not show any evidence of magnetic order, see Fig.2, which is in strong contradiction with the apparent behaviour of bulk measurements [1].

It is worth mentioning that, up to our knowledge, this compound is the best realization of a one dimensional structure containing Pr^{4+} ion (which is usually present as Pr^{3+}, or in mixed valence compounds, or in 3D nets). From the magnetic point of view, while transition metal 1D systems with few electrons have been extensively studied, *e.g.* Haldane (S=1) and Spin Peierls quantum spin systems (S=1/2), no evidence of one-*f* electron chain system has been a subject of devoted research, in part probably due to the scarce presence of the f^1 rare earth electronic configuration (Ce^{3+} is extremely unstable respect to the oxidized Ce^{4+}, that is non magnetic).

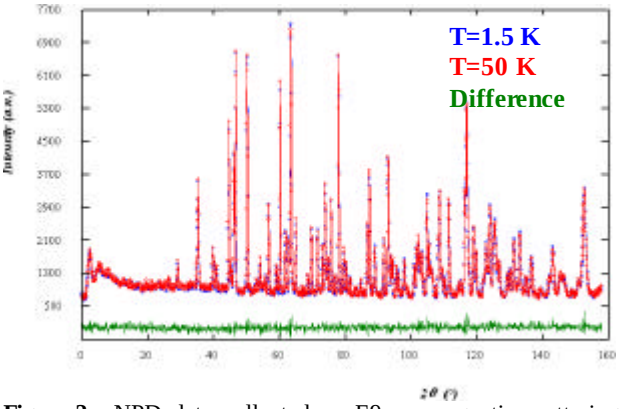


Figure 2.- NPD data collected on E9 no magnetic scattering evidence.

The questions to solve are weather Pr^{4+} is really magnetically 3D-ordered in this compound at T_N~3.2K with an anomalous reduced value of its magnetic moment, well below $0.5\mu_B$ (around our detection limit on powders at E6) while it should be about $gJ=2.14\mu_B$. Or either it remains as a pure 1D magnetically correlated system provided that there is no easy link between the chains. In such a case one could expect an anomaly in the magnetic excitation spectra of this material. On the other hand, Pr^{4+} f^1 ($^2F_{5/2}$) ground state in any crystal field symmetry lower than cubic (G_7 & G_8) should split into Kramers doublets which makes not possible a non magnetic CF ground state, by contrast with the case of Pr^{3+} f^2 ($^3H_4$). The next interesting step is to get information about both the crystal field splitting and spin dynamic in this system measuring the relation S(Q,?) *vs* energy transfer in INS spectra.

[1] J. Hernández-Velasco, to be published, 2005.

	EXPERIMENTAL REPORT **Magnetization steps and phase separation in CMR systems $Pr_{0.5}Ca_{0.5}Mn_{1-x}M_xO_3$ (M = Cr, Ni, Ti; $x \leq 0.03$)**	Proposal N° EF Instrument **E6** Local Contact J. Hernández-Velasco
Principal Proposer: Experimental Team:	J.L. García-Muñoz, N. Bellido, C. Frontera Instituto de Ciencia de Materiales de Barcelona CSIC J. Hernández-Velasco, BENSC-HMI Berlin *current address:* F.CC.Químicas Univ.Complutense Madrid	Date(s) of Experiment 21-27.4.04 & 3-6.5.2004

Date of Report: 15.2.2005

After the discovery of colossal magnetoresistance (CMR) effect, the study of manganese perovskites ($R_{1-x}A_xMn_{1-y}M_yO_3$, R= Rare earth, A= Sr, Ca) has concentrated many efforts. The competition and coexistence of metallic/ferromagnetic (FM) and insulating/antiferromagnetic (AFM) phases is at the origin of the CMR and the unusual step-like phenomena under field observed in manganite compounds (in polycrystalline and single crystal forms). Besides the CMR, one of the most celebrated phenomena of these compounds is the charge/orbital order (CO/OO). CO is classically interpreted as an ordered localization of mobile e_g electrons leading to an ordered distribution of Mn^{3+} and Mn^{4+} ions in the lattice, it is characterized by an insulating behaviour of the compounds and by the stabilization of an AFM structure at low temperature. During the last years the substitution of manganese by a series of other metals in $R_{1-x}A_xMn_{1-y}M_yO_3$, with M=Fe, Cr, Co, Ni, Ti, Mg, Al, Ga, In, Sn, etc. has revealed surprising behaviour [1]. Under some substitutions the effect is a very quick loose of CO. For instance, $Pr_{0.5}Ca_{0.5}MnO_3$ is CO while $Pr_{0.5}Ca_{0.5}Mn_{0.97}Cr_{0.03}O_3$ (with just a 3% of substitution) is FM and metallic (and thus without CO) at low temperature. The stabilization of ferromagnetism has been linked to the electronic configuration of the substituting ion. Ions with active *d* electrons like Cr^{3+} ($3d^3$) show stronger effects than those with *d*-shell half-filled $3d^5$ (Fe^{3+}) fully filled d^{10} (Ga^{3+}, In^{3+}, Sn^{3+}) or empty d^0 (Sc^{3+}, Ti^{4+}). Another amazing effect of the B-site substitution is the apparition of very sharp steps in the magnetization (and resistivity) *vs* field curves (measured after ZFC) in some of these compounds [2], specially $Pr_{0.5}Ca_{0.5}Mn_{1-y}M_yO_3$ with M= Co, Ni, Ga, and Ti.

The study of this behaviour in relation with the electronic structure of the substituted element is the subject of this work. Thus we have studied the "stair like" magnetization process in some B-site substituted manganites $Pr_{0.5}Ca_{0.5}Mn_{1-y}M_yO_3$ with M= Ti, Ni, Cr ($0 \leq y \leq 0.05$). For this we collected powder diffraction data on these compounds at zero field and different temperatures (that will be refined together with synchrotron X-ray data) as well as at different applied field H=5T (VM3). We are intended to characterize the low temperature state and to monitor the avalanches by studying the changes of the intensity of the AFM peaks and the FM ones.

We have shown the coexistence (at low T) of three different domains at a micrometer-scale: FM, AFM-CE and pseudo-CE, being mostly the first. Isothermal (T= 2.0K) magnetization and resistivity measurements show the sudden growth of FM-metallic regions under field. Neutron powder diffraction data evidences the growth of FM domains at expenses of CE and pseudo-CE ones in an irreversible way *vs* H [3]. See Fig.1 (M_y = $Ni_{0.05}$).

In addition, beside the importance of the electronic configuration of the ion introduced, other more sophisticated underlying mechanisms for the stabilization of FM domains have been recently proposed [4]. A sudden martensitic growth of FM microclusters in the OO AFM matrix seems at the basis of the ultra-sharp jumps in the low T *M(H)* and *r(H)* curves of very poor doped manganites. Moreover, we recall that multi-scale phase separation is frequently found in non homogeneous manganites. However we have observed that on warming above the magnetic ordering T, the original state of the sample is fully recovered but the phase separation mechanism has different kinetics than upon cooling.

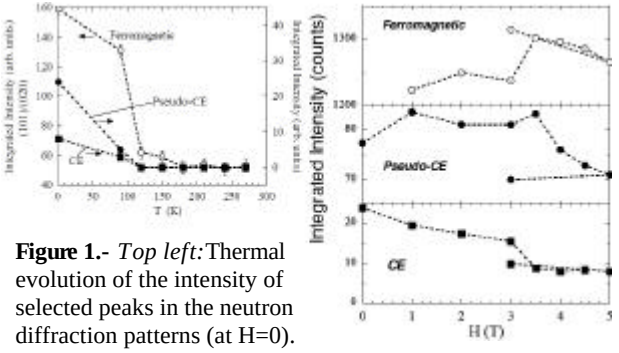


Figure 1.- *Top left:* Thermal evolution of the intensity of selected peaks in the neutron diffraction patterns (at H=0). FM: (101)/(020); Pseudo-CE: (1 ½ 0); CE magnetic peak: (½ ½ 1). *Right:* Evolution under H of the intensity at 2K of the same reflections, which shows the changes associated to the sudden melting of mesoscopic CO domains under field.

[1] A. Bernabé et al. *Appl. Phys. Lett.* **71**, 3907 (1997).
[2] R. Mahendiaran et al. *Phys. Rev. Lett.* **89**, 286602 (2002).
[3] J.L. García-Muñoz, N. Bellido, C. Frontera, J. Hernández-Velasco et al. *J. Appl. Phys.* **in press**, 2005.
[4] K.H.Ahn, T.Lookman, A.R.Bishop, *Nature* **428**, 401 (2004)

BENSC	**EXPERIMENTAL REPORT** **Canted magnetic structure of** **$Fe(N_3)_2$(bpy-d8)**	Proposal N° EF Instrument E6 & E9 Local Contact Stüßer, Többens
Principal Proposer: Experimental Team:	Ralf Feyerherm, HMI Berlin Norbert Stüßer, HMI Berlin Daniel Többens, HMI Berlin	Date(s) of Experiment E6: 6.-9. Mai 2004 E9: 8./9. Feb. 2004

Date of Report: 10.01.2005

Transition metal ions form coordination compounds with a large variety of organic molecules. Many organic ligands quite effectively transmit magnetic exchange interactions between the metal centres, although the exchange pathway usually includes more than one nonmetal atom and the metal-metal distance is much larger than in conventional magnets. Moreover, chemistry allows to tailor molecule-based materials with various topologies, ranging from zero-dimensional (0D) objects like dimers via 1D chains to 2D- and 3D-networks. Therefore, a variety of magnetic topologies can be realized in these systems. This makes this class of materials an ideal playground for tailoring magnetic properties.

An instructive example studied by neutron diffraction at HMI is $Fe(N_3)_2$(4,4'-*bpy*), an iron compound built of the azido ion, N_3^-, and *bpy* = bipyridine ($C_{10}N_2H_8$). In this material, Fe-*bpy*-Fe chains are linked to four neighbouring equivalent chains by N_3^- groups, forming a complex *chiral* 3D-network (see Figure 1). While the *bpy* molecule has proven to be magnetically inactive in former studies on related materials, the N_3^- groups transmit antiferromagnetic interactions between the Fe^{2+} ions through a distance of 5.83 Å. Consequently, long-range magnetic ordering is observed below T_C = 20 K in this compound. Magnetization measurements already indicated a quite exceptional behaviour of $Fe(N_3)_2$(4,4'-bpy), namely, that it is a *canted antiferromagnet* producing *weak ferromagnetic* behaviour with an unusually large ferromagnetic component of 0.7 μ_B, making this material a true molecule-based magnet [1].

Based on the magnetic structure solved by neutron diffraction (see Figure 1, bottom), we suggest that the associated giant spin canting of 10° is a direct result of the chiral symmetry of the lattice (space group $P4_12_12$). This lattice involves a 90° screw axis parallel *c*, leading to an alternation of the orientation of the local easy axis, which is assumed to be parallel to the N_{bpy}-Fe-N_{bpy} bonds. The local anisotropy would favour a 90° alignment between the moments linked by the N_3^- groups, while the antiferromagnetic interaction favours a 180° alignment. Therefore, the actual angle of 160° can be regarded as the result of the competition between anisotropy and the antiferromagnetic exchange interaction.

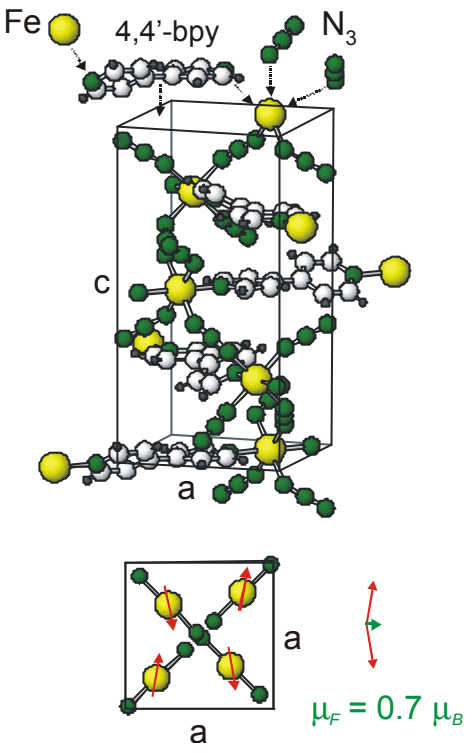


Figure 1: (top) Crystal structure of the molecular magnet $Fe(N_3)_2$(4,4'-bpy). It possesses a complex chiral 3D network structure, involving a 90° screw axis along c. (bottom) The magnetically ordered structure solved by neutron diffraction. Here, besides the Fe atoms only the N from the bipyridine are shown. The corresponding N-Fe-N bonds define the local easy axis. The large canting of 10° is caused by the anisotropy.

[1] A. Fu *et al.*, Chem. Eur. J. **8** (2002) 2239

	EXPERIMENTAL REPORT Structural and magnetic studies of spinel oxides Part 1. Iron substituted lithium-manganese oxides	Proposal N° CHE-01-1456 Instrument **E9** Local Contact **M. Tovar**
Principal Proposer: Experimental Team:	E. Wolska, AMU Poznan, Poland E. Wolska, P. Piszora, J. Darul, W. Nowicki, AMU, Poznan, Poland M. Tovar, HMI Berlin	Date(s) of Experiment 21.04.-27.04.2004

Date of Report: 27.10.2004

Lithium-manganese oxide, $LiMn_2O_4$, exhibits at room temperature a cubic spinel structure (*Fd3m*) with Li^+ ions occupying the tetrahedral *8a* sites, and 1:1 mixture of Mn^{3+} and Mn^{4+} ions randomly distributed over the octahedral *16d* Wyckoff's positions. The Jahn-Teller distortion of $Mn^{3+}O_6$ octahedra induces, however, a reversible first order structural phase transition at about 280K, that turned out to perturb the functioning of $LiMn_2O_4$ as a cathode in rechargeable lithium batteries [1,2]. Powder neutron diffraction has been used to study the nature of the structural transition, the relation between the charge ordering of Mn^{3+} and Mn^{4+} ions and magnetic spin ordering at low temperatures, as well as the cation distribution over the spinel A and B sublattices.

Partial substitution of Fe^{3+} for Mn^{3+} ions in the $LiMn_{2-x}Fe_xO_4$ system, for $0 < x < 0.1$, first lowers the transition temperature, and then totally restrains the structural phase transition, stabilizing the cubic spinel structure [3].

Neutron diffraction experiments, in the temperature range 2K–300K, were undertaken for samples with a stoichiometry of $LiMn_2O_4$, $LiFe_{0.025}Mn_{1.975}O_4$, $LiFe_{0.075}Mn_{1.925}O_4$ and $LiFe_{0.10}Mn_{1.90}O_4$, using the E9 instrument.

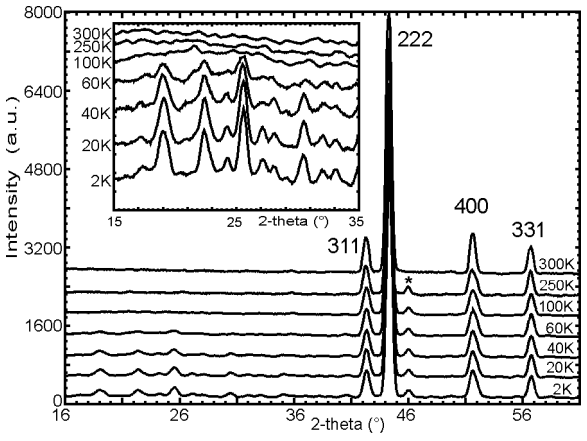


Fig.1. *Neutron powder diffraction patterns of $LiMn_2O_4$ in the temperature range of 2K-300K, revealing the temperature dependence of "magnetic peaks" at 2q=15°-35°; l=1.80306Å ; (*- superstructure reflection).*

Temperature evolution of the neutron diffraction pattern of $LiMn_2O_4$ is presented in Fig.1. A series of well defined "magnetic" Bragg peaks appears at the temperature 2K-60K, suggesting the existence of magnetic long-range order. A set of reflections in the low angular range was previously observed for the lithium-manganese spinel below 65K, suggesting the transition from paramagnetic to the antiferromagnetic state [4].

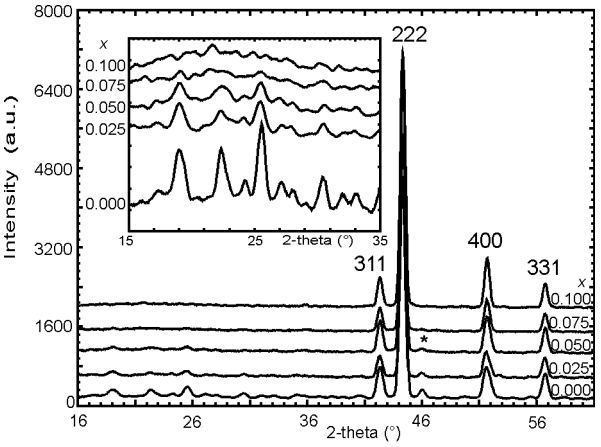


Fig.2. *Neutron powder diffraction patterns of the $LiFe_xMn_{2-x}O_4$ series, recorded at the temperature of 2K, showing the effect of Fe^{3+} substitution on the intensity of "magnetic reflections".*

The neutron diffraction patterns in Fig.2. illustrates the stabilization effect of Fe^{3+} substitution on the cubic spinel structure of $LiFe_xMn_{2-x}O_4$. In samples with $LiFe_{0.075}Mn_{1.925}O_4$ and $LiFe_{0.1}Mn_{1.9}O_4$ stoichiometry only the cubic spinel phase could be detected down to the temperature of 2K. The diffraction patterns in the 2θ region of 15°-35° display the extinction of the low-temperature reflections, with the increase of Fe^{3+} content. The disappearance of antiferromagnetic ordering might be suggested, which is contradicted by the results obtained from susceptibility measurements [5]. The Fe^{3+} ions presumably induce some changes in the cation distribution over the spinel sublattices [6].

References:

[1] J. Rodriguez-Carvajal, G. Rousse, C. Masquelier, M. Hervieu,, Phys. Rev. Lett. 81 (1998) 4660.
[2] V. Massarotti, D. Capsoni, M. Bini, P. Scardi, M. Leoni, V. Baron, J. Appl. Crystallogr. 32 (1999) 1186.
[3] E. Wolska, W. Nowicki, J. Darul, P. Piszora, M. Knapp, Appl. Cryst. Proc.XIX Conf. (2004) 412.
[4] J. E. Greedan, C. R. Wiebe, A.S. Wills, J. R. Stewart, Phys. Rev. B 65 (2002) 4424.
[5] E. Wolska, M. Tovar, B. Andrzejewski, W. Nowicki, J. Darul, P. Piszora, N. Knapp, Solid State Sciences (submitted).
[6] S. M. Woodley, C. R. A. Catlow, P. Piszora, K. Stempin, E. Wolska, J. Solid State Chem. 153 (2000) 310.

BENSC	**EXPERIMENTAL REPORT** **Structural and magnetic studies of spinel oxides Part 2. Effect of Li for Mn substitution on the $LiMn_2O_4$ structure**	Proposal N° CHE-01-1570 Instrument **E9** Local Contact M. Tovar
Principal Proposer: E. Wolska, AMU Poznan, Poland		Date(s) of Experiment
Experimental Team: W. Nowicki, J. Darul, AMU, Poznan, Poland M. Tovar, HMI Berlin		21.07.-26.07.2004

Date of Report: 27.10.2004

The spinel $LiMn_2O_4$ has attracted large attention as a low-cost, safe and non-toxic cathode material. However, disadvantages have been reported, including the irreversible capacity loss, associated with Jahn-Teller distortion and structural transformations appearing below the room temperature [1]. These problems could be resolved by stabilization of the cubic spinel structure by doping cations into $LiMn_2O_4$ lattice [2].
Partial substitution of Li for Mn in the $Li_{1+x}Mn_{2-x}O_4$ depresses the phase transition temperature due to reduction of Mn^{3+}/Mn^{4+} ratio. Lithium-rich spinels show better rechargeable cycle performance than $LiMn_2O_4$ [3].
Powder neutron diffraction has been used to study the location of light atoms, i.e., Li^+, in the A and B spinel positions, as well as the whole lithium content in the lattice.
Neutron diffraction data, in the temperature range from 2K to 300K, were taken for spinel samples with a stoichiometry of $LiMn_2O_4$, $Li_{1.025}Mn_{1.975}O_4$, $Li_{1.10}Mn_{1.90}O_4$ and $Li_{1.025}Fe_{0.10}Mn_{1.875}O_4$, using the E9 instrument.

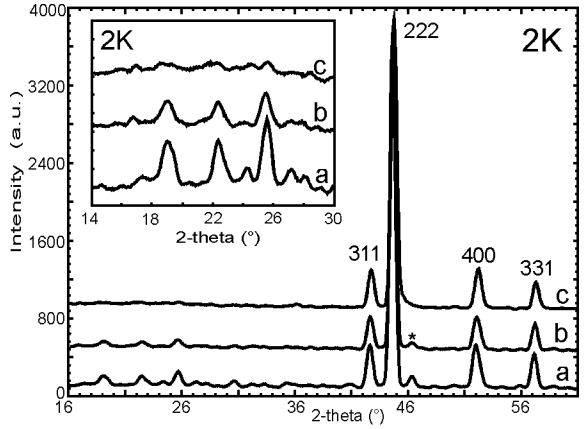


Fig.1. *Neutron powder diffraction patterns of lithium-manganese oxides, recorded at the temperature of 2K: (a) $LiMn_2O_4$; (b) $Li_{1.025}Mn_{1.975}O_4$; (c) $Li_{1.10}Mn_{1.90}O_4$, revealing the lithium-content dependence of "magnetic peaks" at 2q= 15°-35°; l=1.80306Å ; (*- superstructure reflection).*

For the first sample a structural phase transition from cubic (*Fd3m*) to orthorhombic (*Fddd*) structure occurs at 280K, whereas $Li_{1.025}Mn_{1.975}O_4$ undergoes a transition from cubic (*Fd3m*) directly to tetragonal ($F4_1/ddm$) at about 220K. In $Li_{1.10}Mn_{1.90}O_4$ no phase transition could be observed, and the cubic spinel structure was retained down to 10K [3]. The low-angular "magnetic" Bragg peaks [4] , well defined on the $LiMn_2O_4$ diffraction pattern, decrease with increasing Li^+ content, and disappear on the $Li_{1.10}Mn_{1.90}O_4$ pattern (Fig.1.)

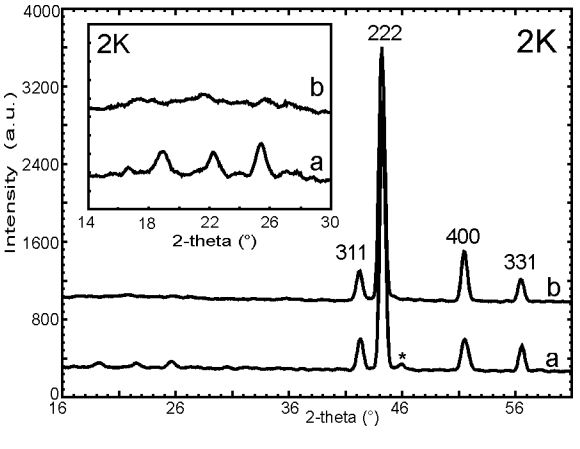


Fig.2. *Neutron powder diffraction patterns of (a) $Li_{1.025}Mn_{1.975}O_4$ and (b) $Li_{1.025}Fe_{0.1}Mn_{1.875}O_4$, recorded at the temperature of 2K, showing the effect of Fe^{3+} substitution in the lithium-rich spinel, on the intensity of "magnetic reflections".*

The effect of simultaneous substitution with small quantities of Li^+ and Fe^{3+} on the stabilization of cubic spinel structure, has been presented in Fig.2.
The doping with Fe^{3+} ions in a lithium rich spinel $Li_{1.025}Mn_{1.975}O_4$, not only restrains the structural cubic→tetragonal phase transitions, but also reduces totally the "magnetic reflections" observable in the region of 2θ=10°-35°. Evolution of these peaks with the Li^+ and Fe^{3+} substitution might suggest a different magnetic spin ordering. Full explanation of such effect requires additional neutron powder diffraction experiments, first of all with preparations containing higher Fe/Mn molar ratio.The magnetic structure and the long-range magnetic ordering in the $Li_{1+x}(Mn,Fe)_{2-x}O_4$ spinel solid solutions remains controversial. Further investigation on the magnetic properties of the system are indispensable.

References:

[1] V. Massarotti, D. Capsoni, M. Bini, P. Scardi, M. Leoni, V. Baron, J. Appl. Crystallogr. 32 (1999) 1186.
[2] H. J. Bang, V. S. Donepudi, J. Prakash, Electrochim. Acta 48 (2002) 443.
[3] E. Wolska, P. Piszora, J. Darul, W. Nowicki, J. Phys. Chem. Solids 65 (2004) 223.
[4] J. E. Greedan, C. R. Wiebe, A.S. Wills, J. R. Stewart, Phys. Rev. B 65 (2002) 4424.

BENSC	**EXPERIMENTAL REPORT** **Crystal and magnetic structure of $La_{1-x}Ca_xMnO_3$ for 0.1<x<0.2**	Proposal N° PHY-01-1472 PHY-01-1454 Instrument E6-E9 Local Contact: D. Argyriou
Principal Proposer: Experimental Team:	M. Pissas, IMS, NCSR "Demokritos" D. Stamopoulos, IMS, NCSR, "Demokritos"	Date(s) of Experiment Jan. 2004

Date of Report: 5/3/05

We studied the crystal and magnetic structure of the $La_{1-x}Ca_xMnO_3$ compound for ($0.11 \leq x \leq 0.175$) using stoichiometric samples. The phase diagram deduced from neutron diffraction experiments is seen in Figure 1.

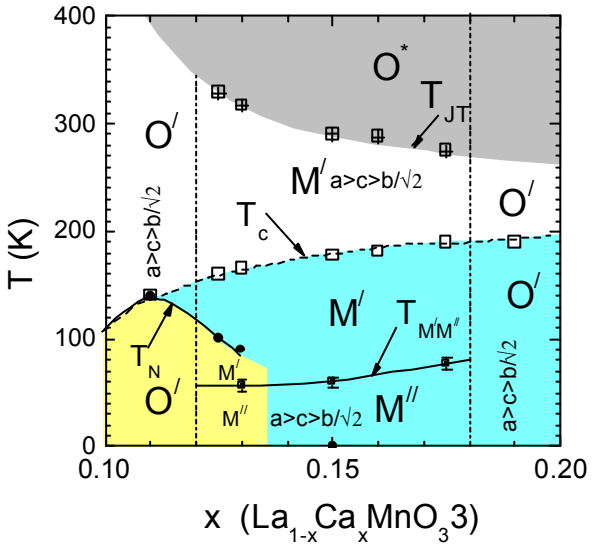


Figure1. Ferromagnetic insulating part of the phase diagram of $La_{1-x}Ca_xMnO_3$ compound. The light yellow region corresponds to the CAF regime, and the light blue to the FMI regime.

For x<0.13 the system's ground state is insulating canted antiferromagnetic. For $0.13 \leq x \leq 0.175$ below Jahn Teller transition temperature (T_{JT}) the crystal structure undergoes a monoclinic distortion. The crystal structure can be described with P $2_1/c$ space group which permits two Mn sites. The unit cell strain parameter s=2(a-c)/(a+c) increases for $T<T_{JT}$, taking the maximum value at the Curie point, and then decreases. Below $T_{M'M''} \cong$ 60K s abruptly changes slope and finally approaches T=0 with nearly zero slope. Figure 2 shows neutron diffraction data for the x=0.11 sample coming from E6 instrument. These data are compatible with a canted magnetic structure. The antiferromagnetic component is the so called A-structure with S$\|$a-axis, while the ferromagnetic components are within b-c plane. For x>0.13 the magnetic structure becomes ferromagnetic.
Figure 3 shows representative results for x=0.15 sample, extracted from neutron diffraction data, from both E6 and E9 instruments. Similar results have also been taken for other samples.

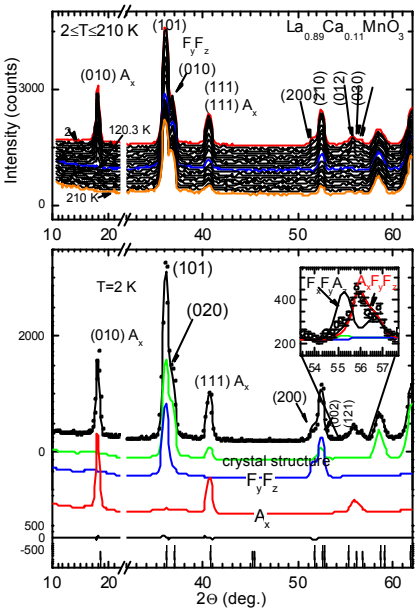


Figure 2 Upper panel: Selected portion of the neutron powder diffraction patterns for x=0.11 sample. Lower panel: Decomposition of the neutron diffraction pattern as T=2 K. Shown are the profiles coming from the A- antiferromagnetic, the ferromagnetic and crystal structures. The inset shows the observed and calculated profiles for the Bragg peaks (210), (012) and (030) based on the models $F_xF_yA_z$ and $A_xF_yF_z$.

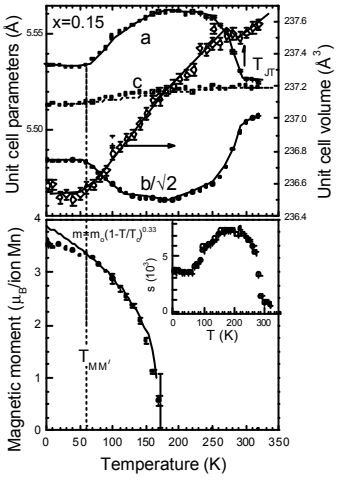


Figure 3. Upper panel: Temperature variation of the lattice parameters and unit-cell volume for x=0.15 sample. Lower panel: Temperature variation of the ordered ferromagnetic moment. The inset shows the temperature variation of the spontaneous orthorhombic strain.

	EXPERIMENTAL REPORT **Spin lattice coupling in β-MnO_2**	Proposal N° PHY-01-1571 Instrument **E9** Local Contact D. M. Többens
Principal Proposer: Experimental Team:	M. Regulski, Inst. of Exp. Phys. Univ. Warsaw M. Regulski, Univ. Warsaw W. Slawinski, Univ. Warsaw D. M. Többens, HMI Berlin	Date(s) of Experiment 2004-08-13

Date of Report: 2005-01-06

β-MnO_2 is an important model Mn oxide material, which in principle should contain Mn^{+4} ions only. The description of the magnetic ordering in β-MnO_2 is important in the context of the magnetic properties of colossal magnetoresistive manganites. Recent neutron diffraction [1-3] and magnetic X-Ray diffraction [4-5] studies on β-MnO_2 shows that well known model of magnetic structure in this material proposed by Yoshimori [6] needs some corrections.

β-MnO_2 has a tetragonal rutile-type crystal structure with *a*=4.3980 Å, *c*=2.8738 Å [7] and space group *P4₂/mnm*. Each unit cell contains two Mn^{+4} ions (e.g. one at position (0,0,0)) and four O^{-2} ions (e.g. one at position (x,x,0)). The changes of magnetic structure and lattice parameters of β-MnO_2 in function of the temperature were investigated at HMI in our previous experiment [1-3]. The precise determination of the temperature dependence of the oxygen position parameter *x* would provide valuable information.

Neutron powder diffraction experiments were performed by using E9 diffractometer operating at a neutron wavelength of 1.3076 Å. Due to limited beam time (we got only one day) we decided to do measurements only at five different temperatures. We performed measurements at 10 K, 70 K, 86 K, 96 K and 285 K. Each measurement took about 4 hours. In order to increase statistics we used 15 mm container, so we performed measurements using 18.5 g of the sample.

Our sample of β-MnO_2 gives an anisotropic broadening of the Bragg peaks. To refine the structural parameters we used our own Rietveld-refinement software [8] which allows to include anisotropic broadening effects to the refinement. Table 1 shows structural parameters refined at T=285 K.

Table 1.

a [Å]	4.39787(4)
c [Å]	2.87305(3)
O occupancy	0.986(1)
B_{Mn} [$Å^2$]	0.14(3)
B_O [$Å^2$]	0.22(1)
x	0.30526(8)

The refined value of the parameter x is determined with better accuracy than in [9]. Present data confirms previous results - β-MnO_2 has an incommensurate magnetic structure and the structural parameter *c* has minimum near the Néel temperature.

W acknowledge the support by the European Commission under the Access to Research of the Human Potential Programme (contract number RII3-CT-2003-505925), and the support by the Committee for Scientific Research (Poland).

1) M. Regulski, R. Przenioslo, I. Sosnowska, J.-U. Hoffmann, Phys. Rev. B 68 (2003) 172401.
2) M. Regulski, R. Przenioslo, I. Sosnowska, J.-U. Hoffmann, J. Phys. Soc. Jpn. 73 (2004) 3444.
3) M. Regulski, R. Przenioslo, W. Slawinski, J.-U. Hoffmann, BENSC Experimental Reports 2003 (2004) 14.
4) H. Sato, K. Wakiya, T. Enoki, T. Kiyama, Y. Wakabayashi, H. Nakao, and Y. Murakami, J. Phys. Soc. Jpn. 70 (2001) 37.
5) H. Sato, Y. Kawamura, T. Ogawa, Y. Murakami, H. Ohsumi, M. Mizumaki, N. Ikeda, Physica B 329-333 (2003) 757.
6) A. Yoshimori, J. Phys. Soc. Japan 14 (1959) 807.
7) D.B. Rogers, R.D. Shannon, A.W. Sleight, J.L. Gillson, Inorg. Chem. 8 (1969) 841.
8) M. Regulski, Program YARRP (2004).
9) H. Baur, Acta Cryst. B32 (1976) 2200.

	EXPERIMENTAL REPORT **Spin-State Transition in $Nd_{1-x}Ba_xCoO_3$ System**	Proposal N° PHY-01-1572 Instrument **E9** Local Contact D.Többens / V.Sikolenko
Principal Proposer: Experimental Team:	A.P.Sazonov, ISSSP NAS, Minsk, Belarus I.O.Troyanchuk, ISSSP NAS, Minsk, Belarus V.Sikolenko, HMI Berlin H. Szymczak, Instiute of Physics, PAS	Date(s) of Experiment 16.07 – 19.07.2004

Date of Report:

Perovskite cobalt oxide $LaCoO_3$ is considered to undergo a transition from the low-spin (LS, t^6_{2g}) to the intermediate-spin (IS, $t^5_{2g}e^1_g$) state of trivalent cobalt (Co^{3+}) ions at 100 K [1]. In addition to this transition, a metal-insulator (MI) transition gradually takes place at $T_{MI} \sim 500$ K [2]. A model that the disappearance of the orbital ordering of the IS state leads to the MI transition was proposed on the basis of the band calculation in the LDA + *U* approximation [3]. This suggests a close relation between the spin state and the MI transition. It was recently reported that $LnCoO_3$ (Ln = Nd, Sm and Eu) undergo the MI transition at $T_{MI} \sim 600$ K similarly to $LaCoO_3$ [1]. If the model of the MI transition based on the band calculation is applicable to these cobalt oxides, a spin state transition should also take place up to the MI transition in $LnCoO_3$. It should be noted that both spin-state and metal-insulator transitions in cobaltites may also be induced by charge carriers doping, replacing Ln^{3+} for Sr^{2+}, Ca^{2+} or Ba^{2+}. Under such a type of doping both ferromagnetic and metallic states develop simultaneously [6].

The concentrational spin-state transitions in La-based compounds have been studied using neutron diffraction experiment, however the results make difficulties for interpretation partly due to strongly inhomogeneous state of samples nearly spin-glass – ferromagnet transition [6]. On the other hand, we have determined that the $Nd_{1-x}Ba_xCoO_3$ solid solutions are chemically homogeneous up to $x = 0.3$ [7]. We have obtained homogeneous $NdCoO_3$ and $Nd_{0.78}Ba_{0.22}CoO_3$ samples.

The neutron powder diffraction data were collected at the E9 diffractometer with the wavelength 1.798 Å. The neutron patterns were refined by the Rietveld method using Fullprof program.

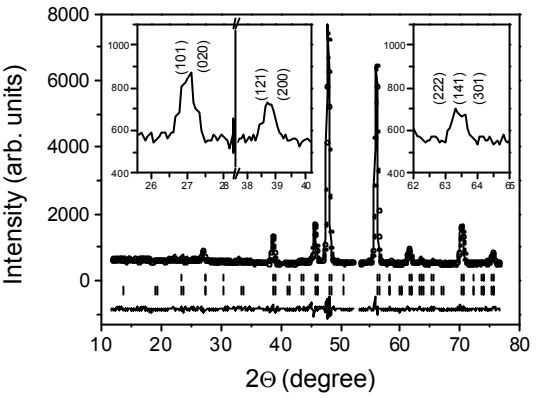


Fig.1 Refinement of the NPD patterns of $Nd_{0.78}Ba_{0.22}CoO_3$ at 3 K. The inset shows some magnetic contributions into peaks.

Both pattern were good refined in orthorhombic space group *Pbnm*. $NdCoO_3$ has no magnetic ordering in the temperature range 3 –560 K, whereas doping with 22 % Ba^{2+} leads to appearance of FM ordering below 140 K. Fig. 1 shows Rietveld refinement of $Nd_{0.78}Ba_{0.22}CoO_3$ at the $T = 3$ K.

REFERENCES

[1] M. Imada *et al.*, Rev. Mod. Phys. 70, 1039 (1998).
[2] S. Yamaguchi *et al.*, Phys. Rev. B 54, R11022 (1996).
[3] M. A. Korotin *et al.*, Phys. Rev. B 54, 5309 (1996).
[4] J. Y. Chang *et al.*, Physica B 329-333, 826 (2003).
[5] M. Itoh *et al.*, Physica B 281&282, 510 (2000).
[6] R. Caciuffo *et al.*, Phys. Rev. B 59, 1068 (1999).
[7] D. D. Khalyavin *et al.*, Inorganic materials 39, 1092 (2003).

	EXPERIMENTAL REPORT Neutron diffraction measurements of rare earth-Fe-Co-V intermetallic compounds	Proposal N° PHY-01-1581 Instrument **E9** Local Contact Daniel Toebbens
Principal Proposer: Experimental Team:	Mergia, Konstantina, N.C.S.R. "Demokritos" Gjoka, Margariti, N.C.S.R. "Demokritos" Messoloras, Spyros, N.C.S.R. "Demokritos" Toebbens, Daniel, HMI Berlin	Date(s) of Experiment 22/9/2004 – 26/9/2004

Date of Report: 3/1/2005

The rare-earth transition-metal intermetallic compounds have attracted great interest because they can be regarded as new candidates for permanent magnet applications. In order to understand the magnetic properties of these families and to develop new hard magnet materials a study on structure and magnetic properties of these novel 3:29 rare-earth transition metal intermetallic compounds is necessary.

$Tb_3(Fe_{1-x}Co_x)_{27.4}V_{1.6}$ compounds for x=1.0, 0.8 and 0.6 were fabricated. X-ray diffraction measurements showed that instead of the 3:29 phase a disordered variant of the hexagonal Th_2Ni_{17}-type structure is formed [1]. The magnetization versus temperature curves for x=1.0 show two transition temperatures: one at $T_c \approx 767$ºC corresponding to the 2:17H and the other at $T^* \approx 667$ºC, which could be attributed to either spin reorientation phenomena or domain wall motion [2]. The transition at T* is not present for x=0.8 and 0.6.

Neutron diffraction measurements were performed on $Tb_3(Fe_{1-x}Co_x)_{27.4}V_{1.6}$ compounds for a) x=1.0 at room temperature (RT), 667ºC (T*) and 837ºC (above Curie temperature), b) x=0.8 at room temperature and at 837ºC and for x=0.6 at room temperature.

In fig.1 it is presented the neutron diffraction patterns from the compound $Tb_3Co_{27.4}V_{1.6}$ at room temperature, at T*=667ºC and at T=837ºC. At RT spectrum aluminium peaks are present from the sample environment. The low statistics at high temperatures do not allow for any distinguished difference between the spectra at T=667 and 837ºC.

For the x=0.8 compound the neutron diffraction patterns are presented in fig.2 at RT and at T=837ºC to eliminate the magnetic scattering. It seems that heating the sample above its T_c the hexagonal 2:17 phase is not stable. Analysis of the diffraction spectra is still in progress for the determination of the crystal and magnetic structure of the above mentioned compounds.

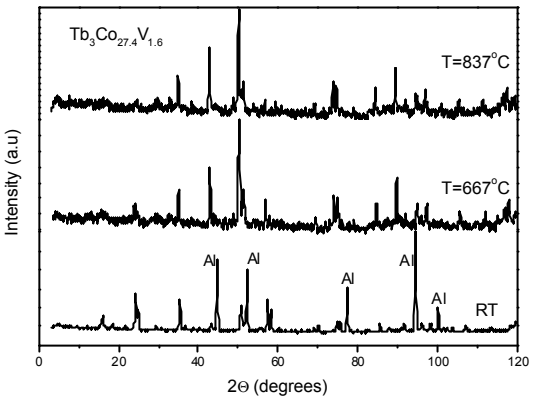


Fig. 1. Neutron diffraction patterns from $Tb_3Co_{27.4}V_{1.6}$ compound at room temperature, T=667°C and 837°C.

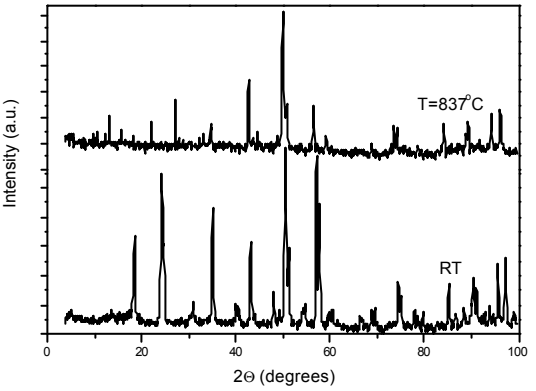


Fig. 2. Neutron diffraction patterns from $Tb_3(Fe_{0.2}Co_{0.8})_{27.4}V_{1.6}$ compound at room temperature and at T= 837°C.

References

[1] D. Hadjiapostolidou, M. Gjoka, C. Sarafidis, E. Pavlidou, T. Bakas and O. Kaogirou, submitted for publication.

[2] O. Kalogirou, C. Sarafidis, M. Gjoka and G. Litsardakis. J. Magn. Magn. Mater. 247 (2002) 34.

	EXPERIMENTAL REPORT Crystal structure and magnetic ordering in Fe-doped In_2S_3	Proposal N° MAT-01-1447 Instrument **E9** Local Contact D. Többens
Principal Proposer: Experimental Team:	A. Krimmel, Univ. Augsburg, 86159 Augsburg A. Krimmel D. Többens, HMI Berlin	Date(s) of Experiment 8. – 12. Jan. 2004

Date of Report: *

In_2S_3 is a large gap semiconductor that has attracted interest as a window material in thin-film photovoltaic devices. From low temperatures up to 693 K it crystallizes in a tetragonal (space group $I4_1/amd$) defective spinel structure in which In ions are located at the Wyckoff positions (8*e*), (8*c*) and (16*h*), respectively, and sulfur is distributed among three inequivalent (16*h*) sites [1-3]. All sites are fully occupied. In search for new materials revealing magnetic and semiconducting properties, we have synthesized the new compound $Fe_{0.5}In_{1.5}S_3$. Characterization by x-ray powder diffraction (T=300 K) showed single phase material. The diffraction pattern could be well described by the normal cubic spinel structure with a statistical distribution of Fe and In among the (8*a*) (1/8,1/8,1/8) and (16*d*) (1/2,1/2,1/2) sites respectively and sulfur at the (32*e*) (*x,x,x*) position with *x*=0.258 close to the value of the ideal spinel structure *x*=0.25. Magnetic measurements showed a Curie-Weiss law with the full effective paramagnetic moment of Fe^{3+} at elevated temperatures. At low temperatures, a cusp in the susceptibility with a corresponding FC-ZFC splitting, as well as a distinct frequency shift in the AC-susceptibility are characteristics of a spin glass state.

In order to discriminate between the normal cubic spinel structure and its tetragonal variant and to determine the cation distribution, as well as to look for possible magnetic contributions, high-resolution neutron powder diffraction studies have been performed on the diffractometer E9 for temperatures 1.5 K < T < 300 K. A standard configuration with an incident neutron wavelength of λ=1.8 Å and an angular step width of 0.078° has been chosen. The data have been corrected for detector efficiency by a vanadium standard and were analyzed by Rietveld refinment employing the FULLPROF programm [4]. An immediate result of this neutron diffraction study was the confirmation of single phase material. As shown in Fig. 1, the neutron powder diffraction patterns confirmed the normal cubic spinel structure of $Fe_{0.5}In_{1.5}S_3$. Within the experimental accuracy no magnetic scattering contributions could be detected in agreement with a low temperature spin glass state. Refining the structure by assuming a distribution of Fe and In ions according to the nominal stoichiometry among the (8a) and (16e) positions respectively results in a fully occupied (16e) site whereas the (8a) site is only occupied to 70% and exhibits 30% vacancies. No significant strucural changes have been observed within the covered temperature range. A more detailed data analysis is currently in progress.

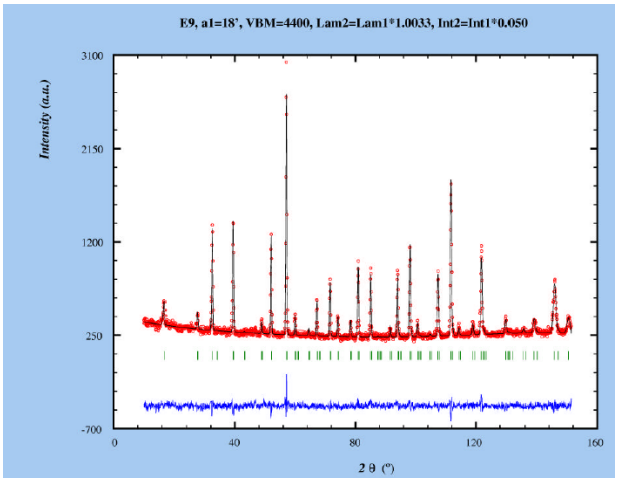


Fig. 1 Neutron powder diffraction pattern of $Fe_{0.5}In_{1.5}S_3$ at T=1.6 K (red circles, observed intensities) and corresponding structural refinment (black line, calculated intensities), as well as difference (blue line at the botton) assuming the normal cubic spinel structure.

References:

[1] G. A. Steigmann, H. H. Sutherland and J. Goodyear, Acta Cryst. **19**, 967 (1965)
[2] R. Diehl, R. Nitsche and C.-D. Carpentier, J. Appl. Cryst. **6**, 497 (1973)
[3] L. Aldon ez al., Phys. Rev. B **58**, 11303 (1998)
[4] J. Rodriguez-Carvajal, Physica B **192**, 55 (1993)

	EXPERIMENTAL REPORT **Variable Temperature PND study of $Na_{0.73}CoO_2$**	Proposal N° EF Instrument **E9** Local Contact
Principal Proposer: Experimental Team:	D.N. Argyriou, HMI Berlin C.J. Milne, HMI Berlin N. Aliouane, HMI Berlin	Date(s) of Experiment 22–3–04 and 3–6-04

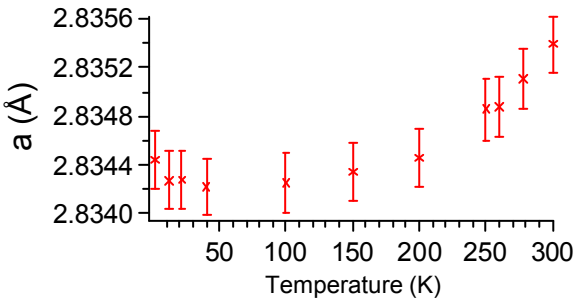
Date of Report: 8 – 12 - 04

The discovery of superconductivity in the layered, hydrated cobaltate Na0.35CoO2.yH2O [1] has fuelled intense research. The stoichiometry of this superconductor was recently revised [2] to account for a lower than expected Co valence if solely controlled by Na content. This missing charge is accounted for by the incorporation of H_30^+ on hydration. The actual cobalt valence was found to be similar to that of the parent $Na_{0.7}CoO_2$ compound. This implies that superconductivity on hydration may be the result of tuning of electronic correlations present in the parent phase.

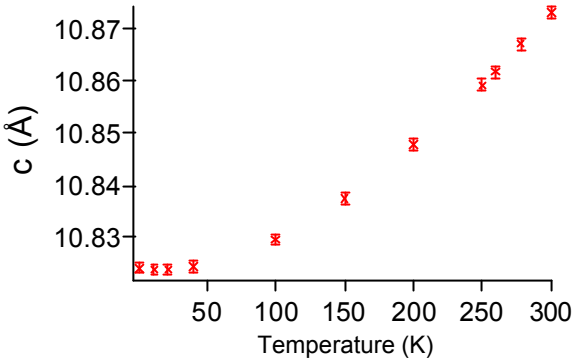
On the basis of this we have performed variable temperature powder neutron diffraction experiments on a sample of composition $Na_{0.73}CoO_2$ (Na:Co determined by NAA).

Rietveld analysis of the collected data (20K, 50K, 200K, 230K, 260K and 280K) showed no additional peaks outside those anticipated for the $P6_3/mmc$ space group.

Analysis of the obtained lattice parameters shows the a axis to decrease slightly from 280K (2.8354Å) down to 100K (2.8342Å) where the value plateaus before showing a slight increase below 50K.



The temperature dependance of the c axis is more pronounced with the value decreasing (from 10.88Å) down to 75K (10.82Å) before plateauing.



No type of magnetic ordering was observed in these powder neutron diffraction experiments. We found no evidence of lattice anomalies associated with anomalies in the specific heat and resistivity reported elsewhere.[3,4] This points towards a weak charge-lattice coupling for this series of materials.

[1] K. Takada et al., Nature 421, 53 (2003).
[2] K. Takada et al., J. Mater. Chem. 14, 1448 (2004).
[3] T. Motohashi *et al.*, Phys. Rev. B **67**, 64 406 (2003).
[4] T. Motohashi *et al.*, Appl. Phys. Lett. **79**, 1480 (2001).

	EXPERIMENTAL REPORT **Structure of hydrated Na_xCoO_2**	Proposal N° EF Instrument **E9** Local Contact
Principal Proposer: Experimental Team:	D.N. Argyriou, HMI Berlin C.J. Milne, HMI Berlin N. Aliouane, HMI Berlin	Date(s) of Experiment 11 – 12 - 03

Date of Report: 8 – 12 - 04

The discovery of high temperature superconductivity in layered copper oxides [1] has fuelled the search for similar properties in layered compounds containing other transition metals. These attempts had yielded only Sr_2RuO_4 [2] until the recent discovery of superconductivity at around 5K in a compound of stoichiometry $Na_xCoO_2.yH_2O$(x~0.35 and y~1.3) [3].

From a structural perspective, the most fascinating aspect of this new superconductor is the triangular like network of superconducting CoO_2 sheets and the structural changes involved during the hydration step in which H_2O is inserted to the structure. This insertion of water is critical to the observation of superconductivity.

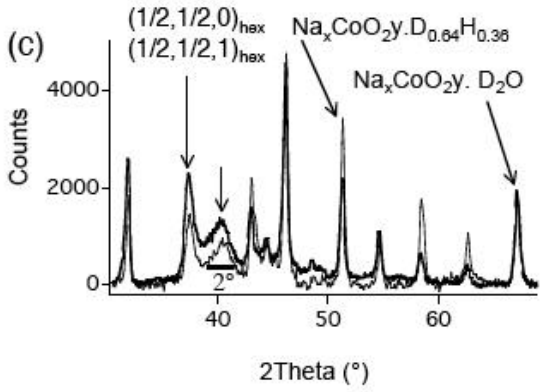


Fig. 1 Neutron diffraction patterns of deuterated and mixed H2O/D2O hydrated samples.

The elucidation of the structure of this superconductor is hampered by incoherent neutron scattering of H and by a substantial degree of proton disorder. To overcome these problems we utilised the fact that H has a positive scattering length whilst D has a negative scattering length. We hydrated the parent compound with a mixture of H_2O and D_2O such that the ratio of H:D gave an overall scattering length, for the protons, of zero. By this procedure only O atoms of the intercalated species effect the diffraction pattern (fig. 1).

From these data we were able to determine that the O atoms of the water molecules are organised around the Na ions so as to form double triangular prisms with three O atoms above and three below the Na sites (fig. 2). This coordination is typical of alkali metal hydrate [4] compounds and has implications for the superconducting phase diagram.Our model shows that variation of x over a relatively wide range can be accomodated without the need for additional water.

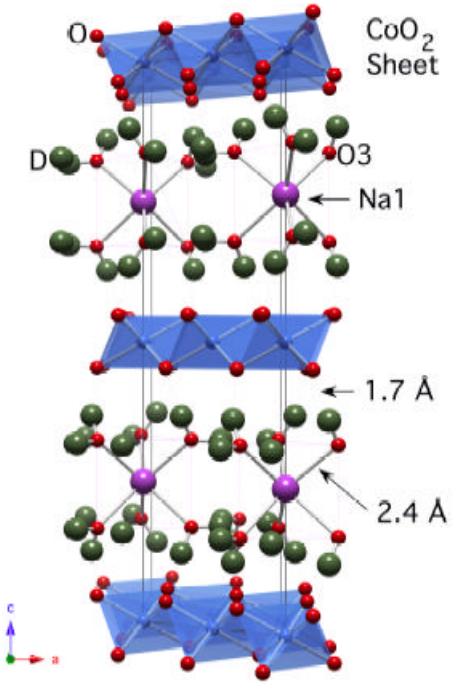


Fig. 2: The structure of the superconducting $Na_xCoO_2.yH_2O$. Certain bond lengths are shown.

[1] J.G. Bednorz and K. Mueller, Physica B 64, 189 (1986).
[2] Y. Maeno et al., Nature 372, 532 (1994).
[3] K. Takada et al., Nature 421, 53 (2003).
[4] S. Obst et al., Journal of Physical Chemistry 100, 15677 (1996).

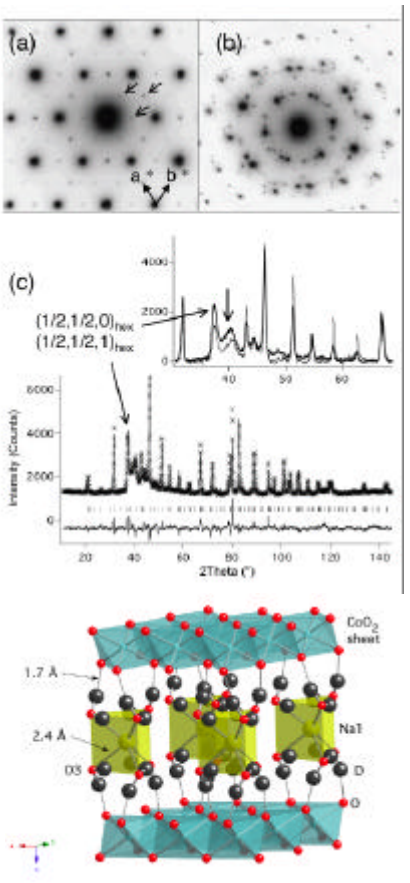
	EXPERIMENTAL REPORT **Crystal Structure of Superconducting $Na_xCoO_2.yD_2O$**	Proposal N° EF Instrument **E9** Local Contact Dimitri Argyriou
Principal Proposer: Experimental Team:	Dimitri Argyriou, HMI Berlin Nadir Aliouane, HMI Berlin Chris Milne, HMI Berlin	Date(s) of Experiment July/2003 Jan/2004

Date of Report: 9/10/04

The tuning of Na content in the alkali layered cobaltate Na_xCoO_2 results in remarkable changes in its physical behaviour, ranging from magneto-thermoelectricity at x=0.75[1] to charge ordering at x=0.5[2, 3] and 5K superconductivity at x=0.3 after intercalation of H_2O.[4] This interesting combination of physical phenomena occurs within a structural motif reminiscent of geometrically frustrated systems. Here, CoO_2 sheets are constructed by edge sharing CoO_6 octahedra, forming a quasi-2D triangular net. The exact mechanism of superconductivity within this triangular motif is currently the topic of extensive scientific inquiry, as it holds the possibility of realizing Anderson's Resonating Valence Bond model.

To unravel the complexity of its crystal structure and gain insight into parameters that are critical in establishing a superconducting phase diagram, we clearly need to establish the true translational symmetry of $Na_xCoO_2 \cdot yH_2O$. To this end, we have performed electron diffraction (ED) (see fig. 1a-1b) and neutron powder diffraction (NPD) measurements (fig. 1c), the latter employing isotopic H-D substitutions. Both sets of data clearly establish that the dominant ordering mode is a doubling of the hexagonal unit cell along both a and b. Our analysis shows that Na-atoms coordinate with D_2O to form an ordered network of NaO_6 triangular prisms. (fig. 1d) This model can account well for the intense Bragg reflection in the neutron data at 2.8 Å. ED also shows a number of different superstructures, suggesting significant Na-inhomogeneities (fig. 1b). These additional ordering modes are most likely the origin the of a broad distribution of scattered intensity at 2.6 Å, a common feature of all the neutron data published thus far. Our double-cell model is able to accommodate a variable amount of Na within the same water framework, strongly suggesting that $NaxCoO_2 \cdot yH_2O$ is not a line compound. Our evidence of more than one Na/water ordering mode within a presumably coherent CoO_2 network should open a serious debate about the true nature of the superconducting phase.

[1] Y. Wang, et al., Nature 65, 423 (425).
[2] Q. Q. Huang, et al.,cond-mat/0402255 (2004).
[3] I. Mukhamedshin, et al.,cond-mat/0402074 (2004).
[4] K. Takada, et al., Nature 422, 53 (2003).



(d)

Fig. 1: (a-b) ED patterns from $Na_{0.35}CoO_2.yD_2O$. The arrows in (a) indicate the cell doubling reflections. (c) Neutron powder diffraction data measured at 2K from $Na_{0.35}CoO_2.yD_2O$, and Rietveld fit of the double hexagonal cell model. The inset in (c) depicts a portion of the neutron diffractogram from the $Na_{0.35}CoO_2 \cdot yD_2O$ (heavy line) and $Na_{0.35}CoO_2 \cdot y(H_{0.641}D_{0.359})_2O$ (light line). This sample provided data in which the proton scattering was eliminated as b(H,D)=0. (d) The structure of the superconducting phase.

	EXPERIMENTAL REPORT **Magnetic Transitions in TbMnO3. Part 1**	Proposal N° EF Instrument **E9** Local Contact Dimitri Argyriou
Principal Proposer: Experimental Team:	Dimitri Argyriou, HMI Berlin Nadir Aliouane, HMI Berlin Chris Milne, HMI Berlin	Date(s) of Experiment May/2004

Date of Report: 9/10/04

The perovskite manganite $TbMnO_3$ has received significant amounts of attention due to its magneto-thermoelectric properties.[1] This material undergoes an ordering to an incommensurate magnetic state at T_N(Mn)~45K, while Tb-spins order at T_N(Tb)~9K. On cooling below 45K the incommensurate propagation vector for the Mn ordering changes with temperature, but locks in an incommensurate value of (0,0.285,0) at T_{lock}=35K. At T_{lock} a peak in the dielectric constant of this material is found indicating a transition from a paraelectric to a ferroelectric phase. Application of magnetic field can lead to additional ferroelectric transitions below 45K.

Although perovskite manganites have been investigated intensively over the past years, little is known about the structural properties of small rare earth manganites, such as $TbMnO_3$, or the details of their magnetic structure-which are indeed very complex. [2]

In this experiment we have used the E9 powder diffractometer to collect high-resolution powder diffraction patterns as a function of temperature to map out the various magnetic transitions in TbMnO3. We then used high counting statistics measurements to obtain high quality data for Rietveld analysis. The sample was obtained using the floating zone method. Here a large rod of sintered $TbMnO_3$ was re crystallized providing a high quality crystalline boule. Part of the boule yielded single crystals of TbMnO3 that were used for other experiments, while another part of the boule was crushed to a fine powder to provide a sample for this experiment.

The survey of the transitions in $TbMnO_3$ was conducted by measuring 20 minute patterns at 2K steps from 1.5 till 50 K. The data are illustrated as a colour waterfall plot in fig. 1. The appearance of new lines at T_N(Mn) and T_N(Tb) is also illustrated in the figure and appear to be in agreement with previous results. We have analysed the data by the

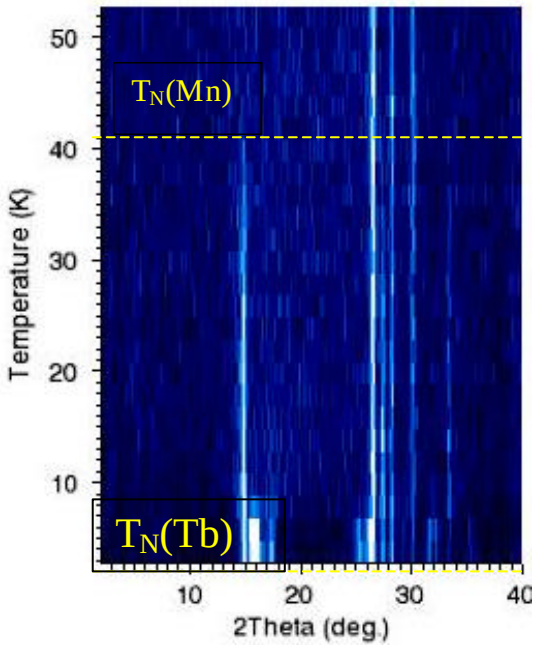


Fig. 1: Temperature dependent neutron powder diffraction measurements of $TbMnO_3$.

Rietveld method using models of the crystal and magnetic structure from previous analysis of powder measurements.[3] Our data fits very well a sinusoidal modulations of the E-type magnetic structure. However our single crystal measurements showed the presence of additional magnetic and structural reflections that are too weak to be observed in the powder data. This observation points towards the presence of a subtle crystallographic distortion of $TbMnO_3$ and a much more complex magnetic structure that require significant input from high quality single crystal data.

[1] Kimura et al. Nature 426, 55 (2003).
[2] Kimura et. al. Phys. Rev. B 68, 060403(R) (2003).
[3] Quezel, et al. .Physica B 86–88, 916–918 (1977).

BENSC	**EXPERIMENTAL REPORT** **Magnetic Transitions in TbMnO3. Part 2**	Proposal N° EF Instrument **E2** Local Contact J-U. Hoffman
Principal Proposer: Experimental Team:	Nadir Aliouane, HMI Berlin Dimitri Argyriou, HMI Berlin Chris Milne, HMI Berlin	Date(s) of Experiment May/2004

Date of Report: 9/10/04

The perovskite manganite $TbMnO_3$ has received significant amounts of attention due to its magneto-thermoelectric properties.[1] This material undergoes an ordering to an incommensurate magnetic state at T_N(Mn)~45K, while Tb-spins order at T_N(Tb)~9K. On cooling below 45K the incommensurate propagation vector for the Mn ordering changes with temperature, but locks in an incommensurate value of (0,0.285,0) at T_{lock}=35K. At T_{lock} a peak in the dielectric constant of this material is found indicating a transition from a paraelectric to a ferroelectric phase. Application of magnetic field can lead to additional ferroelectric transitions below 45K.

Although perovskite manganites have been investigated intensively over the past years, little is known about the structural properties of small rare earth manganites, such as $TbMnO_3$, or the details of their magnetic structure-which are indeed very complex. [2]

In this experiment we have used the E2 flat cone diffractometer and a 8x20 mm cylindrical single crystal to measure a sheet of reciprocal space (bc-plane) of $TbMnO_3$ as a function of temperature to map out the various magnetic transitions in TbMnO3. The sample was obtained using the floating zone method.

A part of the data obtained on E2 as a function of temperature are shown in fig. 1. Below T_N(Mn) we find the presence of incommensurate reflections with propagation vector $(0,q_{Mn},l)$ where q_{Mn}~0.28. In addition we find reflections also with propagation vector $(0,1- q_{Mn},l)$. While we expect that the incommensurate reflections will have a q, -q symmetry the observation of the 1-q type reflections suggests that magnetic structure of $TbMnO_3$ exhibits additional periodicities. This is illustrated further with the observation of a $1-3q_{Mn}$ and $3q_{Mn}$ reflections at 12K.

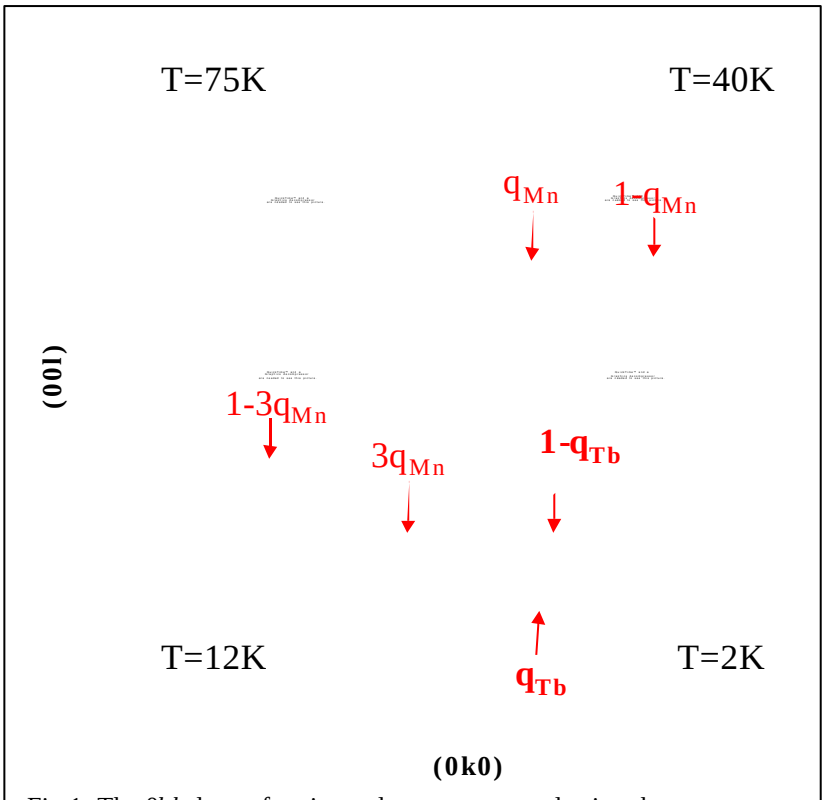


Fig 1: The 0*kl* plane of reciprocal space measured using the neutron diffractometer E2 from a TbMnO3 single crystal at 75,40,12 and 2K. Reflections due to the ordering of Mn and Tb spins are labeled.

Below T_N(Tb) we find the presence of additional reflections associated with the ordering of Tb spins. These reflections are also incommensurate with propagation vector $(0,q_{Tb},l)$, q_{Tb}~0.41.

We are currently in the process of developing models to describe the complex magnetic structure of $TbMnO_3$.

[1] Kimura et al. Nature 426, 55 (2003).
[2] Kimura et. al. Phys. Rev. B 68, 060403(R) (2003).
[3] Quezel, et al. .Physica B 86–88, 916–918 (1977).

	EXPERIMENTAL REPORT **Field Induced Magnetic Transitions in $TbMnO_3$**	Proposal N° EF Instrument **FLEX/E4** Local Contact
Principal Proposer: Experimental Team:	Nadir Aliouane, HMI Berlin Dimitri Argyriou, HMI Berlin Chris Milne, HMI Berlin	Date(s) of Experiment FLEX-July/2004 E4-Sept/2004

Date of Report: 9/10/04

The perovskite manganite $TbMnO_3$ has received significant amounts of attention due to its magneto-thermoelectric properties.[1] This material undergoes an ordering to an incommensurate magnetic state at T_N(Mn)~45K, while Tb-spins order at T_N(Tb)~9K. On cooling below 45K the incommensurate propagation vector for the Mn ordering changes with temperature, but locks in an incommensurate value of (0,0.285,0) at T_{lock}=35K. At T_{lock} a peak in the dielectric constant of this material is found indicating a transition from a paraelectric to a ferroelectric phase. Application of magnetic field can lead to additional ferroelectric transitions below 45K.

In this experiment we have used FLEX and E4 to investigate a magnetic field induced transitions in TbMnO3, with field along the three principal crystallographic directions. On FLEX we used the VM-1b vertical field magnet and mounted our crystal in the bc-plane. This allowed us to monitor characteristic incommensurate reflections as a function of temperature and field (H||a). On E4 we used the horizontal field magnet HM2. Measurements were collected by cooling the samples under various fields.

We found that fields H||a<10T had little effect on T_N(Mn), while T_N(Tb) appears to increase significantly with temperature. Also T_{lock} decreases by several Kelvin as the field is increased up to 6T.

Most dramatic changes were found for H||a. Here at H=10 and 14T we found a phase transition to a commensurate magnetic phase. In Fig. 1 we show the measurement of the A-type reflection (0,q_{Mn},1) as a function of temperature in a field of 10T. The behaviour of the propagation vector of ths reflection is fairly typical as of the zero field measurements in that the q-vector varies with cooling and locks at 28K. Just below the locking temperature the propagation vector varies discontinuously to q_{Mn}-1/4, with a brief co-existence regions of the commensurate and incommensurate q-vectors. This 1-order transition to a q=1/4 phase is also evident for the 1-3qMn reflections plotted as contours in fig. 1. Current analysis suggest that the magnetic arrangements of Mn spins for the q=1/4 phase are up-up-down-down although the relative phase between the Mn spins is not know.

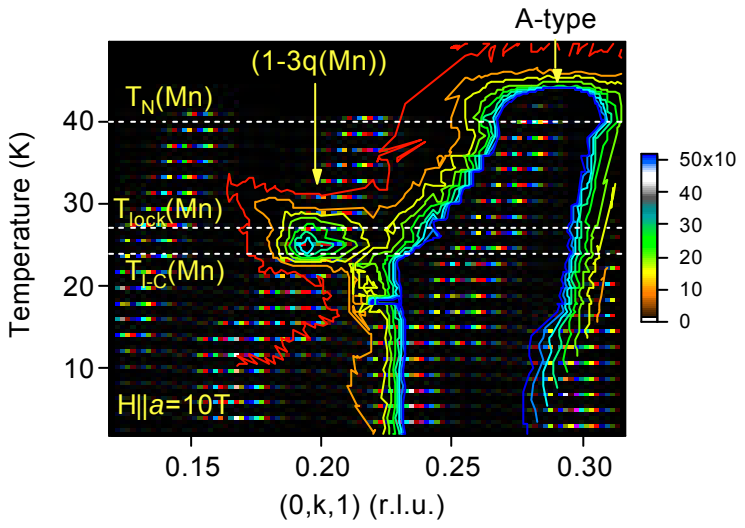


Fig. 1: Temperature depednece of neutron diffraction scans from a single crystals of TbMnO3 along the (0,k,1) direction. Intensity here is ploted as color. The variation of the weaker (0,1-3q(Mn),1) reflection is as contours that range from 50 to 450 counts in increments of 50.

On E4 for H||b we found an additional phase at 4T with propagation vector q_{Tb}=1/3. Further studies and analysis to understand the behaviour of $TbMnO_3$ are continuous

These measurements illustrate that the complex magnetic structure of TbMnO3 is frustrated and small perturbations (10T=ΔE~6K) can relieve this frustration leading to new magnetic phases We speculate that this transition should have a structural component.

[1] Kimura et al. Nature 426, 55 (2003).

BENSC	**EXPERIMENTAL REPORT** **Field-induced transition between magnetically disordered and ordered phases in underdoped $La_{2-x}Sr_xCuO_4$**	Proposal N° **PHY-02-0406** **PHY-02-0404** Instrument FLEX/V2 Local Contact Peter Vorderwisch
Principal Proposer: Experimental Team:	B. Khaykovich, Massachusetts Inst. Tech. S. Wakimoto, University of Toronto R. J. Birgeneau, University of Toronto M. A. Kastner, Massachusetts Inst. Tech. Y. S. Lee, Massachusetts Inst. Tech. K. Yamada, Tohoku University, Japan	Date(s) of Experiment Oct. 27-Nov. 16, 2003

Date of Report: December 22, 2004

We observed a magnetic-field-induced transition between magnetically disordered and ordered phases in slightly under-doped $La_{2-x}Sr_xCuO_4$ with x=0.144. Static incommensurate spin-density-wave order is induced above a critical field of about 3 T, as measured by elastic neutron scattering. Our results allow us to constrain the location of a quantum critical point on the phase diagram.

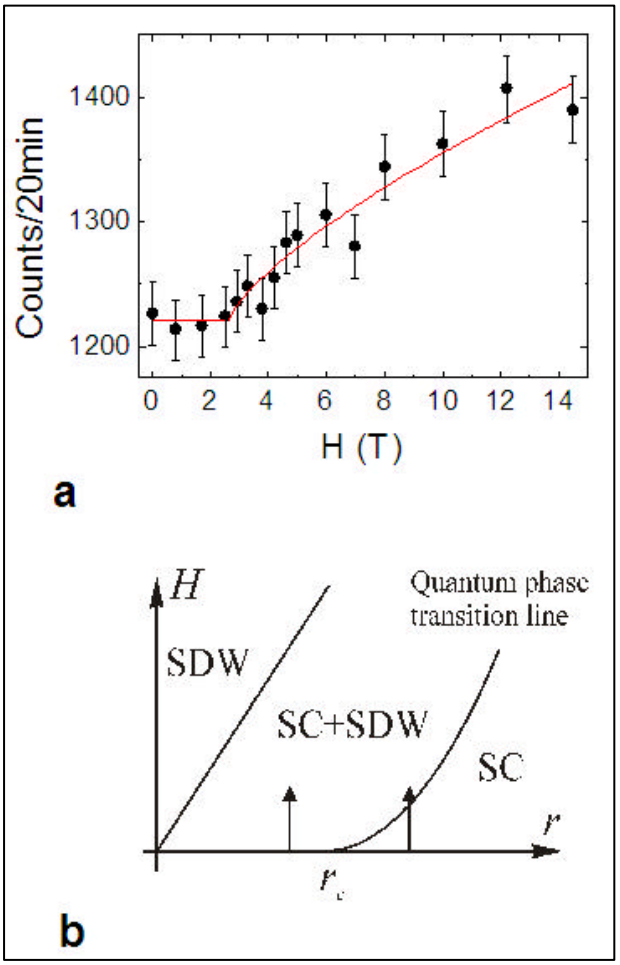


Fig. 1 (a) Field dependence of the magnetic Bragg peak corresponding to the incommensurate SDW peak at Q = (1.125,0.125,0). Every point is measured after field cooling at T = 1.5 K. The data are fitted to $I=I_0+A|H-H_c|^{2\beta}$ above H_c, as expected near a second-order phase transition. Here I_0 is a constant background, H_c= (2.7 ± 0.8) T and β = (0.36 ± 0.10) are fitting parameters. The fit is shown as a solid curve in Fig. 1a.
(b) A fragment of the theoretical phase diagram, adopted from Demler *et al.*, Phys. Rev. Lett. **87,** 067202 (2001). The vertical axis is the magnetic field and the horizontal axis is the coupling strength between superconductivity and magnetic order. The behavior of $La_{2-x}Sr_xCuO_4$ with x=0.144 corresponds to the right vertical arrow in the phase diagram.

These results appeared in the preprint cond-mat/0411355:

B. Khaykovich, S. Wakimoto, R. J. Birgeneau, M. A. Kastner, Y. S. Lee, P. Smeibidl, P. Vorderwisch, and K. Yamada *„Field-induced transition between magnetically disordered and ordered phases in underdoped $La_{2-x}Sr_xCuO_4$".*

The preprint is submitted, full text is available at http://arxiv.org/abs/cond-mat/?0411355

	EXPERIMENTAL REPORT **Dynamics of bond-alternating quantum S=1 chains in the high-field state**	Proposal N° PHY-02-408 Instrument **V2** 02-433 Local Contact P. Vorderwisch
Principal Proposer: Experimental Team:	A. Zheludev, Oak Ridge Natl. Lab, USA L.-P. Regnault, CEA Grenoble, France M. Hagiwara, RIKEN, Saitama, Japan P. Vorderwisch, HMI Berlin, Germany	Date(s) of Experiment 12.01. - 25.01.2004

Date of Report: 26.01.2005

NTENP is a quasi-1D S=1 antiferromagnet that is structurally similar to the extensively studied Haldane gap system NDMAP. Unlike NDMAP though, the chains in NTENP feature bonds of alternating strength. The ground state is a dimerized phase [1], rather than the Haldane state realized in NDMAP. The two ground states differ in their so-called hidden symmetry. This distinction is a very subtle one and the corresponding topological string order parameter is unobservable. For this reason both NENP and NTENP can be expected to have very similar gapped excitation spectra, thermodynamic properties, etc. Moreover, in strong applied fields a Bose condensation of magnons occurs in both types of spin chains, and leads them into one and the same (in terms of preserved symmetries of the wavefunction) magnetized high-field state. The spin dynamics at high fields can thus also be expected to be very similar. Our experiments on the V2 spectrometer in fields up to 14.5 Tesla demonstrate that this is *not* the case.

Previous work on NDMAP has clearly demonstrated the *triplet* nature of spin excitations in the high-field ordered state [2]. As the field is increased from zero, the triplet of Haldane gap modes is subject to Zeeman splitting. The lowest-energy mode softens at some critical field, at which long-range antiferromagnetic order sets in. Above the critical field the lower mode *persists*, and its gap *re-opens*: there are *three* distinct gapped excitations, just as below H_c.

The observed behavior of NTENP is quite different. At zero field three gap modes are observed at the 1D AF zone center with gap energies 0.97, 1.13 and 2.0 meV. Upon applying a modest field of H~6T the two lower modes behave as in NDMAP, but the upper mode *vanishes*. The lowest-energy mode goes soft at the critical field H_c=11.5T (Fig. 1 a,b). However, above H_c the gap in this mode does *not* reopen. In fact, this branch disappears altogether, and there remains *only one* long-lived excitation (Fig. 1c). This disappearance of the lower mode is not a polarization effect: scans in several Brillouin zones have shown that the "middle" mode is indeed the only coherent excited state that survives at $H>H_c$.

Comparing the behaviors of NTENP and NDMAP, we conclude that the spin dynamics of anisotropic Haldane and dimerized S=1 chains are qualitatively different in high fields. More details on the experimental study and a discussion of the underlying physics can be found in [3].

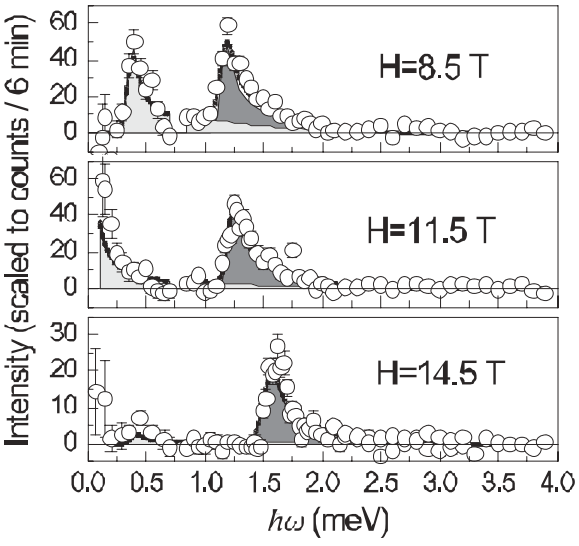


Fig.1: Inelastic energy scans measured at T=100 mK in NTENP at the 1D AF zone-center (1.1,0,1.5) for H=8.5 ($<H_c$), 11.5 ($\sim H_c$) and 14.5 T ($>H_c$).

[1] A. Zheludev, T. Masuda, B. Sales, D. Mandrus, T. Papenbrock, T. Barnes, S. Park, Phys. Rev. B **69**, 144417 (2004). Y. Narumi, M. Hagiwara, M. Kohno, and K. Kindo, Phys. Rev. Lett. **86**, 324 (2001).

[2] A. Zheludev, et al, Phys. Rev. B **69**, 054414 (2004); Phys. Rev. B **68**, 134438 (2003); Phys. Rev. Lett. **88**, 077206 (2002) and references therein.

[3] M. Hagiwara, L. P. Regnault, A. Zheludev, A. Stunault, N. Metoki, T. Suzuki, S. Suga, K. Kakurai, Y. Koike, P. Vorderwisch, and J. H. Chung, **cond-mat/0501207**

	EXPERIMENTAL REPORT **Magnetic instability in $Ca_{1.5}Sr_{0.5}RuO_4$**	Proposal N° PHY-02-0430 Instrument **V2 Flex** Local Contact K. Habicht
Principal Proposer: Experimental Team:	Paul Steffens, Universität Köln Markus Braden, Universität Köln Klaus Habicht, HMI	Date(s) of Experiment 18.-25.5.2004

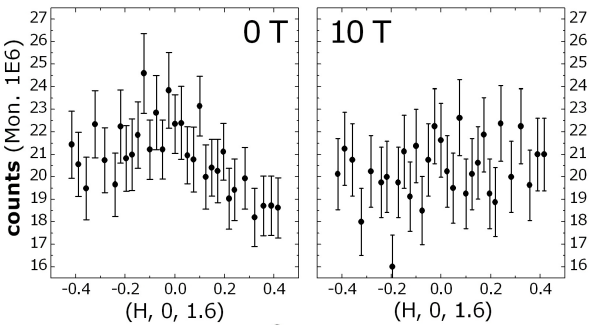
Date of Report: 30.11.2004

Depending on the composition, i.e. the Ca/Sr-mixture, the layered ruthenates $Ca_{2-x}Sr_xRuO_4$ has very different and exciting properties. At high Sr-content, especially in the well-known spin-triplet superconductor Sr_2RuO_4, incommensurate fluctuations at the wave vector (0.3,0.3,0) dominate the excitation spectrum [1]. At lower Sr-concentration one finds strong incommensurate fluctuations at (0.2,0,0), which are probably related to a change of the Fermi surface topology [2]. At even lower *x* (x=0.2-0.5) one finds metamagnetic behaviour [3]. At x=0.5 (this coincides with the onset of the tilt distortion of the structure) the macroscopic susceptibility has its maximum value. Its high value is not in quantitative agreement with the so far known neutron scattering results: despite their large width and excessive overlap with q=0, the incommensurate fluctuations – as far as they were studied until the time of the experiment – may only account for part of this value. They may, however, explain the extremely high electronic specific heat, which is also a very remarkable feature of this compound. Other very recent experiments without magnetic field have given indication for a crossover in the excitation spectrum towards ferromagnetism at very low temperatures and energy transfers.

The purpose of this experiment on V2 was the examination of the effect of a magnetic field on the excitation spectrum. The high susceptibility of this compound, the finding of a moment of $0.5\mu_B$ in a polarized neutron scattering experiment [4] and the fact that in the metamagnetic compounds (x=0.2) a field of 7T is sufficient to cause a crossover to a ferromagnetic-like state, led us to the expectation that in a strong magnetic field we should be able to observe the crossover towards a more ferromagentically dominated fluctuation spectrum. The experiment was performed with the crystal (x=0.62) oriented in 100/001 direction. The fluctuations are rather independent of Q_L, so only Q_H-scans were performed (at Q_L=1.6). In order to avoid possible influence of scattering angle dependent background variation, the scans were programmed as pure rocking (A3) scans. Scans with an energy transfer of 0.3, 0.5, 1.0 and 1.5 meV were performed without and with a magnetic field of 10T, respectively (at T=1.5K).

The main problem of this measurement was that the signal turned out to be too weak to obtain reasonable counting rates with the available sample volume and the increased background due to the magnet. Therefore, no quantitative results could be obtained.

However, an interesting difference between the spectra with and without field could still be seen: Without field, the spectral weight is concentrated at low energies, while no signal could be resolved at 1.5meV energy transfer. In contrast, at B=10T, the signal was absent – within statistics – at low energy, but some weak contribution seems to grow at 1.5meV. A comparison of two energy scans on top of the signal gave a similar result, however, in this case the difference was not significantly larger than statistical error. As an example for our data, the figure below shows the data at 0.3 and 0.5 meV (Sum) with and without applied magnetic field. The expected enhancement of low energy ferromagnetic fluctuations could not be seen, because the circumstances did not allow an additional measurement at lower field. Most likely a magnetic field of 10T opens a gap in the excitation spectrum, thereby shifting spectral weight to higher energies.



[1] Y. Sidis et al., Phys. Rev. Lett. 83, 3320 (1999); M. Braden et al., Phys. Rev. B 66, 064522 (2002)
[2] O. Friedt et al. PRL 93, 147404 (2004)
[3] S. Nakatsuji et al., Phys. Rev. Lett. 90, 137202 (2003) ; M. Kriener et al., cond-mat 0408015 (2004)
[4] A. Gukasov et al., Phys. Rev. Lett. 89, 087202 (2002)

	EXPERIMENTAL REPORT **Spin Dynamics in the S=1/2 Quantum Spin System NH_4CuCl_3**	Proposal N° PHY-02-431 Instrument **V2** Local Contact K. Habicht
Principal Proposer: Experimental Team:	Ch. Rüegg, LNS, ETH Zurich & PSI Ch. Rüegg, LNS, ETH Zurich & PSI M. Oettli, LNS, ETH Zurich & PSI M. Allan, ETH Zurich	Date(s) of Experiment 2.2.-19.2. 2004

Date of Report: 7.1. 2005

Elastic and inelastic neutron scattering experiments have been performed on the dimer spin system NH_4CuCl_3, which shows plateaus in the magnetization curve at *m=1/4* and *m=3/4* of the saturation value [1]. Two structural phase transitions at T_1~156 K and at T_2=70 K lead to a doubling of the crystallographic unit cell along the *b*-direction and as a consequence a segregation into different dimer subsystems (A, B and C). Long-range magnetic ordering is reported below T_N=1.3 K. The magnetic field-dependence of the excitation spectrum identifies successive quantum phase transitions of the dimer subsystems as the driving mechanism for the unconventional magnetization process in agreement with a recent theoretical model [2]. For a detailed discussion of the results (including specific heat measurements in collaboration with Prof. M. Meissner at BENSC) see Ref. [3].

INS experiments have been performed above T_N on the triple-axis spectrometer V2. Energy scans have been measured at the AF zone center Q=(0 0 1) r.l.u. The results are presented in Fig. 1 (closed circles). At T=1.8 K>T_N two excitations, denoted in the following by B and C, are observed in zero-field at E_B~1.6 meV and E_C~3.0 meV, which show linear Zeeman splittings as a function of the applied magnetic field. At temperatures below T_N the excitation energies do not change within experimental error (from TASP, SINQ, open circles in Fig.1). A linear fit to the data collected at T=1.8 K yields E_B=1.593(5) meV, g_B=1.95(4) for the lower mode and E_C=2.987(9) meV, g_C=2.04(2) for the higher mode. The corresponding critical fields for the closing of the spin energy gaps are H_B=14.1(4) T and H_C=25.3(4) T. An additional mode linearly increasing with field is observed for H>H_A, with H_A=4.9(2) T and g_A=2.05(3). We therefore conclude that in NH_4CuCl_3 the first plateau sets in, when the subsystem A is completely polarized along the field direction [2,3]. Accordingly the second plateau starts, when also the subsystem B reaches its complete saturation. The magnetization rises at the edge of the first (second) plateau, when the individual spin gaps of the dimer subsystem B (C) are closed and field-induced magnetic ordering occurs, similar to the soft-mode transition reported for $TlCuCl_3$. The energy splittings observed at T=0.13 K and T=1.8 K are identical, i.e., they are not affected by the onset of magnetic ordering. This directly proves that 75% (B and C) of the spin system remain in a gapped singlet state whereas 25% (A) order. We further interpret the mode linearly increasing above H_A as the field-induced opening of a spin gap for the subsystem A in the *m*=1/4 plateau.

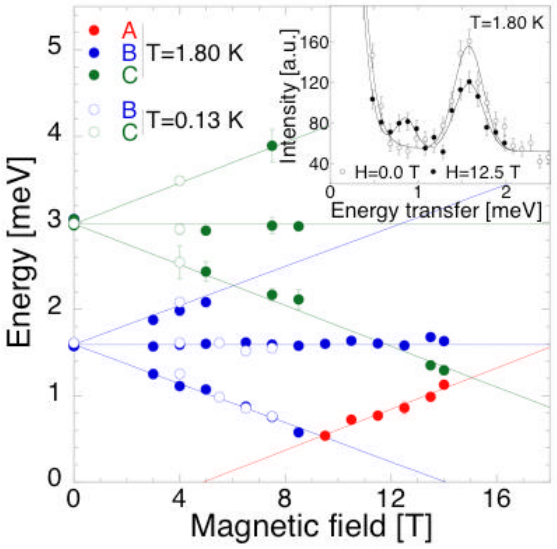


Figure 1: Field-dependence of the spin dynamics in NH_4CuCl_3 measured at Q=(0 0 1) r.l.u., T=1.8 K and T=0.13 K. Solid lines represent linear fits described in the text. Inset: INS spectra measured at H=12.5 T and in zero-field.

[1] W. Shiramura *et al.*, J. Phys. Soc. Jpn. **67**, 1548 (1998).

[2] M. Matsumoto *et al.*, Phys. Rev. B **68**, 180403 (2003).

[3] Ch. Rüegg *et al.*, Phys. Rev. Lett. **93**, 037207 (2004).

	EXPERIMENTAL REPORT **Effect of a Magnetic Field on the Spin Gap in Superconducting $Nd_{1.85}Ce_{0.15}CuO_{4+d}$**	Proposal N° PHY-02-432 Instrument **V2** Local Contact Oleg Sobolev
Principal Proposer: Experimental Team:	Patrick Mang, Stanford University	Date(s) of Experiment March 30 - April 10, 2004

Date of Report: February 8, 2005

The interplay between multiple, possibly competing, order parameters has made understanding the high-T_c copper-oxide superconductors extremely challenging[1]. Much theoretical[2–10] and experimental work[11–18] has tried to understand the mixed phase of the cuprates that exists when a field is applied perpendicular to the copper-oxygen planes. Along with adjusting the chemical composition, such studies provide a crucial second means of mapping the complex multi-dimensional electronic and magnetic phase-diagram of the cuprates. The high-T_c cuprates are doped antiferromagnets with several distinct magnetic phases throughout the chemical phase diagram, and magnetic fluctuations are believed by many to be responsible for the superconducting pairing mechanism. Previous studies have identified an enhancement of static spin-density wave order[11,12], increased low-energy magnetic fluctuations[13], and a suppression of the resonance peak with magnetic field[14] in hole-doped cuprates. The electron-doped materials potentially offer a different paradigm for magnetic-field effects, and as the upper-critical field is about six times lower (~10 T)[19] than for the hole-doped systems, measurements can be performed in new, higher regimes of H/H_{c2}. The purpose of this experiment was to determine the effect of a magnetic field on the spin gap of electron-doped $Nd_{1.85}Ce_{0.15}CuO_{4+d}$, and to compare it to the effect seen in hole-doped materials.

An earlier study reported that a gap in the magnetic fluctuation spectrum at the antiferromagnetic zone center (p,p) forms below T_c [20]. The magnitude of the gap increased with decreasing temperature, reaching a maximum value of 2? ˜ 4.5(1.6) meV for a T_c = 25 K sample of $Nd_{1.85}Ce_{0.15}CuO_{4+d}$ (NCCO). The size of the gap was found to correlate with T_c for two different NCCO samples, and for a previously studied sample of $La_{2-x}Sr_xCuO_4$. The low-temperature value of the spin gap was reported to follow the relation $2? = 2k_BT_c$. Given that the formation and energy scale of this spin gap is closely connected with T_c, it should also be possible to perturb the gap with a magnetic field, which will concomitantly weaken the superconducting order. A different study, also on superconducting $Nd_{1.85}Ce_{0.15}CuO_{4+d}$, previously reported a magnetic-field-induced enhancement of the elastic magnetic scattering at (p,p)[15]. This was interpreted to be indicative of a quantum phase transition to a longrange-ordered antiferromagnetic state. However, this interpretation has been challenged on the basis of additional elastic contributions to the magnetic scattering intensity that arise from an extrinsic secondary phase[16,21]. In this experiment we concentrated exclusively on the inelastic magnetic spectrum, focusing on the spin gap, which dramatically minimizes the effects discussed in Ref. 21.

Scans were performed around (p,p) with and without a magnetic field at several energy transfers and temperatures. Unforunately, the relatively low flux at HMI caused the required count times to be prohibitively long. Count times of greater than 20 hours per point were used, but we can only conclude from the data a consistency with the results of Ref 20. A magnetic-field effect was not ruled out, and we plan to continue this experiment at other higher-flux facilities. However, the data taken at HMI is not of high enough quality to include in publication.

1 Sachdev, S. Colloquium: order and quantum phase transitions in the cuprate superconductors. Rev. Mod. Phys. 75, 913–932 (2003).
2 Sachdev, S. & Demler, E. Competing orders in thermally fluctuating superconductors in two dimensions. Phys. Rev. B 69, 144504 (2004).
3 Demler, E., Sachdev, S. & Zhang, Y. Spin-ordering quantum transitions of superconductors in a magnetic field. Phys. Rev. Lett. 87, 067202 (2001).
4 Franz, M., Sheehy, D. E. & Tesanovic, Z. Magnetic field induced charge and spin instabilities in cuprate superconductors. Phys. Rev. Lett. 88, 257005 (2002).
5 Chen, Y. & Ting, C. S. Magnetic-field-induced spin-density wave in high-temperature superconductors. Phys. Rev. B 65(18), 18051 (2002).
6 Zhu, J. X., Martin, I. & Bishop, A. R. Spin and charge order around vortices and impurities in high-Tc superconductors. Phys. Rev. Lett. 89, 06700 (2002).
7 Ghosal, A., Kallin, C. & Berlinsky, A. J. Competition of superconductivity and antiferromagnetism in a d-wave vortex lattice. Phys. Rev. B 66, 214502 (2002).
8 Andersen, B. M., Hedegard, P. & Bruus, H. Checkerboard local density of states in striped domains pinned by vortices. Phys. Rev. B 67, 134528 (2003).
9 Zhang, S. C. A unified theory based on SO(5) symmetry of superconductivity and antiferromagnetism. Science 275, 1089–1096 (1997).
10 Chen, H. D., Hu, J. P., Capponi, S., Arrigoni, E. & Zhang, S. C. Antiferromagnetism and hole pair checkerboard in the vortex state of high Tc superconductors. Phys. Rev. Lett. 89, 137004 (2002).
11 Lake, B. et al. Spins in the vortices of a high-temperature superconductor. Science 291, 1759–1762 (2001).
12 Khaykovich, B. et al. Effect of a magnetic field on long-range magnetic order in stage-4 and stage-6 superconducting La2CuO4+y. Phys. Rev. B 67, 054501 (2003).
13 Lake, B. et al. Antiferromagnetic order induced by an applied magnetic field in a hightemperature superconductor. Nature 415, 299–302 (2002).
14 Dai, P., Mook, H. A., Aeppli, G., Hayden, S. M. & Do?gan, F. Resonance as a measure of pairing correlations in the high-Tc superconductor YBa2Cu3O6.6. Nature 406, 965–968 (2000).
15 Kang, H. J. et al. Antiferromagnetic order as the competing ground state in electron-doped Nd1.85Ce0.15CuO4. Nature 423, 522–525 (2003).
16 Mang, P. K., Larochelle, S. & Greven, M. Spurious magnetism in high-Tc superconductor. Nature 426, 139 (2003).
17 Alff, L. et al. A hidden pseudogap under the 'dome' of superconductivity in electron-doped high-temperature superconductors. Nature 422, 698–701 (2003).
18 Sonier, J. E. et al. Superconductivity and field-induced magnetism in Pr2-xCexCuO4 single crystals. Phys. Rev. Lett. 91, 147002 (2003).
19 Wang, Y. et al. Dependence of upper critical field and pairing strength on doping in cuprates. Science 299, 86–89 (2003).
20 Yamada, K. et al. Commensurate spin dynamics in the superconducting state of an electrondoped cuprate superconductor. Phys. Rev. Lett. 90, 137004 (2003).
21 Mang, P. K. et al. Phase decomposition and chemical inhomogeneity in Nd2-xCexCuO4. Phys. Rev. B 70, 094507 (2004).

BENSC	**EXPERIMENTAL REPORT** **Field-Induced Static vs Dynamic Magnetism in Underdoped LSCO**	Proposal N° PHY-02-0451 Instrument V2/Flex Local Contact Oleg Sobolev
Principal Proposer: J. Mesot LNS, PSI & ETH, Switzerland Experimental Team: R. Gilardi LNS, PSI & ETH, Switzerland H.M. Ronnow LNS, PSI & ETH, Switzerland		Date(s) of Experiment 28.6-4.7.2004

Date of Report: 30.11.2004

Aim of the experiment:

In underdoped LSCO (x=0.10) it has been shown that static incommensurate antiferromagnetism (AF) can be induced by a magnetic field down to the lowest temperatures [1]. Our recent INS measurements on LSCO samples of identical doping indicate that the low-energy spin excitations as well are strongly affected by the application of a magnetic field, but only in an intermediate temperature range (10 K < T < 30 K) [2]. In order to clarify the relation between the field-induced spin excitations and elastic signal, we performed elastic neutron scattering measurements as a function of temperature and magnetic fields on the same sample used for our INS experiment.

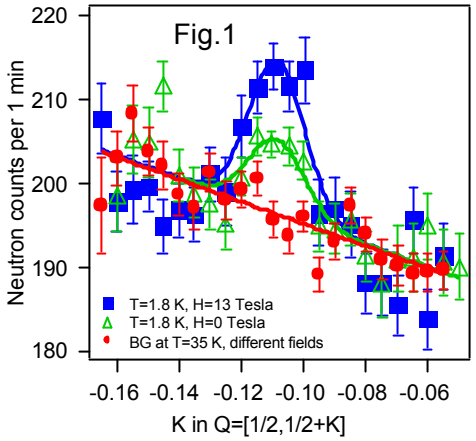
Experimental:

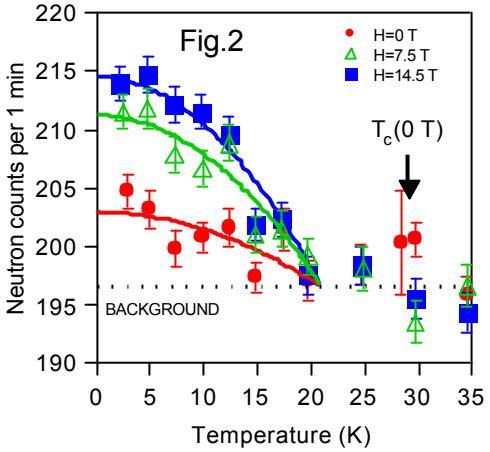
Two LSCO (x=0.10,T_c=29 K) crystals cut from a single crystal with a total mass of 3.86 g have been co-aligned and mounted in a 15 Tesla vertical magnet. The energy was fixed to 7.5 meV and a tunable PG-filter was used to eliminate higher-order reflections.

Results:

In Fig.1 are shown **Q**-scans through one incommensurate peak performed at H=0 and 13 T at base temperature (1.8 K) and at 35 K (>T_c). The sloping background was found to be field- and temperature-independent. In zero field, a weak incommensurate elastic peak is observed. The peak intensity doubles under the application of a magnetic field of 13 Tesla (field-cooled). In Fig.2 are shown temperature scans performed at the peak position for three different fields (H=0, 7.5 and 14.5 T). Both the zero-field and field-induced elastic signals appear below about 20 K (lines are guides to the eye). Another interesting result is that the field-induced signal at 7.5 Tesla is comparable to the field-induced signal at 14.5 Tesla. This means that the signal is strongly enhanced at low fields and then saturates at higher fields.

In general, our measurements are in agreement with those reported by Lake *et al.* [1]. However they observed field-induced signal below T_c=29 K, while we observed it below





about 20 K (<T_c). Therefore, it is probable that the onset temperature of the elastic signal is sample/doping dependent, and not directly related to the onset of superconductivity. This might complicate the interpretation of the field-induced signal as being due to AF vortex cores [3,4].

It remains a challenge to understand our results in relation to the previous INS study: while the elastic signal is increased by the application of a magnetic field down to 2 K, the spin excitations were found to be enhanced by a field only in a finite temperature range [2].

References:

[1] B. Lake *et al.*, Nature **415** (2002) 299
[2] R. Gilardi *et al.*, to be published
[3] D.P. Arovas *et al.*, PRL **79** (1997) 2871
[4] E. Demler *et al.*, PRL **87** (2001) 067202

BENSC	**EXPERIMENTAL REPORT** **Magnon linewidth studied by resonant spin-echo**	Proposal N° PHY-02-0453 Instrument **V2/FLEX** Local Contact K. Habicht
Principal Proposer: Experimental Team:	M. Enderle, ILL, Grenoble M. Enderle, S. Klimko (ILL, Grenoble) K. Habicht, P. Smeibidl (HMI Berlin)	Date(s) of Experiment 12.8.-28.8.2004

Date of Report: 7.1.2005

TMMC alias $(CD_3)_4NMnCl_3$ is a well-known magnetic model for one-dimensional antiferromagnetism, with interactions dominating along the c-axis, while the interactions in a-(or b) direction are more than 10^4 times smaller. The Mn^{2+} moments are pure spins 5/2, giving rise to mainly Heisenberg character. Dipole-dipole interaction leads to a small easy-plane type anisotropy with an excitation gap of 0.8meV for out-of-plane fluctuations. The low-temperature zero-field excitations are well-described by one-magnon excitations in linear spin-wave theory, with no visible broadenings beyond experimental resolution [1,2]. Above the Neel temperature (T_N=0.85 K) a broadening of the 0.8 meV was observed towards higher T, which was not further analysed in [2]. Earlier line width measurements with standard triple axis spectrometry yielded a linewidth which essentially grows proportional to temperature [3]. Here we investigated the linewidth of the 0.8 meV gap mode as a function of temperature with a 50 times better precision of the linewidth determination than that of Heilmann [2].

FLEX/NRSE was set up with vertically focused PG monochromator (RM=35.27), horizontally focused PG analyser (RA=-17.69), high-k_i polarisers in k_i before the sample and in k_f between analyser and detector. k_i =1.9913Å^{-1} was kept fixed and measured by spinecho on the direct beam. The scattering sense was SM/SS/SA= -1/-1/-1. We used mostly non-bootstrap mode (4¼ mode).

The OP-mode at (201) 0.8meV was measured with the B_0 fields in both arms parallel, i.e. the ¼-flip of the spin-echo-plane was achieved by the OP-mode. The polarisation of the OP-mode at t = 0 was determined directly at the inelastic position by measuring with two orthogonal neutron polarisations at the sample. For this purpose the ingoing resp. outgoing neutron spin was rotated by small fields in k_i and k_f perpendicular to the scattering plane. The rotations were adjusted on a nearby magnetic Bragg peak.

We find a *non-linear* relation between linewidth and temperature. At the base temperature of the dilution insert, the zone-center mode has a Lorentzian damping constant G~8±3μeV, which remains *constant* with increasing temperature over a wide T-interval, far beyond the magnetic phase transition. Between 2 K and 3 K, far above T_N (~0.85K), we observe *a sudden increase* of the linewidth of this mode. Our *preliminary* analysis is displayed in the figure. The solid line is a guide to the eye. Our figure includes the 4 K and 8 K data of Heilmann et al. at an equivalent wave vector, which we refitted in order to take into account their experimental resolution (fixed by their 1.5 K data).

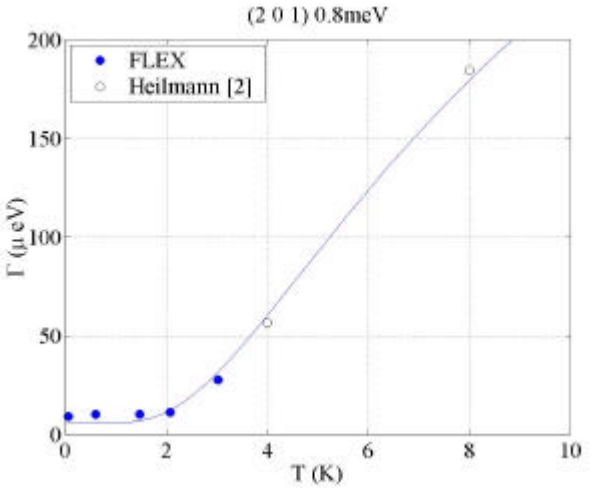


Fig.1 Linewidth of the 0.8 meV mode of TMMC as a function of temperature. Cf. text.

[1] M.T. Hutchings et al., PRB 5, 1999 (1972).
[2] I.U. Heilmann et al., PRB 24, 3939 (1981).
[3] M. Steiner et al., Adv. Phys. 25, 87 (1976).

	EXPERIMENTAL REPORT **Magnetic-field dependence of martensitic transformation temperatures in Ni_2MnGa**	Proposal N° PHY-02-458 Instrument **V2/FLEX** Local Contact Peter Vorderwisch
Principal Proposer: Experimental Team:	Stephen M. Shapiro, Brookhaven Nat. Lab. Stephen M. Shapiro, Brookhaven Nat. Lab. Peter Vorderwisch, HMI Berlin (SF1) Peter Smeibidl, HMI Berlin (BENSC)	Date(s) of Experiment 15.-26. Sept. 2004

Date of Report: 10 January 2005

The martensitic transformation temperature of the ferromagnetic shape-memory alloy Ni_2MnGa is – in contrast to the Curie temperature (T_C) - strongly sensitive to deviations from the stoichiometric composition. Whereas composition dependent transformation temperatures (and corresponding changes in crystal structures) have been extensively studied, the effect of a magnetic field on transformation temperatures has been less investigated. Published experimental findings, based on various methods, differ in magnitude and even in sign for the temperature change under equivalent magnetic fields.

In a previous neutron diffraction experiment [1], performed with the BENSC instrument E4 and the vertical magnet VM3, we have measured the intensities of fundamental and superstructure reflections when passing the transformation on cooling (with a martensite start temperature M_S) and on heating (with an austenite start temperature A_S) for a single crystal of stoichiometric Ni_2MnGa. In addition the field dependence of the transition temperature (T_I) to the intermediate modulated phase can also be measured.

We have now extended these diffraction measurements (using V2/FLEX) for additional applied-field values. As field-dependent temperature changes were found to be small, we have used a set-up with a thermometer directly attached to the sample, in addition to the (normally used) reading of the sample stick temperature on which the previous (E4) experiment had to rely.

This set-up also allowed DSC (*differential scanning calorimetry*) scans in which the sample temperature was monitored under a constant cooling or heating rate. The exothermic transformation on cooling (and endothermic transformation on heating) allowed the determination of M_S (and A_S). Typical DSC scans, shown in Fig.1, also show a narrowing of the transformation temperature range under an applied field. In Fig.2, the results from DSC (closed symbols) and neutron diffraction (open symbols) measurements are summarized. The observed field-dependence can (at least qualitatively) be understood in terms of a Clausius-Clapeyron equation with a field-dependent magnetization change at the transformation.

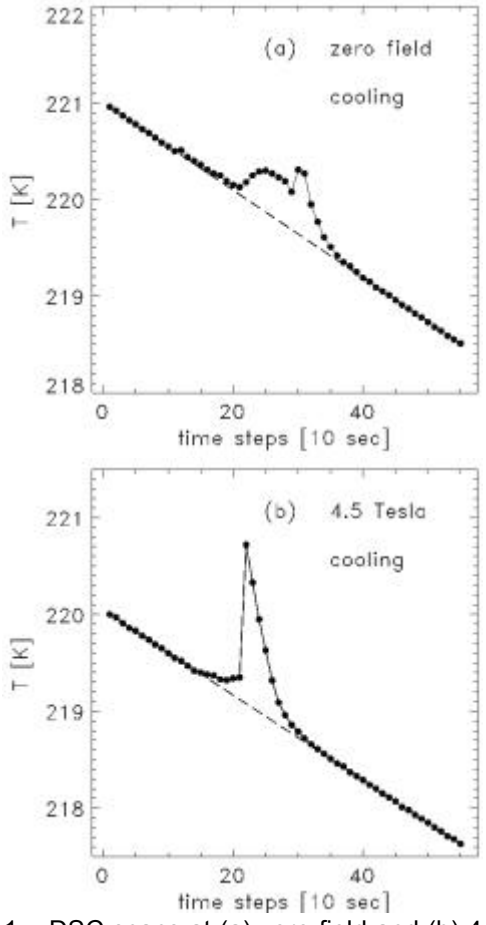


Fig.1 DSC scans at (a) zero field and (b) 4.5 T

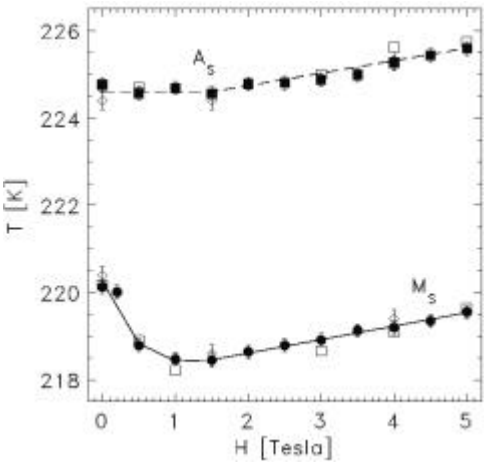


Fig. 2 Field dependence of the transformation temperatures (open symbols: neutron data, closed symbols: DSC data)

[1] BENSC Experimental Reports 2003, HMI-B 595

BENSC	**EXPERIMENTAL REPORT** **Pressure dependence of the magnetic phase diagram in MnSi**	Proposal PHY-04-0938 Instrument **V4** Local Contact E. Garcia-Matres
Principal Proposer: Experimental Team:	L.Pintschovius, Forschungszentrum Karlsruhe D. Reznik, Forschungszentrum Karlsruhe C. Pfleiderer, Universität Karlsruhe	Date(s) of Experiment 20 April –26 April

Date of Report: 22 September

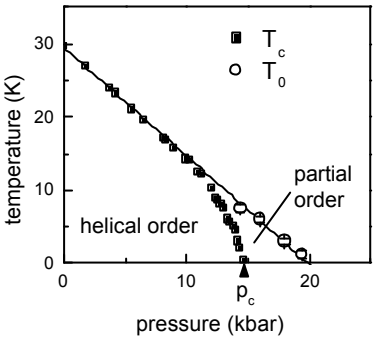


Fig. 1 The magnetic phase diagram of MnSi as a function of pressure. The full symbols denote results of macroscopic (susceptibility, resistivity) measurements. The open symbols denote the onset of partial magnetic order observed by neutron scattering. The data point at p = 19.5 kbar was obtained in the present experiment.

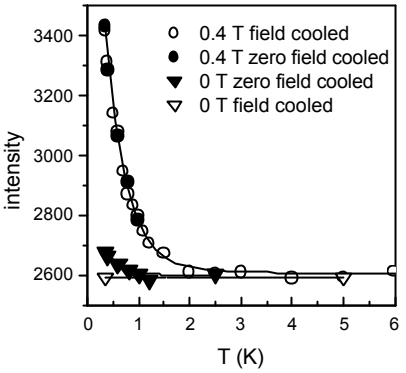


Fig. 2 Integrated intensity at the position of the magnetic Bragg peak corresponding to helical magnetic order as a function of temperature. The sample was under a pressure of 19.5 kbar. Measurements were done with and without a transverse magnetic field.

MnSi is an itinerant ferromagnet which orders at T_c = 29.5 K at ambient pressure. The ferromagnetic order is rather complex because of the presence of a long wavelength helical modulation. T_c is reduced on applying pressure and seems to vanish at the critical pressure p_c = 14.6 kbar as inferred from macroscopic measurements. However, neutron scattering experiments performed both at LLB and at HMI revealed that a certain magnetic order survives to considerably higher pressures. The observed magnetic order is, however, not complete in that the propagation vector of the helical modulation does not point along the (111)-direction as at ambient pressure but shows a broad angular distribution around the (110)-direction.

The actual experiment was performed at an even higher pressure than before, i.e. p = 19.5 kbar. The observed transition temperature of about 1 K (Fig. 2) corresponds to the trend observed at lower pressures (Fig. 1). Even the lowest temperature attainable with the He^3-cryostat was not low enough to saturate the ordered moment. A sizeable signal was observed only after aligning the helices along a direction perpendicular to the beam with the help of magnetic field > 0.4 T. After switching off the field, the intensity of the magnetic satellite decreased strongly in intensity. We found that this decrease was due to a broadening of the magnetic mosaic distribution. Measurements with polarized neutrons demonstrated that the magnetic order, although being weak at this high pressure, is still helical (Fig. 3).

The reported experiment completes our study of the magnetic phase diagram of MnSi, at least with respect to static magnetic order. The question remains why the non-Fermi liquid behavior observed in MnSi sets in at the critical pressure p_c = 14.6 kbar, but continues to much higher pressures than those for which we observe some static magnetic order. This might be due to the persistance of strong magnetic fluctuations which, however, remains to be shown.

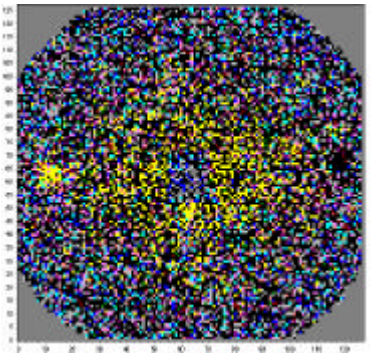


Fig. 3 SANS pattern measured with polarized neutrons on a MnSi sample at T = 0.3 K under a pressure of 19.5 kbar. The pattern shown is the difference intensity for spin up and spin down. The bright (dark) spot in the left (right) hand part of the pattern is indicative of helical magnetic order. A horizontal field of 0.6 T was applied prior to the measurement to align the helices in a direction perpendicular to the beam but was then switched off.

	EXPERIMENTAL REPORT SANS STUDY OF THE MAGNETIC PHASE SEPARATION IN $Pr_{0.66}Ca_{0.33}MnO_3$	Proposal N° PHY-04-0941 Instrument V4 Local Contact E. Garcia Matres
Principal Proposer: Experimental Team:	BRULET A., LLB CE Saclay Gif sur Yvette SIMON Ch., CRISMAT Caen SAUREL D., CRISMAT LLB	Date(s) of Experiment 22-26 04 2004

Date of Report: 19 02 2005

In manganites compounds, like $LaMnO_3$, substitution of trivalent cations by divalent ones rises to a competition between ferromagnetic (F) and antiferromagnetic (AF) order. A large variety of metamagnetic and metal-insulator transitions can be observed, as in the $Pr_{1-x}Ca_xMnO_3$ series. For compositions close to x=0.33, a spectacular property is observed: the colossal magneto-resistance (CMR)[i]. Though this effect is qualitatively explained, its colossal amplitude still remains a puzzling question. Recently, a theory of the electronic phase separation[ii-iii] has considered the percolation of a metallic F phase in an insulating AF matrix.

The crucial questions of these CMR compounds are: what are the different phases? Which ones are varying? From a detailed analysis of neutron diffraction measurements, Radaelli et al.[iv] has proposed the coexistence of three phases: (1) AF with charge plus orbital ordering, (2) F and (3) disordered orbital glass. Among different techniques, SANS is well suited to describe the transformation of AF into F phase at scales of few nm[v].

We are studying a $Pr_{0.67}Ca_{0.33}MnO_3$ crystal. Its magnetization curves at low temperatures are different (Figure 1). While at 2K, a jump is observed around 5T, a continuous transformation occurs around 3.5T and 5T at 10K and 30K respectively. In order to study this peculiar transformation, we have performed SANS experiments on V4 at HMI at 2K with a cryomagnet (up to 6T), using polarized neutrons and flipping method in order to properly separate the nuclear signal (normally weak except crystal defects of nm size) from the magnetic signal of the sample. Three experimental configurations have been used (0.4nm, 12m, 4m and 1.6m) allowing to cover the broad q range of interest: $5\ 10^{-2}$ - 2 nm^{-1}. Since almost no difference was measured between "up" and "down" spectra (nuclear signal weak or depolarization), we added both. After classical data treatment and reduction, the absolute scattering intensities have been fitted following $I(q) = A(q) + B(q) * \sin^2 a$ where α is the angle between the magnetic field and the scattering vector q. We thus obtain A(q) and the purely magnetic signal B(q). At 2K, the magnetic signal B(q) (see Figure 2) remains constant, up to a sudden change around 5T, as expected from the M(H) curve (Figure 1). A first striking result observed whatever the temperature, is that A(q), which normally corresponds to the nuclear signal (thus constant), is the decreasing when the field increases (figure 3b), even while B(q) remains constant at low field values (figure 3a). These results undoubtedly mean that the A(q) signal arises from a non magnetic phase of the sample. The concomitant increase of magnetization observed furthermore shows that this phase displays a huge susceptibility. This observation can be understood by assuming the existence of a third phase, confirming the assumption of Radaelli et al.[iv] But this phase, which would correspond to the low distorted ROO phase, is also composed of F clusters.

Besides, the oriented magnetic part $I_B(Q)$ of the scattered intensity is decreasing when increasing the magnetic field (figure 2). This result is not that expected. Indeed, the magnetic field tends to increase the magnetism as shown on the magnetization curves (figure 1). Furthermore, all the curves, while diminishing, have the same shape: they are homothetic. This behavior is not much in favor of a percolation theory. Indeed, we would expect some changes of shape, thus of the scattering curve, at the percolation threshold. Looking more at the data, we observe in the intermediate Q ranges, a Q^n dependence of scattering function with around 1.5 (see figure 2)[vi]. No peculiar shape except that of an excluded volume linear polymer chain (n=1.67) has such characteristic behavior. Such a shape was recently proposed by Viret et al.[vii], who argue that localized charge carriers hop in a self avoiding walk fashion, giving ferromagnetic filaments of nanometer diameter. Going on the analogy with the polymer physics, we have some difficulties to understand to absence of screening effect on scattering curve for concentrations of F phase larger than 35%. We think that the exponent value is rather intermediate between n=2, corresponding to disk-shaped objects as we proposed before (the red cabbage structure[v]), and n=1 corresponding thin rod like objects. As compromise, we have described this peculiar structure with fractal objects. A quantitative analysis of the magnetic scattering measured at 2K gives some typical sizes of nanometric F clusters (r=1nm R_g~15nm) of fractal dimension n~1.5 in an AF matrix.

More studies of the structure and its evolution upon applied field are under progress by combining SANS and magnetization measurements at 10K and 30K and also on different compounds in the CMR region of the phase diagram of $Pr_{1-x}Ca_xMnO_3$.

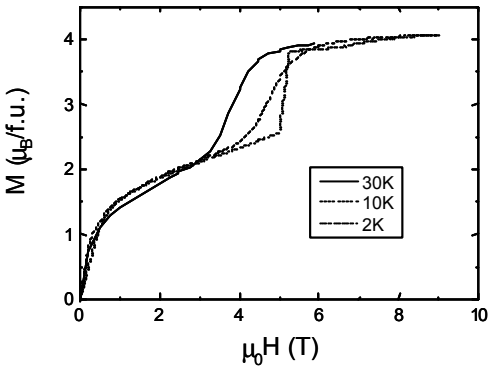


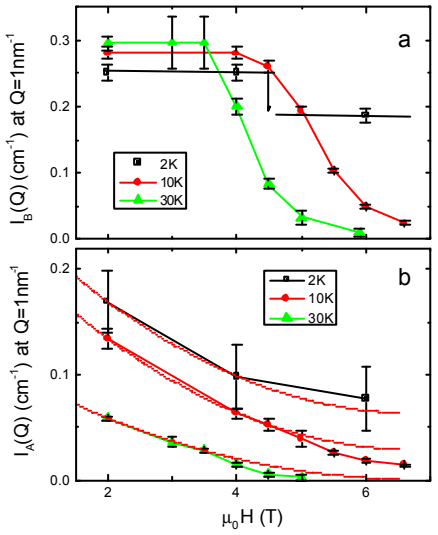
Figure 1. Magnetizeation versus magnetic field of $Pr_{0.67}Ca_{0.33}MnO_3$ crystal

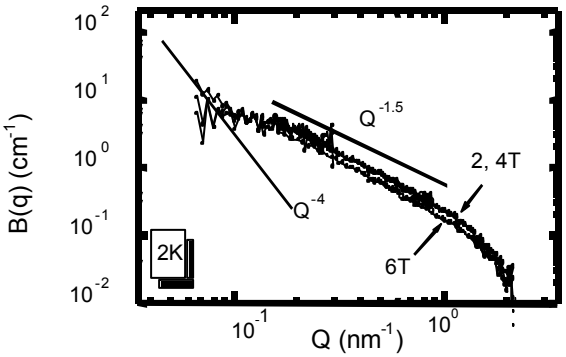
Figure 2. Evolution versus field of scattering intensities A(q) and B(q) (see text) of $Pr_{0.67}Ca_{0.33}MnO_3$ crystal at 2K.

Figure 3. Magnetic part of the scattering intensity of $Pr_{0.67}Ca_{0.33}MnO_3$ crystal at 2K.

---

[i] For a review, see *Colossal Magnetoresistance, Charge Ordering and Related Properties of Manganese Oxides*, edited by C. N. R. Rao and B. Raveau (World Scientific, Singapore, 1998)
[2] L.P. Gor'kov et al., JETP Let. **67**, 985 (1998)
[iii] A. Moreo et al., Science **283**, 2034 (1999). D. Khomskii, Physica B **280**, 325 (2000).
[iv] P.G. Radaelli et al., Phys. Rev. B **63,** 172419 (2001).
[v] Ch. Simon et al., Phys. Rev. Lett. **89**, 207202 (2002). S. Mercone et al., Phys. Rev. B **68**, 094422 (2003).
[vi] In our previous paper[v], we found a value of n around 2, but with a slightly different data analysis: We looked at the scattering intensity perpendicular to the field, subtracted with the saturated signal measured at 6.6T.
[vii] M. Viret et al., Phys. Rev. Lett**93,** 217402 (2004).





	EXPERIMENTAL REPORT SANSPOL Investigation of Highly Concentrated Surfactant Stabilized Magnetic Nanoparticles Dispersions	Proposal N°CHE-O4-945 Instrument V4 Local Contact A. Wiedenmann
Principal Proposer: Experimental Team:	Piero, Baglioni, Univ. Florence (IT) Massimo Bonini, Univ. Florence (IT) Francesca Betti, Univ. Florence (IT) Albrecht Wiedenmann, HMI Berlin (DE)	Date(s) of Experiment 29.03.04 – 02.04.04
	Date of Report:	05/01/05

Aim of this experiment was to evaluate the effect of the magnetic properties of the particles dispersed in a ferrofluid (i.e. a stable suspension of magnetic particles) on their self-assembly behaviour.

It is well known that some ferrofluids form chain-like aggregates under an applied magnetic field, while some others don't [1]. Moreover, evidence of the spontaneous formation of these structures in absence of a field, predicted by de Gennes and Pincus more than 35 years ago [2], has been recently reported [3].

Unfortunately, a clear understanding of this process is lacking in the literature, especially in terms of a precise evaluation of the parameters driving the formation of these aggregates.

The magnetic moment of the particles dispersed in the ferrofluids is certainly one of the most important parameters. Therefore we synthesized in the same conditions ferrofluids differing only by the chemical composition of the dispersed particles ($CoFe_2O_4$, $MnFe_2O_4$, $FeFe_2O_4$). In fact, iron oxide nanoparticles have long been of scientific and technological interest because of their peculiar properties. In particular, the magnetic behaviour of the MFe_2O_4 spinels can be molecularly engineered by adjusting the chemical identity of the bivalent cation M^{2+} [4].

In order to investigate the effect of the particle size, the synthesis of the iron oxide nanoparticles was performed in two solvents. In more details, an high-temperature solution phase reaction of iron(III) acetyl-acetonate, $Fe(acac)_3$, manganese(II) acetyl-acetonate, $Mn(acac)_2$ and cobalt(II) acetyl-acetonate, $Co(acac)_2$, with 1,2-hexadecanediol in the presence of oleic acid and oleyl-amine was performed. Phenyl ether and benzyl ether were alternatively used as reaction media, leading to different particle sizes.

In figure 1 the SANSPOL intensities of two ferrofluids constituted by $CoFe_2O_4$ particles prepared with phenyl and benzyl ether are shown. As expected, the size of the particle is different. Moreover the scattered intensity of the sample prepared in phenyl ether increases at lower Q values as it typically happens when chain-like aggregates are present.

Similar results were obtained for $MnFe_2O_4$ and $FeFe_2O_4$ samples.

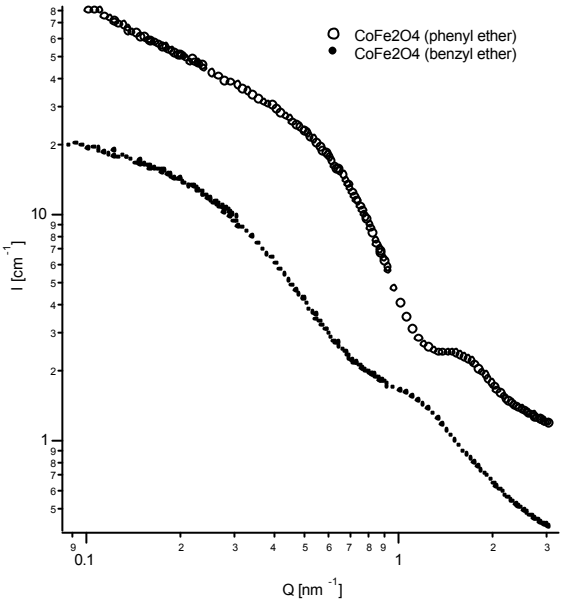


Figure 1. SANSPOL curves of two ferrofluids constituted by $CoFe_2O_4$ particles (the open-circle curve is offset for clarity of presentation).

References

[1] Liu, J.; Lawrence, M.; Wu, A.; Ivey, M. L.; Flores, G. A.; Javier, K.; Bibette, J.; Richard, J. *Phys. Rev. Lett.* **1995**, *74*, 2828-2831.

[2] De Gennes, P. G.; Pincus, P. A. *Phys. Kondens. Mat.* **1970**, *11*, 189-198.

[3] Butter, K.; Bomans, P. H. H.; Frederik, P. M.; Vroege, G. J.; Philipse, A. P. *Nat. Mater.* **2003**, *2*, 88-91.

[4] Sun, S. H.; Zeng, H.; Robinson, D. B.; Raoux, S.; Rice, P. M.; Wang, S. X.; Li, G. X. *J. Am. Chem. Soc.* **2004**, *126*, 273-279.

	EXPERIMENTAL REPORT **Clustering in Magnetic Bulk Metallic Glasses**	Proposal N° PHY-04-954 Instrument V4 Local Contact Elvira Garcia-Matres
Principal Proposer: Experimental Team:	Robert Robinson, Bragg Institute, ANSTO Elliot Gilbert, Bragg Institute, ANSTO Robert Woodward, School of Physics, The University of Western Australia Dehong Yu, Bragg Institute, ANSTO	Date(s) of Experiment 17 – 23 May 2004

Date of Report: December 1, 2004

In this work we measured the Small Angle Neutron Scattering from $Pd_{40}Ni_{22.5}Fe_{17.5}P_{20}$ amorphous ribbons as a function of temperature and applied magnetic field. The aim of this work was to determine the presence and size of chemical and magnetic inhomogeneities and to assess whether the magnetic order is due to local clusters, or some other collective effect.

We had previously proposed that these materials based on bulk metallic glass are not truly amorphous and that their magnetic behaviour is associated with large-scale chemical inhomogeneities within the alloy that may lead to clustering of magnetic ions. The existence of clusters could then be used to explain the observed superparamagnetic behaviour. On cooling, frustration due to competing interactions between clusters results a spin glass-like system. Experimental detection of clusters, and estimates of their size, would provide a means of confirming or discrediting this hypothesis.

All measurements made were conducted using an unpolarised beam using a superconducting cryomagnet to provide the magnetic field and temperature control.

The scattering was measured over a fixed q range of $0.266 \leq q / nm^{-1} \leq 0.951$ in zero field and a field of 300 Oe between 5 K and 300K.

Several phase transitions were observed in the experiments. However, attempts to more precisely define these transition temperatures in zero field between 200 and 300 K using smaller temperature steps was unsuccessful - SANS data collected was not reproducible (see Figure 1). Similar effects were observed for the sample at 300 Oe. Furthermore, a comparison of the results obtained at HMI were made with earlier results obtained at NIST. However no simple scaling relationship enabled the data to be matched.

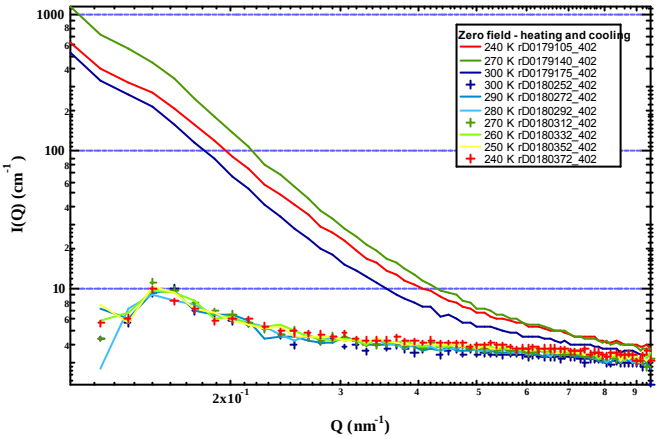


Figure 1. Small angle neutron scattering spectra for $Pd_{40}Ni_{22.5}Fe_{17.5}P_{20}$ amorphous ribbons in zero field. The first three spectra were obtained during heating from 5K, whilst the others were obtained during cooling from 300K following the application and removal of a 300 Oe field.

The inability to repeat the scattering measurements is worrying. It is possible that the source of this is a hysteresis effect in the sample although this is unlikely particularly at higher temperatures. It is more likely that there was some error in either the setting of the field (remanent fields in the magnet) or the temperature (thermal lag).

	EXPERIMENTAL REPORT **Searching for ferromagnetic clusters in paramagnetic phase**	Proposal N° PHY-04-1020 Instrument **V4** Local Contact Elvira García-Matres
Principal Proposer:	Herrero-Albillos Julia. Universidad de Zaragoza	Date(s) of Experiment
Experimental Team:	Campo, Javier. CSIC Garcia Vinuesa, Luis Miguel. Universidad de Zaragoza Bartolome, Fernando. CSIC	20/08/2004 - 24/08/2004

Date of Report: 30/09/2004

$ErCo_2$ is a ferrimagnet with a first order para to ferri transition at T_c= 32 K. When a magnetic field is applied, the Er magnetic moment is parallel to the applied field at all temperatures. The Co sublattice is polarized parallel to the applied field at high temperatures and it orders antiparallel below T_c. Results from X-ray Magnetic Circular Dicroism and magnetic measurement made us to propose the development of ferimagnetic clusters in the paramagnetic phase. The aim of this proposal was to use SANSPOL in order to prove the existence of such clusters and to determine its correlation length. We asked for 9 days at Instrument V4, and committee gave us 3 days in August 04.

An horizontal cryomagnet was employed to achieve the temperature and field environment required and the sample holder was a thin quartz cell of 10 mm in diameter. In order to explore the largest q range available in the instrument we decided to measure with a sample to detector distance of 1.2, 4 and 12 meters. Transmission and dispersion of the empty hole, water, cadmium, the empty cell and the powered sample were measured for all the distances.

Neutron absorption of the sample is very high, making necessary to increase the accumulation time specially in the paramagnetic phase. To acquire good data of the sample, six to eight hours were needed for each temperature. The experiment run reasonably well allowing us to measure SANSPOL at 10 temperatures.

On the other hand, the magnetic field on our instrument was interfering the neighbouring instrument, so we could only perform experiments in the low field range or the phase diagram (1 Tesla).

Preliminary data treatment points to the existence of an important SANS signal in the antiparallel paramagnetic phase. However, measurements at zero field and in the higher field range of the phase diagram are indispensable to experimentally proof the existence of the ferrimagnetic clusters. Exhaustive data analysis is currently being performed on the obtained difractograms.

In order to complete the experiment, we have submitted a proposal (OPS No: 4682) this September. We propose to measure SANSPOL in the same powdered sample, as a function of temperature (20-200 K) at 0 and 5 T to explore the high and the low part of the magnetic phase diagram.

During the performance of the experiment we were supported by E. García-Matres, M. Kamel and A. Heinemann.

	EXPERIMENTAL REPORT **SANS studies of Nd Fe Co Al alloy in the melt**	Proposal N° EF-SF3.Nano Instrument: V4 Local Contact A. Wiedenmann
Principal Proposer: Experimental Team:	O. Perroud, E. García-Matres, A.Wiedenmann O. Perroud E. García-Matres, A.Wiedenmann HMI Berlin	Date(s) of Experiment 26.05 – 02.06.2004

Date of Report: 06.01.2005

Various studies of the hard magnetic properties in ferromagnetic Nd-Fe-Co-Al alloys have been reported in recent years [2]. In our previous SANS experiments we have analysed the magnetic inhomogeneities present in alloys of different compositions[1]. The hard magnetic properties seem to result from pinning of magnetic domain walls at Nd-rich nanoparticles embedded in a Fe-rich crystalline phase [1, 3].

The aim of the present small neutron scattering investigation was to analyse the nanostructure of the $Nd_{60}Fe_{20}Co_{10}Al_{10}$ alloy as a function of temperature. We intended to explore the transformation of the nano-particles by in-situ SANS measurements during heating from room temperature (amorphous solid) to 1050°C, where the alloy should be in the homogenous liquid state. The melting point of the alloy is 870°C. Small-angle neutron scattering were carried out at the instrument V4 at zero magnetic field. The experiment was equipped with a high temperature furnace.

$Nd_{60}Fe_{20}Co_{10}Al_{10}$ ingots were prepared by melting 99.9% pure Nd, Fe, Co and Al in an arc-melting furnace under argon atmosphere. The bulk cylinder of 3mm diameter were obtained by ejecting the melt into a copper mould. The sample were cut in small pellets and enclose into a quartz tube under argon atmosphere. The sample have been measured first at room temperature to confirm the structure of the sample.

The radially averaged scattering intensity plotted in Fig. 1 showed a strong decrease in the Q range above 0.1 nm^{-1} between RT and 400°C, which is well below the first crystallisation temperature. This decrease must therefore be ascribed to the disappearance of the magnetic contrast of the (paramagnetic) Nd nanocrystals at the Curie temperature ~220°C where the ferromagnetism of the host disappears.

The low Q behaviour did not change significantly up to 400°C which shows that the overall morphology was not modified.

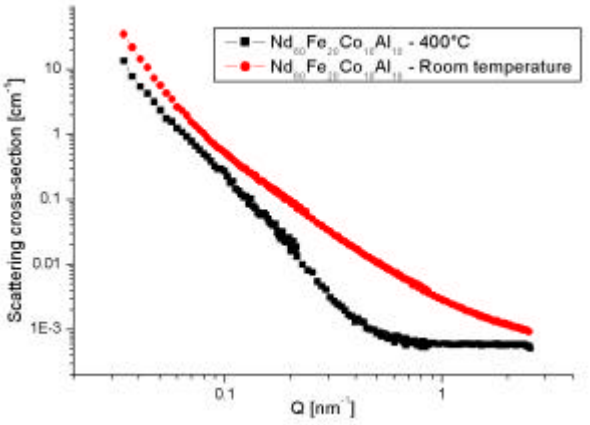


Fig.1 Radially averaged SANS curves at room temperature and 400°C, the decrease of the intensity in the Q range between 0.1 nm^{-1} and 2 nm^{-1} is due to the disappearance of the magnetic contrast of the nanoparticles at the Curie temperature of the ferromagnetic host.

Unfortunately, due to a chemical reaction between the sample and to quartz tube the sample did not melt completely even at 1050°C. Therefore we could not follow the evolution of the microstructure upon further heating beyond the melting temperature.

This work is supported by DFG-Wi-1153/3-1

References

[1] E. García-Matres et al, Physica. B 350 e315-e318 (2004)
[2] A. Inoue et al, Mat. Transactions JIM V37-2 99-108 (1996)
[3] G. Kumar et al, J. of Alloys and Compounds 248 309 (2003)
[4] O. Perroud et al BENSC reports 2004

	EXPERIMENTAL REPORT **10T high magnetic field studies of $Nd_{60}Fe_{20}Co_{10}Al_{10}$ alloys by SANSPOL**	Proposal N° EF Instrument **V4** Local Contact E. García-Matres
Principal Proposer: Experimental Team:	E. García-Matres HMI Berlin A. Wiedenmann HMI Berlin E. García-Matres HMI Berlin O. Perroud HMI Berlin	Date(s) of Experiment 9. – 14. Sept 2004

Date of Report: 15.12.2004

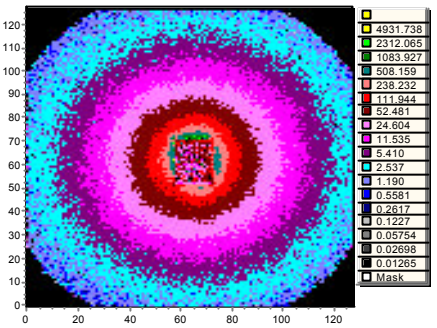
$Nd_{60}Fe_xCo_{30-x}Al_{10}$ (0 < x < 30) bulk amorphous rods exhibit a two-phase microstructure comprising of Nd-rich and Fe-rich phases. These alloys prepared by different methods, show different magnetic behaviour [1]. The as-cast cylinder exhibits hard magnetic properties with relatively high coercitivity. Measurements of the macroscopic magnetization show two Curie temperatures at T_{c1}= 50K and T_{c2} = 495 K attributed to the Nd-rich crystallites and metastable U-phase [2].

Bulk amorphous $Nd_{60}Fe_xCo_{30-x}Al_{10}$ alloys have been studied by Small Angle Scattering using polarized neutrons (SANSPOL). This technique allows us to accurately separate the contribution from nuclear and magnetic scattering which is essential in these measurements due to the weak magnetic effect.
Previous experiments were performed at different temperatures and with variable magnetic field up to 6 T. We were able to analyse these data [3] assuming pinning of magnetic domains resulting from the presence of Nd-rich nanocrystals. However, the experiments performed at 6T revealed a weak orientation of the magnetic domains along the field but the sample does not reach the saturation value. The aim of our experiment is to increase the magnetic field in order to observe an orientation of the magnetic domains along the magnetic field.

Small angle neutron scattering with polarised neutrons were carried out at the V4 instrument at the Hahn-Meitner-Institut. The experiment was equipped with the VM1 vertical cryomagnet which reaches a magnetic field until 15 T. Due to the magnetic environment around the instrument, only 10 T measurements were allowed and since the magnetic field was interfering the neighbouring instrument, during the last two days only 8 T measurements were done.

It is important to point out that after some tests, it was the first experiment realized by these extreme sample environments at V4. The experiments were performed at 5K and 150K with an applied magnetic field between 1T and 10T.

a) 5K 1T



b) 5K 10T

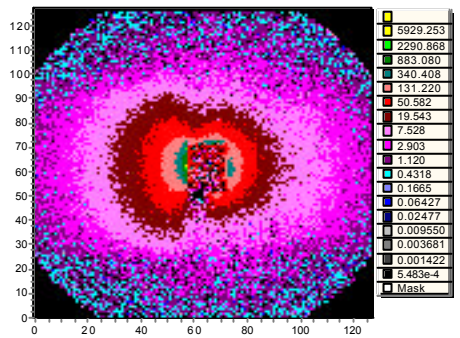


Fig.1 shows the two-dimensional pattern of $Nd_{60}Fe_{20}Co_{10}Al_{10}$ measure at the same temperature 5K and 1T and 10T, respectively.

This work is supported by DFG-Wi-1153/3-1,2.

References

[1] A. Inoue et al., Mat. Transactions JIM V37-2 (1996)99-108
[2] G. Kumar et al., J. of Alloys and Compounds 248 (2003) 309.
[3] E. García-Matres et al Physica. B 350 e315-e318 (2004)

	EXPERIMENTAL REPORT Field variation technique and Langevin behaviour of Co-ferrofluids	Proposal N° EF-SF3. Nano Instrument **V4** Local Contact
Principal Proposer: Experimental Team:	A. Wiedenmann, A. Heinemann A. Wiedenmann, A. Heinemann, HMI Berlin	Date(s) of Experiment 30.04.04-03.05.04

Date of Report: 10.01.2005

SANSPOL is an excellent tool to obtain detailed information about the composition of separated magnetic nanoparticles [1]. The next step is to use this method to attain access to multi-particle structures. New experiments [2,3,4] with concentrated ferrofluids showed a wide range of structure formation under the influence of an external magnetic field

We performed SANSPOL experiments on a concentration series of a Cobalt based ferrofluid prepared by a new technique [5]. From the most diluted sample we extracted the single particle information. This provides us with all microscopic data for the single particles (fig. 1).

In order to evaluate possible ordering phenomena we propose a new representation of the SANSPOL difference $(I^+ - I^-)/\sin^2 a$ iso-intensity lines as a function of $Q = |\mathbf{Q}|$ and the angle a between **H** and **Q**. In the case of an isotropic system we expect straight horizontal lines in the plane such as approximately observed in fig. 3a Any deviation from horizontal iso-intensity lines must therefore result from anisotropic structure factor S(Q,a). (fig. 3b and 3c) shows the occurrence of anisotropic patterns after applying different magnetic fields.

Work supported by DFG priority program SPP1104.

References:

[1] A. Heinemann and A. Wiedenmann, J. Appl. Cryst. **36** (2003), 845-849.
[2] A. Wiedenmann, A. Hoell, M. Kammel and P. Boesecke J. Phys. Rev. E **68** (2003), 031203
[3] A. Heinemann, A. Wiedenmann, *Journal of Magnetism and Magnetic Materials* 2004 (in press)
[4] A. Wiedenmann, A. Heinemann, *Journal of Magnetism and Magnetic Materials* 2004 (in press).
[5] H. Bönnemann, W. Brijoux, R. Brinkmann, N. Waldhöfer, N. Palina and H. Modrow, Inorganica Chimica Acta 350 (2003) Appl. Cryst. **36** (2003) 617-624.

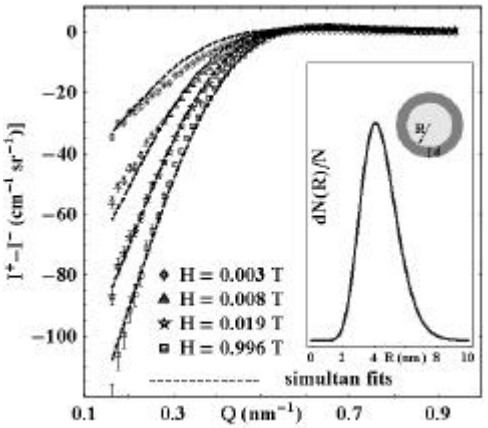


Figure 1: Data points and fit results (dashed lines) for the 0.5 vol.% Co-ferrofluid sample..

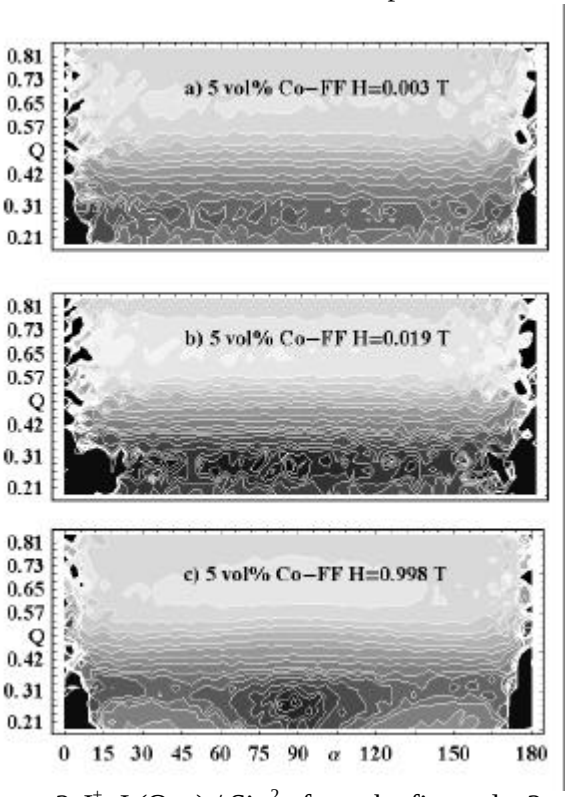


Figure 2: $I^+ - I$ (Q, a) / $\sin^2 a$ from the fit results 2a and the experimental data 2b and 2c for the most diluted sample of 0.5 vol.% Co- ferrofluid in two different external magnetic fields.

BENSC	**EXPERIMENTAL REPORT** **Low dimensional magnetic correlations in R_2BaMO_5 (R=Y, Ho; M=Co, Ni) studied by SANS**	Proposal N° EF Instrument **V4** Local Contact J. Hernández / E. García
Principal Proposer: Experimental Team:	J. Hernández-Velasco, HMI Berlin (BENSC) E. García-Matres, HMI Berlin (BENSC) J. Hernández-Velasco *current address:* F.CC.Químicas Univ.Complutense Madrid	Date(s) of Experiment 30.6.04 - 4.7.2004

Date of Report: 15.2.2005

We have determined previously the magnetic structures of *Immm*-Ho_2BaMO_5 (M^{2+}= Co, Ni) and studied *Immm*-Y_2BaNiO_5 oxide by means of neutron diffraction at zero and applied field. The former, Ho compounds, are magnetically ordered below T_N, at this critical temperature both the R^{3+} and M^{2+} sublattices become ordered, $\boldsymbol{k}$= [½,0,½] being the propagation vector. However the latter is not a 3D magnetic system down to 1.5 K, provided that Y^{3+} is a non magnetic cation, and does not promote the interchain interactions between the Ni-O-Ni- linear paths present in the crystal structure, then remaining 1D-AF.

Furthermore, all the studied *Immm*-R_2BaMO_5 present 1D-AF correlations in the M^{2+} sublattices well above T_N. But differences are found due to the spin quantum numbers S_{Ni}= 1 and S_{Co}=3/2. The former is a quantum integer spin chain, and so exhibits the dynamical properties of a Haldane-system, *i.e.:* Energy gap in the magnetic excitation spectrum, $\Delta \propto S{\cdot}exp(-\pi S)$ separating the non magnetic singlet ground state from the first excited triplet state, and exponentially decaying correlations. The latter is a half integer spin chain: It should show gapless excitations and power-law decay in the spin correlations. A crossover between quantum-spin systems (S = ½, 1) and a classical dynamic behaviour (S = 2, 5/2) is expected for the S= 3/2 chains in their spin-wave-like dispersion spectra.

On the other hand, neutron diffraction patterns at $T>T_N$ show only nuclear scattering due to the low dimensional nature of these AF correlations, but we expected the coherence length to be on the SANS scale and to evidence the crossover to 3D ordered states. The second aim of the proposal was to determine the influence of an applied magnetic field on these correlations. This last topic was unsuccessful due to beam-time constrains, shadowing effects of VM3 cryomagnet in V4 detector at the closest distance (~1m) to sample position and malfunction of HM1 suffering valve freezing, so the whole measurement was performed at H=0. Nevertheless, the first and main issue has been addressed as we have found a direct evidence of these interactions. See scattering curves on Fig.1.

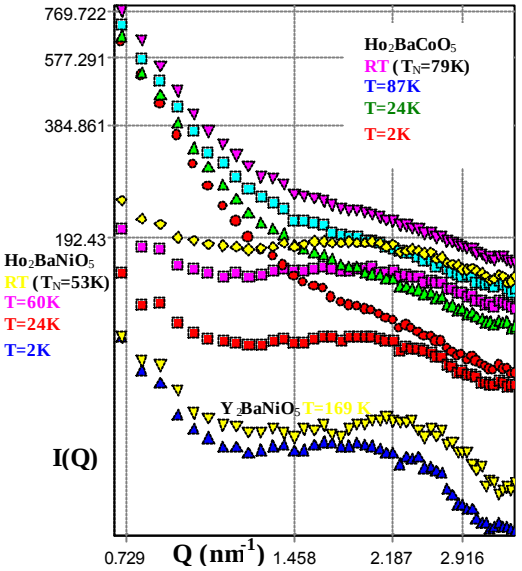


Figure 1.- SANS isotropic data plot for the 3 compounds at some different temperatures. Intensity *vs Q* in log-scale.

It is worth noting the broad peaks with maximum intensity upturn around Q~2.7 nm^{-1}, which corresponds to a dimension about 23Å, *i.e.* 6 times the crystallographic $\boldsymbol{a}$-axis, which is the short 3.8 Å M-O-M distance within the chains, and agrees quite well with the correlation length inferred from INS.

Moreover, the scattered intensity in a wider Q-range extends in some way proportionally to the magnetic moment corresponding to each system, being the highest for the Co oxide and the lowest for the yttrium nickelate, as it could be expected due to the non magnetic rare earth. But even more striking is the fact that the reduction of intensity when T is decreased below T_N in Ho compounds proceeds in the same fashion as the ordered magnetic moments grow towards saturation shown by neutron diffraction (μM^{2+} reaches saturation faster than μHo^{3+}). In contrast, Y_2BaNiO_5 does not illustrate marked changes in the T range of the measurement, remaining just the anomaly that we ascribe to the low dimensional correlations in the Ni^{2+} sublattice. Notice at low T, that the intensity measured in Ho_2BaNiO_5 is comparable to that for the Y oxide and even lower, which is specially marked at the high Q region ($\xi \rightarrow \infty$ and the magnetic intensity condenses in Bragg elastic peaks out of the SANS window).

	EXPERIMENTAL REPORT **Dynamics of spin freezing in the re-entrant spin glass FeNiMn. II**	Proposal N° PHY-03-300 Instrument **V5** Local Contact C. Pappas
Principal Proposer: Experimental Team:	V. Wagner, PTB Braunschweig J. Hesse, TU Braunschweig C. Pappas, HMI Berlin J. Klenke, HMI Berlin V. Wagner, PTB Braunschweig	Date(s) of Experiment 13.12. -19.12.2003

Date of Report: 11.01.2005

In the invar alloy $(Fe_{0.65}Ni_{0.35})_{1-x}Mn_x$ – a well known RSG system /1/ -we measured the magnetic form factor $s(Q)$ and the magnetic intermediate scattering function $s(Q, t)$ for a sample close to the critical Mn-concentration (x_c = 0.139), below which the sample can form a spin glass state upon cooling from the ferromagnetic state. The aim has been to check whether the magnetic behaviour would approach the *Q-independent* relaxation behaviour of a classical spin glass when x approaches x_c. A more ferromagnetic sample with x= 0.113 studied in the previous experiment /1,2/ displayed a remarkable *Q-dependent* diffusive behaviour even in the re-entrant spin glass state. In the experiment presented here a similar behaviour, however, somewhat less *Q*-dependent, was observed for a sample with x = 0.139 ± 0.001. Decreasing depolarization of the transmitted beam indicated that the sample was slightly ferromagnetic (T_c< 200 K) and gradually lost the ferromagnetic order for T < 90 K. The intermediate scattering function and the form factor were determined by paramagnetic NSE techniques for 0.3 nm^{-1} < Q < 1.3 nm^{-1} and 40 K < T > 200 K. Fig.1 shows the time evolution of the normalized function

$$S(Q, t) = s(Q, t)/s(Q) = \exp[(-gt)^n] \quad (1)$$

Stretched exponentials fitted to the data describe the time dependence quite well. The spin diffusive behaviour found in the ferromagnetic phase (T > 100K) is still observed in the RSG pase (T < 90 K), which is a mixed phase of simultaneous ferromagnetic and spin glass order. At 40 K the spins are almost completely frozen within the time window observed in the experiment.
In summary the same behaviour of the spin dynamics was observed for the two Mn-concentrations studied in the previous and the present experiment. Spin diffusion resulting in a *Q*- dependence of $s(Q,t)$ is present and appears to be inherent to a mixed RSG – phase of FeNiMn.

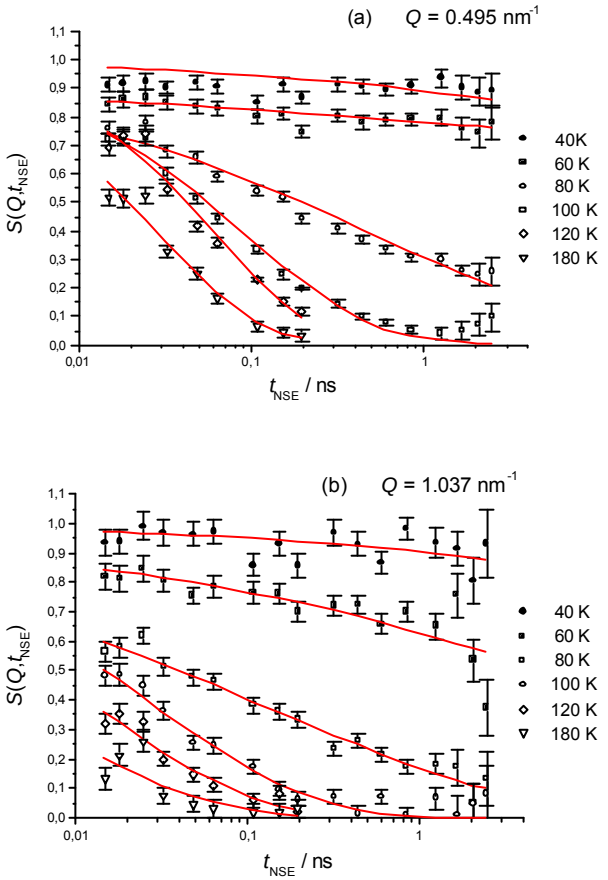


Fig 1: The normalized intermediate scattering function $S(Q,t_{NSE})$ of $Fe_{0.65}Ni_{0.35})_{0.86}Mn_{0.14}$ weakly depends on the scattering vector: (a) Q = 0.495 nm^{-1}, (b) Q = 1.037 nm^{-1}. The lines result from fitting equ.1 to the data.

References:

/1/ J. Hesse, Hyperfine Interactions **47** (1989) 357 –378

/2/ V. Wagner et al., HMI Experimental Report PHY 03-0223 (2003

/3/ V. Wagner et al., Physica B 350 (2004) e1051-e1054

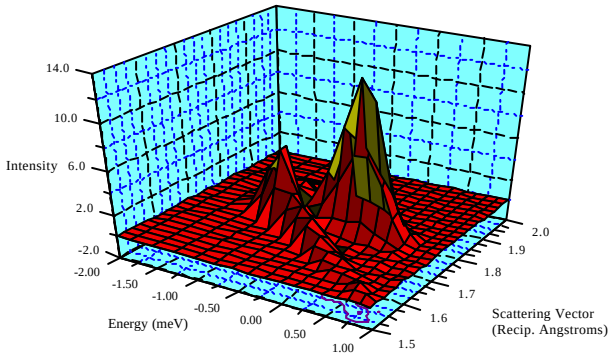
	EXPERIMENTAL REPORT **ToF analysis of the transverse magnetic fluctuations in $Mn_{0.9}Cu_{0.1}$**	Proposal N° PHY-03-333 Instrument **V5 SPAN** Local Contact C Pappas
Principal Proposer: Experimental Team:	Trevor Hicks, Monash University, Australia Stephen Harker, Monash University, Australia	Date(s) of Experiment 15-28 Jun 2004

Date of Report: 05 January 2005

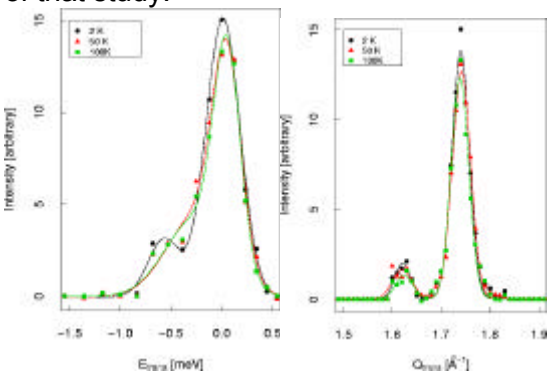
Mn-Cu is a face centred slightly tetragonal antiferromagnet with the first antiferromagnetic reciprocal lattice point at 001. The moments are parallel to the *c* direction, so that there is no magnetic Bragg intensity at 001. Nevertheless there is considerable magnetic intensity at 001, which has been inferred from susceptibility measurements to be due to components of the moment perpendicular to the antiferromagnetic direction.

Previous triple axis spectrometer measurements [1] indicated that the magnetic intensity at 001 consisted of at least two components: a narrow one less than 0.5 meV wide and a broad one greater than 1.5 meV wide. As the temperature increases both broaden and intensity shifts from the narrow one to the broad one.

The present work was performed on SPAN at HMI and was undertaken to further understand the energy spectrum and polarisation dependence of the scattering. The diagram below is a plot of intensity vs **Q** vector and energy transfer in the vicinity of the 001 for the polarisation parallel to **Q** and neutron spin down at 2 K. The scattering around 001 is seen at zero energy but an entirely unexpected feature is seen at smaller **Q**'s and across a number of energies. The ridge of intensity may indicate a coherent excitation which was not seen in the triple axis experiment.



The temperature dependence of the scattering is shown below, for **P** parallel to **Q** spin down for cuts at Q=1.74 $Å^{-1}$ (left) and for a zero energy transfer cut (right). There is a decrease in the intensity with temperature for the quasielastic peak centred at 001. This is in some agreement with the TAS measurements if this peak is associated with the narrow peak of that study.



The polarisation dependence is different for the two features. The smaller inelastic feature has a normal behaviour for magnetic scattering. That is all the intensity is in the **P** parallel to **Q** difference and none in the **P** $\perp$**Q** difference. The zero energy feature shows a quite different behaviour in that there is considerable intensity in the **P** $\perp$ **Q** difference. This was observed previously and attributed to a possible chiral component in the magnetic defect scattering contributing to the zero energy peak at 001.

1. B. Hennion, T.J. Hicks, Y. Sidis, and I. Mirebeau, *J.M.M.M.* **226-230**, 512 (2001).

BENSC	**EXPERIMENTAL REPORT** **Field-induced twisted state in Fe/Cr multilayers**	Proposal N° **PHY-04-972** Instrument **V6** Local Contact **Dr. Marita Gierlings**
Principal Proposer: Experimental Team:	Meersschaut, Johan; K.U.Leuven Meersschaut, Johan; K.U.Leuven L'abbe, Caroline; K.U.Leuven Almeida, Francisco; K.U.Leuven	Date(s) of Experiment 9-01-2004 through 17-01-2004

Date of Report: 5-01-2005

The objective of the experiment was the observation of a field-induced twisted state in a bilinearly coupled Fe/Cr superlattice of 22 repetitions, grown on MgO (001) through DC-magnetron sputtering. This twisted state occurs at low applied field values, and is believed to be the signature of a surface spin-flop. Previous magnetometry measurements performed on this sample along the hard magnetization axis showed a discontinuity in the magnetization loop for an applied field of approximately 40 mT, and micromagnetic calculations explained this discontinuity with a surface spin-flop transition.

Polarized Neutron Reflectometry was identified as a suitable technique for obtaining the spin profile of the system, due to its depth-sensitivity. Furthermore, the spin profile could promptly be predicted with use of micromagnetic calculations and used to simulate the reflectivity curves.

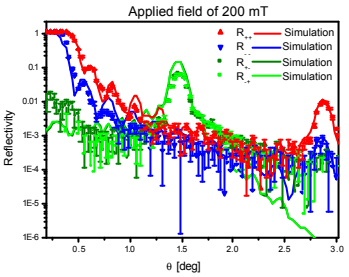
For this experiment, the magnet available at the V6 setup was mounted, as well as the polarizer and analyser. The experiment consisted in four spin-analysis reflectivity measurements. Polarized neutron reflectivity curves were recorded at four values of the external applied magnetic field. The chosen external applied field values were 30 mT, 60 mT – below and above the estimated surface spin-flop transition point –, 200 mT, and 600 mT (in saturation).

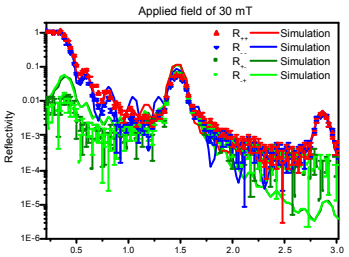
From the analysis of reflectivity curves, the complete layer resolved spin configuration could be reconstructed.

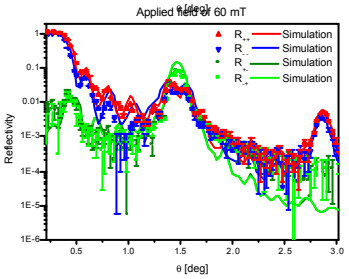
The figures to the right show obtained measurements, with exception of the saturated sample measurement.

When the sample is saturated, a ferromagnetic Bragg peak was observed, indicating that all the layers have their moment parallel to the field. Decreasing the field to 200 mT, moments were found to lay alternately along both crystalline easy axes, albeit still turned towards the external field. At 60 mT, the spin-flop transition yields a splitted half-order Bragg peak due to a stacking fault present in inner ferromagnetic layers. At a field of 30 mT, the moments are in the non-symmetric field-induced state, showing both field-parallel (non spin-flip) and orthogonal (spin-flip) projections in the PNR spectrum, and no longer showing the splitting from the previously existing stacking fault.

In conclusion, this experiment agrees with others which demonstrate the existence of an observable surface spin-flop in Fe/Cr (001) superlattices, being the added sensitivity to anisotropy, when measuring along the hard axis, shown to ease the direct detection of the surface spin-flop.







BENSC	**EXPERIMENTAL REPORT** **Polarized neutron reflectivity on exchange bias nanostructures**	Proposal N° PHY-04-973 Instrument **V6** Local Contact Dr. M. Gierlings
Principal Proposer: Experimental Team:	Dr. Temst Kristiaan, VSM, K.U.Leuven, Belgium Dr. Popova Olena, VSM, K.U.Leuven, Belgium Drs. Loosvelt Hugo, VSM, K.U.Leuven, Belgium Dr. Gierlings Marita, HMI Berlin, Germany	Date(s) of Experiment 17/01/04 – 25/01/04

Date of Report: 27/02/04

The present work is the continuation of proposal N° PHY-04-897 where the magnetization reversal mechanism in exchange biased rectangles was studied. Part of the present beamtime was dedicated to the investigation of the training effect in 1 × 4 μm^2 Co/CoO rectangles with 10 µm period (sample previously used in experiment PHY-04-897). For this purpose, the sample was field cooled in 0.4 T to 10 K. Then the first hysteresis loop and two training loops were cycled with external magnetic field and the spin-flip signal was monitored near the first and second coercive fields. Though the statistics are rather poor, it is still possible to affirm that the magnetization reversal mechanism along the descending branches of two training hysteresis loops is different from that of the initial loop, i.e. the reversal along the training loop occurs by magnetization rotation.

Two additional samples were measured during this beamtime: 5 × 5 μm^2 and 3 × 3 μm^2 Co/CoO squares with 15 µm period. These squares covered 11% and 4% of the substrate, respectively. The shape anisotropy of the samples in this case has been decreased in comparison to the previously used rectangle structures.

As the amount of the magnetic material on the sample was so small and arranged in a periodical structure, only the off-specular reflection configuration has been used for the measurements.

First of all, the optimal angular range for the off-specular satellite peak was found carrying out a Θ - 2Θ scan at magnetic saturation. Then the detector was adjusted to the off-specular reflection and a field sweep was performed in the range from –0.475 T to 0.475 T. In all experiments the external cooling and measurement magnetic field were applied along the edge of the squares. Spin analysis of the neutrons detected by a position-sensitive detector was carried out.

The positive (negative) part of the hysteresis loop has been measured after positive (negative) field cooling of the sample. The magnetisation reversal mechanisms in the samples with different structure size were found to be different along two hysteresis curve branches: domain nucleation and domain wall motion in the descending branch and magnetization rotation in the ascending branch. The outcome of this experiment for 5 × 5 μm^2 squares is shown in Fig. 1a and b. No spin flip signal is observed at the first coercive field (descending hysteresis branch). The spin flip signal is present, however, at the second coercive field (ascending branch). The results are similar for the sample with 3 × 3 μm^2 squares.

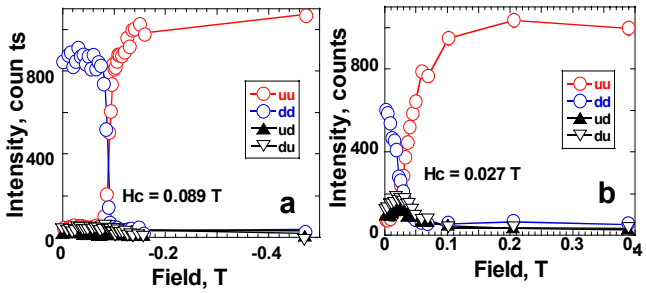


Fig. 1. Magnetic field scans for 5 × 5 μm^2 squares in off-specular configuration. All measurements have been performed with the applied field parallel to the edges of the squares. The cooling field was also applied along the edges of the squares. The measurements have been carried out: a) from the first remanence through the first coercivity field up to negative saturation; b) from the second remanence through the second coercivity field up to positive saturation.

One of the goals of the experiment was to study in detail the magnetization behaviour in the field region between the first remanence and first coercivity (on the descending branch). A 'dip' in the magnetometry hysteresis loop was observed in this field range. In the 'dip' region, apart from the increased noise in the non-spin-flip components, no other effect has been observed by PNR (Fig. 2).

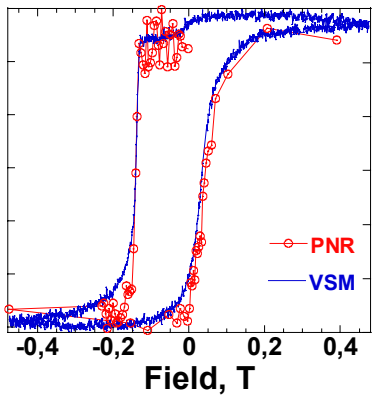


Fig. 2. Vibrating sample magnetometry and PNR hysteresis loops for the sample with 3 × 3 μm^2 squares within 15 µm period. No 'dip' in the PNR curve is observed.

Unfortunately, it was impossible to perform PNR measurements on the sample with smaller squares (1 × 1 μm^2) because of low magnetic contribution to spin-dependent scattering (0.4% surface magnetic coverage).

BENSC	**EXPERIMENTAL REPORT** **Polarized neutron reflectivity on exchange bias patterned structures**	Proposal N° **PHY-04-1054** Instrument **V6** Local Contact Dr. Marita Gierlings
Principal Proposer: Experimental Team:	Dr. Popova Olena, VSM, K.U.Leuven, Belgium Dr. Popova Olena, VSM, K.U.Leuven, Belgium Dr. Gierlings Marita, HMI Berlin, Germany	Date(s) of Experiment 09/09/04-18/09/04

Date of Report: 18/10/04

New physical phenomena become apparent when a pattern is created in a ferromagnetic film on micron or submicron scale, i.e. the magnetic material is confined to a well-defined array of dots or wires. In particular, patterning affects exchange anisotropy in antiferromagnetic/ferromagnetic structures. Our research group is interested in the influence of the structuring on exchange bias in Co/CoO wires.

The goal of the present experiment was to examine the magnetization reversal mechanism in the case of the non-collinearity of the shape anisotropy (created by the patterning), exchange bias and measurement field directions. All the measurements were performed in off-specular geometry using position-sensitive detector.

First of all, the optimal angular range for the off-specular satellite peak was found carrying out a Θ - 2Θ scan at positive remanence (Fig. 1). Then the detector was adjusted to the off-specular reflection and a field sweep was performed in the range from –0.475 T to 0.475 T. Spin analysis of the neutrons detected by a position-sensitive detector was carried out.

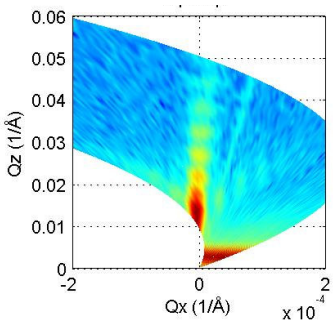
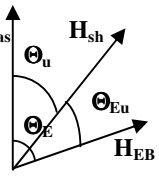


Fig. 1. (Q_x, Q_z) intensity map for up neutrons scattered from the Co/CoO wires in positive remanence.

Four polarized neutron reflectivity experiments have been successfully performed on a sample covered by Co/CoO wires with strong shape anisotropy. In each experiment either the angle between shape and exchange anisotropy axes Θ_{Eu} or the angle between exchange anisotropy and field applied during the measurement Θ_E have been varied. The four neutron cross-sections Ruu, Rdd, Rdu, Rud have been recorded along initial and training hysteresis loops of the wires. This allowed us to determine the magnetization reversal mechanism for all measurement configurations and to point out the influence of the non-collinearity of shape and exchange anisotropy on the reversal along both initial and training hysteresis loops.

Experiment	Θ_u	Θ_{Eu}	Θ_E
1	45°	0°	45°
2	45°	90°	45°
3	0°	45°	45°
4	45°	45°	0°



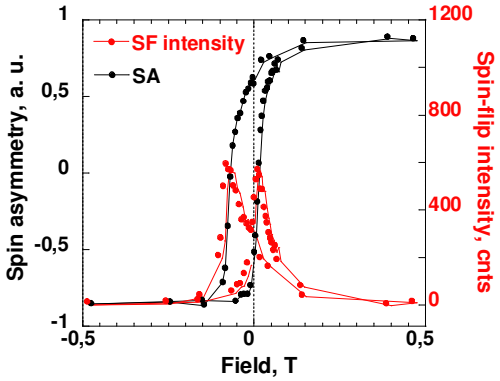


Fig. 2. Spin asymmetry and spin-flip intensity as a function of the applied magnetic field for the configuration where shape and exchange anisotropy axes were parallel and made an angle of 45° with the measurement field direction.

Magnetization of the wires reverses by rotation in all cases except along the descending branch of the initial loop in the configuration where unidirectional exchange anisotropy is parallel to the measurement field direction (experiment 4). Exchange bias field decreases for the increasing angle between shape and exchange anisotropies. When the angle between shape and exchange anisotropies Θ_{Eu} is 90°, the exchange bias is erased after first (initial) measurement. Further data analysis is in progress.

To our knowledge, this is the first experiment of such kind on the system where both ferromagnetic and antiferromangetic layers are patterned.

	EXPERIMENTAL REPORT **Polarised neutron reflectivity measurements on Cr/Gd multilayers**	Proposal N° PHY-04-1056 Instrument **V6** Local Contact Marita Gierlings
Principal Proposer: Experimental Team:	Mergia, Konstantina, N.C.S.R. "Demokritos" Messoloras, Spyros, N.C.S.R. "Demokritos" Baczewski, Tomasz, Polish Academy of Science	Date(s) of Experiment 22/9/2004 – 26/9/2004

Date of Report: 6/1/2005

Rare earth - transition metals (RE/TM) based multilayers provide novel magnetic properties. The magnetic coupling between layers can be varied, giving rise to a variety of magnetic structures which are sensitive on individual elements, the spacer thickness, interface quality and interdiffusion. Questions have arisen about the correlation between magnetic and chemical structure and the stability and uniformity of the magnetic coordination [1]. In addition RE/TM multilayers in which the layer thicknesses are quite small and comparable with the lattice parameters of metals have attracted attention as specific ferimagnets [2].

Polarised neutron reflectivity measurements were carried out on [Cr(20 Å)/Gd(30 Å)]×15 multilayer grown by Molecular Beam epitaxy on MgO single crystal substrate and with a cover layer of chromium. It consisted a continuation experiment where in the initial experiment a [Cr(30 Å)/Gd(30 Å)]×15 multilayer on MgO was studied [3]. The sample was field cooled in a magnetic field of 0.5 T and the spin up and down reflectivities were measured on the two-dimensional position sensitive detector (PSD). Although we were interested only in the specular reflectivity the PSD was utilised due to misalignment problems of the single detector with respect to the sample angular position.

The integral of the y-projections on the 2D detector was calculated to get the specular intensity. The spin up and down reflectivities at 10 K and at an applied magnetic field of 0.5 T are presented in fig. 1. Afterwards the sample was warmed at room temperature and the polarised neutron reflectivity is presented in fig.2. As it is expected no difference between spin up and spin down reflectivity is observed since the Curie temperature of Gd is a little below room temperature. The position of the Bragg peak at Q=1.17 nm^{-1} corresponds to a bilayer thickness of 53.7 Å which is very close to the nominal value of 50 Å.

Simulations of the data are underway in order to estimate if there is any induced moment on the Cr layer.

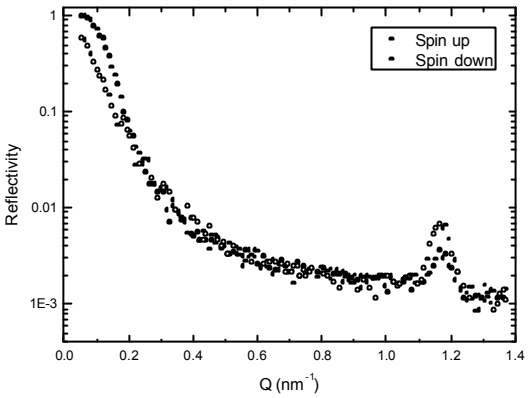


Fig. 1. Polarised neutron reflectivity curves from [Cr(20 Å)/Gd(30 Å)]×15 multilayer at T=10 K and at a magnetic field of 0.5 T.

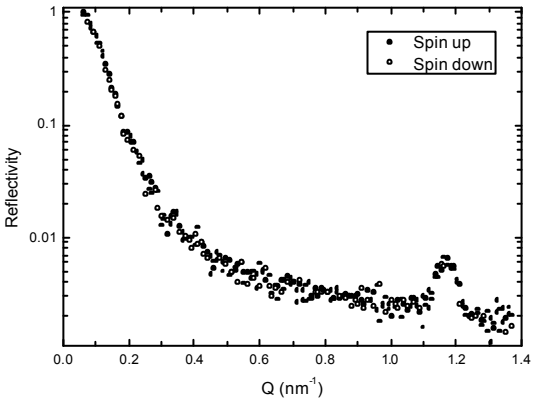


Fig. 2. Polarised neutron reflectivity curves from [Cr(20 Å)/Gd(30 Å)]×15 multilayer at room temperature.

References

[1] M. Loewenhaupt, W. Hahn, Y.Y. Huang, G.P. Felcher and S.S.P. Parkin, J. Magn. Magn. Mater. **121** (1993) 173-176

[2] R.E. Camley and R.L. Stamps, J. Phys: Condens. Matter. **5** (1993) 3727.

[3] K. Mergia, L.T. Baczewski, S. Messoloras, S. Hamada, T. Shinjo, H. Gamari-Seale, J. Hauschild, Appl. Physics A, **74** (2002) S1520.

	EXPERIMENTAL REPORT **Diffuse scattering of cation-doped zirconia-oxynitrides**	Proposal N° CHE-01-1440 Instrument **E 2** Local Contact Jens-Uwe Hoffmann
Principal Proposer: Experimental Team:	Ines Kaiser-Bischoff, LMU München, Kristallogr Ines Kaiser-Bischoff, LMU München J.-U. Hoffmann, BENSC, HMI Berlin/Uni Tübingen	Date(s) of Experiment 21.04. – 28.04.04

Date of Report: 04.01.2005

Zirconia, ZrO_2 doped with cations (e.g. Y, Sc, Ca) and/or anions (e.g. N) shows a high ionic conductivity based on oxygen vacancies. The analyzing of the diffuse scattering gives information about the short range order (SRO) of anions, cations and vacancies. Different layers of the [1-10] zone of four different single crystals have been investigated with $\lambda = 0.91$ Å.

Sample 1: $Zr_{0.83}Y_{0.17}O_{1.68}N_{0.158}$, which was measured first in 1999 at RT (OTH-01-735), was investigated at four temperatures (400, 800, 1000 and 1200°C). At RT, this sample shows a characteristic distribution of the diffuse scattering which is typical for cubic stabilized zirconia: diffuse maxima are parts of global diffuse phenomena such as bands perpendicular to ⟨111⟩ [1]. These diffuse phenomena do not disappear at high temperatures, but become slightly weaker. The intensity distributions were successfully fitted with the program TVtueb (written for the instrument E2) using a model based on random vacancies and radial displacements of the surrounding atoms (Fig. 1). These displacements increase with increasing temperature.

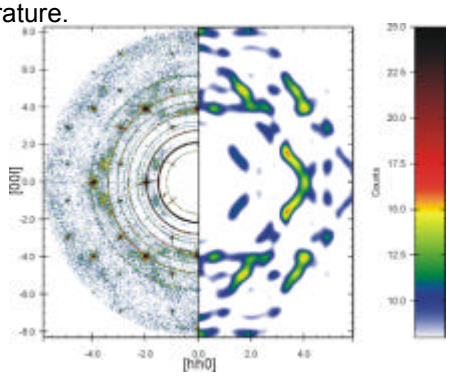


Fig. 1

Sample 2: $Zr_{0.82}Sc_{0.18}O_{1.91}$ crystallises in R-3. At RT, it does not show the typical diffuse scattering of cubic zirconia, but the distribution of the intensities of the superstructure reflections reflects these features (see CHE-01-1250). The sample was measured at three temperatures (400, 1000, 1200°C). The rhombohedral long range order (LRO) disappears, and it transforms in a cubic phase with rhombohedral SRO represented by the typical diffuse phenomena (Fig. 2) at 1000 and 1200°C. During cooling short scans at a fixed Ω position have been performed allowing the phase transition to be determined to be around 600°C.

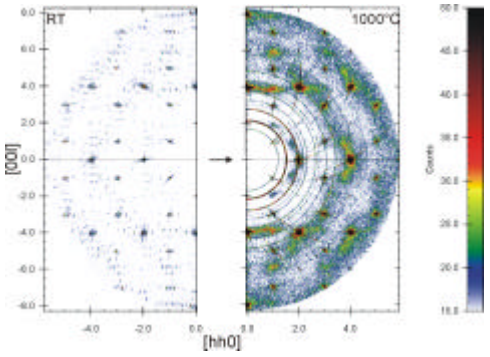


Fig. 2

Sample 3: $Zr_{0.85}Ca_{0.15}O_{1.85}$ (cubic) shows the typical diffuse scattering but in contrast to Y-doped material the diffuse maxima within the global features are more separated and their shape is different (Fig. 3). The refinements using the mentioned model could not separate the maxima. Correlations of two vacancies in different directions were not successful. There are additional diffuse maxima at positions of tetragonal Bragg reflection caused by a tetragonal SRO. This has to be related to the ageing process, because old measurement of this sample within our group (nearly 10 years ago) did not show this phenomenon.

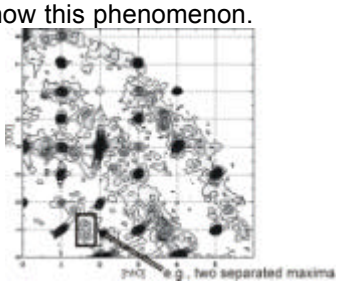


Fig. 3

Sample 4: This sample (sample 3 doped with nitrogen) shows similar diffuse scattering as sample 3. Unfortunately, it was no single crystal. But it could be seen that the tetragonal SRO is disappeared.

Conclusion: The characteristic distribution of the diffuse scattering can be described very well with the defect model concerning the Y- and/or N-doped samples. But for the Ca-doped samples this model has to be revised.

This work is supported by DFG (Bo1199/2-2) within the SPP “Substitutionseffekte in ionischen Festkörpern”.

[1] I. Kaiser-Bischoff, H. Boysen, F. Frey, J.-U. Hoffmann, D. Hohlwein and M. Lerch, *J.Appl. Cryst*, 2005, in press.

	EXPERIMENTAL REPORT **Neutron diffraction on amorphous silicon sesquioxide (Si_2O_3)**	Proposal N° CHE-01-1561 Instrument **E2** Local Contact T. Lonkai
Principal Proposer: Experimental Team:	A. Hohl, Darmstadt University of Technology, Darmstadt, Germany A. Hohl, TU Darmstadt, Germany T. Lonkai, HMI Berlin, Germany	Date(s) of Experiment 25.08.2004-29.08.2004

Date of Report: 11.02.2005

On the way to detailed structural models for silicon sub-oxides we investigate amorphous silicon sesquioxide Si_2O_3, which is a single-phase material in contrast to disproportionated amorphous silicon monoxide SiO [1]. Si_2O_3 is produced in our institute according to the procedure given by Belot *et al.* [2] and Hagenmayer *et al.* [3]. This is to our knowledge the first time that neutron data on Si_2O_3 is presented.

Neutron diffraction was carried out at the instrument E2 at BENSC. In this measuring time two samples could be measured with sufficient statistics, i.e. a native (unannealed) powder sample and a powder sample, which had been annealed earlier in vacuum for one hour at 600 °C. Evaluation of radial distribution functions was performed by using the Reverse Monte Carlo program MCGR [4]. The real space resolution was limited to $2\pi/k_{max} \approx 0.57$ Å by the maximum momentum transfer at E2 limited to about $k_{max} \approx 11$ Å^{-1}.

For both samples we can identify the peaks for Si-O near 1.5-1.6 Å, for Si-Si near 2.4 Å, and for O-Si-O and Si-O-Si near 2.7-2.8 Å (Figs. 1-2). The Si-O-Si chain seems to be limited to not too large Si-O-Si angles. The peak near 3.4 Å can be related to Si-Si-O chains, as it is not present in radial distribution functions for disproportionated SiO [1]. Differences in the curves for the two samples may be measurement artefacts due to low resolution. A high amount of defects and a high degree of disorder particularly within the native sample may cause some broadening and loss of intensity for a peak [1].

However, we expect to obtain clearly resolved partial radial distribution functions for Si_2O_3 from simultaneous evaluation of a set of diffraction data measured by neutron diffraction, X-ray diffraction, and electron diffraction likewise this has been done by us for SiO [1]. To our experience the combining of three independent datasets will provide lowered dependence from data quality.

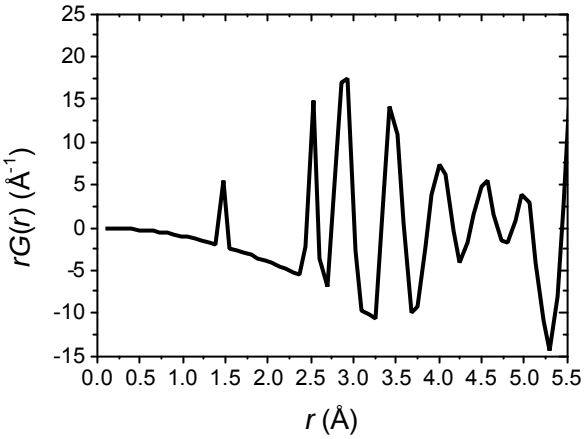


Fig. 1. Total radial distribution function $rG(r)$ for native Si_2O_3.

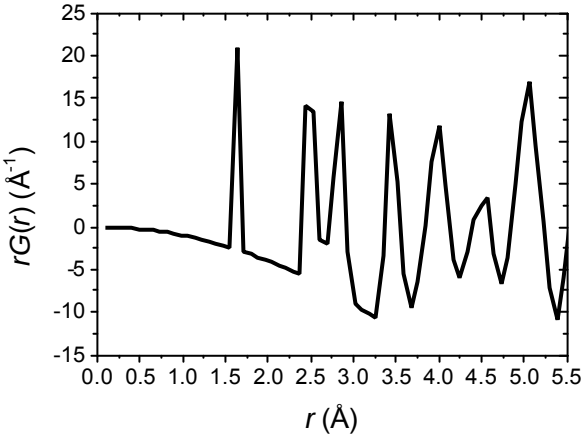


Fig. 2. Total radial distribution function $rG(r)$ for Si_2O_3 annealed at 600 °C.

[1] A. Hohl, T. Wieder, P.A. van Aken, T.E. Weirich, G. Denninger, M. Vidal, S. Oswald, C. Deneke, J. Mayer, and H. Fuess, J. Non-Cryst. Solids **320** (2003) 255.
[2] V. Belot, R. J. P. Corriu, D. Leclercq, P. Lefèvre, P. H. Mutin, A. Vioux, and A. M. Flank, J. Non-Cryst. Solids **127** (1991) 207.
[3] R. M. Hagenmayer, B. Friede, and M. Jansen, J. Non-Cryst. Solids **226** (1998) 225.
[4] P. Zetterström and R. L. McGreevy, Physica B **276-278** (2000) 187.

BENSC	**EXPERIMENTAL REPORT** Structural and magnetic phase transitions of potassium-holmium double tungstates	Proposal N° PHY-01-1441 Instrument E4 Local Contact Dr. Karel Prokes
Principal Proposer: Experimental Team:	Dr. Mieczyslaw Tadeusz BOROWIEC, Institute of Physics, Polish Academy of Sciences, Warsaw Dr. Karel Prokes, HMI Berlin Vadim Sikolenko, HMI Berlin	Date(s) of Experiment 03.05.2004-09.05.2004

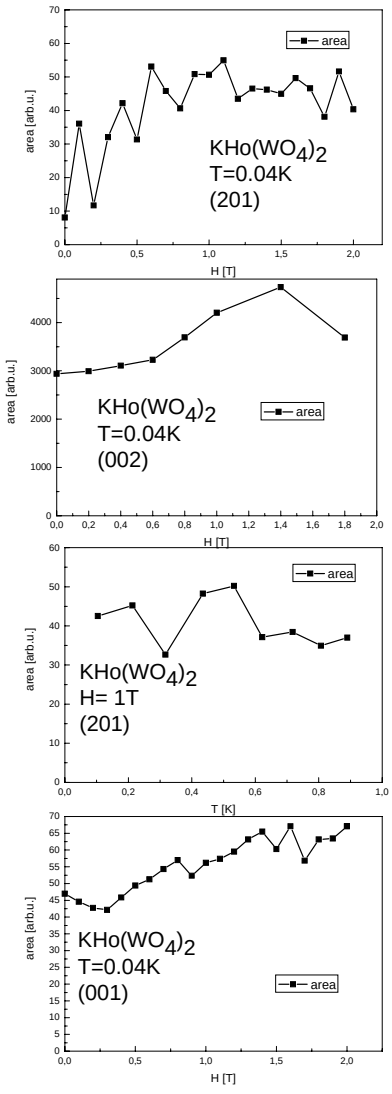
Date of Report: 20.01.2005

The alkali-dysprosium double tungstates $ARe(WO_4)_2$ (AReW), where A is alkali ion, Re=Dy, Er, Ho, Nd, belong to the class of magneto-elastics with interrelation between magnetic and elastic ordering. Scientific interest is connected with structural and magnetic phase transitions observed for them. For KHoW the spontaneous structural phase transition (SPT) of the cooperative Jahn-Teller effect (CJTE) type was observed at 5.6K in several experiments. The problem of the magnetic phase transition (MPT) for KHoW was still open. In specific heat (including specific heat in magnetic field) and susceptibility experiments without doubt the induced magnetic phase transition was found at 0.4K for H=1T and 0.33K for H=0.1T.

The neutron scattering experiment, in the frame of this project was directed to solve the problem of existence and conditions of the spontaneous/induced MPT for KHoW single crystal and to determine the structure of the magnetic state for it, if it exists. Our earlier neutronographic results obtained for KHoW were only clear for magnetic field 1T at T=0.05K: some small additional magnetic peaks were observed. The peaks were small and wide but on the correct positions.

For neutron scattering experiments on oriented single crystal the set of selected temperatures, magnetic fields and directions was following: T= 40, 60, 104. 213. 317, 435, 533, 622, 718, 807, 890mK, 1.7K, 10K; H= 0-2.0T with step 0.1T, directions 001, 200, 002, -202, 201, 20-1, -204, 400, -404, 40-1, 40-2, 60-2, 60-4. The choice of above temperature and magnetic field values is connected with our erlier experimental results of specific heat, susceptibility experiments and earlier neutronographic experiments on powdered and single crystals on E2 instrument.

The results obtained for oriented KHoW single crystal for wavelength 2.4A on instrument E4 do not confirm of existence of spontaneous magnetic phase transitions (up to 40mK). The existence of induced magnetic phase transitions is confirmed (at temperature below T=0.4K). In this last case some properties indicate the ferromagnetic ordering (especially for higher magnetic fields). The Figures present the temperature and magnetic dependences for some choosed directions. It must be underlined that existence of reflex on 001 direction is not clear for C2c symmetry.



	EXPERIMENTAL REPORT **Critical fluctuations in orientational glass $(NH_4I)_x(KI)_{1-x}$**	Proposal N° **PHY-01-1377** Instrument **E5** Local Contact M. Reehuis
Principal Proposer: Experimental Team:	M. Ohl, FZ Jülich M. Ohl, FZ Jülich M. Reehuis, HMI Berlin, MPI Stuttgart	Date(s) of Experiment 28.10.-16.11.2003

Date of Report: 24.11.2004

NH_4I:KI and its deuterated isomorphs have attracted much attention during the last years. $(NH_4I)_x(KI)_{1-x}$ forms at intermediate compositions $0.55 < x < 0.8$ at low temperatures the e-phase with trigonal crystal structure in $R\bar{3}m$ [1]. In going to lower ammonium concentrations the orientational order of the NH_4^+-tetrahedra decreases and an orienttational glass phase appears.

From preliminary Fourier-transform infrared measurements the question arises, whether this orientational glass state affects the lattice dynamics in means the optical and acoustic phonon branches, as predicted by the Lyddane-Sachs -Teller relation. We know from preliminary dielectric measurements that the deuteration isomorphs $(ND_4I)_x(KI)_{1-x}$ forms as well as the protonated mixed crystal system an orientational glass state. These crystals were predestinated for phonon investigations caused by their less incoherent scattering.

In order to investigate the thermal motions of the NH_4^+-tetrahedra in the mixed crystal system $NH_4I)_x(KI)_{1-x}$ with an ammonium concentration close to an orientational glass state, we examined a single crystal of $(NH_4I)_{0.4}(KI)_{0.6}$ with the dimensions of 1.9 × 1.9 × 4.5 mm^3. 14 data sets were collected on the four-circle diffractometer E5 at different temperatures between 10 and 75 K. With the neutron wavelength l = 0.89 Å a total of 93 unique reflections could be measured for each temperature. In Fig. 1 it can be seen that below the phase transition at 50(1) K, from the cubic ($Fm\bar{3}m$) into the lower symmetric trigonal structure, the reflection 5 0 0 spontaneously appears. Not any anomaly could be observed for the in the cubic symmetry allowed reflections 2 0 0 and 12 0 0 at 50 K. The intensity of the 2 0 0 between 10 and 75 K remains unchanged, whereas that of the 12 0 0 is continuously increasing down to 10 K. This can be ascribed to the fact that the thermal motions of the atoms are more and more frozen with lowering temperature. This effect especially is stronger pronounced for reflections with larger $\sin q/l$-values.

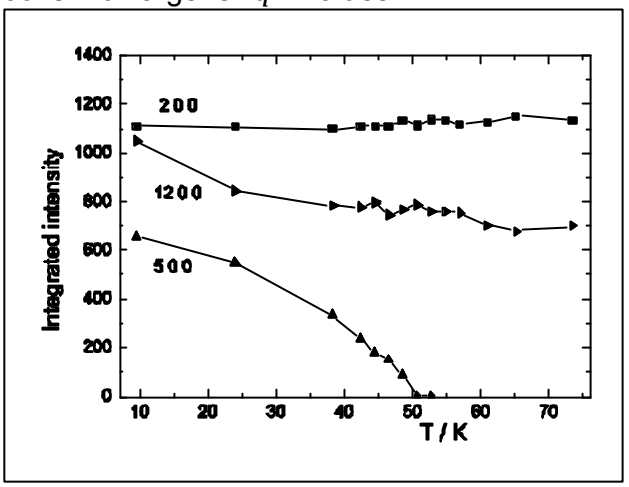


Fig. 1. Temperature dependence of the integrated intensities of some prominent Bragg reflections.

From the crystal structure refinements of the data sets we expected to determine the temperature factors U with a good accuracy. However, not any anomaly could be observed close to the phase transition temperature of 50 K. But here it has to be mentioned that the data quality suffered from the relatively strong absorption cross section caused by the incoherent scattering of the hydrogen in the sample. This was the reason, that we were not able to measure precisely the weak reflections, especially the superstructure reflections close to the phase transition temperature and those collected at higher $\sin q/l$-values. However, we gained more insight to observe the temperature factors U directly at the phase transition temperature. In order to avoid absorption effects it seems more promising to investigate deuterated samples. This may allow us finally to decide whether critical fluctuations of the NH_4-tetrahedron may accompany the phase transition into the glass like the e-phase.

[1] M. Paasch, G.J. McIntyre, M. Reehuis, R. Sonntag, A. Loidl, Z. Phys. B **99** (1996) 339.

	EXPERIMENTAL REPORT The ordering of ammonium in ferroelectric phase II of b-$LiNH_4SO_4$	Proposal N° PHY-01-1483 Instrument **E5** Local Contact: Dr.A.Loose
Principal Proposer: Experimental Team:	L.S.Smirnov, FSUE SSCRF ITEP, Moscow A.Loose, HMI, BENSC, Berlin L.S.Smirnov, FSUE SSC RF ITEP, Moscow	Date(s) of Experiment: 17.05.04-07.06.04

Date of Report: 04.09.2004

The β-$LiNH_4SO_4$ (or LAS) undergoes the series of phase transitions:phaseI(Pmcn)⇔459.6K⇔phaseII($P2_1cn$)⇔284K⇔phaseIII($P2_1/c$)⇔27K⇔phaseIV(Cc).

The crystal structures of all phases were determined only with the help of X-ray single crystal diffraction. The hydrogen positions in phasesII were determined in [1]. The N-H bond lengths and H-N-H angles for phase II were scattered in the region 0.71~1.08 Å and 96~119°, respectively. Tetrahedra of SO_4 and LiO_4 are almost regular in phasesII. The differential Fourier synthesis of phaseII showed that one well defined peak could be assigned as H4 ($\Delta\rho\approx0.5$ e$Å^{-3}$), H1, H2 and H3 could correspond to three peaks among five weak peaks ($\Delta\rho\approx0.3$ e$Å^{-3}$) around N. Two-site disordered model for ammonium ion was not accepted as the reality and further ordered model was analyzed with 4 peaks among the six ones to form a regular tetrahedron. However thermal parameters for hydrogen atoms H1 and H3 were significantly larger than ones for H2 and H4. The analysis of the result of differential Fourier synthesis and hydrogen thermal parameters led to the conclusion that ammonium ion in phase II is partially disordered. The results of X-ray crystal structure study of phase II of LAS had not given definite presentation about orientational positions of ammonium ion.

The refinement of hydrogen positions in LAS in recent study is carried out with the help of single crystal neutron diffraction on E5 diffractometer. Experimental conditions, obtained lattice parameters and R-factors are presented in Table 1.

Table 1. Crystal and refinement data

Substance	β-$LiNH_4SO_4$
Temperature	298 K
Radiation	neutron
Wavelength	0.8839 Å
Space group	$P2_1cn$, Z=4
a	5.2666(5) Å
b	9.0973(9) Å
c	8.7584(9) Å
α	90°
β	90°
γ	90°
Number of reflections (measured/unique)	1929/858
Number of variables	100
R-factor(using |F|)	0.072
wR-factor (using |Y|)	0.057

The refined atomic positions in LAS at RT are presented in Table 2.

Table 2. The refinement of atomic positions in β-$LiNH_4SO_4$ at room temperature.

Atom	x	y	z
Li	0.2515(17)	0.08775(57)	0.32238(55)
S	0.25069(95)	0.41661(35)	0.20263(35)
O1	0.2521(12)	0.40349(54)	0.03906(25)
O2	0.34528(75)	0.28169(24)	0.26895(43)
O3	-0.00821(60)	0.44501(25)	0.25616(27)
O4	0.41757(76)	0.53741(23)	0.25044(29)
N	0.75569(68)	0.28438(17)	0.49957(14)
H1	0.8316(34)	0.18785(92)	0.50843(81)
H2	0.5773(16)	0.2666(15)	0.4840(14)
H3	0.8373(18)	0.33651(70)	0.41020(64)
H4	0.7887(49)	0.34662(69)	0.59391(63)

The obtained bond lengths for phase II of LAS and the comparison with results of x-ray study in [1] are presented in Table 3.

Table 3. The determined bond lengths in β-$LiNH_4SO_4$ at room temperature (phase II).

Atoms	Bond lengths, Å neutron	Bond lengths, Å x-ray [1]
S-O1	1.4376(38)	1.450(2)
S-O2	1.4463(44)	1.461(2)
S-O3	1.4649(57)	1.475(2)
S-O4	1.4683(49)	1.472(2)
mean	1.454	1.464
Li-O1	1.8995(53)	1.892
Li-O2	1.8911(60)	1.888
Li-O3	1.9396(75)	1.937
Li-O4	1.9257(92)	1.938
mean	1.914	1.914
N-H1	0.968(11)	1.08(7)
N-H2	0.9632(93)	0.71(7)
N-H3	1.0111(69)	0.91(8)
N-H4	1.0166(74)	1.04(4)
mean	0.99	0.93

Thus obtained by single crystal neutron diffraction the hydrogen positions showed in the result that the N-H bond lengths indeed are scattered in the region 0.96-1.02 Å and that is significantly less than in [1]. The results of differential Fourier synthesis and hydrogen thermal parameters will be presented in the publication.

1. H.Mashiyama, H.Kasano, J.Phys.Soc.Japan, 62 (1993) 155.

	EXPERIMENTAL REPORT **Exact determination of the deuteron positions of $ND_4(ND_3)_3Cl$**	Proposal N° CHE-01-1484 Instrument **E5** Local Contact Dr. Anja Loose
Principal Proposer: Experimental Team:	Thomas Rossmeier, Universität Regensburg Thomas Roßmeier	Date(s) of Experiment 19 Apr – 10 May 2004

Date of Report: 12/22/2004

The quality of the X-ray data allowed the tentative localisation of most of the hydrogen atoms in these compounds; however, for a precise characterisation of the hydrogen bonds and for a meaningful comparison with theoretical investigations, neutron diffraction data are necessary.

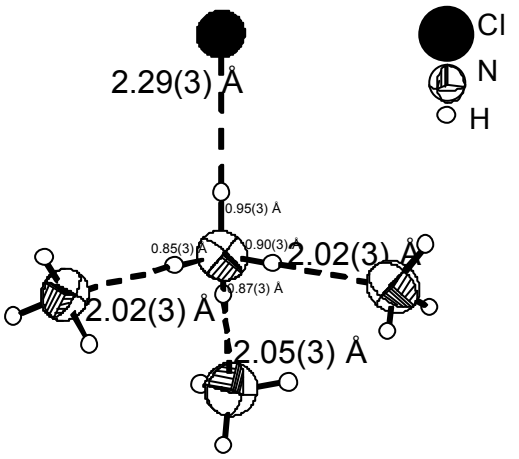
The aim of the experiment is the exact determination of the deuteron positions of the analogous deuterated Ammine-Ammonium complex $ND_4(ND_3)_3Cl$ by collecting neutron diffraction data of a single crystal with the 4-Circle Diffractometer (E5).

Consequently, $ND_4(ND_3)_3Cl$ crystals were obtained from ND_4Cl and ND_3 and transferred into sealable vanadium containers. These precooled vessels (N_2) were transported in temperature-controlled containers to Berlin and mounted on the 4-Circle Diffractometer (E5). Following that, a sample temperature of less than -10 °C was achieved in short time (5 minutes), due to the thermal instability of the crystals.

The Figures show the central ion-paired molecular unit of the crystal structure of $NH_4(NH_3)_3Cl$ and $ND_4(ND_3)_3Cl$ with the distances and angles that resulted from our X-ray single crystal study and from the neutron single crystal study. The central ammonium ion is connected to three ammonia molecules and the chloride counter ion, via hydrogen bonds. $ND_4(ND_3)_3Cl$ crystallises in the orthorhombic space group $P2_12_12_1$ (Nr. 19), a = 8.497(1) Å, b = 8.890(1) Å, c = 8.732(1) Å and forms colourless regular box-shaped crystals, for which an edge length of ca. 5 mm is readly achievable.

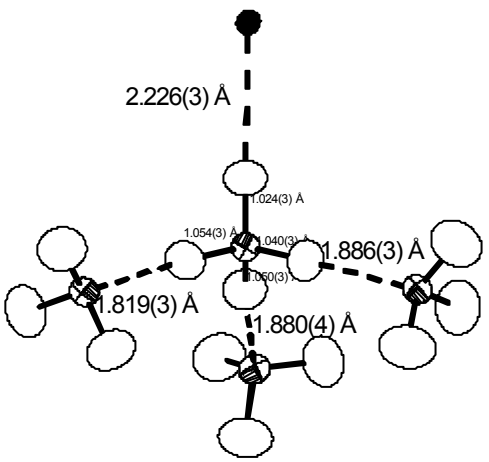
Temperature: 10 K, μ: 0.1231 mm^{-1}, Goodness-of-fit F^2: 1.225, electron density min/max: 2.076/-1.993 e $Å^{-3}$, R1 = 0.0554, wR2 = 0.1433 (all data), reflexes/restraints/parameter: 1672/0/165.

$NH_4(NH_3)_3Cl$



Cl···N: 3.232(2) Å; **N···N:** 2.865(3)-2.920(3) Å
DHA-angle: 168(2)-178(2)°
ORTEP-plot: 80% probability

$ND_4(ND_3)_3Cl$



Cl···N: 3.234(2) Å; **N···N:** 2.872(2)-2.928(2) Å
DHA-angle: 168.3(3)-176.3(3)°
ORTEP-plot: 80% probability

	EXPERIMENTAL REPORT Hydrogen Compounds and Intermetallic Phases	Proposal N° CHE-01-1467 Instrument E6 Local Contact N. Stüßer
Principal Proposer: Experimental Team:	G. Auffermann, MPI CPfS Dresden W. Bronger, TH Aachen G. Auffermann, MPI CPfS Dresden N. Stüßer, HMI Berlin	Date(s) of Experiment 17.05. – 20.05.2004

Date of Report: 22.12.2004

Cs_3OsD_9 was synthesized by the reaction of cesium deuteride with osmium powder at 870 K above a deuterium pressure of 1500 bar [1].

The atomic arrangement of the metal atoms (Cu_3Au-type structure) was derived from Guinier diffractometer (Huber G645) investigations on powdered samples. To determine the deuterium positions neutron diffraction experiments were carried using TAS I at the Riso National Laboratory at room temperature. These investigations confirmed the arrangement of the metal atoms and additionally revealed the positions of the deuterium atoms [1]. The structure of $Cs_3D[OsD_8]$ is shown in Fig. 1. The positions of the deuterium ligands within the $[OsD_8^{2-}]$-polyhedra can be crystallographically described with a statistical occupation of two 24-fold positions.

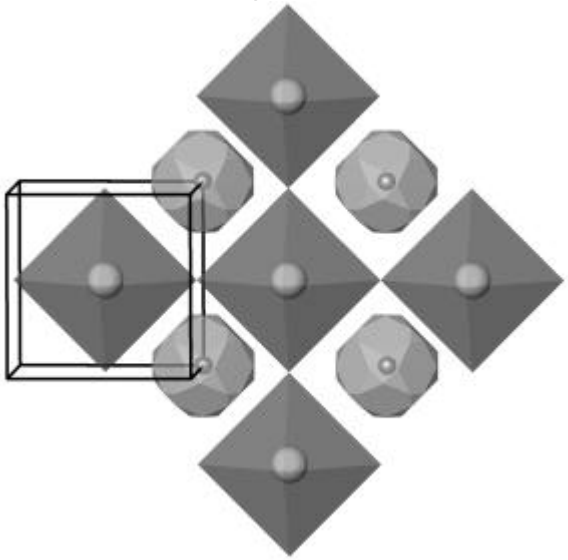


Fig. 1: Cs_3OsD_9; atomic arrangement at room temperature showing the three-dimensional framework structure of corner-sharing cesium octahedra, centred by deuterium ions and the $[OsD_8^{2-}]$-polyhedra, in which the positions of the ligands are statistically occupied.

Strongly related structures were found for the compounds $Rb_3D[ReD_9]$ and $Cs_3D[ReD_9]$ [2,3]. Therein, the extraordinary behaviour of hydrogen ligands is evident in the dynamic properties and is responsible for numerous phase transitions. In the high temperature modifications (HT) the mobility of hydrogen leads a statistical occupation of the ligands positions whereas in the low temperature modifications (LT) an ordered arrangement occurs [4]. Therefore neutron diffraction experiments on $Cs_3D[OsD_8]$ were carried out as a function of temperature using the E6 diffractometer (HMI Berlin). The data show a splitting of the reflections below 110 K. Additionally, weak reflections are observable (s. Fig. 2). The pattern at 2 K can be indexed with an orthorhombic metric: $a_{LT}=a_{HT}v2$, $b_{LT}=a_{HT}v2$, $c_{LT}=2a_{HT}$. The complete structure refinement is still in progress.

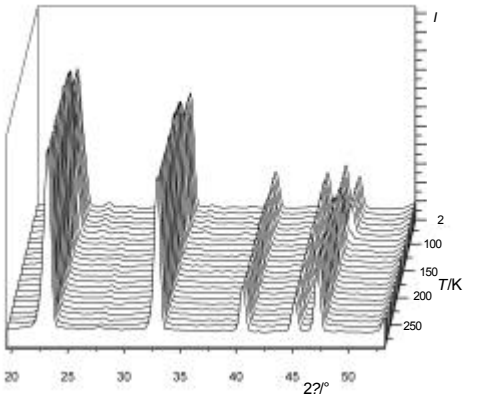


Fig. 2: Cs_3OsD_9; Neutron diffraction profiles as a function of temperature taken at the diffractometer E6 (HMI Berlin, λ = 2.4415(3) Å). The sample was located in a vanadium container of 6 mm diameter; measuring region: 19.5° < 2Θ < 53.1°, measuring time 1h each scan.

References

[1] W. Bronger, T. Sommer, G. Auffermann, P. Müller, J. Alloys Comp. **330-332** (2002) 536.

[2] W. Bronger, G. Auffermann, Z. Anorg. Allg. Chem. **625** (1999) 1147.

[3] G. Auffermann, W. Bronger, Z. Anorg. Allg. Chem. **628** (2002) 2159.

[4] W. Bronger, G. Auffermann, Chem. Mater. **10** (1998) 2723.

	EXPERIMENTAL REPORT Metal – Nitride – Hydrides	Proposal N° CHE-01-1562 CHE-01-1450 Instrument E9 Local Contact D. M. Többens
Principal Proposer: Experimental Team:	G. Auffermann, R. Kniep, MPI CPfS Dresden G. Auffermann, MPI CPfS Dresden R. Chemnitzer, MPI CPfS Dresden D.M. Többens, HMI Berlin	Date(s) of Experiment 15.06. – 25.06.2004 20.09. – 22.09.2004

Date of Report: 01.10.2004

In the course of our studies on the existence of diazenides in the binary system Sr – N we observed a successive insertion of $[N_2^{2-}]$ - dumbbells into the crystal structure of Sr_2N [1]. Neutron diffraction experiments were carried out on single phase products (Sr_4N_3, SrN, SrN_2) and led to their complete crystal structure determinations [2, 3].

The extension of this work to the investigation of the insertion of hydrogen into the host structure of Sr_2N led to single phase products of $(Sr_2N)H$ [4], whereas former investigations by *H. Jacobs* [5] only led to a "two phase model" with $(Sr_2N)D$ besides Sr[ND] with anomalous temperature factors for D (B_{iso} increases with decreasing temperature) [5].

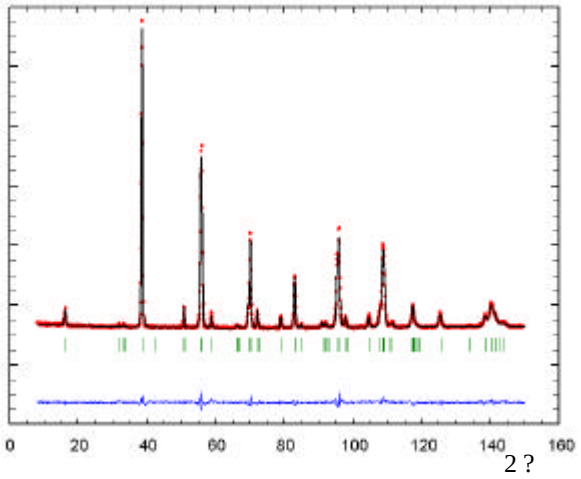


Fig. 1: Neutron powder diffraction pattern of $(Sr_2N)D$ at 297K (observed (red), calculated (black) and difference (blue) profiles, green ticks mark the Bragg positions).

Table 1: Structural parameters of $(Sr_2N)D$ ($R\bar{3}m$, 60 reflections).

		2 K	297 K
Lattice (Å)	*a*	3.8125(2)	3.8208(2)
	c	18.8384(7)	18.8828(8)
Sr in (6*c*)	*z*	0.2387(1)	0.2387(1)
	B_{iso} (Å^2)	0.0 (1)	0.81 (4)
N in (3*b*)	B_{iso} (Å^2)	0.08 (4)	0.77 (5)
D in (3*a*)	B_{iso} (Å^2)	1.22 (5)	2.19 (8)
R_{Profil}/R_{Bragg}		0.060/0.049	0.052/0.036

Neutron diffraction investigations were carried out at 298 K and 2 K on single phase samples of $(Sr_2N)D$, using the powder diffractometer E9. Structure refinements (Fig. 1) were performed applying the program FULLPROF [6]. The results do not show any anomalies (Table 1). The Sr - D and Sr - N distances at 297 K are 2.839(1) Å and 2.592(1) Å, respectively.

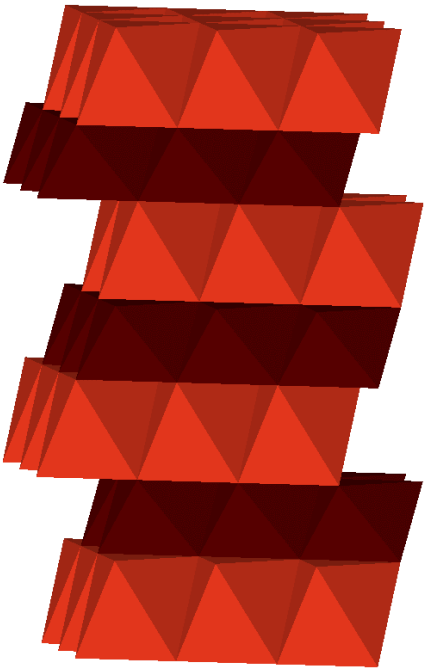


Fig. 2: Crystal structure of $(Sr_2N)D$. Along [001] the octahedral holes between the strontium layers are alternatively filled with nitrogen (dark red) and deuterium (light red), respectively.

References:

[1] N. E. Brese, M. O´Keeffe, *J. Solid State Chem.* 87 **(1990)** 134.
[2] G. Auffermann, Yu. Prots, R. Kniep, *Angew. Chem. Int. Ed.* 40 **(2001)** 547.
[3] Yu. Prots, G. Auffermann, M. Tovar, R. Kniep, *Angew. Chem. Int. Ed.* 41 **(2002)** 2288.
[4] R. Chemnitzer, G. Auffermann, D.M. Többens, R. Kniep, *Z. Anorg. Allg. Chem.* in preparation.
[5] Th. Sichla, F. Altdorfer, D. Hohlwein, K. Reimann, M. Steube, J. Wrzesinski, H. Jacobs, *Z. Anorg. Allg. Chem.* 623 **(1997)** 414.
[6] J. Rodriguez-Carvajal, LLB, Saclay FULLPROF.2K Version 2.70 **(2004)**.

	EXPERIMENTAL REPORT **Oxygen/Nitrogen Order in doped Tantalum Oxynitride Compounds**	Proposal N° CHE-01-1448 Instrument **E9** Local Contact Michael Tovar
Principal Proposer: Experimental Team:	Schilling, Heikko, TU Berlin Schilling, Heikko, TU Berlin Lerch, Martin, TU Berlin Tovar, Michael, HMI Berlin	Date(s) of Experiment 03. Feb – 07. Feb 2004

Date of Report: 20.11.2004

Oxynitride materials are promising candidates for future applications as nitrogen ion conductor materials (sensors) and colour pigments. Doped tantalum oxynitride compounds are of special interest because of their high nitrogen content compared to previously investigated oxynitrides of zirconium (fluorite-type structures). The determination of nitrogen/oxygen ordering by neutron scattering is essential for an understanding of the physical properties (e.g. electrical and optical) of these materials.

Doped tantalum oxynitride materials can be prepared by ammonolysis of the corresponding oxides. These oxides were synthesized as X-ray amorphous powders by the citrate method.

Single phase samples (X-ray diffraction) were obtained with the following compositions (chemical analysis):

1) $Y_{0.20}Ta_{0.80}O_{1.09}N_{0.81}1_{0.10}$, dark brown, fluorite-type structure, SG $Fm\bar{3}m$
2) $Y_{0.25}Ta_{0.75}O_{1.20}N_{0.70}1_{0.10}$, dark brown, fluorite-type structure, SG $Fm\bar{3}m$
3) $Sc_{0.35}Ta_{0.65}O_{0.48}N_{1.11}1_{0.41}$, brown, bixbyite-type structure, SG $Ia\bar{3}$
4) $Sc_{0.50}Ta_{0.50}O_{1.25}N_{0.50}1_{0.25}$, brown, fluorite-type structure, SG $Fm\bar{3}m$
5) $Sc_{0.15}Ta_{0.85}O_{1.30}N_{0.70}$, yellow, anatase-type structure, SG $I4_1/amd$
6) $Mg_{0.05}Ta_{0.95}O_{1.15}N_{0.85}$, orange, anatase-type structure, SG $I4_1/amd$

Neutron data were collected at the instrument E9 (wavelength 1.797 Å). The 2T-range was up to 160° with a step width of 0.05°. Measurements were carried out at room temperature (samples 1 – 6) and between 400°C and 1000°C in intervals of 100°C (sample 6) under vacuum using a high-temperature furnace.

Measurements of the Y-containing fluorite-type phases resulted in patterns with very broad reflections probably due to inhomogeneity of the samples. Rietveld refinements could not be performed with these two data sets. No superstructure reflections could be detected so far.

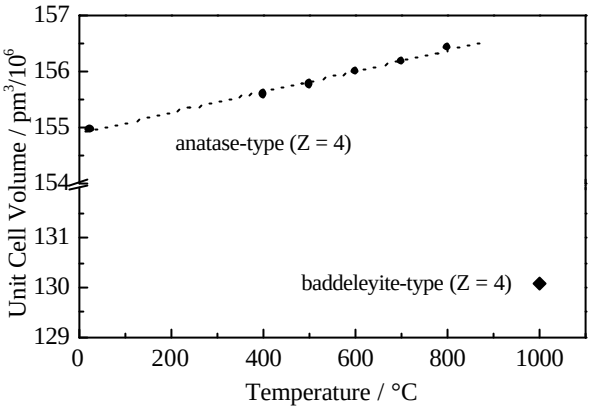


Fig. 1: *Thermal expansion and anatase to baddeleyite phase transition of* $Mg_{0.05}Ta_{0.95}O_{1.15}N_{0.85}$

Neutron diffraction data of the Sc-containing phases could be analyzed by joint refinements with XRD data. For $Sc_{0.35}Ta_{0.65}O_{0.48}N_{1.11}1_{0.41}$ the bixbyite-type structure could be established.

The phase $Sc_{0.50}Ta_{0.50}O_{1.25}N_{0.50}1_{0.25}$ showed superstructure reflections which were not detected in XRD patterns. They correspond to the bixbyite-type structure. Thus, the bixbyite-type super-structure with its anion vacancy ordering is likely to be present in the whole range of Sc-doped cubic tantalum oxynitrides $Sc_xTa_{1-x}(O,N)_y$; $0.33 = x = 0.75$; $1.7 = y = 1.9$.

Anion ordering in an anatase-type compound AXY can be described in three of the maximal non-isomorphic subgroups of $I4_1/amd$: $I\bar{4}m2$, $I4_1md$, and Imma – resulting in three different ordering schemes. Rietveld refinements with the neutron diffraction data of $Mg_{0.05}Ta_{0.95}O_{1.15}N_{0.85}$ show no advantage for the anion ordered structures. Theoretical calculations on this problem are at work.

Temperature dependent measurements of the same sample show clearly that the baddeleyite-type phase resulting from a first order phase transition at about 900°C has fully ordered anions similar to TaON [1].

[1] D. Armytage, B. E. F. Fender, J. Solid State Chem., 77, 67-71, (1988)

	EXPERIMENTAL REPORT **Structure and anion ordering in $BaPbO_{3-d}$**	Proposal N° PHY-01-1452 Instrument **E9** Local Contact M. Tovar
Principal Proposer: Experimental Team:	S. Schorr, University Leipzig, IMKM S. Schorr, University Leipzig, IMKM A. Franz, University Leipzig, IMKM M. Tovar, HMI Berlin	Date(s) of Experiment 10. 2. – 18. 2. 2004

Date of Report: 14. 2. 2005

The ABO_3 perovskite structure reveals a large tolerance for the variety of substitutions at both A and B sites and for a wide range of cation and vacancy ordering. This has led to a number of discoveries of useful chemical and physical properties. Particularly the oxygen deficit influences the electrical conductivity critically. Oxygen measurements are challenging. The references give either none or incorrect data. The amount of oxygen deficiency is influenced by sample preparation, calcination temperature and atmosphere used for synthesizing and annealing.
Tetravalent Pb partly changes to more stable divalent Pb caused by insertion of vacancies in the anion sublattice.
$BaPbO_{3-x}$ samples were synthesized from barium and lead oxalates. These oxalates were homogenized dry as well as in an aqueous suspension followed by calcination in air using an optimised temperature profile (up to 850°C). Afterwards the perovskites were annealed in vacuum, air and oxygen atmosphere and at different temperatures (up to 800°C) which corresponds to different oxygen fugacities. The variation of homogenization methods yields homogeneous powder with various oxygen deficiencies (x = 0.5(1) – 0.1(1)) up to fully occupied anion sites ($BaPbO_3$). Depending upon different sample preparation technique a orthorhombic (Imma) structure with two different oxygen sites or a monoclinic (I2/m) structure with three different oxygen sites was reported.
Neutron powder diffraction experiments were performed at the high resolution powder diffractometer E9 (λ=1.7969Å) at room temperature and at lower temperatures (1K, 50K) in order to study the structure and relevant oxygen occupancy of different oxygen sites.

Rietveld refinements (FULLPROF) were done on all diffractograms using the monoclinic (s.g. I2/m) and the ortho-rhombic (s. g. Imma) structure model resulting in comparable fit qualities (tab. 1).

atmosph.	monoclinic		orthorhombic	
	R_{Bragg}	χ^2	R_{Bragg}	χ^2
Oxygen 1K	4.78	2.34	5.12	3.06
Oxygen 300K	5.12	3.35	5.05	2.05
Vacuum 1K	4.25	3.01	5.05	3.54
Vacuum 300K	6.66	4.81	4.55	2.81
Air 300K	4.99	3.79	4.66	2.81

Tab. 1: R_{Bragg} and χ^2 values of Rietveld refinments

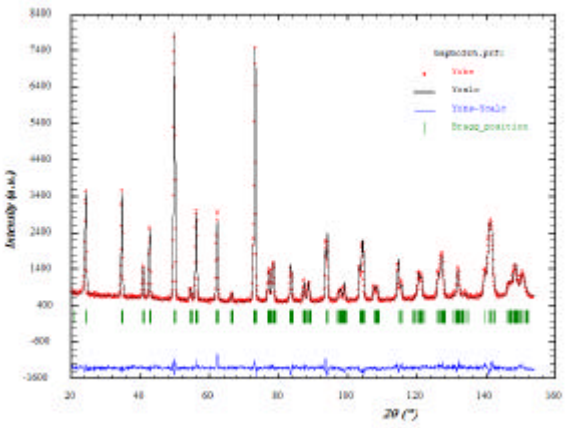


Fig. 1: refinement pattern for $BaPbO_3$ annealed in oxygen

These results have to be compared with synchrotron radiation data and results from Temperature Programmed Reduction to get full information about the structure.

	EXPERIMENTAL REPORT **Structure and cation ordering in the solid solution system $BaPbO_3$- $BaSnO_3$**	Proposal N° PHY-01-1563 Instrument **E9** Local Contact Michael Tovar
Principal Proposer: Experimental Team:	A.Franz, University Leipzig, IMKM A.Franz, University Leipzig, IMKM S.Schorr, University Leipzig, IMKM M.Tovar, HMI Berlin	Date(s) of Experiment 10.09.04-15.09.04

Date of Report: 07.01.05

The ABO_3 perovskite structure reveals a large tolerance for the variety of substitutions at both A and B sites and for a wide range of cation and vacancy ordering. This has led to a number of discoveries of useful chemical and physical properties.
Particularly the oxygen deficit influences the electrical conductivity critically. Oxygen measurements are challenging. The references give either none or incorrect data. The amount of oxygen deficiency is influenced by sample preparation, calcination temperature and atmosphere used for synthesizing and annealing.
The samples were synthesized from barium and lead oxalates. Those oxalates were homogenized dry as well as in an aqueous suspension followed by calcination in air using an optimised temperature profile (up to 850°C). The starting materials $BaPbO_{3-x}$ and $BaSnO_3$ are monoclinic and cubic respectively.
Neutron powder diffraction experiments were performed at the high resolution powder diffractometer E9 (λ=1.7969Å) at room temperature. The aim was to study cation ordering and transition of the crystal system in correlation with the stoichiometry.
Rietveld refinements (FULLPROF) were done on all diffractograms using monoclinic (I2/m), orthorhombic (Imma) and cubic (Pm-3m) structure models.
Figure 1 shows the decrease of the line splitting while the Sn content increases from Sn20 ($Ba(Pb_{0.8}Sn_{0.2})O_{3-x}$) to Sn100 ($BaSnO_3$). This is an indication of a crystal system transition from monoclinic to cubic.

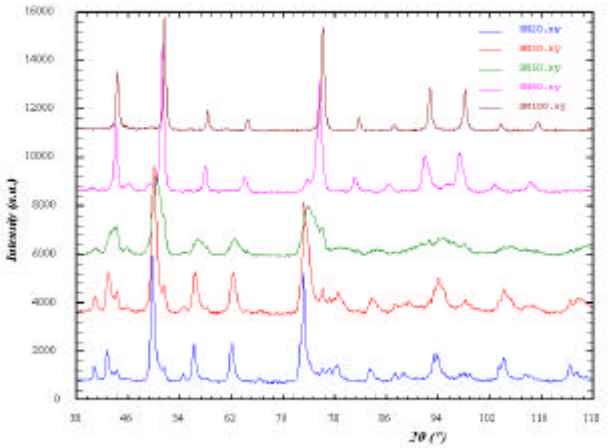


Fig.1 changing line splitting in $Ba(Pb_xSn_{1-x})O_{3-x}$

The Rietveld refinements gave best results by using a 2 phased structure model in case of Sn20 and Sn30 (orthorhombic and monoclinic). Sn80 is single phased cubic with small impurities of SnO_2. Refining the Sn100 sample led to a pure single phased $BaSnO_3$ (cubic).
Sn50 showed a mutiphase mixture.This is an indication for a miscibility gap at this mixing ratio.
That all samples showed an average grain size of approximately 280Å, is the reason for non satisfying chi^2 (11,7) and R-Bragg (12,4) values. Whether the change of the sample preparation or the improvement of the strucure model will lead to better relults has to be studied in future.

	EXPERIMENTAL REPORT **Structure Investigation of the Kesterite-Stannite Series, Cu_2FeSnS_4 – Cu_2ZnSnS_4**	Proposal N° PHY-01-1565 Instrument **E9** Local Contact Michael Tovar
Principal Proposer: Experimental Team:	Susan Schorr, University Leipzig Susan Schorr, University Leipzig Michael Tovar, HMI Berlin	Date(s) of Experiment 10. 8. – 13. 8. 2004

Date of Report: 7. 1. 2005

Stannite (Cu_2FeSnS_4, sg $I\bar{4}2m$) is one of the-best known sulfide minerals, not only because of its economical importance as a tin ore, but also because of its structural and physical characteristics. The Zn-analogue Kesterite, Cu_2ZnSnS_4, is closely related, but assigned to a different space group ($I\bar{4}$). The both structures are topological identical, but differ in the distribution of the metal atoms. In particular, in the Stannite structure Fe is located at the origin (2a) and Cu at 4d (0, ½, ¼). On the other hand in the Kesterite structure, Cu occupies the 2a (0, 0, 0) and 2d (0, ¼, ¾) position, Zn is located at 2c (0, ½, ¼). Owing to the different populatopn at 2c and 2d, the mirror plane parallel to (110) is lost, resulting in space group $I\bar{4}$. In both structures, Sn is located at 2b (0, 0, ½), the sulfur atoms lie on the (110) mirror plane at 8i (x, x, z) for Stannite and 8g (x, y, z) for Kesterite respectively. Thus the both structures are based on different distributions of Cu, Zn and Fe among the crystallographic positions (0,0,0), (0,½,¼) and (0,¼,¾).

The studies presented here deal with the join between Kesterite and Stannite, $Cu_2Zn_xFe_{1-x}SnS_4$. Structural studies of this series were done up to now using X-ray diffraction, notwithstanding the problem of the electronic similarity of the elements Cu, Zn and Fe. The powder samples were prepared by solid state reaction of the elements in sealed evacuated silica tubes at 750°C. The chemical composition was determined using an electron microprobe (Cameca SX 100) where $CuFeS_2$ and ZnS have been used as standards.

Neutron powder diffraction experiments were performed at the high resolution powder diffractometer E9 (λ=1.797 Å). Structural parameters were obtained by Rietveld analysis (FullProf software package) of the data using the space groups $I\bar{4}2m$ and $I\bar{4}$ as structural model.

The lattice parameter (Fig. 1) depend linear on the chemical composition, showing the transition from $I\bar{4}2m$ to $I\bar{4}$ occurs between 0.6<x<0.8

Figure 2 shows, that for 0<x<0.5 Zn may occupy the Fe site (2a) only, but with higher Zn content some Zn occupies the Cu site (4d) too. The constant behaviour of the latter for x>0.5can be explained by a Cu Fe anti site occupation (note that $b_{Fe}>b_{Cu}>b_{Zn}$). A simultaneous refinement of neutron and X-ray powder diffraction data is ongoing, which will strengthen this results.

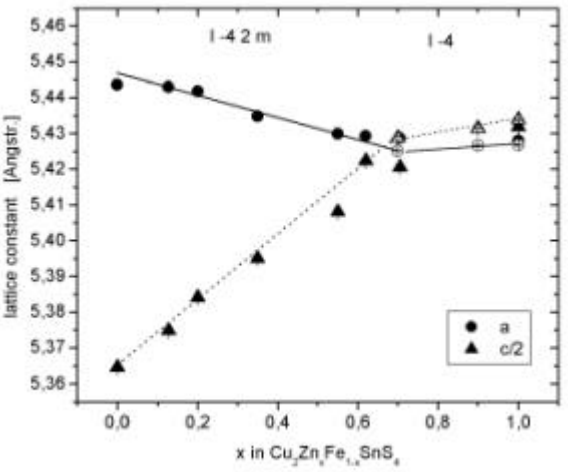


Figure 1: Lattice parameter of $Cu_2Zn_xFe_{1-x}SnS_4$ in dependence on the chemical composition. Open symbols refer to the sg $I\bar{4}$, the lines should guide the eye.

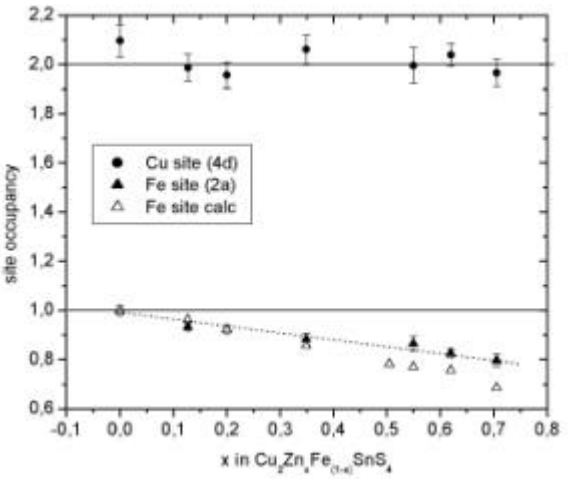


Figure 2: Occupancy of the 4d and 2a position within the sg $I\bar{4}2m$. The calculated occupancies refer to the assumption that Zn occupies the 2a site only.

	EXPERIMENTAL REPORT **Phase diagram of $Sr_{(x)}Ba_{(1-x)}TiO_3$ solid solutions**	Proposal N° PHY-01-1575 Instrument E9 Local Contact M. Tovar
Principal Proposer: Experimental Team:	A. Naberezhnov, PTI S-Petersburg, Russia E. Smirnova PTI S-Petersburg, Russia M. Tovar, HMI Berlin	Date(s) of Experiment 16/09 – 20/09 2004

Date of Report: 26/12/2004

$SrTiO_3$ (STO) is so-called incipient (virtual) ferroelectrics with extrapolated Curie-Weiss temperature T_0 ~ 40 K. However the ferroelectric phase transition (PT) is not achieved in this compound due to quantum fluctuations playing an important role in the suppression of PT. At the same time STO shows also antiferrodistorsive (AFD) instability due to the rotation of BO_6 octahedra, resulting in the PT at 105 K with doubling of unit cell. Energy difference between paraelectric, ferroelectric (FE) and AFD states are very small. This is the reason why quantum fluctuations can stabilize the paraelectric phase against the ferroelectric one.

It has been shown that Ca, Pb and Cd impurity ions in A-sublattice indeed induce the ferroelectric PT with a very small critical concentration (quantum limit) x_c of about 0.002. In the most interesting and practically important case of Ba impurities the data are contradictory and the value of x_c given by different authors varied from 0.002 to 0.09.

Recent dielectric and ultrasonic studies [1] has shown that the critical concentration x_c of ferroelectric state in $(1-x)SrTiO_3$ - x $BaTiO_3$ (SBT) is equal to about 0.015. Crossover to normal ferroelectric state takes place at the Ba concentration about 4% (0.04) and three ferroelectric PTs (cubic-tetragonal-orthorhombic-rhombohedral) were observed in this system for x>0.06. At x = 0.06 there is only one AFD PT and this PT is accompanied by the change of specific heat and elastic constants. It was found that AFD phase transition disappears above x_{c1}=4%, when the line of the AFD transitions crosses the line of the ferroelectric transitions. However these results are in a contradiction with the data of Ménoret et al [2], who performed combined neutron diffraction and dielectric study of SBT systems and proposed the phase diagram with $x_c=x_{c1}$=0.09.

To clarify the situation we have studied the temperature evolution of the intensity and the lineshape of peaks in Bragg and superstructure positions (h+½ k+½ l+½) at x=0.02 in the temperature span 5 K – 160 K and at x=0.04 from 5 K up to 70 K (for lack of beam time) at λ= 1.79738 Å. It is known that below temperature of AFD PT the intensity of superstructure peaks is proportional to the square of the order parameter and in a case of the suppressed PT diffuse scattering gives the information about the short range AFD correlations.

The principal results are:

1 – For SBT with x=0.02 (SBT2) we did not observe any traces of AFD PT at 60 K as it follows from the paper [1]. According to our data the temperature of this PT is of about 100 K and agrees with the result of the paper [2].

2 – In a vicinity of several Bragg peaks we have observed the intensive and temperature independent (in the range 5 K – 120 K) diffuse scattering. At present time the origin of this scattering is not clear but possibly it appears due to elastic strains.

3 – For SBT with x=0.04 (SBT4) at low temperature the intensity of scattering in superstructure positions was essentially smaller than we have expected based on the results of paper [2]. The weak superstructure peaks we have observed up to 45 K, but at 70 K the structure corresponds to the high temperature paraelectric structure of SBT2. In temperature diapason 5 – 45 K we did not observed any visible modification of Bragg peak lineshape pointed out of ferroelectric PT. This result is in agreement with paper [1] and our result obtained for SBT with x=0.06 at 1.5 K [3].

It is absolutely clear that for comprehension of current situation it is necessary to study the temperature evolution of structure SBT solid solutions at x = 0.03, 0.06-0.07 and 0.12.

References

1. A.V. Sotnikov, E.P. Smirnova, V.V. Lemanov, R. Kunze, and M. Weihnacht, Journal of Conference Abstracts (Cambridge), v.8 (1), 318 (2003)
2. C. Ménoret, J.M. Kiat, B. Dkhil, M. Danlop, Y. Dammark, and O. Hernandez, Phys. Rev. B65, 224104 (2002)
3. A.I. Beskrovny, S.B.Vakhrushev, A.I.Kurbakov, A.A.Naberezhnov,N.M.Okuneva,E.P.Smirnova, Neutron diffraction study of the $Sr_{0.98}Ba_{0.02}TiO_3$ solid solution structure, 2nd European Conference on Neutron Scattering, 1-4 September 1999, Budapest, Hungary

	EXPERIMENTAL REPORT	
BENSC	**Crystal structure and vacancies order in chalcopyrite related semiconductors CuX_nY_m** **(X=In, Ga; Y=S, Se; *n*=1, 3, 5; *m*= 2, 5, 8)**	Proposal N° EF Instrument **E9** Local Contact J. Hernández-Velasco
Principal Proposer: Experimental Team:	D. Fuertes-Marrón, SE2 HMI Berlin J. Hernández-Velasco, SF2-BENSC HMI Berlin *current address:* F.CC.Químicas Univ.Complutense Madrid	Date(s) of Experiment 30/31.3.04 & 9.8.2004

Date of Report: 15.2.2005

$CuInSe_2$ and $CuGaSe_2$ are materials of high interest in the field of thin-film photovoltaics and solar cell applications, which have demonstrated high conversion efficiencies. It has been reported that ordered vacancy chalcopyrite type CuX_3Se_5 layer exists in the surface of the $CuXSe_2$ films and it is responsible of enhancing the properties of photovoltaic devices. X-ray and electron diffraction studies have shown the presence of forbidden reflections for the basic $CuXSe_2$ structure in the richest X phases, however unambiguous determination of the crystal framework in CuX_3Se_5 has not been carried out. Thus the goal of the experiment is to study the structural properties of selected members of the so-called "ordered-vacancy (also ordered-defect) compounds" of I-III-VI_2 Cu-containing chalcopyrites. Whereas theoretical studies led to postulate the existence of an internal stabilisation mechanism in Cu-poor I-III-VI_2 by periodic arrangement of defect pairs, held as ultimate responsible for experimentally found deviations from ideal 1:1:2 stoichiometry towards 1:3:5 or 1:5:8 compositions of such samples, while maintaining the chalcopyrite structure, the analysis of XRD results reported so far does not exclude other possibilities. Recently published EXAFS studies on $CuIn_3Se_5$ report on its chalcopyrite structure, claiming cation-anion site disorder as responsible for the discrepancies in bond-lengths in earlier studies. Our study is aimed to extend the structural analysis to $CuGa_3Se_5$, $CuGa_5Se_8$, $CuIn_3Se_5$, and $CuIn_5Se_8$ combining Neutron diffraction data with XRD, LEED, AES and STM measurements using Synchrotron radiation.

Cu-containing chalcopyrites (hereafter CIGS) are direct semiconductors with high absorption coefficients and energy gaps ranging between 1-2 eV, well suited to be used as p-type absorber layers in nowadays topmost efficient solar cell devices based on thin-film technology (approaching 20 % energy conversion efficiency from heterostructures of the type Mo/CIGS/CdS/ZnO). The main functional heterojunction CIGS/CdS plays indeed a central role in the performance of chalcopyrite-based solar cells. It was proposed that the electrical p-n junction of such devices actually lies buried in the absorber, the surface of which is in turn inverted into n-type by the formation of an ordered vacancy compound, with composition in the 1:3:5 range. Since then, experimental proof of the existence of such compounds, since long time postulated, were reported both as crystalline and polycrystalline samples, see. Fig. 1. The physical relevance of such phases lies also in connection with the activation of self-compensation mechanisms showing up in CIGS, as a function of the position of the Fermi level in the energy gap with respect to an absolute energy scale. This phenomenon is central for the understanding of the electronics (including doping) of these compounds, largely dominated by native defects. Acceptor-like V_{Cu} is considered the main responsible for the p-type doping, and according to the accepted model, the enthalpy of formation of such point defect decreases (and eventually becomes negative, i.e. leading to spontaneous formation) as the amount of certain group-III-antisite-donor-like point defects increases. As a result, Cu-poor compositions (*i.e.* 1:3:5) would be favoured. This self-compensation mechanism is believed to prevent the achievement of n-type conductivity in $CuGaSe_2$ (CGSe) by native doping, as spontaneous formation of acceptors balances out whatever minor tendency towards donor-like defect formation, keeping the Fermi level lying within the lower half of the band gap (thus preserving p-type). Indeed, no evidence of n-type conductivity has been found so far for the particular case of $CuGa_3Se_5$ single crystals. For these reasons, it appears thus attractive to combine both issues, namely the formation of phases at the near-surface region showing compositions close to that of 1:3:5 compounds, and the self-compensation mechanism leading to a rearrangement of the native-defect chemistry of the material, in a single model accounting for the experimental findings. In order to look for such link, the basic knowledge of the structural and electronic properties of 1:3:5 and 1:5:8 "defect compounds"is mandatory. In this sense, the analysis in progress of the neutron diffraction measurements on the bulk materials (see Figure 1 below) could help to the straightforward determination of subtle details in the crystal structure.

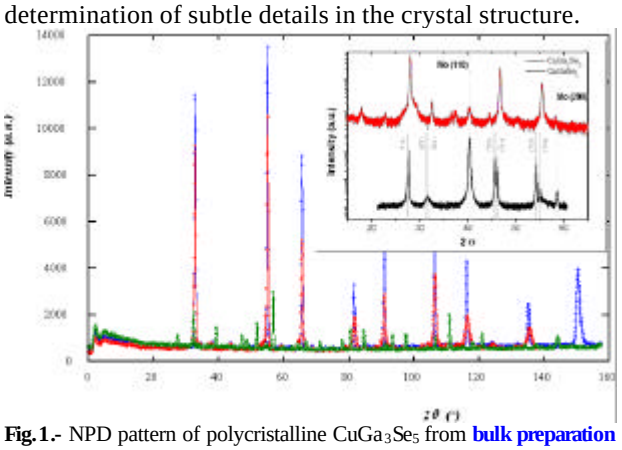


Fig.1.- NPD pattern of polycristalline $CuGa_3Se_5$ from **bulk preparation** and from **powder of CVD** removed from glass foils. Non isostructural sulphide $CuIn_5S_8$. **Inset:** XRD spectra of $CuGaSe_2$ thin films grown on Mo-coated glass substrates (in log-scale). Lower scan: standard slightly Ga-rich film, as used for solar cells. Upper scan: sample grown under high Ga-excess, with a composition in accordance with $CuGa_3Se_5$, revealing superstructure-associated peaks and the absence of the characteristic doublet reflections (220)/(204) and (312)/(116).

EXPERIMENTAL REPORT

Study of paramagnetic crystals of family $A_2CuCl_4 \cdot 2H_2O$ (A = NH_4, K, Rb) – A combination of quasielastic neutron scattering with broadband dielectric spectroscopy

Proposal N°: EF
Instrument: V3
Local contact: A. Buchsteiner

Principal proposer: A. Buchsteiner, HMI Berlin
Experimental team: A. Buchsteiner, HMI Berlin
M. Slaboszewska, Institute of Physics, Adam Mickiewicz University, Poznan

Date(s) of Experiment: 12.07. – 17.07.2004

Date of report: 06.01.2005

The crystal family $A_2CuCl_4 \cdot 2H_2O$ (A = NH_4, K, Rb) has a very interesting structure with the Cu ion at the centre of a distorted octahedron being bonded to two water molecules, two short-bonded Cl atoms and two long-bonded Cl atoms.

Single crystals of $(NH_4)_2CuCl_4 \cdot 2H_2O$ show a strong anomaly in their dielectric dispersion, whereas a Debye dispersion was observed for other members of the crystal family. Additionally, samples cut out perpendicular to the tetragonal axis show a huge dielectric dispersion, but samples which were cut out parallel to the tetragonal axis do not.

While $(NH_4)_2CuCl_4 \cdot 2H_2O$ has two energetically equivalent configurations, $K_2CuCl_4 \cdot 2H_2O$ and $Rb_2CuCl_4 \cdot 2H_2O$ are isostructural crystals.

With decreasing temperature the ordering of the NH_4^+ tetrahedra has been observed [1].

We wanted to show, that the abnormal dielectric behavior can be related to the diffusive motions of protons.

The crystal structure of $(NH_4)_2CuCl_4 \cdot 2H_2O$ has been determined at room temperature by X-ray and neutron diffraction [2].

In order to enlighten the reason for the orientation dependent effects we measured deuterated and non-deuterated single crystals in two different orientations, [100] and [001], respectively, each orientation at 3 temperatures: 210 K, 250 K, 320 K, plus additionally at 5 K to get the resolution function.

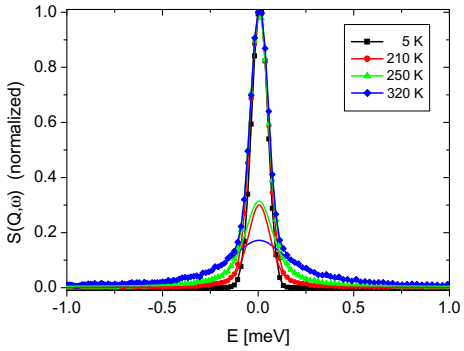
The measurements were done with a resolution of about 93 μeV (FWHM).

All data showed a distinct quasielastic broadening. For a first analysis we fitted all data with a phenomenological model consisting of a single Lorentzian function convoluted with the Gaussian resolution function plus an additional constant background. The quasielastic contribution was Q-independent, thus resulting from localized motion, see the figure at top right for an example.

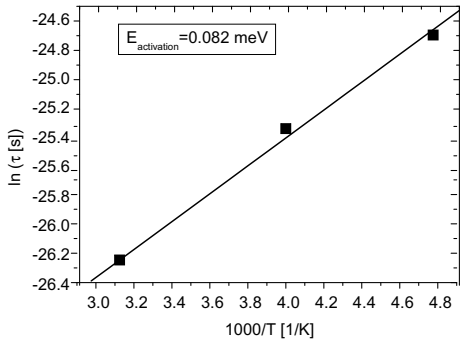
As the broadening is present in the H_2O samples and in the D_2O samples as well with identical parameters, the quasielastic contribution stems probably from the rotation of the NH_4-groups. This contribution was present for all samples and all orientations.

We will try to apply a model of n-fold jumps on a circle, probably with n=4, to prove this assumption.

Contrary to our expectations, we did not find any orientation dependent effect for all the above described measurements. We did also not see any translational diffusion of water in any of the crystals.



The widths of the quasielastic contribution were the same for all samples and showed an Arrhenius like temperature behavior (210K: 0.035 meV, 250K: 0.065 meV, 320K: 0.165 meV (half-width half-maximum); times: 18.9 ps, 10.1 ps, 4 ps).



To check if there are different motions in a different time window, we did one measurement with a broader resolution of about 287 μeV. We found another motion (0.24 meV), but again a clearly localized one. Also with this resolution we did not see any orientation dependency.

Up to now, we could not clarify where the strong orientation dependency could come from, which was found for the dielectric properties.

We plan to further investigate the system with Raman scattering to get more information about the motions of the NH_4^+ ions.

[1] H. Suga et al., Bull. Chem. Soc. Jap. **38** (1965) 1007
[2] R. Chidambaram et al., Acta Cryst. B **26** (1970) 827
[3] M. Slaboszewska et al., Ferroelectrics, in press

	EXPERIMENTAL REPORT **Surfactant Aggregate Structure in SBA-15 Silica Nanopores**	Proposal N° CHE-04-0935 Instrument **V4** Local Contact Uwe Keiderling
Principal Proposer: Experimental Team:	Gerhard H. Findenegg, TU Berlin Gerhard H. Findenegg, TU Berlin Taegyu Shin, TU Berlin U. Keiderling, HMI Berlin	Date(s) of Experiment 21.-25. Jan 2004

Date of Report: 25. March 2004

We are studying the structure of surfactant aggregates in the pores of SBA-15, a periodic mesoporous silica with two-dimensional (2D) hexagonal arrangement of cylindrical pores of uniform size (pore radius ca. 4 nm). Two alternative structural scenarios were envisaged: (i) surface micelles that are loosely attached to the silica surface, or (ii) an adsorbed layer of uniform thickness that is strongly coupled to the pore walls.

Samples were prepared by contacting the silica powder with a surfactant ($C_{12}E_5$ or $C_{12}G_1$) and a H_2O/D_2O mixture of a scattering length density (SLD) equal to that of the silica matrix. In "mixing-type" samples, surfactant loadings corresponding to the plateau of the adsorption isotherm in SBA-15 were chosen. Lower surfactant loadings were reached by subsequent equilibration with known amounts of the H_2O/D_2O solvent ("washing-type" samples). A new aluminium cell suited for samples of a paste-like consistency was tested. It was found to be very suitable for these measurements.

Our SANS experiments furnished the following results: (i) The Bragg peaks caused by the regular pore structure of the SBA-15 matrix are completely quenched when the pore space is filled with a contrast matching H_2O/D_2O mixture (SLD ρ_0 = $3.7x10^{10}$ cm^{-2}) (Fig. 1, lower curve); (ii) The most prominent Bragg peaks of SBA-15 reappear when the surfactant is adsorbed in the pore space: In the example shown (Fig. 1 upper curve), the (*11*) peak at 1.112 cm^{-1} becomes almost equally strong as the (*10*) peak at 0.642 cm^{-1}. This indicates that the pore walls are decorated by the surfactant and implies that the surfactant is forming an adsorbed layer. Significant changes in I(q) occur when the contrast-matching H_2O/D_2O was replaced by pure D_2O (ρ_0 = $6.5x10^{10}$ cm^{-2}): In particular, the first peak is enhanced relative to the second peak.

Specific differences in the scattering curves were found between the surfactants $C_{12}E_5$ or $C_{12}G_1$. However, this may be due in part to difficulties in sample preparation with the glucoside $C_{12}G_1$.

We adopt the "three-density-level" model of ref. 1 to simulate the scattering curves, where ρ_0, ρ_1 and ρ_2 denote the SLD of the liquid core, adsorbed film and matrix, resp., assuming sharp changes in SLD at the radii r_1 (core radius) and r_2 (pore radius), with $h = r_2 - r_1$ the film thickness. This simplistic model accounts for the observed differences in I(q) between D_2O and H_2O/D_2O in terms of the form factor of a core-shell cylinder, which exhibits pronounced minima at certain values of q (Fig. 2): For ρ_0 = $3.6x10^{10}$ cm^{-2} (a value close to the SLD of the contrast matching H_2O/D_2O), the first minimum of the form factor appears close to the first Bragg peak of SBA-15, but this minimum in the form factor is missing for ρ_0 = $6.5x10^{10}$ cm^{-2} (pure D_2O), which immediately explains the observed differences in the intensities of the (10) and (11) Bragg peaks.

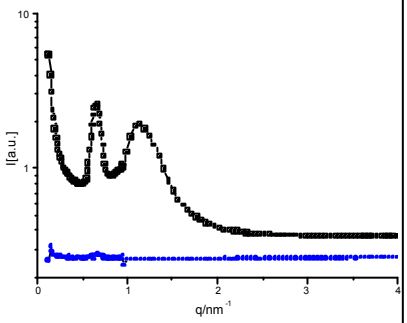


Fig. 1. I(q) for SBA-15 immersed in contrast-matching H_2O/D_2O mixture (lower curve); I(q) for SBA-15 sample loaded with surfactant in the same H_2O/D_2O solvent mixture (upper curve)

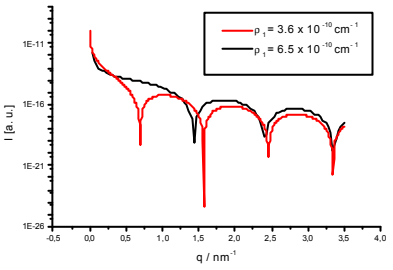


Fig. 2. Effect of SLD of core (ρ_0 = 3.6 or 6.5) on I(q) of a core-shell cylinder: r_1, r_2 = 3, 4 nm, ρ_1, ρ_2 = 1.5 and $3.7x10^{10}$ cm^{-2}

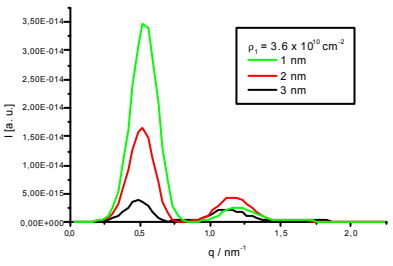


Fig. 3. Simulation of I(q) for surfactant films in SBA-15 (r_2 = 4 nm), film thickness h = 3, 2, 1 nm SLD: ρ_0, ρ_1, ρ_2 = 3.6, 1.5, $3.7x10^{10}$ cm^{-2}

(1) M. Impéror-Clerc, P. Davidson , A. Davidson, *J. Am. Chem. Soc.* **122** (2000) 11925

BENSC	**EXPERIMENTAL REPORT** **Surfactant Aggregate Structure in SBA-15 Silica Nanopores**	Proposal N° CHE-04-1011 Instrument **V4** Local Contact Uwe Keiderling
Principal Proposer: Experimental Team:	Gerhard H. Findenegg, TU Berlin Gerhard H. Findenegg, TU Berlin Taegyu Shin, TU Berlin U. Keiderling, HMI Berlin	Date(s) of Experiment 26 – 29. Jul 2004

Date of Report: 17. September 2004

We are studying the self-assembly of surfactants in the pores of SBA-15, a periodic mesoporous silica with two-dimensional (2D) hexagonal arrangement of cylindrical pores of uniform size, using SANS. As an extension of our first experiment [1] we now investigated the influence of surfactant head group size and shape on the self assembly in the pores. Three nonionic surfactants of equal alkyl chain length, viz. decyl penta(ethylene glycol) ($C_{10}E_5$), decyl glucoside ($C_{10}G_1$) and decyl maltoside ($C_{10}G_2$) were studied in SBA-15 materials of pore diameter ca. 8 and 9 nm.

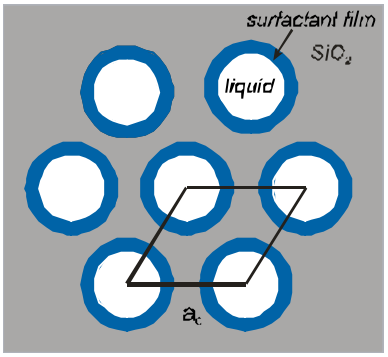


Fig. 1: Model of a 2D hexagonal array or cylindrical pores with an adsorbed surfactant film an the pore walls.

SANS curves of SBA-15 samples in D_2O exhibit Bragg peaks caused by the periodic pore structure of SBA-15. The intensities of the individual peaks are changed in a characteristic way by the adsorption of the surfactant, which may form either a uniform film or discrete surface aggregates at the pore walls. Fig. 2a compares SANS curves for SBA-15 equilibrated with $C_{10}G_1$, $C_{10}G_2$ and $C_{10}E_5$. The former two, which are weakly adsorbed, cause no significant changes of the peak intensities of SBA-15. $C_{10}E_5$, which is strongly adsorbed, causes a significant decrease in the intensity of the first Bragg peak (*10*) and strong enhancement of the second peak (*11* and *20*). When D_2O is replaced by a H_2O/D_2O mixture of equal scattering length density as the silica matrix (Fig. 2b) the scattering curve for $C_{10}G_2$ resembles that of a micellar solution of this surfactant [2], suggesting the existence of isolated surface micelles in the pores.

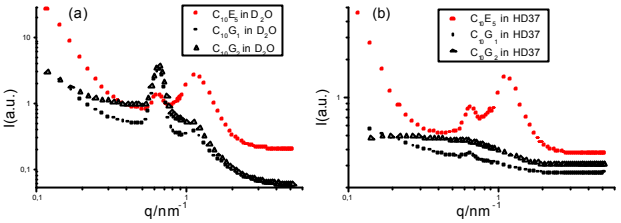


Fig. 2. SANS curves for SBA-15 equilibrated with the surfactants $C_{10}G_1$, $C_{10}G_2$ and $C_{10}E_5$: (a) in D_2O; (b) in contrast-matching H_2O/D_2O.

The SANS curves are analysed in terms of a model function I(q) which combines the structure factor of the 2D hexagonal assembly of pores with a form factor of the surfactant aggregates. For the strongly adsorbed surfactants $C_{10}E_5$ and $C_{12}E_5$ the form factor of a core-shell cylinder [3] was adopted to model a uniform surfactant film at the pore walls. In this three-phase model the parameters $?_1$, $?_2$ and $?_3$ denote the scattering length densities (SLD) of the liquid core, adsorbed film and silica matrix, and we assume sharp changes in SLD at r_1 (core radius) and r_2 (pore radius), with $r_2–r_1$ = h the film thickness. As seen in Fig. 3, this model reproduces the main features of the experimental SANS curves in both contrast scenarios. Specifically, it accounts for the observed enhancement of the second Bragg peak relative to the first peak in the case of strong adsorption. A quantitative analysis of all SANS data is in progress.

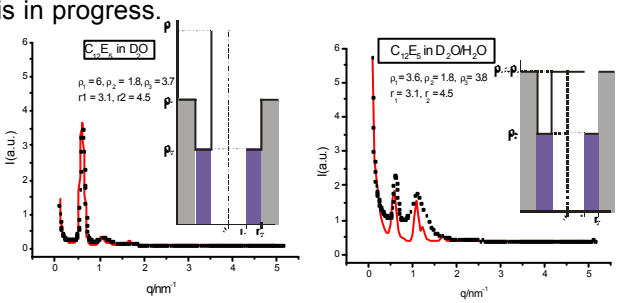


Fig.3 SANS curve with corresponding form factor model (core-shell cylinder) [3] for $C_{12}E_5$ in D_2O (left) and H_2O/D_2O (right)(!:experiment, _:fitting)

[1] G.H. Findenegg, T.G. Shin, BENSC Experimental Report 2004, CHE.04-0935

[2] A. Möller, P. Lang, G.H. Findenegg, U. Keiderling, *J. Phys. Chem. B* **102** (1998) 8958

[3] M. Impérort-Clerc, P. Davidson, A. Davidson, *J. Am. Chem. Soc.* **122** (2000) 11925

BENSC	**EXPERIMENTAL REPORT** **NRSE Investigation of Phonon Lifetimes in the conventional Superconductor Nb**	Proposal N° PHY-02-438 Instrument V2-NRSE Local Contact K.Habicht
Principal Proposer: Experimental Team:	K. Habicht, F. Mezei, HMI Berlin T. Keller, MPI f.FKF, Stuttgart, FRM-II,Garching B. Keimer; MPI f. FKF, Stuttgart S. Bayrakci; MPI f. FKF, Stuttgart K. Habicht; HMI Berlin; TU-Darmstadt	Date(s) of Experiment 04.05.– 09.05.2004

Date of Report: 03.01.2005

Within the standard BCS theory of superconductivity, interactions between electrons and phonons play a fundamental role. The phonons with energy less than twice the superconducting energy gap 2Δ show an abrupt change in lifetime as the temperature passes through the transition temperature T_C, as has been confirmed by standard inelastic neutron scattering experiments in a few favorable cases [1, 2].

The neutron resonance spin-echo technique (NRSE) is well suited to overcome the resolution limits of the standard spectroscopic techniques, since it can resolve energy transfers within the resolution ellipsoid of a background three-axis spectrometer. Phonons relevant for the electron-phonon interaction are usually dispersive, so the spin-echo focusing technique with tiltable fields must be used.

The experiment performed was an extension of previous NRSE measurements on single-crystal niobium. Though being well studied with respect to its phonon dispersion as well as the change of linewidth at T_C = 9.2 K for selected TA phonons [2], the contribution to the electron-phonon interaction at lower phonon wavevectors q is impeded due to lack of wavevector-resolution. The experimental results reported here protrude into a q-range inaccessible with conventional TAS spectroscopy.

As in the previous experiment, the TAS was operated in a configuration with scattering senses (SM=-1, SS=-1, SA=+1) in order to minimize the effects of the curvature of the dispersion surface. The transverse Q-resolution was about 0.015 • $^{-1}$ FWHM at fixed incident k_i = 2.0 • $^{-1}$. Second- order contamination is substantially suppressed by the curved neutron guide. No additional collimators were used.

The required tilt angles of the RF coils were calculated from Born-von-Kàrmàn fits to data taken in previous experiments. For the [0.025 0.025 0] T_1 phonon investigated, tilt angles θ_1 = -31.3° and θ_2 = 27.4° were used. A cylindrical crystal (10 mm diameter, 30 mm long) was mounted with the [100] axis perpendicular to the scattering plane.

Fig. 1 displays the temperature dependence of the phonon linewidth as obtained from the raw data normalized to the polarization measured in the direct beam. No correction for sample mosaicity was applied. The new data rules out the possibility that the change of linewidth 2Γ = 60(26) μeV with temperature is related to anharmonic effects.

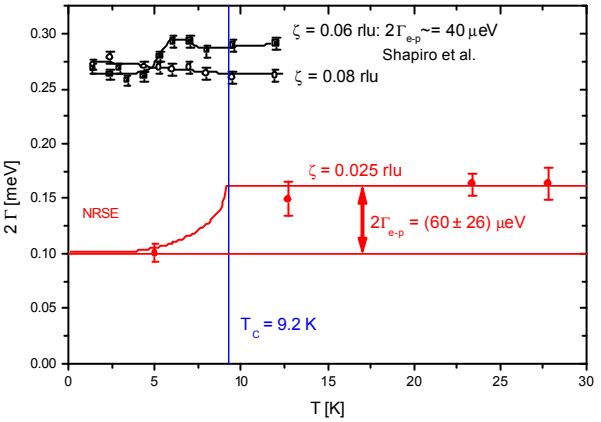


Fig. 1: Linewidth of the [0.025 0.025 0] T1 phonon as a function of temperature. NRSE data (full circles, red) in comparison to the data of [2] (full squares and open circles, black). Below T_C the line through the NRSE data represents the temperature dependence of the linewidth as given by Bobetic [4]; above T_C the linewidth is assumed to be constant.

[1] J.D. Axe, G. Shirane, Phys. Rev. Lett. **30**, 6, 214 (1973).
[2] S.M. Shapiro *et al.*, Phys. Rev. B **12**, 11, 4899 (1975)
[3] K. Habicht, R. Golub, T. Keller, J.Appl.Cryst. **36**, 1307 (2003)
[4] V.M. Bobetic, Phys Rev., **136**, A 1535 (1964).

BENSC	**EXPERIMENTAL REPORT** **Phonon dispersion in the martensitic phase of ferromagnetic Ni_2MnGa**	Proposal N° PHY-02-440 EF Instrument **V2/FLEX** Local Contact Peter Vorderwisch
Principal Proposer: Peter Vorderwisch, HMI Berlin Experimental Team: Stephen M. Shapiro, Brookhaven Nat. Lab.		Date(s) of Experiment 13. - 21. July 2004

Date of Report: 10 January 2005

The ferromagnetic shape-memory alloy Ni_2MnGa undergoes a martensitic transformation which, for compositions close to stoichiometric, is from a cubic Heusler (austenite) structure to a tetragonally distorted and twinned (martensite) structure with c/a = 0.94.

The phonon dispersion curves measured in the austenite phase exhibit a pronounced softening in the transverse acoustic TA_2 branch, at a wave vector **q**=ζ[110] where ζ ≈ 0.33, which is a precursor to the transition.

In the tetragonal martensite phase, the corresponding branch (in [110] direction) shows a (less pronounced) anomaly at a wave vector ζ ≈ 0.4, whereas no anomaly has been observed in [101] direction.

Recent ab initio calculations [1] of the phonon dispersion relation (at zero temperature) in the austenite and martensite phase confirm the phonon instabilities in [110] directions. For the [101] direction, however, the calculated phonon dispersion predicts a kink in the TA_2 branch at ζ≈0.4 (arrow in Fig.1). We extended the previous experiment [2], with a sample of stoichiometric composition, in search of this anomaly.

As in previous experiments a magnetic field is used to produce a single martensite variant. Experimental data, obtained with the horizontal-field magnet HM1, are shown in Fig. 2. Within experimental accuracy, the predicted 'kink' cannot be observed. Further experiments to measure the acoustic branches (using thermal neutron triple-axis-spectrometry) out to the zone boundary are in progress.

[1] C. Bungaro et al., Phys. Rev. B 68 (2003) 134104

[2] BENSC Experimental Reports 2003, HMI-B 565, p. 74

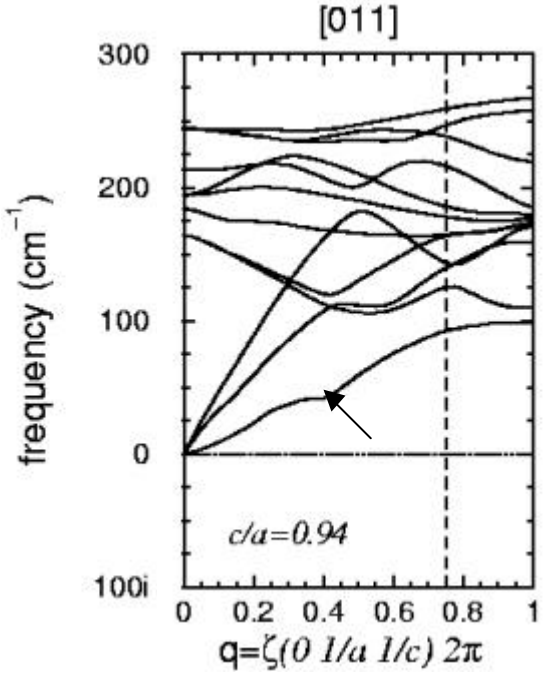


Fig. 1 *Ab initio* calculation of the phonon dispersion along the [101] direction (at T=0) in the martensite phase [1]. The TA_2 branch is that with lowest frequency.

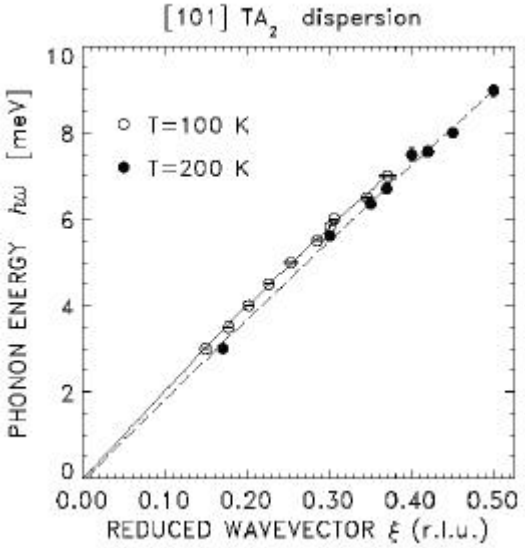


Fig. 2 Experimental phonon dispersion for the TA_2 branch along the [101] direction at T=100 K and T=200 K

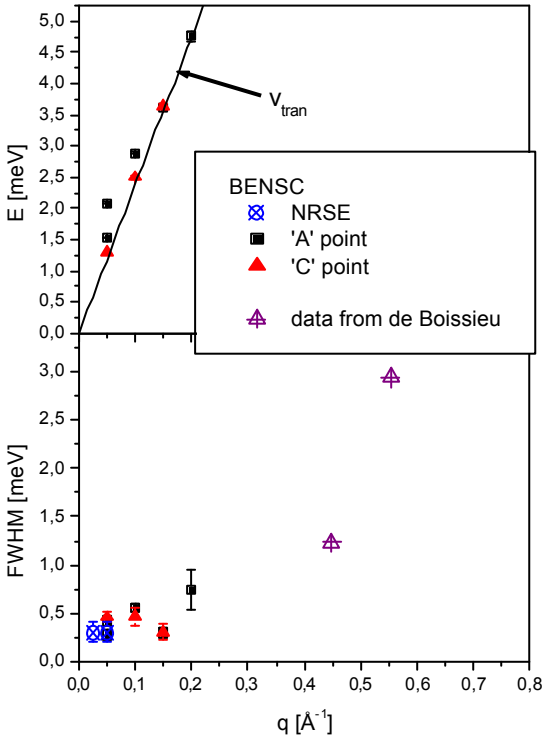
BENSC	**EXPERIMENTAL REPORT** **Triple Axis Study of the Intrinsic of Phonons in i-AlPdMn**	Proposal N° PHY-02-372 Instrument **V2** Local Contact K.Habicht
Principal Proposer: Experimental Team:	**R. A.Brand, Universität Duisburg-Essen** **K. Habicht, HMI Berlin** **T. Keller, MPI Stuttgart**	Date(s) of Experiment Feb. 16-25, 2003

Date of Report: 16/02/2005

We have studied the acoustic phonon lifetimes at small reduced scattering vector *q* in the icosahedral quasicrystal i-AlPdMn. The sample used has previously been prepared at Jülich and used in the thesis of N. Schramchenko [4]. We have measured the lifetime of the TA mode at small reduced *q* starting from the (18,29) reflection along the 5-fold axis at room temperature.
Previous triple-axis inelastic neutron scattering [1] and our own inelastic x-ray scattering experiments [2] have shown that the longitudinal acoustic (LA) phonon linewidth G is not measurably broadened for small *q*, but that it becomes very large for *q* larger than about 0.4 nm. We found that the transverse acoustic (TA) linewidth increases quadratically with *q*. We performed a neutron resonant spin echo (NRSE) experiment previously to study the limit of small-*q* region. We used the triple-axis instrument V2 at the Hahn-Meitner Institute with NRSE option [3]. This resulted in the following partial results:

- The NRSE-determined mosaic spread of our sample at this reflection is about 4.38' ± 0.03', showing the very high quality of the sample.
- The correlation time determined at q =0.025 and 0.050 $Å^{-1}$ was about 4 ps, equivalent to about a linewidth of 0.3 meV.
- .This linewidth is larger than that expected from previous INS experiments [1], and because of the ample quality it cannot be due to the mosaic spread.

In this experiment we used V2 in the usual triple-axis mode in order to study the region between the NRSE result and the results of de Boissieu. We were able to study at two different reflections, denoted in the Fig. 1 as A an C. The comparison with the results of de Boissieu shows that there is a smooth variation in the linewidth starting at about 0.25 meV near zero q increasing roughly quadratically.



[1] M.de Boissieu et al., J.Phys. Conden. Matter **5** (1993) 4945.
[2] M.Krisch et al., Phys. Rev. B **65** (2001) 134201.
[3] R. Gähler et al, Physica B **180-181** (1992) 899.
[4] N.Shramchenko, thesis, LLB, CEA Saclay, Gif sur Yvette, 2001

	EXPERIMENTAL REPORT **Study of the Aromatic H-bond in NH_4- and ND_4-Tetraphenylborate**	Proposal N° EF Instrument **V3** Local Contact Margarita Russina
Principal Proposer:	Niina Jalarvo, HMI Berlin	Date(s) of Experiment
Experimental Team:	Arnaud Desmedt, CNRS - Université de Bordeaux I Ruep Lechner, HMI Berlin Ferenc Mezei, HMI Berlin	26.7.2004-1.8.2004 18.9.2004-21.9.2004

Date of Report: 8.1.2005

With respect to the aromatic hydrogen bonds, tetraphenylborate salts are a particularly interesting substance class. The simplest member of this category, ammonium tetraphenylborate $NH_4B(C_6H_5)_4$ (hereafter called ATPB), represents a prototypical system to understand aromatic H-bonds.

Previously quasielastic incoherent neutron scattering (QENS) experiments have been performed with ATPB sample in temperature range 20-300K, with energy resolutions of 50μeV, 100μeV and 200μeV [1]. The quasielastic component has been explained considering models for ammonium ion reorientations. However, an additional narrow quasielastic component at the higher temperatures (T>200K), has been observed. Our suggestion is that it might originate from phenyl ring motions. The goal of the present experiment was to investigate the origin of this additional quasielastic component using the deuteration of the ammonium ion in ATPB as a tool.

We have measured both ATPB and ATPB-d4 (the latter is the ammonium deuterated sample) in temperature range from 150K to 350K. The used experimental energy resolutions were 100μeV and 30μeV with the exposure times of 12h and 24h respectively.

The deuteration percentage of the ammonium ions in ATPB-d4 was found to be 77% from the QENS data. Thus the quasielastic component originating from ammonium ion reorientations is markedly weakened, as can be noticed from figure 1, where the quasielastic spectra of the ATPB-d4 (b) and, for comparison ATPB (a) are shown. We have reproduced the QENS data with a model including a contribution for ammonium ion rotations around a C2-axis and another contribution for phenyl ring torsions. The phenyl ring torsions have been described as a twist around a rotation axis (which passes through two opposite corners of the hexagonal shaped phenyl ring) by angle α. Since with the used energy resolution the neutron flux was relatively weak, we have grouped the spectra from all the angles together in order to obtain better statistics. This excludes the possibility to study the Q-dependence of the phenyl ring motions, which could provide additional information. However, the fitted model is in good agreement with the experimental data, giving a value α=7.4°±2° for the twist angle.

[1] Jalarvo et al. BENSC Experimental Reports 2002. Dynamics of the aromatic H-bond in ATPB.

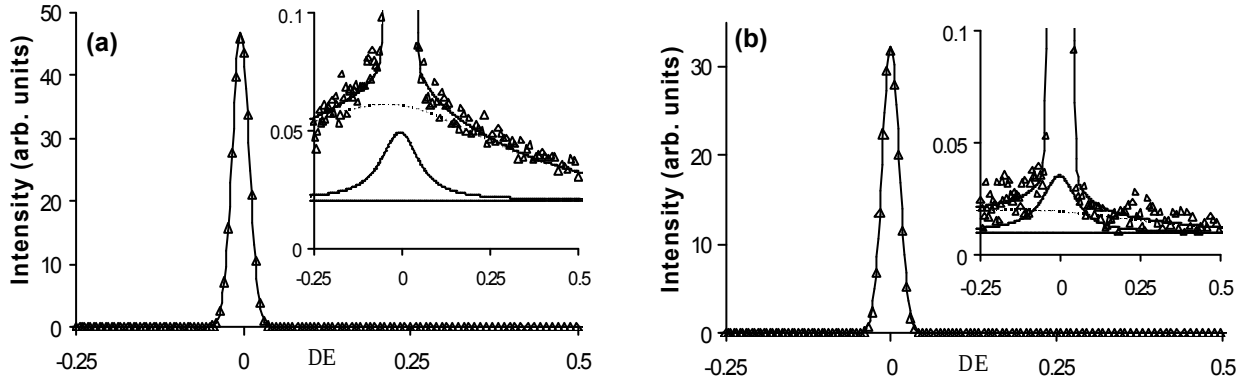


Figure 1. *The QENS spectra of ATPB (on the left hand side) and ATPB-d4 (on the right hand side), at T=300K and at DE=30meV. The spectra from all angles were grouped together in order to obtain better statistics, the grouping results in an averaged Q-value of 1.03Å^{-1}. The triangles present the measured data and the solid line is the fitted scattering function. In the inserts we show the rescaled quasielastic contribution, which has been fitted with two Lorentzian functions, due to the ammonium reorientations around a C2-axis (the dashed Lorentzian function) and the phenyl ring torsions (the solid Lorentzian functions). The solid straight line is the fitted background.*

	EXPERIMENTAL REPORT SANS Structural Characterisation of Pillared Layered Catalysts	Proposal N° CHE-04-876 Instrument **V4** Local Contact U. Keiderling
Principal Proposer: Experimental Team:	Theodore Steriotis, NCSR "Demokritos" Adriana De Stefanis, I.S.M.N. C.N.R. Georgia Charalambopoulou, NCSR "Demokritos" U. Keiderling, HMI Berlin	Date(s) of Experiment 11-12/11/2003

Date of Report: 06/01/2005

A layered material is considered pillared when its internal surface has been greatly expanded by insertion of a chemical moiety linked to at least one sheet of the material. Traditionally, the pillaring process has been-and still is-mainly concerned with inorganic moieties, where the pillar is a nano-oxide particle usually derived from a cationic polyoxohydroxy metal species. Pillared inter-layered clays (PILCs) and related pillared materials have over the past decade been utilized in catalysis, sorption and separations. Although numerous studies have been carried out, their structure is not fully resolved yet, the major reason being their high heterogeneity.

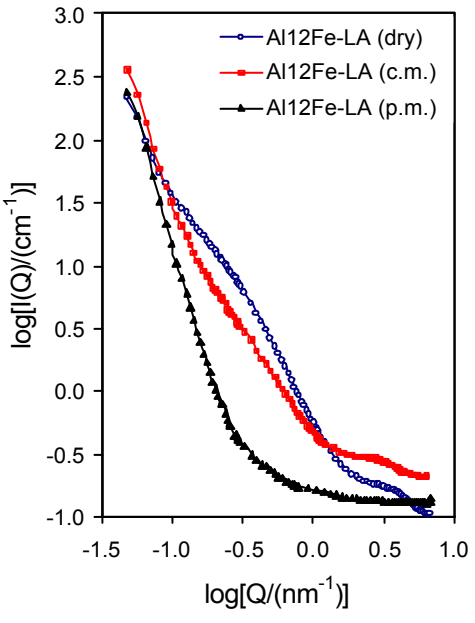
PILCs are in principle a three-phase system (clay sheets, pillars, pores) and the decoupling of structural information for each phase is a challenging task. On the other hand, small angle scattering (SAS) is a powerful tool for structural characterization of porous materials in the nanoscale region, especially when combined with the contrast matching technique.

In a previous small angle neutron scattering (SANS) experiment in V4 (CHE-04-548-December 07-11, 2000) we have employed contrast-matching (CM) SANS to independently resolve the structure of each phase in alumina-pillared smectites (mainly montmorillonites, beidelites and bentonites). Additional measurements have been carried out on commercial and novel restructured clay catalysts. Using this technique pores were filled with appropriate ratios of H_2O/D_2O that match the neutron scattering length density of each phase (clay, pillars) so that the scattering curve results only from the non-contrast matched phase.

In this continuation experiment we have expanded the same approach to different families of pillared natural as well as synthetic clays. We have specifically performed SANS and CM SANS experiments on a series of parent, pillared and pillared/ion exchanged saponites and laponites. The saponite (SA) family consists of the parent clay and its restructured and restructured/ion exchanged (with Ca and Ba) derivatives and also Al- and Fe/Al- pillared SA. The pillared samples were measured before and after calcination. Apart from the parent laponite (LA) this family includes Na- and V- Al13 as well as Al12M (M=Ga, In, Fe) pillared samples. The graph attached presents a typical example of the spectra obtained for the same material (Al13Fe pillared laponite) under different contrast conditions (c.m.: clays matched, p.m.: pillars matched).

SANS measurements were also carried out for MCM-36 type molecular sieves. These materials are currently used as new Fluid Catalytic Cracking (FCC) catalysts mainly due to their tunable acid-base properties and the combination of zeolitic microporosity with mesoporosity originating from swelling the layered precursor of zeolite MCM-22 with cations and subsequent pillaring of the layers with silicate polyoxocations.

Finally, the SANS spectra of traditional (FSM-16) and novel (FSM10, FSM10/16) Folding Sheet Mesoporous Materials (FSMs) were recorded. The FSMs are mesoporous silica materials with highly ordered pores and have attracted considerable interest in the field of adsorption science and catalysis chemistry. They are prepared by intercalation of quarterly ammonium surfactant as a template in a layered sodium silicate, kanemite.



	EXPERIMENTAL REPORT **Slow Dynamics of Co_2RuO_4**	Proposal N° PHY-03-0332 Instrument **V5** Local Contact C. Pappas
Principal Proposer: Experimental Team:	G. E. Granroth,ORNL/SNS D. L. Abernathy, ORNL/SNS G. Ehlers, ORNL/SNS S. E. Nagler, ORNL/CNS	Date(s) of Experiment 20 Apr – 30 Apr. 2004

Date of Report: Dec. 7, 2004

We study systems where geometrical frustration and quantum fluctuations inhibit magnetic order. Specifically our study on SPAN was performed to elucidate the time scales of the dynamics in a spin glass like state of the compound Co_2RuO_4. This compound is a spinel with the tetrahedral (A) sites are occupied by S = 3/2 Co^{2+} ions, ½ the octahedral (B) sites are occupied by S = ½ Ru^{3+} ions, and the other ½ of the B sites are occupied by Co^{3+} in the low spin (S =0) state. The Co^{3+} ions also provide a strong exchange path between the A sites. Between the Spin structure and the S=1/2 ions on the B sites this material is a strong candidate for both geometrical and quantum fluctuation related disorder.

Bulk susceptibility [1] measurements show that the system enters a frozen state, near a temperature T_f = 15 K. Preliminary neutron diffraction and inelastic studies confirm the presence of this state and also suggest the B sites do not participate in this state. The experiment we performed on SPAN clarified these issues.

An incident wavelength of 6.5 Å was used and the detector bank A3 was positioned to accept a momentum transfer (q) window between 1.27 $Å^{-1}$ and 1.57 $Å^{-1}$. This window is well matched to a peak in S(q) corresponding to short range correlations among the A sites. Measurements were performed at temperatures around T_f. A separate run with a spin ice sample ($Ho_{1.7}Y_{0.3}Ti_2O_7$) was used as a completely frozen standard to normalize the intermediate scattering function (S(q,t)).

The preliminary results of the analysis are shown in Figure 1. Overall the measurements show that the dynamics of the sample move through the time window of the spectrometer in the studied temperature range (2 -25 K). For T < 20 K S(q,t) does not reach zero in the time window of the Spin-Echo Measurement. This result indicates that dynamics with a time scale t > 2 ns are present as the sample is cooled. The sloped curve at all temperatures indicates a wide distribution of time scales in the system consistent with a Spin Glass. However a combined analysis of this data and previously taken time of flight data is required before a more definitive statement can be made. Finally for the lowest temperatures, S(q,t)/S(q,0) does not go to 1 at the shortest times. This result indicates that dynamics on a time scale faster that t = 0.015 ns exist in the system also. Part of this fast fluctuating moment can be attributed to the paramagnetic Ru^{3+} ions in the system. However they will contribute no more than 25% to the total S(q). Since the measurement was performed where S(q) was a maximum for the A site contributions, the B sites will contribute less than the possible maximum. Therefore, some of the A site spin fluctuations in the frozen state are faster than the observation window. The complete analysis of this data is currently in progress.

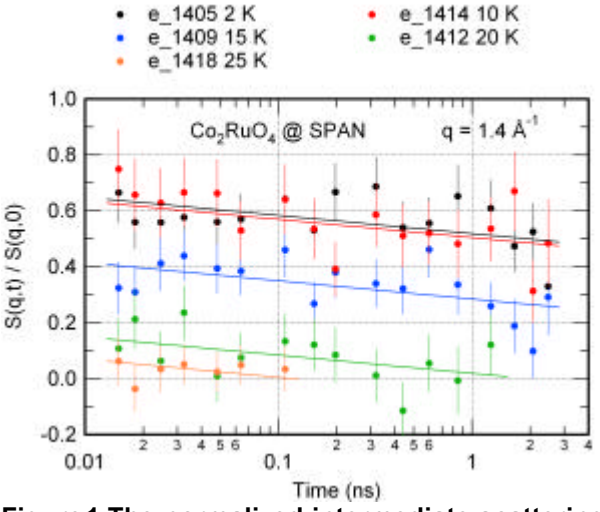


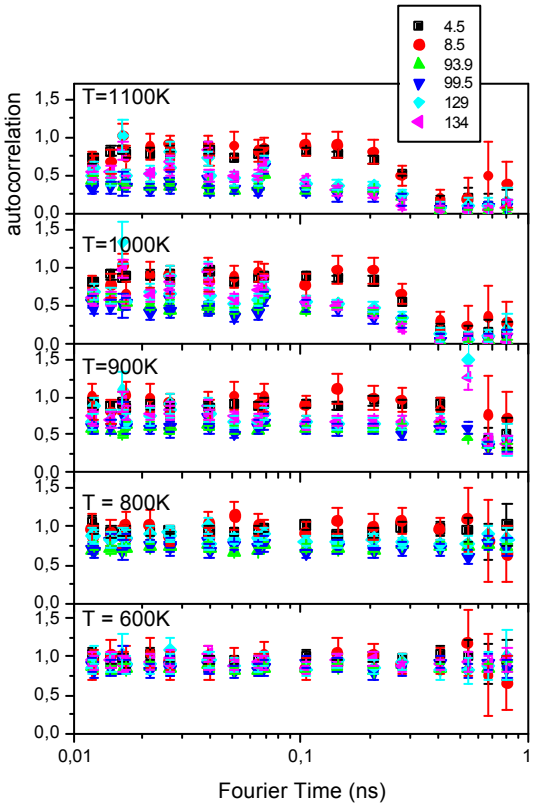
Figure 1 The normalized intermediate scattering function as a function of temperature.

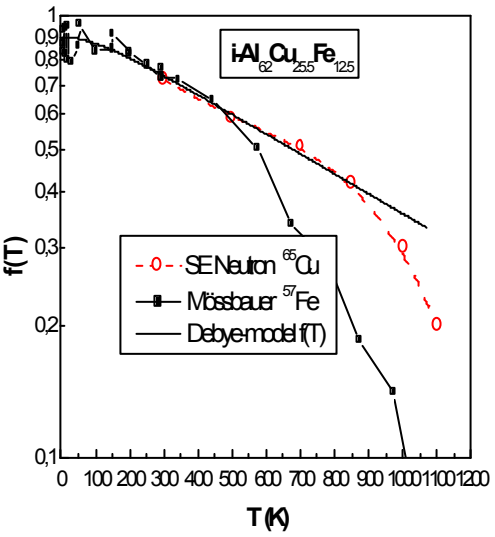
[1] D. Mandrus, V. Keppens, and B. C. Chakoumakos, Mat. Res. Bull., **34**, 1013 (1999).

BENSC	**EXPERIMENTAL REPORT** **Phason Dynamics in the Icosahedral Quasicrystal i-AlCuFe**	Proposal N° PHY-03-363 Instrument **V5** Local Contact Pappas
Principal Proposer: Experimental Team:	Richard A. Brand, Universität Duisburg-Essen Richard A. Brand, Universität Duisburg-Essen Catherine Pappas, HMI Berlin Carlos Fehr, HMI Berlin	Date(s) of Experiment Sept. 2004

Date of Report: 03.02.2005

We have investigated the temperature dependence of the self-correlation function in icosahedral AlCuFe using neutron spin echo (SE) neutron scattering. What we wish to investigate is the phason dynamics present in this quasicrystal above 600K. In order to separate the different atomic contributions (Al, Cu and Fe), we proposed to study 3 different isotopic compositions (natural isotopes, one containing 65Cu, and one containing 57Fe). We were able in this experiment to investigate the first two samples. The graphics below show the preliminary results for the sample with 65Cu. The plot on the left shows the thermal evolution of the self-correlation from 600 to 1100K. Evidently, the results at 600K are purely elastic. At higher temperatures, there is a gradual evolution towards decorrelations above ca. 0.1 ns (probably corresponding mainly to Cu jumps). The Q dependence will also be deduced from the angle-dependent results. For this, we still must do some computations on the background level for the smallest two and largest two angles shown. But the Debye-Waller factor calculated from the results, shown on Fig. 2 to the right is very encouraging. It shows first of all as black squares the previous Mössbauer results. The decrease above 600K demonstrates the added iron phason dynamics over and above phonons. The pure phonon effects are shown a solid line as calculated from inelastic neutron scattering results. This decrease is interpreted as evidence of iron atoms participating in phason jumps. The red circles show the Debye-Waller effect as calculated from the SE autocorrelation at long times for the 65Cu-sample. This isotope strongly weights the copper contribution. It is clear that the iron Mössbauer (black squares) and SE results (red circles) show that there are two different phason jump behaviours active in icosahedral AlCuFe quasicrystals. Further work will be done on the other isotope (57Fe) after the SE instrument is reinstalled in the new guide hall.





	EXPERIMENTAL REPORT **Investigation of DaPP static structure factor temperature evolution**	Proposal N° EF Instrument **E2** Local Contact J.U. Hoffmann
Principal Proposer: Experimental Team:	F. Mezei and O. Russina O. Russina, F. Mezei, HMI Berlin J.-U. Hoffman, T. Lonkai, HMI Berlin	Date(s) of Experiment 18-24.07.2004

Date of Report: 15.01.2005

The neutron diffraction data of DaPP, collected at the E9 diffractometer in 2003 indicate a strong increase of the static structure factor S(Q) at low Q (including the first peak, in the region around and below 1.1Å^{-1}) upon heating. This rise of order is remarkable and is related to the increase of interchain correlation in the melt state as compared to the glassy one. The goal of our experiment on E2 was to explore the temperature evolution of this phenomenon, collecting the diffraction pattern in smaller temperature steps across Tg.

The use of PG 002 Monochromator crystal (?=0.241 nm) allows to collect the static structure factor S(Q) from 0.23Å^{-1} to 3.5Å^{-1}. The sample was transferred in the slab aluminium cell with the thickness 1.2 mm. The data have been collected from 29 K (glassy state), across the glass transition (Tg=240K), up to the 340K (melt). Below 200K the spectra were collected with 50K step, above 200K up to 260K – every 10K, and from 260K up to 320K (above the glass transition) every 5K. Selected spectra are shown in Fig.1 in the region of the main peak.

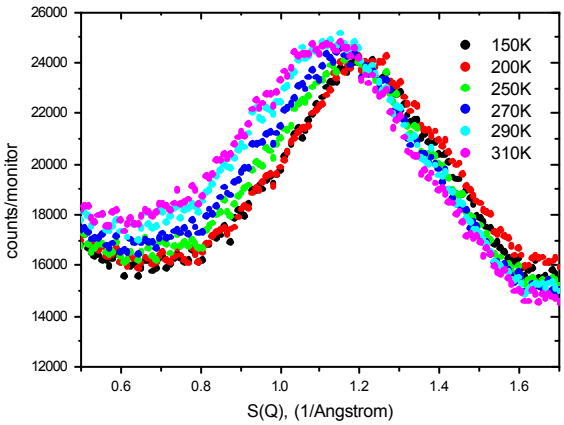


Fig.1. *The temperature evolution of the first diffraction peak of S(Q) on DaPP (see text for details).*

While the peak position moves to smaller Q-values already below Tg, the first significant increase of intensity appears at 240K only. The rise of the peaks amplitude occurs *continuously*, without showing some "jump". The behaviour is reversible: the spectra, collected upon heating and upon cooling at the some temperature fall on each other.

To give a glance into the origin of this phenomenon we took advantage of the analyser crystals available on E2 and explore the partial $S_{part}(Q)$, limited by the analyser window from –13meV up to 4 meV. In this way the neutrons, scattered on the high frequency vibrational modes remain outside of the analyser window and their contribution to the S(Q) could be estimated.

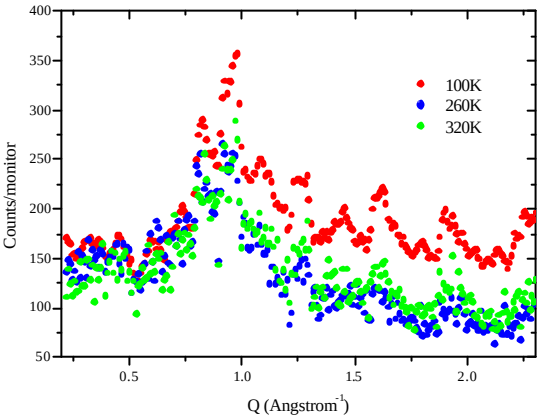


Figure 2. The diffraction pattern of DaPP, collected with the analyser crystal (see text for details.)

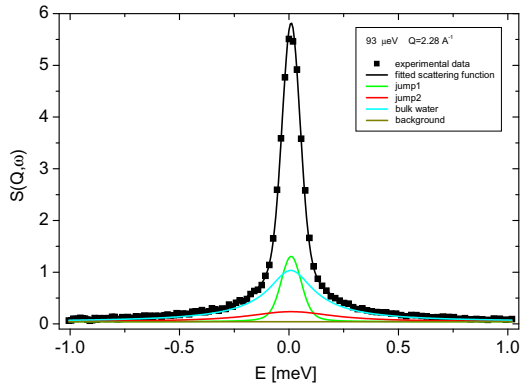
The diffraction patterns collected with the analyser crystals are presented in Figure 2. $S_{part}(Q)$ shows a different temperature behaviour for the data at small Q (below 1.1Å^{-1}) and high Q (above 1.1Å^{-1}), in agreement with S(Q) temperature behaviour. While the strong decrease in $S_{part}(Q)$ in the high Q-range is related to the decay of the static structure upon heating, the relative constant level of S(Q) in the small Q region indicates some additional scattering contribution. This is in agreement with the inelastic neutron data collected on DaPP (Report **PHY-03-360)** which reveals the dynamic nature of this phenomenon and highlight the atomic correlation on a quite short time scale (shorter that 1ns).

BENSC	**EXPERIMENTAL REPORT** **Water mobility in graphite oxide**	Proposal N°: PHY-03-318 Instrument: V3 Local contact: A. Buchsteiner
Principal proposer: Experimental team:	A. Lerf, Walther-Meissner-Institut, Garching A. Lerf, Walther-Meissner-Institut, Garching A. Buchsteiner, HMI	Date(s) of Experiment: 28.06. – 04.07.2004

Date of report: 09.01.2005

In the past few years a detailed study of the static structure of graphite oxide was carried out. This was mainly done by NMR investigations and lead to a new structural model of graphite oxide [1], [2].
The layer distance of graphite oxide increases with increasing humididy level giving raise to different spacings of the carbon layers in the range from 6 Å to 12 Å. As a consequence appear different motions of water and functional groups. Information about the mobility of the water molecules is not yet complete but crucial for the understanding of the structure of the carbon layers as well as the intercalation process.
The degree of hydration and the kinetics of water uptake depends crucially on the preparation and aging conditions.
We investigated two samples with different humidties, 35 % and 70 %, respectively, giving raise to layer distances of 8.0 Å and 11.2 Å.
The temperature behavior was measured in the range between 240 K and 320 K.
All samples showed a quasielastic contribution. Together with the results from the previous experiment we could show, that the character of the water does not change with humidity level until the amount of water is high enough to build bulk water.
In order to describe the dynamic behavior we had to find a model suitable to describe the experimental scattering function. A first rough analysis revealed that we have at least two different quasielastic contributions whose widths are not Q-dependent for small and medium humidities and encounter a third strong contribution at high humidity with a strong Q-dependency.
We did not find any hint for a translational motion of the interlayer water.
The experimental scattering function was then fitted with a combination of a bulk water model [3] (only in the case of the sample with highest humidity) and a model describing two different jumps between two equivalent places [4] plus an additional constant background, see the top right picture for an example. The jump distances were 1.46 Å (jump 1) and 3.05 Å (jump 2), respectively.
Deducing from the activation energies, the jump distances and the temperature behavior we assign the short jumps to 180°-flipping motions of isolated water molecules encapsulated in the interlayer space between the functional groups attached to the carbon grid. This type of motion is comparable to that of water molecules in the monolayer hydrate of halloysite [5], but shows a lower activation energy than the latter.

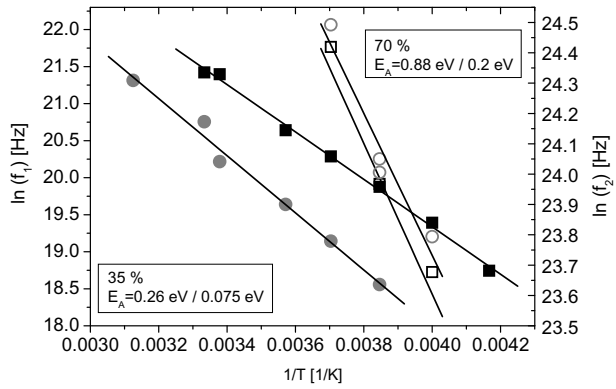
It seems also reasonable to assign the long jumps to jumps of the OH-groups involved in hydrogen bonds with epoxide functions of the neighbouring graphite oxide layers.



The investigation of temperature behavior revealed an Arrhenius dependency for both jumps

$$\tau = \tau_0 \exp\left(\frac{E}{kT}\right) \quad \rightarrow \quad \ln\left(f_{\max}\right) = -\frac{E}{k}\cdot\frac{1}{T} + \text{const.},$$

where E_A is the activation energy, τ and $f_{\max}$ are the relaxation time and the relaxation frequency, respectively.
The figure below shows the Arrhenius plot for both jump motions at both humidities and the resulting activation energies as well (squares: jump 1, circles: jump 2).



[1] A. Lerf et al.; Phys. Chem. B **102** (1998) 4477
[2] A. Lerf et al.; Solid Stat. Ion. **101-103** (1997) 857
[3] J. Teixeira et al.; Phys. Rev. A **31**/3 (1985) 1913
[4] M. Bée; Quasielastic neutron scattering; Adam Hilger (1988)
[5] M. Cruz et al; J. Chem. Phys. **69** (1978) 2018

BENSC	**EXPERIMENTAL REPORT** **The study of changes in pyridinium cation dynamics in (bis)thiourea pyridinium bromide inclusion compound**	Proposal N° PHY-03-0323 Instrument V3 Local Contact A. Buchsteiner
Principal Proposer: Experimental Team:	**P. Czarnecki, University Poznan** **P. Czarnecki, University Poznan** **A. Marczak, University Poznan** **A. Buchsteiner, HMI Berlin**	Date(s) of Experiment 5-8 April , 2004

Date of Report: 27.12.2004

Thiourea is known to form inclusion compounds with many inorganic salts, but with only a few organic salts. One of the representatives of the latter is a complex with pyridinium salt $(SCN_2H_4)_2$ – $(H_5C_5NH)^+Br^-$. The thiourea molecules are arranged to form ribbons in which they are connected through hydrogen bonds. Four such ribbons form a channel of a square cross-section, hosting pyridinium cations. At the site where four channels meet a smaller channel forms hosting the bromide anion. The structures of the compound have been resolved by X-ray diffraction method [1]. On decreasing temperature the compound reveals sequence of the phase transitions: Cmcm(I)(T_1=180K)→$Cmc2_1$(II) (T_2=150K)→$P2_1cn$(III). To verify the reorientation models of the pyridinium cation in thiourea host molecule we performed quasielastic neutron scattering (QNS) measurements at BENSC.

Because the broadening of quasielastic component was easy to measure in few hours, we were able to record the spectra at ten different temperatures: 130 K, 160 K, 180 K, 200 K, 220 K, 240 K, 270, 296 K, 310 K and 330 K using resolutions of 93 meV. The spectra were recorded at about 5 hours at each temperature. The spectrum of vanadium and the spectrum of the empty cell were also recorded to get resolution function. All the spectra of our compound display a very nice quasielastic broadening except the spectrum at 130 K. The lack of broadening at 130 K clearly shows that at low temperature phase (III) the reorientations of the pyridinium cation disappear *or* there are no cation reorientations faster than 10^{-9} s. The result confirms the order-disorder type of the low temperature phase transition. From the preliminary fittings we found that the correlation time dependends on the temperature according to Arrhenius low (Fig 1.) and the activation energy of the reorientation is about 2 kJ/mol (20.7 meV). From our earlier dielectric measurements [2] we expected higher activation energy. The results obtained show that the cation reorientation is more complex than we expected.

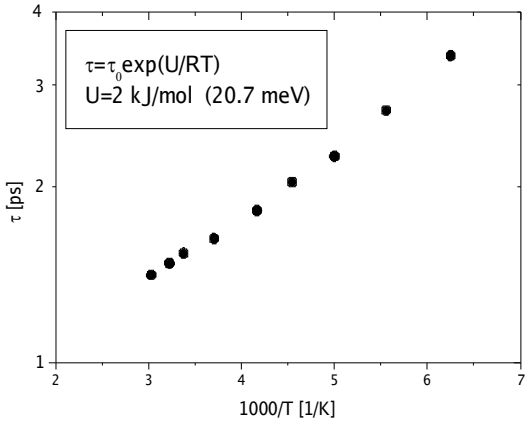


Fig. 1 . The relaxation time (log scale) dependence on the reciprocal temperature.

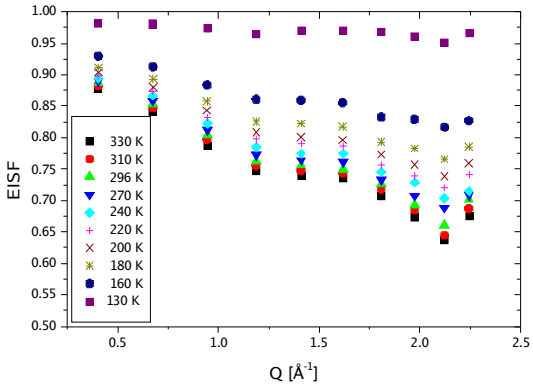


Fig. 2. EISFs for thiourea pyridinium bromide at ten temperatures

We hope that so strong quasielastic broadening is caused by the wobbling or in-plane libration of the pyridinium cation. The modelling of the movement of the pyridinium cation is currently under progress.

[1] K.Prout, S.J. Heyes, C.M. Dobson, A. McDaid, T. Maris, M. Muller and M. J. Seaman, Chem. Mater. 12, 3561 (2000)

[2] A. Marczak, P. Czarnecki, S. Mielcarek, Z. Naturforsch. 59a, 857-860 (2004)

	EXPERIMENTAL REPORT **Ordering upon melting: the effect of the fast dynamics on the order**	Proposal N° **PHY-03-322** Instrument **V3 (NEAT)** Local Contact M.Russina
Principal Proposer: Experimental Team:	A. Triolo, CNR-Messina, Italy O.Russina, HMI Berlin F.Mezei, HMI Berlin M.Russina, HMI Berlin	Date(s) of Experiment 3-10.05.2004

Date of Report: 15.01.2005-01-15

Neutron diffraction characterisation of the structure of deuterated atactic polypropylene (DaPP) –[CH2-CH(CH3)]$_n$ demonstrates different temperature evolution of the local and intermediate range order (IRO) across transition from the glassy state to the melt.

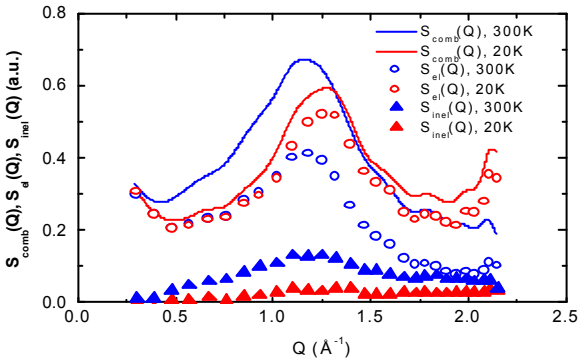
The local range order appears as a peak around 3.2 Å^{-1} in S(Q) and reflects the atomic space correlation between closer neighbours inside the chain [1]. The nearest neighbour interchain distance is reflected in the peak around 1.1 Å^{-1}. While the intramolecular peak does not show significant change with temperature, the intermolecular peak moves to smaller Q values and its amplitude increases with temperature. The shift of the latter peak position is mainly related to density change. However the rise of its amplitude is remarkable and indicates an increase of the atomic correlation on the IRO scale in the melt state as compared to the glassy one. Since the static structure factor, S(Q), is defined as the integral of the dynamic structure factor, **S(Q,**w**)**, over all the energy exchanges [1]: S(Q)= $\int S(Q,\hbar w)d\hbar w$, it is complicate to rationalise this experimental evidence on the basis of the diffraction data only.

In order to experimentally access the dynamic structure factor, S(Q, ω), we investigated DaPP at the time of flight spectrometer NEAT using an incoming beam with λ=5.4 Å, with instrumental resolution of ca. 70 μeV. S(Q,ω) has been measured at different temperatures ranging from the glassy state (20, 150 and 200 K) to the melt (300 and 340K). As can be expected, the integral of S(Q,ω) over all the accessible energy range, **S$_{int}$(Q)**, reproduces the same trend of the diffraction spectra: the IRO's amplitude rises with temperature!

In order to understand if this behaviour has a purely static structural origin, the Elastic Structure Factor, **S$_{el}$**(Q)=S(Q,ω~0), has been calculated as a integral of S(Q,ω) inside the instrumental resolution. This quantity is related to all those atomic correlations, which are characterised by a relaxation time longer than ca. 1 nanosecond and generally considered as responsible for the static structure The IRO peak position shifts with temperature in agreement with the diffraction data. On the other hand, S$_{el}$(Q) *decreases* continuously with increasing temperature over the whole Q-range. This observation might be expected on the basis of the temperature dependence of the Debye-Waller factor, but gives no indication of the increasing of order!

The time of flight data, S(Q,ω) evidence a strong increase in scattering intensity in the small energy exchange range (ΔE<1.5 meV). This scattering is associated to the so-called fast dynamics, with a characteristic time in the picosecond range and its existence is a general feature of dynamics in glass formers. In order to evaluate the role played by this dynamic process on the observed behaviour of S(Q), we evaluated **S$_{inel}$**(Q), defined as the integral of S(Q, ω) between 0.04 and 1.1 meV. The corresponding data are reported in Figure 1. The inelastic scattering signal shows a strong Q dependence: S$_{inel}$(Q) has a maximum around 1.1 Å^{-1} similarly to S(Q). The temperature dependence of the combination of this inelastic contribution to the elastic structure factor, **S$_{comb}$** (Q), shows similar trend to the static structure factor. *This result implies that the fast dynamic process probed by S$_{inel}$(Q) is responsible for the anomalous behaviour observed in the temperature dependence of the static structure factor.*

Figure 4. Temperature dependence (red symbols for T=20 K, blue symbols for T=300 K) for the different structure factors defined in the text (see the text for details).



References

[1] A.Triolo et al, Expérimental Report, BENSC 2003, 132.

[2] Mezei, F. *Liquids, Freezing and Glass Transition*; Elsevier Science Publishers B. V.: Amsterdam, 1991 (J. P. Hansen, D. Levesque and J. Zinn-Justin Eds., Les Houches, Session LI)

	EXPERIMENTAL REPORT On the nature of the fast process in B_2O_3	Proposal N° **PHY-03-360** Instrument **V3 (NEAT)** Local Contact M. Russina
Principal Proposer: Experimental Team:	A. Triolo, CNR-Messina, Italy O. Russina, F. Mezei, HMI Berlin M. Russina, HMI Berlin	Date(s) of Experiment 16-26.08.2004

Date of Report: 15.01.2005

An essential issue in the physics of the glass transition is the nature of the so called β-process, which appears on the picoseconds scale. This process has been predicted by mode coupling theory [1] and later experimentally found in the microscopic dynamics of many glassy systems, such as $Ca_{0.4}K_{0.6}(NO_3)_{1.4}$, OTP, $ZnCl_2$, polybutadiene [2-5] et cetera. Since then the fast β-process was found to be a universal feature of the dynamics in glass formers The β-process manifests himself upon increasing temperature close and above Tg trough an anharmonic increase of intensity at low frequency (i.e. small energy transfer) in Raman and QENS scattering spectra. Its main features are quite different from those of the slow α-relaxation: the relaxation time for the β-process depends only slightly on temperature, while the relaxation amplitude increases with temperature, especially above the glass transition temperature Tg.

The goal of the experiment was to study the β-process strong glass former B_2O_3. In an attempt to carefully explore the features of the β-process, we investigated a representative strong glass former, such as B_2O_3. Our previous Neutron Spin Echo measurements showed that in this system, α- and β-processes are well separated on a time scale as a consequence of the slow temperature dependence of diffusive process.

Data have been collected in a wide range of temperatures including glassy and liquid state ($300 < T(K) < 1080$), using the high temperature furnace available at the NEAT spectrometer. Due to technical limitations, it was not possible to access higher temperatures. Instrumental configuration with λ=8.5Å and λ=6.0Å with elastic energy resolution $\Delta\omega$=60μeV for both wavelengths, have been used, which allowed to cover the range of Q from $0.13Å^{-1}$ to $1.34Å^{-1}$ and $0.18Å^{-1}$ to $1.9Å^{-1}$ respectively.

As one might expect, above Tg, the fast β-process appears as a broad quasi elastic contribution, without, however, leading to an appreciable broadening of the elastic central line. This effect is a consequence of the strong character of this glass former.

As the sample state changes from the glassy to the liquid one, the static structure factor, S(Q), considerably changes (Figure 1). The main peak position shifts to lower Q, presumably as a consequence of density changes. Moreover, the scattering intensity at low Q values substantially increases, thus indicating the progressive development of ordering.

In order to model the temperature and momentum transfer dependence of dynamics in B_2O_3, applying proper corrections [6] for multiple scattering effects (which affect the low Q portion of the spectra), we collected data at two wavelengths (namely λ=6.0 and 8.5 Å). The correcting procedure also requires a precise knowledge of sample transmission at the different wavelengths: the corresponding measurements were collected at the SPAN spectrometer. This time consuming analysis, which is devoted to the understanding of the nature of the β-process, is presently in progress. Such a precise data treatment is necessary in order to properly model the low Q portion, distinguishing between the different proposed mechanisms of vibration and relaxation. In fact though in the past a description of dynamics in B_2O_3 has been reported [7], yet no proper account has been given for the low Q region, which is fundamental to understand long range collective motions.

[1] W.Götze, Z.Phys.B 60 (1985), 195 ; W.Götze, W.Sjörgen Rep.Prog.Phys.55 (1992)242
[2] F.Mezei, et al., Phys.Rev.Lett 85 (2000) 5669
[3] A.Tölle, rep.Prog.Phys.64 (2001) 1473
[4] O.Russina, et al., Appl.Phys.A 74 (2002) 1192
[5] B.Frick, et al., Phys.Rev.Lett. 64 (1990) 2921
[6] M.Russina, et al. Phys.Rev.Lett 84(2000) 3630
[7] Engberg et al., PRB58, 9087 (1998)

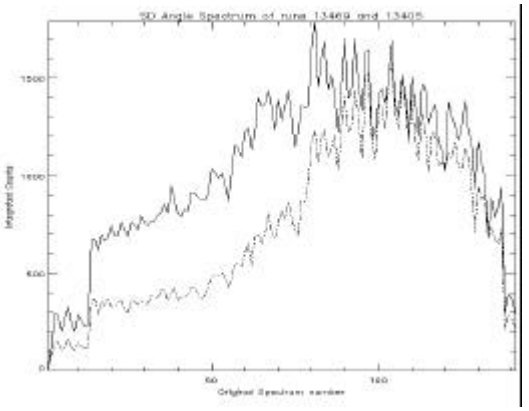


Figure 1. Total integral of the scattering intensity over the accessible dynamic window at 300 K (dashed line) and 1080 K (continuous line)

	EXPERIMENTAL REPORT **Diffusive Relaxation Processes in Liquid Ethylene Glycol**	Proposal N° PHY-03-336EF Instrument V3/NEAT Local Contact J. Pieper
Principal Proposer: Experimental Team:	O.Sobolev, HMI Berlin A.Novikov, IPPE, Obninsk, Russia J. Pieper, HMI Berlin	Date(s) of Experiment 27-29.03.2004 23-27.06.2004

Date of Report: 5.01.2005

Ethylene glycol (HO-CH_2-CH_2-OH, EG) is the simplest diatomic alcohol, which is used mainly as an antifreeze and for organic syntheses. Besides its technological importance, it is of great interest as a glass forming molecular liquid with three-dimensional H-bond network. Our previous attempts to analyze the microscopic dynamics of liquid EG by neutron scattering are presented in Ref. [1,2]. The main aim of this experiment was to study the diffusive relaxation processes in liquid EG by quasielastic neutron scattering.

The measurements were performed with the time-of-flight spectrometer NEAT at sample temperatures 296 K, 323 K, 348 K, 373 K and 393 K. Incident neutron energies were 1.278 meV (with an elastic resolution ΔE ~ 30 μeV) and 1.936 meV (ΔE ~ 100 μeV). The data were collected in the Q range of 0,24 Å^{-1} – 1.6 Å^{-1}. A standard flat sample of 0.2 mm thickness was used, resulting in a transmission of about 92%. Multiple scattering was calculated using FISC program [1,2].

The quasielastic scattering data were fitted in the energy domain by the Fourier transform of Kohlrausch-Williams-Watt function corrected for the instrumental resolution (Gaussian with dispersion σ_{res}):

$$I(Q,t) = \exp(-(t/t_w)^b)\exp(-s_{res}^2 t^2/2)$$

The stretching parameter β was found almost Q-independent, and its temperature dependence is also weak: β=0.63±0.04 at T = 296 K and β=0.69±0.04 at higher temperatures. The relaxation time τ_w obtained from the fitting procedure can be approximated by the power low $t_w = t_0 Q^{-g}$ (Fig. 1) with the exponent parameter γ = 2.4 and $\tau_0(T) \propto \eta$ (Fig. 2).

The similar Q- and T-dependencies was found earlier for other glass-forming systems. The values of β and γ are comparable to those obtained for glycerol (β = 0.61 and γ = 2.2) [3].

The power low dependence of the relaxation time τ_w with $\gamma = 2/\beta$ is typical for polymers [4].

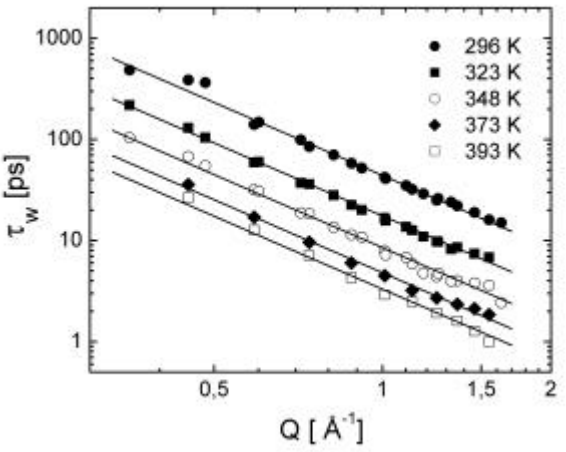


Fig. 1 Relaxation time τ_w (symbols) and the power-low fit $t_w = t_0 Q^{-g}$ (lines).

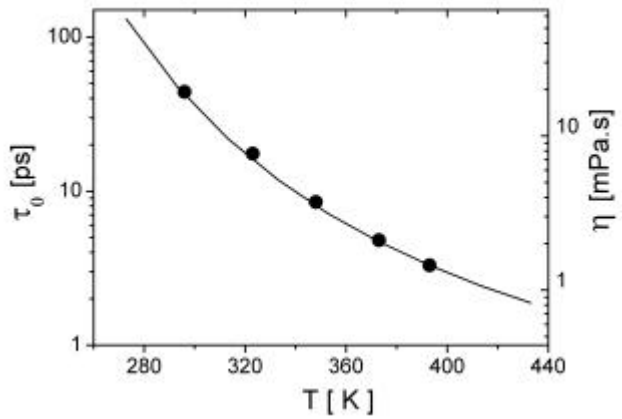


Fig.2 Relaxation time τ_0 (points) and viscosity (line).

References

[1] A.G.Novikov et al., Appl.Phys. A 74 (2002) S502

[2] A.G.Novikov et al., Physica B 350 (2004) e363

[3] J.Wittke et al., Phys. Rev. E 54 (1996) 5364

[4] J.Colmenero et al., J.Phys.: Cond. Matt 11 (1999) A363

BENSC	**EXPERIMENTAL REPORT** **Controlled grafting from nano-silica beads**	Proposal N° PHY-04-0940 Instrument **V4** Local Contact Daniel Clemens
Principal Proposer: Experimental Team:	El Harrak, LLB, Saclay Boué, Carrot, Oberdisse, Jestin, LLB Saclay	Date(s) of Experiment 06-09 February 2004

Date of Report: 15 Mars 2004

We have developped controlled grafting of polystyrene chains on nano-silica beads suspended in organic solvent (dimethylacetamide, DMAc). We used the "grafting from" method: after grafting the initiator(silanisation followd by an overgrafting reaction), we conduct the polymerization directly from the surface allowing for a better controlled layer density. We use controlled radical polymerisation (namely, Atom Transfert Radical Polymerization, ATRP), and try to keep the stability of the colloidal suspension. The purpose of the proposal was to follow by SANS the several steps of the grafting procedure with a particular focus on the evolution of the scattering from the initial state of the polymerisation, where the reaction is not started, to the final state.

A first series of results is about the aggregation state of silica beads. We match the scattering length density of the solvent to the one of the polymer, using a mixture of hydrogenated/deuterated DMAc.

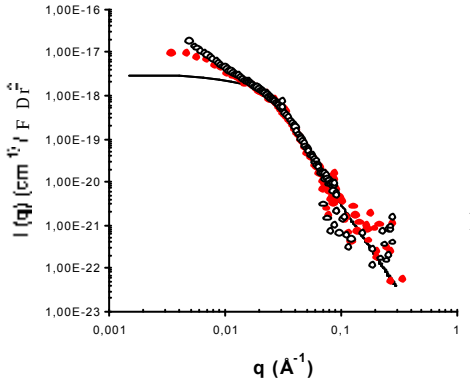


Fig.1

Fig.1 shows two interesting scattering curves for the initial state (open circles) and the final state of the polymerisation procedure (full circles). The full line is the polydisperse form factor fit of the naked silica deduced from preliminary SANS measurements at LLB (<R>=50.9Å, σ=0.365). At the initial step, when any polymer is formed, the low-q scattering, larger than the calculation for the individual particle, indicate the presence of large aggregates. At the end of the polymerisation, the scattered intensity, shows clearly a diminution of the intensity, i.e. of the aggregates size, compared to the initial state. By extrapolation of the intensity at q=0, in absence of interactions between aggregates, we find a number of particles per aggregates equal to 3. In summary, grafting polymer on silica spheres has reduced aggregation and stabilized the colloidal dispersion.

A second series of SANS measurements investigates the structure and conformation of grafted polymer on particles. We used the possibility of matching the solvent to silica beads. Fig. 2 presents the scattering curves for grafted particles with hydrogenated and deuterated polymer. We observe at large q a slow decrease, with a slope (~1.65) characteristic of large q polymer scattering. We also observe at lower q ~ 0.02 $Å^{-1}$ a shoulder, clearly noticeable for D polymer, but also present for H polymer. Though the silica is mached, this shoulder is at the same q than for Fig. 1, and is thus close to correspond to the form factor of the beads. One can expect that grafted polymer particles scatter like hollow spheres larger than the native beads. This implies a shift of the shoulder towards low qs, which is not observed. This comes certainly from the following: we have non grafted initiators in solution in order to keep a high enough concentration of radicals during polymerisation. This induces the presence of free chains, the fraction of which can only be estimated from the ratio of grafted initiator to free initiators. Note also that a simple subtraction of the free polymer scattering contribution ignores all kinds of interaction between grafted and free chains. Some difficulty to observe the grafted chains can also come from the aggregation of the beads at the beginning of the polymerisation (see Fig. 1 for the H polymer sample; in Fig.2 for the D polymer sample, and silica matching, we also observe strong low q scattering).

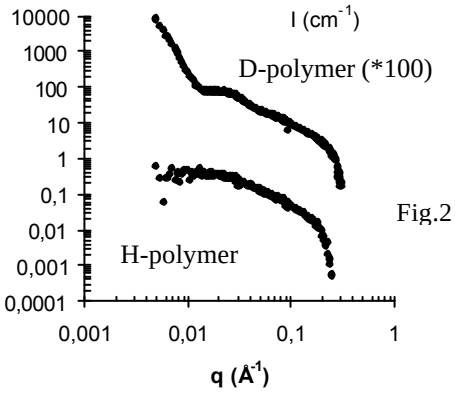


Fig.2

In conclusion, this experiment shows first the necessity to control aggregation of the silica particles before initiating polymerisation. This prompted us to lead a series of stability tests recently, hence we determined precisely the conditions for a well dispersed suspension, should now be characterized by future SANS experiments. Second, it suggests that conformation of grafted chains will be accessible by a physical separation (centrifugation) of the free residual polymer.

	EXPERIMENTAL REPORT Controlled grafting from nano-silica beads	Proposal N° PHY-04-1021 Instrument **V4** Local Contact Daniel Clemens
Principal Proposer: Experimental Team:	G. Carrot, LLB J. Jestin, LLB F. Boué, LLB	Date(s) of Experiment 29.07-1.8.2004

Date of Report: 10.01.2005

We have developed controlled grafting of polymer chains on nano-silica beads suspended in solution. We used the "grafting from" method: after grafting the initiator, we conduct the polymerisation directly from the surface allowing for a better controlled layer density. We used controlled radical polymerisation (namely, Atom Transfer Radical Polymerisation, ATRP), and try to keep the stability of the colloidal suspension. The purpose of the proposal was to follow the several steps of the grafting procedure by SANS and to characterise the form factor of the grafted nano-beads when the reaction is ended. The proposal described a polymerisation in organic solvent (dimethylacetamide, DMAc) with polystyrene. More recently, similar reactions have been developed in aqueous solvent (water) using a hydrophilic monomer (2-dimethylamino ethyl methacrylate, DMA). For reasons of time and opportunity, we decided to test this new system during the SANS run on V4 in July.

The silica particles are LUDOX TMA stabilized in water. At first, we measured the scattered intensity of a dilute solution of the particles before grafting (about 1% in volume). The recorded spectrum is presented in figure 1. The experimental data are well fitted by a hard sphere model with a log normal law of polydispersity. Results of the adjustment gives a mean radius <R> = 123 Å with a dispersion $\sigma = 0.16$.

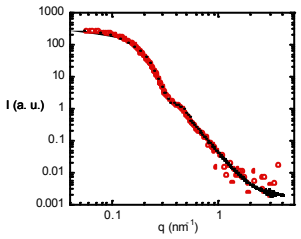


Fig.1

The polymerisation reaction is initiated as follow. The initiator is fixed onto the particles by electrostatic interaction and the initiator-grafted-particle system is mixed with the monomer. The polymerisation reaction is started by addition of the $Cu^{I}Br$ catalyst. Chemical analysis gives a conversion rate of 40% and indicates a well controlled reaction. During the "grafting-from" polymerization, several samples have been taken at different stages of the polymer conversion: typically, (i) just before the reaction is starts, (ii) at one or two intermediate states and (iii) at the end of the reaction. Using contrast variation method, we could measure separately the scattered intensity due to the silica beads, by matching the polymer scattering length, and the intensity due to the polymer, by matching the silica.

Fig 2. shows four scattering curves for four states of the polymerisation process (from (i) to (iii)) in polymer matching conditions (scattering from silica). At the initial step, when no polymer is formed, the low-q scattering indicates the presence of large aggregates. At the end of polymerization, the low-q scattered intensity shows clearly a diminution traducing a decrease of the size or the fractal dimension of theses aggregates. In summary, grafted polymer on silica particles leads to a desaggregation of the colloidal dispersion.

A second series of SANS measurements investigates the structure and conformation of the grafted polymer chains. We used the possibility of matching the solvent to silica beads. Fig. 3 presents the scattering curves of the grafted particles at different states of the reaction. The first spectra of this series should be theoretically a flat signal (absence of polymer and matching of silica) but shows nevertheless an increase at low-q which indicates that the matching is not perfect. In spite of this, the following curves present remarquable oscillations: the maxima q-values can be related to larger sizes than the one of the elementary silica particle. The maxima of the oscillations seem to be shifted to lower q-values when polymerization proceeds. This can be the signature of the growth of the polymer layer around the particle.

Fig. 2

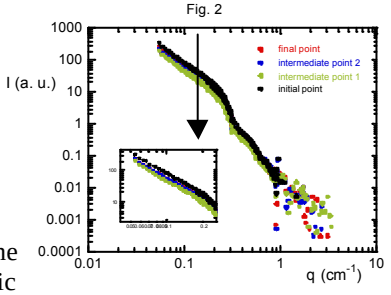
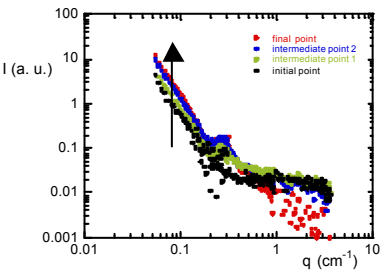


Fig. 3



In conclusion, this experiment is a very encouraging test to develop a complete study of polymer grafting from silica particle, **in aqueous solutions** . It shows the need for control of particles aggregation at the successive stages of the grafting procedure. This should be done by tuning the physical-chemical parameters (pH, salinity) with still best synthetic conditions, to keep convenient polymer conversion.

BENSC	**EXPERIMENTAL REPORT** **Tuning the hydrophobic interaction to act on the capacity of a polyelectrolyte to unfold a protein**	Proposal N° OTH-04-0942 Instrument V4 Local Contact Jörg Haug
Principal Proposer: Experimental Team:	Cousin Fabrice, LLB Gummel Jérémie, LLB, Cousin Frabrice, LLB Boué Francois, LLB, Haug Jörg, HMI Berlin	Date(s) of Experiment 03/02/04 to 06/02/04

Date of Report: 12/03/04

Mixing polyelectrolytes and proteins of opposite charges leads to the formation of complexes. When PSSNa and lysozyme are mixed, it instantaneously forms a turbid gel. However, this gel progressively becomes clear in a case of a PSSNa excess. We have shown nevertheless that this is due to an unfolding of lysozyme. Suspecting hydrophobic forces to be responsible of such unfolding (PSSNa has a PS hydrophobic backbone), we decided to change the charge rate f of the PSSNA which both decrease the electrostatic interactions and increase hydrophobic interactions.

In this experiment, we use three charge rates f (f = 0.5 ; 0.7 ; 0.9) for short PSSNa chains (Mw parent = 10000). Two concentrations of lysozyme and PSSNa are studied : one with **an excess of proteins** ([lysozyme] = 40g/L [PSSNa] = 0.1M/L) and one with **an excess of PSSNa** ([lysozyme] = 20g/L [PSSNa] = 0.3M/L ; 40g/L 0.1M). For each sample, we either match the signal of lysozyme (in a 43%D_2O/57%H_2O buffer), either the signal of PSSNa (in a 100%D_2O buffer).

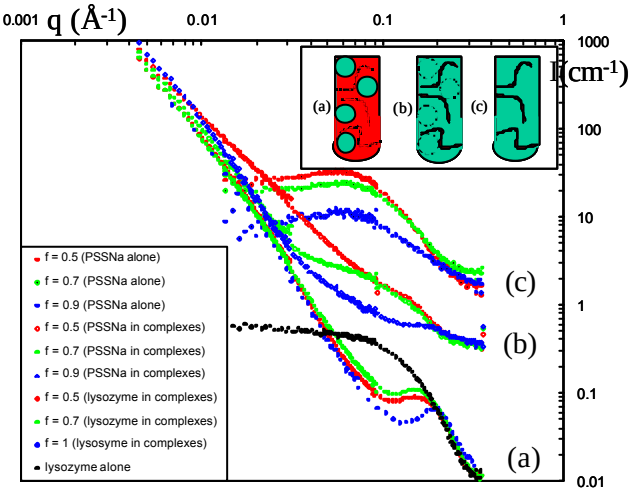


Figure 1 : Protein in excess ([lysozyme] = 40g/L [PSSNa] = 0.1M/L). Spectra for PSSNa in complexes are magnified by a factor 10 and spectra for PSSNa alone by a factor 100 for clarification.

Protein excess : Figure 1 compares spectra of complexes to pure lysozyme and PSSNa solutions at the same concentration. The shape of the spectra for proteins are exactly the same as the protein alone at high q, which means that the protein stays in its native form (a). For the highest charge rate, there is a peak at 0.2 $Å^{-1}$ that corresponds to a protein-protein contact and I(q) decays at smaller q as q^{-4}. The mixtures form thus dense complexes. For the lowest f, spectra are similar apart from the position of the correlation peak which is shifted towards low q : lowering f prevents lysozyme-lysozyme contact. The signal of PSSNa within the complexes is similar to the one of lysozyme at small q (b), indicating that lysozyme and PSSNa are included together within larger dense complexes. Especially the correlation peak q^* which is observed on pure PSSNa solutions in semi-dilute regime is no longer observed (compare b and c). The primary structure of PSSNa chains have thus disappeared.

PSSNa excess : Spectra of figure 2 shows features for this concentration. The form factor of lysozyme within the complexes at high q differs from the one of pure lysozyme solutions (a). Lysozyme has been unfolded by PSSNa. At low q, the signal is flat which means that unfolded proteins are no longer aggregated, except for f = 0.7 due to slower kinetics (a).

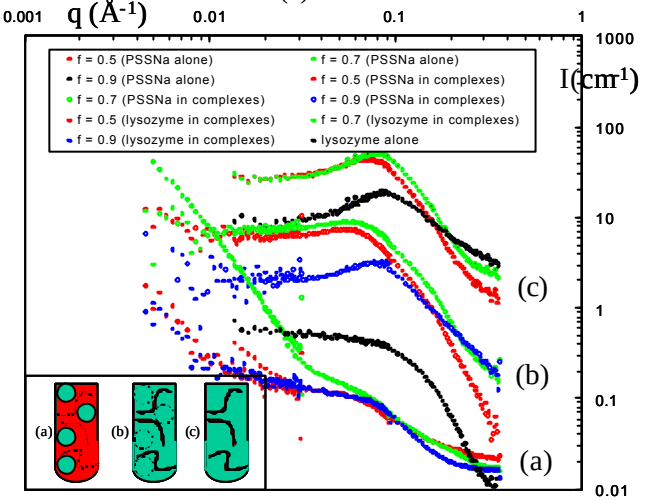


Figure 2: PSSNa in excess ([lysozyme] = 20g/L [PSSNa] = 0.3/L). Spectra for PSSNa in complexes are magnified by a factor 10 and spectra for PSSNa alone by a factor 100 for clarification.

The correlation peak of polyelectrolyte solutions is still visible (b). The network formed by PSSNa in semi-dilute regime is thus partially conserved. Nevertheless its position q^* is shifted towards low q (compare b and c). This results from an interaction with unfolded protein that locally contract PSSNa. This interaction is clearly evidenced by the fact that spectra of lysozyme within the complexes present a shoulder at the same q^* as PSSNa within complexes (compare a and b). Lysozyme and PSSNa have the same characteristic distance in the sample. The hydrophobic interaction seems to play a huge role in the PSSNa-unfolded lysozyme interaction : the less the charge rate, the more the shift of q^*. Interaction is thus stronger (more contraction of PSSNa) when hydrophobic interaction is increased and electrostatic interaction is decreased.

	EXPERIMENTAL REPORT **Huge polymer build with recognition groups directed Hydrogen bonds self-assembly**	Proposal N° CHE-04-0943 Instrument V4 Local Contact A.Brandt
Principal Proposer: Experimental Team:	D.Sarazin, ICS Strasbourg France J.M.Guenet, ICS Strasbourg France A.Brandt. HMI Berlin Allemagne J.M.Lehn. ISIS Strasbourg France	Date(s) of Experiment 20-23/07/2004

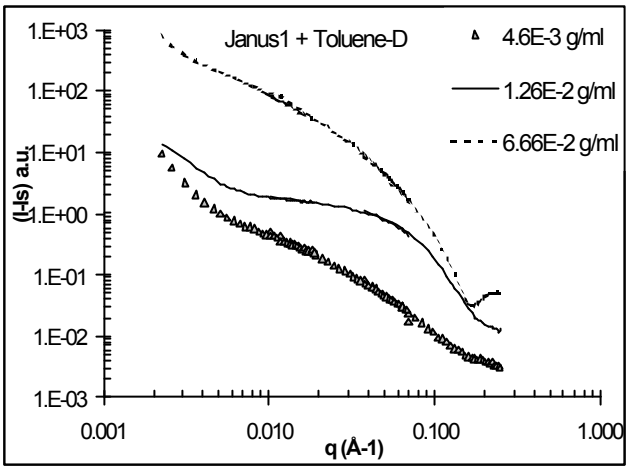
Date of Report: 27/07/2004

Self-assembly has proven to be a valuable process to target large structures with new properties. A way to study the different steps of their organization is to study their interactions with electromagnetic radiation. The scattering spectrum of the media lead to the determination of the molecular dimensions and may be used to follow the kinetic of self-assembly or growth in their dispersing media. So in the course of our studies on supramolecular polymers based on hydrogen bonding of the janus generation (initiated and synthesized by professor J.M.Lehn at ISIS laboratory, Strasbourg) we investigated dilute solutions from short to large wave vector q ranging from 10^{-3} to 1 $Å^{-1}$. Using MALLS at ICS. SAXS at ESRF SANS at ILL and HMI. That janus elementary unit lead to ribbon like growth structure depicted in the following drawing with high molecular dimension (Mw= 2. 10^7 g.mole $^{-1}$, Rg = 300 nm). The kinetic is driven by the close association rules very similar to the well-known polycondensation leading to a polymolecularity ratio Mw/Mn = 2. The thermal behavior of the mixture given by the second virial coefficient is A2 = 0 at room temperature, which is called the theta temperature by Flory and the solution consequently behave as pseudo-ideal. The polymer assembly thus exhibits its unperturbed dimensions influenced only by short-range interactions between neighboring recognition groups.

By lowering of the temperature and for concentration c> c^* we enter the gel phase for reversible thermal physical gelation of the janus self-assembly.

We measured also a persistence length b=140nm and a molecular weight per unit length M_L = 570 g (mol.A) $^{-1}$, which lead to the pitch of the monomer unit equal to p=2.4

At the ILL center on the D11 apparatus at a wave length of 6Å ; we pointed out new signatures for the structural factor at higher concentration near the physical gel threshold showing the onset of oscillation of well-organized assemblies see figure



The aim of the experiments performed at HMI on the V4 line at a wavelength of 4.5Å is to extend the range of the wave vector q. This should magnified the view on the details of the structure and will increase the accuracy on the determination of structural parameters used for the comparison with the theoretical form factor in dilute solution.

In fact neutron scattering turns out to be a powerful tool for tackling this question because of its non-destructive character and also because the usual accessible range of scattering vectors allows one to probe the cross-section of these threads in solution. This makes absolute calibration possible and one can find out whether one is dealing with filaments or with threads or if a thin ribbon-like structure of thickness *d* is obtained. The conclusion are still puzzling.

At this stage the experiments at V4 are given as a success. It is a part of a continuing investigations of the physical properties of hydrogen-bond self-assembly in solution.

We are grateful to the members of the scientific secretary for making our stay at HMI so easy.

	EXPERIMENTAL REPORT **The Effect of Particulate Addition on Surfactant Stabilised Emulsions**	Proposal N° CHE-04-0949 Instrument V4 Local Contact Daniel Clemens
Principal Proposer: Experimental Team:	Terence Cosgrove, University of Bristol Chau Chan, University of Bristol Cécile Dreiss, University of Bristol Daniel Clemens, HMI Berlin (BENSC)	Date(s) of Experiment 16th-18th July 2004

Date of Report: 7th January 2005

Aim

The first aim was to compare the adsorption of the Pluronic block copolymer F127 onto "hard" and "soft" particles (polystyrene latex and poly(dimethylsiloxane) emulsion droplets, respectively). A polymer layer will form in the hard particle case, however, it is possible that the hydrophobic block of the Pluronic will penetrate into the emulsion droplet in the "soft" particle situation. The second objective was to investigate the effect of particulate addition to surfactant stabilised PDMS oil in water emulsions. The stabilising polymer layer in some cases is scavenged by the particles leading to the destabilisation of the emulsion. Another possibility may be the enclosure of particles within the emulsion droplets. The study utilised the contrast match method, where the scattering from the particle and oil droplet in turn were matched to that of the solvent so that scattering from the adsorbed layer only, was observed.

Sample Materials and Conditions

The Pluronic surfactant F127 is a triblock copolymer consisting of poly(ethylene oxide)-poly(propylene oxide)-poly(ethylene oxide) units, in the ratio of PEO_{100}-PPO_{65}-PEO_{100}. The PEO blocks are hydrophilic, whilst the PPO blocks are hydrophobic. The polystyrene particles were prepared via surfactant-free emulsion polymerisation. Two types of latex were utilised, a 75% deuterated latex, and a 100% hydrogenous latex; this was in order for a contrast match condition to be met for both the polystyrene and the PDMS oil in the emulsions. The F127 stabilised PDMS emulsions were prepared via the base catalysed hydrolysis of dimethyldiethoxysilane. The samples were dispersed in H_2O/D_2O mixtures and measurements were conducted at 25°C and ambient pressure.

Preliminary Results

The scattering from the bare polystyrene latex (Figure 1) was fitted to a polydisperse hard sphere model using a non linear least squares fitting program.

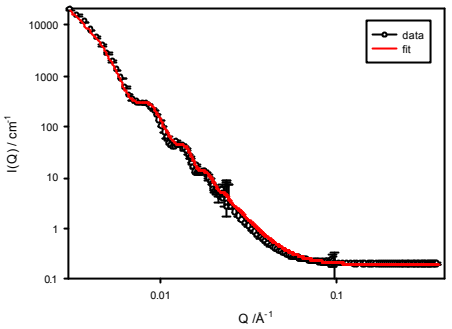


Figure 1. Scattering from a 6% bare hydrogenous polystyrene particles in 64% D_2O.

The particle radius was found to be 662Å with a log normal distribution of 0.06.

The scattering from the F127 in solution, and also adsorbed onto latex is shown in Figure 2.

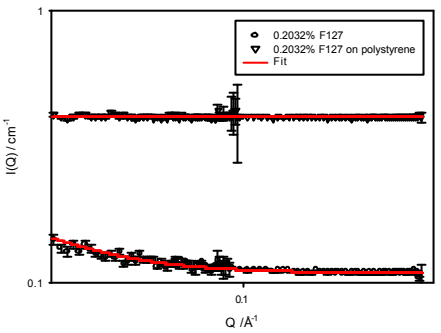


Figure 2. The data for a 0.2032% F127 solution (circles) and with 6% contrast matched polystyrene latex added (triangles).

The scattering from the bulk F127 solution was fitted to a Guinier/Debye model for polymers from which the radius of gyration was found to be 77Å. The adsorbed layer scattering was fitted using the scattering from the bulk F127 solution as a correction. The data was analysed in terms of a thin polymer shell, using an exponential profile for the adsorbed layer which showed a very low volume fraction of 0.01% polymer at the surface. The adsorbed amount was 0.27mgm^{-2}. The data for the F127 stabilised PDMS emulsions and the scattering observed after the addition of polystyrene particles is under analysis. This will reveal the adsorbed layer conformation on the emulsion droplet and the changes that occur upon addition of polystyrene latex particles.

	EXPERIMENTAL REPORT **Silicate-based nanoparticles and their interactions with PDMS melts and solutions**	Proposal N° CHE-04-0952 Instrument V4 Local Contact Daniel Clemens
Principal Proposer: Experimental Team:	Cécile Dreiss, University of Bristol Terence Cosgrove, University of Bristol Chau Chan, University of Bristol	Date(s) of Experiment 18-21 July 2004

Date of Report: January 2005

Silicate-based nanoparticles are frequently used as reinforcing agents in polymers such as poly(dimethylsiloxane) (PDMS). The interactions in these systems are complex and a wide range of behaviours dependent on particle size and molecular weight of the polymer have been reported. The aim of this broad project is to investigate the interactions of silicone resins with PDMS. We plan to study in particular the influence of the ratio of the size of the particles and the polymer on the inter-particle structure factor.

Materials

A series of fractionated trimethylsilyl-treated polysilicate nanoparticles is available, where the size of the particles is systematically varied. In this experiment, the bulk resin (non fractionated material) was used for the preparation of the samples.

Experimental set-up

Three sample-detector distances were used: 16m, 4m and 1m, with a neutron wavelength of 6.05 Å to cover a Q-range from 0.003 to 0.37 $Å^{-1}$.

The scattering from seven fractions of the silicate-based resins was measured, with molecular weights ranging from 2k to 27k. Their size and shape was characterised by dispersing them in deuterated toluene to achieve maximum contrast. 3% w/w solutions were prepared; this concentration was considered high enough to achieve sufficient signal from the resins and low enough to avoid the influence of inter-particle interactions. However, the data collected at the highest detector distance were quite noisy (data not shown here). The scattering curves (Fig.1) clearly show increasing particle size with increasing molecular weight. From a simple Guinier analysis, radii of gyration ranging from 7.5 to 21.4 Å are obtained. The lower molecular weight fractions could be fitted to a spherical shape with a lognormal distribution of sizes. The polydispersity was found to increase significantly with increasing molecular weight and the spherical model gave a poor fit in the lower Q-range for the larger particles (Fig. 1), revealing asymmetry in shape.

Solutions of the bulk resin were made in deuterated toluene with volume fractions from 10% to 40% v/v. At these high concentrations, a good signal was obtained. Curiously, the influence of the structure factor is hardly visible (possibly due to the very small size of the particles?) and we suspect that multiple scattering is taking place at the highest concentration. Dispersions of particles in PDMS melts were also measured. Hydrogenous PDMS of 100k and 5k was used, giving weak contrast and rather poor statistics at low Q. However, the effect of the concentration is clearly seen in the data, but no clear structure peak is visible, even at the highest concentration of 40% v/v. Current work is aimed at finding a suitable model to fit the data and compare the interactions in the polymer melt with those in solvent media.

Further experiments are planned using deuterated PDMS and the fractionated resins of varying particle size.

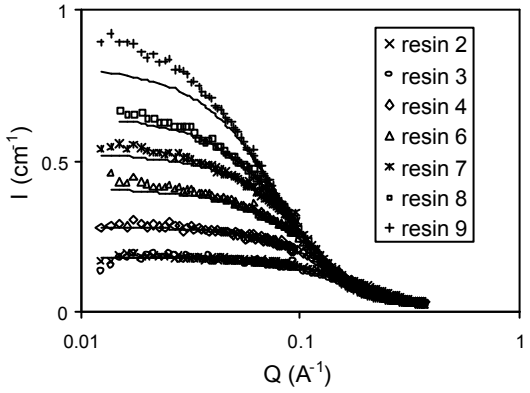


Figure 1 Dilute solutions of the resins (3% w/w) in deuterated toluene.

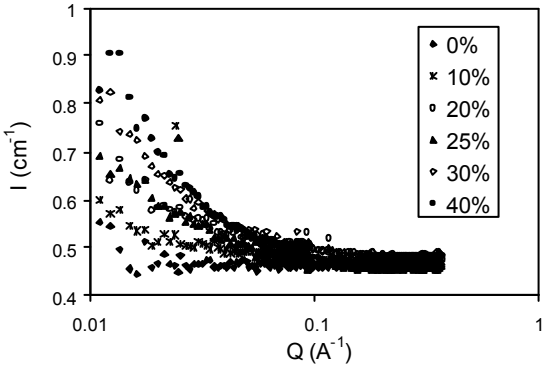


Figure 2 Bulk resin at various concentrations in 100k cross-linked PDMS.

BENSC	**EXPERIMENTAL REPORT** **Surface effects from doping liquid crystals**	Proposal N° **PHY-04-1058** **PHY-04-1035** Instrument **V4, V6** Local Contact U Keiderling, R Steitz
Principal Proposer: Experimental Team:	Robert Richardson, University of Bristol Yuk Gyn Joanna Lau, Institut Laue-Langevin U. Keiderling, HMI Berlin	Date(s) of Experiment 16-18 Aug 2004 19-23 Aug 2004

Date of Report: 01 Dec 2004

The adsorption of polydimethylsiloxane (PDMS) to the silicon oxide surface from liquid crystal solvent was characterised using neutron reflectivity. A fully deuterated PDMS of molecular weight approximately 60,000 (actual weight awaiting analysis) was mixed into liquid crystal 4-n-pentyl-4'-cyanobiphenyl (5CB) at 1%, 5% and 10% concentrations. The 5CB has a nematic-isotropic phase transition at 35°C. The mixtures were warmed and agitated before being sandwiched between two silicon substrates, one of which was polished and one which was rough. A native oxide layer was present on the polished surface. Reflectivity measurements were made at the polished silicon-PDMS/5CB mixture interface as a function of temperature. It was found that there was no difference between the pure 5CB and 1% PDMS/5CB mixture suggesting that PDMS is completely soluble in 5CB at all temperatures between 30°C and 70°C and does not adsorb to the silicon oxide surface. For the 5% and 10% PDMS/5CB mixtures, a critical edge can be seen at $Q \sim 0.012 Å^{-1}$ corresponding to the critical edge of pure deuterated PDMS with a scattering length density of $5.038e^{-6} Å^{-2}$. This shows that PDMS is not completely miscible with 5CB at all temperatures between 30°C and 70°C and thus some remained out of solution and formed a thick layer, very rich in PDMS, on the silicon surface. It is expected that PDMS is much more soluble in 5CB at higher temperatures so that the PDMS rich layer at the silicon interface should decrease. However, due to temperature limitations of the bath, these were not measured. Further experiments should be carried out with a lower molecular weight PDMS so that temperature dependence of the adsorption of PDMS can be fully investigated. Figure 1 shows the overall results.

A small angle neutron scattering study was run in parallel with the reflection measurements. However, results do not indicate immediate differences between the samples and do not show any temperature variance. The fact that all mixtures show similar behaviour to pure 5CB suggests that the samples were not mixed enough during cell filling. Repeated measurements need to be made for any conclusive results.

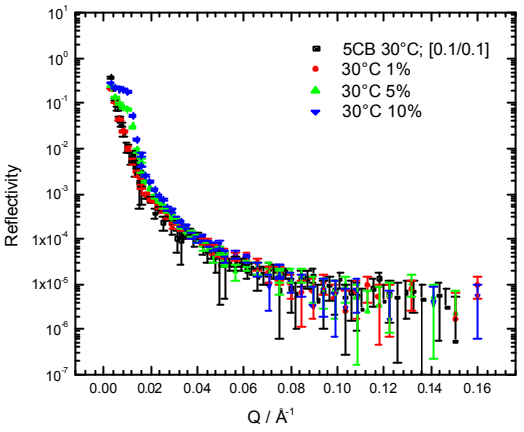


Figure 1 Overview of reflectivity results

	EXPERIMENTAL REPORT **Nanoscale dynamics of a strong glass former across its glass transition**	Proposal N° PHY-03-334 Instrument **V5 (SPAN)** Local Contact C.Pappas
Principal Proposer: Experimental Team:	A. Triolo, CNR-Messina, Italy O.Russina, HMI Berlin F.Mezei, HMI Berlin C. Pappas and C.Fehr, HMI Berlin	Date(s) of Experiment 02.02.-16.02.2004

Date of Report: Jan. 2004

Boron oxide belongs to the class of strong glass formers that has been identified by Angell to characterise the response of glass dynamics to temperature, as one approaches the glass transition. As opposite to so called fragile glass formers, the strong ones display simple Arrhenius-like temperature dependence for viscosity and other diffusive quantities in the neighbourhood of Tg. Such temperature dependence is then much less strong than in fragile glasses. It is of interest to rationalise the fragile-strong behaviour of glasses and relate it to microscopic features of the materials. For this reason we undertook an investigation of B_2O_3, trying to investigate novel features of its strong glass behaviour. In particular, in the present report, we will describe the first Neutron Spin Echo data collected on glassy and liquid B_2O_3.

The glass temperature of B_2O_3 is ca. 530 K. As a consequence of the strong character, the slow process associated to diffusive motions, often

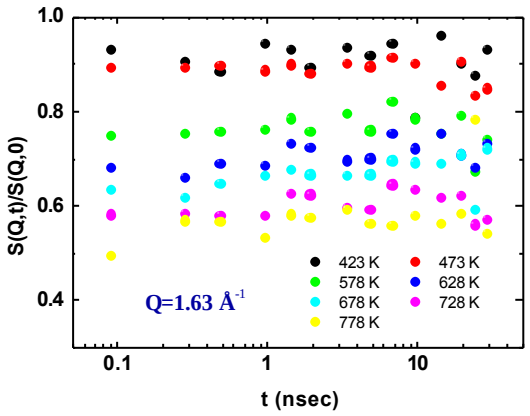


Figure 1. Neutron Spin Echo data collected form B_2O_3 at Q=1.63 $Å^{-1}$.

indicated as a-process, has a low (Arrhenius) temperature dependence. The consequence is that in order to fully access the α-process by NSE (0.1< t(nsec)< 20), one needs to explore dynamics at very high temperature. This creates a number of technical difficulties, given the highly corrosive nature of molten B_2O_3. Accordingly, we had to use a platinum cell and, due to the foaming effect associated to the melting of crystalline B_2O_3 special care had to be paid to the glassy sample preparation, which took more than 10 days.

The static structure factor of B_2O_3 has been investigated in the past (e.g. Engberg et al.; Phys. Rev. B 58, 9087 (1998)). We are presently focusing our attention on the Q range between 1.19 and 1.63 Å-1. In Figure 1 we plot the Neutron Spin Echo spectra collected for Q=1.63 Å-1, corresponding to the position of the first interference peak in B_2O_3. The data cover a temperature range between 423 K and 778 K and are normalised for the data set at T=300 K (that was the lowest temperature that was accessible using the furnace employed in our experiment). A distinct temperature dependence of the dynamic structure factor can be appreciated, though the accessible dynamic range does not allow detecting the shape of the relaxation associated to the a-process. In Figure 2, we report the so called non-ergodicity factor, corresponding to the constant value of the plateau observed in the three data sets collected on B_2O_3, as normalised to the data set at 300 K. These data follow a linear trend in agreement with the Mode Coupling Theory. Work is now in progress in order to further rationalise the observed results.

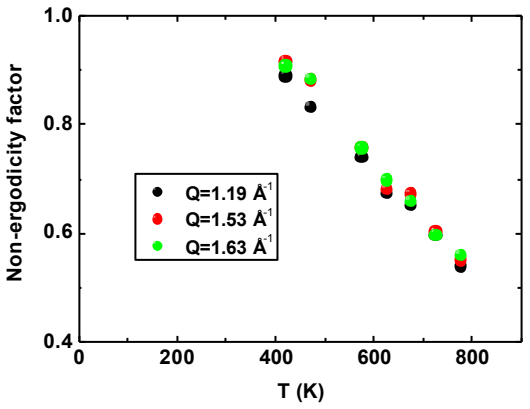


Figure 2. Temperature dependence of the non ergodicity factor obtained from NSE data from B_2O_3 at three different Q values.

	EXPERIMENTAL REPORT **Characterization of Trehalose Aqueous Solutions by Neutron Spin Echo as a function of temperature and concentration**	Proposal N° PHY-03-302 Instrument V5 Local Contact Carlos Fehr
Principal Proposer: Experimental Team:	Magazù Salvatore, University of Messina Migliardo Federica, University of Messina	Date(s) of Experiment 1. - 8.12. 2003

Date of Report: 7/02/2005

We used the V5-SPAN spectrometer to collect neutron spin echo (NSE) data on trehalose and sucrose/water (H_2O and D_2O) solutions as a function of temperature.
In the V5 configuration used for the experiment the incident wavelength was λ_o=6.5Å, scanning a Q range of 0.4÷1.5 Å^{-1}.
In Fig. 1, as an example, a comparison between the NSE intensities of deuterated trehalose and sucrose water solutions at T=293K and at Q=0.6 Å^{-1} is shown.
The fitting procedure has been carried out according to the Kohlrausch-Williams-Watts (KWW) function:

$$S_{self}(Q,t) = f(Q)\exp\left[-\left(\frac{t}{\tau_w}\right)^{\beta}\right] + BKG$$

where β is the stretching parameter describing the shape of the relaxation function ($0<\beta\leq 1$) and τ_w is the relaxation time.

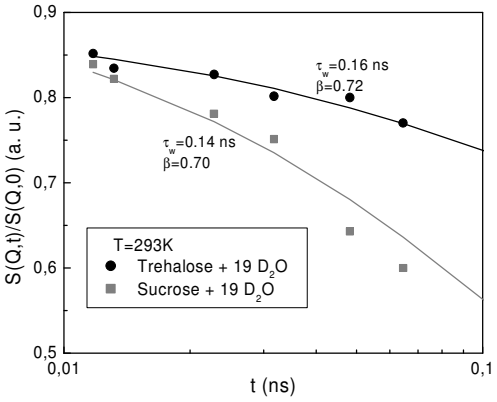


Fig. 1

Molecular Dynamic Simulation results have been obtained in order to perform a comparison with NSE findings. The simulation results in comparison with those obtained by the NSE spectra are shown in Fig. 2.

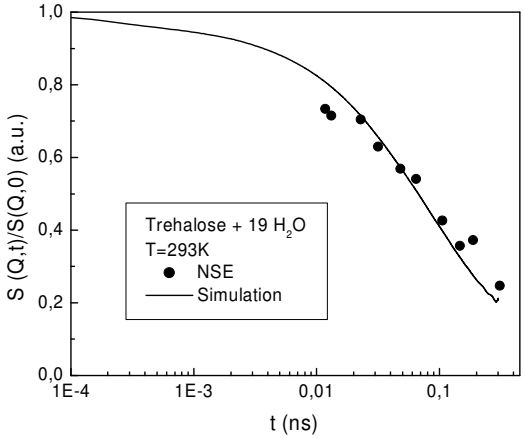


Fig. 2

In conclusion, NSE measurements on partially deuterated and hydrogenated samples make possible to characterise the dynamics of the entire solute-solvent system and to compare the experimental findings with those obtained by MD simulation. The results highlight that the disaccharide-water system is characterised by a strong solute-solvent coupling.

	EXPERIMENTAL REPORT **Biocomposite planar polyelectrolyte multilayers as a tool to understand different DNA transport systems**	Proposal N° BIO-04-1002-LT Instrument V6 Local Contact Krastev,R.
Principal Proposer: Experimental Team:	Gromelski, S.; MPI-KGF, Golm, Germany Gromelski, S.; MPI-KGF, Golm, Germany Krastev R., HMI Berlin; MPI-KGF, Golm, Germany	Date(s) of Experiment 20.05 - 28.05.2004

Date of Report: 22.12.2004

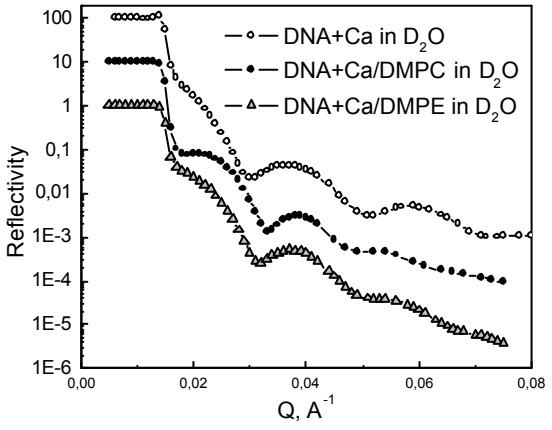
The usage of natural viruses as drug delivery vehicles is a quite controversial research topic. Due to the pathogenicity of the parental viruses it is supposed to assemble an „artificial virus“. Hollow polyelectrolyte (PE) capsules, built by layer-by-layer technique on a soluble template, can be used as model systems for artificial viruses. To guarantee an uptake of such capsules into the cell, the capsules are covered by a lipid bilayer. Unique information about the interaction between the three components at their individual interfaces, i.e. PE/lipid, PE/aqueous phase or lipid/aqueous phase can be achieved by neutron reflectometry (NR). Cationic lipids form easily stable and structured complexes with DNA[1,2]. Unfortunately cationic lipids are frequently toxic for cells, which exclude their use in the construction of artificial viruses. Complexes composed of neutral or negatively charged lipids offer an alternative as they are completely non-toxic. The neutral lipids do not interact with DNA directly, but the interaction can be mediated by divalent cations[3,4]. Recent studies on lipid monolayers at air/water interfaces using infrared reflection absorption spectroscopy (IRRAS) and grazing incidence X-ray diffraction (GIXD) showed that DNA can couple to zwitterionic DMPE (1,2-dimyristoyl-phosphatidylethanolamine) monolayers in presence of magnesium[1].

NR experiments were carried out in a solid/liquid experimental cell in θ/2θ geometry. The reflectivity from the sample was scanned over the whole range of incident angles of the incoming beam. The measurements were performed on a silicon block covered by a $(PSS/PAH)_6$DNA cushion (PSS Poly Styrene Sulfonate, PAH Poly Allylamine Hydrochloride and calf thymus DNA). The block was prepared, dried and stored in lab atmosphere for several days before measurements.

In the performed experiments the adsorption of the zwitterionic lipids a) DMPC and b) DMPE in presence and absence of calcium on a polyelectrolyte cushion covered with calf thymus DNA was studied. The experiments were performed above the phase transition temperature of the lipids - for DMPC at 26°C and for DMPE at 55°C. The lipid was adsorbed from dispersion with a concentration of 0,5 mg/mL and size of the vesicles prepared by ultrasonication and followed extrusion 50 nm. The lipid was adsorbed onto the DNA terminated polyelectrolyte cushion, resulting in the formation of a smooth bilayer. In a following step non-adsorbed lipids were washed out with D_2O. It was observed that the DNA terminated polyelectrolyte cushion has a thickness of 335 Å, independent of the temperature (26°C or 55°C).

a) The adsorption of DMPC resulted in a 65 Å thick bilayer only if calcium was present. (figure) In the absence of calcium no bilayer was formed. That shows that calcium plays a crucial role in the PC/DNA interaction. It is supposed that calcium turns the zwitterionic lipid bilayer cationic.

b) DMPE was only adsorbed in presence of calcium, forming a bilayer with a thickness of 48 Å. An additional in-situ adsorption of DNA on top of the lipid bilayer was not successful at the experimental temperature of 55°C.



[1] P. L. Felgner, T. R. Gadek, M. Holm, R. Roman, H. W. Chan, M. Wenz, J. P. Northrop, G. M. Ringold and M. Danielsen, *Proc. Natl. Acad. Sci. U. S. A.*, 1987, **84**, 7413.

[2] J. O. Rädler, I. Koltover, T. Salditt and C. R. Safinya, *Science*, 1997, **275**, 810

[3] V. G. Budker, A. A. Godovikov, L. P. Naumova and I. A. Slepneva, *Nucleic Acids Res.*, 1980, **8**, 2499.

[4] D. Huster, G. Paasche, U. Dietrich, O. Zschörnig, T. Gutberlet, K. Gawrisch and K. Arnold, *Biophys. J.*, 1999, **77**, 879.

[5] S. Gromelski, G. Brezesinski, *Phys. Chem. Chem Phys*., 2004**, 6**, 5551

	EXPERIMENTAL REPORT **Adsorption of B18 peptide on hydrophilic charged surfaces**	Proposal N° CHE-04-907-LT Instrument V6 Local Contact R.Krastev
Principal Proposer: Experimental Team:	S. Rocha, MPI, Golm, Germany S. Rocha, MPI, Golm, Germany R.Krastev, HMI Berlin, Germany/TU Berlin G.Brezesinski, MPI, Golm, Germany	Date(s) of Experiment 21 – 22 May 2004

Date of Report: 15.12.2004

Fusion peptides promote the fusion of membranes and hence are functional at interfaces. Surface interaction may lead to peptide conformational changes and may induce their aggregation. Fusion peptides such as B18 form amyloid fibrils at lipid membranes. B18 is the sequence 103 to 120 of the protein bindin, found in the sperm cells of the purple sea urchin.

The adsorption of B18 at a concentration of 4.8 µM and pH 7.4 on positively and negatively charged polyelectrolyte multilayer (PEM) films was characterized by neutron reflectometry (NR). The reflectivity of the pure PEM films in D_2O was first measured. The subphase was exchanged by a solution of the peptide in aqueous buffer solution, which was exchanged by D_2O after 12 hours. Figure 1 shows the NR profile of the positively charged PEI(PSS/PAH)$_6$ film before and after exposure to B18 solution. No differences in the position and amplitude of the Kiessig fringes were observed, indicating that the thickness and composition of the film were unchanged.

The effect of B18 on the negatively charged PEI(PSS/PAH)$_6$PSS film can be seen in Figure 2. B18 exposure resulted in a shift of the position of the minima to smaller *q* values, indicating an increase in the film thickness. The reflectivity curve was fitted by two-layer model. The first layer represents the silicon oxide and the second one the PEM film. The thickness of the film was 358 Å. The reflectivity profile of the film after B18 adsorption was also best fitted with a two-layer model. This shows weak contrast between PEM film and the adsorbed B18. In this case the second layer corresponds to the film plus B18 and had a thickness of 369 Å (Table 1) Hence B18 adsorption resulted in a thickness increase of 11 Å.

On a hydrophilic surface, the extent of adsorption of a protein is determined by the balance between electrostatic attraction and repulsion in the adsorbed layer. At pH 7.4, B18 carries a net positive charge. Most likely, the absence of B18 adsorption on the positively charged film is due to electrostatic repulsion, whereas adsorption on the negatively charged film is driven by electrostatic attraction.

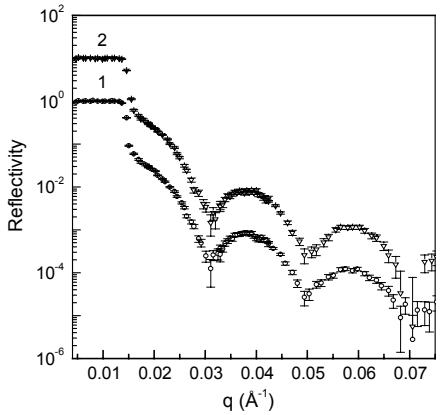


Figure 1*: NR curves of PEI(PSS/PAH)$_6$ film in D_2O (1) before and (2) after exposure to B18 solution. The curves are offset vertically for clarity.*

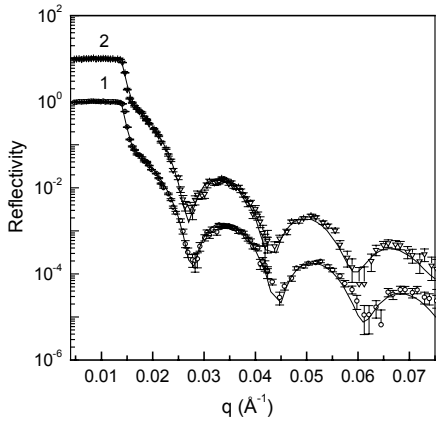


Figure 2*: NR curves of PEI(PSS/PAH)$_6$PSS film in D_2O (1) before and (2) after exposure to B18 solution. The curves were fitted using parameters of Table 1 (continuous line). The curves are offset vertically for clarity.*

layer	**d (Å)**	**ρ (10^{-6} Å^{-2})**	**σ (Å)**
silicon oxide	8 ± 2	3.41 ± 0.10	9 ± 3
before B18 adsorption			
film	358 ± 1	3.79 ± 0.10	23 ± 4
after B18 adsorption			
film + peptide	369 ± 1	3.79 ± 0.10	25 ± 1

Table 1: P*arameters used to fit the reflectivity profile of PEI(PSS/PAH)$_6$PSS and B18. d, ρ and σ are the thickness, scattering length density and roughness, respectively.*

	EXPERIMENTAL REPORT **Adsorption of amyloid beta (1-40) peptide on hydrophilic positively charged polymer**	Proposal N° CHE-04-907-LT Instrument V6 Local Contact R.Krastev
Principal Proposer: Experimental Team:	S. Rocha, MPI, Golm, Germany S. Rocha, MPI, Golm, Germany R.Krastev, HMI Berlin, Germany/TU Berlin G.Brezesinski, MPI, Golm, Germany	Date(s) of Experiment 20 – 21 May 2004

Date of Report: 15.12.2004

Amyloid β-peptide (Aβ) is found in neuritic plaques and cerebrovascular deposits that characterize Alzheimer's disease [1]. The reasons for the conversion of correctly folded peptide into pathological aggregates are unclear. Since in physiological environments many processes occur at interfaces, strong surface interactions may be responsible for damaging the native structure of the peptide and lead to its aggregation. Previous results have shown that Aβ does not adsorb on hydrophilic non-charged and negatively charged surfaces [2].

Here the study is extended to hydrophilic positively charged surfaces. The adsorption of Aβ (1–40) on PEI(PSS/PAH)$_6$ film was studied by neutron reflectometry (NR). The experiments were performed in θ/2θ geometry on the reflectometer V6. The solid/liquid experimental set-up was employed. The film was prepared by layer-by-layer deposition on a silicon block [3].

The structural parameters of the pure film were first determined by measuring their reflectivity profiles in D_2O. The subphase was then exchanged by a solution of Aβ (1–40) in D_2O at a concentration of 4.6 μM and pD 7. The profile of PEI(PSS/PAH)$_6$ film changed after exposure to Aβ solution (Figure 1). A pronounced shift of the position of the minima to lower *q* values was observed in the reflectivity curve after 12 hours adsorption time. This is an evidence that the thickness increased, indicating the formation of an additional layer on the PEI(PSS/PAH)$_6$ film. The reflectivity curve of the bare film was fitted with a two-layer model, using the program Parratt 32. The first layer represents the silicon oxide layer and the second one the bare film. A scattering length density of 4.1 x 10^{-6} Å^{-2} and a thickness of 308 Å were obtained for the pure film (Table 1). The reflectivity curve after Aβ adsorption was fitted adding an additional layer to the previous model. However, it was found that the surface coverage was not uniform. The best fit was obtained with a surface coverage of 0.6, suggesting that the peptide adsorbs as patches dispersed over the surface at distances larger than the correlation length of the neutrons. According to the fitting parameters the patches have a scattering length density of 3.4 x 10^{-6} Å^{-2} and a thickness of 20 Å (Table 1).

The electrostatic attraction between a charged surface and oppositely charged protein is often the driving force for protein adsorption on the hydrophilic solid substrate [4]. At pD 7, partial deprotonation of the histidines residues of Aβ is expected to occur and hence the net charge of the peptide at this value is negative. The fact that Aβ adsorbs on the positively charged film suggests that electrostatic attraction between the peptide and the PAH surface occurs.

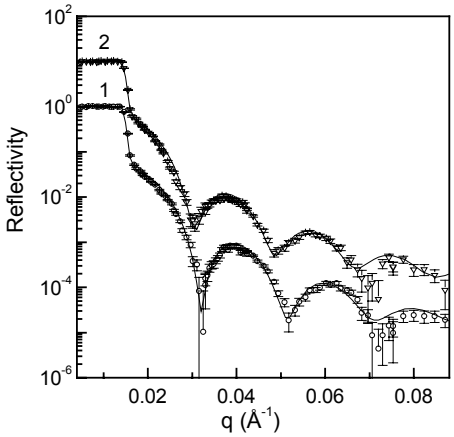


Figure 1: *NR curves of PEI(PSS/PAH)$_6$ film covered Si substrate in D_2O (1) and in solution of Aβ (2). The curves were fitted using parameters of Table 1 (continuous line). The curves are offset for clarity.*

layer	d (Å)	ρ (10^{-6} Å^{-2})	σ (Å)
silicon oxide	6 ± 4	3.48 ± 0.41	3 ± 2
film	308 ± 2	4.10 ± 0.04	2 ± 1
peptide	20 ± 1	3.40 ± 0.07	17 ± 1

Table 1: *Structural parameters used to fit the reflectivity profile of the system PEI(PSS/PAH)$_6$ and Aβ. The surface coverage of the peptide layer was 0.6. d, ρ and σ are the thickness, scattering length density and roughness, respectively.*

1. D. J. Selkoe, *Physiol. Rev.* 81 (2001) 741.
2. S. Rocha et al BENSC Experimental Report 2003
3. G. Decher, *Science* **277** (1997) 1232.
4. C. A. Haynes, W. Norde, *Colloids surf. B* **2** (1994) 517.

	EXPERIMENTAL REPORT PEO-PPO-PEO Triblock Copolymers at the Polymer/Water Interface, part II	Proposal N° CHE-04-913 LT Instrument **V6** Local Contact Roland Steitz
Principal Proposer: Experimental Team:	R. Sedev, Univ. South Australia, R. Steitz, G.H. Findenegg, TU Berlin M. Izerrouken, CRND, Algeria R. Steitz, TU Berlin and HMI Berlin	Date(s) of Experiment 23.-29. 8. 2004

Date of Report: 23.12.2004

In aqueous solutions PEO-PPO-PEO triblock copolymers of ethylene oxide (EO) and propylene oxide (PO) behave as polymeric surfactants whose size can be tailored to meet specific requirements. Their adsorption at the solid/liquid interface is relevant to the wetting and spreading of surfactant solutions, steric stabilization of suspended particles or emulsion droplets, modification of the solid surface affinity for protein adsorption, etc.

The aim of this project is to explore the influence of the surface energetics on the adsorption of such triblock copolymers. Here, we focused on the adsorption of $EO_{122}PO_{56}EO_{122}$ (F108) to deuterated poly(methyl methacrylate), d-PMMA, spin-coated on silicon blocks. Three coatings, S1-S3, were investigated. The neutron reflectivity of the coatings against vacuum revealed smooth and homogeneous films. The layer thickness was 30 nm (34 nm for S3) and their SLD was $(6.6 \pm 0.1)\cdot 10^{-6}$ Å^{-2}.

The adsorption of F108 from aqueous solution to the d-PMMA surface was carried out as follows: Initially the reflectivity of the d-PMMA/D_2O interface was recorded as a reference. Then the flow cell was emptied, washed and re-filled with a sample solution (0.1-2.0 wt% F108; 0.5 wt% NaCl) and the reflectivity of the d-PMMA/solution interface was monitored again.

The reflectivity curves of S1/D_2O and S1/sample solution (01.wt-% and 2 wt-% F108 in D_2O) were found identical thus revealing that the F108 did not adsorb to the interface. This finding was rather unexpected. A subsequent measurement against H_2O showed a strong damping of the Kiessig oscillations from the d-PMMA coating. Similar results were obtained from sample S2 (see Fig. 1): Here, we started off with a calibration measurement against H_2O, followed by measurements against pure D_2O, sample solution in D_2O and subsequently against H_2O, in that order. The chosen contrast in the reference measurements against H_2O before and after F108 incubation highlights the d-PMMA coating. From the comparison of the two reflectivity curves it is obvious that the d-PMMA film changed in the course of the experiment.

With sample S3 we tracked that behavior. After assembly of the flow cell the d-PMMA/liquid interface was rinsed three times with pure H_2O before the reference measurement, S3/H_2O, was taken. Interestingly, this first calibration curve of S3 (see Fig. 2) was closely matching the second calibration curve of sample S2 against H_2O (see Fig. 1). It is

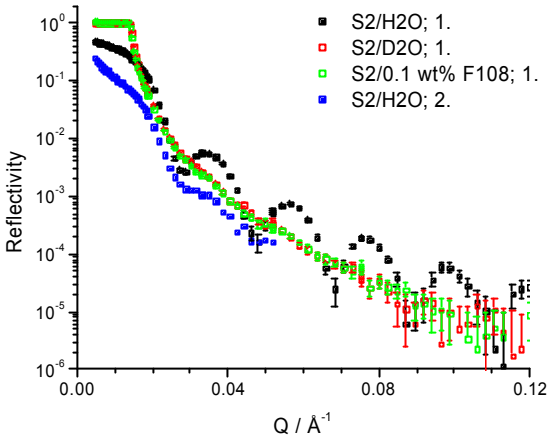


Fig. 1: Reflectivity curves from S2. For details see text.

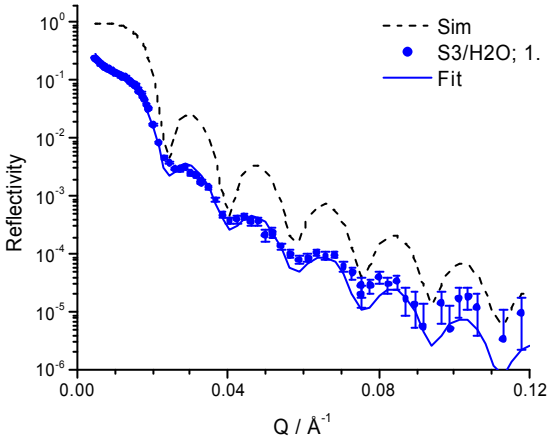


Fig. 2: Reflectivity curves from S3. For details see text.

very different from the expected curve (Sim in Fig. 2), calculated on the basis of an unperturbed d-PMMA coating with the parameters as obtained from the preceding measurement against vacuum. Detailed analysis (Fit in Fig. 2) proofed destruction of the d-PMMA coating leaving 90% of the surface area of the underlying silicon substrate uncovered. The comparison of Fig. 1 and 2 shows that the d-PMMA coatings are unstable against rinsing, i.e. multiple displacement of the liquid phase.

The origin of this instability is currently unclear. It has to be overcome before future experiments can return to the original goal of the project.

	EXPERIMENTAL REPORT **How bound is bound water in swollen polyelectrolyte multilayers?**	Proposal N° PHY-04-964 Instrument **V6** Local Contact Roland Steitz
Principal Proposer: Experimental Team:	John E. Wong, Regine v. Klitzing, TU Berlin John E. Wong, S. Schemmel, TU Berlin R. Steitz, TU Berlin and HMI Berlin	Date(s) of Experiment 20.-28. 4. 2004

Date of Report: 19.01.2005

The sequential layer-by-layer adsorption of polyanions and polycations to build polyelectrolyte multilayers has triggered enormous interest in their potential uses in a wide range of fields, from photonic to pharmaceutical applications. It is imperative to have a good understanding of the influence of environmental parameters on such multilayer assemblies. Polyelectrolyte multilayers are known to swell in water or water vapor. Recently, it has been found that swelling depends on the charge effect of the outer layer. In the PAH/PSS system, assemblies with PSS outermost layer swell more than those with PAH outside. Neutron reflectivity conducted on this effect in addition indicated two kinds of water, bound with different strength within the films. Beside an unexpected two-step kinetics of swelling, the reflectivity curves against vacuum before and after re-hydration in D_2O vapor did not overlap. It was only after subsequent re-hydration in saturated H_2O vapor that the final reflectivity curve against vacuum and the very first reflectivity curve against vacuum superimposed. This finding suggested a slow exchange of protons between the amine group of PAH and the water vapor phase [1].

In the neutron reflectivity experiments reported here we crosschecked above hypothesis with two chemically different systems, (I) $(PDADMAC/PSS)_8$, and (II) $(PAH/PSS)_8$. Both systems were prepared on silicon wafers from 0.25 mol/l NaCl solutions, containing 0.01 mol (monomer) of the respective polymer. From the chemical formula of PDADMAC, there is no possibility of proton exchange with the environment.

Figure 1 shows the reflectivity curves obtained from system I against vacuum (a), D_2O vapor (b), and vacuum (c) in that order. From the increased number of Kiessig fringes in the spectrum against D_2O vapor there is a pronounced swelling of the multilayer film. The water uptake is fully reversible as the comparison of curve (a) and (c) reveals. This is not true for system II, see figure 2. As in our previous experiment [1], the reflectivity curves against vacuum before and after re-hydration in D_2O did not overlap. Once again, it was only after subsequent re-hydration in liquid H_2O that the final reflectivity curve against vacuum, (d), and the very first reflectivity curve against vacuum, (a), superimposed.

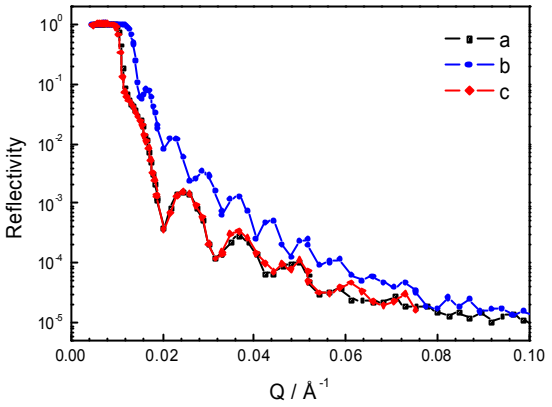


Fig. 1: Neutron reflectivity of coating (I) against vacuum (a), D_2O vapor (b), and vacuum (c) in that order.

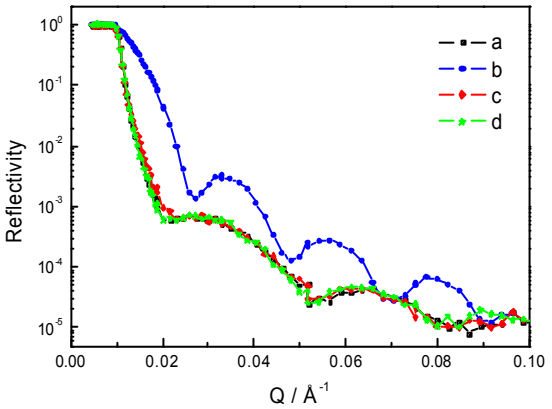


Fig. 2: Neutron reflectivity of coating (II) against vacuum (a), D_2O vapor (b), vacuum (c) and vacuum after immersion in liquid H_2O (d) in that order.

In conclusion, the conducted experiments proof a slow exchange between mobile protons in system II and the corresponding environment on the time scale of hours. It is these protons that might be identified as strongly bound water in polyelectrolyte films.

[1] BENSC Experimenal Report PHY-04-822 (2003).

BENSC	**EXPERIMENTAL REPORT** **Density depletion at the interface between hydrophobic surfaces and water**	Proposal N° CHE-04-895; CHE-04-966 Instrument **V6** Local Contact Dr. R. Steitz
Principal Proposer: Experimental Team:	M. Grunze, Univ. Heidelberg M. Maccarini, Univ. Heidelberg R. Steitz, HMI & TU Berlin	Date(s) of Experiment 7-8 Jan, 2004, 9-14 Aug, 2004

Date of Report: 26 Nov 2004

Sample preparation. Self assembling monolayers (SAMs) of deuterated dodecanthiol ($C_{12}D_{25}$) and protonated mercapto undecanol ($C_{11}OH$) were adsorbed on polycrystalline thin Au films (~60 nm) evaporated on quartz wafers with 3 nm Ti as adhesion promoter. The films (~12 Å thick) were precisely characterized and stored in an inert gas atmosphere (Ar). The hydrophobic sample had an advancing contact angle of 107°, the hydrophilic 40°.

Experimental The refl. were measured first in vacuum for each sample in order to estimate the thickness of the layer sequences, then in contact with degassed D_2O and d-octane.

Results and discussion: Fig. 1 shows the refl. data for the hydrophobic sample in contact with D_2O and d-octane. The two profiles are sensibly different. In the inset we report $\Delta R_{norm}=(R_{D2O}-R_{d\text{-}oct})/R_{D2O}$, i.e. the difference between the two refl. normalized to that measured in D_2O. Since the two liquids have very similar scattering length density, different structural properties of the interfacial liquid must be invoked to explain the difference. As predicted by theoretical studies[1], a layer of water with reduced density, i.e. a depletion layer in contact with a hydrophobic surface is supposed. On the contrary, this depletion layer should be absent in the case of apolar solvent in contact with hydrophobic surface in view of the relative affinity. The latter system can therefore be thought as a zero depletion reference. Therefore, the extent of the depl. layer can be quantified independently of the SAM parameters by fitting the interfacial water and the SAM as a single box (see Fig. 2), and by making the difference between the depletion lengths d_2 [2] obtained in contact with D_2O and that in contact with d-octane. By doing this, we avoid the ambiguities resulting from applying the Nevot-Croce approach in the case of layers whose thickness is of the same order of the roughness. From our analysis the difference in depletion length is 1.4 Å. In the inset of Fig 1 we show also the $\Delta R_{norm}=(R_{depl}-R_{no\text{-}depl})/R_{depl}$ calculated for the same layers sequence with and without a depl. layer of 1.4 Å. The agreement with the ΔR_{norm} experimentally determined is remarkable.

The refl. of the hydrophilic sample did not show any appreciable difference for water and apolar solvent.

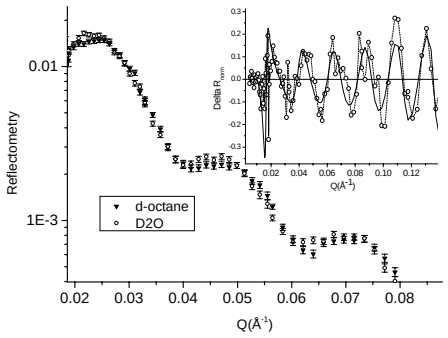


Figure 1. *Reflect. of the hydrophobic sample against d-octane and D_2O. Inset: ΔR_{norm} calculated (solid line) and from experiments (symbol and dotted lines)*

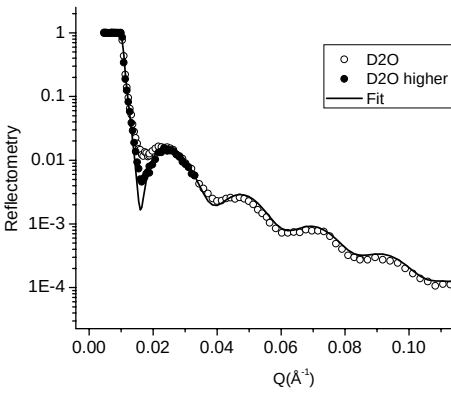


Figure 2. *Fit of the refl. assuming 1-box model. Two different resolutions were used in the experiments. The full symbols represent a scan with higher resolution.*

[1] Lum et al. J. Phys. Chem. B, 103, 4570 (1999)
[2] S. I. Mamatkulov et al. Langmuir, 20, 4750 (2004)

	EXPERIMENTAL REPORT **Chemical Switching of Model Cell Membrane - Substrate Interactions with Weak Polyelectrolytes**	Proposal N° PHY-04-0968 Instrument **V6** Local Contact Dr. R. Steitz
Principal Proposer: Experimental Team:	Dr. Motomu Tanaka, TU München Florian Rehfeldt, Emanuel Schneck, Kirstin Seidel, TU München Dr. Roland Steitz, HMI Berlin	Date(s) of Experiment 01.06.04 – 06.06.04

04. 01. 2005

This project aims at chemical "switching" of interaction between a model cell membrane and ultrathin films of weak polyelectrolyte brushes by pH titration under physiological conditions. To achieve a high polymer chain density, we transferred insoluble monolayers of the amphiphilic diblock copolymers onto hydrophobized silicon. The copolymer, (poly-(DMAEMA-b-MMA)) with 50 % of "switchable" DMAEMA block (DB 50) was synthesized by S.P. Armes (Univ. Sussex).

In earlier experiments (HMI Report 2002, 2003) we demonstrated the reversible and reproducible switching of the thickness, roughness and hydration properties of DB 50 layers at the solid/liquid interface due to pH titration. Based on these results, this beamtime was dedicated to study the interactions between model cell membranes (phospholipid bilayers) and the DB 50 film at charged/uncharged states.

Prior to the experiments at V6, specular x-ray reflectivity experiments of DB 50 films deposited at different lateral pressures were performed at the HMI to optimize the lateral polymer chain density. Furthermore, homogeneous spreading of a lipid bilayer was verified with fluorescence microscopy experiments at TU München (Figure 1).

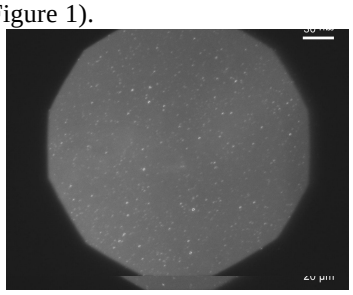


Figure 1: Fluorescence image of a DB 50 film homogeneously covered with a lipid membrane (pH=5.5).

Figure 2 shows the reflectivity of a DB 50 film before and after incubation with a lipid suspension at pH=5.5. Clearly the change in the global shape of reflectivity curves can be identified, corresponding to the deposition of a protonated layer. A six box model fit (Si, d-PMMA, DB 50, D_2O, bilayer, and D_2O) using the values fitted before incubation lead to a thickness of the lipid layer of 24 Å. Although this value seems to be rather small, it is still reasonable from the different scattering length densities of fully protonated hydrocarbon chains and hydrophilic headgroups, which are hydrated with D_2O. In fact, as it is impossible to separate these three (head-tail-head) layers, the roughness of the lipid membrane was found to be relatively large (σ = 14 Å). Moreover, the obtained data are better explained by including another D_2O layer into account, suggesting the existence of a pure D_2O reservoir (with the thickness of 14 Å) between hydrated DB 50 and the lipid membrane.

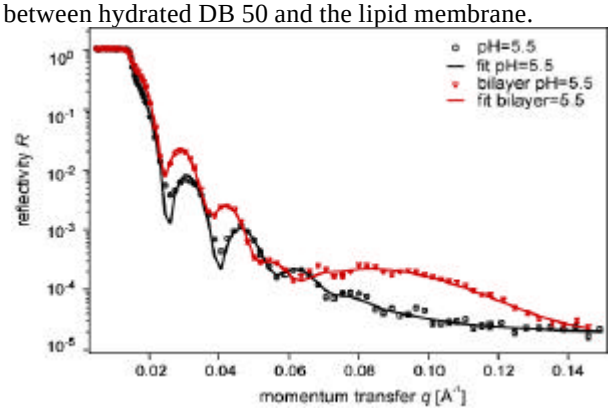


Figure 2: Reflectivity of the DB 50 polymer layer before (black) and after (red) deposition of a lipid membrane.

Switching of the subphase pH to 8.5 resulted not only in change in polymer chain conformation (as observed previously) but also in a clear increase in the thickness of the D_2O spacer to 30 Å. Figure 3 shows the scattering length density profiles for both pH conditions and a sketch of the model system.

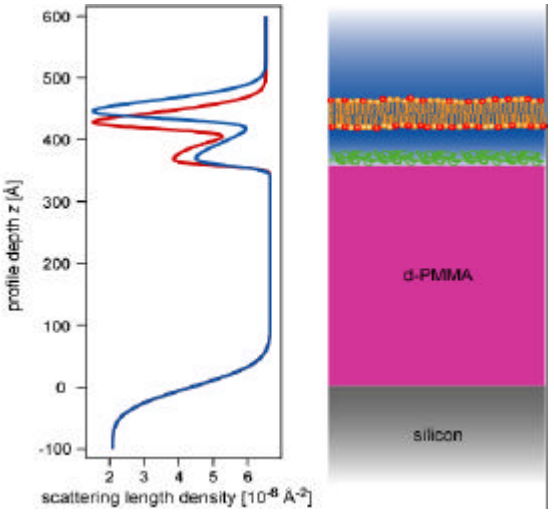


Figure 3: Scattering length density profile for pH=5.5 (red) and pH=8.5 (blue) together with a sketch of the model system.

The obtained results demonstrate the advantages of weak polyelectrolyte brushes against other strong polyelectrolytes for the fine-tuning of interfacial interactions between biological materials and solid substrates.

	EXPERIMENTAL REPORT **Critical and multilayer adsorption from alkane + perfluoroalkane mixtures**	Proposal N° PHY-04-0977 Instrument **V6** Local Contact Roland Steitz
Principal Proposer: Experimental Team:	James Bowers, University of Exeter, U.K. Ali Zarbakhsh, Queen Mary, U. of London John Webster, ISIS Ian McLure, University of Sheffield	Date(s) of Experiment 1-8 April 2004

Date of Report: 21 April 2004

Interesting adsorption behaviour occurs as the liquid–liquid coexistence curve of a binary liquid mixture is approached. As coexistence is approached along a path of constant composition on the appropriate side of the coexistence curve, a thick film of the preferentially adsorbed component builds up. The thickness l of this multilayer adsorbed film is expected to grow as $l \sim |T - T_{sep}|^{-1/3}$, where T_{sep} is the coexistence temperature. A special situation arises when the critical solution point is approached. In this region the behaviour of the system is governed by composition fluctuations. Here, the thickness of the adsorbed film scales with the correlation length ξ of the composition fluctuations, and behaves as $l \sim \xi \sim |T - T_c|^{-0.305}$, where T_c is the critical temperature. However, despite the similarity in the film thickness divergence, the analytical behaviour of the composition profiles is different. Critical adsorption possesses a now-established power-law dependence, $\phi(z) - \phi(\text{bulk}) \sim z^{-0.52}$, where ϕ is the volume fraction composition and z is the coordinate normal to the interface, whereas the less frequently examined multilayer adsorption profile is considered to be either a slab or an exponentially decaying profile, and the nature of this profile remains open.

We have recently performed neutron reflectivity measurements on V6 that will aid the examination of the nature of such critical and multilayer adsorption profiles. Alkane + perfluoroalkane mixtures provide suitable systems for the study of such phenomena, and, accordingly, we have examined the adsorption from mixtures of (1–x) hexane-d_{14} + x perfluorohexane, where x is the perfluorohexane mole fraction, to an octadecyl-coated silicon substrate. Reflectivities have been measured for mixtures with x = 0.36 (critical composition), 0.5 and 0.65 as a function of temperature upon approach to the coexistence curve. Selected data for the x = 0.36 and 0.65 mixtures are shown in the figures below to indicate the observed trends. Note that the changes in reflectivity are more pronounced for x = 0.65 and rather subtle (closer to the total reflection edge) for x = 0.36. Data analysis will focus on determining the power-law decay, exponential decay, or slab-like nature of the adsorbed films and how the adsorption profiles vary with distance from the critical point and from coexistence.

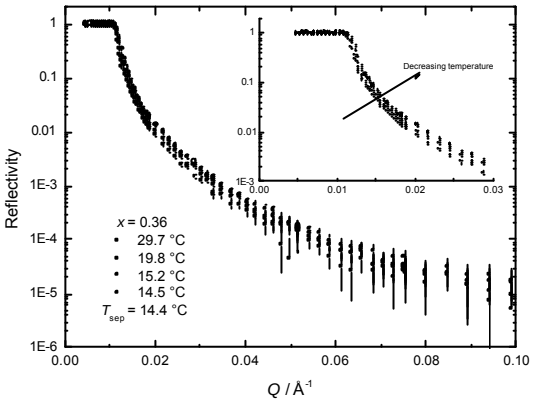


Fig. 1. x = 0.36 (critical adsorption).

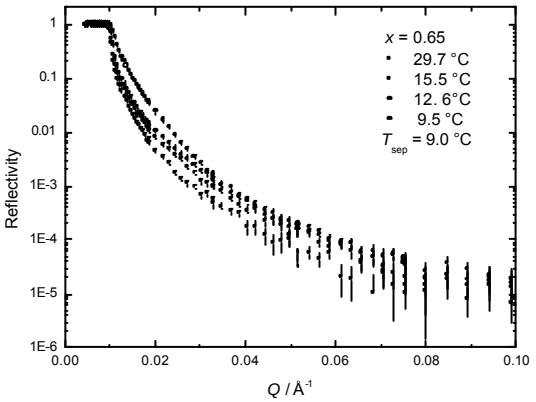


Fig. 2. x = 0.65 (multilayer adsorption).

	EXPERIMENTAL REPORT **Hydration of lipid layers on polyelectrolyte multilayer support**	Proposal N° CHE-04-976 Instrument V6 Local Contact R. Krastev
Principal Proposer: Experimental	C. Delajon, Uni. Strasbourg / MPI KG C. Delajon, Uni. Strasbourg / MPI KG R. Krastev, HMI Berlin / TU Berlin	Date(s) of Experiment 30.04. – 04.05.2004

Date of Report: 20.12.2004

Biomimetic surfaces with tailored properties are a major object of application oriented biophysical studies. We studied the formation of a planar biomimetic model membrane made of a DMPC lipid layer and supported by polyelectrolyte multilayers (PEM). Neutron reflectometry (NR) experiments were performed to study the characteristics of the formed lipid layers. It allows the thickness of the samples h, as well as their Scattering Length Densities (SLD) ρ to be obtained. The later is related to the composition of the samples.

Two samples were prepared by covering silicon wafers with a PEI/(d-PSS/PAH)$_6$ PEM cushion using the Layer-by-Layer deposition technique [1]. Sample 1 was kept as it is for reference experiments. Sample 2 was covered with an additional lipid layer prepared by immersion in an extruded DMPC lipid vesicle solution followed by an extensive rinsing and dust-free nitrogen drying. All measurements were performed in a solid-air measurement cell. Two sets of experiments, in H_2O saturated vapours and in dry atmosphere, were carried out. The reflectivity curves together with the best fits to the data are shown on Fig. 1. The data of the best fits are summarised in Table 1.

Upon exposure to H_2O vapours the thickness of the sample 1 increases with around 30 % and its SLD decreases. The amount of adsorbed in the sample H_2O is estimated to be around 32 %. The values correspond well to the prior experiments [2]. Detail fits to the reflectivity curves of sample 2 did not enable to distinguish between the polymer and the lipid layer. That is why only a one-box model was used to fit the data. Upon exposure to H_2O vapours an increase in the sample thickness of around 27 % was observed and a decrease in its SLD which relates to around 30 % H_2O adsorption. This result shows that the adsorption/desorption of H_2O in the PEM cushion is not affected by the presence of DMPC layer on top of it.

We observe a thickness decrease in case of sample 2 in comparison with sample 1, although the decoration with a lipid layer was confirmed by X-ray analysis and should lead to an increase of the overall thickness. This phenomenon has already been observed for the similar samples in D_2O vapours [2] and was initially attributed to a non-equivalent exposure time of both samples to the vapours. This explanation is no longer valid, as the exposition time parameter was carefully checked in the present set of experiments.

A better explanation for the deswelling observed after the lipid decoration may be the lack of affinity between PAH and DMPC, and the hydrophilicity difference between PAH and d-PSS. Indeed, *in situ* deposition of DMPC onto PAH and d-PSS terminated polymer blocks at the solid-liquid interface revealed the formation of a lipid bilayer only in the case of d-PSS terminated samples [3].

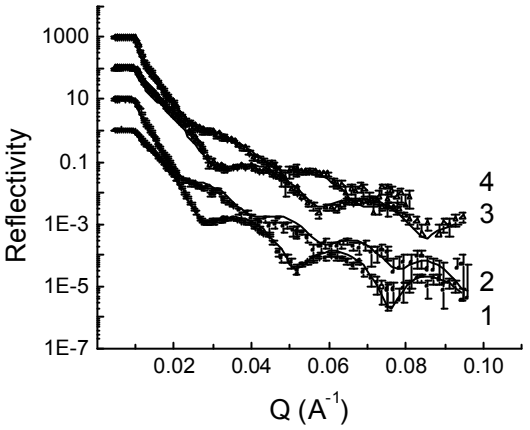


Figure 1: *NR curves together with the best fits to the data. 1+2) Sample 1 in dry N_2 and in H_2O vapours respectively; 3+4) Sample 2 in dry N_2 and in H_2O vapours respectively.*

Table 1:

	In dry N_2		In H_2O vapours	
	h, Å	?, x 10^{-6} Å^{-2}	h, Å	?, x 10^{-6} Å^{-2}
PEI/(d-PSS/PAH)$_6$ (Sample 1)	252	3.41	328	2.49
PEI/(d-PSS/PAH)$_6$/DMPC (Sample 2)	224	3.30	283	2.43

References:

[1] Decher, G. Science **277** (1997) 1232

[2] Delajon, C., Krastev, R. HMI Exp. report 2003 CHE-04-859 LT

[3] Delajon, C., Krastev, R., Gutberlet, T., Möhwald, H., to be submitted

	EXPERIMENTAL REPORT **Soft supported lipid layers for adsorption studies of Aβ(25-35)**	Proposal N° BIO-04-997 LT Instrument V6 Local Contact R. Steitz
Principal Proposer: Experimental Team:	Silvia Dante, TU Darmstadt and HMI Berlin Thomas Hauß, HHU Düsseldorf / HMI Roland Steitz, TU Berlin and HMI Berlin Sebastian Schemmel, TU Berlin	Date(s) of Experiment 22.-28.6.2004

Date of Report: 21.12.2004

To gain information on the adsorption of small peptides, like the beta-amyloid Aβ(25-35), in/on lipid membranes, we have developed a method to prepare model membranes (stacked lipid layers) via fusion of small unilamellar vesicles onto a polymer coated substrate. In particular, the interaction of the peptide with the lipid membrane may be driven by electrostatic forces, since Aβ carries a positive charge, and the natural neuronal membrane is negatively charged. We chose therefore to utilize charged polyelectrolytes (PE) to coat the substrate, and we investigated the adsorption process of negatively charged and neutral vesicles. Substrates were prepared by coating silicon wafers with a layer of poly(ethylene imine) followed by six bilayers of poly(styrene-sulfonate)/poly(allyl amine-hydrochloride) with terminal PSS layer, $(PSS/PAH)_6/PSS$, negatively charged, (I), or without, $(PSS/PAH)_6$, positively charged, (II), by self-assembly technique. As model lipids a mixture of d-DMPC (fully deuterated, neutral) and d-DMPS (chain deuterated, negatively charged), 90:10 mol/mol, was chosen. The vesicles were prepared by extrusion with 100 and 50 nm filters at a concentration of 0.3 - 0.53 mg/ml in D_2O. Alternatively, purely hydrogeneous, unilamellar DMPC vesicles were prepared by ultrasonication.

Neutron reflectivity measurements were performed on the Si/PE coating/liquid interface prior to and after incubation with vesicle solution for 1h and subsequent rinsing with pure D_2O (or H_2O), The setup of the experiments is shown in Fig. 1.

There was no difference in the reflectivity curves of the PE coating (I) against D_2O, prior to and after incubation with (a) mixed d-DMPC/d-DMPS vesicles and (b) pure d-DMPC vesicles. This finding is not unexpected for case (a) as there is electrostatic repulsion between vesicles and coating. It is rather unforeseen for case (b) where the driving force of vesicle fusion is of entropic nature. Control measurements against H_2O after incubation with d-DMPC vesicles, with enhanced sensitivity against the adsorbed d-DMPC layer, proofed no net adsorption of lipids to the PE coating.

Identical results were obtained from PE coating (II) against mixed d-DMPC/d-DMPS vesicles, when prepared by extrusion through a 50 nm filter.

It was only when PE coating (II) was exposed to DMPC vesicles in D_2O, that were prepared by ultrasonication, that vesicle fusion to the soft polymer cushion occurred. Fig. 2 shows the successful assembly of the soft-supported lipid membrane at the solid-liquid interface. The observed left-shift of the Kiessig fringe positions in the corresponding neutron reflectivity curve reveals a thickness of the adsorbed DMPC bilayer of about 47 Å. Detailed analysis revealed a water content of ca. 44% by volume. Although the lipid layer is well pronounced and easily formed its water content is rather high. This suggests a patchwork structure of lipid-covered and lipid-free regions in the adsorbed layer. Higher lipid densities (close to full coverage) have to be achieved before a model system is established. Upcoming experiments will focus on this aspect.

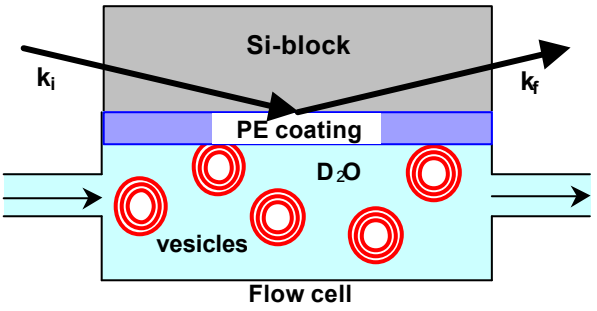


Fig. 1: Sketch of the experimental setup.

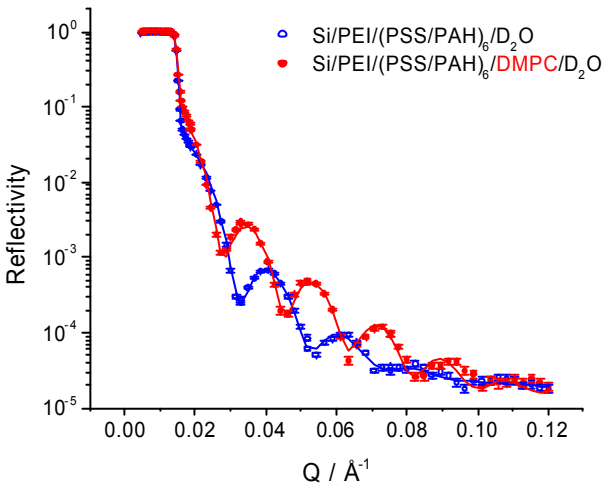


Fig. 2: Reflectivity curves from PE coating (II) (d = 304 Å) before and after incubation with lipid vesicles. Solid lines are fits to the data.

	EXPERIMENTAL REPORT **Temperature dependent water depletion at a hydrophobic solid/liquid interface**	Proposal N° CHE-04-998 LT Instrument **V6** Local Contact Roland Steitz
Principal Proposer: Experimental Team:	R. Steitz, G.H. Findenegg, TU Berlin S. Schemmel, TU Berlin R. Steitz, TU Berlin and HMI Berlin	Date(s) of Experiment 28.-30. 5. 2004

Date of Report: 29.12.2004

Neutron reflectivity experiments conducted on the interface of deuterated polystyrene, d-PS, thin films and heavy water, D_2O, revealed a depletion of water at the d-PS/D_2O interface. Reduced water density (90% bulk water density) was found in 2-5 nm thick boundary layers as a function of air saturation of the water sample and on the time elapsed after contacting it with the hydrophobic surface [1]. These findings are corroborated by MD simulations on an alkane slab immersed in water [2]. The latter study predicted a pronounced increase in thickness of the depletion layer with elevated temperature.

In 2004 we stepped out for an experimental cross-check on above prediction with d-PS films, spin-coated on silicon substrates, in contact with heavy water, D_2O. Reference measurements were conducted on the d-PS samples against air, prior and after exposure to the liquid phase. The d-PS coated silicon single crystals served as the top of a flow cell made up by a Teflon trough. The cell was embedded in an aluminum housing water-thermostatted by a HAAKE F6 circulating bath. The neutrons (λ = 4.66 Å) assessed the d-PS/liquid interface through the silicon backing with a typical reflectivity run consuming 7h of beamtime.

Figure 1 shows the reflectivity curves obtained from d-PS coating 3 against degassed D_2O as a function of sample temperature. The Kiessig fringes in the spectra reveal non-vanishing scattering contrast, i.e. water depletion, at the interface at all temperatures. It is the amplitude of the oscillations which decays with increasing sample temperature.

Detailed analysis reveals an increase in depletion layer thickness from 3.6 nm at 23°C to 4.4 nm at 67°C. However, also the water density in the depletion layer increases from 91 to 95% bulk water density. The corresponding depletion length d_2 thus decreases from 3.1 ± 0.7 Å to 2.3 ± 0.8 Å. The latter result is opposed to the MD results by Mamatkulov and Netz [2], who predicted a moderate increase in d_2 from 2.5 to 2.7 Å in the temperature range 27 to 67°C.

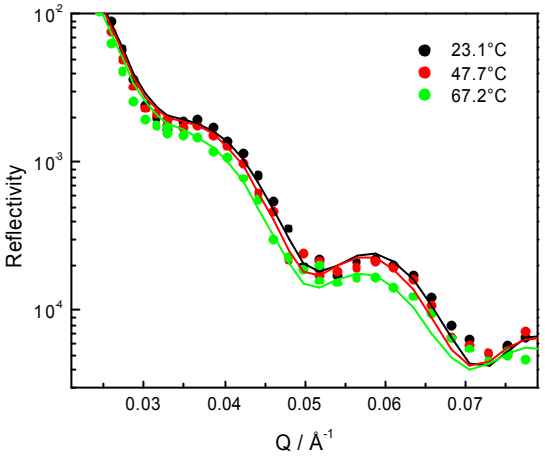


Fig. 1: Neutron reflectivity (close-up) from the interface of coating d-PS 3 against D_2O as a function of sample temperature. Solid lines are best fits to the data.

$$d_2 \approx \left(1 - Nb_{layer}/Nb_{bulk}\right) \cdot d_{layer}$$

After cooling to 23°C d_2 increased again to 3.6 ± 1.2 Å. Also the polymer coating itself changed in the course of the experiment: While its total thickness (27.5 ± 0.1 nm) remained constant, its average scattering length density decreased. This can be taken as the onset of a de-wetting from the silicon substrate where roughening on the length scale of visible light cannot be excluded (the d-PS film was opaque after the experiment where it was transparent before). One may speculate whether it is these structural changes in the d-PS coating that are responsible for the observed increase in the depletion length against D_2O after cooling to room temperature again.

[1] R. Steitz et al., Langmuir 19 (2003) 2409.

[2] S.I. Mamatkulov et al., Langmuir 20 (2004) 4756.

	EXPERIMENTAL REPORT **Influence of the Confinement on the Amount of D_2O Absorbed in Polyelectrolyte Films**	Proposal N° CHE-04-1004 Instrument V6 Local Contact R.Krastev
Principal Proposer: Experimental Team:	R. Krastev, MPI KG, Golm, Germany R. Krastev, MPIKG,Golm/HMI,Berlin, Germany N. C. Mishra, MPIKG, Golm, Germany	Date(s) of Experiment 20 – 27 July 2004

Date of Report: 12.01.2005

The concentration of mobile components in nano-structured systems may depend on the dimension of the system. When two semi-infinite phases are separated by a thin layer the thermodynamical properties of the layer are different than those of the bulk material. This difference leads to changes in the thickness of the thin layer, well described by the DLVO theory in the case of easy deformable (fluid) materials. In the case of stiff materials this effect might create exchange of mobile components between the thin layer and its surrounding. Such a dependence should appear, if the dimension of the system under consideration comes into the range of the action of the surface forces (less than 15 nm). Then the chemical potential becomes function of the dimensions and the concentration of a mobile component will change. We checked this hypothesis in the case of the water absorption in polyelectrolyte multilayers (PEM) with different thickness.

Four PEM films were prepared on Si wafers by LbL technique from poly(ethylenimine) (PEI), poly(allylamine hydrochloride) (PAH) and poly(sodium 4-styrenesulfonate) (PSS). The film structure was $PEI(PSS/PAH)_n$ where n = 1, 2, 4 and 6. Neutron reflectometry (NR) experiments were performed at 23 °C in gas tight cell in dry and near to 100 % r.h. (saturated D_2O vapour atmosphere) at the reflectometer V6. The reflectivity curves in D_2O vapour atmosphere are shown on Figure 1. A linear increase in the film thickness with the number of (PSS/PAH) polyelectrolyte bilayers was observed (Figure 2). The amount of D_2O absorbed in the PEM was also calculated knowing the scattering length density of the material in dry and wet state. We observed decrease in the D_2O content upon increase the number of PE layers. Only the first point in the dependence (PEM with one PE bilayer) deviates from the trend. This might be an effect of lower precision of determination of the SLD of that sample (see Fig. 1) or its non-homogeneous structure which consists of many empty voids.

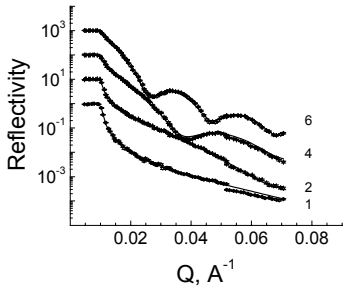


Fig 1: *NR curves in 100% r.h. D_2O atmosphere for samples with 1, 2, 4, and 6 (PSS/PAH) bilayers.*

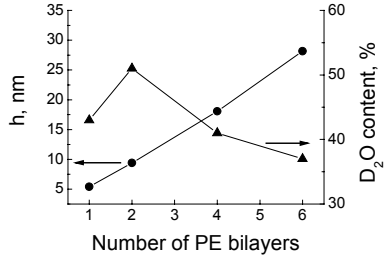


Fig. 2: *PEM thickness (●) and D_2O content (▲) as a function of the number of PE bilayers*

The observed effect can be explained by changes in the bulk density of the PEMs or increased chemical potential of D_2O which results in its reduced amount. More precise answer will be found when other methods for surface characterisation (e.g. X-ray reflectometry) is used to complement the present results.

BENSC	**EXPERIMENTAL REPORT** **Internal Order of Polyelectrolyte Multilayers**	Proposal PHY-04-1049 Instrument V6 Local Contact Roland Steitz
Principal Proposer: Experimental Team:	Christiane A. Helm, Physik, Uni Greifswald Manesh Gopinadhan, Physik, Uni Greifswald Heiko Ahrens, Physik, Uni Greifswald Jens-Uwe Günther, Physik, Uni Greifswald	Date(s) of Experiment 13.-19.7.04

Date of Report: 3.1.05

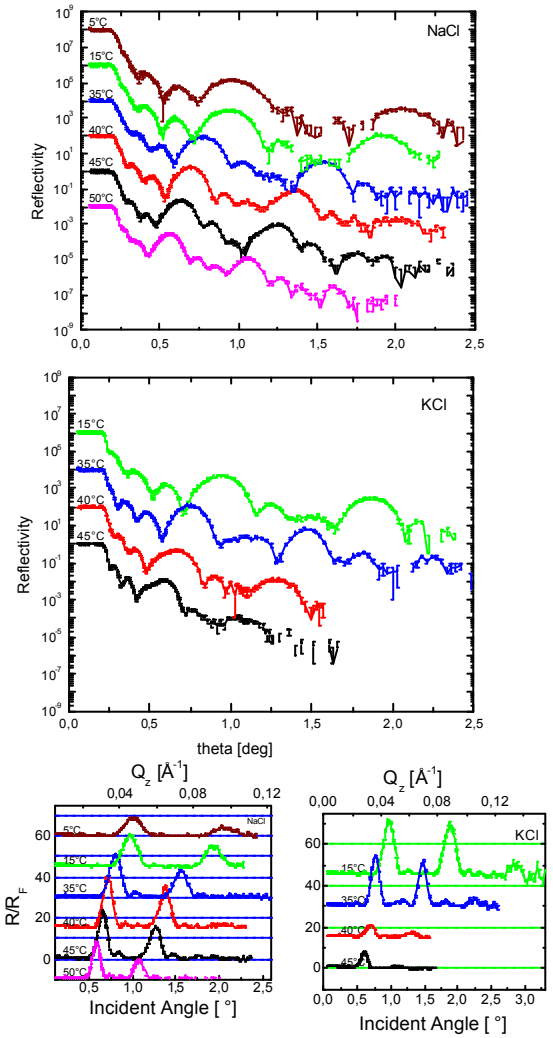


Fig. 1. Neutron reflectivity curves of polyelectrolyte multilayers, PEI{(PSS/PAH)$_3$PSS$_d$/PAH}$_4$(PSS/ PAH)$_3$ prepared from 1 M KCl (top) and 1 M NaCl (center) solution at different temperatures (as indicated). The films consisted of polystyrene(sulfonate) (PSS) and poly(allylamine hydrochloride) (PAH) with selectively deuterated PSS-layers. Bottom: The same data, yet normalized relative to the Fresnel-Reflectivity.

Self-assembly processes of polyelectrolytes involving electrostatic interactions can be used to build-up multi layered materials with unique properties. The basic principle is the sequential adsorption of positively and negatively charged polyelectrolytes[1, 2].

Polyelectrolyte adsorption onto an oppositely charged interface is determined by electrostatic and secondary interactions.[3, 4] On increase of the salt concentration in the deposition solution, both the polyelectrolyte coverage and the thickness of the adsorbed layer increase, features which are attributed to the screening of the electrostatic force.[2] However, little is known about the nature, the origin and the influence of the secondary forces[4, 5]. The solvent quality declines on temperature rise, it can be varied systematically. We found that the thickness per layer pair increases by about 75%[5], if the temperature of a solution containing 1 M monovalent salt is varied between 5 and 45°C, a finding confirmed by neutron reflectivity (cf. Fig. 1).

Since the segmental distribution of one polyelectrolyte layer exceeds its thickness[1], the monomer density is constant along the surface normal for both polycations and polyanions. The interpenetration of consecutive layers is attributed to the formation of ion contact pairs, which are responsible for the pronounced stability of multilayers. If the salt concentration[5] in solution or its temperature[6] are varied (in the latter case below 35°C), the internal roughness amounts to 40% of the thickness of a polycation/polyanion pair. At temperatures exceeding 35°C, the internal roughness is larger, which is attributed to the approaching precipitation temperature.

The films shown in Fig. 1 were organized in a superlattice of 7 perprotonated layers and 1 perdeuterated layer in 4 repeat units, the selectively deuterated PSS layers provide contrast. They were prepared from 1 M KCl solution (precipitation at 55°C) and 1 M NaCl (no precipitation). At low temperatures, oscillations which measure the film thickness as well as two Bragg peaks can be discerned. With NaCl in the subphase, the peaks vary in intensity, yet can always be found. With KCl the approach of precipitation temperature leads to the loss of the third Bragg peak, and eventually to the disappearrance of the second. These structural data indicate that polyelectrolyte molecules adsorb in a collapsed state onto the oppositely charged film surface, stratification is no longer prominent.

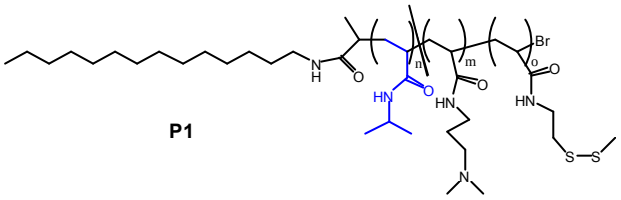
Literature

1. Decher, G., *Science*, 1997. **277**: p. 1232-1237.
2. Schönhoff, M., *Curr. Opin. Colloid Interface Sci.*, 2003. **8**: p. 86-95.
3. Netz, R.R. and J.-F. Joanny, *Macromolecules*, 1999. **32**: p. 9013-9025.
4. Shiratori, S.S. and M.F. Rubner, *Macromolecules*, 2000. **33**: p. 4213-4219.
5. Büscher, K., et al., *Langmuir*, 2002. **18**: p. 3585-3591.
6. Gopinadhan, M., et al., *Macromolecules*, 2005. **subm.**

	EXPERIMENTAL REPORT **Novel Lipopolymer Supported Lipid Bilayers**	Proposal N° CHE-04-1051 Instrument **V6** Local Contact Dr. Rumen Krastev
Principal Proposer: Experimental Team:	Dr. Patrick Theato, University of Mainz Dr. Patrick Theato, University of Mainz Dr. Rumen Krastev, HMI Berlin	Date(s) of Experiment 14.08.04 – 17.08.04

Date of Report: 15.12.04

Polymer supported lipid membranes are very attractive models of the biological membrane. Many fruitful approaches have been proposed to prepare such very sophisticated nano assemblies. [1] End-functionalized lipo-polymers are a novel class of polymers tuned as supports for lipid membranes. Recently, we could synthesize end-functionalized lipopolymers based on poly(N-isopropylacrylamide) which has a lower critical solution temperature (LCST). [2]



***Scheme 1**: Structure of lipopolymer **P1** investigated in this study.*

It was the purpose of the present study to investigate such a thermosensitive lipopolymer (**P1**) at different temperatures. Especially the stability of the supported membrane at higher temperatures was of interest. Thus, the following series of neutron reflectometry experiments were performed: gold coated silicon block in D_2O (Si/Au/D_2O) at T=26 °C and T=60 °C, adsorbed **P1** layer onto the gold coated silicon block (Si/Au/**P1**/D_2O) at T=26 °C and T=60 °C, and DMPC vesicles fused onto this lipopolymer monolayer (Si/Au/P1/DMPC) at T=26 °C and T=60 °C.
As reference measurements bare gold coated Si blocks were measured at T=26 °C and T=60 °C. It turned out, that the same reflectometry curves were measured for both temperatures. In the following a monolayer of P1 was adsorbed onto the gold surfaces, resulting in a thin about 12 Å thick polymer film. However, the thickness of the gold layer was with 1400 Å too thick to obtain a good resolution with such a thin polymer film. Nevertheless, it could be recorded that at T=60 °C the polymer film collapses to a dehydrated polymer film.

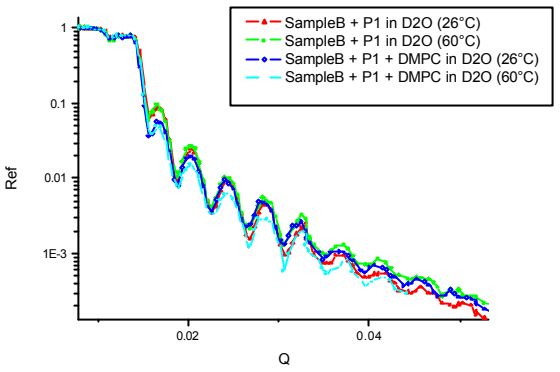


***Figure 1**: Neutron reflections of **P1** and **P1**+DMPC at T=26 °C and T=60 °C.*

Much more pronounced was the change in thickness after fusing a lipid bilayer onto the **P1** monolayer. Clearly a thickness increase of 40 Å could be observed at T=26 °C, proving the nano-assembly of a lipid bilayer on a polymer support.
Most interesting was the decrease in thickness upon temperature increase to T=60 °C. It resulted in a thickness comparable to the origin **P1** monolayer at T=60 °C. Thereby, we were able to show for the first time that the polymer **P1** is capable to act as a reversible support for lipid bilayers. This will open new possibilities in the field of potential biosensor applications. [3]
To conclude, we were able to investigate monolayers of a thermosensitive lipopolymer P1, which is capable to act as a new reversible support for lipid bilayers.

References:
[1] E. Sackmann, *Science*, **1996**, *271*, 43.
[2] P. Theato, R. Zentel, *Macromolecular Bioscience*, **2002**, *2*, 387
[3] P. Theato, R. Krastev, in preparation.

	EXPERIMENTAL REPORT **Neutron Reflectivity and calcium-induced modification of a phospholipid/polymer layer**	Proposal N° PHY-04-1070-LT / EF Instrument **V6** Local Contact R. Krastev
Principal Proposer: Experimental Team:	Ropers M.H., INRA Nantes (France) Ropers M.H., INRA Nantes (France) Krastev R., HMI Berlin	Date(s) of Experiment 29.06.04 to 02.07.4

Date of Report: 06.08.04

Interactions between surfactants and polymers may occur either in a direct way between two oppositely charged molecules or through a divalent cation such as calcium. We analysed by neutron reflectivity the adsorption of a pectin (natural negatively charged polysaccharide) onto a dimyristoyl phosphatidic acid layer via assumed calcium bridges, the lipid layer being itself anchored on a polymer cushion modifying a silicone wafer. The interest of such cushions lies in the formation of a liquid-like interface for the phospholipid and the measurement of the thickness in a reduced q-range.

The measurements were performed on a silicone wafer modified by a PEI/$(PSS/PAH)_{6.5}$ layer (PolyEthyleneImine PEI, PolyStyreneSulfonate PSS and PolyAllylamine Hydrochloride PAH) according to the method initiated by Decher (*Science, 277 (1997) 1232-1237*) and studied by Steitz et al. (*Coll. Surf. A 163 (2000) 63-70*). The temperature was fixed to 25°C. Dimyristoyl phosphatidic acid DMPA was spread onto polymers from a solution of multilamellar vesicles (C=1mg/ml) sonicated at 50°C for several hours until getting a clear solution. We have considered a pectin made of mainly galacturonic acid units partially methylated (77%) which does not gel in the considered conditions. The cell was rinsed after each deposition with a salty D_2O solution (NaCl 25mM or $CaCl_2$ 2mM) to remove non adsorbed molecules and get optimal contrast.

The thickness of the polymer cushion as well as the phospholipid layer were extracted from the adjustment of the curves with a single box model. The contact of the polymer with the solution of vesicles leads to the formation of a 76Å-thick phospholipid layer with a low roughness onto a less rough polymer layer (Figure 2). The lipid layer thickness value agrees with the parameters of a single hydrated DMPA bilayer (*Schalke et al. BBA 1464 (2000) 113-136*) but it was impossible to adjust the curve with more than 1 layer (referring to tails and hydrated heads). The roughness increases in presence of calcium and the polymer layer is more compact while the bilayer thickness stays constant. Calcium may interact more strongly with sulphonate groups of PSS than with phosphates of DMPA and have penetrated into the polymer cushion. The complexation between two neighbouring sulphonate groups or two sulphonate groups belonging to two different layers may also occur (a hydrated PAH layer is however roughly 30Å thick) and the conformational rearrangement result in a rougher material. The introduction of a pectin charged with calcium induces a surprising thinning of the phospholipid bilayer. Either the conformation of the phospholipid changed or the hydrated layer between the polymer and the phospholipid disappears.

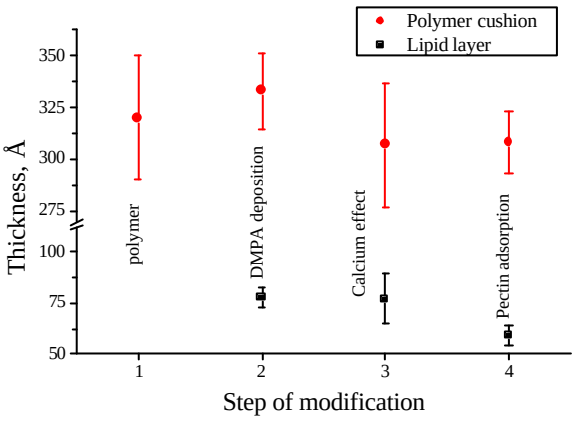


Figure 2. Thickness of the polymer and the phospholipid layers as a function of the consecutive steps of treatment. The error bars refer to the values of roughness.

BENSC	**EXPERIMENTAL REPORT** **Pretreatment dependent water depletion at a hydrophobic solid/liquid interface**	Proposal N° PHY-04-1072 LT Instrument **V6** Local Contact Roland Steitz
Principal Proposer: Experimental Team:	R. Steitz, G.H. Findenegg, TU Berlin S. Schemmel, TU Berlin R. Steitz, TU Berlin and HMI Berlin	Date(s) of Experiment 28.-31. 3. 2004

Date of Report: 28.12.2004

Neutron reflectivity experiments conducted on the interface of deuterated polystyrene, d-PS, thin films and heavy water, D_2O, revealed a depletion of water at the d-PS/D_2O interface. Reduced water density (90% bulk water density) was found in 2-5 nm thick boundary layers as a function of air saturation of the water sample and on the time elapsed after contacting it with the hydrophobic surface [1].

In 2004 we continued above line of experiments on the interface of d-PS films, spin-coated on silicon substrates, in contact with a less hydrophilic liquid phase, namely deuterated methanol, CD_3OD. Reference measurements were conducted on the d-PS samples against vacuum and D_2O, prior and after exposure to CD_3OD. The d-PS coated silicon single crystals served as the top of a flow cell made up by a Teflon trough. The neutrons (λ = 4.66 Å) assessed the d-PS/liquid interface through the silicon backing with a typical reflectivity run consuming 10h of beamtime.

Figure 1 shows the reflectivity curves obtained from d-PS coating 2 against vacuum (1), degassed D_2O (1), CD_3OD (not shown), degassed D_2O (2) and vacuum (2) in that order. The Kiessig fringes in the spectra against heavy water reveal non-vanishing scattering contrast, i.e. water depletion, at the interface.

Although the reflectivity curves against vacuum are identical, the curves against D_2O are not. There is a clear reduction in Kiessig oscillation amplitude after intermediate exposure to CD_3OD. Detailed analysis reveals a 3 nm thick liquid boundary layer of 86% bulk water density prior to displacement of D_2O by CD_3OD and a 4 nm thick boundary layer of 96% bulk water density afterwards. The corresponding depletion length

$$d_2 = \left(1 - Nb_{layer}/Nb_{bulk}\right) \cdot d_{layer}$$

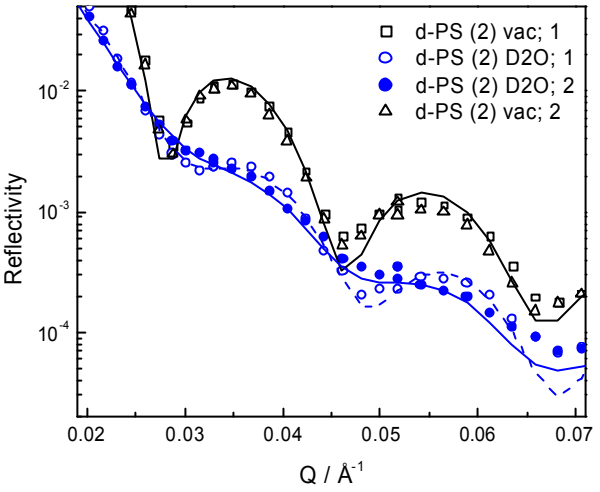


Fig. 1: Neutron reflectivity from the interface of coating d-PS 2, against vacuum, D_2O, CD_3OD (not shown), D_2O and vacuum in that order.

changes from 4.3 ± 2.0 Å to 1.8 ± 2.0 Å. Qualitatively similar findings are reported by Simonsen and co-workers who observed a drastic decrease in the number of nanobubbles at the d-PS/liquid interface after displacement of the water phase by ethanol (89% before to 7% surface coverage after) [2].

The depletion length at the interface of d-PS 2 against D_2O measured three weeks later (with intermediate storage of the coating in vacuum) was 3.3 ± 1.5 Å. The polymer coating itself proofed uneffected: Its thickness did not change outside error from the very first measurement with neutrons against vacuum (d_{dPS} = 29.3 nm) to the very last measurement with x-rays against air (29.9 nm). Therefore, we conclude that the reduced depletion length found at the dPS/D_2O interface directly after intermediate exposure of the polymer coating to CD_3OD originates from a remaining, molecular adsorption layer of CD_3OD that promotes wetting between d-PS and D_2O.

[1] R. Steitz et al., Langmuir 19 (2003) 2409´.
[2] A.C. Simonsen et al. J. Coll. Interface Sci. 273 (2004) 291 and private communication.

	EXPERIMENTAL REPORT **Thermal expansion and electroweak interaction in the amino acid L-alanine**	Proposal N° EF Instrument **E9** Local Contact D.N. Argyriou
Principal Proposer: Experimental Team:	H.N. Bordallo, HMI M. Barthès, Université Montpellier II F. Denoyer, Université Paris XI C. Fehr and D.N. Argyriou, HMI	Date(s) of Experiment 24-30/06/2004

Date of Report: 20/10/2004

For the most part, enantiomers have identical physical and chemical properties. However, the difference between enantiomers can have enormous impact, particularly in biological systems. In this way an enantiomer can fit the active site of a specific enzyme producing the desired effect. While, the other one cannot interact with the same site due to a different arrangement of atoms. For the development of medical drugs, which very often are chiral substances, it is extremely important to fully characterize the enantiomers.

As in neutron diffraction the scattering power does not depend upon the number of electrons surrounding the atom, but rather upon the nuclear cross-section, the method is particularly useful for the study of crystal structures containing light elements. Moreover peak shapes from neutron powder diffraction (NPD) are relatively simpler to model than that from synchrotron, allowing for relatively straightforward refinements of structural parameters. With this in mind we started a study to verify if the enantiomers for the chiral amino acid, alanine ($C_2H_4(NH_2)COOH$), display subtle differences in their crystallographic structure, and if their crystal structure evolves in the same way with temperature.

Other than a slightly different melting point, 314 ˚C for L-alanine and between 291 - 295 ˚C for D-alanine, recent temperature-dependent longitudinal ultrasonic attenuation and velocity showed indications that while D- alanine crystal undergoes a reversible second-order phase transition at 247 K, L-alanine has a step-like attenuation transition around the same temperature [1]. In opposition, a recent work presented evidence that small differences observed in the DSC measurements become smaller upon successive recrystallization [2]. These findings bring back to surface contradictory arguments to the possibility predicted by A. Salam that this phase transition could be related to a break of the as C_α-H bond where the H atom becomes a superconductive atom [3].

Our results on hydrogenated L-alanine, obtained using the ID10A beam line at ESRF and the present NPD measurements of deuterated L-alanine using the high-resolution powder diffractometer E9 at HMI, ruled out the hypothesis of a conventional structural phase transition in L-alanine [4].

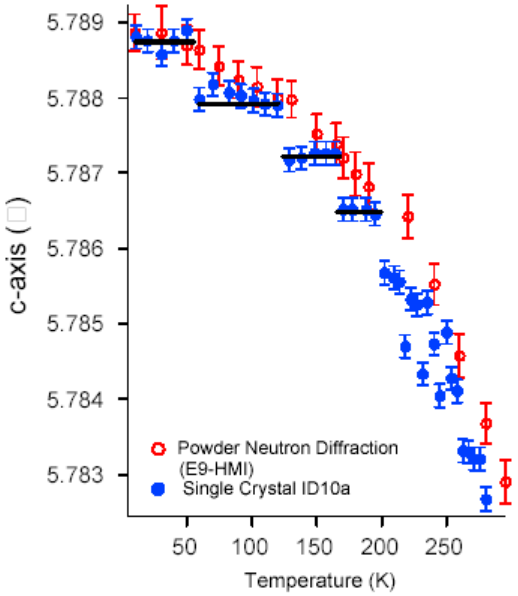


Fig 1:Temperature dependence of the *c*-lattice parameter of L-alanine measured on warming, using single crystal sample on ID10A (closed symbols) and NPD on the E9 diffractometer at HMI (open symbols). The error bars are typically 1.5 10^{-4}. The neutron data has been analyzed by the Rietveld method. One notices that *c* decreases in a succession of steps and plateaus.

Our initial analysis points to a subtle changes to the H-O bond lengths of the protons in the NH_3 group and the O-atoms of the CO_2, that can possibly lead to a compression of the *b*-axis and an expansion of the *c*-axis on cooling. Furthermore, we also confirm that the sample history plays an important role in L-alanine, in the present study the violations to the $P2_12_12_1$ structure occurring at several points on the diffraction pattern were not observed as previously reported [5].

[1] W. Wang et al, Phys. Chem. Chem. Phys. **5** 4000 (2003)
[2] R. Sullivan et al., J. Phys. Chem A **107** 6674 (2003)
[3] A. Salam, Phys. Lett. B, **288** 153 (1992); H. Zepik et al.,Science **295** 1266 (2002)
[4] M. Barthes, et al European Phys. J. B **37** 375 (2004)
[5] H.N. Bordallo et al, BENSC Report (2003)

	EXPERIMENTAL REPORT **Interaction of NK-2 with POPC**	Proposal N° BIO-01-1488 Instrument **V1** Local Contact Thomas Hauß
Principal Proposer: Experimental Team:	Dr. Regine Willumeit, GKSS, Geesthacht Sebastian Linser, Frank Förster, GKSS, Geesthacht	Date(s) of Experiment 13.06.-01.07.2004

Date of Report: 13.12.2004

Introduction

Antimicrobial peptides perform defensive functions in eukaryotic and prokaryotic cells. They are relatively small molecules whose action is fast and lethal towards a large spectrum of pathogens. These peptides seem to evade many drug-resistance mechanisms that are typical with the use of conventional antibiotics, and can therefore serve as alternative antibiotics. Studies suggest that they interact with the membrane and that their activity is intimately related to their membranolytic potential. However, the molecular details of the mechanism are poorly understood. The NK-2 peptide, which corresponds to a fragment of the NK-lysin protein from natural killer-cells, is a potent antibiotic peptide. It has good antibacterial properties and virtually no haemolytic or cytotoxic activity, and the objective of this project is to analyse the interaction of this peptide with model membranes. So far we investigated the position of the peptide in multilamellar membranes of POPE (palmitoyl-oleoyl phosphatidal-ethanolamine) and POPG (palmitoyl-oleoyl phosphatidal-glycerol) which are the main components of bacterial membranes. In order to test the influence of the peptide on erythrocyte membranes in this work we used POPC (palmitoyl-oleoyl phosphatidal-cholin) as model system.

Methods

The peptide was added to multilamellar liposomes of POPC in a fully protonated version and as partially deuterated derivatives in a molar ratio of 100:1 lipid:peptide. The deuterated labels were induced at positions Isoleucine-2 [I2D] and Leucine-23 [L23D] as well as in both positions. The solution was then dried at room temperature on quartz plates. The samples were equilibrated at 20° C in 100% D_2O, 100% H_2O, 50% D_2O and 20% D_2O for at least 24 hours and measured for 17 -20 hours. From the diffraction data the phases and amplitudes were calculated at 8% D_2O.

Results

From biosensor measurements a weak interaction with POPC lipids was deduced[1]. Therefore contrary to pervious measurements with POPE and POPG in which a strong or deep interaction was detected we expected the signal from the deuterated amino acids on the surface of the membrane. From the data analysis a completely different result was obtained (figure 1).

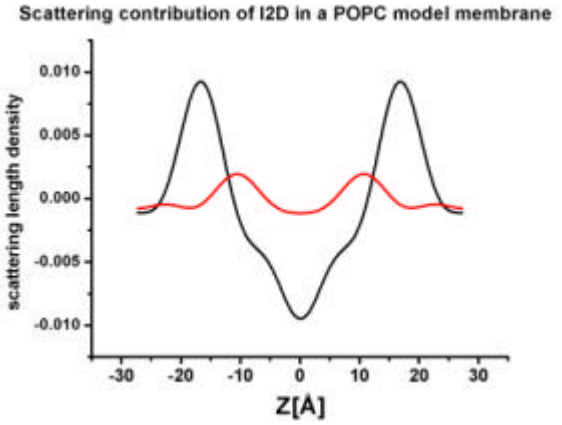


Figure 1: Result for NK-2 in a POPC membrane
As an example the scattering contribution of the deuterated Isoleucine-2 is displayed here. The black curve represents the scattering length density profile of a POPC membrane. The repeat distance was measured to be 55 Å.

It seems that also in this case the peptide is inserting into the membrane. A reason for this could be the lack of water which leads to a significant thinner repeat distance (9 Å less than in excess water). This could mean that the peptide is 'pushed' into the membrane. For the other lipids (POPE and POPG) this thinning of the repeat distance in the neutron experiments was not observed.

References

1. Schröder-Borm, H., Willumeit, R., Brandenburg, K. & Jörg, A. (2003). Molecular basis for membrane selectivity of NK-2, a potent peptide antibiotic derived from NK-lysin. *BBA* 1612, 164-171.

	EXPERIMENTAL REPORT **A neutron diffraction study on nucleolipid membranes**	Proposal N° BIO-01-1600 Instrument **V1** Local Contact T. Hauss, S. Dante
Principal Proposer: Experimental Team:	Piero Baglioni, Dept. of Chemistry and CSGI, University of Florence, Italy F. Baldelli Bombelli, University of Florence Silvia Milani, University of Florence, Italy	Date(s) of Experiment 20.07.04-29.07.04

Date of Report: 07/01/2005

Soft matter scientists are becoming increasingly interested into lipid bilayers/DNA interactions in order to design more efficient supramolecular arrays that can target oligonucleotides to cells in non-viral gene therapy. In this field a considerable scientific relevance concerns the study of self-assembling properties of phospholiponucleosides, a peculiar class of synthetic compounds, that merge auto-aggregation features of lecithin to the biological functions of nucleosides. We have currently extended our work to the study of membranes formed by 1-palmitoyl-2-oleoyl-phosphatidylnucleosides (POPN), whose self-assembled structures represent interesting examples for the development of surfaces able to display biological functionalities amplified in a supramolecular arrangement.

Aim of this proposal was a neutron diffraction investigation of POP-Adenosine and POP-Uridine lamellar phases prepared from vesicle dispersions. This method is suitable to monitor the formation of adducts with water-soluble biomolecules (i.e. polynuceotides) and overcome the difficult and lengthy hydration of films prepared spreading a $CHCl_3$ solution.

The lipids were enzymatically synthesized in our laboratory. 100-nm unilamellar liposomes were prepared by repeated extrusion through polycarbonate filters. The vesicle dispersion was let dry on quartz slides and then hydrated at controlled isotopic vapor composition and humidity. Figure 1 shows the curves obtained for POPU hydrated with 50% D_2O.

The main goal in the use of neutron diffraction was to infer the profile of the scattering length density of the molecules in the bilayer in order to track on the mesosocopic scale the structural changes induced by polar head chemical nature (base orientation, polar head hydration). A parallel FTIR linear dichroism investigation performed in our laboratory has stressed a better orientation for POPUridine lamellar stacks prepared in ste same way as for neutron diffraction experiments.

FTIR linear dichroism is particularly useful when combined to neutron diffraction because it gives information on higher resolution (i.e. submolecular) scale.

The experimental results, shown in Figure 1 for POPU, confirm the better ordering of this lyotropic phase (five diffraction orders obtained) with respect to POPA (three diffraction orders with broad Bragg peaks). Even with these limitations liposomal preparation has proven to be the best way to obtain equilibrium hydrated lamellar phases for POPA.

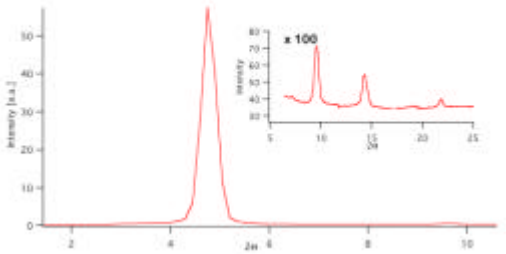


Figure1: Raw data of POPU lamellar stacks swollen in 50% D_2O

The smectic period was found to be substantially similar (56.1 Å POPA and 55.9 Å for POPU). However the different hydration degree implies a different bilayer thickness, certainly connected with polar head nature and interaction pattern with neighboring molecules.

The scattering length profile, determined for POPU bilayers (figure 2) combined with FTIR data gives a complete picture of the molecules arranged in bilayers.

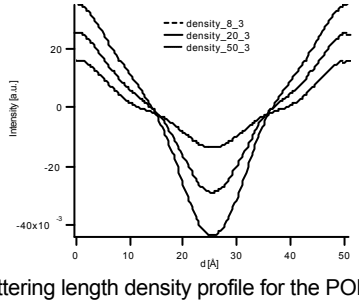


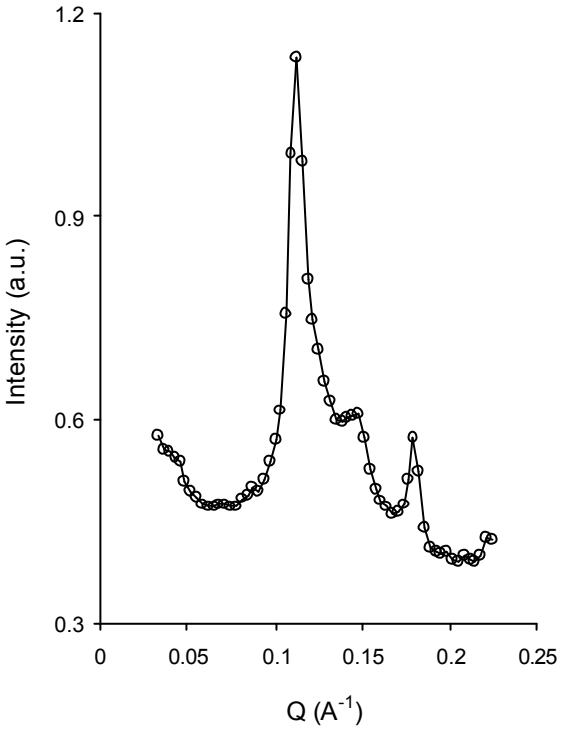
figure2: Scattering length density profile for the POPU sample

	EXPERIMENTAL REPORT Skin lipid organisation	Proposal N° BIO-01-1601 Instrument V1 Local Contact Dr. Th. Hauss
Principal Proposer: Experimental Team:	Joke Bouwstra, Leiden University Gert Gooris, Leiden University Georgia Charalambopoulou, NCSR Demokritos Theodore Steriotis, NCSR Demokritos Thomas Hauss, HMI Berlin	Date(s) of Experiment Sep 16 – Sep 26, 2004

Date of Report: January 10, 2005

Skin is a very complex organ whose main role is to protect the body from the various physical, chemical or pathogen environmental challenges. Its barrier function is associated with the lipid organisation in the outer layer of epidermis, the stratum corneum (SC). The main lipid classes of SC include cholesterol (CHOL), ceramides (CER) and free fatty acids (FFA), while nine ceramide types (CER1-CER9) have been identified in human SC. All these lipids form an exceptional organization of lamellar phases, among which the one with 13 nm periodicity (long periodicity phase - LPP) is considered to be crucial for skin's barrier properties. Our group has achieved, as confirmed by X-ray diffraction, to reproduce *in vitro* the lipid organization of SC, including the characteristic LPP, with mixtures based on CHOL, FFA and natural as well as a unique set of synthetic CER costume synthesized for our research. The presence in the lipid mixtures of CER1, a ceramide with a unique molecular structure comprising of a linoleic acid bound to a long chain (33 carbon atoms) ω-hydroxy fatty acid, has been shown to be a prerequisite for the formation of the LPP, the molecular organisation of which is still a matter of strong debate. Neutron diffraction is a useful tool for the localisation of perdeuterated linoleic of CER1 in the LPP domain (in a proposed molecular model this perdeuterated chain has a very characteristic position in the repeating unit of the lamellar phase); this knowledge in combination with the scattering density profiles is expected to unravel the molecular organization of this phase.

In experiment BIO-01-1601 two types of lipid samples (with protonated and deuterated CER1, respectively) with composition CER:CHOL:FFA= 2:1:1 (this scheme mimics the lipid organisation in human SC), were used. Phase assignment was studied through measuring both types of samples hydrated in three different compositions of D2O/H2O mixtures (50%, 20% and 8% D2O) as well as in pure D2O. After the determination of the optimum experimental conditions (sample environment, experimental set-up) through a systematic series of control measurements, Diffraction intensities were recorded with rocking scans, around the expected Bragg positions.



In general, the diffraction pattern of the deuterated samples (attached figure) revealed the structure of SPP (Short Periodicity Phase, corresponding to a spacing of ca. 5.6 nm) up to the 3^{d} order, the 1st order of LPP as a shoulder and several peaks that might indicate higher order LPP reflections. On the other hand, the profiles of the protonated samples were less detailed; although the SPP was clearly visible (peaks at 5.59 and 2.76 nm), the signal from LPP was rather weak in this case.

The analysis and interpretation of the obtained results is not straightforward and further measurements have been planned.

	EXPERIMENTAL REPORT **Fusion peptides and the inverted hexagonal phase in phospholipids**	Proposal N° BIO-01-1487 BIO-01-1386 Instrument **V1** Local Contact Thomas Hauß
Principal Proposer: Experimental Team:	Jeremy Bradshaw, University of Edinburgh Kia Balali-Mood, University of Edinburgh Thomas Hauß, HMI Berlin (BENSC)	Date(s) of Experiment 17.05.04 – 01.06.04

Date of Report: 16.12.04

In these experiments, we studied the bilayer interaction of islet amyloid polypeptide (IAPP). The data have been written up and submitted for publication.

A number of extracellular proteins can misfold spontaneously and aggregate to form ß-sheet rich amyloid deposits characteristic of a variety of "protein misfolding" diseases, most notably Alzheimer's disease. While the precise molecular basis of such conditions is unclear, strong arguments are emerging to implicate organ-specific amyloidogenic proteins, particularly oligomeric intermediates on the pathway to amyloid fibril formation, in disease pathogenesis. Human islet amyloid polypeptide (hIAPP), a peptide hormone secreted by pancreatic beta cells, often forms amyloid deposits in patients affected by NIDDM (non-insulin dependent or type 2, maturity onset, diabetes mellitus).

Unlike human IAPP, rat IAPP (rIAPP) is inert. Sequence variations in IAPP are strongly associated with the ability of the peptide to form amyloid, and susceptibility to NIDDM. However, mice expressing the hIAPP transgene do develop a NIDDM-like disease.

The membrane-active form of hIAPP is currently poorly defined. In the present study, we identified the membrane-associated form of hIAPP in stacked phospholipid bilayers using neutron diffraction. We directly tested the hypothesis that hIAPP oligomers span the bilayer, and our findings are consistent with the idea that oligomeric hIAPP is associated with the formation of transmembrane channels. rIAPP was excluded from the membrane, as predicted, and rifampicin, an inhibitor of the membrane activity of hIAPP [5], prevents membrane insertion.

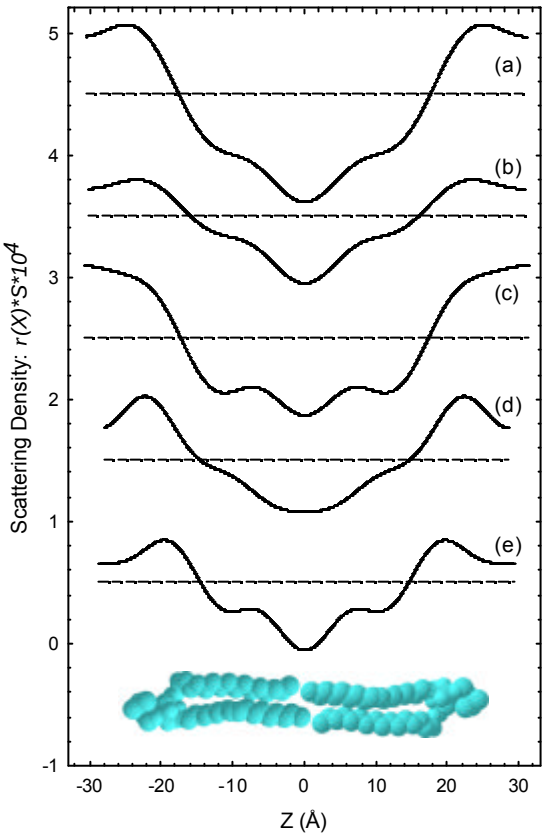


Figure: Neutron scattering length density profiles of phospholipid bilayers: (a) 50:50 (mol) mixture of POPE and POPS; (b) 50:50 (mol) mixture of POPE and POPS with 1% (mol) hIAPP; (c) 50:50 (mol) mixture of POPE and POPS with 1% (mol) rIAPP; (d) 50:50 (mol) mixture of POPE and POPS with 1% (mol) rifampicin; (e) 50:50 (mol) mixture of POPE and POPS with 1% (mol) hIAPP and 1% (mol) rifampicin hIAPP. The structure factors for bilayers hydrated with 8% 2H2O were used to calculate the profiles, since water of this isotopic composition has a net neutron scattering length density of zero. The profiles have been displaced vertically, for clarity. A pair of lipid molecules is also shown, for orientation.

	EXPERIMENTAL REPORT **Interaction of Alzheimer's ß-amyloid(1-42) peptide with cholesterol-containing membranes**	Proposal N° BIO-01-1602 Instrument **V1** Local Contact Thomas Hauß
Principal Proposer: Experimental Team:	Jeremy Bradshaw, University of Edinburgh Richard H. Ashley, University of Edinburgh Kia Balali-Mood, University of Edinburgh	Date(s) of Experiment 09.08.04 – 21.08.04

Date of Report: 06.01.05

Many degenerative diseases, including Alzheimer's disease and type II diabetes mellitus, are characterised by deposits of "cross beta" fibrils of disease-specific amyloidogenic proteins in affected tissues and organs. Extracellular amyloid may play a key role in pathogenesis, and it has been hypothesised that pre-fibrillar, oligomeric forms of amyloidogenic proteins are membrane-active and toxic to cells. Having tested some of these ideas using islet amyloid polypeptide (IAPP), a hormone that forms amyloid deposits in many patients affected by type II diabetes, we extended our work to Alzheimer's ß-amyloid(1-42), a major component of the extracellular amyloid plaques in the brains of patient's suffering from Alzheimer's disease. In other experiments, oligomeric, not monomeric or fibrillar, ß-amyloid(1-42) was membrane-active, in line with our central hypotheses, and at least one small molecule inhibitor, rifampicin, prevented membrane activity. We also confirmed a key role for membrane lipids, including cholesterol. The aim of this study was to determine whether neutron diffraction could be used to obtain detailed structural information about the location of the ß-amyloid(1-42) peptide in cholesterol-containing lipid bilayers in the presence and absence of rifampicin.

Mixtures of dry palmitoyl-oleoyl phosphatidylcholine and cholesterol were dispersed in a minimally-buffered aqueous solution of appropriately aged, fibril-free peptide oligomers, or in buffer alone. The resulting multilamellar liposomes were then deposited and dried onto quartz glass slides. Some of the samples also contained rifampicin at a peptide:rifampicin ratio of 1:1 (molar). Up to 5 orders of diffraction were collected on the V1 membrane diffractometer

The Bragg peaks were less intense when the lipids were prepared in aqueous medium rather than from chloroform dispersions, and showed increased mosaic spread, although the calculated lamellar spacing of the multibilayers was unaltered. Inclusion of the peptide did not increase the lamellar spacing significantly, but the mosaic spread increased (as previously noted for amyloid ß-peptide fragment 25-35 [1]), suggesting that the full-length peptide disrupted the lattice orientation of the cholesterol-containing multibilayer system. This was partially reversed in the presence of rifampicin (Figure 1), and could potentially reflect peptide-induced domain formation, or a phase transition in the phospholipid component. Despite these changes, we were able to obtain complete data sets for several multibilayers at 3 different relative humidities. The scaled and corrected data were phased by fitting all structure factor amplitudes for each 8% D_2O sample to a single continuous transform [2], followed by straight-line fitting to 8%, 20% and 50% D_2O samples [3]. Transbilayer water profiles were calculated by Fourier difference analysis. The peptide introduced additional scattering in the region of the hydrophobic core, which was partially reversed by rifampicin. Overall, lamellar neutron diffraction appears to offer substantial potential for further studies of the interaction of ß-amyloid(1-42) with cholesterol-containing membranes in the presence and absence of inhibitors.

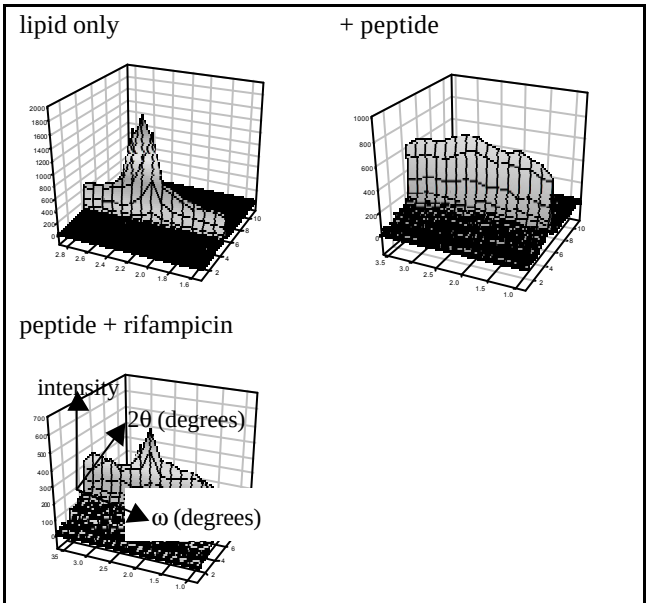


Figure 1. Examples of rocking curves (? scale, sample rotation) around the first Bragg peak (2? scale). Note marked broadening of the rocking curve with peptide, partially reversed by rifampicin.

1. Dante, S., Hauss, T., Dencher, N.A. (2003) Biochemistry 42, 13667-13672.
2. Darkes, M.J.M., Bradshaw, J.P. (2000) Acta Cryst. D56, 48-54.
3. Bradshaw, J.P., Davies, S.M.A., Hauss, T. (1998) Biophys.J. 75, 889-895.

	EXPERIMENTAL REPORT **Transport Properties of Hydrated Stratum Corneum**	Proposal N° BIO-03-288 Instrument V3 Local Contact Dr. J. Pieper
Principal Proposer: Experimental Team:	Theodore Steriotis, NCSR Demokritos Georgia Charalambopoulou, NCSR Demokritos Jörg Pieper, HMI Berlin	Date(s) of Experiment November 2003

Date of Report: January 19, 2005

The main resistance to the penetration of various substances through skin, the largest organ of human organism, resides within the superficial 15-50 μm layer of epidermis, the Stratum Corneum (SC). SC is a highly complex biological membrane with a heterogeneous structure that consists of keratin-filled flat cells, the corneocytes, surrounded by an extended lipid bilayer phase. Native SC can be hydrated to different degrees depending on both endogenous and exogenous factors, while the respective water content modulates its barrier function. The water sorbed by SC can be distinguished in three forms, i.e. bound, weakly bound and bulk water, the dynamic properties of which are quite different. The multiplicity of diffusion mechanisms is further increased by the anisotropy of SC structure imposing different transport routes parallel and perpendicular to the membrane plane. As a result, diffusion studies in SC are very complicated and there is a need to combine several techniques to unravel the pertinent behaviour.

As a first approach, complementary QENS and PFG-NMR measurements were previously employed in order to investigate the microscopic dynamics of water in fully hydrated SC (equilibrated at 100 % relative humidity, RH). PFG-NMR results showed that the translational diffusion coefficient of weakly bound water is different for diffusion parallel and perpendicular to SC plane. Using the respective data as input, QENS data for two sample orientations and two different energy resolutions were fitted by a model, which accounts for all three aforementioned types of water exhibiting both, rotational and translational diffusion, as well as SC matrix (described phenomenologically by a rotational motion). As both QENS and PFG-NMR data pertained to all three aforementioned water forms, their relative concentrations were determined by independent H_2O sorption experiments. Even though the above model lead to a realistic picture of the hydrated SC system, it was not possible to experimentally determine the dynamics of the individual water phases.

In experiment BIO-03-288, an attempt was made to further extend the study to SC samples hydrated at different, lower RH-levels in order to separate effects from firmly bound and other types of hydration water. In this respect, there were used SC samples hydrated at (a) RH=23% (ca. 6% H_2O content) aiming to address the effect of bound water only, and (b) RH=58% (ca. 12% H_2O content) where both bound and weakly bound water are present. In order to isolate the "hydration water" contribution from the rest of the scattered intensity, SC samples of identical geometry and equal weight were hydrated over the vapor of appropriate H_2O and D_2O solutions, respectively, for each of the two aforementioned hydration levels. To ensure full comparability with the QENS data obtained from the fully hydrated samples, the water transport was again studied in porcine samples, at room temperature and as a function of orientation for two different resolutions (ΔE = 0.093 meV and ΔE = 0.066 meV), while an additional measurement at ΔE = 0.032 meV was performed for the samples corresponding to 58%RH.

It should be noted that the above experiment was also complemented by PFG-NMR (Univ. Leipzig) as well as Back-Scattering (BSS, FZ Jülich) measurements in an effort to obtain an, as much as possible, complete set of data that will ultimately allow the formulation of a sufficiently accurate and comprehensive model of water diffusion in SC tissue. The analysis and interpretation of the individual results and mainly their conjugation has been proven laborious, and is thus still in progress.

	EXPERIMENTAL REPORT **Elastic Resolution Spectroscopy of protein solutions, stability of lactalbumin**	Proposal N° BIO-03-317 Instrument **V3** Local Contact A. Buchsteiner
Principal Proposer: Experimental Team:	Doster, Wolfgang, TU München Buchsteiner, Alexandra, HMI Berlin	Date(s) of Experiment 17.5.04

Date of Report: 20.1.05

The goal of this experiment was to explore the molecular motions of α-lactalbumin and its calcium-depleted form within a wide range of time scales. The heat denaturation temperatures of the apo- and calcium bound form can differ by 50 degrees. The acid form has as a more open structure and is even less stable than the apo-protein. The experiment will establish, whether a local disturbance at the Ca-binding site, can affect the global plasticity of the protein structure, as measured by dynamic neutron scattering. Since experiments are mainly performed in solution, the solvent will give a sizeable contribution to the spectrum. Due to fast motion of water, the respective spectrum will be a broad line. To minimize this problem we planned to focus on the elastic region of the spectrum employing “elastic resolution spectroscopy”. One measures the elastic (zero energy transfer) regime and modifies the resolution of the spectrometer within a wide range to gain time information.

Native and calcium-depleted lactalbumin samples were observed in concentrated D_2O-solutions at the incident neutron wavelengths of 5 and 12 A. The chopper speed was varied between 1000 and 20 000 rpm. Thus the spectral resolution could be changed from 8 to 900 μeV, corresponding to a time scale from 1 ps to 140 ps. The experiment worked very well and a complete set of data could be obtained. With calcium-depleted lactalbumin one observes slightly enhanced quasielastic scattering in comparison with the native probe. An unexpected finding was the broadening of the central line in addition to quasielastic scattering. The broadening is larger than expected for translational protein diffusion, a preliminary analysis suggests that rotational diffusion could be significant. These results require to analysing the complete spectrum separating several spectral components, which is in progress.

BENSC	**EXPERIMENTAL REPORT** **Study of the influence of the pressure on the structure and dynamics of BPTI**	Proposal N° BIO-03-0319 Instrument NEAT (V3) Local Contact Pieper J, Buchsteiner A.
Principal Proposer: Experimental Team:	Appavou M.-S , LLB CEA Saclay France Bellissent-Funel M.-C, LLB CEA Saclay France Annighöfer B., LLB CEA Saclay France Pieper J., Buchsteiner A., HMI Berlin (BENSC)	Date(s) of Experiment 18/04/04 to 04/05/04

Date of Report: 02/12/04

We have studied the influence of pressure on the structure and the dynamics of a small protein belonging to the enzymatic catalysis : the bovine pancreatic trypsin inhibitor or BPTI. Using a copper-beryllium high pressure cell which can sustain a pressure value of 6000 bar, we have performed small angle neutron scattering experiment with NEAT (V3) spectrometer in the SANS configuration in order to observe the evolution of the radius of gyration (λ = 5.1 Å, 0.004 $Å^{-1} < q < 0.2$ $Å^{-1}$) and the shape (λ = 2 Å, 0.01 $Å^{-1} < q < 0.5$ $Å^{-1}$) of the protein under pressure from atmospheric pressure up to 6000 bar.

We have also performed quasielastic neutron scattering experiments with the QENS configuration of V3 (λ = 5.1 Å, 93 µeV FWHM resolution) in order to investigate the global motions and internal dynamics of BPTI between atmospheric pressure and 6000 bar. In the Guinier regime, SANS results were analysed in terms of evolution of the radius of gyration as a function of applied pressure (figure1). We have observed some effect of this physical parameter on the global structure of BPTI since 3000 bar with a reduction of the radius of gyration from 15.2 Å down to 13.8 Å at 6000 bar. A transition is observed between 5000 and 6000 bar. This influence of pressure is not reversible since the initial value of radius of gyration is not recover when the sample is turn back at 1 bar.

Extending the range of wavevector to higher q values, we have observed using simple models to fit the form factor, a change of the shape of the BPTI when pressure is applied : the protein adopts a spherical shape rather than an ellipsoid shape when pressure increases from atmospheric pressure up to 3000 bar. Increasing pressure above 5000 bar induces a partially unfolded state of BPTI because form factors at 5000 and 6000 bar can be better fitted by a model of micelles. This model is composed by a collapsed spherical shaped core surrounded by a corona of disordered structures, as gaussians chains. We have observed a transition in the shape of the molecule because of the change in the proportion of spherical form factor contribution and gaussian chain form factor contribution at these high pressure values. BPTI keeps a spherical shape once the pressure is released, indicating the irreversibility of the pressure-induced structural changes on the protein.

Influence of pressure is evident on global diffusion and internal dynamics of BPTI in solution. Indeed, intermediate scattering functions I(q,t) calculated from the dynamical structure factors S(q,ω) show a slowing down of the dynamics as a function of applied pressure (figure 3). These I(q,t) were fitted with a sum of exponentials with two relaxation times τ_1 and τ_2 describing global diffusion and internal dynamics respectively. *Data analysis is still in progress*

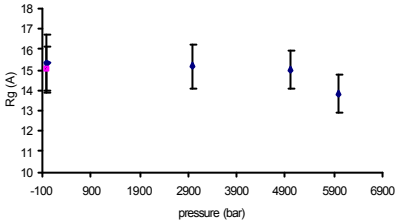


Figure 1: evolution of Rg as a function of pressure.

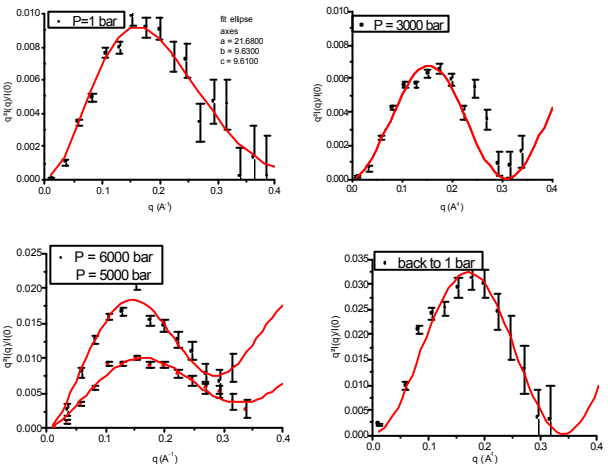


Figure 2: Kratky plot ($q^2I(q)$ vs q) at different pressure.

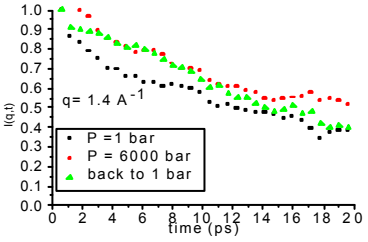


Figure 3: I(q,t) at 1 bar, 6000 bar and after pressure release.

	EXPERIMENTAL REPORT **Dynamics of immobilized myoglobin the folding/unfolding transition**	Proposal N° BIO-03-0320 Instrument **NEAT** Local Contact Jörg Pieper
Principal Proposer: Experimental Team:	Longeville Stéphane, Laboratoire Léon Brillouin, CEA Saclay Haouz Ahmed, Institut Pasteur, Paris Pieper Jorg, HMI Berlin	Date(s) of Experiment 23 May – 3 June 2004

Date of Report: Januar 2005

The knowledge of macromolecular structure is fundamental but not sufficient to understand the mechanisms responsible for protein stability. Studying internal protein dynamics could help to understand some of the mechanism of biological function and to specify the role of fluctuation in the folding/unfolding transitions of proteins.

Internal fluctuations knowledge of protein is very scarce, imprecise and very difficult to obtain. Few attempts have successfully shown the possibility to measure the protein dynamics and their influence on biological functions [1,2,3]. Protein dynamics is shown to be necessary for the catalytic activity of enzymes [1]; it is partially responsible of their stability [2]; it also participates to specific protein-DNA recognition [3].

Measurement of internal dynamics of protein by inelastic neutron scattering can be performed either on hydrated powders or in solution. In the first case, beyond the difficulty to control hydration and homogeneity of the sample, the limited layer of water molecules reduces the amplitude of fluctuations. In the second case, the signal is perturbed by the diffusion of the molecules [4] and one need to introduce both a decoupling hypothesis and a diffusion model to analyze the data [5].

In order to circumvent these problems we have studied the dynamics of myoglobin immobilized by intermolecular glutaraldehyde bridges. These molecules are trapped by direct covalent bonds between the neighboring proteins. The diffusion then gets outside the spectrometer window (even at high wave vectors) but we keep an aqueous environment for the protein, and hence there is no reduction of internal fluctuation amplitudes. In such samples, the physiological properties of protein are kept but the creation of intermolecular bonds induces an increase of folding/unfolding transition temperature without apparent structural modifications [2]. Our particular interest is to study the pretransitionnal fluctuations in the folded and molten globule states.

Experiments have been performed on the TOF spectrometer NEAT with rather bad energy resolution (FWHM 200 μev) to study the 0.1-10 mev range in the dynamical fluctuations. We also simultaneously followed used the Multi-detector in SANS mode to check the possible evolution of the structure of the solution and/or molecular form factor during the experiment. The spectrometer setup was set to perform time-of-flight diffraction experiments [6], only the two choppers close to the sample were used to pulse the beam (1000 rpm) and the double trumpet system was removed and replaced by collimating devices.

The data analysis and modelisation is under progress. TOF-Diffraction analysis is a very time demanding process because of the very huge amount of data. Preliminary analysis of the quasielastic spectrum show significant changes in the dynamics when approaching the molten globule state

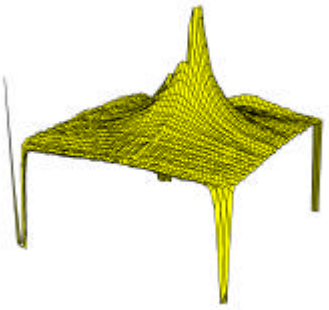


Figure 1: contour map of Immobilized myoglobin measured on the multi-detector of NEAT, the neutron intensities of the 512 tof channels have been summed.

[1] Zavodskay P., Kardos J. , Svingro A.., and Petsko G.A., Proc. Natl. Acad. Sci. USA, **95** (1998) 7406-7411.

[2] Haouz A., Glandières J.-M. and Alpert B. Febs letters. (2001) 25313, 1-5.

[3] Zargarian L., Le tilly V., Jamin N., Chaffotte A.., Gabrielsen OS., Toma F., and Alpert B. (1999) **38** Biochemistry 1921-1929.

[4] S. Longeville, W. Doster and G. Kaly, Chem. Phys. **292** (2003) 413-424.

[5]J. Pérez, J. M. Zanotti and D. Durand, Biophysical Journal, **77** (1999) 454-469.

[6] B. Rufflé, J. Ollivier, S. Longeville and R.E. Lechner, Nucl. Inst. and Meth. In Phys. Res. A 449 (2000) 322-330.

	EXPERIMENTAL REPORT **Using QENS to explore the dynamics of serine proteases**	Proposal N° BIO-03-355 Instrument NEAT Local Contact J. Pieper
Principal Proposer: Experimental Team:	A. Zychlinsky, MPI for Infection Biology M. Ingersoll, MPI for Infection Biology H.N. Bordallo, HMI Berlin T. Hauß and E. Garcia-Matres, HMI Berlin	Date(s) of Experiment 9-15/08/2004

Date of Report: 27/10/2004

Here we report the results of the first study of the proteins elastase (NE) and cathepsin G (CG) performed at the HMI. Both NE and CG belong to a large family of serine proteases with sequence and structural similarity but with very different biological functions. The basis for the difference in substrate specificity is not yet understood.

CG, like NE, is an abundant serine protease in neutrophil granules. The structures obtained through X-ray crystallography of these two proteins are nearly identical [1]. Yet, CG does not cleave virulence factors of enteric bacteria [2]. We put forward the idea that is the dynamical behavior of NE and CG that determines their specificity.

In order to test this hypothesis we performed a quasi-elastic neutron scattering (QENS) experiment, using NEAT at HMI. To cover the time range of protein dynamics that operate between nano and pico-seconds, we used 2 different energy resolutions, 93 and 10 μeV. The experiments were performed at room temperature with the sample placed directly inside the sample chamber. The sample cell, containing protein dissolved in 100 mM Tris D_2O buffer with a nominal concentration of 4 ± 0.5 mg/ml, was placed at 135° to the direction of the incident neutron beam.

In order to evaluate our data we implemented LAMP, so that NEAT data can now be read and analyzed using this program [3]. The time-of-flight spectra are showed in figure 1 (for λ=15.3Å). The spectra were corrected for scattering from the buffer, standardized to vanadium, and converted to the differential scattering cross section.

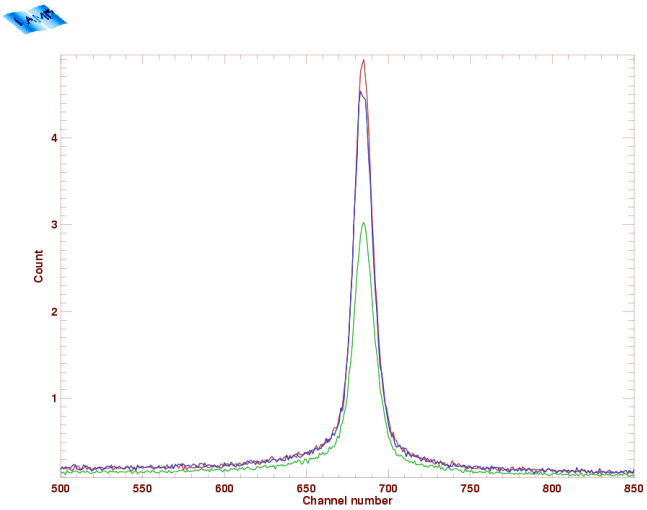


Fig. 1. (red line) NE plus buffer, (blue line) CG plus buffer and (green line) buffer signal from the time-of-flight data. Each channel number represent 14.65 μs, with the elastic peak (ω = 0) situated at about channel 685; T=300K.

Although our enzymatic assays showed that the samples had very low activity, and we are aware now that a systematic study of the effects influencing activity is needed, the observation of a significant peak situated at about channel 685, corresponding to the elastic peak (ω =0) and the quasi-elastic component, makes our results especially promising. In the near future, with active enzymes, we will likely show that indeed, the different function of NE and CG can be correlated to their dynamics.

[1] Yv. Weinrauch et al Nature **417**, 91 2002.
[2] C. Mattos et al, Nat Struct Biol **1**, 55 1994; P. Hof et al EMBO J **15**, 5481 1996.
[3] H.N. Bordallo and S. Rols, private communication.

	EXPERIMENTAL REPORT **Picosecond internal dynamics of lysozyme embedded in a glucose matrix as affected by thermal unfolding**	Proposal N° BIO-03-359 Instrument **V3** Local Contact Jörg Pieper
Principal Proposer: Experimental Team:	Alessio De Francesco, Università Perugia Alessandro Paciaroni, Università Perugia Jörg Pieper, HMI Berlin	Date(s) of Experiment 09.09. – 16.09.04

Date of Report: 10/01/2005

It is well known that sugars play an important role in conditioning the protein dynamics and thermal stability and that these effects could be at the basis of their use as cryo-protectors and as essential additives to improve the long-term storage and delivery of biopharmaceuticals (Klibanov, 2001; Brumfiel, 2004). That is why we have investigated the melting process of lysozyme embedded in this different organic solvent and in the present experiment in glucose.

We have measured quasielastic neutron scattering spectra of lysozyme embedded in glucose as a function of the temperature. The incident neutron wavelength was 5.1 A providing an elastic energy resolution of about 0.1 meV. In particular, we measured the sample at T=200K to collect purely inelastic spectrum, and at 300K, 330K, 360K, 410K and 440K to follow the quasielastic signal before and after thermal unfolding (T_{unf}=400K). The sample was also measured after denaturation at 300K to investigate the effect of disrupting the protein structure on the dynamics.

In Fig. 1 we show the spectra (in arbitrary units) collected for the samples at 200K, 300K, 330K, 360K and 410K (from the bottom to the top in the figure). At 200K the spectrum is characterised by the presence of a well visible inelastic bump, elsewhere called boson peak, is centred at around 3.8 meV. At 300K a quasielastic signal superimpose to the inelastic peak, despite the temperature is still below the dynamical transition of the system (~330K).

Such a quasielastic signal increases as a function of the temperature and quite remarkably above the unfolding, thus indicating that thermal denaturation has an effect on the protein dynamics in the picosecond timescale.

In Fig. 2 we show the comparison between the spectrum of the sample at 300K before and after the unfolding, respectively lower and upper spectrum. Such comparison established that the changes in protein dynamics observed upon melting are irreversible. In fact, the unfolded sample exhibits a larger quasielastic signal, thus confirming the effect of denaturation on increasing the protein fast atomic mobility.

The nature (geometry and characteristic times) of the motions involved in such an effect is at the moment under investigation.

Brumfiel, G. 2004. *Nature* 428:14-15.
Klibanov, A. M. 2001. *Nature*. 409: 241-246.

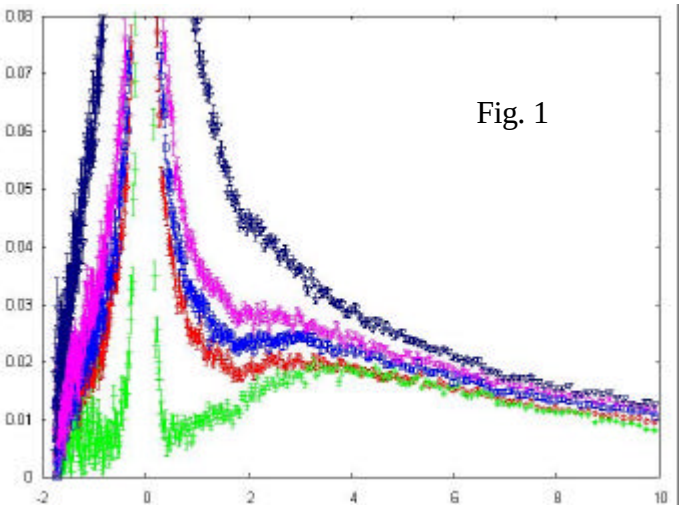


Fig. 1

E (meV)

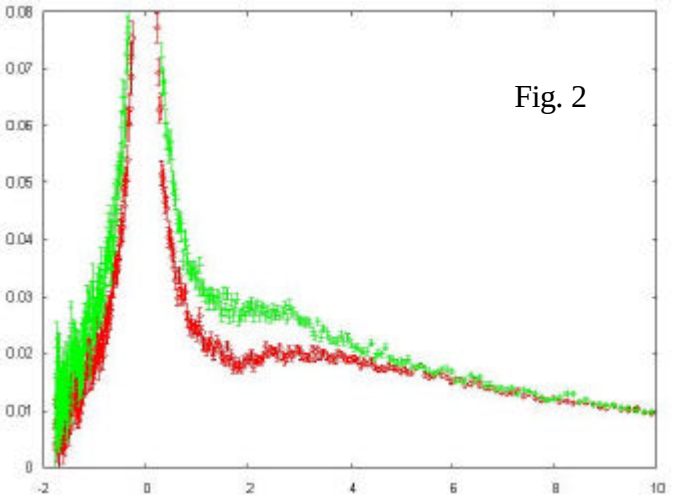


Fig. 2

E (meV)

	EXPERIMENTAL REPORT **Protein Dynamics in the Monomeric Light-Harvesting Complex II of Green Plants**	Proposal N° BIO-03-EF Instrument **V3** Local Contact: J. Pieper
Principal Proposer: Experimental Team:	J. Pieper, HMI Berlin J. Pieper, R. E. Lechner, HMI Berlin K.-D. Irrgang, Max-Volmer-Institut, TU Berlin M. Rätsep, FI Tartu (Estonia)	Date(s) of Experiment 03.12. – 10.12.2003

Date of Report: 10.01.04

The pigment-protein complex LHC II is the major antenna complex of green plants. Its function is to absorb light in a broad spectral range as well as to efficiently transfer excitation energy to reaction center complexes, where the photochemical processes of photosynthesis take place.
Quasi- and inelastic neutron scattering (QENS, INS) can contribute information on two aspects which are of great importance for light absorption and excitation energy transfer in antenna complexes: i) the low-frequency vibrational modes and ii) the internal flexibility of the protein matrix [1].
In the present experiment solubilized monomeric LHC II was studied in a temperature range from 40 to 280 K by QENS. As described previously for trimeric LHC II [2], two different incident neutron wavelengths of 2.0 (~20 meV) and 5.1 Å (~3.2 meV) were chosen in order to measure inelastic spectra for energy gain and loss of the neutron. The corresponding elastic energy resolutions were 921 and 93 µeV, respectively.
Monomeric LHC II complexes were solubilized in a D_2O-containing buffer solution, so that the contribution of the solvent had to be determined by separate experiments. Figure 1 shows INS spectra of solubilized LHC II (upper full line) and buffer solution (lower full line) obtained with an incident wavelength of 5.1 Å at 80 K. The former and latter spectra exhibit apparently different shapes with maxima at about 2.5 and 6 meV, respectively. The dashed line is the difference spectrum corresponding to monomeric LHCII.
The average atomic mean square displacement $<u^2>$ obtained from the data of monomeric LHC II (Fig. 2) exhibits deviations from a purely linear temperature dependence above 120 and 240 K (regions B and C in Fig. 2) due to the onset of internal protein motions. The transition temperatures correlate well with drastic changes in the fluorescence properties of LHC II as will be discussed in ref. [3].

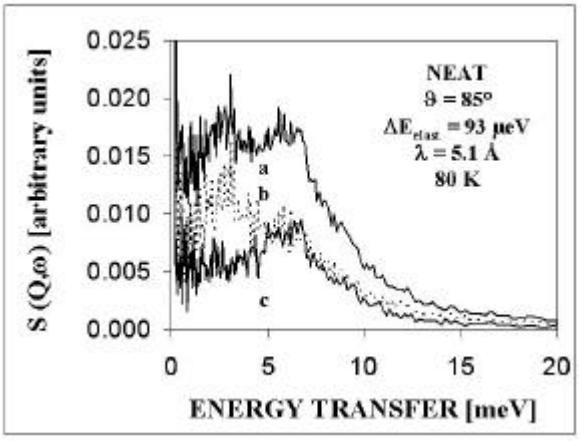


Figure 1
INS spectra of solubilized monomeric LHC II (a, upper full line) and buffer solution (c, lower full line) obtained with an incident neutron wavelength of 5.1 Å at 80 K. The dashed line is the difference spectrum (monomeric LHCII).

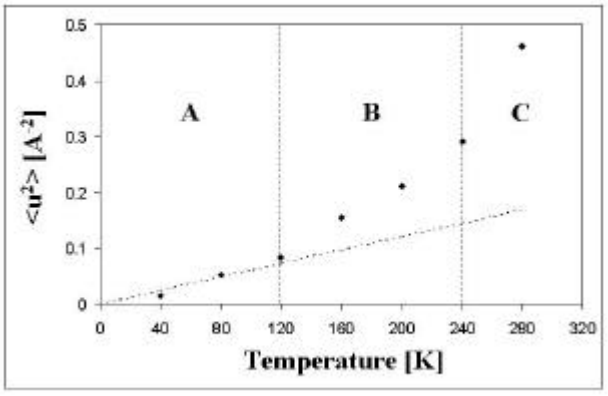


Figure 2
Temperature dependence of the average atomic mean square displacement <u2> (left scale) of monomeric LHC II (full diamonds).

References:

1. Pieper, J.; Schödel, R.; Irrgang, K.-D.; Voigt, J.; Renger, G., J. Phys. Chem. B (2001), 105, 7115-7124
2. Pieper, J.; Irrgang, K.-D.; Renger, G.; Lechner, R.E., J. Phys. Chem. B (2004), 108,10556
3. Pieper, J.; Irrgang, K.-D.; Rätsep, M., Lechner, R.E., to be published

	EXPERIMENTAL REPORT **Structural Organization of Photosystem II Membranes of Green Plants**	Proposal N° BIO-03-EF Instrument **V3** Local Contact: J. Pieper
Principal Proposer: Experimental Team:	J. Pieper, HMI Berlin J. Pieper, A. Buchsteiner, HMI Berlin R. E. Lechner, Th. Hauß, HMI Berlin M. Weß, G. Renger, TU Berlin	Date(s) of Experiment 02.06. – 06.06.2004

Date of Report: 10.01.05

Photosynthesis is a fundamental physiological process in nature representing the transformation of solar radiation into storable chemical energy. This photochemical process of all oxygen evolving photoautotrophic organisms (cyanobacteria, algae and green plants) comprises the light-induced cleavage of water and fixation of carbon by formation of a carbohydrate $(CH_2O)_n$ under release of oxygen (for a review see ref. 1). The key steps of photosynthetic water cleavage take place in a multimeric membrane-bound protein complex referred to as Photosystem II (PS II). The reaction pattern of PS II is characterized by a high degree of specific coupling between structural dynamics and function. Recent findings revealed that dehydration (2) as well as lowering of temperature leads to blockage of individual redox reactions of PS II (3).

Recently, we have investigated the protein flexibility of PSII as a function of temperature and hydration degree. A preliminary analysis of the data showed that a significant quasielastic contribution is present only for T> 230 K and for r.h. > 45 %, i.e. exactly the values where the PS II redox reactions are activated (4). These findings suggest that the functionality of PS II is strongly correlated with the protein flexibility.

A deeper understanding of these effects requires information on the structural organization of PS II membrane fragments and the location of hydration water molecules.

To address this point, TOF-diffraction measurements using a white incident neutron beam were carried out for PS II membrane fragments. The samples were hydrated using D_2O vapors of well-defined relative humidities (r.h.) from 57 - 90 %. In addition, a vacuum dried sample as well as the incoherent background were studied. The sample preparation protocol was identical to that used for the preceding QENS studies. The results show a complex structure with peak positions depending on the hydration degree of the sample. The observed structure is qualitatively similar to that reported for intact thylakoids (5). A more detailed analysis is in progress (6).

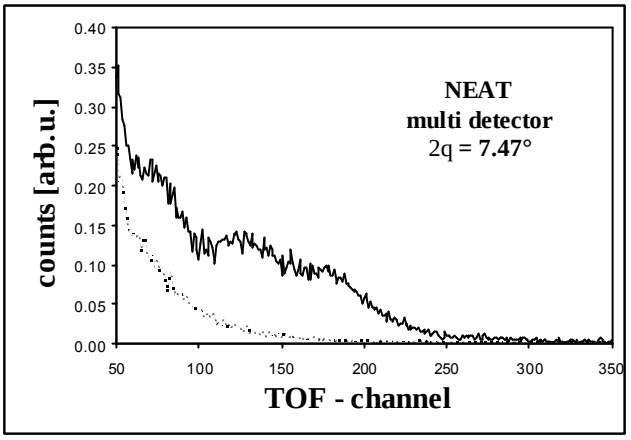


Figure 1
TOF-diffraction using the NEAT multi detector for PSII membrane fragments (full line) hydrated with D2O at 57 % r.h..fit. The dashed line gives the incoherent background.

References:

1. G. Renger, Biochim. Biophys. Acta 1503 (2001) 210-228
2. O. Kaminskaya, G. Renger, V. A. Shuvalov, Biochemistry 42 (2003) 8119-8132
3. Garbers, F. Reifarth, J. Kurreck, G. Renger, F. Parak, Biochemistry 37 (1998) 11399-11404
4. Kühn, P., Pieper, J., Kaminskaya, O., Eckert, H.-J., Lechner, R., Shuvalov, V, Renger, G., Photosyn. Res., in press
5. Posselt et al., in preparation
6. Pieper, J.; Buchsteiner, A.; Weß, M.; Hauß, Th.; Lechner, R.E.; Renger, G., to be published

	EXPERIMENTAL REPORT **Light-Induced Protein Dynamics in Bacteriorhodopsin**	Proposal N° BIO-03-EF Instrument **V3** Local Contact: J. Pieper
Principal Proposer: Experimental Team:	J. Pieper, HMI Berlin J. Pieper, A. Buchsteiner, R. E. Lechner, HMI Th. Hauß, Uni Düsseldorf & HMI Berlin N. Dencher, TU Darmstadt	Date(s) of Experiment 10.12. – 22.12.2003 15.06. – 20.06.2004

Date of Report: 11.01.04

Bacteriorhodopsin (BR) is a light-driven proton pump bound in the purple membrane of *halobacterium salinarum* [1,2]. Absorption of a light quantum by BR initiates the so-called photocycle corresponding to a well-defined sequence of protein-chromophore conformations (intermediates). The intermediates of BR are characterized by specific absorption maxima and decay times ranging from 500 fs to 15 ms. In the time course of the photocycle one proton is pumped through the membrane creating a net transport from the cytoplasmic to the extracellular side of the membrane. This vectorial proton transport requires a conformational change in the M-intermediate so that its structure of differs from that of the ground state [3].

The internal protein dynamics of BR in its dark state has already been thoroughly studied by QENS (see e.g. ref 4 and references therein). However, information on the effect of the conformational changes on protein dynamics during the photocycle is scarce and difficult to obtain. A straightforward, but technically challenging approach is to synchronize a pulsed QENS-measurement with repetitive light excitation at room temperature and selectively probe the protein dynamics in the ground state and different intermediates in a time-resolved manner. Accordingly, a special optical setup and electronics allowing for time-resolved data acquisition and synchronized laser excitation have been developed (see Fig. 1). Likewise, excitation conditions and time-course of the photocycle have been thoroughly characterized before the actual experiment.

The protein dynamics of BR was studied in the dark state as well as with laser excitation in the ground state (BR_{568}) and in the M-intermediate by QENS experiments with an incident neutron wavelength of 5.1 Å and an elastic energy resolution of 93 µeV. While the EISF obtained for the dark and ground state of BR is similar within experimental error, the EISF for the M-intermediate is lower by ~5 % at higher Q (Fig. 2). The latter finding indicates higher protein flexibility in the M-intermediate.

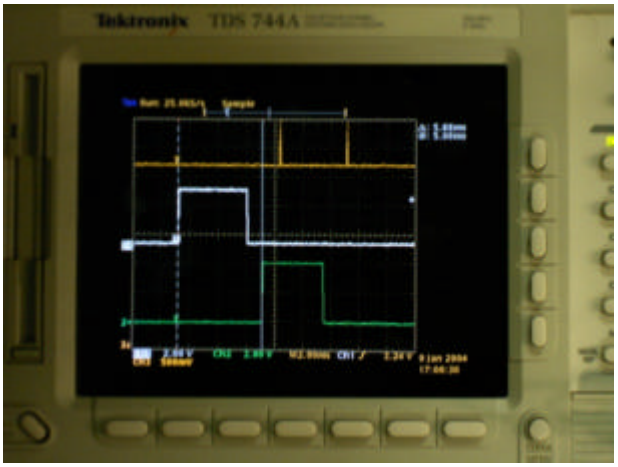


Figure 1

The relative location of master trigger (center), laser (green) and neutron pulses (yellow) for the case of the M-intermediate.

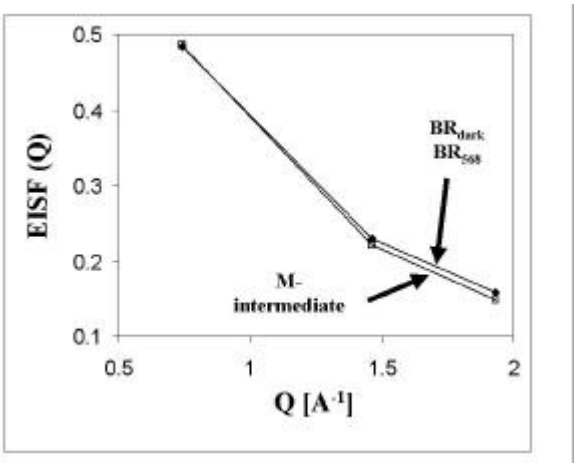


Figure 2

EISF from QENS spectra of BR in the dark, ground state (BR_{568}) and M-intermediate obtained with an incident wavelength of 5.1 Å.

References:

1. R. R. Birge , Biochim. Biophys. Acta 1016 (1990) 293.
2. J. K. Lanyi, , J. Phys. Chem. B 104 (2000) 11441.
3. N. A. Dencher, D. Dresselhaus, G. Zaccai, G. Büldt, Proc. Nat. Acad. Sci. USA 90 (1989) 9669.
4. J. Fitter, R. E. Lechner, N. A. Dencher, J. Phys. Chem. 103 (1999) 8036.

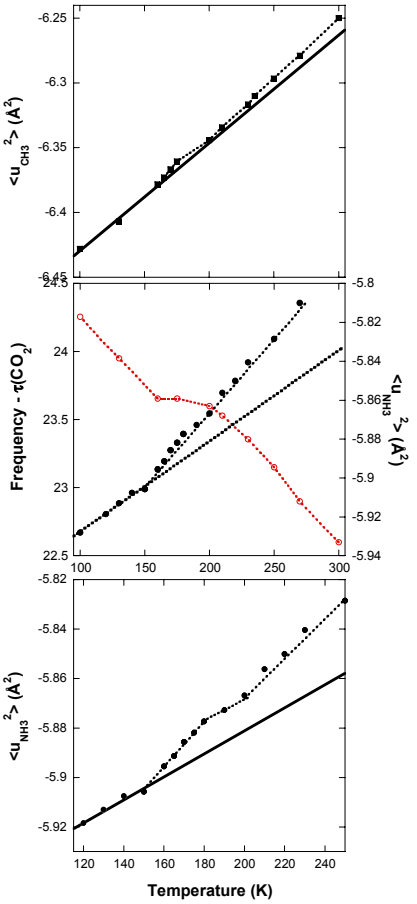
	EXPERIMENTAL REPORT **Dynamical transition in the amino acid L-alanine**	Proposal N° EF Instrument **NEAT** Local Contact A.Buchsteiner
Principal Proposer: Experimental Team:	H.N. Bordallo, HMI Berlin M. Barthès, Université Montpellier II F. Denoyer, Université Paris XI C. Fehr, J. Pieper, A. Buchsteiner, HMI Berlin	Date(s) of Experiment 21-26/09/2004

Date of Report: 21/10/2004

The role of dynamics in enzyme function is a subject of increasing interest. Trying to address such issues at the molecular level, changes in the internal dynamics of proteins as a function of solvent conditions have been examined using several techniques X-ray diffraction, INS, other spectroscopies and simulations have demonstrated the existence of a so-called dynamical transition; i.e. a qualitative change in the nature of internal motions of proteins, generally at about 220 K [1]. Below the transition, the internal motions are thought to be essentially harmonic, while above their anharmonicity contributes and, at physiological temperatures, dominates the internal fluctuations. While it is well accepted that solvent can strongly influence protein structure and dynamics, up to now experiments to test the comportment of isolated amino acids have not been done.

With this in mind we started a series of experiments on alanine, one of the amino acids serving as building blocks for proteins. Here we report on the continuation of a selective deuteration study of the dynamics of each hydrogen group in polycrystalline L-alanine ($C_2H_4(NH_2)COOH$). The experiments were performed using NEAT at HMI from 100 to 300K [2]. Between 100 and 190 K no quasi-elastic component was observed implying a solid like behavior, whereas the development of quasi-elastic signal above 190K suggests the onset of a "liquid like" motion on alanine. Furthermore the observation of a boson peak is a sign of orientation disorder [3,4] what corroborates with our recent diffraction experiments [5].

The figure shows the evolution of the mean-square displacement of each the hydrogen group and the evolution of the $\tau(CO_2)$ group (red line). Since the S(Q) signal arises manly from the incoherent neutron scattering from hydrogen atoms, the elastic intensity follows the expression $\ln[S(Q)=-\langle u_H^2\rangle Q^2$. We can observe that $\langle u_H^2\rangle$ increases steadily with increasing temperature. But near 150K and again near 200K the line breaks indicating the excitation of new degrees of freedom.



One needs to ask what physical mechanisms are responsible for this new excitation and if they are correlated to the torsional jumps observed in protein. A more detailed analysis is under way, but we would like to point out that both the $\tau(NH_3)$ [6] and $\tau(CO_2)$, as shown here, present discontinuities at the same temperatures where breaks on the evolution of the mean-square displacement were observed.

[1] See for example W. Doster et al, Nature **337** 754 (1999)
[2] H.N. Bordallo et al, BENSC Report (2003)
[3] E. Whalley and J.E. Berthe, J. Chem. Phys. **46** 1264 (1967)
[4] H. Leyser et al, PRL **82** 2987 (1999).
[5] M. Barthes, et al European Phys. J. B **37** 375 (2004); and experimental report on E9 results.
[6] M. Barthes et al. J. Chem. Phys. A **106** 5230 (2002)

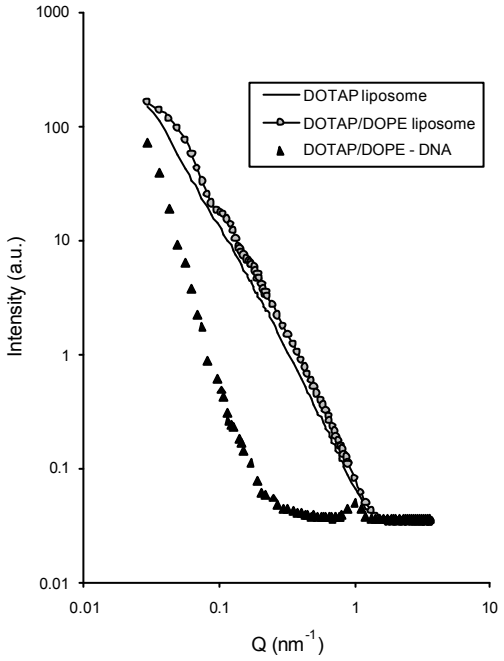
	EXPERIMENTAL REPORT **Supramolecular Organisation in Gene Delivery Complexes**	Proposal N° BIO-04-0944 Instrument V4 Local Contact Dr. U. Keiderling
Principal Proposer: Experimental Team:	Theodore Steriotis, NCSR Demokritos Georgia Charalambopoulou, NCSR Demokritos Thomas Hauss, HMI Berlin Uwe Keiderling, HMI Berlin	Date(s) of Experiment July 12 – July 16, 2004

Date of Report: January 11, 2005

Somatic gene therapy is based on the transfer of extra-cellular DNA into the nuclei of target cells, aiming to replace a defective or adding a missing gene. The current trend is to develop synthetic non-viral "carriers" able to bind and safely deliver DNA. Great attention has been given to positively charged vectors (e.g. cationic liposomes, CLs, and polymer polycations), which can form complexes with the negatively charged DNA.

Despite the intense research, the relationship between the structural details of the complexes and the DNA delivery function is far from being established. Although the self-assembly mechanisms and the resulting molecular arrangement of the complexes determine the overall efficiency of the system, information on the internal organisation of the complexes are seldom found in the literature. The internal 3-D organisation of polycation-DNA complexes is not known at all, while a first approach to resolve structural details of some CL-DNA complexes was carried out by means of Small Angle X-ray Scattering (SAXS). The use of neutrons is very well suited for the study of such systems because the scattering length densities of protonated lipids (or polymers) are significantly different from that of D_2O.

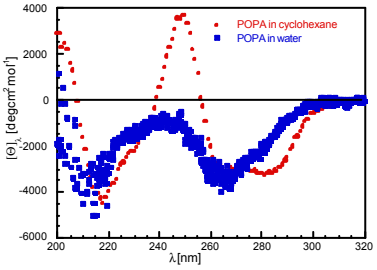
In order to study simultaneously the bulk properties and the internal organisation of the CL-DNA and polymer-DNA complexes a series of contrast variation SANS experiments on a series of cationic precursors and their DNA complexed analogues was performed in experiment BIO-04-0944. The samples were selected carefully in order to represent different major groups of DNA transfer vectors that are showing distinct behaviour in several physicochemical and biological experiments: DNA was complexed with 4 types of cationic precursors (DOTAP and DOTAP/DOPE liposomes as well as PLL and PEI polymers), by using +/- charge ratios of 0.5, 2 and 4 in different H_2O/D_2O mixtures, namely pure D_2O (best overall contrast) and 70% D_2O (DNA matched). A neutron wavelength of 0.605 nm and three sample-detector distances were used (1, 4 and 16 m) in order to cover a Q-range between 0.03 and 3.68 nm^{-1}. It should be noted that the longer than originally expected measurement times did not allow the study of the whole range of scheduled samples. This has definitely hindered the analysis and interpretation of the obtained results, which is still in progress. The most interesting behavior was rather observed in the case of the lipoplexes. The pure liposome solutions (without the presence of DNA) made by the univalent cationic lipid DOTAP resulted in a rather smooth scattering pattern (see attached figure), while the corresponding spectra of (1:1) DOTAP/DOPE water mixtures indicated that the neutral helper-lipid DOPE induces the formation of globules (no Bragg reflection was detected also in this case).



Interestingly, the addition of increasing quantities of DNA led progressively to the condensation of the separate lipid bilayer particles into a multi-lamellar structure characterized by the peak at 1.0 nm^{-1}.

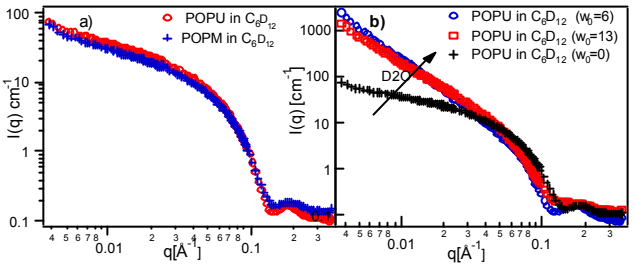
	EXPERIMENTAL REPORT **Reverse phases of phosphatidylnucleosides**	Proposal N° BIO-04-946 Instrument **V4** Local Contact Astrid Brandt
Principal Proposer: Experimental Team:	D. Berti, University of Florence F. Baldelli Bombelli University of Florence F. Betti, University of Florence P. Baglioni, University of Florence	Date(s) of Experiment 23/07/04-26/07/04
		Date of Report:

The systems under investigation in this proposal were the ternary system composed of POPN/water/oil, where POPN are Palmitoyl-oleoyl-phosphatidyl-nucleosides, (with n=adenosine, uridine or the 1:1 mixture of the two nucleosides). POPN are synthetic nucleolipids, whose self-aggregation in direct phases has been studied for some years by us. More recently we have been interested in reverse phases, where water droplets are dispersed in oil by a monolayer of closely packed amphiphilic molecules. Water content can be controlled by phase composition; moreover, the shape of aqueous nanodomains depends upon surfactant chemical nature, oil kind and water content. The motivation to investigate self-assembly in reverse phases lies in the interest for expression of base-base interactions in aggregates with negative curvature and in the possibility to use water pools as nanocompartments where water-soluble macromolecules, such as nucleic acids can be included. Experimental evidence gathered in our laboratory suggests that, upon curvature inversion, a completely different pattern of base-base interaction occurs. As an example in fig. 1 we compare circular dichroic spectra of POPA dispersed in cyclohexane and in water, where bilayered vesicles are formed. The presence of a positive Cotton effect for RMs indicates that the inverted curvature of the lipidic film enhances stacking interactions between bases.



Therefore, an investigation of the structural properties on the nano and mesoscale appears to be in order. The samples measured in this SANS experiment are formed by water addition to POPN solutions in cyclohexane, at constant surfactant volume fraction for all of the three polar head structures above mentioned. Three different water contents have been measured for each system, w_0=0, 6, 13 ([water]/[POPN]).

Moreover both hydrogenated and deuterated cyclohexane have been employed. A parallel QELS investigation on binary phases suggests the presence of two relaxation modes, whose nature (diffusive and/or possibly collective) is currently under investigation.



The measurements had been carefully planned to get a self-consistent picture, even thanks to contrast variation techniques. Due to some problems with the detector electronics, we have lost about 33% of beam time and the results are not a complete set. (backlog requested). Indeed this problem hampered the determination of the phase diagram of the three systems. Some preliminary conclusions can however be drawn. The binary systems show strong similarities for POPU and POPM, while POPA exhibits some major deviations that can be traced back to a higher stacking constant of the base. While binary systems can be conveniently represented by a core-shell ellipsoidal form factor, water dispersion in hydrophilic domains of POPU causes a structural transition to discoidal shapes.

This behavior is in contrast with experimental data available for w/o lecithin microemulsions, where a transition from wormlike micelles to spherical droplets has been found upon water addition. Even if the full set of data will be necessary to draw some conclusive remarks, the interplay between self-assembly and base-base interaction is clear and worth further investigations

BENSC	**EXPERIMENTAL REPORT** **A SANS study of the porosity of biogenic silica from the fustules of diatom species**	Proposal N° BIO-04-0953 Instrument V4 Local Contact Albrecht Wiedenmann
Principal Proposer: Experimental Team:	Chris Garvey, ANSTO Chris Garvey, ANSTO John Ferris, ANSTO Jorg Haug, HMI Berlin	Date(s) of Experiment 9/2/04-11/2/04

Date of Report: 7/1/05

Diatoms are microscopic algae that synthesise intricate silica cell walls, called frustules. Apart from the intrinsic aesthetic appeal of these objects the ability of diatoms to synthesise a number of well-defined pore classes and morphologies in intracellular conditions is of technological interest. The pores and their pattern in the diatom are highly characteristic of the species of diatom (Figure 1). We have been using small angle neutron scattering to study the internal structure of bulks samples of these materials

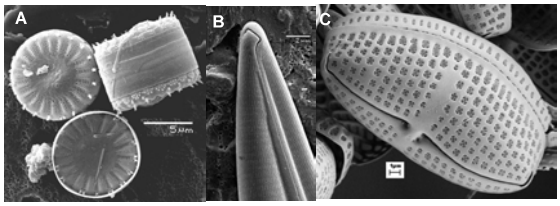


Figure 1 Scanning electron micrographs of **A)** *Cyclotella meneghiniana*, **B)** *Seminavis robusta and* **C)** *Achnanthes subsessilis* (Micrographs courtesy Mathew Phillips, University of Technology Sydney).

In contrast to man-made porous silica, where it is much more difficult to produce monodisperse pore size distributions, these structures are produced under normal intracellular physiological conditions. The basic unit for the assembly of frustules is generally accepted to be colloidal scale silica which are synthesised in silica deposition vesicles (SDV's). Three main mechanisms have been postulated for templating:

1. A precise moulding mechanism where silica is deposited uniformly onto a scaffold from SDV's.
2. A mechanism whereby silica nucleation occurs on the scaffold that is followed by diffusion limited reaction.
3. A phase separation model guided by the electrostatic interaction between charges on the scaffolding and negatively charged silica particles.

Scattering patterns have been collected from bulk samples with sample path lengths 4.00 to 0.2 mm for each of the species shown in Figure 1 . A path length of 0.25mm represented the maximum path length before changes in the scattering pattern could be observed. The slope of data followed Porod behaviour over a wide q-range (Figure 2) and report BIO-04-961.

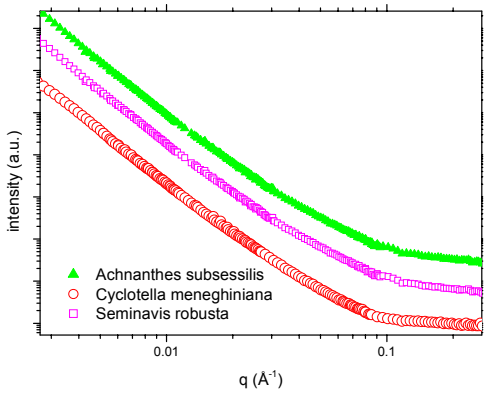


Figure 2 SANS data from 0.2 mm thick samples of frustules from each diatom species showing the similarity of the scattering curve over a range of q-values.

The observation of Porod like behaviour would seem to preclude mechanism 2, diffusion limited reaction, as a mechanism for templating. Currently we are investigating the absolute intensity scale for Figure 2 . The surface area per gram of material was measured by fitting the BET isotherm to the adsorption of N_2 to a known mass of frustules (Table 1).

Table 1 Specific surface areas determination of diatom frustules from BET isotherm fitted to N_2 sorption.

Diatom species	BET specific surface area ($m^2.g^{-1}$)
Achnanthes subsessilis	15.70 ± 0.16
Cyclotella meneghiniana	9.51 ± 0.06
Seminavis robusta	9.61 ± 0.06

BENSC	**EXPERIMENTAL REPORT** **A USANS study of the porosity of cultured diatoms**	Proposal N° BIO-04-0961 Instrument **V12a** Local Contact Wolfgang Treimer Markus Strobl
Principal Proposer: Experimental Team:	Dr Chris Garvey, ANSTO Dr Chris Garvey, ANSTO Dr John Ferris, ANSTO Dr. Markus Strobl, HMI Berlin	Date(s) of Experiment 01 Feb – 08 Feb. 2004

Date of Report: 27th June 2004

This experiment aimed at determining the pore size distributions of the silica frustules from cultures of three species of diatoms (microalgae). Samples were therefore silica powders that contained three or four well defined pore size distributions. In TEM and SEM micrographs produced from the three species of diatoms clear differences in the pore sizes and shape were apparent. While certainly pore sizes in the q-range of the experiment are visible in micrographs the intention is to use data from this study to examine the internal porosity of a bulk sample and the construction of this material at a nanoscale.

A critical issue in the interpretation of scattering patterns from these samples is the maximum thickness of sample which can used without multiple scattering effects becoming apparent in the small angle scattering. A number of samples of increasing thicknesses were packed to known densities. It was found that the scattering pattern did not change above a thickness of ~2mm. All subsequent experiments were carried out with this sample thickness.

Figure 1 shows the slit smeared neutron scattering patterns obtained from the three diatom species. The three curves are similar in the higher q-range. The slope in the higher q-range is ~1.5. The curves are quite different in the smaller q-range with a number of clear features visible. The length scales correspond to clear periodic features in the SEM micrographs and may be due to constructive interference of radiation scattering from the these features.

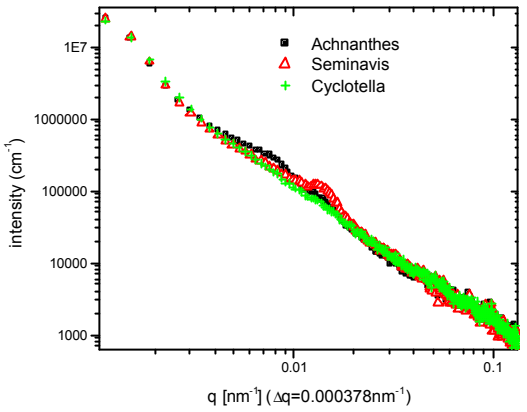


Fig. 1 Slit smeared scattering curves from samples consisting of frustules of three diatom species.

Current analysis of the scattering curves has slit smeared pin-hole data from the V4 instrument on the same samples[1] to provide data over a wide q-range. An abstract has been submitted to present a preliminary analysis of the data[2].

[1] BENSC Experimental report Bio-04-0953.
[2] Garvey, C.J., and Ferris, J., "Small angle neutron scattering (SANS) and TEM studies of the internal porosity of three cultured diatom frustules." International Conference on Biological Physics, Gothenburg (2004).

	EXPERIMENTAL REPORT **Adsorption of S-protein on polyelectrolyte multilayers**	Proposal N°: BIO-04-971 Instrument V6 Local Contact R.Krastev
Principal Proposer: Experimental Team:	J.L. Toca-Herrera, BOKU, Vienna, Austria J.L. Toca-Herrera, BOKU, Vienna, Austria R.Krastev, HMI Berlin/MPI KGF, Golm, Germany	Date(s) of Experiment 13.02.-15.02.2004

Date of Report: 20.03.2004

Crystalline bacterial cell surface layers (S-layers) are composed of a single protein or glycoprotein, and exhibit oblique, square or hexagonal lattice symmetry. They have the ability to assemble into a closed lattice during all stages of cell growth and cell division. Therefore, they can be considered as one of the most common outermost cell envelope components of the prokaryotic organisms (bacteria and archaeda), and represent the simplest biological membranes developed during evolution [1]. Isolated S-layer subunits are able to assemble into (mono)molecular arrays on lipid films, liposomes and solid supports. In the present study, we studied the assembly of S-layers onto solid support covered with polyelectrolyte (PE) multilayer films.

S-layer protein of *B. sphaericus CCM 2177* (SbpA) has been used to cover three samples – bare Si-substrate and two Si samples covered with PE multilayers. The negatively charged Poly(sodium 4-styrenesulfate) (PSS) and the positively charged Poly(allylamine hydrochloride) (PAH) were used as PEs. An initial layer of Polyethylene imine was added as well. The samples were prepared using the layer-by-layer technique (LbL) [2], which allows the deposition of multiple layers in a controlled fashion, due to the electrostatic interaction. The following PE samples were studied – PEI/$(PSS/PAH)_6$ which assures positive charge at the surface and PEI/$(PSS/PAH)_6$PSS, which creates negative charge at the surface due to the adsorption of a last additional layer of PSS. The experiments were performed in the solid-liquid experimental cell available at HMI. First the neutron reflectometry curves from the bare preliminary prepared solid supports against D_2O were collected. Then the solution of the S-protein in 0.5M Tris/HCl (pH 9) buffer in H_2O was introduced in the cell and left for the adsorption of the protein. After 1 hour the solution was exchanged with pure D_2O and the NR curves against pure D_2O were collected.

The results are shown in the figures (curves1 and 2). Both figures show change in the film thickness upon exposure to the S-protein solution. An increase of the thickness with 13-15 nm is attributed to formation of a bilayer of S-layer on the solid supports. This result coincides with earlier obtained data from AFM studies. A difference in the Scattering Length Density (SLD) of the S-layers was observed. A SLD of around $4.8x10^{-6}$ Å^{-2} is obtained in the case of the PSS terminated layers. This result suggests formation of a low density S-layer filled with D_2O. In the case of the PAH terminated layer the SLD was calculated to be around $2.8x10^{-6}$ Å^{-2} which shows formation of a densely packed protein layer which includes small amount of D_2O. The results obtained for the bare Si substrate (not shown) are similar to that of the PAH terminated PE layer.

Another experiment was performed to study the influence of the ion content on the properties of the S-layer. The D_2O was exchanged with 10 mM solution of EDTA in H_2O. It was washed with fresh D_2O after 4 hours and the NR curve was collected again. The result is shown on figure 1 curve 3. The curve is similar to that of the bare PSS terminated substrate and shows that the S-protein layer was desorbed from the substrate. Our preliminary conclusion is that the effect is due to the lack of Ca^{2+} ions which were blocked by EDTA.

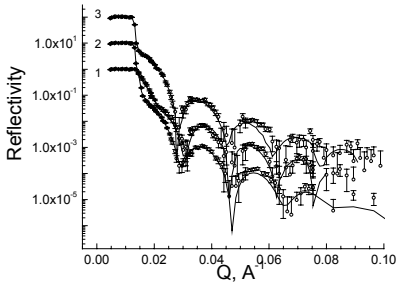


Fig. 1*: NR curves of PSS terminated PE multilayer: 1) bare substrate; 2) after 1 h adsorption of S-protein; 3) after exposure of the already formed S-layer to 10 mM EDTA solution. All curves are collected against pure D_2O.*

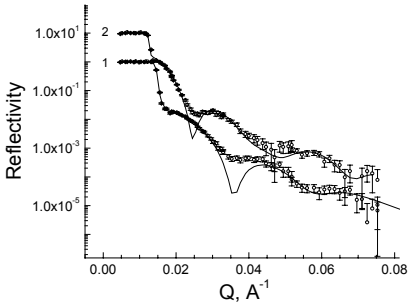


Fig. 2: NR curves of PAH terminated PE multilayer: 1) bare substrate; 2) after 1 h adsorption of S-protein

1. U. B. Sleytr, M. Sara, D. Pum, B. Schuster, *Progress in Surface Science*, **68** (2001) 231
2. G. Decher *Science,* **277** (1997) 1232

	EXPERIMENTAL REPORT **Thermal stability and effect of the external magnetic field on 7M modulated structure in non-stoichiometric Ni-Mn-Ga ferromagnetic martensite**	Proposal N° MAT-01-1444 Instrument **E2** Local Contact J.-U.Hoffmann.
Principal Proposer: Experimental	N.Glavatska, Institute for Metal Physics, Kiev, Ukraine I.Glavatskyy, Institute for Metal Physics, Kiev, Ukraine J.-U.Hoffmann, HMI Berlin	Date(s) of Experiment 27.04-7.05.2004

25.05.2004

Present investigation concerns neutron diffraction study of structure martensitic phase and its temperature stability within the whole range of martensite as well as effect of magnetic field on twinned martensite structure rearrangement in off-stoichiometric high-temperature Ni-Mn-Ga Heusler alloy $Ni_{2.053}Mn_{1.105}Ga_{0.842}$. Studied specimen has temperatures of martensite-austenite transformation A_s= 330K, M_s= 322K and Curie point T_c= 370K.

Experiment: During the experiment performed on E2 diffractometer (with λ= 0.239 nm) the single crystalline specimen was aligned to have (001) plane coinciding with scattering plane. Crystal structure was studied in the temperature interval from T=330K down to 50K.

Results.

The unit cell in martensite in the studied single crystal is determined as slightly monoclinic (3^0 declination) with inconsistent 7-layered modulation and lattice parameters: ***a′***=***b′***=0.6649 nm, ***c′***=0.5547 nm at 300K. Lattice modulation M(7) is observed in directions [101] and [10-1]. 7M martensite remains stable within the studied temperature range.

Temperature dependence of martensite lattice parameters ***a*** and **c** is opposite (**Fig.1**). This behaviour causes strong change of the lattice distortion of martensite – from 0.157 at 330K to 0.185 at 50K (**Fig.2**). This strongly affects the twin boundary mobility, i.e. max possible shape memory value increases at the same time as critical stress magnetic field value needed to move the twin boundary rises until they finally become immovable.

Fig.3 shows effect of applied magnetic field (H=2T) on the crystal structure of martensite – peak intensity changes due to twin variant rearrangement (the key of the magnetic shape memory), as it was found to have realised 4 twinned martensite variants in the initial state. Thus, the studied alloy seem to be very perspective for magnetic shape memory effect.

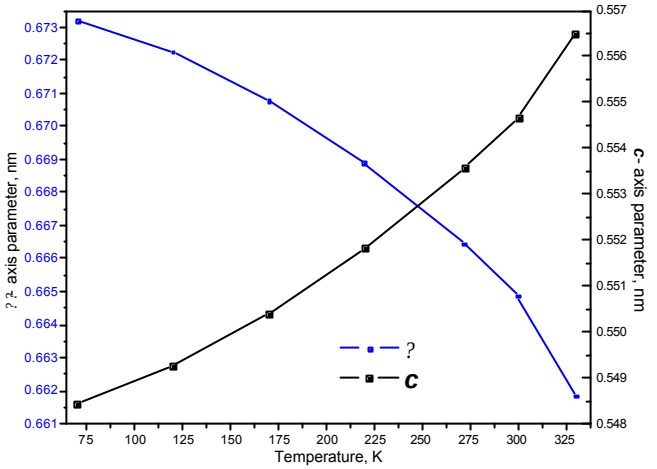


Fig.1 Lattice parameters of martensite vs temperature

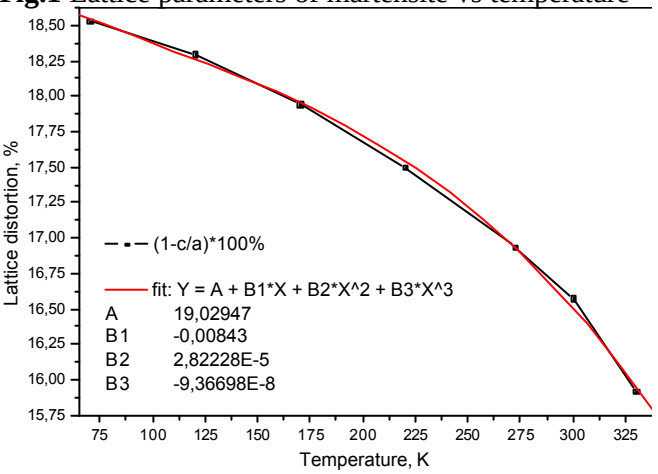


Fig.2 Temperature dependence of lattice distortion

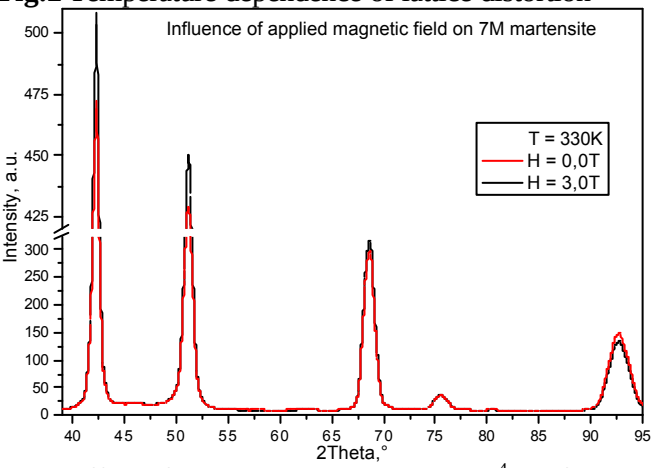


Fig.3 Effect of external magnetic (H=2*10^4Oe) field on twinned martensite structure.

BENSC	**EXPERIMENTAL REPORT** **Residual stresses in ball bearing rings, -comparison of Neutron and X-ray diffraction measurements**	Proposal N° MAT-01-1491 MAT-01-1391 Instrument **E3** Local Contact Tobias Poeste
Principal Proposer: Experimental Team:	Thomas Hirsch, IWT A. da S. Rocha and T. Hirsch, IWT T. Poeste and R. Schneider, HMI Berlin	Date(s) of Experiment 284th of April to 06th of May 2004

Date of Report: 10th of February 05

1 Introduction

A combination of X-ray- and neutron diffraction was used to identify residual stress distributions over whole ball bearing rings' cross sections. Investigated residual stress distributions were generated by different manufacturing steps in the manufacturing route of a ball baring ring (SFB 570 - "Distortion Engineering"). Results are presented in this report for machining and quenching steps.

2 Experimental Description

Ball bearing rings were manufactured from the steel 100Cr6 with following chemical composition in mass-%: 0.966 C; 0.0236 Si; 0.48 Mn; 0.008 P; 0.005 S and 1.58 Cr. Rings with dimensions D.int.= 133mm, D.external= 145 mm, 26mm height have been manufactured according to industrial standards. They were machined to their final dimensions by a turning process. A ferritic perlitic microstructure with spheroidized carbides was observed in the machined cylinders. Some of the rings have been austenitized and symmetrically quenched by a gas nozzle field with a gas velocity per nozzle of 150m/s. After quenching, mixtures of martensite and 10 to 15 Vol% occur over the whole cross section. Residual stresses were measured in one cross section at a marked 0° position of the outer circumference of the rings. In the neutron diffraction experiments, volume elements of approximately 1,5x1,5x1,5mm were defined by the slits' choice. X-ray RS measurements were executed in the IWT-Bremen using Cr-kα radiation and the standard $\sin^2\Psi$ method. X-ray RS depth's profiles were performed by measurements after successive electro-chemical layer removals. Different samples from the rings were produced for the d_0 measurements: powder, thin plates and cubes. The powder was prepared by a hand grinding process. Thin plates (0.5mm thickness) from the radial direction of the rings and cubes (3x3x3mm) were prepared by EDM and electropolishing of their surfaces. As a second way to establish d_0, residual stresses measured over the whole cross section combining X-ray and neutron diffraction were checked for the balance of stresses.

3 Results

Figure 1 presents results for the machined ring. As measured by X-rays, a high gradient of residual stresses exists in the surface layer. The RS are about 350MPa at surface and change from tensile to compressive at about 0.06mm from the surface. The RS become less compressive for higher distances from surface and from neutron RS measurements they are around zero for 0<z<2,5 mm. The results of X-rays and neutron diffraction measurements were checked by the RS balance over the cross-section for the hoop and axial direction. They show that axial residual stresses in the center are shifted a little bit towards compression while the hoop stresses are a little bit too high in tensile.

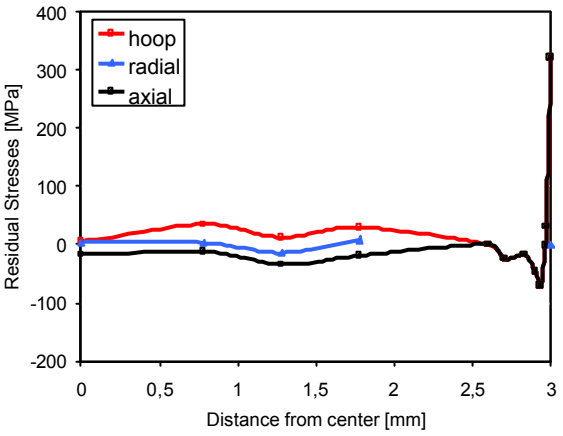


Fig.1: Residual stresses measurements by neutron and X-rays for a ring after machining.

In a quenched ring, compressive stresses of +50 MPa were measured by X-rays at the surface. Neutron diffraction measurements exhibited high scatter due to the diffraction lines with low intensity and high FWHM values.

4 Consequences

A detailed review will be given in a paper. The next experiments will be extended to other steps of the manufacturing route including carburizing of cylinders for which a d_0 gradient must be taken into account. Some experiments should be repeated.

BENSC	**EXPERIMENTAL REPORT** **The impact of grain size on residual stress measurement in welded components**	Proposal N° MAT-01-1493 Instrument **E3** Local Contact R. Schneider
Principal Proposer: Experimental Team:	Robert Charles Wimpory, HMI (formerly JRC) Carsten Ohms JRC – IE, Westerduinweg 3, 1755 LE, Petten, NL	Date(s) of Experiment 5th till the 10th Feb 2004

Date of Report: 14.01.2005

Two nominally identical rectangular double-V-weldments of austenitic steel (100mm x 30mm x 12mm) were investigated. One had an average grain size of 50-60 µm (stainless steel grade 347) and the other an average of 200 µm (stainless steel grade 304) in the base material. 3-dimensional stress measurements were performed at specimen mid-thickness along a line transverse to the welding direction (see fig. 1). Locations were tested in the base material, HAZ (heat affected zone) and within the weld itself.

Diffraction methods are strongly sensitive to the average grain size within the material. Too large a grain size can cause erroneous strain values emerging from the diffraction data.

E3 was suitable for these measurements because it offered the use of a 2 dimensional area detector to identify less problematic test positions and because it offers the possibility to rock the specimen during testing. It can be seen in fig2. that oscillating the omega table during measurement vastly improved the scatter in the data caused by large grains. Oscillating continuously +/- 10 degrees produces a smooth measurement curve compared to the large scatter obtained when measuring without oscillation.

Fig. 3 shows that the strain in the longitudinal direction between the large grain 304 and smaller grain 347 specimens are very similar. The large grain measurement however still exhibits a little scatter. Better agreement can be seen in the residual stress in fig. 4 where the scatter appears to have been averaged out more. All strains were measured with +/- 10 degrees omega oscillation and measurements were made based on the 311 reflection with a neutron wavelength of 1.3729 Å.

By using omega oscillation it has been possible to circumnavigate the grain size problem and to measure the stress field within coarse grained materials.

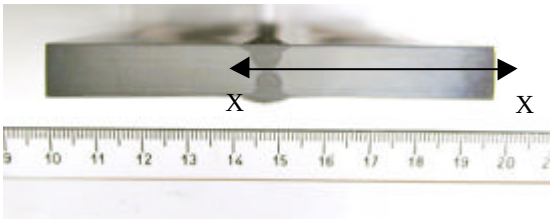


Fig. 1 Cross section of the double-V weld specimen.

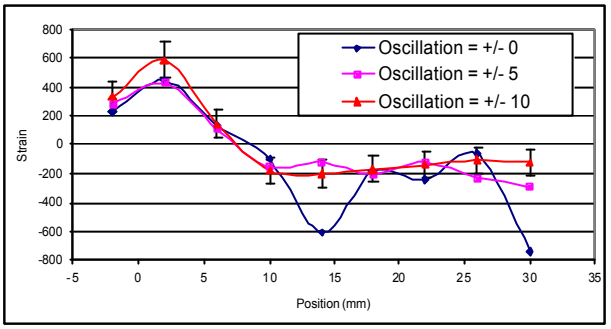


Fig. 2 Longitudinal strain in 347 specimen as a function of Omega oscillation.

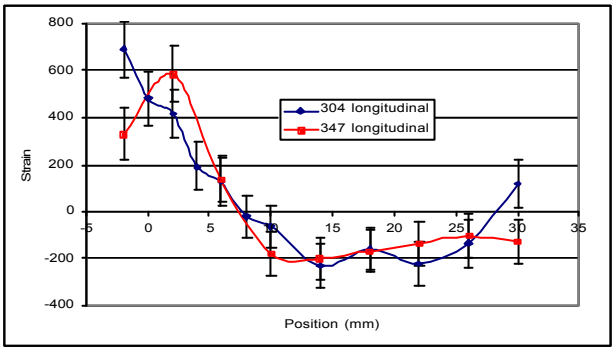


Fig. 3 Longitudinal strains in 347 and 304 specimen with +/10 degree omega oscillation.

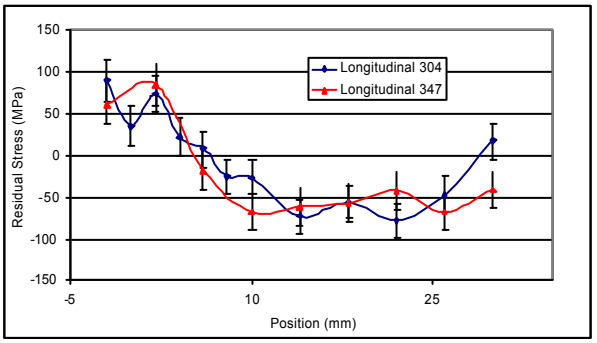


Fig. 4 Longitudinal stresses in 347 and 304 specimen with +/10 degree omega oscillation for all strains.

	EXPERIMENTAL REPORT **Effect of Fatigue Crack Propagation on Residual Stresses in a 2024 Aluminium Weld Coupon**	Proposal N° **MAT-01-1495** Instrument **E3** Local Contact Rainer Schneider
Principal Proposer: Experimental Team:	**Lyndon Edwards - The Open University, U.K.** **S. Pratihar, Jeffrey M. L. Tan - Open University** **T. Poeste, R. Schneider, F. Henkel - HMI Berlin**	Date(s) of Experiment 12th - 22nd July 2004 (10 days)

Date of Report: 5th January 2005

Introduction

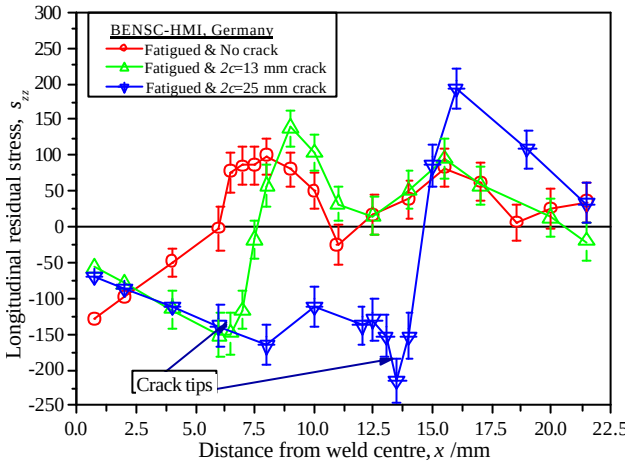
This experiment aims to study the effect of the fatigue crack propagation on the redistribution of the original residual stress field induced in weld coupon. Plates of 2024 aluminium alloy, commonly used in aerospace industry, were welded using the Variable Polarity Plasma Arc technique (VPPA). The joined plates were subsequently skimmed and fabricated into dog-bone coupon. Starting with a central notch introduced in the specimen, fatigue cracks were grown under controlled constant ?K. To achieve the requirements of safety design optimisation and maintenance, it is necessary to track the changes of residual stress with response to fatigue cyclic loading and crack propagation in and out of the Heat-Affected-Zone (HAZ). The effect of the redistributed residual stress can then be assessed by aircraft damage tolerance analysis using linear elastic fracture mechanics methodology.

Experiment

With take-off angle at $2T_M$ = 65° of vertical focusing Cu (220) flat monochromator, a 1.37 Å wavelength was used. The gauge volume $2\times2\times2mm^3$ was used to probe along the mid-thickness of the specimen starting from the centre notch where the crack firstly initiated. The the 2Θ = 69.939º was used to define the scattering vector *Q* corresponding to the directions of strain measured, which is perpendicular to the diffracting plane. A complete set of three principal residual strains were probed in 3 specimens of different crack lengths.

Results and Discussion

Three samples of 8mm thick VPPA coupons of different crack sizes of 0, 13 & 25 mm, were measured successfully. The data corresponding to fatigued by without crack was actually measured 40mm away from the crack plane of specimen containing 2*c* = 13mm crack. Our initial analysis indicates that the residual strain does redistribute due to propagation of cracks. The amount of redistribution is the greatest for longer crack sizes. This is understandably due to higher number of cyclic loadings that promote further crack extension coupled with successive re-equilibrating of stress field when the crack grows.



	EXPERIMENTAL REPORT **Residual Stress Relaxation in Fatigued Cold-Expanded Holes**	Proposal N° **MAT-01-1496** Instrument **E3** Local Contact Rainer Schneider
Principal Proposer: Experimental Team:	**Lyndon Edwards - The Open University, U.K.** **Jeffrey M. L. Tan, S. Pratihar - Open University** **T. Poeste, R. Schneider, F. Henkel - HMI Berlin**	Date(s) of Experiment 23rd July 2004 till 2nd August 2004 (9 days)

Date of Report: 5th January 2005

Introduction

The present work aims to study the relaxation of beneficial residual stress field around fatigue-cracked cold-worked fastener holes in aerospace aluminium alloy plate. The cold-working of holes were performed by a new patented technology called StressWave™, which shows great potential of efficiency and effectiveness in automatic bulk production of metallic joints in airframes. To achieve the requirements of safety design optimisation and maintenance, it is necessary to track the changes of residual stress with response to fatigue cyclic loading and crack propagation in the material. Subsequently, based on the fracture mechanics approach, the HMI data will be used for fatigue life modelling of related mechanical components.

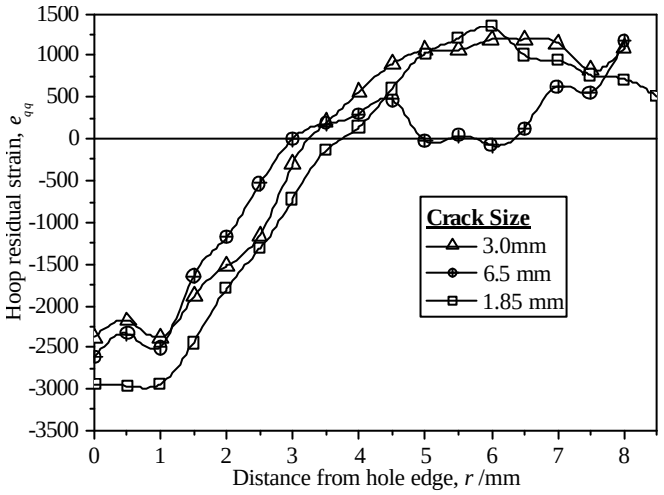
Experiment

With take-off angle at $2T_M$ = 65° of vertical focusing Cu (220) flat monochromator, a 1.37 Å wavelength was used. The gauge volume $2\times2\times2mm^3$ was used to probe along the mid-thickness of the specimen starting from the hole edge. The material of the specimen is 2024 aluminium alloy widely used in aerospace industry. The angle 2Θ = 69.939° was used to define the scattering vector *Q* corresponding to the directions of strain measured, which is perpendicular to the diffracting plane. For the present specimen geometry, the cold-working process of the hole was optimised by finite-element analysis. Then, uniaxial fatigue loading was applied on the specimen to grow fatigue cracks. Only the residual strains in the hoop and radial direction for 3 specimens of different crack lengths were measured.

Results and Discussion

1. Three samples of F6.35mm cold-worked holes, of different crack sizes of 1.85, 3 & 6.5* mm, were measured successfully. Our initial analysis indicates that the residual strain relaxed during the propagation of cracks starting from the hole edge.

*(the last specimen was partially measured in the 2nd direction i.e. radial)



2. The data also shed the light on the effectiveness of the remnant residual stress of particular crack size, which is still safe to allow further crack propagation before requiring structural maintenance.

3. Following from the successful quantification of residual strain in cold-worked hole specimen with crack, a complete distribution of residual stress is desirable for complex 3D crack shape, and this requires more measurement at the different thickness location and other strain directions of the specimen.

BENSC	**EXPERIMENTAL REPORT** **Stress Gradients below the Surface of a Model Rocket Nozzle**	Proposal N° MAT-01-1635 Instrument E3 Local Contact Tobias Poeste
Principal Proposer: Experimental Team:	Michael Hofmann, FRM II, TU Munich Tobias Poeste, TU Berlin Michael Hofmann, FRM II, TU Munich Rainer Schneider, HMI Berlin	Date(s) of Experiment February 9th, 2005

A model rocket nozzle (figure 1) was investigated using neutron diffraction on E3. The main interest of the measurement was the in depth residual stress state of the outer Ni layer of the nozzle after the final fabrication process. Using the (311) reflection of Ni we were able to extract strain data at two different points of the component up to 8 mm depth in the Ni coating. Due to the high absorption of Ni and relative large neutron path length through the material in the hoop direction, however, full analysis of the residual stress state was only possible in one of those points.



Figure 1 Model rocket nozzle.

	EXPERIMENTAL REPORT **Study of the R-Phase Structure in NiTi Shape Memory Alloys**	Proposal N° MAT-01-1449 Instrument **E9** Local Contact D.M. Többens
Principal Proposer: Experimental Team:	Prof. Wolfgang Schmahl, Ruhr-Universität Bochum Prof. Wolfgang Schmahl, Ruhr-Universität Bochum, Germany Dr. Jafar Khalil-Allafi, Sahand University of Technology, Tabriz, Iran	Date(s) of Experiment 28.07-31.07.2004

Date of Report: 13.12.2004

A 13 mm diameter rod of $Ni_{50.8}Ti_{49.2}$ was purchased from Memory Metalle, Weil am Rhein. A sphere of 12 mm diameter and two small pieces of 30 mg were machined from the as-received material. In order to have The R-phase in this material both the sphere and the small pieces were solution annealed at 850°C for 20 minutes, water-quenched, and subsequently aged at 400°C for 150 minutes. Figure 1 shows DSC (differential scanning calorimetry) chart of NiTi aged material.

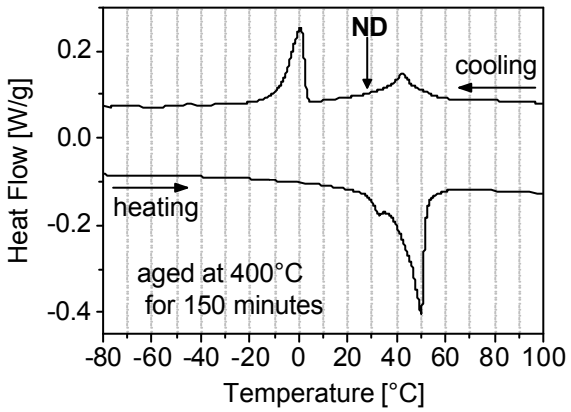


Figure 1: DSC chart of aged $Ni_{50.8}Ti_{49.2}$.

During cooling two step martensitic transformations occur. First of all the high temperature phase austenite with B2 structure and Pm3m symmetry transforms to R-phase with trigonal structure. In the second step both R-phase and remaining austenite transform to martensite with B19' (monocline) structure. On heating reverse transformations occur.

Neutron diffractograms of the spherical sample were collected at room temperature on the E9 instrument using the wavelength 1.79668 Å. The effect of texture on the diffraction intensities was minimized by suspending the NiTi sphere on an air cushion, which was generated by an air current issued from a 4 mm opening at the bottom of a calotte-shaped recess in a perspex rod of 20 mm diameter. The air flow has to be limited to the minimum which is sufficient to suspend the sphere, such that fluctuations in air currents lead to a random rotation of the sphere. Larger currents cause more permanent rotations around axes of inertia, since a mechanically made sphere will never by exactly spherical. The NiTi sphere was dipped into boiling water just before it was placed on the sample holder, to make sure it was in the R-phase state by entering the martensitic hysteresis loop from high temperature (see Figure 1). The Rietveld refinements were performed using the GSAS code including a spherical harmonic correction for remaining texture effects (Figure 2).

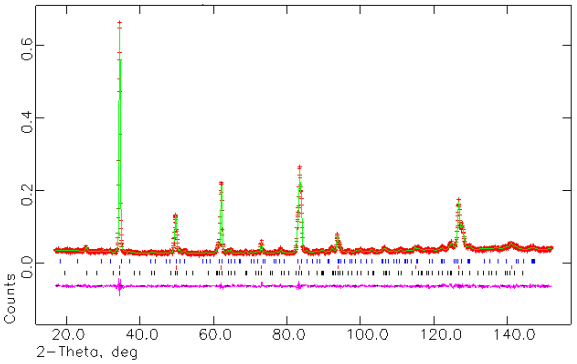


Figure 2: Neutron diffractogram for the aged $Ni_{50.8}Ti_{49.2}$ sample along with calculated diffraction profiles.

Space groups considered by us in refinements of the R-phase structure, P $\bar{3}$1m, P $\bar{3}$, and P3, all belong to a group-subgroup chain originating in Pm3m as a common supergroup. The results show clearly that the R-phase has a trigonal structure with P $\bar{3}$ symmetry.

The structure of the B19' phase was also refined ($P2_1/m$ symmetry) on texture free data, obtained in the same way.

BENSC	**EXPERIMENTAL REPORT** **Neutron powder diffraction line broadening and corrosion products of an electrochemically cycled $LaMMNi_{3.55}Co_{0.75}Mn_{0.4}Al_{0.3}$ battery electrode material**	Proposal N° MAT-01-1458 Instrument **E9** Local Contact M. Tovar
Principal Proposer: Experimental Team:	Peter A. Georgiev, UNI Salford, Salford, UK P.A. Georgiev, UNI Salford, Salford, UK M. Tovar, BENSC, HMI, Berin D.L. Ross, UNI Salford, Salford, UK	Date(s) of Experiment 28-29/03/2004

Date of Report: 26/11/2004

The present neutron diffraction study is part of an extensive investigation of the structure thermodynamics, hydrogen diffusion kinetics and electrochemistry of a commercial $LaNi_5$-type of hydrogen storage material. Although replaced by the Li-ion technology in portable applications such as mobile phone and laptop batteries, there is still great interest in these types of materials due to their low cost, simple manufacturing process, easily engineered thermodynamical properties and potential application in large hydrogen storage systems and fuel cells.

The aim of the experiment was to observe the effects on the material microstructure caused by a prolonged electrochemical cycling in a 6M KOH water electrolyte and to identify the eventual corrosion products. Accordingly, two samples were measured. The neutron powder diffraction pattern of the as produced material is shown in Fig.1a. A single P6/m m m phase of the compound with lattice parameters a=5.008 Å and c=4.051 Å was observed. In Fig. 1b is shown the pattern of the same material after 120 charge/discharge cycles performed in a vented cell at 40°C and down to -0.6V (v.s. Hg/HgO/6MKOH ref. Electrode) cut-off voltage during each discharge process. Crystal structure refinement of each of the observed phases was performed using the program FULLPROF [1]. Two main differences were observed in the diffraction patterns of the two materials. Firstly, the pattern of the cycled material clearly contains more than one phase. The refinement was carried out including $La(OH)_3$ phase and pure Ni-phase with an average domain size of about 100 Å estimated from the diffraction lines broadening. Secondly, the almost 10% decrease in the width of the peaks of the main phase suggests that residual stress relaxation processes take place during the associated with the charge/discharge crystal lattice expansion/contraction.

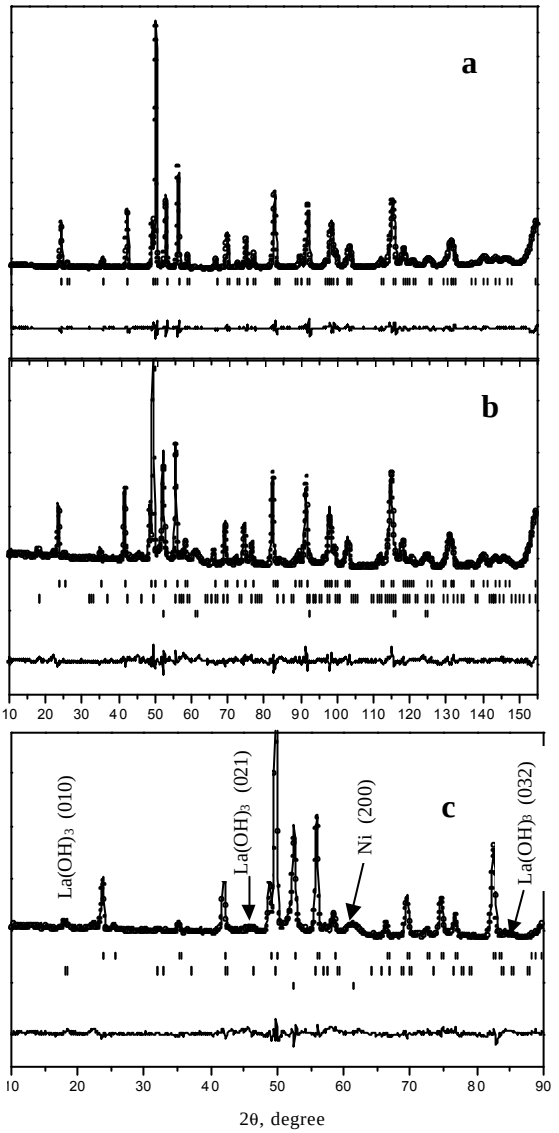


Fig. 1. Neutron powder diffraction pattern of the untreated AB_5 material is shown in a), b) the same for the electrochemically cycled sample, and c)-the main crystallographic reflections of the $La(OH)_3$ and pure Ni phases are indexed.

[1] J. Rodríguez-Carvajal, in: Presented at the XV Congress of Int. Union of Crystallography, Satellite Meeting on Powder Diffraction, Toulouse, France, 1990, p. 127.

[2] G.W. Beal et al. J. In. and Nuc. Chem. **39**, 65, 1977

BENSC	**EXPERIMENTAL REPORT** **Phase analysis of Ni-Fe-base superalloys**	Proposal N° MAT-01-1566 / 1453 Instrument **E9** Local Contact Dr. D.M. Toebbens
Principal Proposer: Experimental Team:	Dr. habil. Ralph Gilles, TU München Dr. R. Gilles, Dr. M. Hoelzel, TU München / TU Darmstadt, Dr. D. Mukherji, ETH Zürich, D. del Genovese, IWF TU Braunschweig, Dr. P. Strunz, PSI, Dr. D.M. Toebbens, HMI Berlin	Date(s) of Experiment 17.08.04 – 23.08.04

Date of Report: 04.01.05

The beam time corresponding to MAT-01-1566 was partly used as a continuation of MAT-01-1453 for studies on Ni_3Al based γ' particles which were extracted from W-rich Ni-base superalloys (see MAT-01-1453) and for studies on superalloys based on Inconel 706.

Superalloy Inconel 706 is used in gas turbine discs because of its outstanding creep and rupture properties combined with its high tensile strength at temperatures up to 650 °C. A modified η stabilisation heat treatment was applied on Inconel 706 in this study to obtain high amounts of inter- and intragranular η precipitations. The formation of the η phase is accompanied by a considerable decrease in tensile strength, but has beneficial impact on the creep rupture strength. Neutron diffraction was performed using the powder diffractometer E9 with a wavelength of λ = 1.797 Å. To minimise texture effects, the measurements have been divided into several scans with different sample orientations. Rietveld refinement was applied to analyse the experimental data, using the software package of FullProf (Fig.1). The reflections other than from the γ matrix (fcc) reflections could be described by the η phase with space group $P6_3/mmc$, having an ordered Ni_3Ti structure with Ni (Fe, Cr) atoms distributed on (0,0,0) and (1/3, 2/3, 1/4) sites, while Nb (Ti, Al) atoms occupy (1/2,0,0) and (-1/6, -1/3,0) sites. Prior X-ray diffraction studies were unsuccessful for the identification of η precipitations, supposedly because not enough η particles had suitable orientations on the surface for measurements in Bragg-Brentano geometry.

The superalloy named DT 706 can be described as a modified Inconel 706. The modified alloy is designed to stabilize the γ' phase over γ'' phase by altering the (Al+Ti)/Nb ratio. Neutron diffraction patterns of direct-aged DT 706, taken at E9, were analysed by Rietveld refinement to reveal a weight fraction of γ' of about 20 wt.% and a γ/γ' lattice mismatch of + 0.38 %. In contrast to previous X-ray studies the small γ' superlattice reflections, which do not overlap with fcc matrix reflections, were clearly visible (Fig 2).

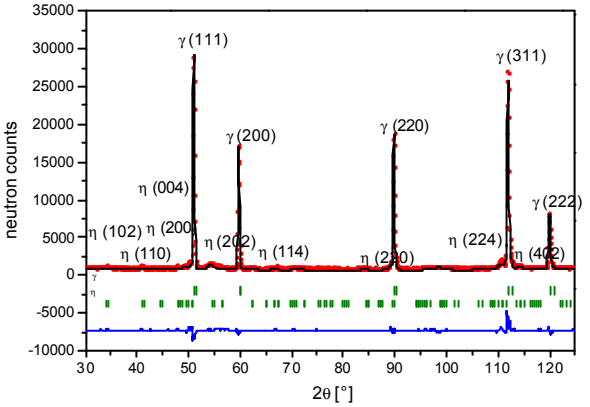


Figure 1: Measured and calculated diffraction patterns for Inconel 706 MST 5000a.

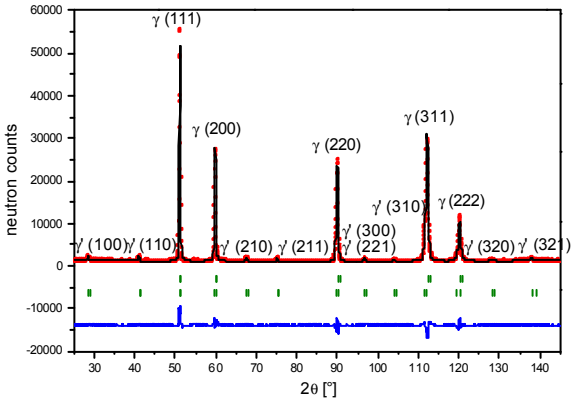


Figure 2: Measured and calculated diffraction patterns for DT 706.

BENSC	**EXPERIMENTAL REPORT** **MECHANISM OF FORMATION AND STRUCTURE OF ZEOLITE LTA COLLOIDS**	Proposal N° MAT-04-873 Instrument **V4** Local Contact U. Keiderling
Principal Proposer: Experimental Team:	J.D.F. Ramsay (IEM CNRS Montpellier France) J.M. Condre (IEM CNRS Montpellier France) T. Steriotis (Demokritos NCSR Greece) U. Keiderling (BENSC Berlin Germany)	Date(s) of Experiment 13/11-17/11/2003

Date of Report: 15/12/200

A possible route of formation of composite nanostructured layer of porous materials is the sol-gel process. This relies on the use of mixed colloidal nanoparticles. Our interest here is the mechanism of formation and structure of composites of

(a) Zeolite/Boehmite and

(b) Zeolite/Zirconia.

Here we report SANS results on mixed sols and solid composites measurements on V4 (at 4.57Å, detector distances of 16m, 4m and 1m). SANS results for simple component powder are illustrated in Fig.1. These confirm the shape and size of the particles as determined in other studies [1, 2]

To study the stability and interactions of mixtures, we needed to establish contrast matching points for each individual component (see e.g. Fig.2.). Results for mixed sols are illustrated in Fig.3. More detailed analysis of these results show that the mixed colloids are stable and homogeneous. A comparison with theoretical prediction band on the SANS of single components indicates that significant interaction occurs in the Zeolite/Boehmite mixture.

The critical stage of nucleation could determine substantially the mechanical properties of final composite. Formation of the oriented layer is due to relative nano-size and affinity between both colloids.

1. J.D.F. Ramsay and al. Farad.Disc.Chem.Soc., 1978, **65**, 65-75

2. J.N. Watson and al. J.Chem.Soc.Farad.Trans, 1998, **94,** 2181-86

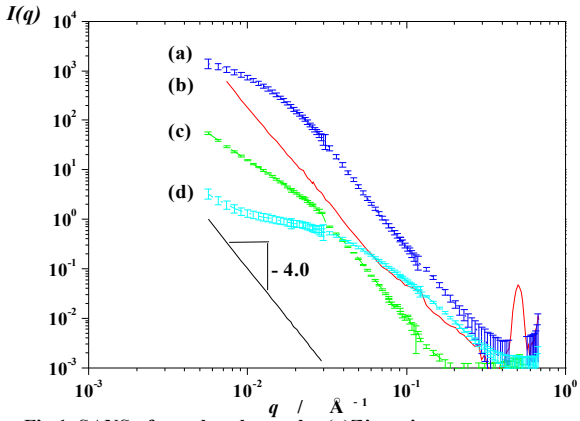


Fig.1. SANS of powdered samples (a)Zirconia, Zeolite (b)24hours (c)12 hours synthesis, (d)Dispersible Boehmite

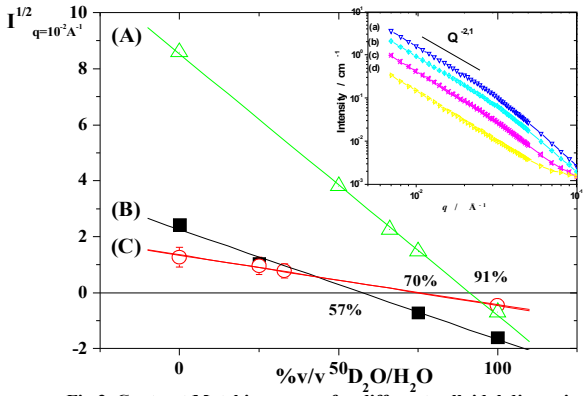


Fig.2. Contrast Matching curves for different colloidal dispersions in H2O/D2O mixtures (A)Zirconia, (B)Zeolite, (C)Boehmite Inset shows full SANS curves for Boehmite colloids dispersed in different H2O/D2O mixtures (a)00%, (b)25%, (c)33%, (d)100%

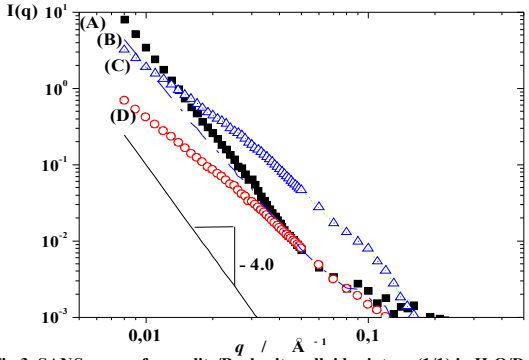


Fig.3. SANS curves for zeolite/Boehmite colloid mixture (1/1) in H_2O/D_2O=50% Theorical mixture (B) is calculated with Zeolite(A) and Boehmite(D) Experimental mixture (C) is a composite

	EXPERIMENTAL REPORT **Synergism effects between Ni and Cu on the radiation susceptibility of RPV model alloys**	Proposal N° MAT-04-0937 Instrument **V4** Local Contact U. Keiderling
Principal Proposer: Experimental Team:	A. Ulbricht, FZ Rossendorf e.V. A. Ulbricht, FZ Rossendorf e.V. U. Keiderling, HMI Berlin	Date(s) of Experiment 02.-05.04.2004

Date of Report: 03.11.2004

After the formation of a high point-defect content of vacancies and self- or solute interstitial atoms during neutron-induced displacement cascade processes, the radiation susceptibility of a reactor pressure vessel (RPV) steel is expressed in its capability of defect clustering. These fine-scaled features are the essential micro-structural changes and the reason for the enhanced material ageing under irradiation. SANS provides statistically reliable results about their size distributions and contents in macroscopic volumina. A possible cluster composition can be derived from the ratio of their magnetic and nuclear scattering intensity. Therefore, the samples of 0.8 mm thickness were placed in a magnetic field perpendicular to the incident neutron beam (λ= 0.6 nm) with a diameter of 7.5 mm; two sample-detector distances of 1.1 and 4 m were adjusted covering a range of the scattering vector from 0.2 to 3 nm^{-1}.

The SANS results can be summarized as follows:

The mean irradiation defect radius (approx. 1.0 nm) is not changed by the composition of the the RPV model alloy.

The volume fraction of defects increases with the copper content and also with the Ni content.

The evolution of the defect content for a model alloy is not linear in response to the irradiation damage values of displacement per atom (see fig. 1).

The defect type is not uniform. The average composition of defects is changed with increasing of neutron fluence (different ratios in magnetic and nuclear scattering).

The content of Cu is the most essential parameter controlling the radiation susceptibility. Ni rich alloys have a higher radiation susceptibility as Ni poor steels with the same content of deleterious elements as Cu.

The radiation-induced defects dissolve gradually and completely disappear after annealing at 475 °C (748 K). The dissolution kinetics follows a relation of Arrhenius-type (see fig. 2). The measured activation energy, E_A, approx. agrees with the activation energy for vacancy migration in iron. It is believed that the dissolution kinetics is determined by vacancy migration. The complete mechanism of dissolution is, of course, more complex.

The synergism of Ni and Cu have a catalytical effect on the radiation defect formation. Cu precipitates were not found.

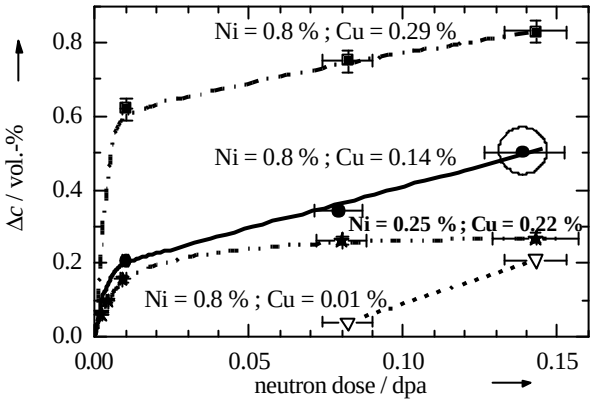


Fig. 1: Volume fraction, Δc, versus neutron dose for model alloys with different chemical composition.

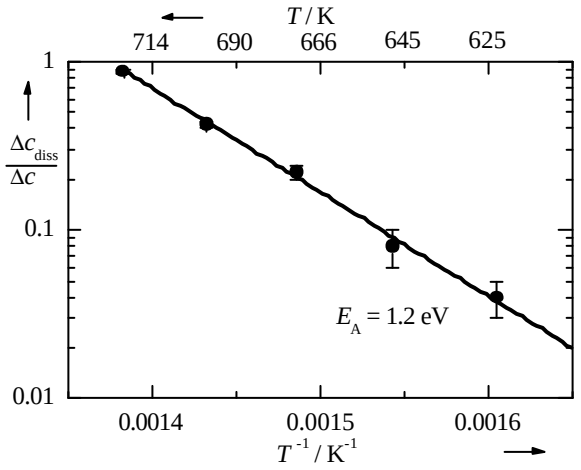


Fig. 2: Arrhenius plot of the volume fraction of defects dissolved, Δc_{diss}, for the material state covered by the circle in fig. 1 as a function of inverse annealing temperature, T^{-1}.

	EXPERIMENTAL REPORT **Solution treatment of the single-crystal Ni-base superalloy Re_{81}**	Proposal N° MAT-04-955 Instrument **V4** Local Contact J. Haug
Principal Proposer: Experimental Team:	P. Strunz, NPI Rez near Prague P. Strunz, NPI Rez; D. Mukherji, ETH Zürich J. Rösler, TU Braunschweig R. Gilles, TU München	Date(s) of Experiment 2.-6.6.2004

Date of Report: 9.12.2004

The strong partitioning of Re to matrix in the third-generation commercial single crystal superalloys leads to a heavy segregation between the dendrite and the interdendrite region. It is the main cause for a narrow solution window in Re containing alloys, which typically require several step solution treatments. In addition to the highest solution treatment temperature (typically above 1300°C), the holding at lower temperatures and the rate, at which the temperature is increased, can play an important role during the dissolution of γ' precipitates.

In our previous in-situ SANS experiments at elevated temperatures, the heat treatment cycle leading to a homogeneous element distribution in the polycrystalline superalloy Re13 was optimized [1]. It involved a long hold at 1290°C. The aim of the proposed experiment was to determine a reliable solution-treatment procedure for an experimental single-crystal superalloy Re81 containing Re using in-situ SANS.

During the SANS experiment, two samples of Re81 (Ni-6Al-8.4Ta-7.5Re in wt.%) were tested using ILL-type high-temperature furnace. The in-situ thermal history of the first Re81 sample (figure) differed from the exposure of the second sample by holding at 1290ºC for 16 hours. The thermal histories were identical otherwise.

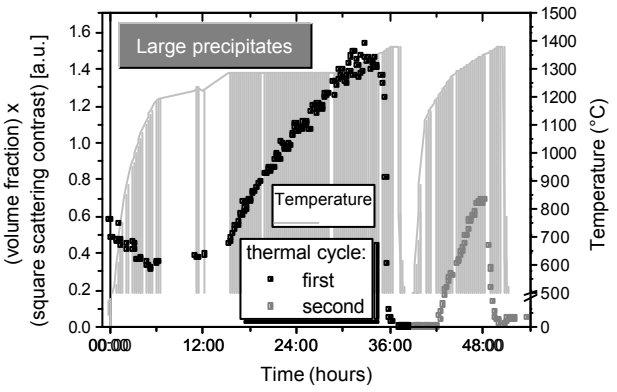
Figure shows the evolution of the volume fraction times square of scattering contrast for the largest precipitates (dissolution of which is the most difficult). Each point in the graph represents one evaluated SANS curve. The dissolution of majority of the large precipitates was reached at 1369ºC for hold and at 1374ºC for the non-hold sample, respectively. For comparison, the melting point is 1400ºC. However, small decrease of the total scattering probability (and thus volume fraction of remaining inhomogeneities) continues up to 1381ºC, which was also the highest temperature tested in the experiment.

Both samples were exposed to a second thermal cycle as well directly after the first one was finished. In this second cycle, majority of precipitates is dissolved already at 1360ºC, confirming thus a successful homogenization caused by the first applied thermal cycle. However, the dissolution is not so steep (in dependence on the temperature) in the final period as in the case of the first cycle and the complete removal of all inhomogeneities is reached again only at 1381ºC.

The SANS measurement in Re81 clearly showed that the holding at 1290ºC shifts the final solution temperature towards lower values by 5K. However, the microstructure evolution at the elevated temperatures significantly differs from the previously studied polycrystalline Re13 and Re31 superalloys. Solution treatment of the Re81 is easier than that of polycrystalline Re31 and Re13. In fact, a long hold at temperatures (around 1290ºC) is not essential in this case in order to homogenize the alloy, although such a hold decreases slightly the solution temperature. The reason for such a difference can be twofold:
a) compositional difference between Re81 and Re13, or
b) grain boundaries in Re13, which are not present in the single-crystal Re81.

However, a very similar behaviour (a gradual increase of volume fraction times square of scattering contrast) as for polycrystalline Re13 and Re31 alloys was observed during the hold at 1290ºC as well as for the further temperature increase up to 1350ºC (see the figure). It can be most consistently explained – in the same way as for the polycrystalline superalloys - by slow diffusion between dendritic and interdendritic regions [1].

[1] P. Strunz, D. Mukherji, R. Gilles, J. Rösler and A. Wiedenmann: Mat. Sci. Forum, Vols. 426-432 (2003), pp. 821-826



BENSC	**EXPERIMENTAL REPORT** **Solution treatment of the single-crystal Ni-base superalloy CMSX4**	Proposal N° MAT-04-1018 Instrument **V4** Local Contact J. Haug
Principal Proposer: Experimental Team:	P. Strunz, NPI Rež near Prague P. Strunz, NPI Rež; D. Mukherji, ETH Zürich J. Rösler, TU Braunschweig R. Gilles, TU München	Date(s) of Experiment 23.-26.9.2004

Date of Report: 7.1.2005

Precipitate microstructure of superalloys is formed by heat treatment, the first step of which is called solution treatment. In-situ SANS study of solution treatment for the commercial single-crystal superalloy CMSX4 containing rhenium was carried out. On the basis of experience obtained in the past with experimental Re-containing nickel-base superalloys [1, 2], significant contribution of SANS to optimization of the solution-treatment procedure for this complex commercial superalloy was expected. Such knowledge can help to improve the characteristics of the superalloy, to cut down the heat treatment cost as well as to understand better the precipitate dissolution at high temperatures.

In Fig. 1a and b, rough evaluation of the extensive SANS data for two of altogether three measured samples is plotted (a detailed evaluation is currently being carried out). The displayed parameter, i.e. the maximum intensity of the measured data at Q=0 (for SDD=16m and λ=19.6 Å) in dependence on time and temperature, is an inverse quantity to the scattering probability. With decreasing volume fraction of precipitates and their scattering contrast, this quantity should increase, reaching a maximum when all the precipitates are dissolved.

The in-situ SANS experiment revealed, that neither the standard solution treatment (ST, i.e. 1277–1280–1296–1304–1313–1316-1318°C, each step for 2hr [3]) nor prior holding (16 hours) at 1214 or 1282°C, followed by standard ST, is able to dissolve the largest precipitates or the γ/γ' eutectics in the interdendritic regions. An additional increase in temperature up to 1337°C was necessary to fully solutionize the superalloy CMSX4. This temperature was the same for both cycles (i.e. the ones including 1214 or 1282°C hold, seemingly having no influence on the γ' dissolution temperature). In the temperature region above 1335°C, a danger of incipient melting already exists as the solidus temperature reported for ST CMSX4 is between 1341 and 1344°C [3].

The hold at lower temperature (1214 or 1282°C) has an influence on the scattering probability and its evolution with time. Its increase during holding (see Fig. 1a) is most likely due to increase of the scattering contrast of remaining gamma prime phase in the sample brought about by diffusion of the elements (particularly Re) between dendritic and interdendritic regions [2]. The hold at 1282°C has an evident influence on the homogeneity of elemental distribution in CMSX4 alloy. Homogeneity is of equal importance as dissolution of precipitates [4]. The use of holding at 1282°C should be therefore considered.

Microstructural characterization of in-situ treated samples by EM is planned in order to assess the degree of inhomogeneity by an independent method.

[1] D. Mukherji, P. Strunz, R. Gilles, J. Rösler, A. Wiedenmann and H. Fueß, Applied Physics A 74 (2002), 1074-1076
[2] P. Strunz, D. Mukherji, R. Gilles, J. Rösler and A. Wiedenmann, Mat.Sci.Forum, Vols. 426-432 (2003), 821-826
[3] B. Wilson: http://web.clas.ufl.edu/CLAS/jur/0502/wilsonpaper.html
[4] G.E.Fuchs: Mat.Sci.Eng A300 (2001) 52-60.

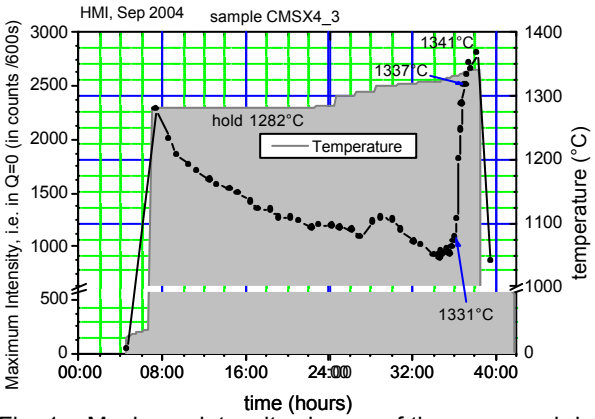


Fig. 1a. Maximum intensity change of the measured data at Q=0 corresponding to the temperature cycle including hold at 1282°C.

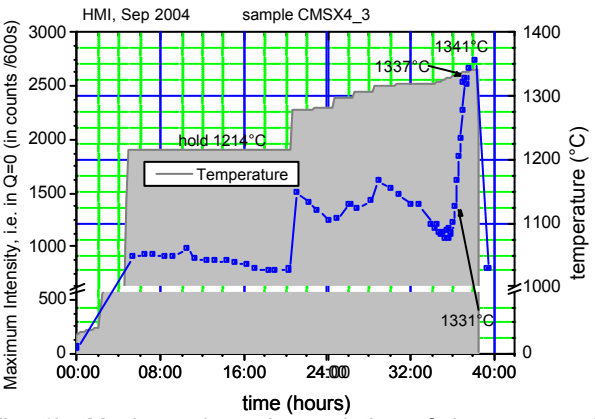


Fig. 1b. Maximum intensity evolution of the measured data at Q=0 corresponding to the temperature cycle including hold at 1214°C.

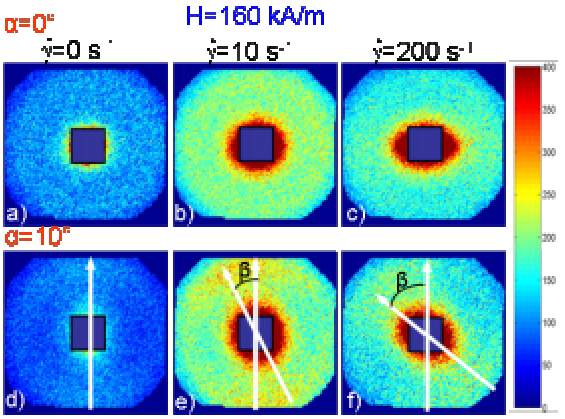
	EXPERIMENTAL REPORT **Investigation of the microstructure of ferrofluids using Small Angle Neutron Scattering**	Proposal N° MAT-04-1012 Instrument V4 Local Contact A. Wiedenmann M. Kammel
Principal Proposer: Experimental Team:	Stefan Odenbach, ZARM University of Bremen Loredana Pop, Oliver Brunke, Harald Engler ZARM University of Bremen Martin Kammel, HMI Berlin	Date(s) of Experiment 14.09-19.09.2004

Date of Report: 1.12.2004

Ferrofluids, stable suspensions of nanometer size particles in proper carrier liquids, can be magnetically controllable using moderate magnetic field strengths. Due to their normal liquid behaviour, coupled with superparamagnetic properties they are useful for a wide area of applications, bringing solution to a lot of highly demanding scientifical and technological problems as well as to important medical tasks.

In the presence of magnetic fields, ferrofluids show an increase of viscosity of several hundred percent compared to the viscosity without magnetic field, the so called magnetoviscous effect. Rheological experiments have shown that the magnitude of the effect is determined by the ability of particles for chain formation resulting in significant changes in the fluids microstructure due to the presence of magnetic fields and shear flows. To correlate the rheological behaviour of ferrofluids to their microstructure, small angle neutron scattering experiments were carried out. The experiments were performed in a magnetic field range from 0 to 160 kA/m, directed parallel to the neutron beam (α=0°) and with a deviation of 10 degree relative to the neutron beam (α=10°) for the rheometer rotated in the horizontal plane. The shear rates were varied within the range from 0 to 200 s^{-1}. The measurements were made for a scattering vector in the range from 0.01 to 0.93 nm^{-1}. A cobalt based ferrofluid, (Co100-04, supplied by Bönnemann / MPI-Mülheim) with particle diameter of about 7.5 nm was investigated. The obtained results indicate formation of small structures only, which is in accordance with the rheological data and with previous SANS results obtained for ferrofluids with small particles, i.e. with reduced capability to form chains. The second sample was a high concentrated, Co91-02 (3.5 vol.%), cobalt based ferrofluid with large particles (diameter of about 10nm), from the same source. Under the influence of the magnetic field, chains aligned parallel to the field direction are formed. Due to the orientation of the field relative to the neutron beam, the obtained scattering pattern is isotropic (fig.1a). A fit applied to the radial averaged scattering curve for this situation gives as results the same mean particle size and concentration as it was obtained from magnetisation measurements. A shear flow applied to the sample induces a local vertical deviation of the chains resulting in a horizontal anisotropy of the scattering patterns (1b). For α=10°, in the presence of a magnetic field, a vertical anisotropy of the scattering pattern can be observed, indicating the presence of chains aligned parallel to the field, with magnetic moments orientated along the chains (1d). A shear flow produces horizontal anisotropy, and therefore the resulting anisotropy is deviated (fig.1e). With increasing the shear rate, the deviation of the chains increases also, fact confirmed by the appearance of a stronger horizontal anisotropy (fig. 1c), i.e. a higher deviation angle ß (fig.1f). The experimental results are in a good agreement with numerical simulations. To obtain detailed results about the length and deviation of the chains, an implementation of a 2D data analysis program (A. Heinemann, HMI) is in progress.

Fig.1 Scattering patterns for Co91_02



BENSC	**EXPERIMENTAL REPORT** **In-situ SANS study of microstructure homogenization in wrought Ni-base superalloy**	Proposal N° MAT-04-1031 Instrument **V4** Local Contact U. Keiderling
Principal Proposer: Experimental Team:	J. Zrník, TU Košice P. Strunz, NPI Rež near Prague; J. Zrnik, TU Košice; P. Hornák, TU Košice U. Keiderling, HMI Berlin	Date(s) of Experiment 20.-22.9.2004

Date of Report: 7.1.2005

The wrought nickel-base superalloy EI698VD has to resist complex thermo-mechanical loading in gas turbine for a long period. The demand for lifetime extension tends to alloying additions as well as to structural improvements of gamma-prime precipitate characteristics resulting from a heat treatment. In-situ SANS can be helpful in understanding of high-temperature microstructure evolution during the heat treatment, particularly of homogenization process (i.e. precipitate dissolution) [1]. This first step of the heat treatment governs the uniformity of precipitation and influences thus greatly the ability to resist the deformation process. An optimization of homogenization procedure (including dissolution of carbides) for EI698VD superalloy using in-situ SANS was carried out.

A rough evaluation of the SANS data for two in-situ measured samples is plotted in Fig. 1 and 2. The displayed parameter, maximum intensity of the measured data in Q=0 (SDD=16m, λ=19.6 Å) in dependence on time and temperature, is an inverse quantity to the scattering probability. It has to increase with decreasing volume fraction of gamma prime precipitates and carbides.

During the first couple of hours of in-situ measurement, a decrease of maximum intensity on temperature increase occurs (caused by the increase of the diffuse scattering, eventually by the growth of precipitates at intermediate temperatures). Then, the gamma prime precipitates are dissolved at the standard solution temperature of EI698VD superalloy equal to 1100°C (see Fig. 1). The solution process is rather fast and the hold at this temperature does not bring any additional dissolution of precipitates for the small sample investigated (there could be, however, a technological need for a longer hold when performing the solution treatment of large structural parts of turbine made of EI698VD).

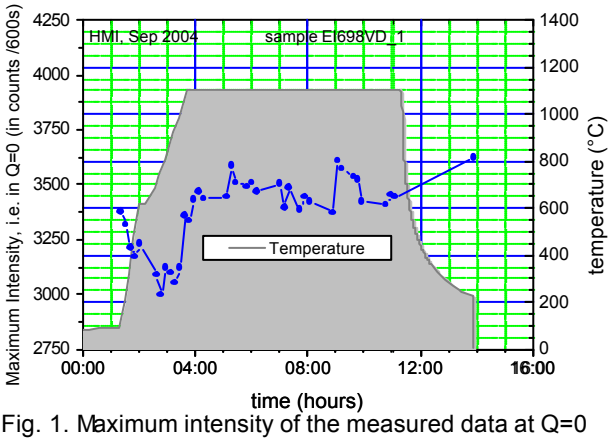


Fig. 1. Maximum intensity of the measured data at Q=0 for the sample hold at 1100°C.

However, the further measurement (Fig. 2) revealed that the temperature increase up to 1300°C still causes a gradual decrease of the scattering probability. Since this decrease is significant, it has to be caused by dissolution of additional inhomogeneities, most probably carbides (MC) which are stable to higher temperatures. In case the creep properties improvement is required, the increase of the solution temperature of the superalloy up to 1250°C can be recommended.

For this second sample (Fig. 2), a significant increase of the scattered intensity (i.e. decrease of the transmitted intensity at Q=0) on cooling to RT indicates a formation of a significant amount of precipitates. As such a strong increase does not occur for the first sample (Fig. 1), these precipitates are most probably carbides created again after their dissolution.

The integral scattered intensity was also measured on sample cooling from the solution treatment to room temperature. It has been found that the gamma prime phase start to precipitate at around 950°C.

[1] P. Strunz , D. Mukherji, R. Gilles, A. Wiedenmann, J. Rösler and H. Fuess: J. Appl. Cryst. 34 (2001) 541-548

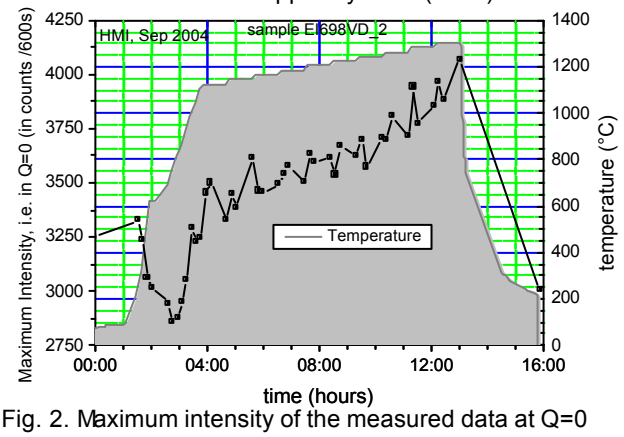


Fig. 2. Maximum intensity of the measured data at Q=0 for the sample heated up to 1300°C.

	EXPERIMENTAL REPORT SANSPOL structure studies of Cobalt - ferrofluids	Proposal N° EF-SF3. Nano Instrument **V4** Local Contact M. Kammel
Principal Proposer: Experimental Team:	M. Kammel,A. Wiedenmann, A. Heinemann A. Wiedenmann, HMI Berlin A. Heinemann, HMI Berlin M. Kammel, HMI Berlin	Date(s) of Experiment 27.8.-29.8.2004

Date of Report: Jan. 2005

We investigated a new series of cobalt ferrofluid samples[1], prepared by thermolysis of $Co_2(CO)_8$ in the presence of $Al(C_2H_5)_3$, After the preparation a smooth oxidation of the samples gives access to air stable samples. The Co particles were coated by Korantin SH. Earlier Small Angle Neutron Scattering experiments showed a complex composition for such a ferrofluid without smooth oxidation [2].

In order to evaluate the unknown ferrofluid structure and size distribution as well as the magnetic nanostructure after the smooth oxidation we performed Small Angle Neutron Scattering studies with polarised neutrons (SANSPOL) [3] at the instrument V4. Using polarised neutrons with a wavelength λ =0.6nm, a range of momentum transfer **Q** between 0.04 nm^{-1} and 4 $nm^{-1}$was couvered. A horizontal magnetic field up to 1.0T and perpendicular to the incoming neutrons was applied on the samples. This allowed an exact calculation of the structural parameters in the fitting procedure and the accurate separation of magnetic and nonmagnetic parts of the scattering intensities.

Three different samples in toluene and kerosene were investigated. The figures 1 and 2 shows the 2 dimensional SANSPOL scattering data of the Cobalt ferrofluid with a smooth oxidation. The analysis of the scattering intensities perpendicular to the applied magnetic field gives in all measured samples evidences for a nonmagnetic layer of a cobalt-oxide on the surface of the cobalt-core.

Work supported by DFG project Wi 1151/2-2 in the frame of priority program SPP1104.

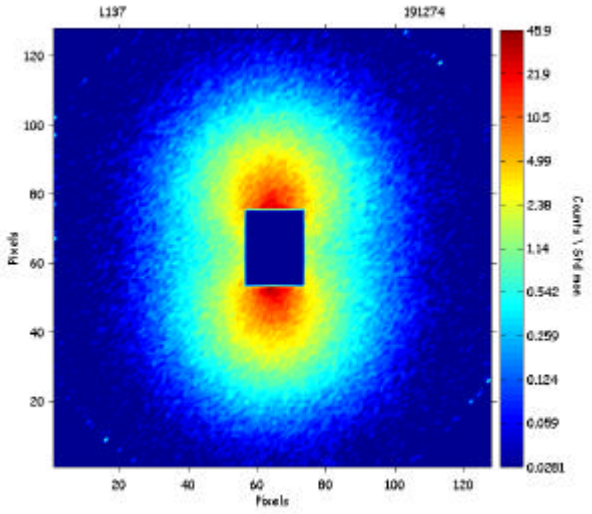


Fig. 1: 2-dim SANSPOL scattering intensity I^- for the Co – ferrofluid in kerosine as solvent (MA-137).

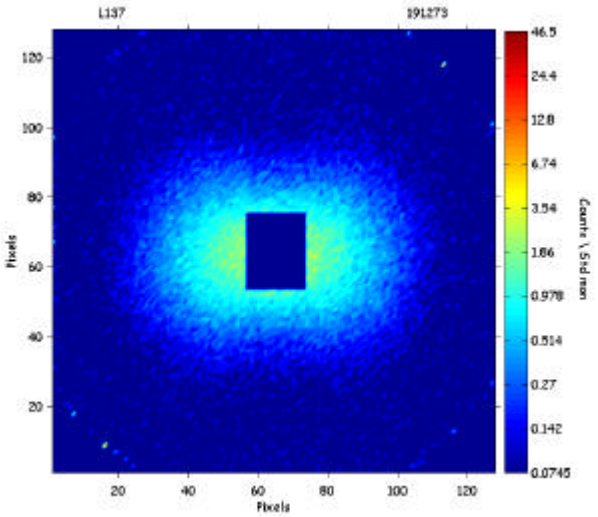


Fig. 2: 2-dim SANSPOL scattering intensity I^+ for the Co – ferrofluid in kerosine as solvent (MA-137).

References:
[1] H. Bönnemann, W. Brijoux, R. Brinkmann, N. Matussevitch, H. Modrow, N. Palina, N. Waldöfner, Inorganica Chimica Acta 350 (2003) 617-624.
[2] A. Wiedenmann, A. Hoell, M. Kammel, J Magn Magn Mater252 (2002) 83-85.
[3] A. Wiedenmann, Mat. Science Forum, 312-314 (1999) 315-324.

BENSC	**EXPERIMENTAL REPORT** **Crystallization behaviour of amorphous $Al_{94-x}Ni_6La_x$ (x=4-7) alloys**	Proposal N° EF Instrument **V4** Local Contact J. Haug
Principal Proposer: J. Haug, M. Wollgarten, HMI/SF3 Experimental Team: J. Haug, K.L. Sahoo		Date(s) of Experiment 17.01.-20.01.2004 23.06.-29.06.2004

Date of Report: 05.01.05

In the ongoing search for light-weight structural materials, Al-based amorphous and nano-crystalline alloys, mainly of composition Al-Ni-RE (RE=Y, La, Ce), with high specific strength, good ductility, high hardness, good wear and corrosion resistance, have attracted intensive reserach activities [1]. For the properties of these alloys the crystallization mechanism is a important factor.

With SANS on V4 facility it is possible to use a heating stick for in-situ measurements from RT to 300°C. Three samples with different compositions were investigated ($Al_{89}Ni_6La_5$, $Al_{87}Ni_6La_7$, $Al_{87}Ni_5La_7Cu_1$) at two sample detector distances (1, 4 m) with λ=0.605 nm. After completing the in-situ experiment a measurement at 16, 4 and 1 m was carried out.

The course of the in-situ experiment is shown in Fig. 1 for a sample detector distance of 4 m. At heating from RT to 210°C a rapidly increase of the intensity at 4 m at 130°C can be observed. During isothermal treatment the increase in intensity is reduced. After cooling down to RT and measure at 16 m there is no change in intensity for the 4 m run.

Fig. 2 reports the SANS curves for the $Al_{89}Ni_6La_5$ sample between RT and 210°C and at the end of heating for all three distances. The scattering cross section obtained at the end of the annealing procedure shows a shoulder at Q≈0.4 nm^{-1} and maximum at Q≈0.08 nm^{-1}, which indicates at least two predominant particle sizes. During heat treatment the intensity in the range 0.1 nm^{-1} ≤ Q ≤ 0.9 nm^{-1} increases and the shoulder is shifted to smaller Q-values. This points to an increase in size of the small precipitates during heating.

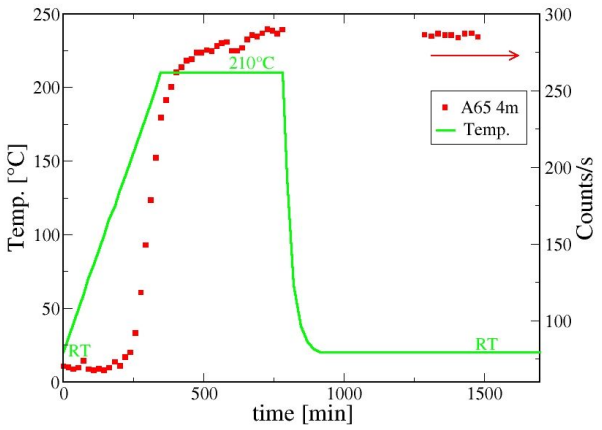


Fig. 1: *Intensity and temperature during the in-situ measurement of $Al_{89}Ni_6La_5$.*

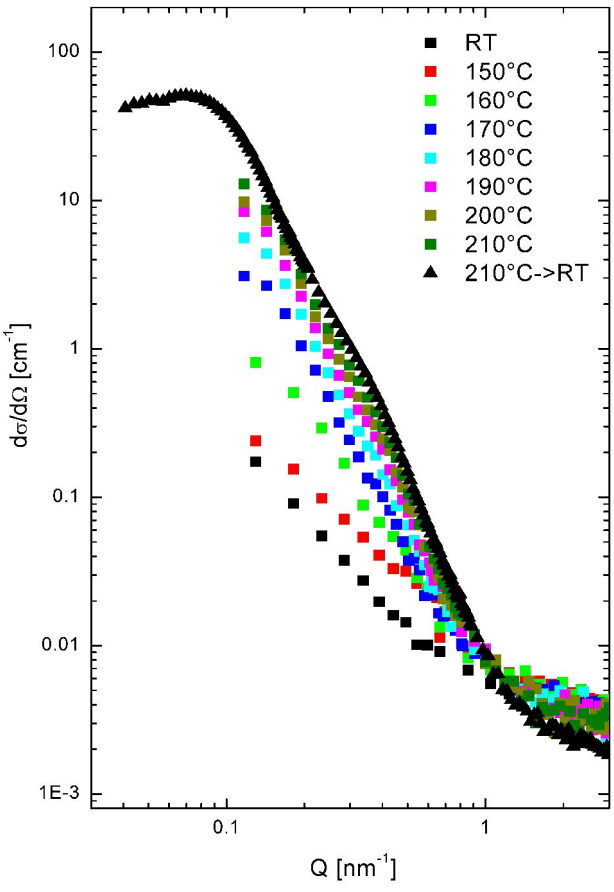


Fig. 2: *SANS curves from sample $Al_{89}Ni_6La_5$.*

References:

[1] A. Inoue, Progress in Materials Science 4 (1998) 365-520

	EXPERIMENTAL REPORT **Low temperature behaviour of ordering phenomena in Ferrofluids**	Proposal N° EF-SF3.Nano Instrument **V4** Local Contact A. Wiedenmann
Principal Proposer: Experimental Team:	A. Wiedenmann, HMI Berlin A. Wiedenmann, HMI Berlin A. Heinemann, HMI Berlin	Date(s) of Experiment 03.05-.09.05. 2004

Date of Report: 04.01.2005

Ordering phenomena have been observed previously in concentrated Ferrofluids when a magnetic field was applied [1,2]. The aim of the present SANSPOL study was to elucidate the formation of this pseudo crystalline particle arrangement as a function of magnetic field and temperatrure. For this purpose the Ferrofluid sample "MFT" containing 6 vol.% Co-particles stabilized with C_{21}-H_{39}-NO_3 and dispersed in a viscous technical oil "L9" has been investigated by SANSPOL using a horizontal cryomagnet HM1. The set-up of the cryomagnet on a turntable allowed the magnetic field to be applied perpendicular or parallel to the incoming neutrons. The temperature has been varied between 10K and RT. Cooling of the sample has been performed in zero field or in an applied field up to 1T. At different temperatures hysteresis loops have been measured between -1T and +1T.(see Fig.1). Several problems occurred during the measurements. First, the programming of the field and temperature variation via CAERSS did not work reliably. The magnetic field

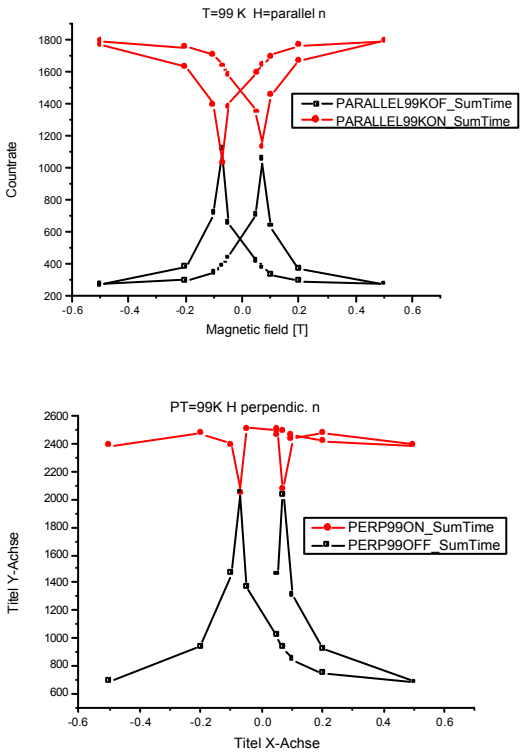


Fig. 1: Hysteresis loops measured in cryomagnet HM1 at 99K with H parallel (upper part) or perpendicular to incoming neutrons. The detector count-rates for flipper ON and OFF are shown as function of H.

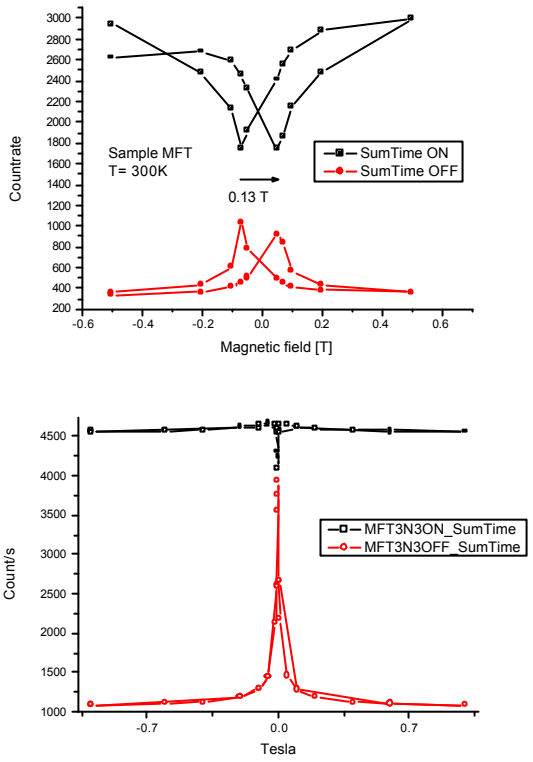


Fig. 2: Field dependence of detector count-rates for flipper ON and OFF measured at 300 K with cryomagnet (upper part) and with electromagnet (lower part).The hysteresis observed in the cryomagnet is an artefact due to anormal behaviour of the superconducting coils.

had to be set manually using very slow ramp-up rates in order to prevent quenching of the cryomagnet. Even in the manual mode it turned out that the current applied to the superconducting coils did not correspond to the value indicated before operating the heating –contact. The result was an apparent hysteresis much larger than known from calibration measurements of the order of 0.13 T as shown in Fig.1. This value was found to be independent of temperature and on the direction of the magnetic field. In the electromagnet no hysteresis was observed while in the cryomagnet a strong hysteresis occurred (Fig 2). Test measurements with a hall-probe confirmed that the current really present in the superconducting coil differred from the value indicated before operating the heat-switch. These problems prevented a quantitative analysis of these data.

[1] A. Wiedenmann, A. Hoell, M. Kammel, P. Boesecke, Phys. Rev. E **68**(2003) 031203
[2] A.Wiedenmann, A. Heinemann ,JMMM (2005) in print

	EXPERIMENTAL REPORT **Field dependence of ordering phenomena in ferrofluids**	Proposal N° EF-SF3.Nano Instrument **V4** Local Contact **A. Wiedenmann**
Principal Proposer: Experimental Team:	A. Wiedenmann, HMI Berlin A. Wiedenmann, HMI Berlin A. Heinemann, HMI Berlin	Date(s) of Experiment 04.-0.9.05.2004

Date of Report: 04.01.2005

The Ferrofluid sample "MFT" containing 6 vol.% Co-particles stabilized with C_{21}-H_{39}-NO_3 and dispersed in a viscous technical oil "L9" has been investigated by SANS in a horizontal magnetic field up to 1.1 T applied perpendicular to the incoming neutrons. In zero magnetic field the isotropic average of the SANS intensities (Fig. 1) a Q^{-1} behaviour is observed at low Q which is well described by a random orientation of cylindrical objects formed by a spontaneous arrangement of about 3-4 particles in the attractive head-to-tail conformation. The evolution of the ordering phenomena was quantitatively analysed from the SANSPOL difference pattern

$$I(-) - I(+) = 4F_M F_N L(x) \sin^2 S(Q,a),$$

which arises solely from magnetic particles. At H=1T six distinct peaks occur at Q_1 at azimuth angles φ ±30, ±90° and ±150°, respectively, and two peaks at Q_3 at ± 90 (Fig. 2) which represent the pseudo-crystalline hexagonal order as found before [1]. The structure factors have been fitted simultaneously on the 2-D SANSPOL difference patterns by using four 2-D Gaussians (solid lines in Fig. 2). A strong decrease of the inter-plane distance and only a minor change of the

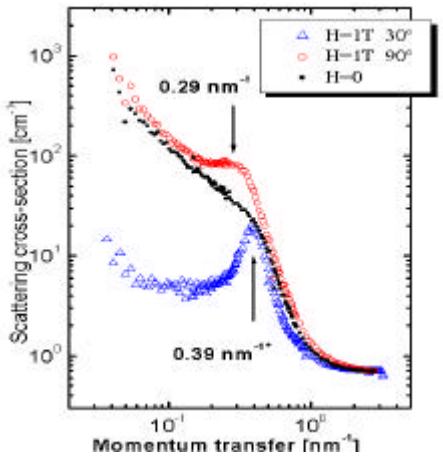


Fig. 1: SANS intensity of MFT: The isotropic average at H=0 (full points)is characteristic for segments of chains while at H=1T peaks observed in sectors of 10° at φ=30°(triangles) and 90°(open circles) define the hexagonal ordering.

in-plane nearest-neighbour distance were observed with increasing field. The overall densification of the ordered domains must be dominated by an increase of the correlations between neighbour layers. The areas ($=N_1\Delta\eta^2$) of the 2D-Gaussian peaks, Fig. 3, increase with H according the Langevin function L(x) (solid line).

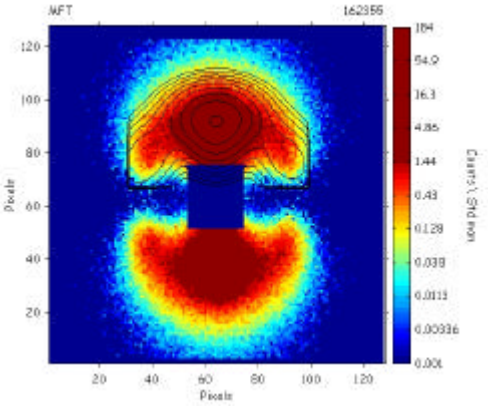


Fig. 2: SANSPOL difference pattern I(-)-I(+)of MFT in H=1T.The solid iso-intensity lines in the upper hemisphere represents a 2D-Gaussion fit of the peaks at Q_1 and Q_3 which define of the pseudo-crystalline hexagonal ordering.

In the sector at φ=30° the scattering contribution from chain segments $N_2\Delta\eta^2$ decreases rapidly, despite an increase of the magnetic contrast Δη (Fig.3).

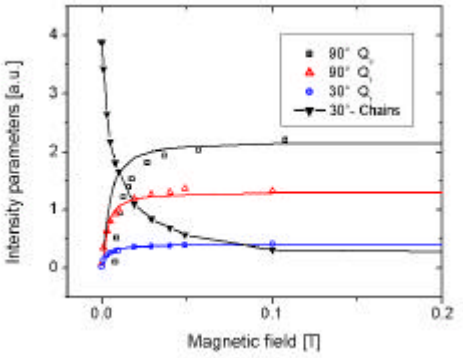


Fig. 3: Field dependence of the corresponding scattering contributions show that chain segments (solid triangles at φ=30°) are aligned along H while hexagonal ordering (peak area at Q1 and Q3-open symbols) is set up according to the Langevin behaviour (solid line).

This indicates clearly that the uncorrelated chain segments are aligned along the direction of the magnetic field already at very low values of H. However, with increasing H the chains aligned along H do not grow in lengths, instead lamellar arrangements are formed which become more and more correlated giving rise to the broadened peaks in Fig. 2 and Fig. 3.[2]

[1] A. Wiedenmann, A. Hoell, M. Kammel, P. Boesecke, Phys. Rev. E **68**(2003) 031203
[2] A.Wiedenmann, A. Heinemann ,JMMM (2005) in print

BENSC	**EXPERIMENTAL REPORT** **Time dependence of field induced ordering in concentrated Ferrofluids studied by SANS**	Proposal N° EF-SF3.Nano Instrument **V4** Local Contact **A.Wiedenmann**
Principal Proposer: Experimental Team:	A, Wiedenmann, HMI Berlin A. Wiedenmann, HMI Berlin U. Keiderling, HMI Berlin J. Haug, HMI Berlin	Date(s) of Experiment 05.-09.04. 2004

Date of Report: 05.01.2005

Previous Small Angle Neutron Scattering in concentrated Co-ferrofluids has revealed a pseudo-crystalline hexagonal ordering of the core-shell nanoparticle induced by an external magnetic field [1]. The aim of this proposal was to follow the onset and decay of the local ordering when the field is switched on and off. Using the list mode of the detector electronics [2,3] time resolved SANS has been performed for the first time on the V4 instrument in a stroboscopic mode in order to establish the kinetics of these processes.

The power supply of the electromagnet has been operated in cyclic mode allowing to ramp up and down the current from zero to nominal values between 50 A and 100 A corresponding to magnetic field between 0.25 T (a) and 0.5 T (b). The field was held at the nominal values Hmax and H=0 during a hold period between 5 s (a) or 10 s (b). A trigger signal from the electromagnet allowed the magnetic field to be synchronised with the data acquisition and to regroup the data in a free choice of the number and widths of time slices. The total measuring time was 12 h which allowed to regroup the data with good statistics in 128 *128 detector channels in time slices of 100 ms(a) or 200 ms (b). Measurements have been performed with non-polarised neutrons at one geometry (detector distance of 4m ,collimation 4m and λ = 0.6 nm) where the field induced peaks can be best observed. Due to the low ramp-up rate of the magnetic field we did not try to follow systematically the kinetics of ordering process. However, we observe the final scattering pattern already after the first time slice of 0.2s when the field is ramped up to 0.5T, i.e. the ordering process was too fast to be observed by this technique. The disordering kinetics could be well followed on this sample. In Fig. 1 the regrouped 2D time-frame SANS patterns of the sample MFT3N1 in a horizontal magnetic field of H=0.5 T applied perpendicular to the incident beam are presented at different times after switching off the field starting from the time where the field. was zero. In Fig. 2 the intensities averaged in a 10° sector are presented as a function of Q at 30° from the horizontal field for time slices of 0.1 s. The correlation peak around Q=0.38 nm^{-1} present in the maximum field smears out continuously after switching off the field which reflects the sluggish decay of the magnetic correlations with time.

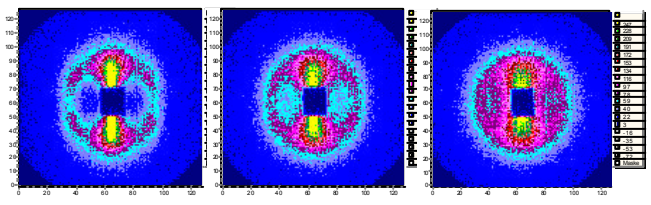


Fig. 1:SANS intensities of MFT3N1 after switching off the horizontal magnetic field t=0(left) , t=2s(middle) t=5s (right).

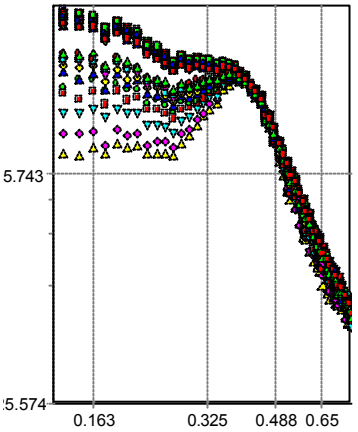


Fig. 2 : Time dependent decay of the SANS intensities at an angle of 30° to the horizontal magnetic field of Fig.1 (yellow triangle: t=0, green circle: t=5 s.)

We will have to analyse the time dependence of the intensities for the different samples as a function of the scattering vector ***Q*** in order to obtain the kinetics of the underlying disordering process. A first analysis revealed an exponential decay with time constants of the order of 1-5 s.

The present experiment demonstrated successfully how SANS allowed the nature of magnetic ordering of nanosized objects to be visualised during magnetic relaxation processes on a time scale of few hundred ms.

*) The project is supported by DFG Project Wi 1151/2 in the frame of the Priority program SPP 1104 (2000-2006)

[1] A. Wiedenmann, A. Hoell, M. Kammel, P. Boesecke Phys Rev. E 68 (2003) 031203, 1-10
[2] U. Keiderling , A.Wiedenmann, J.Haug BENSC report 2004
[3] J.Haug ,U. Keiderling , A.Wiedenmann, BENSC report 2004

	EXPERIMENTAL REPORT SANS with polarisation analysis on Ferrofluids using ^{3}He filter	Proposal N° EF-SF3.Nano Instrument V4 Local Contact A.Wiedenmann
Principal Proposer: Experimental Team:	A. Wiedenmann, HMI Berlin A. Wiedenmann, A. Rupp (HMI); W. Heil, Uni Mainz	Date(s) of Experiment 10-15.6.2004

Date of Report: 04.01.2005

When polarised neutrons are used four types of scattering process are to be distinguished, two for conserving the neutron spin ++, -- (snf) and two with reversal of the spin by the scattering +-, -+ (sf). For the case of *non perfect alignment* of the superparamagnetic single domain particles the four scattering cross-sections $d\sigma/d\Omega_{ij}(Q,\alpha)$ (i, j= +, -) have been derived for the general case where the scattering vector **Q** may form any angle α with the applied magnetic field H. The scattering contributions are regrouped as [1]

$$d\sigma/d\Omega_{ij}(Q,\alpha) = A_{ij}*S(Q,\alpha) + B_{ij} F_M^2(Q). \qquad (1)$$

Nuclear and magnetic contrasts lead to different values of the weighting functions A_{ij} and B_{ij} (table 1.) depending on the technique used [1]. The first term in Eq. (1) is a contribution which is affected by nuclear and/or magnetic inter-particle correlations defined by

Table 1 : Weighting functions for the scattering contributions of inter-particle correlations A_{ij} and of moment misalignment B_{ij} respectively with the abbreviations: a=L(x)/x and b=[L2(x)-1+3L(x)/x)], where L(x) is the Langevin function.

Process	A_{ij}	B_{ij}	B_{ij} (H? 0)
POLARIS			
I(- -)	$[F_M L(x) \sin^2? + F_N]^2$	a $\sin^2?$ - b $\sin^4?$	1/3 $\sin^2?$
I(++)	$[F_M L(x) \sin^2? - F_N]^2$	a $\sin^2?$ - b $\sin^4?$	1/3 $\sin^2?$
I(+-), I(+)	$[F_M L(x) \sin? \cos?]^2$	a (2-$\sin^2?$)-b $\sin^2? \cos^2?$	1/3(2-$\sin^2?$)
I(--)-I(++)	$F_N F_M L(x) \sin^2?$	0	0
SANSPOL			
I(-)	$[F_M^2 L^2(x)+2 F_M F_N L(x)]\sin^2? + F_N^2$	a -b $\sin^2?$	2/3
I(+)	$[F_M^2 L^2(x)-2 F_M F_N L(x)]\sin^2? + F_N^2$	a -b $\sin^2?$	2/3
I(-) - I(+)	$F_N F_M L(x) \sin^2?$	0	0
SANS			
I(Q)	$F_M^2 L^2(x) \sin^2? + F_N^2$	2a- b $\sin^2?$	2/3

S(Q,α), while the second term results solely from non-perfect alignment of the magnetic moments of individual particles. In a pilot experiment on a 6 vol. % Co Ferrofluid sample uni-axial polarization analysis (POLARIS) has been performed on neutrons scattered in the 2 dimensional detector using a prototype of ^{3}He filter [2]. The sample was measured in a weak magnetic field of B = 0.05T applied perpendicular to the neutron beam which gives rise to a partial misalignment of the particle moments and hence to disordering sf scattering confirming the non-zero contributions B_{ij} of table 1. In the 2D patterns of $I(-)_{POLARIS}$ which is mainly due to sf

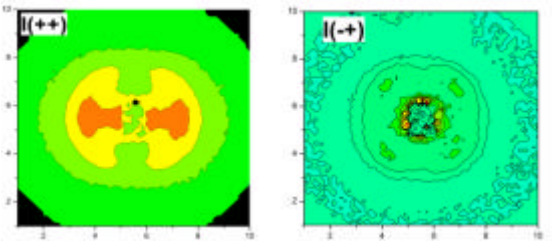


Fig. 1: 2D-POLARIS in 6vol.%Co-FF in vertical field H=0.05T. The peaks at ±30°,150° in the sf channel (I-+)(rhs) are purely of magnetic origin while those in snf channel I(++)(lhs) at 90°have nuclear and magnetic contributions.

scattering (Fig. 1 rhs) are clearly distinguished at Q_1 for α =±30° and ±150°. This coherent sf scattering results solely from *magnetic* inter-particle correlations in agreement with the predictions of table 1. We note that such sf contributions can only be observed when spin analysis is performed on all neutrons scattered in the xz plane of a 2D detector. In the classical set-up for uni-axial spin analysis where only special orientations of Q parallel and perpendicular to H are analysed this contribution is missing. In fact, $I(-)_{POLARIS}$ integrated over Q_1± 10 % and plotted against the angle α (upper part of Fig. 4) shows the overall oscillations (solid line) according to the $(F_M L(x)\sin\alpha\cos\alpha)^2$ behaviour of A_{ij} in table 1 which results from the magnetic form-factors alone. Subtracting this function from the experimental curve one extracts the structure factor (S(Q)-1) shown in lower part of Fig. 4. The data deviate significantly from zero at the angles marked by arrows i.e. α=±30, ±90 and ±150° expected for the hexagonal symmetry of the local ordering. Despite the rather poor statistics the present POLARIS experiment confirms fully the predictions of table 1.

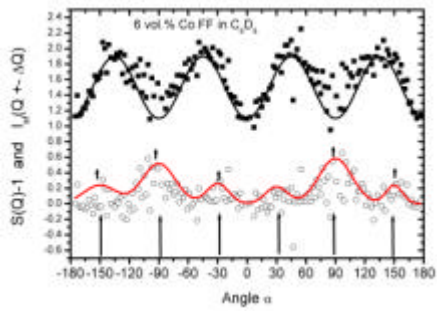


Fig. 4: Spin-flip scattering I_{sf} at Q_1 ±ΔQ as a function of α (full symbols) and the oscillation of $(\sin\alpha\cos\alpha F_M L(x))^2$ (line) in the upper part ;the difference represents S(Q)-1 (open circles) which was fitted with Gaussians corresponding to 6 peaks marked as arrows.

[1] A. Wiedenmann, in press Physica B(2005)
[2] A. Wiedenmann, A. Rupp BENSC report (2002)

	EXPERIMENTAL REPORT Neutron Tomography on White and Polychromic Marbles of Archaeological Interest	Proposal N° MAT-04-1062 Instrument **V7** Local Contact N. Kardjilov
Principal Proposer: Experimental Team:	N.Kardjilov,(HMI), R. Triolo,(Università di Palermo) N. Kardjilov, HMI Berlin A. Hilger, HMI Berlin I. Manke, HMI Berlin	Date(s) of Experiment 15.06 - 17.06. 2004

Date of Report: Jan. 2005

Introduction

Among the natural composites, there is a wide variety of stones used in buildings, monuments, statues and other objects of archaeological or cultural heritage interest. Sandstone, Limestone, Granite und Marbles are the most common stones used for these purposes. Marbles may look very different as far as texture, color, mechanical and physical properties are concerned. This is mainly a consequence of their "formation history". Here it is of archeological interest to link certain types of marbles to the areas and formations they have been taken from. Neutron tomography can provide information about the inner composition which can be used to define a kind of "fingerprint" of different types of white and polychromatic marbles in order to easily identifying their origin. Two different sets of samples were investigated. One from the island of Naxos (Greece) which is a well known source of white marbles and another one from the Villa Adriana (Tivoli, Roma, Italy) where both white and polychromatic marbles are present.

Experiment

The experiments were performed at the high-flux measuring position of the V7 (CONRAD) instrument. The number of the collected tomography projections in a 180° angular interval was 200 which corresponds to an angular rotation step of 0.9°. The exposure time per projection was 0.4 s.

Results

The neutron tomographic reconstruction of a polychromic marble is shown in Fig. 1 a. The presence of high-attenuating areas can be seen in Fig. 1 b. They are related to Kaolinit inclusions [$Al_2Si_2O_5(OH)_4$] in the marble matrix providing a high neutron contrast due to the containment of crystal water in their chemical composition.

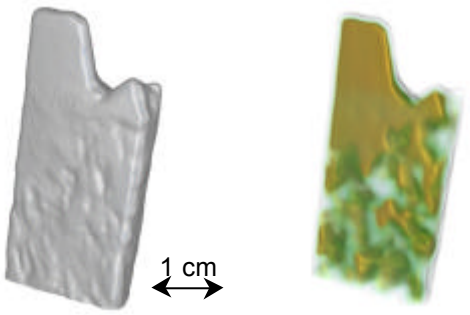


Fig. 1. Neutron tomographic reconstruction of a polychromatic marble sample from Villa Adriana. a) General view of the sample; b) Visualization of the high-attenuating areas in the sample.

The volume fraction of such inclusions in the marble matrix can be used to characterize polychromic marbles. It has been calculated to be approximately 43 % of the whole marble volume.
In the case of the white marble it could be found by the neutron tomographic investigation that the inner volume of the stone is much more homogeneous. Some minerals could be identified on the sample surface, see Fig. 2. Most likely these minerals, whose volume fraction was found to be 4.4 vol. %, are residues of material used to hold the marble in place.

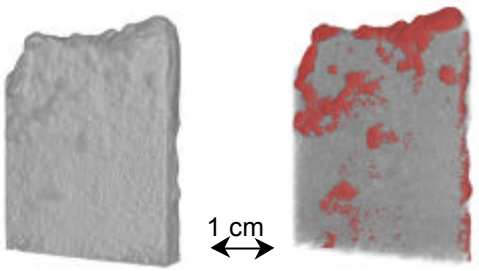


Fig. 2. Neutron tomographic reconstruction of a white marble sample from Villa Adriana. a) General view of the sample; b) Visualization of the high-attenuating areas in the sample.

Acknowledgements

This research project has been supported by the European Commission under the 6th Framework Programme through the Key Action: Strengthening the European Research Area, Research Infrastructures. Contract n°: RII3-CT-2003-505925 (NMI3).

	EXPERIMENTAL REPORT Real-time imaging of diffusion processes in liquid metals	Proposal N° MAT-04-1080 / EF Instrument **V7** Local Contact N. Kardjilov
Principal Proposer: Experimental Team:	A. Griesche, N. Kardjilov HMI Berlin N. Kardjilov, HMI Berlin A. Hilger, HMI Berlin	Date(s) of Experiment 13.09. 2004

Date of Report: Januar 2005

Introduction

In case of diffusion experiments with a classical capillary method in multi component metal melting complicated mass flows can be observed due to the diffusion and convection processes. The so far performed ex-situ analysis leads to a difficult interpretation of the chemical diffusion profiles. The in-situ investigations open the possibility to separate the mass flow process in its convection and diffusion parts. The technical development of the neutron tomography in the last decades allows in-situ diffusion measurements of metal systems which can not be investigated by conventional X-ray radiography because of their high attenuation properties. The use of very small concentration of trace element with high attenuation properties for neutrons (for example Gd) in the investigated metal alloys provides a high contrast for the mass flow process in the radiography image. From the position and the concentration changes of the trace element with the time some conclusions about the nature of the diffusion process can be made.

Experiment

The diffusion process between two metal allows PdNiP and PdNiCuP was investigated. The second alloy was doped with 1% trace material: Gd. The radiography experiment was performed at the high-flux measuring position of the V7 (CONRAD) instrument. The used detector system was based on a standard CCD camera Andor DV 434. The two sample rods with a diameter of ca. 2 mm were placed into a vacuum furnace chamber. The temperature was increased up to the melting temperature for the both alloys of 750 °C. The in-situ images were recorded with a time interval of 10 s and exposure time of 0.3 s. An example radiography image of the diffusion chamber is presented in Fig. 1

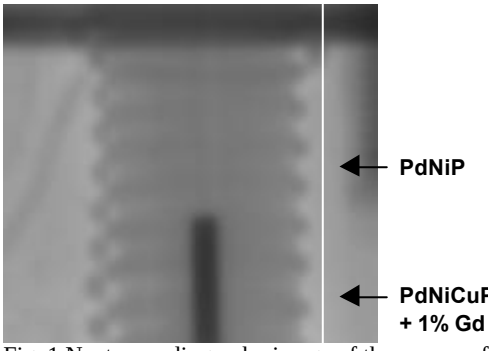


Fig. 1 Neutron radiography image of the vacuum furnace with the two alloys rods before the melting procedure. The profile position is marked by an white line.

For a qualitative analysis of the data an intensity profile through the two rods (marked with an white line in Fig. 1) was extracted for each measuring point. The data are summarized in Fig. 2.

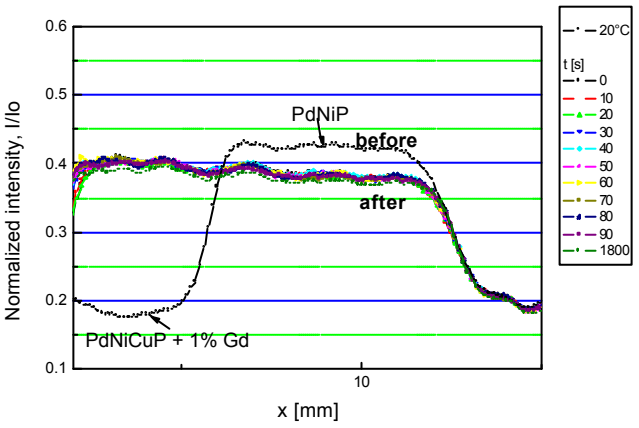


Fig. 2 Intensity profiles through the investigated alloys for different time intervals of the diffusion process.

Conclusions

The change in the diffusion profile before and after the diffusion process is visible in Fig. 2. The diffusion process occurred in the first point of the measurement where the melting temperature was achieved. In the next time intervals the state of the system was stable and no relevant changes were observed, Fig. 2.

The result can be used as a basis for further measurements where the diffusion system will be observed in shorter measuring intervals.

	EXPERIMENTAL REPORT **Investigation of the discharge process in a LiI-battery**	Proposal N° MAT-04-1081 Instrument **V7** Local Contact N. Kardjilov
Principal Proposer: Experimental Team:	I. Manke, HMI Berlin N. Kardjilov, HMI Berlin A. Hilger, HMI Berlin I. Manke, HMI Berlin	Date(s) of Experiment March - September 2004

Date of Report: Januar 2005

Introduction

Because of the low specific weight, Lithium is widely used in the battery industry. Furthermore Lithium possesses one of the highest linear attenuation coefficient for cold neutrons among all the elements of ca. 11.7 cm^{-1}. Hence the Lithium batteries are interesting objects for investigations with neutrons , because the contrast to other battery components is very high.

Normally the content of a battery is gel-like because of the liquid ingredients i.e. the electrolyte. Thus, if cropped the surface pattern is blurred, even if the battery is frozen with liquid nitrogen. Therefore the neutron tomography is a very suited method for non-destructive investigations of discharging processes in a LiI battery intended for a pacemaker device.

Results

The experiment was performed at the high-flux measuring position of the V7 (CONRAD) instrument. The experimental procedure is described elsewhere [1]. This type of battery is made up of several coplanar plates of Lithium and Iodine. Normally it should last up to ten years. To discharge the battery more quickly it has been attached to a 200 kΩ resistor. But it still needs about 6 months to fully discharge the battery.

Figure 1 shows cross sections of a neutron tomography of a Lithium-Iodine-battery. The three pictures in figure 1 represents a tomography slice through the battery before (fig. 1 a) and after (fig. 1 b, c) discharging the battery for about one and two months correspondingly.

After the first month an unexpected dramatic change in the Lithium distribution can be observed. Before discharging, the Lithium distribution (white colored) is relatively smooth as it was expected from the manufacturing specifications. After discharging, the Lithium distribution is no longer smooth, but characterized by strong discontinuities. This is an evidence for a significant material transport in the electrolyte, caused by the chemical reaction between Lithium and Iodine.

This can also be seen in the 3D view in Figure 2.

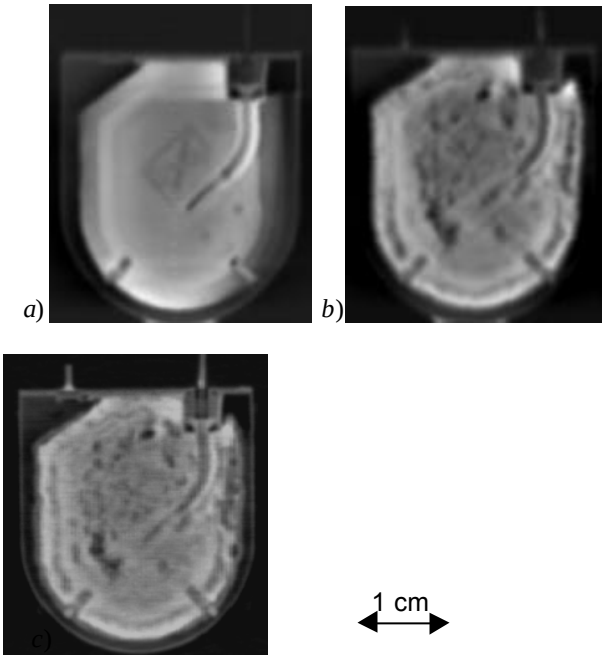


Fig. 1: Cross sections of a tomography of a Lithium-Iodine battery a) before and after b) one and c) two monats discharging time. The material with high attenuation coefficient i.e. the Lithium is white.



Fig. 2: Three-dimensional visualization of a horizontal cross section through the battery discharged after two months.

[1] N. Kardjilov et al, High flux neutron tomography investigation of a LiI battery, BENSC Report 2003

	EXPERIMENTAL REPORT Investigation of geological samples (granite)	Proposal N° MAT-04-1083 Instrument **V7** Local Contact N. Kardjilov
Principal Proposer: Experimental Team:	I. Manke, HMI Berlin, J. Tiedemann, TU Berlin N. Kardjilov, HMI Berlin A. Hilger, HMI Berlin I. Manke, HMI Berlin	Date(s) of Experiment 14.07 – 16.07. 2004

Date of Report: Januar 2005

Introduction

The neutron tomography can be used for geological investigations providing information about the stone formation and the morphological changes in the stone matrix for samples set under extreme conditions - high pressure, temperature changes or water flush.

Experiment

The experiments were performed at the high-flux measuring position of the V7 (CONRAD) instrument. The number of the collected tomography projections in a 180° angular interval was 200 which corresponds to an angular rotation step of 0.9°. The exposure time per projection was 0.4 s.

Results

The density variation and the distribution of minerals in a granite-sample was investigated. This information helps to make conclusions about the formation of granite. In this case the presence of Kaolinit mineral (marked with dark) in Fig. 1 is an evidence that the granite material has underwent a hydrothermal alteration probably due to the flow of hot water through it. In this case the big Feldspar crystals frequently presented in granite have been transformed to Kaolinit by the following chemical reaction: $KAlSi_3O_8 + H_2O \rightarrow Al_2Si_2O_5(OH)_4$.

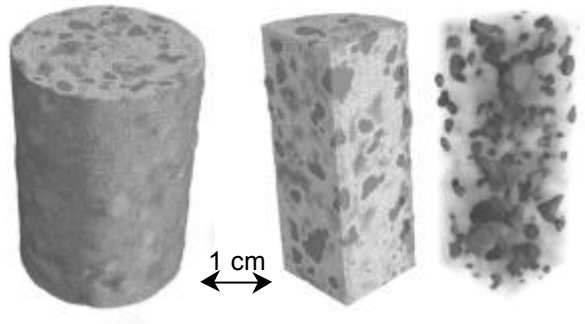


Fig.1 The tomographical reconstruction of the granite cylinder shows the spatial distribution of the mineral Kaolinit. The presence of four hydroxyl groups in the chemical composition leads to a strong contras for Kaolinit crystals in the tomography reconstruction due to high scattering properties of hydrogen.

The quantitative volume fraction of the Kaolinit inclusions (Fig. 1) can be determined easily from the tomographic data even by using the standard segmentation tool of the 3D-rendering software VG StudioMax [1]. It has been calculated to be approximately 5.2 % of the whole granite volume.
In a further experiment the cracks distribution in a granite sample exposed on a high pressure was investigated. In the tomography slices the size and the orientation of the cracks was observed. Some examples for it can be seen in Fig. 2.

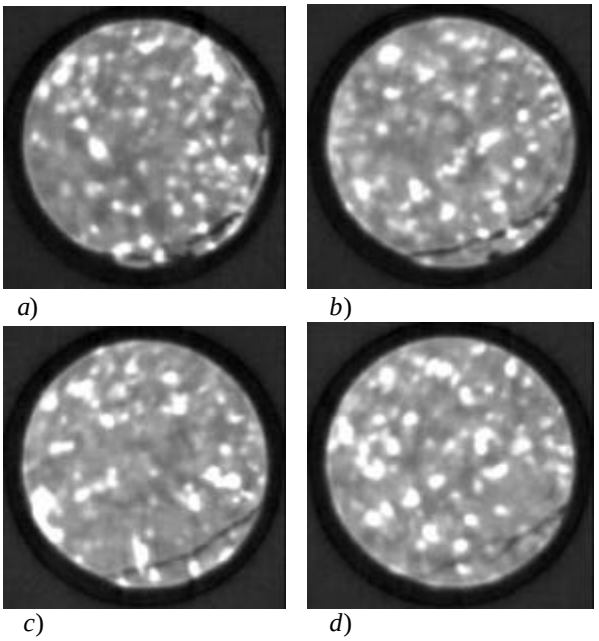


Fig.2 Tomographic slices taken at different height of the granite sample: a) 6 mm, b) 16 mm, c) 24 mm, d) 34 mm

This kind of experiments will help for future to find a precise quantitative classification of different types of geological materials.

References

[1] http://www.volumegraphics.com/

	EXPERIMENTAL REPORT **Neutron tomography of archaeological glass samples**	Proposal N° EF Instrument **V7** Local Contact N. Kardjilov
Principal Proposer: Experimental Team:	F. Rustichelli, F. Fiori, Universita' Politecnica delle Marche, Ancona, Italy, N. Kardjilov, HMI Berlin N. Kardjilov, HMI Berlin A. Hilger, HMI Berlin	Date(s) of Experiment 21.04 - 23. 04. 2004

Date of Report: Jan. 2005

Introduction

Three fragments of glass from approximately the I-II century A.D. stemming from excavations in Altino near Venice, Italy [1] have been investigated at the high flux measuring position of the neutron tomography facility CONRAD at HMI. The Altino archaeological site has a complex stratigraphy, where at least three different historical layers are present, corresponding to ages starting from approximately the VII century B.C.. There is still a large amount of different items which have been recently collected there. In many cases these items have to be handled carefully and destructive analyses or analyses introducing a risk to damage an object are a problematic choice. Even cleaning the samples from clay or earth is a delicate problem. Therefore neutron and X-ray tomography are reasonable techniques to be applied in order to visualize the samples, their inner structure or for example, to look for inscriptions or engravings. Also defects (mainly due to segregation induced by corrosion) and the eventual presence of substructures and finer chromatic domains can be visualized. Fig. 1 and Fig. 2 are images obtained from the 3D reconstruction of a glass sample.

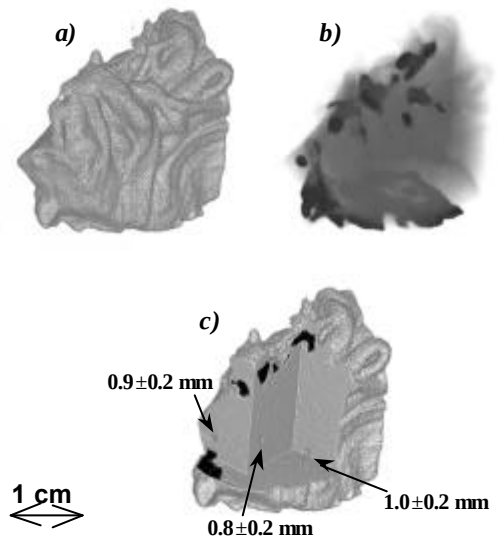


Fig. 1 Neutron tomographic reconstruction of a glass sample from the excavations in Altino. a) General view of the sample; b) high-absorbing areas; c) quantitative analysis of the voids in the glass material.

Experiment and results

In a first qualitative analysis of the neutron tomography data areas of high-attenuation could be clearly identified as can be seen in Fig. 1 b. These areas could be related to earth, clay and minerals containing hydrogen mainly sticking to the sample surface. Also void structures (Fig. 1 c) could be found in the inner region of the sample and their sizes could be determined quantitatively. The voids can also be seen on three tomographic images representing slices at different sample heights, see Fig. 2. The presence of soil in inclusions and on the surface are seen as dark areas in the images. For archeology the information about the size and the distribution of the voids (marked by arrows) in the glass can be a hint concerning the glass production process in the antique.

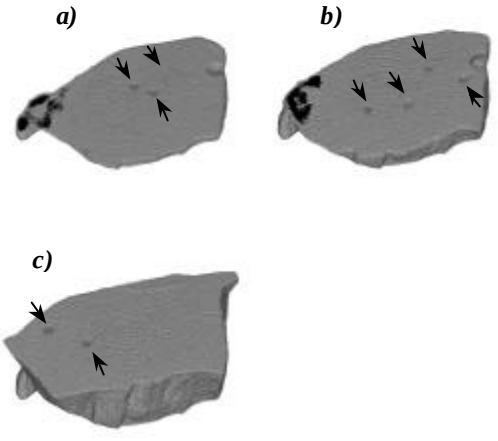


Fig. 2. Tomographic slices taken at a sample height of a) 4.1 mm, b) 6.5 mm and c) 10.7 mm

References

[1] B. M. Scarfi, M. Tombolani, Altino preromana e romana, Musile di Piave 1985

	EXPERIMENTAL REPORT **Neutron tomographies of aviation engine vent pipes**	Proposal N° PHY-04-1074-3 LT Instrument **E8** Local Contact M. Strobl, W. Treimer
Principal Proposer: Experimental Team:	C. Lewis, T. Cable, AAIB M. Strobl, TFH/HMI Berlin A. Hilger, W. Treimer, TFH/HMI Berlin N. Kardjilov, HMI Berlin	Date(s) of Experiment Mar./Apr. 2004

Date of Report: Jan. 05

Introduction

Due to a request from aviation industry together with the British Air Accident Investigation Branch some vent pipes of aircraft engines have been measured tomographically, in order to investigate sedimentations of oil and fuel non-destructively. The E8 beam position was chosen because of the provided monochromatic beam which allows to resolve small density differences and minimizes the danger of activating the samples (low flux) that shall be used for further investigations later on.

Measurement

Two of these vent pipes from different engines have been measured at the E8 beam position. A new monochromator at E8, an asymmetric reflecting (asym. factor b = -0.056) and not edged perfect Si [111] single crystal, provides a highly monochromatic (λ = 0,45(2) nm) flux density of 10^4 $cm^{-2}s^{-1}$ and a beam cross section of 2 x 5 cm^2. The collimation ratio L/D could be measured to be 400 in horizontal and 250 in vertical direction. Therefore different resolutions are achieved for horizontal (125 µm) and vertical (200 µm) directions (see other report in this issue). The vent pipes had an outer diameter of 14.2 mm and a length of more than 20 cm. Therefore only the most interesting parts of them around a knee have been investigated. One tomographic run recording 101 projection images on 180° and 20 min exposure for each of them took 34 h plus about 6 h for open beam and background measurements.

Results

The reconstructed 3-dimensional images of the samples are of good quality and enable some interesting analyses and views for the investigators. The difference between the two pipes concerning sedimentation was obvious. While one tube carried only slight and flat sedimentations on the inner walls the second one was tending to be even blocked by the sediments, which is a severe danger for the engine. This second pipe which was the one of the highest interest for the proposing company respectively the AAIB is represented in the image of Fig. 1.

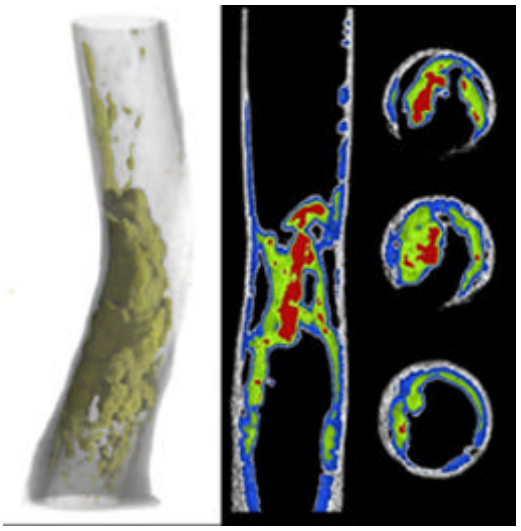


Figure 1 Used vent pipe of aircraft engine including oil and fuel sedimentation

The different colours in the right side images, which are different cuts through the 3-dimensional reconstruction, correspond to different densities. This density information enables experts to learn about the sedimentation history within the pipe. Additionally the structure of the sedimentation and volume fractions can be investigated. Despite the long exposure times the samples have not been activated and could be returned to the company without any restrictions.

This work has been supported by BMBF 03TRE9B6.

	EXPERIMENTAL REPORT **Tomographies of industrially manufactured silver rings**	Proposal N° PHY-04-1074-4 LT Instrument **E8** Local Contact M. Strobl
Principal Proposer: Experimental Team:	F. Rustcchelli, Uni. Ancona; M. Strobl, TFH/HMI M. Strobl, TFH/HMI Berlin N. Kardjilov, HMI Berlin	Date(s) of Experiment Apr./ May 2004

Date of Report: Jan. 2005

Introduction

Some silver rings that had been investigated before in the V12a double crystal diffractometer (DCD) concerning their porosity [1,2] have been measured again but now tomographically. This provided a 3-dimensional resolution and using the E8 position with its monochromatic neutron flux a high density resolution. Compared to other tomographic facilities using a broader wavelength spectrum the density resolution and avoiding the influence of beam hardening (especially for strongly attenuating materials like Ag) are major advantages of the monochromatic beam for tomography. A disadvantage is only the necessary long exposure time as the monochromatic flux is clearly reduced compared to broader spectra.

Measurements

Several rings have been investigated. They had to be mounted on a new and horizontal rotation axis perpendicular to the beam as their diameter (>23 mm) was bigger then the horizontal beam cross section (~20 mm). Additionally the axis of the rings were rotated out of the rotation axis in order to avoid an overlap of the front and back parts of the ring (concerning the beam direction) and hence to enable satisfactorily transmission (Figure 1).

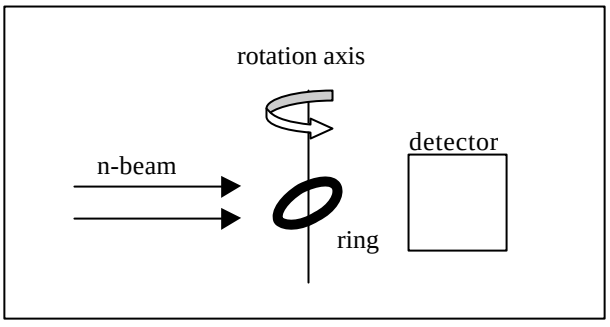


Figure. 1 bird view of schematic set-up

The resolution of the set-up can be given with 125 µm in horizontal and 200 µm in vertical direction. Measurement times for every projection were 40 min and 101 projections have been taken on 180°. For the results one example is represented in Fig. 2.

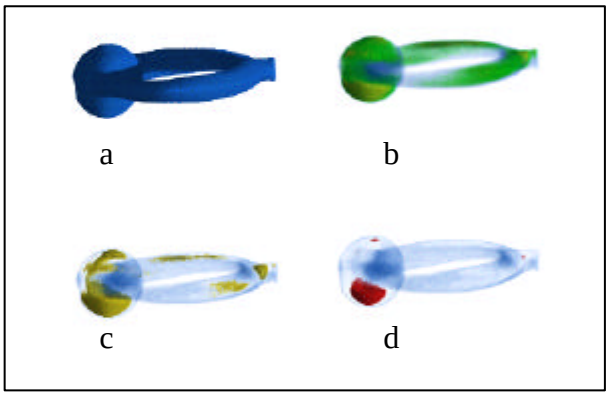


Fig. 2 Reconstruction of silver ring setting lower densities transparent from a) to d)

In the resulting reconstructions it is possible to colour areas of different attenuation (here i.e. areas of different densities) with different colours and to set such defined grey level values transparent in order to see inner details. This is done for the representation in figure 2. The density grows from blue over green and yellow to red coloured areas. Hence areas of different densities and their distribution in the sample volume can easily be identified and analysed. From such kinds of results it shall be tried to find the reasons for inhomogeneous densities in the production process and to avoid them.

This work has been supported by BMBF 03TRE9B6.

References

[1] M. Strobl et al., BENSC-Rep. 2003, p.231
[2] A. Manescu et al., BENSC-Rep. 2003, p.212

	EXPERIMENTAL REPORT **Investigation of Polymer Electrolyte Membrane Fuel Cell (PEMFC) Water Household**	Proposal N° MAT-04-1085 EF Instrument **E8** Local Contact M. Strobl
Principal Proposer: Experimental Team:	I. Manke, (HMI); J. Scholta (ZSW) J. Scholta (ZSW) M. Strobl (TFH), A. Hilger (HMI Berlin) N. Kardilov (HMI Berlin)	Date(s) of Experiment 21.-24. Sept. 2004

Date of Report: 30. Nov. 2004

Introduction

Polymer Electrolyte Membrane Fuel Cells (PEMFCs) are developed worldwide for portable, stationary, and mobile applications.
Whereas at normal operating temperatures of approx. 80 °C no problems concerning water household are experienced, at lower temperatures coexisting phases of gaseous and liquid water are observed. The removal from such liquid phases sometimes causes problems, especially if only small pressure differences are possible due to system boundary conditions. Normally, the possibilities to identify two-phase regions are very limited, and no statement of locations and in- and decrease of the total area can be made.
Neutron radiographic investigation of cells turned out to be a promising method because of the high cross section of hydrogen atoms to neutron scattering which lead to good distinction of liquid water zones within the cell.
This project is initiated to determine the influence of flow field geometries on the water distribution within the cell.

Experimental Procedure

Several single cell were prepared using material combinations excluding steel and plastics as far as possible to avoid excessive absorption caused by those materials. The scheme of the experimental setup is shown in Fig. 1.

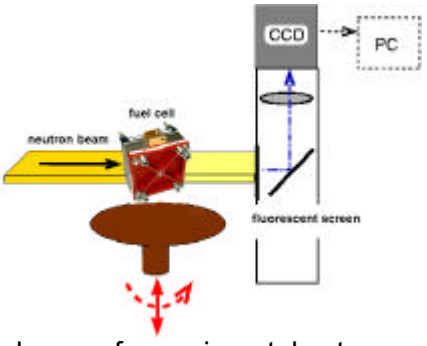
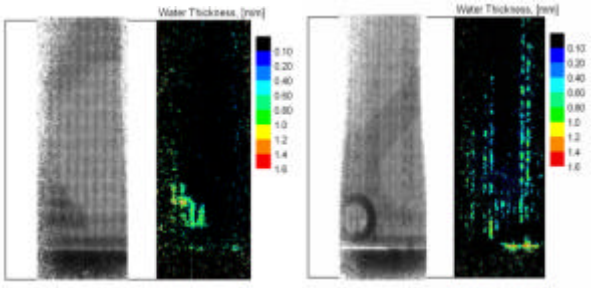


Fig. 1: Scheme of experimental setup

The fuel cell was connected to a hydrogen and air supply which enabled the adjustment of media flows with defined utilization degrees referred to the electrical current through the cell. Exposition times between 1 and 4 min were used to obtain a radiogram of sufficient quality. A systematic variation of cathode utilization between 2 and 60 % was performed.

Results and Discussion



a) b)

Fig. 2: Neutron radiogram of a) standard and b) advanced fuel cell under 'wet' operating conditions

As shown in Fig. 2, the standard cell tends to form water agglomerates under so-called wet operating conditions. The advanced configuration shows smaller agglomerates, but also some areas with flooded channels.
A fuel cell with optimized configuration is shown in Fig. 3. It is shown, that the fully

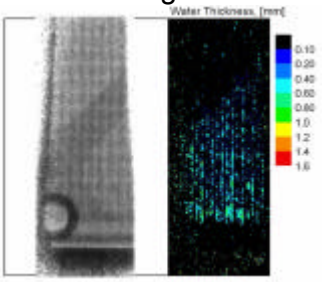


Fig. 3: Neutron radiogram of a fuel cell with optimized flow-field construction under wet operating conditions

flooded zones are replaced with only partially filled areas such that gas flow is not hindered by water droplets.

	EXPERIMENTAL REPORT **Imaging of fibre reinforced low absorbing materials**	Proposal N° MAT-04-1040 Instrument **V12a/E8/V7** Local Contact M. Strobl W. Treimer
Principal Proposer: Experimental Team:	M. Bastürk, ATI; H. Rauch, ATI Wien M. Strobl, TFH/HMI Berlin M. Strobl, TFH/HMI Berlin A. Hilger, TFH/HMI Berlin N. Kardjilov, HMI Berlin	Date(s) of Experiment July 2004

Date of Report: Jan 2005

Introduction

The aim of the proposed experiment was to image the macroscopic inner structure of SiC/SiC_f samples [1] by the means of tomography. SiC/SiC_f is an important material for nuclear fusion experiments such as ITER. The porosity and swelling of the fibres due to manufacturing and high irradiation have to be imaged and investigated to determine the quality of the material. The material has a very low attenuation cross section so that common neutron (and X-ray) tomography fails. Therefore an attempt was made to image a sample of this fibre material with the neutron imaging methods available at the HMI as there are the refraction [2] and USANS contrast [3] tomography at V12, the monochromatic neutron tomography at E8 and the high flux position CONRAD at V7 [4].

Measurements

The sample dimensions were about 3 x 4.5 x 20 mm^3. Measurements have been performed at all of the three instruments. However, the contrast was poor at all of them and taking into account the required resolution the refraction and USANS methods could not achieve enough contrast (also due to high background in the scintillator CCD detector system) in scanned radiographies to perform a tomography (Fig. 1, USANS signal).

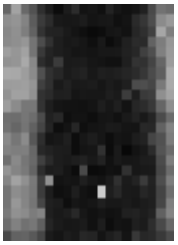


Fig. 1 USANS signal radiography, the object is visible but no additional structure can be identified and image noise is high

The reconstructions of the E8 and V7 measurements are presented in Fig 2 a and b. The contrast is low as well but at least some structures of higher and lower densities can be identified. Whether they represent reliable information or not has to be proved by further data evaluation and comparison of the results and other measurements.



a b

Fig. 2 a E8 monochromatic, b V7 high flux tomography

Mind that 2 a and b have been reconstructed independently and the cuts are not comparable. Brown are higher absorbing areas and their distribution might be related to the direction of fibre bundles.

References

[1] F. Elio et al., Fusion Eng. &Des. 46 (1999), p. 159
[2] M. Strobl et al., NIMB 222 (2004), p 653
[3] M. Strobl et al., Appl. Phys. L. 85, 3 (2004), p. 488
[4] N. Kardjilov et al., BENSC Rep. 2003, p. 209

	EXPERIMENTAL REPORT SANS investigation of microstructural features influencing crack growth in aluminium alloys	Proposal N° MAT-04-1042 Instrument **V12a** Local Contact Markus Strobl
Principal Proposer: Experimental Team:	Dr. Fabrizio Fiori, Univ. Politecnica delle Marche Dr. Adrian Manescu, same as above Vittorio Calbucci, same as above Markus Strobl, HMI Berlin	Date(s) of Experiment 16.08 – 24.08.2004

Date of Report: 28.09.2004

Void nucleation, growth and coalescence are the main micromechanisms of failure in Aluminium alloys. SANS experiments were performed on Al2024 alloy notched and pre-cracked specimens, submitted to different fatigue tests, in order to investigate the influence of microstructure (precipitates, dispersoids and voids) on the crack growth.
The measurements were done in three different points around the crack for each of the four analysed specimens, as presented in the Figure 1 below.

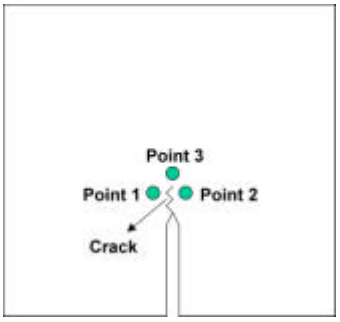


Figure 1. Investigated points

The SANS measurements were performed on the V12a instrument, using a wavelenght of 0.476nm and a beam size defined by a slit having a circular shape with a diameter of 1.8 mm.

The following experimental SANS curves were obtained for the three analysed points:

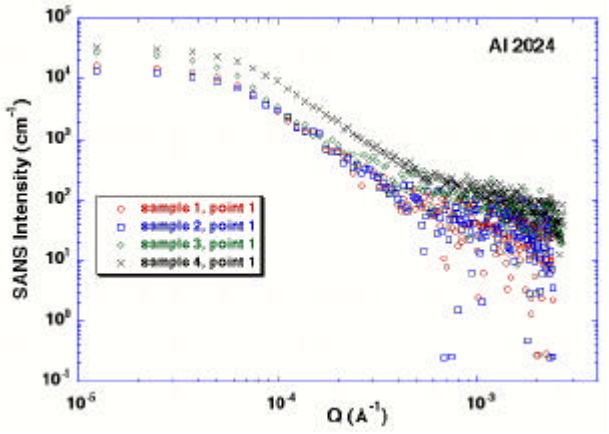


Figure 2. SANS curves for the 1st point

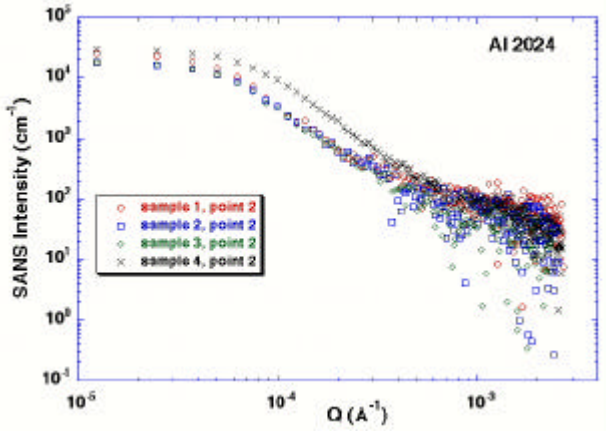


Figure 3. SANS curves for the 2nd point

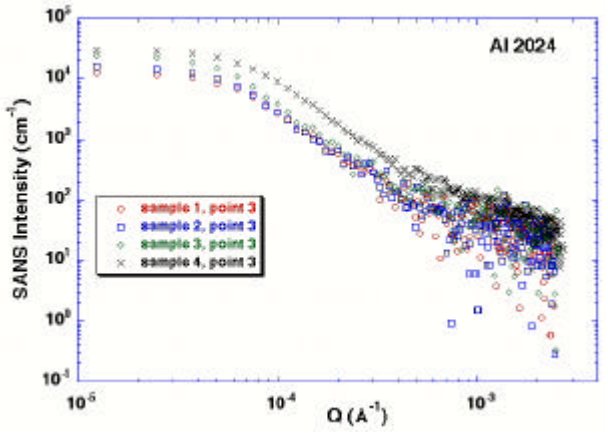


Figure 4. SANS curves for the 3rd point

From the experimentally determined SANS cross section, the particle size distribution and volume fraction will be evaluated.

	EXPERIMENTAL REPORT **Mesoscopic Structure of Marbles**	Proposal N° OTH-04-1043 Instrument V12a Local Contact M. Strobl, W. Treimer
Principal Proposer: Experimental Team:	R. Triolo, Univ. Palermo, F. Lo Celso, Univ. Pal. I. Ruffo, U. Mursia, Carini R. Triolo, Univ. Palermo M. Strobl, TFH/HMI Berlin	Date(s) of Experiment Aug. - Sep. 04

Date of Report: Feb. 05

The effect of metamorphism on the formation and on the characteristics of marbles is not fully understood yet. The formation of marble suggests that the metamorphic evolution leads to the transformation of an original sedimentary carbonate protolith (limestone) into a marble, involving a progressive increase in the dimension of the building single crystals from fractions of microns to mm or cm (macroscale), according to the metamorphic degree. At the microscale level, metamorphism by itself is expected to hardly effect the size of the elementary cell, with the exception of the chemical composition of the rock and any eventual interacting fluids, with special reference to the elements substituting for Ca (Mg, Sr, etc.). However, little is known about the effect of metamorphism on the mesoscale structures, which is the object of the present report. This information is particularly relevant when the provenance of marble objects is involved. The provenance is of key importance to archaeology in so far as artistic, technological or commercial exchange patterns may be correlated to historical events. In addition authentication of works of art in museums is of great concern. We thought that the texture of white marbles is mainly related to the structural features at the mesoscale level, i.e. in the range of dimensions which can be explored by combining ultra small and small angle scattering experiments. We had plans of testing this assumption by studying a small set of white marble samples representative of a variety of metamorphic conditions. In addition, for comparison purposes, also a small number of polychromic marbles was considered. The original proposal was intended to investigate the mesoscopic structure of marble by combining Small Angle (SANS) and Ultra Small Angle Neutron Scattering (USANS) measurements. Overload of beam time requests has allowed us to perform only USANS measurements on a small number of samples.

Figure 1 shows USANS slit smeared data for three samples of marbles from the Carrara area. As expected the different samples are quite similar. Figure 2 shows results for samples of white marbles coming from different locations in Northern Italy. The q dependence indicates different texture of the different samples. Definite conclusions may be drawn only when also SANS measurements will be available. Nevertheless, results obtained seem to point out in the direction of confirming the importance of the mesoscopic structure for fingerprinting purposes. We are currently working on the software to desmear the data and to improve the quality of the fits of the experimental data.

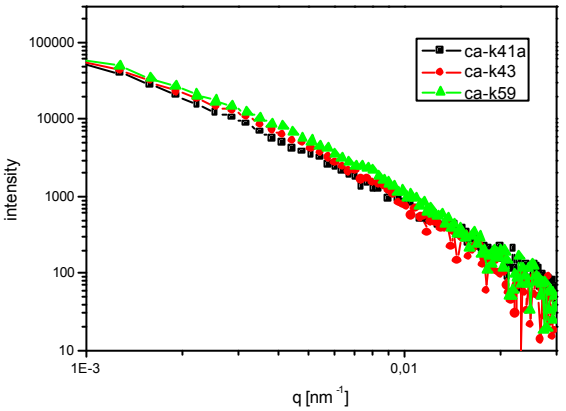


Fig.1 Scattering curves from samples from same area

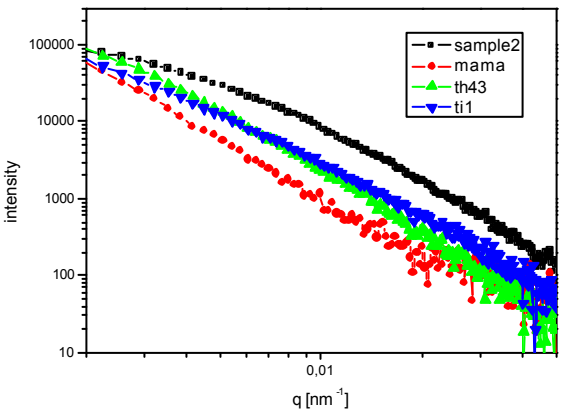


Fig.2 Scattering curves from samples from different areas

	EXPERIMENTAL REPORT **Test and application of refraction and USANS contrast tomography**	Proposal N° PHY-04-1074/5-LT Instrument **V12a** Local Contact M. Strobl, W. Treimer
Principal Proposer: Experimental Team:	M. Strobl, W. Treimer, TFH & HMI Berlin M. Strobl, TFH & HMI Berlin A. Hilger, TFH & HMI Berlin N. Kardjilov, HMI Berlin	Date(s) of Experiment Feb. 04

Date of Report: 9.01.2005

Introduction

Related to a request from aviation industry a special designed dummy was fabricated and measured with the new tomographic refraction and USANS contrast method. The result was compared to the standard tomography performed on the same dummy. Later on also the real sample was measured but as there was a need for three dimensional imaging measurements on the sample have been performed at E8 as well and can be found in another BENSC report.

Measurements

The request concerned a steel tube with inner sediments of oil and fuel. Therefore a dummy was produced using a steel tube of corresponding dimensions i.e. a diameter of 15 mm and a wall thickness of 1 mm. The tube was filled with an Al cylinder with a diameter of 12 mm in an eccentric position. The additional free space within the tube kept three pencil leads with diameters of 300, 500 and 700 µm and was filled with black toner in order to roughly simulate the sediments of oil and fuel in the real sample. This sample was measured by performing a conventional tomography at a high flux position [1] and by recording tomographic scans with a 0.2 mm slit at V12a [2]. From both measurements an attenuation contrast reconstruction was made while from the V12a data also refraction and USANS reconstructions were done. While the reconstruction from the conventional measurement was three dimensional they were just two dimensional for the V12a data. The dummy got activated by the conventional measurement in a way that it has to be kept in an authorised laboratory. The real sample was measured at V12a with an enlarged slit of 0.3 mm in order to decrease the exposure time.

Results

For the dummy the reconstructions have been compared. As can be seen from Fig.1 the USANS image (a) displays only the pencil leads and the edges of the tube (i.e. artefact [3]). The refraction image resolves all components (although the toner is actually invisible). The attenuation image (c) recorded at V12 distinguishes the steel and coal parts as the radiation is monochromatic, while the conventional acquired image (d) hardly gives contrast between different components except for the biggest pencil lead for size and higher density.

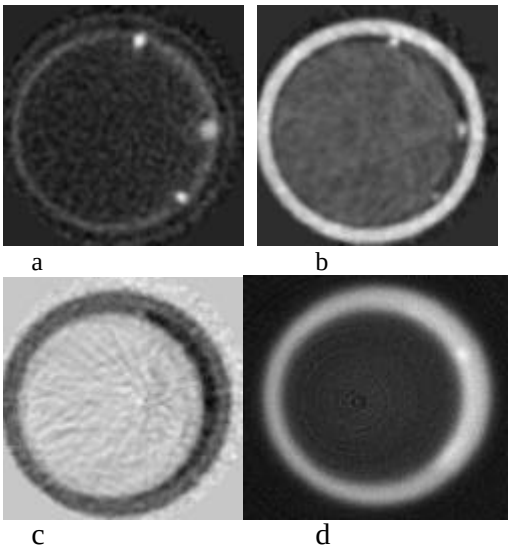


Fig. 1 Different reconstructions of dummy; a) USANS V12a, b) refraction V12a, c) attenuation V12a, d) conv. attenuation



Fig. 2 Combination of attenuation and refraction images V12a

The real sample in Fig. 2 could be resolved by using the refraction image that displays the tube only and the attenuation image without contrast between steel and sediments. The slice represents a mean cross section on a height of 6 mm.

This work has been supported by BMBF 03TRE9B6

References

[1] N. Kardjilov et al., BENSC Rep. 2003, p. 209
[2] Treimer, W. et al., Appl. Phys. Lett. 83, 2, 2003
[3] Strobl, M., Diss., TU Wien, 2003

	EXPERIMENTAL REPORT **Influence of external magnetic fields on ^{3}He filter cells made out of quartz glass**	Proposal N° EF Instrument E1 Local Contact J.Klenke
Principal Proposer: Experimental Team:	V. Hutanu, HMI Berlin V. Hutanu, HMI Berlin A. Rupp, HMI Berlin J. Klenke, HMI Berlin	Date(s) of Experiment 09.02.04 – 15.02.04 23.06.04 – 04.07.04

Date of Report: 20.12.2004

A high reliability of glass cells for polarised ^{3}He to be applied as neutron spin filters is indispensable. Cells must be able to undergo both, many refilling cycles and exposures to various magnetic environments without changing their properties concerning the relaxation of polarised ^{3}He. Jacob at al. [1] demonstrated that the ^{3}He polarisation decay in Pyrex cells can be very sensitive to their magnetic history. This report presents measurements performed on a number of cells made out of quartz glass which show that the phenomenon seems to be characteristic not only to Pyrex, but has a more general origin.

The aim of the measurements was to check whether the effect also occurs in quartz cells, uncoated as well as Cs-coated. Another goal was to found both, a threshold for an external magnetic field at which a remanent influence on the relaxation behaviour of the cell sets in, and a saturation value, above which no further deterioration occurs. The possibility to improve the ^{3}He relaxation time constant T1 of a "magnetised" cell by "degaussing" it was also one of the important aspects of the experiments. Finally, measurements of T1 in oxidised cells were performed to learn more about the influence of Cs oxides and the "ageing" of cells.

A huge decrease (about one order of magnitude) of T_1 occurred due to an even short exposure of the cells to an external magnetic field of 0.7 T. Partial or total restoring of the initial T_1 value could be achieved by a careful degaussing of the magnetised cells.

Fig.1 presents a typical example of the influence of external magnetic fields on the T1 of a Cs-coated cell, while Fig.2 shows the alternation of the magnetic field, applied to degauss the cells, which lead to a total restoring of the initial T1.

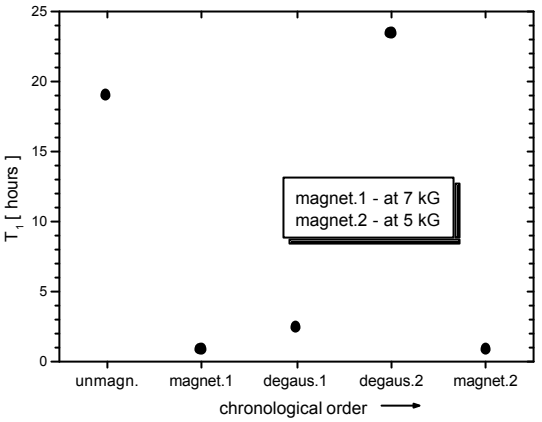


Fig.1 Characteristic relaxation time T1 plotted vs the chronological history of magnetisation in a certain cell.

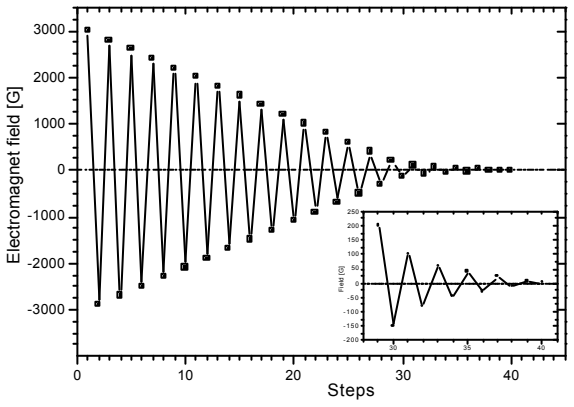


Fig.2 Alternation of a magnetic field; in steps of 100 G, 20 G and 10 G, respectively, in order to degauss a cell.

Acknowledgement

We are grateful to Prof. Heil and his group (University of Mainz) who supplied us with polarised ^{3}He. The work has been supported by the EU through the NMI3 project RII3-CT-2003-505925 (JRA4)

References

[1] R.E. Jacob, S.W. Morgan, B. Saam, J.C. Leawoods, Phys. Rev. Lett. 87 (2001) 143004.
[2] V. Hutanu, A. Rupp, Physica B(in press)

	EXPERIMENTAL REPORT **Phase contrast radiography with monochromatic neutrons**	Proposal N° PHY-04-1074-6 LT Instrument **E8** Local Contact M. Strobl
Principal Proposer: Experimental Team:	M. Strobl, TFH/HMI Berlin M. Strobl, TFH/HMI Berlin	Date(s) of Experiment Sep 2004

Date of Report: Jan. 2005

Introduction

Using phase contrast can enhance the available image information of radiography experiments especially for low contrast materials concerning attenuation. The high phase difference at the edges of a sample causes strong intensity variations in these areas of the image [1, 2]. It was suggested that for phase contrast imaging at least a highly collimated beam (i.e. high spatial coherence) is necessary after it has been shown that even a polychromatic beam can provide phase contrast [3]. However, phase contrast measurements with a comparably low collimation but a highly monochromatic beam have been performed at the E8 instrument.

Measurements

The conditions for the measurements are mainly defined by the asymmetric perfect Si monochromator (as described elsewhere in this issue). The collimation ratio L/D was measured to have a horizontal value of 400 which is very small compared to [3] for example where this value was higher than 10000. However the flux density given was with app. $10^4 cm^{-2}s^{-1}$ a factor of 5 better. The wavelength resolution of the monochromator is of the order of some percent (10^{-2}). Even similar samples like in [3] have been used. The samples were stainless steel capillaries (syringe needles) with diameters of 0.9 mm and 1.2 mm diameter. The images were recorded by a handmonitor-CCD camera system providing a spatial resolution of app. 50µm. Calculations concerning the intensity distribution at different distances have been made. Two different ways of calculation have been used and the results correspond perfectly. On one hand they were based on phase considerations like in [3] and on the other Snellius´ law of refraction was used. However, so far no smearing representing divergence and limited resolution has been applied to the calculation. Hence the comparison to the measured curves is purely qualitative and the curves are scaled (Fig. 1 & Fig.2). However, the typical phase contrast related intensity patterns could clearly be measured. Mind that the contrast is increased at the increased distance of 12 cm between detector and sample (Fig.1).

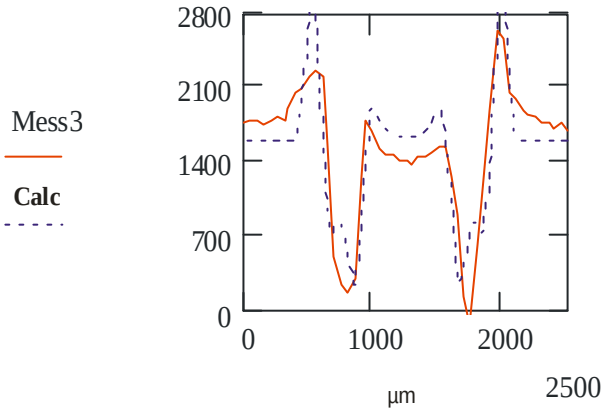


Fig. 1 Intensity pattern at of 12 cm behind the sample

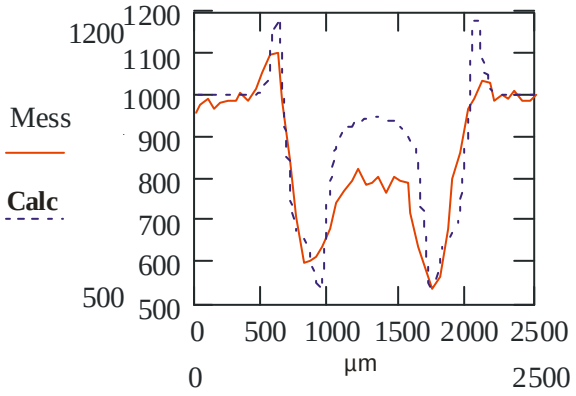


Fig. 2 Intensity pattern at 2 cm behind the sample

This work has been supported by BMBF 03TRE9B6.

References

[1] B. E. Allmann et al., Nature 408 (2000), p. 158
[2] P. Cloetens et al., Appl. Phys. 29 (1996), p. 133
[3] N. Kardjilov et al., NIM A A 537 (2004), p. 519

	EXPERIMENTAL REPORT **Manipulation of the Spin-Fan in NRSE**	Proposal N° PHY-02-388 Instrument V2-NRSE Local Contact K.Habicht
Principal Proposer: Experimental Team:	K. Habicht; HMI,Berlin, TU-Darmstadt K. Habicht; HMI,Berlin, TU-Darmstadt	Date(s) of Experiment 23.04.– 03.05.2004

Date of Report: 03.01.2005

Resolution limiting effects in inelastic neutron scattering experiments using the NRSE technique on a TAS have been studied in detail recently [1]. Theoretical analysis and experimental evidence have identified sample properties, e.g. curvature of the dispersion surface, to be crucial to resolution. Lifetime measurements of dispersive excitations can most easily be performed using the NRSE technique, since the tilted field geometry is simply adapted by rotating RF-flipper coils. This allows to match planes of constant Larmor phase with the slope of the dispersion. However curvature of the dispersion surface within the resolution ellipsoid of the TAS might overshade intrinsic linewidths to some extent. The overall goal is to overcome this effect by a set of correction elements which provide additional Larmor precession such that surfaces of constant Larmor phase distinct from the planar geometry could be realized.

The purpose of this experiment was to show that very simple manipulations of the neutron beam polarization in the NRSE setup can be performed and to study a simple arrangement of Mezei tilt coils situated in between two NRSE RF coils.

The TAS was operated in a direct beam geometry with fixed incident k_i = 1.7 • $^{-1}$. Second-order contamination was suppressed by a tuneable PG filter. No additional collimators were used. The NRSE-option was operated in non-bootstrap mode throughout the experiments. Having the spin-fan oriented perpendicular to the incident beam is a necessary requirement to operate tilt coils between the NRSE coils. The realization of an adiabatic transition from a spin-fan orientation in the scattering plane to a longitudinal geometry, where the spin-fan is oriented perpendicular to the incident beam, using modified coupling coils between the RF coils, failed due to spatial restrictions. However a $\pi/2$ flipper after the first NRSE coil can provide this transition. Using a second $\pi/2$ flipper in front of the second NRSE coil and a solenoid coil in between the two static flippers it could be shown, that this transition can be performed without loss of polarization (see Fig.1). For each setting of the current parameters a spin-echo signal has been measured. The setup was used in similar arrangement in a later NRSE experiment on magnon lifetimes to determine the polarization at spin-echo time τ=0 for mixed SF/NSF signals.

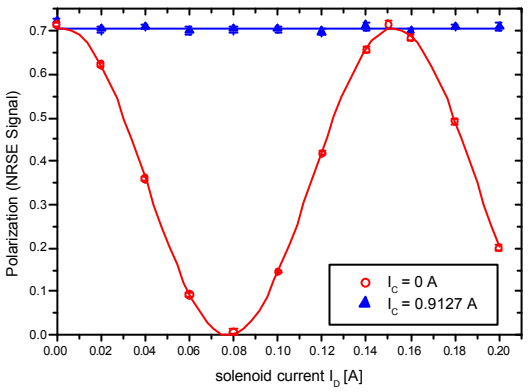


Fig. 1: Polarization of the NRSE signal as a function of the solenoid current with (triangles) and without (open squares) operation of the two $\pi/2$ flippers.

A preliminary test experiment has been performed using two Mezei tilt coils in one arm of the spectrometer, while in the second arm the RF-coils were mechanically rotated to determine the effective tilt angle. Using static currents I ≅ 5 A, maximum tilt angles θ_1 ≅ 7° (15°) could be realized at f_{NRSE} = 100 kHz however with an expected severe loss of polarization which was reduced to 67 % (48 %) of the original value.

This research project has been supported in part by the European Commission under the 6th Framework Programme through the Key Action: Strengthening the European Research Area, Research Infrastructures. Contract n°: RII3-CT-2003-505925.

[1] K.Habicht *et al.*, J.Appl.Cryst. **36**, 1307 (2003)

BENSC	**EXPERIMENTAL REPORT** **Time-resolved SANS listmode data: Generation with detector control program "Mesydaq" and treatment with "BerSANS-PC" data processing software**	Proposal N° EF Instrument **V4** Local Contact U.Keiderling
Principal Proposer:	U.Keiderling, A.Wiedenmann, J.Haug, HMI	Date(s) of Experiment
Experimental Team:		05.04. - 08.04.2004

Date of Report: 04.01.2005

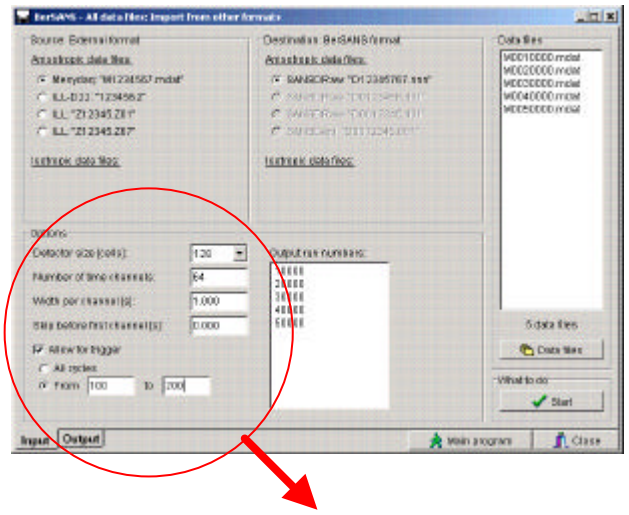
The "BerSANS-PC" data processing software is a unique tool for raw data treatment, data reduction and data visualization, that is being successfully used at the "V4" SANS instrument. As a part of the continuous upgrade of this software, a new option has been implemented to import and pre-process time-resolved listmode data.

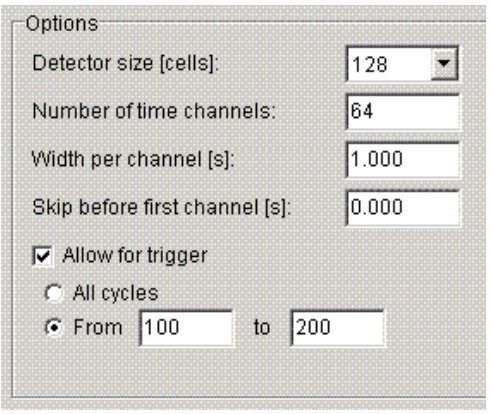
By default, the existing detector control program "Mesydaq" produces 2-dimensional (x,y) histograms of the detector intensity with a spatial resolution of 128x128 pixels, but time-integrated over a pre-defined measurement time of typically 1 min to 20 min per data file. There is also a rudimentary option to gain time-resolved spectra, but limited to a fixed number of 128 channels with a maximum time of 1 ms per channel, allowing only inflexible measurements on very fast processes. However, besides this that program also possesses an implemented function to produce listmode data consisting of full (x,y,time) information for each single neutron. This listmode option has been set to operation within the hardware environment of the SANS instrument. The listmode data are produced by the control program in a sophisticated proprietary format, and easily reach the amount of gigabytes per day. They thus require great efforts for convenient handling and reduction according to the special needs of the user and the experiment. All these requirements are met by the new "BerSANS-PC" listmode option.

There are two basic types of time-resolved measurements. The first type comprises continuous time-dependent processes. With plain histograms time-integrated by the hardware, the user has to predict an expected time-dependence of the experiment, and must set the measurement time per data file accordingly. After the experiment, no further alteration of this time resolution will be possible. In contrast, using listmode data, no primary assumptions have to be made. The user is completely free to reduce the data after the experiment, with any spatial and time resolution desired. The program interface (see figure) provides the option to easily integrate the data into any number of histograms (time channels) with any channel width. There is an extra option to skip a certain time range at the beginning of a listmode file. This offers the possibility to integrate different periods of a single time-dependent process with different time resolutions. Example: If a process turns out to run very fast in the beginning, but then slower, the first part of the process can be histogrammed with a small time channel width, and the remainder of the process can be integrated with a larger time channel width by repeating the import skipping the beginning of the process. There is also an additional option to reduce the spatial resolution from 128x128 to 64x64, to obtain smaller data files if the higher spatial resolution is not required.

The second type of measurements comprises periodical processes. A trigger signal related to the periodicity can be merged in the listmode data during measurement, and then re-extracted during import. This offers the unique possibility to overlay all or some selected cycles of the periodical process, yielding a significant improvement of statistics.

First examples of use of this new feature are given in other experimental reports.





BENSC	**EXPERIMENTAL REPORT** **TOF-SANS on V4 after changing the detector readout system**	Proposal N° EF/SF3nano Instrument **V4** Local Contact J. Haug
Principal Proposer: Experimental Team:	J. Haug, U. Keiderling, A. Wiedenmann J. Haug, U. Keiderling, A. Wiedenmann	Date(s) of Experiment 11.02.-19.02.2004

Date of Report: 05.01.05

The readout system of the position sensitive detector at V4 was changed in 2003 and the new detector software makes it possible to measure with a TOF option. The measurement is restricted to 128 channels and the time per channel can be set to 1µs, 10µs, 100µs and 1ms. To check the correct function of the software in TOF-mode silver behenate (AgBE) powder was used because of its well known Bragg reflection with d=58.378. For the mesurement the velocity selector was put out and the chopper system in the beam position.
To suppress the overlap between fast and slow neutrons the chopper was set to 12Hz. Fig. 1 shows the time-distance diagramm for 3Å and 20Å. The distance between chopper and detector was set to 18.8 m and a resolution of 1ms was used for the 128 histograms.

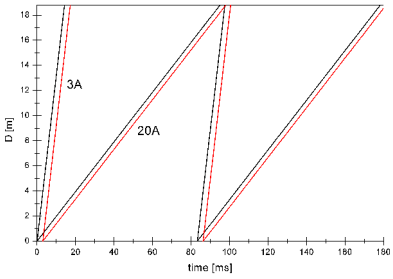


Fig. 1: *Time-distance diagramm for 3Å and 20Å. The black and red lines are the edge of the chopper-slit.*

The AgBE rings of some histograms were used to recieve the wavelength λ (Fig. 2) and by a fit with the formula $\lambda=(h/m_N)\cdot(t/L)$ the wavelength of all histograms were calculated. Radial averageing was made with BerSANS [1] for all histograms. Fig. 3 shows the data of some histograms with a Bragg-peak at Q=1.076nm. By fitting Gaussian functions the Bragg-angle 2θ and FWHM(2θ) were calculated and compared with previous measurements [2,3] in Tab. 1. The FWHM(2θ) of the TOF measurements is smaller resulting from a better wavelength resolution in this case.

References:

[1] U. Keiderling *The new "BerSANS-PC" data processing software* BENSC Rep. 2003
[2] R. Gilles, U. Keiderling, P. Strunz, A. Wiedenmann, H. Fuess Mat. Sci. Forum 321-324 (2000) 264.
[3] J. Haug, A. Wiedenmann *Instrumental resolution on V4 after changing the detector readout system* BENSC Rep. 2003

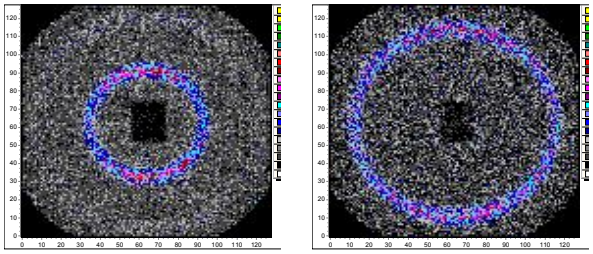


Fig. 2: *2D raw data of the AgBE sample at 24 and 39ms leading to a wavelength of 4.289Å and 7.444Å.*

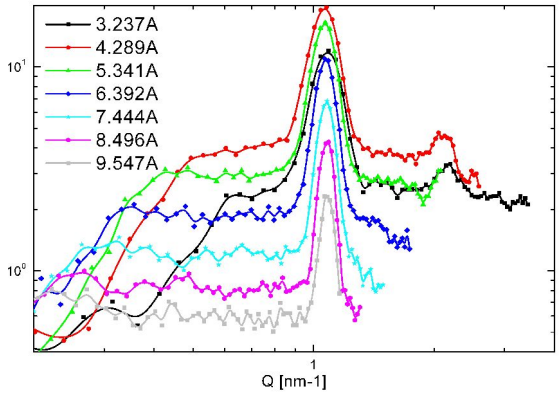


Fig. 3: *Radial averaged SANS data of histograms between 3Å and 10Å.*

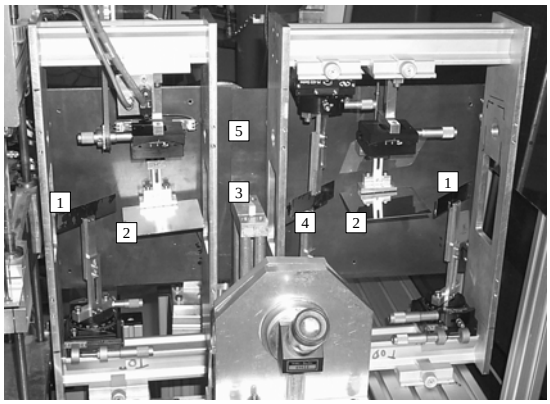
λ [Å]	2θ (001)	FWHM(2θ)
6.05 [2]	5.814	1.222
6.05 [3]	5.879	1.086
5,97 TOF	5,828	0,804
6,39 TOF	6,033	0,802

Tab. 1: *Comparison of the FWHM(2θ) of the TOF with standard measurements.*

	EXPERIMENTAL REPORT **Spin Echo Scattering Angle Measurement (SESAME)**	Proposal N° MAT-04-978 Instrument **V-6** Local Contact Marita Gierlings
Principal Proposer: Experimental Team:	Roger Pynn, Los Alamos National Lab Mike Fitzsimmons, Los Alamos National Lab Helmut Fritzsche, Chalk River Janos Major, MPI, Stuttgart	Date(s) of Experiment June 15 – 22, 2004

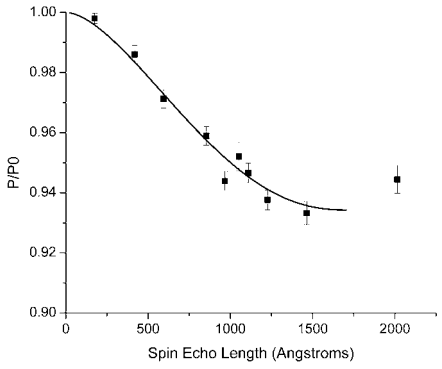
Date of Report: Dec 3, 2004

This experiment is the last of a series of tests of the Neutron Spin Echo (NSE) method applied to the coding of neutron scattering angles. Our implementation of this method uses thin films of Permalloy electrodeposited on silicon wafers as pi/2 flippers, pi flippers and as the precession fields that encode the neutron scattering angles. A photograph of our apparatus mounted on V-6 is shown below:

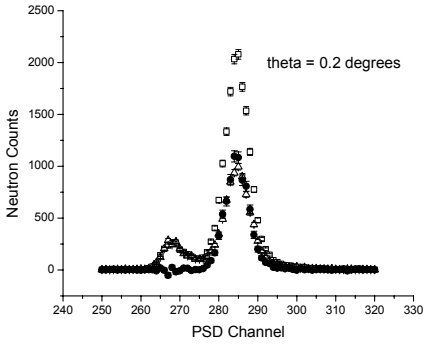


1: pi/2 flippers; 2:precession films; 3: sample; 4: pi flipper; 5: iron plate – part of guide field.

We made measurements of SANS from a dilute suspension of 84 nm diameter poly-styrene spheres in a D_2O/H_2O mixture. The ratio of the spin echo polarizations with and without the sample in the beam is plotted below as a function of the spin echo length (which is the correlation range probed in the sample.) The solid line through the data points is the result (the Patterson correlation function for dilute particles) expected on the basis of the known sample parameters and the collimation on V-6. Note that the NSE method has allowed us to access correlation distances up to 200 nm using 4.6 Å neutrons, something that would be impossible to do with existing SANS instrumentation.



Using the SESAME technique, we have also been able to separate diffuse and specular reflection from a thin-film polymer sample. This separation is shown below for a single setting of the neutron angle of incidence.



The open squares are spin-up data that include specular scattering plus one half of the diffuse scattering. The open triangles are spin-down data that include only diffuse scattering. The filled circles are the difference data i.e. specular scattering only. Note that the small peak to the left is part of the unreflected neutron beam that is not quite blocked by a mask in front of the detector. This peak appears equally in the spin-up and spin-down channels and, like the diffuse scattering, does not contribute to the difference (specular) data. In our experiment, diffuse and specular scattering were separated with an angular resolution of about 0.02º, about 5 times better than the instrumental collimation used.

	EXPERIMENTAL REPORT **Tests of a fast speed camera for real-time imaging**	Proposal N° MAT-04-1079-EF Instrument **V7** Local Contact N. Kardjilov
Principal Proposer: Experimental Team:	N. Kardjilov, HMI Berlin N. Kardjilov, HMI Berlin A. Hilger, HMI Berlin J. Brunner, FRM-2 Garching	Date(s) of Experiment 23-26 June 2004

Date of Report: Jan. 2005

Introduction

Going to short exposure times a lot of parameters can determine the quality of a neutron radiography (NR). In order to compare NR images taken with different detector systems under different conditions the images should be characterized quantitative by some parameters. Four parameters are useful in considering the image quality: the spatial resolution Δx, the time resolution Δt, the noise σ_{bg} and the contrast C. The spatial resolution Δx can be defined as the distance at which two structures can be distinguished, the time resolution Δt is the exposure time of the image. The noise σ_{bg} is the mean graylevel amplitude of the statistical fluctuations of a homogenous area. The contrast C is the graylevel difference between two structures.

Measurements

The aim of the experiments was to investigate the behavior of a fast CCD camera detector by measuring the image noise σ_{bg} for different exposure times Δt. The effect of snapshot accumulation by using software post processing of the images (stroboscopic method) was investigated too.

The measurements were performed at the high-flux measuring position at the V7 (CONRAD) instrument. The available high neutron flux of ~ 10^9 n/cm^{2}s allows radiography experiments with very short exposure times down to 100 µs.

Since the beam divergence is defined by the neutron guide at this beam line [1], the image spatial resolution Δx is determined by the distance between the sample and the detector. The used distance was 3.5 cm which gives a fixed resolution Δx of ca. 500 µm. Other fixed parameter is the image contrast C due to the fact that we used the same sample for all of the measurements – a stationary model air craft engine.

The used detector system was based on the 12-bit triggered CCD camera Sensicam qe double shutter 1376x1040 pixels with a fast electronic shutter allowing exposure times down to 500 ns. The image obtained by the LiZnS scintillator was projected via a mirror and a lens system onto the CCD chip.

The results for three exposure times 0.4 ms, 10 ms and 40 ms and different number accumulated snapshots using the stroboscopic method are shown in Fig. 1. The number of the accumulated snapshots is shown beside the symbols in the graph. The total measuring time was calculated as the number of the added up snapshots multiplied by the exposure time for one snapshot. The standard deviation of the pixel values was calculated for a defined ROI in the final image (see Fig. 2).

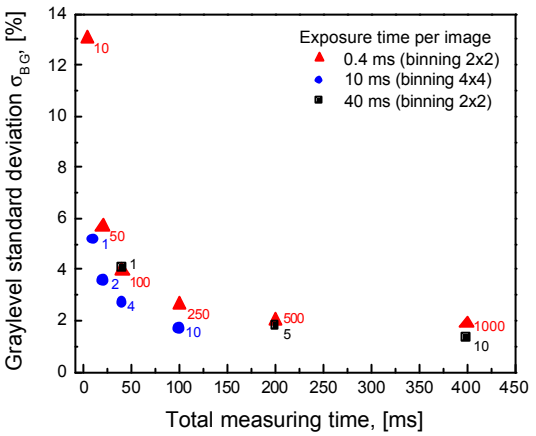


Fig. 1 Statistical characteristics of real-time images recorded at different detector settings.

The final images for different number of accumulated snapshots are shown in Fig. 2.

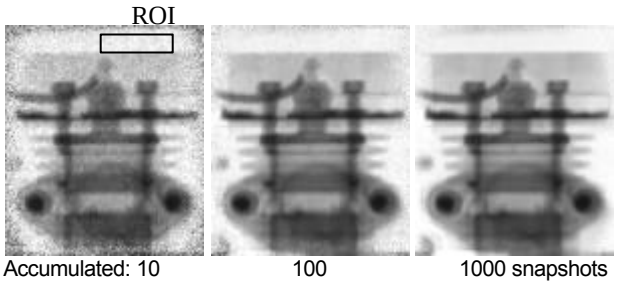


Fig. 2 Images obtained after adding up of different number of stroboscopic snapshots. Exposure time per snapshot: 0.4 ms. The used ROI for the calculation of σ_{bg} is shown in the first image.

[1] N. Kardjilov, A. Hilger, M. Dierik, B. Masschaele, Real-time imaging with cold neutrons, BENSC Experimental Reports 2003, 209

BENSC	**EXPERIMENTAL REPORT** **Testing a crystal for tomographic applications**	Proposal N° PHY-04-1078-5 LT Instrument **E8** Local Contact M. Strobl, W. Treimer
Principal Proposer: W. Treimer TFH/HMI; M. Strobl, TFH/HMI Experimental Team: M. Strobl, TFH/HMI Berlin		Date(s) of Experiment Mar/Apr 2004

Date of Report: Jan. 2005

Introduction

A new perfect Si single crystal monochromator has been installed at E8 instrument position. The crystal was cut for asymmetric reflection by the [111] crystal planes having an angle of 42° to the crystal surface. Hence the asymmetry factor b = -0.056 and the beam cross section reduces from 50 mm x 45 mm to 50 mm x 2.5 mm for a Bragg angle of 45° and a wavelength λ= 0.45(2) nm. This crystal was tested for tomographic purposes i.e. flux density and divergence respectively the collimation ration L/D have been determined. The principal idea was to use this monochromator for conventional attenuation contrast tomography involving the advantages of a monochromatic beam. These are mainly a higher contrast sensitivity and to avoid beam hardening (artefacts), both because the attenuation is wavelength dependent. On the other hand there is a gain in the flux density by the reduction of the beam cross section. Later on it was successfully applied for tomographic purposes reported in different reports within this issue.

Measurements

Open beam measurements have been recorded at different distances from the monochromator. From the images the beam divergence could be estimated to be between 0.15° and 0.2° horizontally and app. 0.24° in vertical direction. Fig. 1 shows the beam at ~2.5 m distance from the crystal. It is clearly possible to identify the overlapping (caused by divergence) front and backface reflections. For tomographic imaging a cross section of 2 x 5 cm^2 or 1.5 x 6 cm^2 can be used although the intensity distribution is inhomogeneous. The flux density of the backface reflection is approximately 2/3 of the more intense frontface which can be given with app. 1 x $10^4 cm^{-2}s^{-1}$. Then measurements with a Gd plate in the beam were recorded and from the horizontal and vertical edges the modulation transfer functions (MTF, Fig.2, 3) have been deduced. This enables to determine the spatial resolution for radiographic and tomographic measurements. Involving the sample detector distance the collimation ratios and the divergence can be calculated as well.

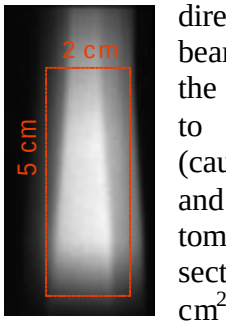


Fig.1 Open beam

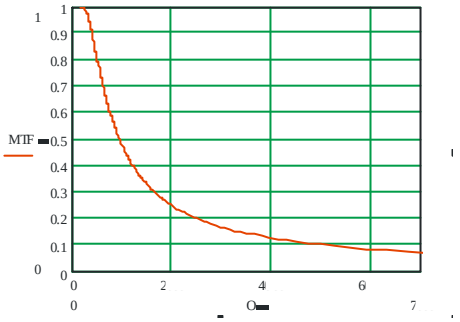


Fig. 2 Vertical MTF (x-axis: line pairs/mm)

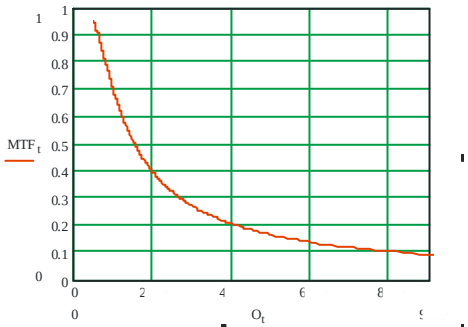


Fig. 3 Horizontal MTF (x-axis: lp/mm)

The results are vertical: L/D = 250, 5 lp/mm and F_{div}= 0.22°; horiz.: L/D = 400, 8 lp/mm and F_{div}= 0.14° although calculations for the guide would give poor 0.8° divergence and hence L/D = 70 only. Spatial resolution of 125 resp. 200 µm can be achieved.

This work has been supported by BMBF 03TRE9B6.

BENSC	**EXPERIMENTAL REPORT** **Synchrotron tomography study on disc chopper coatings**	Proposal N° **EF** Instrument **Beamline**BESSY Local Contact A. Haibel
Principal Proposer: Experimental Team:	J. Peters, HMI Berlin J. Peters, HMI Berlin A. Haibel, HMI Berlin A. Rack, HMI Berlin	Date(s) of Experiment Feb. – Dec. 2004

Date of Report: 7.12.2004

Disc choppers (see fig. 1) allow for the production of well defined neutron pulses and the application of the time-of-flight technique at a continuous source. To guarantee for the desired cut-out of the neutron pulse by the chopper window, the surface of the disc has to have a neutron absorbing coating, for instance gadolinium or boron ^{10}B. The carrier substance of modern discs is often composed of CFRP (carbon fibre reinforced plastic) epoxy. The absorption of the coating depends on the material, its thickness and the homogeneity of the coating layer. A typical requirement is an absorption of > 99.99% at wavelengths ≥ 0.7. These values are also expected for the choppers of the instrument EXED at the HMI.

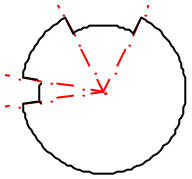


Fig. 1: *Schematical representation of a disc chopper with two windows.*

To check the homogeneity of the coating layer, a tomography study has been carried out at the BAMline at BESSY on three samples with two absorbing coatings, boron and gadolinium. The spatial resolution amounted to 3.6 µm at an incident energy of 15 keV for boron and 30 keV for gadolinium. 900 pictures were taken with an angular increment of 0.2° and a total sample rotation of 180°.

The first measurement (Fig. 2) shows an epoxy support layer (thickness 1.5 mm) coated with ^{10}B layers with a thickness of 0.3 mm on both sides. On the left hand side a coating with various pores is shown, whereas on the right hand side the very precisely produced layer looks homogeneous.

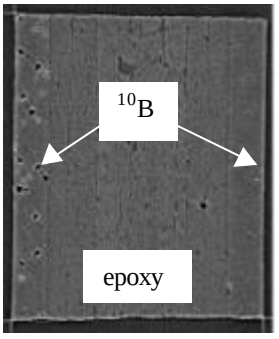


Fig. 2: *Tomographic 2D slice (2x2.5 mm). The homogeneous boron layer can be recognized at the right whereas the left layer shows various pores. Pores with diameters of £ 0.05 mm are admitted by the supplier.*

A second sample, shown in Fig. 3, has an absorbing layer of gadolinium only on one side (thickness 1.064 mm). Various pores are detected, too.

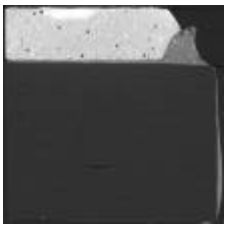


Fig. 3: *Tomographic 2D slice (4x4mm). The gadolinium layer corresponds to the light slice. Various pores in the coating material are detected, too.*

In Fig. 4 a tomographic image of the chopper coating material gadolinium of a real window cut-out is plotted.

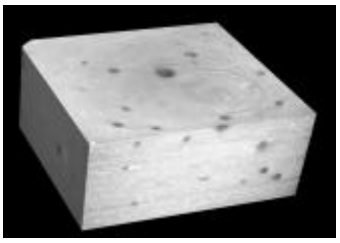


Fig. 4: *Tomographic picture of the chopper coating material gadolinium (1.5x1.5x1mm).*

In all samples pores with a size of 20 to 120 µm were found (see Fig. 5). While in the chopper material made of ^{10}B (red) more small pores and a small pore size distribution occur, the gadolinium chopper material (green) shows a broad pore size distribution and larger pores. For the third chopper material (blue), the lowest porosity was found.

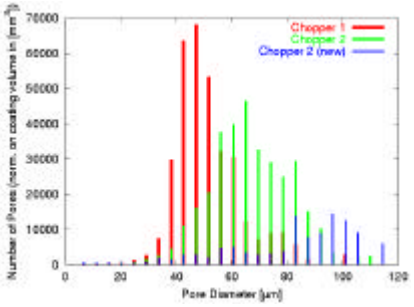


Fig. 5: *Pore size distribution of the three investigated coatings.*

Furthermore in this latter material the pore size distribution is homogeneous enough to guarantee for sufficient absorption .

Theoretically, gadolinium is the better absorber for higher wavelengths (> 0.85 Å), however at these wavelengths the absorption is already that high that all in all boron works more effectively.

BENSC	**EXPERIMENTAL REPORT** **Divergence investigations for 3D refraction contrast tomography**	Proposal N° PHY-04-1074-LT Instrument **V12a** Local Contact M.Strobl, W. Treimer
Principal Proposer: M.Strobl, W. Treimer, TFH/HMI Berlin Experimental Team: M. Strobl, TFH/HMI Berlin		Date(s) of Experiment März, April 2004

Date of Report: 9.01.05

Introduction

Within recent years the method of refraction contrast tomography could be developed successfully at the V12a diffractometer [1,2]. However, this was done without vertical resolution. For most applications a three dimensional tomographic resolution is necessary and it could be shown already that three dimensional resolution is possible as well [3]. While for the horizontal resolution a slit scan defines the resolution, in vertical direction the resolution is dependent on the beam divergence and the newly required 2D detector. Therefore these parameters have been investigated.

Experiments

For that purpose the modulation transfer function (MTF) has been determined from measurements with two different detectors and at different beam conditions. A highly absorbing Gd plate of 250 µm thickness has been used to measure the edge spread function from which the MTF could be calculated. The detectors used were on one hand a state of the art scintillator-CCD-camera system [4] and on the other hand a He3 filled wire chamber detector. In the case of the CCD detector, which provides higher spatial resolution, two different measurements have been performed, with and without a Si wafer collimator (from NOB)[5]. The collimator reduced the vertical divergence to approximately 7 min of arc.

Results

The highly monochromatic flux in the instrument is with approximately 1.2 x 10^3 $cm^{-2}s^{-1}$ very low for tomographic purposes. Therefore exposure times are relatively long. The He3 detector provides a higher efficiency and lower noise (only statistic noise and background) but the resolution is limited. The CCD detector on the other hand has a lower efficiency but as mentioned a higher resolution of at least theoretically app. 100µm. Furthermore the noise is worse as there is additionally read-out noise and dark current from the CCD and a high ? contamination of the recorded images.

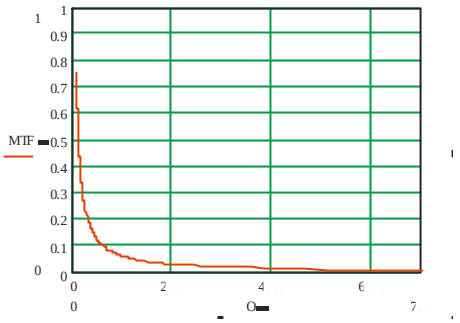


Fig.1 MTF of 2D He detector (x-axis line-pairs/mm)

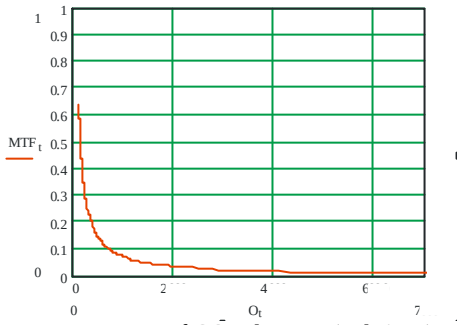


Fig.2 MTF of CCD detector (x: lp/mm)

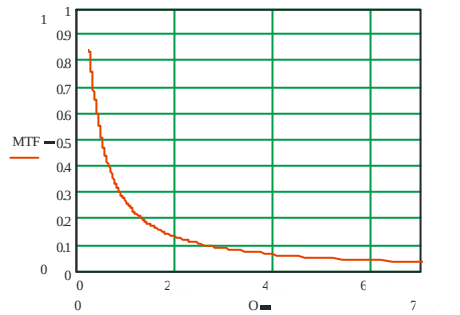


Fig.3 MTF of CCD detector with add. collimation (x: lp/mm)

While for measurements without collimation the resolution is with 0.6 and 0.7 lp/mm for the He resp. the CCD detector comparable there is a huge improvement to 2.6 lp/mm with collimation and CCD. However, collimation reduces the flux down to app. 20%.

This work has been supported by BMBF 03TRE9B6.

References

[1] Treimer, W. et al., Appl. Phys. Lett. 83, 2, 2003
[2] Strobl M. et al., BENSC-Rep. 2003, p.227
[3] Strobl, M. et al. NIMB 222, 2004, p 653
[4] Strobl, M., Diss., TU Wien, 2003
[5] Strobl M. et al., BENSC-Rep. 2003, p.230

	EXPERIMENTAL REPORT **Inelastic Neutron Scattering by Ultrasound. Research by Bonse-Hart Diffractometer**	Proposal N° PHY-04-1044 Instrument V12b Local Contact W.Treimer, M.Strobl
Principal Proposer: Experimental Team:	E.Iolin, Institute of Physical Energetic, Riga E.Iolin, Institute of Physical Energetic, Riga M.Strobl, Hahn-Meitner Institute, Berlin W.Treimer, Hahn-Meitner Institute, Berlin L.Rusevich, Institute of Physical Energetic, Riga P.Mikula, Nuclear Physics Institute, Rez near Prague	Date(s) of Experiment 12.07 - 23.08.2004

Date of Report: 09.11.04

Neutron double crystal diffractometers (DCD) are applied for Ultra Small Angle Scattering investigations. It is known that high frequency (h.f.) ultrasound (AW) applied to perfect crystals leads to increased intensities *Ih* in the diffracted beam. However this increase is accompanied by a loss of resolution. Recently [1] we recorded ultrasonic phonon satellites from exciting the analyzer crystal of a DCD. We continued exciting analyzer AND monochromator crystals simultaneously and observed increased intensities *Ih* and a contrast improvement concerning the satellites [2]. Here we are continuing research of AW application to DCDs and especially for the up-to-date use of many bounce crystals.

We excited h.f. AW in single bounce silicon monochromator and observed AW satellites by means of a 7-bounce analyzer crystal. We were able to record satellites when two transducers at the monochromator were excited simultaneously by two different generators with approximately the same frequency of 70.3 MHz. (Fig.1). This result is important because it is difficult to design large h.f. transducers and to excite a one-mode i.e. coherent AW field in a big crystal.

Furthermore we investigated Back-Face (BF) diffraction [3] at a Si single crystal in order to examine possible deformations created by the cooplant between transducer and crystal. We found that this deformation is moderate and observed satellites in the BF regime (Fig.2).

At last we installed transversal AW transducers on a triple-bounce analyzer and applied h.f. AW. We again observed satellites but with moderate contrast (Fig.3). The contrast and the intensity could be increased by additional excitation of the single bounce monochromator crystal with h.f. AW.

[1] E.Iolin et al., Nucl. Instr. & Methods in Phys. Research A 529, 152, 2004.

[2] E.Iolin, Zh. Tekhn.Fiz. Pis'ma **15,** 52,1989.

[3] Agamalian, M. et al, Phys. Rev. Lett., 81, 602, 1998.

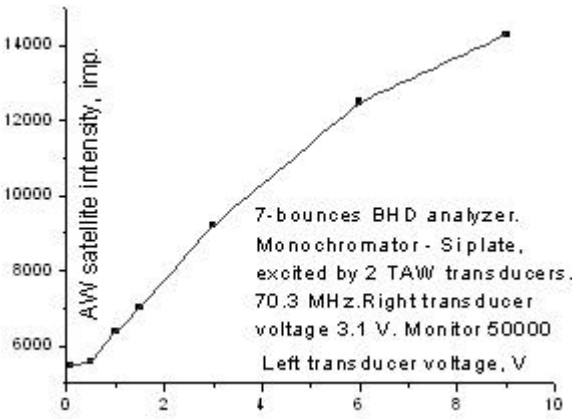


Fig.1 .TAW satellite intensity vs. transducer voltage

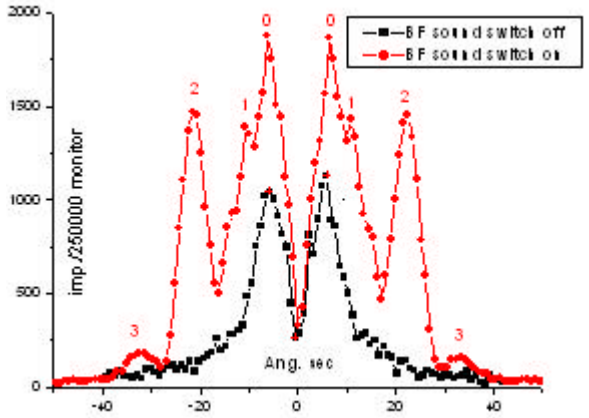


Fig.2. BF scattering of monochromator, TAW, 70.3 MHz. 7-bounces BHD analyzer.

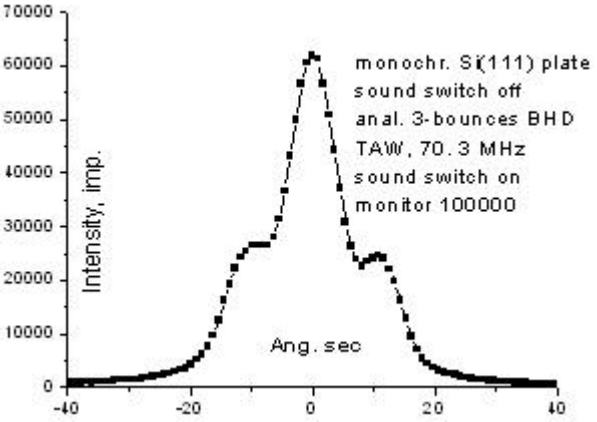


Fig.3 Ultrasonically excited 3-bounce analyzer

BENSC	**EXPERIMENTAL REPORT** **Test of radial cavity neutron spin analyser**	Proposal N° PHY-04-1084 / EF Instrument **V14** Local Contact Th. Krist
Principal Proposer: Experimental Team:	Péter Falus, ANL Argonne, USA Péter Falus, Gian P. Felcher ANL Argonne, USA Alexei Vorobiev , MPI-MF Stuttgart Thomas Krist, HMI Berlin	Date(s) of Experiment 16.-24. 9. 2004

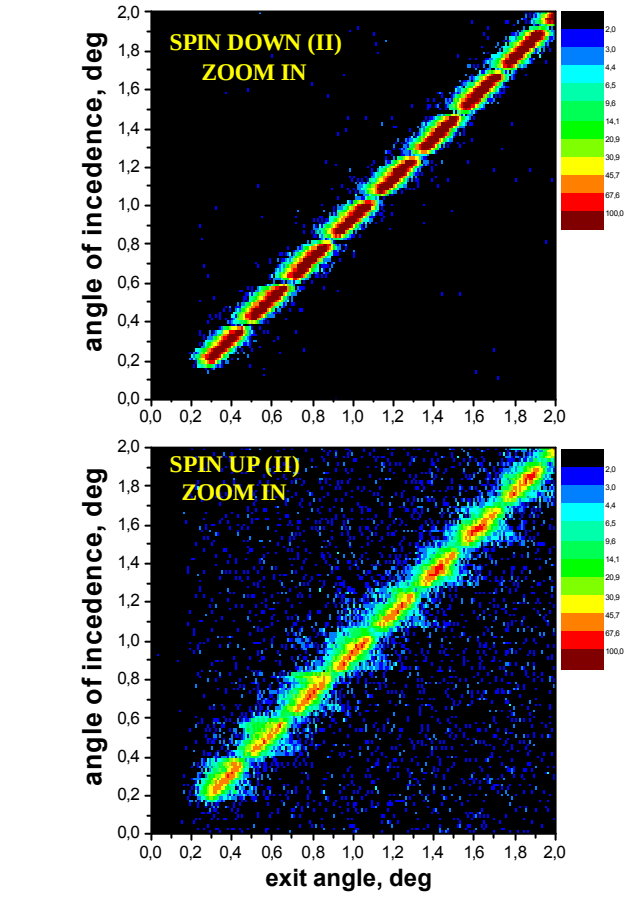
Date of Report: 10. 1. 2005

The aim of this measurement was to test the new spin polarization analyzer for the EVA-SERGIS beam line at Institute Laue Langevin which was built in Berlin. The spin analyzer had to fulfill the following conditions: It should select one of the two spin states of a neutron beam of wavelength 5.5 Å impinging on a horizontal sample and reflected or scattered from the sample. The spin shall be analysed for all neutrons scattered into a detector with an area of 190mm x 190mm at 2.7m behind the sample.

The tests were done at the HMI V14 beamline by illuminating the analyser with a neutron beam of 3x80 mm^2 of 96.6% polarization and 4.7 Å wavelength. The transmitted intensity was recorded by a 2D gas detector from the EVA beamline. Since the analyser has approximately the geometry of a section of cylinder, the illuminated area was changed by rotating the analyser around the sample position. The transmission for the two spin components, the flipping ratio and small angle scattering were recorded while scanning the incoming beam on the analyser. The total intensity recorded on the detector is noted on Fig. 2. versus the position on the analyzer . It is clear from this plot that due to the stacked construction the intensity is blocked at regular intervals. Careful inspection shows that the transmission for the good spin component is more than 0.5 for 65% of the detector area and the corrected flipping ratio is more than 55 for 65% of the detector area. If we note the intensities versus the incident angle (position on the analyser) and the exit angle (position on the detector), we can analyse if the line shapes get distorted by scattering in the analyser. On Fig. 1. the intensities are represented by different colours. An ideal analyser would only have intensity in the diagonal, any off diagonal scattering is small angle scattering and should be eliminated. Although some scattering is visible, it is notable that the Fig 1 plots the logarithm of the intensities and this final analyser design has very small scattering intensities.

The result of these measurements is that analyser fulfills the above mentioned conditions. While large areas of the analyser are blocked by the stacked design, doing each measurement in two steps, shifting the analyser between measurements we can have composite results which allow for a flipping ratio over 55 and transmission above 0.5 for the full area of the 190x190 mm detector.

Fig. 1 (Next column) Transmitted neutron intensity plotted versus incoming and outgoing angle.



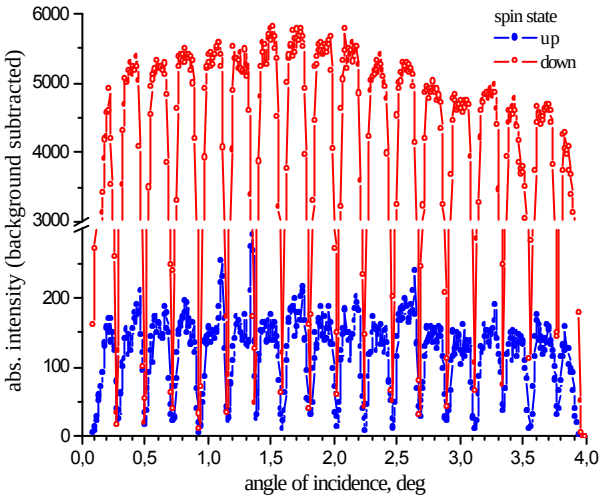


Fig. 2 Transmitted intensity versus position on analyzer. Red – spin down component, blue – spin up component, contaminated by 1.7% of the spin down intensity (94 counts).

	EXPERIMENTAL REPORT **Polarising bender used in transmission**	Proposal N° EF Instrument **V 14** Local Contact Th. Krist
Principal Proposer: Experimental Team:	Th. Krist, HMI Berlin Th. Krist, HMI Berlin	Date(s) of Experiment 2004

Date of Report: 10. 1. 2005

A polarising solid state bender without absorbing layers works as a spin splitter: it transmits both components which are distinguished by different angles and one spin state can be selected by putting a collimator behind the bender at the angle of the beam to be used. In particular, the non deflected component can be chosen thus giving a polarizing device which polarizes a beam without changing the flight path of the desired neutrons.
Such a system was built and tested at BENSC.
For the bender silicon wafers with the dimensions of 50 mm high, 54 mm long and 0.16 mm thick were coated on one side with FeCo-Si supermirrors with m=2.3, where m denotes the ratio of the critical angle of the supermirror to the critical angle of natural nickel. 125 of these wafers were put into a holder which deflects the middle of this stack by one wafer thickness to close the direct line of sight. The supermirrors are subjected to a magnetic field of 1 kG.
The collimator was built from silicon wafers with the dimensions of 50 mm high, 33 mm long and 0.2 mm thick which were coated with a Gd layer. Collimator and bender both cover a beam width of 20 mm.
Experiments were performed at the BENSC reflectometer V14 with a polarised neutron beam and a wavelength of 4.72 Å, a width of 0.4 mm, a divergence of 0.035° and a polarisation of 96.6%. A ^{3}He detector with a slit of 8 mm width was placed 2 m behind the bender. The background was $5 * 10^{-4}$ of the direct beam.
Fig. 1 shows the rocking curve for the collimator normalized to the direct beam. The FWHM is 0.37°. For a channel width of 0.2 mm this corresponds to an effective channel length of 31 mm. The transmission reaches in the maximum 83.5%.
Fig. 2 shows the transmission through the bender at a fixed angle normalized to the direct beam when it is moved perpendicular to the beam, thus testing the homogeneity of performance over the width of the stack of wafers. The transmission amounts to 67.2 ±3.2% over a width of 19mm, i. e. the relative variations amount to ±4.6%. The average flip ratio is above 100.
Fig. 3 shows the rocking curve for the combined system of bender and collimator normalized to the direct beam. Here, the bender was set at the optimal angle and the collimator was put a few cm behind it at the angle with the highest transmission. After this alignment the whole system was rocked in the beam.
The FWHM is the same as for the collimator found in Fig. 1. The transmission reaches in the maximum 54.2%. The flip ratio is above 100 for most of the angular range, the mean value of the flip ratio weighted with the transmitted intensity is 129.5.

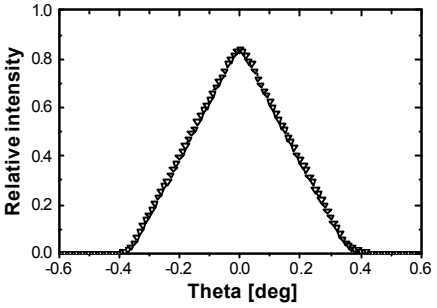


Fig. 1. Neutron intensity transmitted through the collimator described in the text, normalized to the incoming beam intensity.

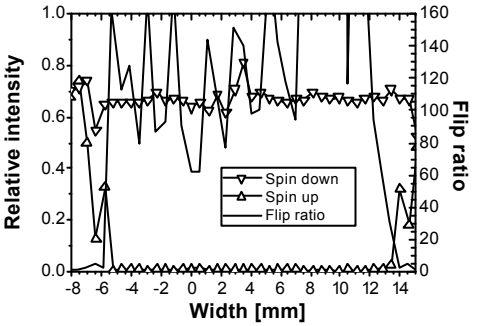


Fig. 2. Neutron intensity transmitted through the bender for both spin states together with the flip ratio for a movement of the bender perpendicular to the beam direction.

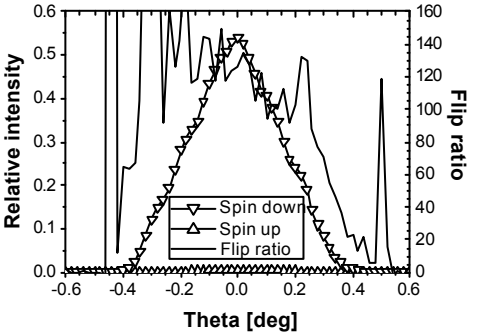


Fig. 3. Rocking curve for the neutron intensity transmitted through both the bender and the collimator, for both spin states together with the flip ratio.

	EXPERIMENTAL REPORT **Recent performance studies of the instrument EXED**	Proposal N° **EF** Instrument **EXED** Local Contact J. Peters
Principal Proposer: Experimental Team:	J. Peters, HMI Berlin J. Peters, HMI Berlin K. Lieutenant, HMI Berlin F. Mezei, HMI Berlin	Date(s) of Experiment Oct. – Dec. 2004

Date of Report: 16.12.2004

Detailed VITESS Monte Carlo simulations of the new time-of-flight powder diffractometer EXED at HMI allows us on the one hand side, to optimise some of the design parameters and on the other hand side and most importantly, to assess the expected performance.

Estimated resolutions could be confirmed by the simulations: The planned resolution of less than $2x10^{-4}$ is feasible for wavelengths above 4 or 5 Å, a resolution of less than $5x10^{-4}$ can be gained over the entire wavelength range using the Fermi chopper (see fig. 1).

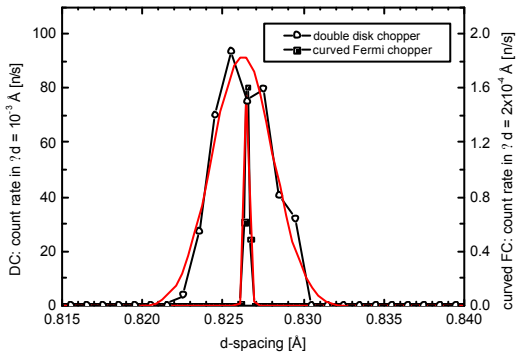


Fig. 1: *Normalised simulated powder pattern results for l = 1.65 Å with the double disk chopper (open circles) and the curved Fermi chopper (full squares) at a scattering angle of 2q = 177°±2°. Gaussian fits are shown as solid lines. The resolution is Dd/d ˜ 5.4 x 10⁻³ and Dd/d ˜ 3.8 x 10⁻⁴, respectively.*

The Monte Carlo simulations of the entire instrument allow for an estimation of the neutron flux at the sample (see fig. 2 which shows the flux for the wavelength bandwidth 0.7 Å < λ < 5 Å).

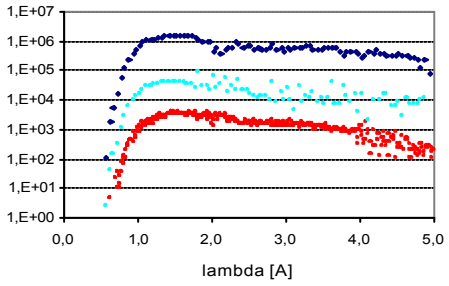


Fig. 2: *Flux at sample (in neutrons/s/cm²/Å) with the double disc chopper (DC), the curved Fermi chopper (FC curved, and the straight Fermi chopper (FC straight).*

The data collection times estimated on the basis of the simulation results also look very promising: standard measurements can be performed in less than 10 min, ultra high resolution measurements, which are currently out of reach for neutron scattering, in about 1.5 days. The data collection times of this instrument are similar to those calculated for the powder diffraction instrument POWGEN3 in the high resolution configuration ($\Delta d/d = 10^{-3}$) planned for the new spallation source SNS in Oak Ridge/US, where typical times of about 120 s for an equivalently simple sample were found.

Finally, $TbMnO_3$ data measured monochromatically at E9 (courtesy of D. Argyriou) were treated with a Rietveld refinement program (FULLPROF) to get the crystal structure. These results were introduced into the VITESS simulation of EXED to get the same powder diffraction pattern (see fig. 3). Both spectra were divided by the corresponding Lorentzian factor and finally the EXED time-of-flight spectrum was reduced by the flux spectrum to make a comparison possible. The simulated data contain no background. One recognizes the peaks at the theoretically predicted positions (green markers), but the higher resolution of EXED, which allows for the seperation of double peaks (small figure).

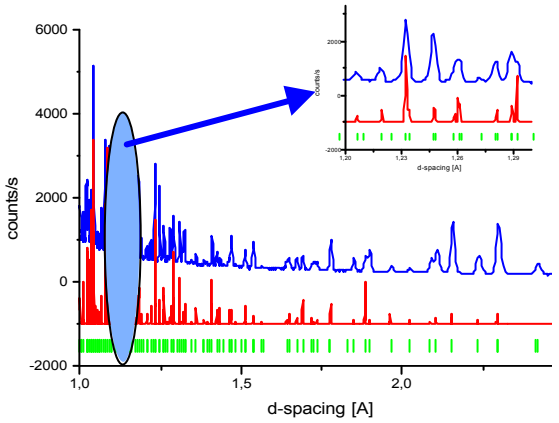


Fig. 3: *$TbMnO_3$ powder diffraction pattern measured at E9 (blue), simulated with the EXED parameters (red) and predicted peak positions (green).*

References

J. Peters, K. Lieutenant, D. Clemens, F. Mezei, Proc of the "European Powder Diffraction Conference" (Prag, 2. - 5. Sep. 04), submitted for publication.

K. Lieutenant, J. Peters, F. Mezei, J. Neutron Res., submitted for publication.

	EXPERIMENTAL REPORT **Study of PNR in relaxor ferroelectrics $PbMg_{1/3}Nb_{2/3}O_3$ by quasielastic neutron scattering**	Proposal N° PHY-02-428 Instrument E1 Local Contact J. Klenke
Principal Proposer: Experimental Team:	A. Naberezhnov, PTI S-Petersburg, Russia J. Klenke, HMI Berlin S. Vakhrushev, PTI S-Petersburg, Russia	Date(s) of Experiment 27/03 – 8/04 2004

Date of Report: 26/12/2004

Relaxor Ferroelectrics (RF) demonstrate a diffuse maximum of dielectric permittivity of extremely high value in a large temperature interval. Lead magnoniobate $PbMg_{1/3}Nb_{2/3}O_3$ can be consider as a model relaxor. At the freezing temperature T_g (~ 230 K) if exhibits the phase transition into a glass-like state as evidenced by divergence of nonlinear susceptibility [1] and nonergodic phenomena [2].

There are several theoretical approaches to describe the properties of relaxors, but practically all of them are based on the assumption of the existence of slowly relaxing polar nanoregions at temperatures much above T_g. Firstly the conception of PNR was proposed by Burns and it was shown that in PMN PNRs are formed at some temperature T_d (~ 630 K - so-called Burns temperature) much higher than T_g. Later it was demonstrated that the formation of the PNR is related to the TO mode softening [3]. However no exact understanding of the microscopic mechanism of the PNR formation exists up to now. The most striking difference of the PNR in relaxors from the precursor clusters in the most compounds undergoing PT is essential difference of the eigenvectors of the soft mode and PNRs. Analyzing the intensity of the diffuse scattering (DS) in the vicinities of the different Bragg peaks one can obtained the information about the eigenvectors of the ionic displacement related to the appearance of this scattering.

The principal idea of this experiment was to study the temperature evolution of 2D-plots of DS in the temperature range from RT up to T_d in the vicinity of several reciprocal lattice points. The measurements have been performed at λ = 2.3971Å and λ = 1.19855Å and at T= 300 K, 347 K, 392 K, 447 K, 494 K and 528 K.

We have observed two components of diffuse scattering: the anisotropic one arising upon cooling well below T_d and the really transverse component.

The 2D-map of anisotropic scattering in the vicinity of the (h00) points looks like a “butterfly” profile elongated in the [110] directions (Fig. 1). On heating to T_d the intensity of this component has essentially decreased and practically disappeared at high temperature. To clarify the possible origin of this scattering, we suggest that the local ferroelectric polarization in PMN is accompanied by local micro-deformations. Then these elastic deformations should result in the Huang scattering. Using the standard approach [4] for describing the wave vector dependence of the scattering intensity and known elastic constants we have constructed the expected distributions for Huang scattering. In Fig.1 the calculated intensity map is indicated by solid curves and is in a good agreement with the “butterfly” shape. So one can believe that this component is the Huang scattering and could be explained by static micro-deformations.

1 – E.V. Colla, E.Yu. Koroleva, N.M. Okuneva, S.B. Vakhrushev J. Phys.: Condens. Matter 4, 3671 (1992)

2 – S. Vakhrushev, B. Kvyatkovsky, A. Nabereznov, N. Okuneva, B. Toperverg Physica B, 156&157, 90 (1989)

3. A. Naberezhnov, S. Vakhrushev, B. Dorner, D. Strauch, and H. Moudden, *Eur. Phys J.***B 11**, 13 (1999)

4. M.A. Krivoglaz „Theory of X-ray and thermal neutron scattering by real crystals“, 1969, New York: Plenum

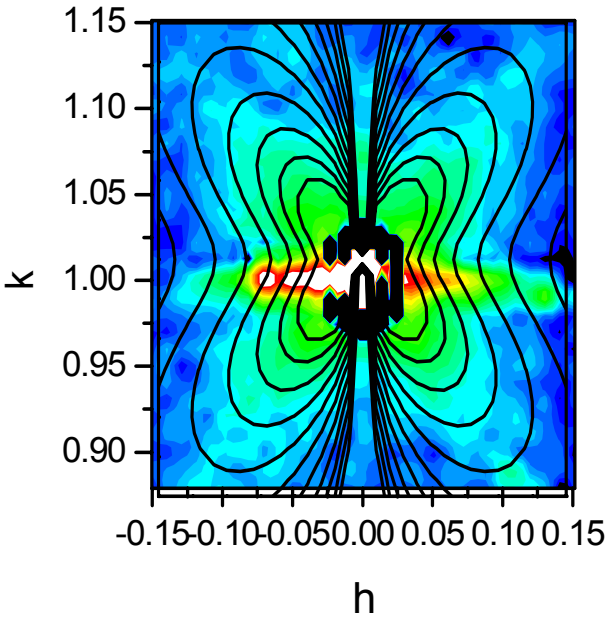


Fig. 1 PMN RT, Black curves - calculated Huang scattering.

	EXPERIMENTAL REPORT **Melting-freezing phase transition in nanostructured mercury**	Proposal N° PHY-01-1443 Instrument E2 Local Contact: J.- U. Hoffmann
Principal Proposer: Experimental Team:	A. Naberezhnov, PTI S-Petersburg, Russia J.- U. Hoffmann, HMI Berlin M. Tovar, HMI Berlin	Date(s) of Experiment 18/05 –25/05 2004

Date of Report: 26/12/2004

The physical properties of materials in a restricted geometry are one of the most interesting topics of the modern solid state physics. The melting-freezing phase transition (PT) of liquid metals in a confined geometry revealed a row of very interesting phenomena. It is shown that the melting and freezing temperatures for In within porous silica with pore diameters between 6 and 141 nm are the always less than the corresponding bulk values and are proportional to inverse diameter of silica pores [1]. The study of melting-freezing PT for Ga in 4 nm porous glasses has shown essential reduction of freezing temperature (T_f) (down to 236 K at cooling) and large temperature hysteresis (~30 K) at melting-freezing process. The widths of temperature span of melting and freezing differ significantly: the freezing process takes place within a narrow interval (step-wise character), whereas the melting process occurs in a wide range of no less 15 K. However at the same time there are no direct experimental data about temperature evolution of structure at the melting-freezing PT for confined metals within porous glasses, although this PT is interesting since usually metals do not wet the porous matrices. Therefore they are more independent of the matrix than wetting liquids.

We have studied the temperature evolution of structure of mercury embedded within porous 7 nm glasses at the freezing-melting PT by neutron diffraction in temperature diapason from RT down 180 K on cooling and heating. The liquid Hg was embedded within porous matrices under high pressure. Unfortunately ~20 % of Hg flown out after taking down the pressure during the storage of samples and ~15 % of mercury formed macroscopic (up to 0.1 mm diameter) drops within internal cracks of porous matrices.

At RT no diffraction peaks were observed in the diffraction patterns. On cooling at temperature diapason 227 K – 208 K we have observed the narrow Bragg peaks from bulk material with the width corresponding to the experimental resolution. At low temperature the additional broad scattering from isolated nanostructured Hg was appeared. These peaks were essentially wider than experimental resolution. The average size of these nanoclusters was about 8 ± 1 nm and corresponded to the mean pore diameter. On heating the additional scattering was practically disappeared above 222 K, and up to the bulk melting temperature the narrow Bragg peaks were observed again. The width of additional scattering did not depend on temperature neither on cooling nor on heating within statistical errors.

We have analyzed the temperature dependences of the intensity of the additional scattering and the obtained results are quite different from those for bulk mercury [2] or thin mercury films [3]. The freezing and melting transitions are essentially broaden and the temperature hysteresis is about 20 K. Using the result about the temperature dependence of average size of mercury nanoparticles we can state that broadening of Bragg peaks due to possible anomalous thermal motions of nanostructured Hg is essentially smaller than the broadening due to size effect.

The obtained results are in a good agreement with our preliminary data [4].

References

1. K.M. Unruh, T.E. Huber, C.A. Huber Phys. Rev. B48, 9021 (1993)
2. A.R. Ubbelode, Melting and Crystal Structure (Clarendon Press, Oxford, 1965)
3. G.S. Zdanov, Fiz. Tverd. Tela (Leningrad) 18, 1415 (1976) [Sov. Phys Solid State 18, 819 (1976)]
4. Yu.A. Kumzerov, A.A. Nabereznov, S.B. Vakhrushev et al, Phys. Rev. **B 52**, 4772 (1995).

	EXPERIMENTAL REPORT Neutron tomography of geological samples	Proposal N° PHY-04-1074-9 LT Instrument **E8** Local Contact M. Strobl
Principal Proposer: Experimental Team:	M. Strobl, TFH / HMI Berlin, J. Walter FZJ/GZG M. Strobl, TFH / HMI Berlin	Date(s) of Experiment Sep 2004

Date of Report: Jan 2005

Introduction

Two carbonate stone samples should be investigated by tomography concerning their microstructures. One of them, sample (a) a marble, consists of crystalline calcite grains with sizes of some hundred µm (Fig. 1), while in the other sample the calcite is more homogeneous but there are some inclusions of mica minerals. As also the pore space between the different grains are of interest but beyond the resolution of neutron tomography complementary synchrotron tomography measurements have been performed. However the results are not available yet.

Measurements

Both samples have been measured in a single tomographic run at the E8 instrument. 100 projection images have been taken over an angle of 180°. The diameter of the cylindrical samples was with 20 mm a bit too big for the beam cross section with approximately the same width. Therefore just an inner part with a radius of 12 mm could be reconstructed without artefacts. The presented tomographic reconstructions represent a square cross section of 10 x 10 mm^2 and a height of 50 mm (Fig. 2).

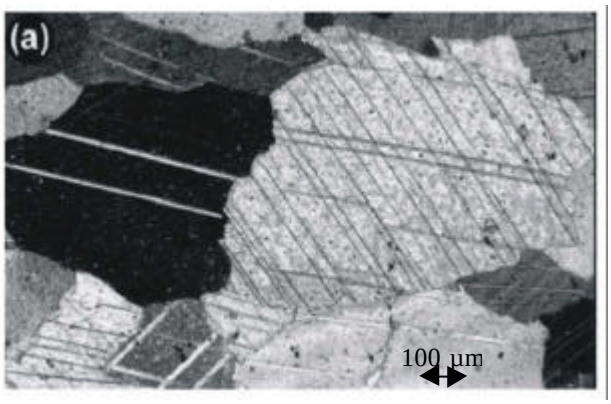


Figure 1 microscopic image of grains of first sample (a)

The result of the reconstruction was surprising especially concerning the first sample (a) which is the upper part of the reconstruction. Although all the grains are of the same phase a grain-like structure was found with clearly higher and less absorbing “grains”.

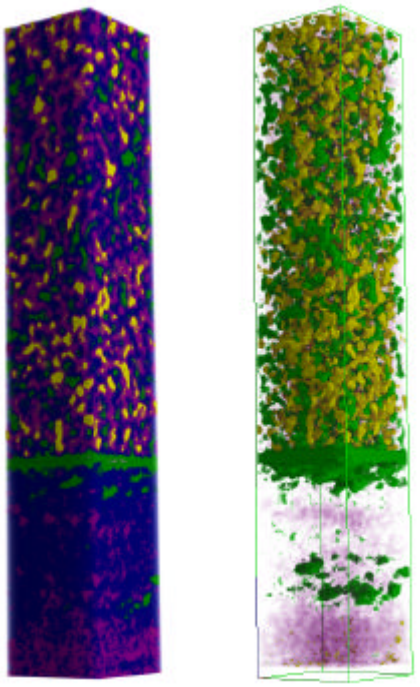


Figure 2 reconstruction of geological samples

In the right side of Figure 2 the medium absorbing parts are defined transparent. There is a green coloured area between the upper and lower part of the reconstruction which is the tape by which the samples are fixed together. In the lower part, the second sample, only the mica minerals remain visible as they are stronger absorbing and hence remain as green coloured areas.

	EXPERIMENTAL REPORT **Investigation of the low energy vibrational density of states in $Fe_{0.3}Y_{0.7}$ and $Fe_{1-x}Sn_x$ (x=0.3, 0.4 and 0.5) ribbons**	Proposal N° PHY-03-0316 Instrument **V3** Local Contact Dr. J. Pieper
Principal Proposer: Experimental Team:	Prof. Dr. Werner Keune, Universität Duisburg-Essen, Duisburg, Germany Prof. Dr. Werner Keune, Uni-Duisburg-Essen Mr. Balaram Sahoo, Uni-Duisburg-Essen Dr. V. Kuncser, NIPM, Bucharest, Romania Dr. J. Pieper, HMI Berlin (BENSC), Germany	Date(s) of Experiment 16.02. – 19.02.2004

Date of Report: 10.01.05

The low energy part of the vibrational density of states (VDOS) of crystalline materials obey the Debye law [$g(E) \propto E^2$]. However, amorphous materials are found not obeying the Debye law. The low energy region (0-10 meV) of the VDOS of amorphous materials show an excess density of states known as the 'boson peak'. The boson peak appears by plotting $g(E)/E^2$ versus E in the low energy region. The atomistic origin of the boson peak is still a mater of debate. Hence, this is the most attractive part of the VDOS in amorphous materials. Although these low energy excitations have been studied more widely in complex biological systems [1] they were observed earlier by inelastic neutron scattering on simple binary metallic glasses such as a-$Mg_{0.7}Zn_{0.3}$ alloy[2].

In the present experiment binary amorphous (a-) $Fe_{0.3}Y_{0.7}$ alloy ribbons were studied at 300 K and 77 K with improved statistics by inelastic neutron scattering (INS). This project is a continuation of the former proposal PHY-03-287. According to [3], two different incident neutron wavelengths of 2.0 Å (incident energy ~20 meV) and 5.1 Å (~3.2 meV) were chosen in order to measure INS spectra for energy gain and energy loss of the neutrons at room temperature. The corresponding elastic energy resolutions were 921 and 93 μeV, respectively. However, for the measurement at 77 K, only 2.0 Å was chosen. The Q-range for NEAT was: 2.0 Å: 0.77-5.8 $Å^{-1}$ and 5.1 Å: 0.3-2.3 $Å^{-1}$.

The sample was placed inside the cryo-furnace at V3 by putting the sample into the slab-shaped aluminum sample holder in argon atmosphere. It was sealed airtight by using indium. The sample and background (empty sample holder) spectra were measured, and preliminary analysis has been partly performed by the standard program at V3. We are in the process of completing the analysis. Figure 1(a) shows INS spectra of a-$Fe_{0.3}Y_{0.7}$ alloy ribbons obtained with an incident neutron wavelength of 2 Å at 300 K.

The density of vibrational states has been calculated and the boson peak has been discovered after preliminary analysis of the spectra. The peak position is found to be at about 4 meV.

Unfortunately, we could not use 3 days of our beam time to extend our measurements to related $Fe_{1-x}Sn_x$ samples due to an early reactor shutdown.

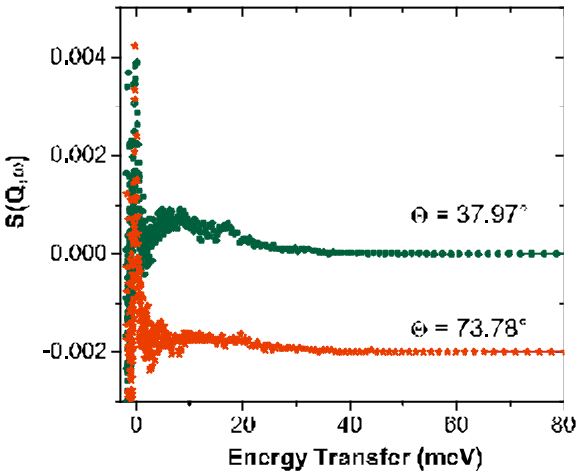


Figure 1.

INS spectra of a-$Fe_{0.3}Y_{0.7}$ alloy ribbons obtained with an incident neutron wavelength of 2 Å at 300 K. The spectra obtained for different angles are grouped into two with average angles of 37.97° and 73.78°. For clarity, the bottom spectrum has been shifted by -0.002 units.

References:

1. see for example, Orecchini A., Paciaroni A., Bizzarri A. R. and Cannistraro S., J. *Phys. Chem. B* (2001), **105**, p. 12150-12156 and references therein.
2. Suck H. B., and Rudin H., (1983) in: *Glassy Metals II*, Beck H. and Güntherodt H. J. (editors) *Topics in Applied Physics* Vol. **53** (Springer, Berlin) p. 217
3. Pieper J., Irrgang K. D., Renger G., Lechner R. E., *J.Phys.Chem.B* (2004), **108**, p. 10556

	EXPERIMENTAL REPORT **Molecular dynamics in triglycine sulphate by cold neutron spectroscopy**	Proposal N° PHY-03-326 Instrument V3 Local Contact Jörg Pieper
Principal Proposer: Experimental Team:	V.Tripadus, IFIN-HH Bucharest A.Radulescu, FRJ-2 Jülich J. Pieper, A. Buchsteiner HMI Berlin	Date(s) of Experiment 09-15.02.04

Using the V3 instrument from the BENSC –HMI we have measured the TOF neutron scattering spectra on a TGS powder sample at different temperatures, both below and under critical point. The measurements were carried out at 93 μeV resolution power, in the Q range allowed by the spectrometer. For every temperature we calculated the incoherent scattering law S(Q,?) using the standard programmes used for this device. TGS is a ferroelectric at room temperature. In this phase below 49.5°C the symmetry is monoclinic with space group $P2_1$ whereas above this critical point the structure gains additional symmetry planes in the space group $P2_1/m$. The elementary cell of TGS contains three distinct glycine molecules denoted with GI, GII and GIII. They are connected between them and SO_4 groups by a network of hydrogen bonds/1,2/. The crucial motions that are involved in phase transition are:

- NH_3-CH_2 reorientational motion of GI glycine molecule around an axis contained in the mirror planes b=1/4 or ¾; this is so cold the flip motion. The characteristic time of this motion is comprised in the range about $1.05 \div 0.85 \times 10^{-11}$s,
- rotational motion oscillations of NH_3 group around its main axis. The energy levels of this motion are associated with the widths of the Lorentz functions that fit the experimental quasielastic scattering law data. Their ratio was constant 4, that correspond to 0 $\rightarrow$2, 0 $\rightarrow$1,energy levels for hindered rotations of amino group in the TGS molecular lattice.

The analysis of the quasielastic line broadening suggests jump rotational diffusion behaviour in restricted volumes. The main parameters involved in this model are: the local diffusion coefficient D_{loc}, the rotational diffusion coefficient D_r, the mean residence time τ_r, the mean jump length r_0 and the dimension of the restricted space L. The values of these parameters obtained from the present experiment are summarised in the Table 1. The value of L was of about 5.5÷6Å. This value is in accordance with the EISF fitting data that presumes that the protons of NH_3- GI perform large amplitude rotational motions on a circle of radius R_1 (around 6 Å) whereas the CH_2-GI protons are rotating on a smaller radius circle R_2. (of about 4.5Å).

Besides these low energy transfer molecular motions, the neutron scattering TOF spectra contain also and other collective and individual motions of TGS lattice dynamics. From the inelastic part of the spectra we have calculated the generalised density of states in an energy range that comprises the acoustic phonon group and other higher energy modes. In Fig. 1 we present this spectrum measured at two temperatures: below and above phase transition critical point. Notable changes were observed in the acoustic part around 4 meV as well as in the range around 18 meV in the frequency spectrum.

T [K]	D_{loc} [10^{-5} cm^{-1}]	τ_r [10^{-12} s]	r_0 [Å]	D_r [10^{-5} cm^2 s^{-1}]
298	1.12	2.99	1.37	1.05
303	1.13	2.87	1.33	1.03
313	1.08	2.64	1.08	0.74
322	1.08	2.44	1.06	0.77
333	1.08	2.35	1.12	0.89
338	1.07	2.27	1.05	0.82

Table 1. The main dynamical parameters obtained from the quasielstic peak according to Hall- Ross model

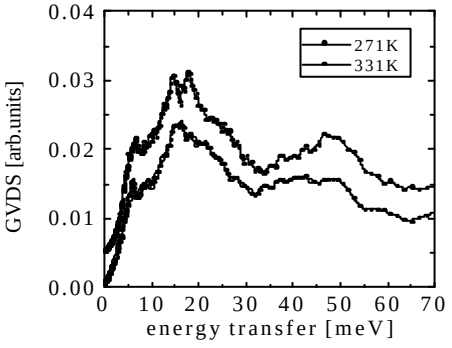


Fig.1. Generalised Phonon Density of States for TGS below and above critical point.

References

1. Genowefa Slorasek , A. Heurer, H.Zimmerman and U.Haeberlen, J.Phys.:Condens.Matter, 1 (1989) 5931-5954
2. Rajul Ranjan Choudhury, R.Chitra and M.Ramanadham, J.Phys:Condens.Matter 15 (2003) 4641-4650

	EXPERIMENTAL REPORT SANS studies on undercooled metals	Proposal N° EF-SF3 Instrument: V4 Local Contact A. Wiedenmann
Principal Proposer: Experimental Team:	O. Perroud, A.Wiedenmann, HMI Berlin O. Perroud, A.Wiedenmann, HMI Berlin	Date(s) of Experiment 15.06 – 22.06.2004 09.08 – 16.08.2004

Date of Report: 10.01.2005

Following the theoretical predictions of Frank in 1952 [1], an icosahedral short-range order should be energetically favoured in undercooled metallic melts. Due to the difficulties to process undercooled liquids up to now only very few direct experimental studies have been reported [2]. In order to determine the structure factor from the presumed icosahedral clusters in the liquid as a function of temperature, we choose to process pure Ni samples and $Cu_{86}Co_{14}$ alloys by in-situ SANS measurements. The liquid were processed without any container and undercooled by using the electromagnetic levitation technique. SANS measurements were carried out at the instrument V4. The electromagnetic levitation furnace of DLR Köln (Institut für Raumsimulation) has been adapted mechanically to the SANS requirements of the V4 instrument.

Sample temperatures had to be controlled manually. Due to the long-time measurement of SANS at different temperatures corresponding different metastable states of undercooled samples, we had to apply shift-work during the experiment. Due to the sample environment, to the sample preparation etc, it was not always possible to keep the samples in a liquid state below the melting temperature. The experiments were performed under high purity environmental conditions. Temperatures were measured by pyrometry. Temperatures up to 1600°C were reached during the experiment for the Ni sample and 1000°C for Cu-Co alloys. With some nickel samples, we achieved undercooling by about 300°C below the melting temperature.

The samples were prepared from constituents of purity better than 99.99%. The Ni samples having a mass of about 1,7 g were cut into cubes with a side of 5mm. The Cu-Co samples having a mass of about 1,3 g were prepared by premelting in an induction furnace into spheres of about 6mm diameter.

The radially averaged scattering intensity of the Ni-sample is plotted in Fig.1. Within the accuracy of the instrument for both the liquid state and the undercooled states the same scattering curves were observed. The background scattering as measured at the end of the in-situ sample treatment is also reported in Fig. 1. This rather high background probably results partly from the sample evaporated during the long term heating and condensed at the windows of the vacuum vessel. However, a clear SANS scattering curve remains after correction for this background which clearly indicates the presence of nanoscaled clusters as well as in the stable liquid phase as in the undercooled liquid phase. The Cu-Co sample shows a qualitative similar behaviour.

A detailed analysis of the size-distributions is under progress.

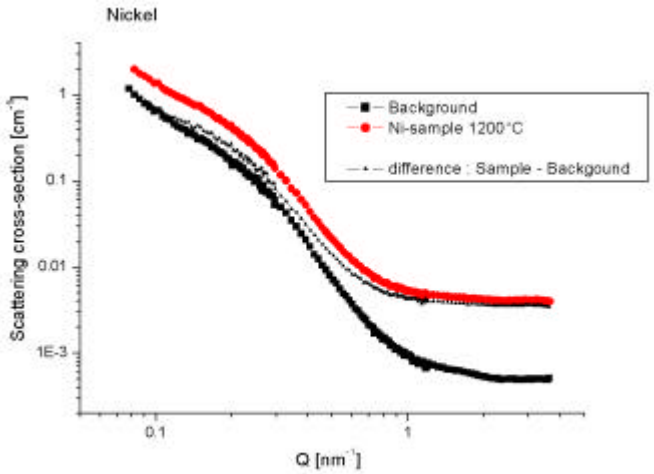


Fig.1 Radially averaged SANS curves of one nickel sample 300°C under the melt point (1200°C) and the background of the experiment after processing the sample. The difference between sample and background scattering indicates the presence of nanoscaled clusters in the liquid and undercooled liquid phases.

This work is supported by DFG-Wi-1153/3-1

References

[1] F.C. Frank, R. Soc. A215(1952) 43
[2] Holland Moritz et al Mater. Sc Eng. A375-377(2004)98-103

	EXPERIMENTAL REPORT **Search for partially ordered structures in very high concentrated Fe_3O_4 based magnetic liquids**	Proposal N° EF-SF3. Nano Instrument **V4** Local Contact
Principal Proposer: Experimental Team:	A. Wiedenmann, A. Heinemann, M. Kammel M. Kammel, A. Heinemann, HMI Berlin	Date(s) of Experiment 25.08.04-28.08.04

Date of Report: 10.01.2005

The formation of ordered or partially ordered structures in magnetic liquids is still under discussion. For Co-based high concentrated (1-3 vol.%)samples SANSPOL technique provided evidence of hexagonal structures [1]. New experiments [2,3] with similar Co-based ferrofluids confirmed this result. Due to the weaker magnetic interaction between the isolated magnetic particles in Fe3O4-based ferrofluids ordering is expected only for very high concentrations of the magnetic cores. With a new preparation technique [4] it was possible to prepare such samples.

We performed SANSPOL experiments to very concentrated Fe_3O_4 based ferrofluids with a magnetic core concentration up to 30vol% in different solvents (water and petroleum) and in different external magnetic fields. Neither in the water based nor in the petroleum based samples we find any evidence of hexagonal structure formation but anisotropic structure factor like in dense packed systems. In further investigations we separate the single particle structure from the diluted sample curves. This investigations should lead us to a systematic approach for the formation mechanism of ordered structures in magnetic fluids.

Work supported by DFG priority program SPP1104.

References:

[1] A. Wiedenmann, A. Hoell, M. Kammel and P. Boesecke J. Phys. Rev. E **68** (2003), 031203
[2] A. Heinemann, A. Wiedenmann, *Journal of Magnetism and Magnetic Materials* 2004 (in press)
[3] A. Wiedenmann, A. Heinemann, *Journal of Magnetism and Magnetic Materials* 2004 (in press).
[4] N. Buske (private communication).

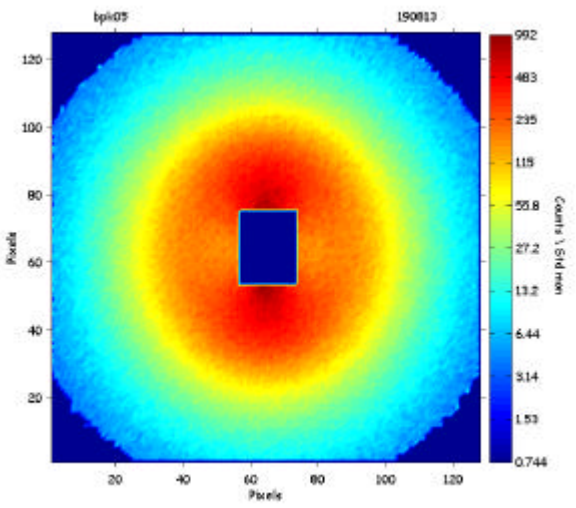


Figure 1: 2-dim SANSPOL scattering intensity (I^{on}) for the 30 vol.% Fe_3O_4 based-ferrofluid sample in petroleum at H = 1 T.

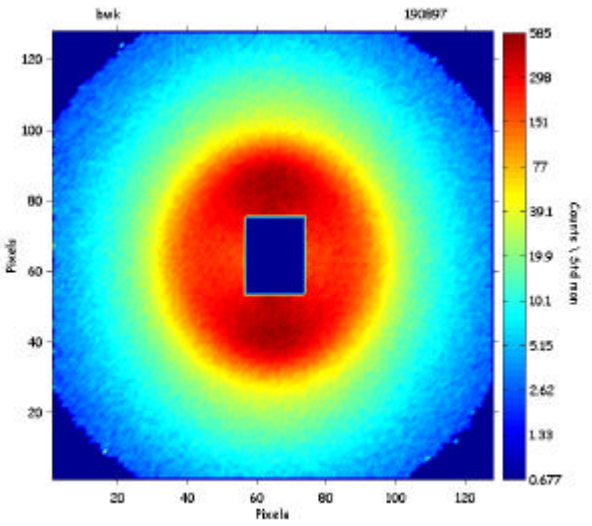


Figure 2: 2-dim SANSPOL scattering intensity (I^{on}) for the 30 vol.% Fe3O4 based-ferrofluid sample with water as solvent at H = 1 T.

	EXPERIMENTAL REPORT **Coherence investigations with Si phase gratings**	Proposal N° PHY-04-1077-LT Instrument **V12a** Local Contact M. Strobl, W. Treimer
Principal Proposer: Experimental Team:	W. Treimer, TFH/HMI; M. Strobl, TFH/HMI M. Strobl, TFH/HMI Berlin	Date(s) of Experiment Mar 2004

Date of Report: Jan 2005

Introduction

It had been shown that the tuning of the full width at half maximum (FWHM) of the resolution function (i.e. rocking curve) of a double crystal diffractometer (DCD) does not significantly influence the lateral coherence of the beam. Only the q-resolution could be improved [1]. The same Si phase gratings that have been used for these measurements have been used once more in order to look at the influence of additional collimation within the DCD onto the lateral coherence width and the diffraction pattern.

Measurements

The phase grating with hexagonal geometry [1] (Fig. 1) was aligned along an axis with a periodicity of d = 4 µm and the diffraction pattern has been recorded with and without additional horizontal collimation. A Si-wafer based collimator was used limiting the divergence at 7 min of arc [2] while the divergence without collimator can be approximated with 0.45° i.e. 27 min of arc.

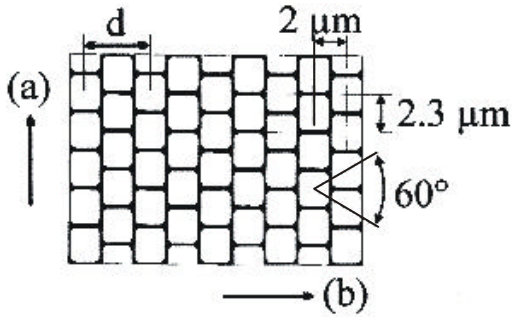


Fig. 1 Si phase grating geometry

As expected the contrast in the pattern measured with the collimator was significantly improved (Fig. 2 and 3), but as the data evaluation is not completed an increase of the lateral coherence can not be numbered yet.

The collimator had to be placed between the monochromator and analyser crystal of the DCD and hence influenced the resolution function of the DCD i.e. the wing intensities of the curve are enhanced. This can clearly be seen in Fig. 3 applying a logarithmic scale.

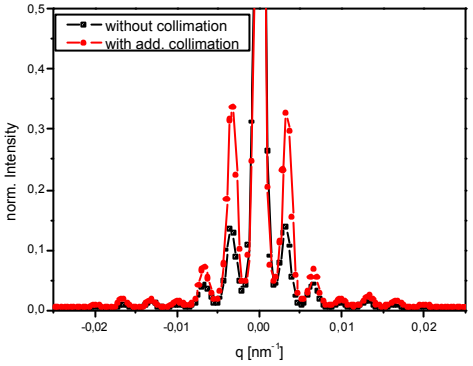


Figure 2 diffraction pattern of grating with and without additional collimation

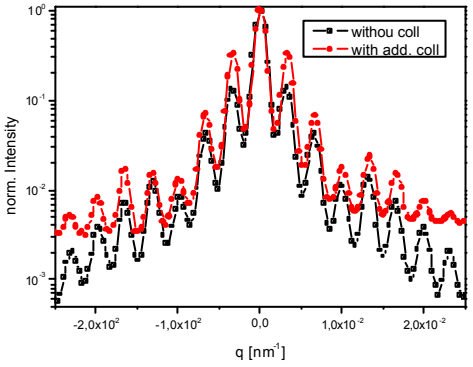


Figure 3 diffraction pattern of grating with and without additional collimation log. scale

This work has been supported by BMBF 03TRE9B6.

References

[1] W. Treimer et al., BENSC Rep.2002, p. 254
[2] M. Strobl et al., BENSC Rep. 2003, p. 230

	EXPERIMENTAL REPORT **Refraction versus USANS by nearly perfect Si crystal surfaces**	Proposal N° PHY-04-1078LT Instrument **V12b** Local Contact W. Treimer
Principal Proposer: Experimental Team:	W.Treimer, TFH Berlin, HMI Berlin M. Strobl, TFH Berlin, HMI Berlin A. Hilger, HMI Berlin A. Qissabi, TFH Berlin	Date(s) of Experiment March - May

Date of Report: 6.1.2005

Perfect Silicon crystals are often used as monochromator and analyzer in high resolution double crystal diffractometer (DCD). In previous measurements we used a perfect Si wedge to shift the range of total reflection within a seven-fold channel cut crystal to reduce the resulting Darwin width down to app. 20% of the natural width of this reflection [1], [2]. The wedge was placed between the 3rd and 4th reflection in the channel cut crystal (see Fig.1) and could be rotated in such a way, that due to refraction the reflected Darwin range was shifted several sec of arc. We used Si because the absorption and the incoherent part of the corresponding cross sections are both negligible. Due to the high angular correlation within this seven-fold channel cut crystal each scattering effect reduces the reflectivity of the channel cut crystal dramatically and therefore also the total intensity in the DCD. To investigate the influence of surface effects of perfect Si crystals which are used in non-Bragg diffracting experiments we measured the scattering from polished and etched surfaces by means of high resolution double crystal diffractometry. Fig.2 and Fig.3 show two different polished surfaces with the corresponding surface profiles. Note the different x-scales of both profiles. To distinguish between refraction and USANS one has to calculate the portion of crystal volume contributing to refraction and the one to USANS.

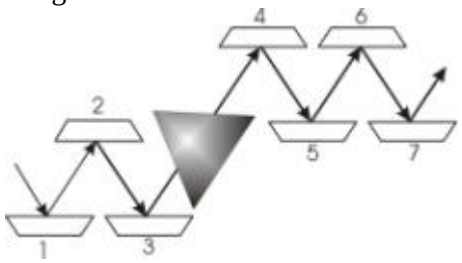


Fig. 1 Seven-bounce channel cut crystal with tuning wedge

We can assume (for this DCD it was measured previously by single slit diffraction) that the width of the coherent front of a neutron wave is of the order of app. 80µm – 100µm. Exactly this part must be taken into account to estimate the contribution to USANS, the other part, refraction can be calculated simply from Snellius' law. Knowing the surface one can determine the angle of refraction and therefore the broadening due to refraction. The angle of incidence to the surface must be less than app. 3° to cause a remarkable deviation from the incident flight direction. Due to the high angular correlation between the monochromator and analyzer of the DCD, each deviation larger than 0.1 sec of arc can be determined. As can be seen from the surface profiles shown in Fig.2 and Fig.3 the angle of incidence for any neutron wave is much larger than 3°, so that refraction due to the surface structure is a rather negligible effect. USANS occurs in the "valleys" of the "scratches" and due to the rather flat "scratch profile" USANS contributes into the "Porod" region, where the scattered intensity is ~ $1/q^4$ which also explains the scattering profile of the rocking curves (s. other report in this volume).

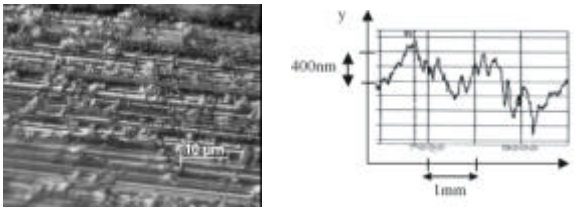


Fig.2 Si surface polished with 180µm grain abrasive paper, right the surface profile

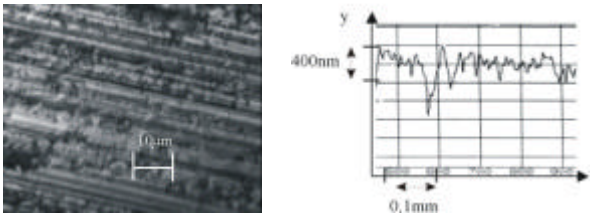


Fig.3 Si surface polished with 47µm grain abrasive paper, right the surface profile

This work was supported by the BMBF project 03TRE9B6

References

[1] W. Treimer, M. Strobl, A. Hilger, Phys. Lett. A 289, (2001) 151 – 154

[2] W. Treimer, M. Strobl, A. Hilger, J. Appl. Physics A 74, (2002) 191 - 193

	EXPERIMENTAL REPORT **Refraction versus USANS from different prepared perfect Si surfaces**	Proposal N° PHY-04-1078LT Instrument **V12b** Local contact W. Treimer
Principal Proposer: Experimental Team:	W. Treimer, TFH Berlin, HMI Berlin A. Qissabi, TFH Berlin M. Strobl, TFH Berlin, HMI Berlin A. Hilger, HMI Berlin	Date(s) of Experiment March – May June-July

Date of Report: 3.1.2005

The preparation of perfect Si crystals for dynamical scattering was studied many years ago. After cutting a crystal slice it was polished and etched to remove the mosaic surface structure which influences the reflectivity of the crystal slab. It was well known, that tiny surface damages distort the neighbouring lattice. This distorted atomic plane changes dramatically the energy flow of radiation, because the dispersion surface around the Bragg condition is in this region strongly curved. Deviations of fractions of sec of arc of the lattice planes cause a change of several degrees of the energy flow. One criterion to control the undisturbed surface is the exact measurement of the full width at half maximum (FWHM) which depends on the undisturbed interaction of radiation with unaffected atomic planes. Any force on the atomic lattice causes a deformation of the net planes. This deformation is proportional to the force that acts on the net planes. The deformation itself causes a broadening of the angular range of acceptance of a perfect lattice, similar to a mosaic structure of mosaic crystals. The integrated reflectivity increases with the mosaic spread in the case of divergent and polychromatic radiation.

The process of surface preparation starts with polishing the surface with decreasing grain size of the abrasive paper. We studied the influence of the preparation state, if differently polished surfaces are etched for different times. As etching liquid we used the composition of 1part 48% HF and 20 parts 65% HNO_3 . The etching rate of this mixture is for an area of 50 cm^2 1 µm / minute. After the Si crystal surfaces were prepared with different abrasive papers (80, 320, 600 and 1200 corresponding to grain sizes of 180, 47, 30, and 17 µm) each surface was etched for 20, 40, 120, 420 and 1020 seconds. Fig.1 shows the first three etching times in comparison to the empty DCD and the effect of no etched surface, just polished with abrasive paper 80. It was indeed highly surprising to see, that in spite of the fact of etching the wings of the rocking curve were enhanced, in contrast to the expectation of a reduction of the wing intensity. The intensity was normalized to 1, however the measuring time for each rocking curve was the same. The full width at half maximum did not change and a pure SANS measurement would not indicate the imperfectness of the sample. Using this crystal as monochromator or analyser in combination with a perfect prepared partner (analyser or monochromator) the FWHM would be increased. It is of fundamental interest to consider the integrated intensities of the wings of the rocking curves. Due to the fact that the absolute intensities of the wings are very low (10^{-3} until 10^{-4} of the peak intensity) we compared the integrated intensities in the angular rage of -50” until - 8” and +8” until +50”. (cp. Fig.2) In the case of SANS (USANS) we observed a maximum scattering for an etching time of ~ 40 sec and not a continuous decrease of the wing intensity.

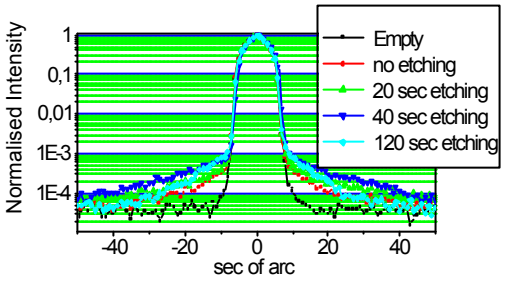


Fig.1 Scattering curves from different etched Si surfaces

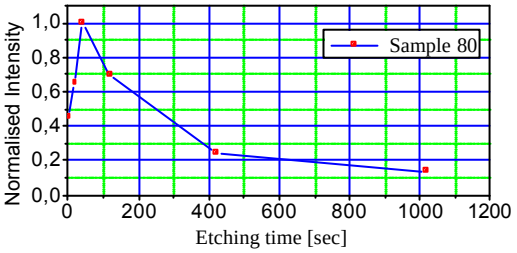


Fig. 2 The integrated intensity of the wings first increases with increasing etching time, contrarily to the expectation of a continuous decrease of surface mosaic structures.

This is reduced for longer etching times and became close to the theory after app. 1000 seconds. This holds for all different prepared surfaces and can be understood by the study of the surface profile after etching. Within the first 40” – 60” the depths of the polishing structure were increased due to the larger surface of the scratches and then they were smoothed and washed out by further etching, getting more likely the ideal crystal structure of the perfect lattice.

This work was supported by the BMBF project 03TRE9B6

	EXPERIMENTAL REPORT Investigations of neutron scattering by surface effects of perfect Si plates	Proposal N° PHY-04-1078LT Instrument **V12b** Local Contact W. Treimer
Principal Proposer: Experimental Team:	Treimer, W. TFH Berlin, HMI Berlin Qissabi, A. TFH Berlin Strobl, M.TFH Berlin, HMI Berlin Hilger, A. HMI Berlin	Date(s) of Experiment March – May June-July

Date of Report: 3.1.2005

It is commonly assumed, that perfect Si plates (with a thickness of app. 1 mm) usually do not contribute to any scattering if no net planes are hit for Bragg reflection. There are measurements, that show deviations from theory of dynamical scattering from perfect crystals in the case of high resolution ultra small angle scattering (USANS) [1], [2]. The measured wing intensity is increased, which was explained by thermal diffuse scattering (TDS) and/or surface small angle scattering. These discrepancies become important if results of experiments performed with a DCD are being falsified. Small angle neutron scattering (SANS) using the well known Bonse-Hart camera is the most prominent example. The sample scattering curve registered with the analyser crystal of the DCD provides information about the scattering objects inside the sample and therefore the precise knowledge of the pure analyser rocking curve (instrumental curve) is of fundamental importance. The DCD as small angle facility is used in many laboratories all over the world and therefore each progress on this subject is of high interest. In addition to this it is of principle interest if the common accepted derivation of the formulae of the dynamical theory for the diffraction pattern given finally by M. v. Laue in his famous book "Röntgenstrahlinterferenzen" is correct or if some additional interactions have to be taken into account to explain these measured deviations of the wing intensity from theory. Within a previous work we could realise for the first time a tail–free Darwin angular profile for a triple Bragg reflected beam [3] - [5]. In this work we show, that the enhanced wing intensity also comes from insufficient prepared Si crystals. This is demonstrated by USANS where the Si crystals act as USANS samples. Knowing from dynamical scattering that extreme small defects cause large changes of the energy propagation in the crystal and therefore contribute to a broadening of the rocking curve, we investigated different states of surface preparation and the effect of surface defects which cause USANS.

The Si samples (app. 30 x 40 x 1) mm^3 were polished with different abrasive papers (grain sizes from 17, 30, 47 and 180 µm), producing surface roughness of 5, 0.3, 0.15 and 0.1 µm (on both sides of the samples. For each surface roughness a precise rocking curve was measured. The results are shown in Fig.1

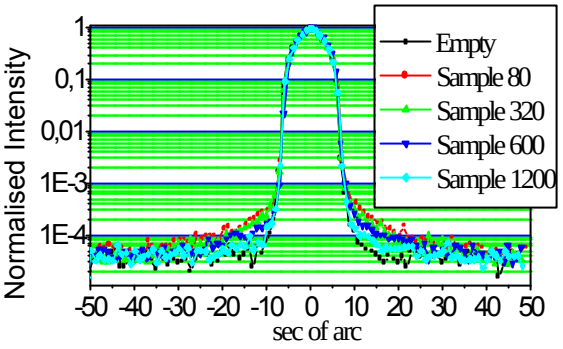


Fig. 1 USANS scattering from different prepared perfect Si crystal surfaces

Despite the fact, that the surface roughness was of the order of 100 nm, there are still contributions to USANS. In the case of channel cut crystals these tiny defects would destroy the perfect Darwin pattern, which is in the case of our seven-fold reflection nearly rectangular.

This work was supported by the BMBF project 03TRE9B6

References

[1] M. Agamalian, G. D. Wignall, R. Triolo (1997), J. Appl. Cryst. **30**, 345 – 352
[2] M. Agamalian, D.K. Christen, A.R. Drews, C. J. Glinka, H. Matsuoka, G.D. Wignall, J. Appl. Cryst. **31**, 235-240 (1998)
[3] A. Wagh, V. C. Rakhecha, W. Treimer, Phys. Rev. Lett. 87, 12, 125504-1 (2001)
[4] Treimer, W., Strobl, M., Hilger, A.; Cryst. Res. & Technology **37**, 7, 727-733 (2002)
[5] Treimer, W., Strobl, M., Hilger, A., Phys. Lett. A **305**, 87-92 (2002)

	EXPERIMENTAL REPORT USANS with Large Area Si Phase Gratings	Proposal N° PHY-04-1041 Instrument **V12a** Local Contact W. Treimer, M. Strobl
Principal Proposer: Experimental Team:	M. Trinker, ATI Wien E. Jericha, ATI Wien M. Strobl, A. Hilger, W. Treimer, HMI Berlin	Date(s) of Experiment 16.-26. June 2004

Date of Report: December 2004

Introduction

Artificial periodic structures have already become a topic of interest for the presentation of USANS performance possibilities [1,2] and also for fundamental quantization aspects in neutron optics [3,4]. Since existing phase gratings manufactured from silicon wafers have rather small patterned areas and/or poorly defined geometry of the single units it was decided to develop Si phase gratings especially for USANS experiments. This was done at the ATI and MISZ in Vienna during 2003 using a so-called RIE (reactive ion etching) process at the cleanroom facilities of the MISZ (Fig. 1).

Experimental

A selection of these gratings was used as scattering samples at the bent crystal setup of the V12a facility at HMI. Each sample was rotated around the vertical axis in steps of 0,5° from -10° to +10° relative to the orthogonal position to the beam and for a each position a full scattering pattern was recorded. An example is shown in Fig. 2.

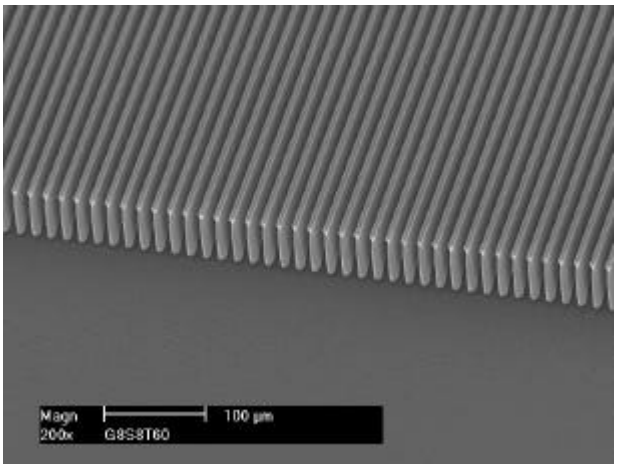


Fig. 1 Si phase grating, period 16 µm, trench depth 60 µm

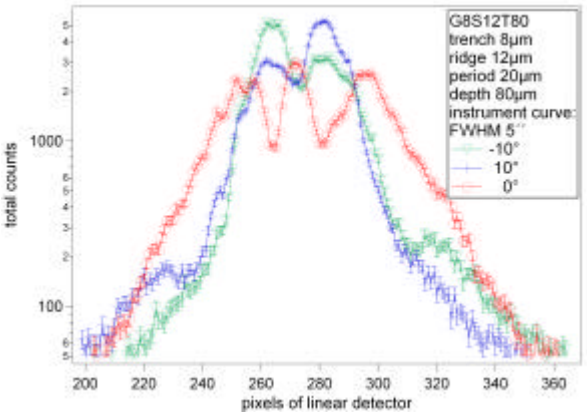


Fig. 2 Scattering patterns at different tilting angles of the grating (-10°, 0°, 10°) around the vertical axis. Grating period 20 µm, trench depth 80 µm

Results

A variety of gratings with lattice constants from 16 µm to 28 µm and trench depths of 40 µm, 60 µm and 80 µm was measured at different tilting angles relative to the neutron beam with a neutron wavelength of 4,76 Å. Since the overall geometry of the gratings is known precisely the scattering data will provide tests for phase grating scattering models as well as properties of this specific instrumental setup.

References

[1] Treimer, W., Strobl, M., Hilger, A. (2001) *Phys. Lett.* **A289**, 151-154

[2] Hainbuchner, M., Villa, M., Kroupa, G., Bruckner, G., Baron, M., Amenitsch, H., Seidl, E., Rauch, H., (2000) *J. Appl. Cryst.* ***33****, 851-852*

[3] E. Jericha, M. Baron, M. Hainbuchner, R. Loidl, M. Villa, H. Rauch *J. Appl. Cryst.* (2003) **36**, 778-782

[4] Rauch, H., Lemmel, H., Baron, M., Loidl, R. (2002) *Nature,* **417**, 630-632

	EXPERIMENTAL REPORT USANS with Large Area Si Phase Gratings Part II	Proposal N° PHY-04-1041 Instrument **V12b** Local Contact W. Treimer, M. Strobl
Principal Proposer: Experimental Team:	E. Jericha, ATI Wien M. Trinker, ATI Wien M. Strobl, A. Hilger, W. Treimer, HMI Berlin	Date(s) of Experiment 16.-26. June 2004

Date of Report: December 2004

For a short description of the motivation and the phase gratings used as samples for the experiment we refer to the related report for the V12a instrument.

Experimental

A selection of phase gratings was measured at the tuneable 7-bounce double crystal setup of the V12b facility. Each sample was oriented perpendicular to the neutron beam and a full diffraction pattern was recorded up to about 10 interference orders. The measurements were carried out in two sets of runs: In the first set we used the untuned instrument with a FWHM of the instrument curve of 6,23 seconds of arc (Fig.1). Interference phenomena were clearly observable (Fig.2), but individual interference orders for several gratings with larger constants of periodicity could not be resolved properly. Therefore we used the tuning option of the V12b instrument to reduce the FWHM of the instrument curve (Fig.1). The effect of tuning on the diffraction pattern may be appreciated by the separated interference peaks shown in the second curve of Fig.2.

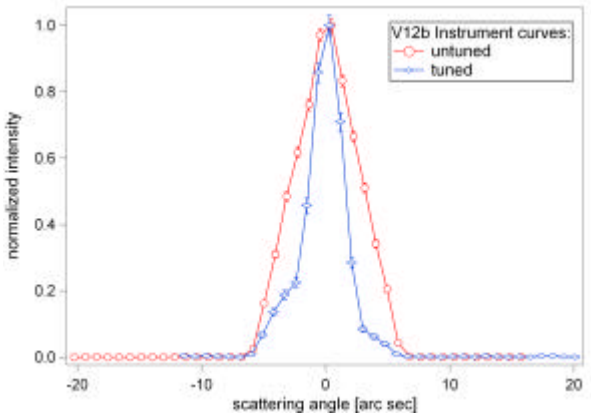


Fig. 1 Instrument curves at different tuning states of the V12b instrument. The broader curve (circles) corresponds to the untuned instrument, the narrow one (diamonds) to the tuned state.

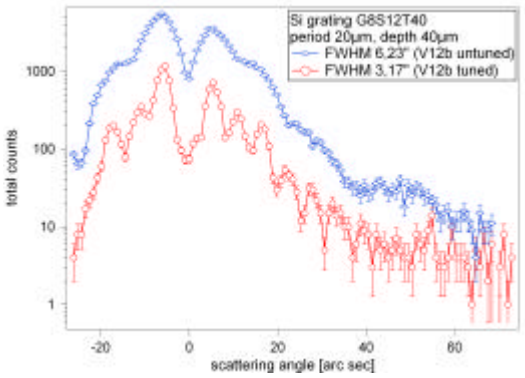


Fig. 2 Scattering patterns at different tuning states of the instrument V12b. FWHM 6,23" (diamonds) and FWHM 3,17" (circles). Grating period 20 µm, trench depth 40 µm

Results

A variety of gratings with lattice constants from 16 µm to 28 µm and trench depths of 40 µm, 60 µm and 80 µm was measured at different tuning states of the instrument with an incident neutron wavelength of 5,25 Å. Similar experiments up to now have been mainly performed with thermal neutrons at wavelengths below 2 Å.

The new measurements at HMI will allow us to test wavelength dependent models of phase grating diffraction. Important quantities in this respect are the position of the interference maxima, the ?-thickness characteristic for the total phase shift and the lateral coherence of the neutron beam.

References

[1] Treimer, W., Strobl, M., Hilger, A. (2001) *Phys. Lett.* **A289**, 151-154

[2] Hainbuchner, M., Villa, M., Kroupa, G., Bruckner, G., Baron, M., Amenitsch, H., Seidl, E., Rauch, H., (2000) *J. Appl. Cryst.* ***33****, 851-852*

[3] E. Jericha, M. Baron, M. Hainbuchner, R. Loidl, M. Villa, H. Rauch *J. Appl. Cryst.* (2003) **36**, 778-782

[4] Rauch, H., Lemmel, H., Baron, M., Loidl, R. (2002) *Nature,* **417**, 630-632

	EXPERIMENTAL REPORT **Search for scission neutrons using angular correlation in fission of U-235**	Proposal N° PHY-05-7 Instrument **V-13** Local Contact Katerina Korobkina
Principal Proposer: Experimental Team:	Danilyan, ITEP, Moscow Pavlov, ITEP, Moscow Karpikhin, ITEP, Moscow Krakhotin, ITEP, Moscow Fedorov, ITEP, Moscow Brakhman, ITEP, Moscow Golub, BENSC, HMI Berlin Korobkina, BENSC, HMI Berlin Wilpert, BENSC, HMI Berlin	Date(s) of Experiment Sept. – Dec. 2003 Feb. – Sep. 2004

Date of Report: 25.12.2004

The problem of scission neutrons existence is one of the unsolved problems in fission physics yet. Scission neutrons are the neutrons emitted by fissile nucleus before its rupture into two fragments. Common technique to search for scission neutrons is the fitting of angular and energy distributions of prompt fission neutrons by two components. The first one is the contribution of fragment's neutrons which predominantly emitted along the fission axis. Angular distribution of the second component is assumed to be approximately isotropic (scission neutrons). This technique gives very contradictory results. The fraction of the second component varies from 1% to 35% depending on the experiment and the assumptions made.

We suppose that the specific angular correlations like as P-odd asymmetry of prompt fission neutron emission:

$$W = \text{Const.}(1 + \alpha \mathbf{S}, \mathbf{n}_{pfn}), \quad (1)$$

where α is the correlation coefficient, S and n_{pfn} are unit vectors in the directions of neutron beam polarization and the momentum of detected prompt fission neutron, will be evidence of the scission neutrons existence, because for neutrons evaporated from fragments coefficient α must be washed out due to summation over a huge number of final states in fission process. Of course, fragment's neutrons are the background which will suppresses the measured asymmetry. It's obvious that this method is free of arbitrary assumptions.

We've performed the measurements of correlation (1) on the polarized cold neutron beam (instrument V-13) of the reactor BER-II of BENSC, HMI. For the first step we searched for the P-odd asymmetry of prompt neutron emission in ^{235}U fission. The set-up consists of the fission chamber, including target and fragment detectors, neutron detectors, electronic modules (CAMAC) and the computer. The target contains 48 mg of $^{235}U_3O_8$ plotted to the both sides of the thick Zr plate. Two multiwire low-pressure proportional counters were situated on both sides of the target to detect fission fragments. They do not distinguish between light and heavy fragments. The neutron beam was polarized in the plane of target, perpendicularly to the direction of beam and to the average direction of momentum of fission fragments. The polarization of the neutron beam was about 85%. The target and fragment detectors were enclosed into aluminum chamber. The chamber was filled by isobuthane up to pressure 10 torr. Two neutron detectors were placed outside the chamber in orthogonal geometry to the beam direction and to the average fission axis at the distance 25 cm from the center of target. These detectors consist of plastic scintillator and photomultiplier. To distinguish between prompt fission neutrons and γ-quanta, the time-of-flight technique was used. The polarization of neutron beam was reversed once per second by the signal from the experiment control module. The data acquisition program collects spectra of the delayed coincidences and data from scalers for both directions of neutron beam polarization. All runs were divided into 15-minutes expositions. We have measured the value

$$A_n^* = (N^+ - N^-)/(N^+ + N^-). \quad (2)$$

Here N^+ и N^- are events sum under the neutron peak in delayed coincidence spectra for opposite directions of neutron beam polarization. The same value for the asymmetry under the gamma peak was also measured. Last one used for checking of the apparatus asymmetry. Moreover, we have changed the direction of guiding magnetic field in the second half of the measurements. No apparatus asymmetry was found. The results for both neutron detectors are shown below.

	$A_n^*(90^0)\cdot 10^5$	$A_\gamma^*(90^0)\cdot 10^5$
Detector 1	+3.5±1.1	+0.7±0.9
Detector 2	+1.9±1.1	–0.9±0.9
Average	+2.7±0.8	-0.1±0.6

Thus we've found P-odd asymmetry of scission neutron emission. The value of asymmetry measured at 90^0 relative to fission axis lies in the interval $1.4\cdot 10^{-5} \le A^* \le 4.0\cdot 10^{-5}$ on 90% c.l.. To find the fraction of scission neutrons it's necessary to measure the asymmetries at the angles 90^0 and 45^0 relative to the fission axis with the accuracy $3\cdot 10^{-6}$.

BENSC	EXPERIMENTAL REPORT Title **Autoradiographs of the painting "The Old Man with the Cane and the Plume Cap" Unknown artist, copy of Rembrandt, 82,5 x 102 cm²**	Proposal Nº Instrument B8 Local Contact Dr. B. Schröder-Smeibidl
	Name(s) Affiliation Principal Proposer: C. Laurenze-Landsberg, Gemäldegalerie Berlin (GMB) Experimental Team: C. Laurenze-Landsberg, C. Schmidt (GMB) L.A. Mertens, Dr. B. Schröder-Smeibidl (HMI)	Date(s) of Experiment April 2004
	Date of Report	8.2.2005

Introduction

The picture "The Old Man with the Cane and the Plume Cap" (Fig. 1a, privately owned) is obviously a relative poorly manufactured copy of a painting of Rembrandt (Fig. 1b, dated 1645) which originally belongs to the Museum of Arts in Lisbon. Surprisingly the X-ray record reveals under the visible painting a further but better performed replica of an other Rembrandt painting "The Preacher Eleazar Swalmius (1637)" which can be seen in the Royal Museum of Fine Arts in Antwerp. To learn more about the genesis, the origin and the artist of this copy the painting was investigated by neutron autoradiography.



Figure 1a: "The Old Man with the Cane and the Plume Cap", Coloured Replica, Private Property
Figure 1b: Black and white photograph of "The Old Man with the Cane and the Plume Cap", H. Rembrandt (1645), Museum of Arts, Lisbon



Figure 2a: X-ray record of "The Old Man with the Cane and the Plume Cap", Replica, Private Property
Figure 2b: black and white photograph of "The Preacher Eleazar Swalmius (1637)", H. Rembrandt (1645), Royal Museum of Fine Arts, Antwerp

Results

The defects in the painting layer of the underlying portrait can be attributed to a longer period between the completion and the over-painting. How much time had elapsed could not be clarified as the defects could be deteriorated because of lack of technique or/and climate fluctuations.

The background contains the pigment smalt. In both portraits the tinge of the incarnates (hands and face) were mixed by naples-yellow including a little bit of vermillion (see Fig 3. revealing Antimony Sb and Mercury Hg). This consistence might be a hint that both portraits are painted by the same artist or that both are made in the same workshop where the application of naples-yellow was a common practice. But the long period between both portraits and the difference in quality contradict the suggestion above.



Figure 3: 3rd neutron autoradiography of "The Old Man with the Cane and the Plume Cap", Replica, unknown artist.

The application of naples-yellow is usually not observed in Rembrandts paintings. Referring to the series of investigations of Rembrandt paintings and paintings which presumably were made in his workshop carried out by the Berlin Picture Gallery naples-yellow was found only in one painting and there not as mixture but as intensive clear yellow colour.

Conclusion

With the utmost probability neither the visible nor the portrait which is recorded by X-rays, can be ascribed to the environment or to Rembrandt himself.

BENSC	EXPERIMENTAL REPORT Title **Autoradiographs of the painting "The Hermit" Unknown artist, 46,6 x 63,3 cm²**	Proposal Nº Instrument B8 Local Contact Dr. B. Schröder-Smeibidl
Name(s) Affiliation Principal Proposer: C. Laurenze-Landsberg, Gemäldegalerie Berlin (GMB) Experimental Team: C. Laurenze-Landsberg, C. Schmidt (GMB) L.A. Mertens, Dr. B. Schröder-Smeibidl (HMI)		Date(s) of Experiment June 2004
	Date of Report	8.2.2005

Introduction

The painting "The Hermit" (Fig. 1) as art work of an unknown artist was suspected of being made by the hand of H. Rembrandt. To clarify the issue of authorship by comparing painting techniques an investigation by the means of neutron autoradiography was carried out.



Figure 1: "The Hermit", Unknown artist, Private Property

Results

In the neutron autoradiography (Fig. 2) the pigments umber and probably azurite or ultramarine (lapis lazuli) are observed containing Mn, Cu or Na, respectively. The blue pigment smalt, the pigment vermillion (Hg) or modern pigments were not detected. Sb of the corresponding Naples-yellow was observed, but this pigment was only applied in later added retouchings.

With respect to the secured knowledge H. Rembrandt has applied smalt as part of mixed colours not earlier than 1640. Therefore there is no contradiction to a creation of this painting in the environment of Rembrandt. In addition, the autoradiography reveals pentimenti, especially in the position of the hands and the book. Originally the hands were located a little bit lower. The pentimenti carried out by umber, the contour lines in the lower part of the dress and the diverse tinge of the background indicate also a draft in umber. In comparison, in early works of Rembrandt sketches and background paintings made by umber are well known.



Figure 2: "The Hermit", 3rd neutron autoradiography

In the lower right part of the picture brushstrokes performed by a pigment containing Cu show clearly the duct and the special handwriting of the artist. This handwriting might be identified with the handwriting of the Dutch painter Govaert Flinck (1615-1660), because there is a remarkable accordance to the results of the neutron autoradiography of the painting "Susanna and the Old Couple" ascribed to G. Flinck (dated 1639/40), which was investigated at the BER II a few years ago. A study of further paintings of Flinck should be carried out to enlighten this issue and to learn more about Flinck's original handwriting.

BENSC	EXPERIMENTAL REPORT Title **Autoradiographs of the painting "The Baptism of a Child" Jan Steen, 85 x 100 cm^2, Cat No. 795D**	Proposal Nº Instrument B8 Local Contact Dr. B. Schröder-Smeibidl
Name(s) Affiliation Principal Proposer: C. Laurenze-Landsberg, Gemäldegalerie Berlin (GMB) Experimental Team: C. Laurenze-Landsberg, C. Schmidt (GMB) L.A. Mertens, Dr. B. Schröder-Smeibidl (HMI)		Date(s) of Experiment ART -05-008 November 2003
	Date of Report	8.2.2005

Introduction

The painting "The Baptism of a Child", by Jan Steen (Fig. 1) belongs to the Berlin Picture Gallery (Cat. No. 795D).

The Dutch Painter Jan Steen (1625/26 – 1679), a contemporary of Rembrandt, is best known for his humorous genre scenes, animated works in which he treats life as vast comedy of manners. Many of his pictures represent taverns and festive gatherings such as in the painting focused in this experiment. In addition, as painter of children he is considered to be unsurpassed which can also be seen in Fig. 1.



Figure 1: "The Baptism of a Child", by Jan Steen, Gemäldegalerie zu Berlin, Cat No. 795D

In the course of the restoration of this picture in 2003 diverse structures in the composition of colours were detected by X-rays which disagree with the visible painting. The neutron autoradiography promised a better and deeper understanding of this issue by visualizing pentimentis and other changes.

Results

The pentimenti recorded by X-rays were understood as more formal changes within the composition of the representation of a baptism of a child. But the pentimenti observed in the neutron autoradiography (Fig. 2) do not display corrections of the presented scence, a genre which demonstrates human misdemeanour according to a saying "The young people twitter as the old people sing".

In the neutron radiography (Fig 2.) a lot of pentimenti were revealed. Originally the platform with the cradle was not provided. At this place a chair was located. The tiled floor was continued under the platform.

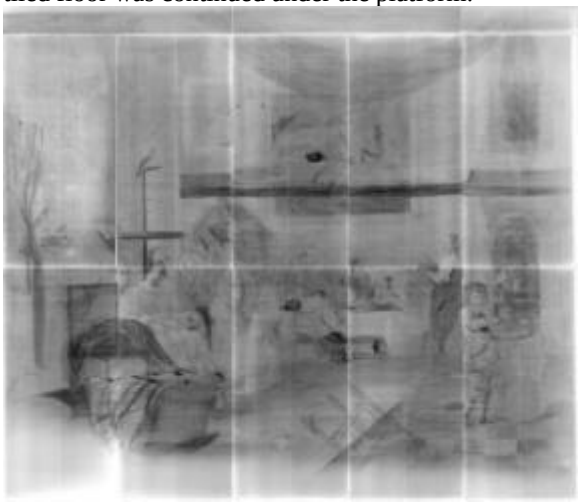


Figure 2: ": "The Baptism of a Child", by Jan Steen, Gemäldegalerie zu Berlin, 1st autoradiography

Especially one thematic modification on the right side of the picture is very enlightening: Behind the originally larger archway the view is open to a palace surrounded by a garden and sculptures, which should establish the manorial reference of the content of the picture. The large painting in the middle of Steen's picture changed during the creation shows two struggling cavaliers and indicates a manorial military context. With these paintings within the picture the artist wanted to strengthen the thematic statement of this presentation. In the visible composition the pictures hanging at the walls on the left and right hand side strengthen now the moral didactic statement of the painting. In conclusion by analogy the presentation of struggling cavaliers has to refer to the content of the painting, too.

Conclusion

The observed pentimenti indicate that Steen has painted over a picture with completely different content. Especially, he has not made changes within the present composition. Further image editing is intended to carry out in order to map and to understand the entire content of this underlying picture.

Part II

LIST OF PUBLICATIONS

Theses	210
Papers	211
Conference Contributions and Seminar Talks	224
Contributions to the BENSC Users' Meeting 2004	235

Theses 2004
Examina

PhD-theses

2003 (supplement)	
Maksimov, I.: **Investigations of the role of disorder in heavy fermion compounds** TU Braunschweig, March 2003	E4
2004	
Baldelli Bombelli, F.: **Physico chemical characterization of liponucleoside micellar solutions. structural and dynamic investigation in presence of molecular recognition between nucleic bases** University of Florence, April 2004	V4
Bonini, M.: **Nanostructured magnetic fluids: synthesis and characterization** University of Florence, April 2004	V4
Dennison, S.R.: **Investigation into the structure function relationship of the membrane interaction of amphiphilic alpha helical antimicrobial peptides** University of Central Lancashire, July 2004	V1
Gilardi, R.: **Inelastic and small angle neutron scattering study of the LSCO high-Tc superconductor in a magnetic field** ETH Zürich, October 2004	V2
Gondek, L.: **Magnetic properties of hexagonal RTIn (R - rare earth, T - transition metal) compounds.** Jagiellonian University, September 2004	E6
Janousova, B.: **Magnetic state instability in intermetallics with f- and d-electrons. RPtSn compounds (R = La - Nd)** Charles University in Prague, Faculty of Mathematics and Physics, September 2004	E4
Kiefer, K.: **Kalorimetrische und Magnetische Untersuchungen am Spin-Peierls System $CuGeO_3$** Universität Saarbrücken, July 2004	V2
Lonkai, Th.: **Elektrische und magnetische Ordnungsparameter im multiferroischen hexagonalen $RMnO_3$-System** Eberhard-Karls-Universität Tübingen, May 2004	E2
Mang, P.K.: **Magnetic, phonon, and structural scattering studies of the electron-doped high-temperature superconducting neodymium cerium copper oxide** Stanford University, June 2004	E4
Pritula, O.: **Quantitative X-ray and neutron phase analysis of Portland clinker** Institute of Inorganic Chemistry, Slovak Academy of Sciences, June 2004	E9
Russina, O.: **Die Untersuchung der mikroskopischen Dynamik am Glasübergang** Technische Universität Berlin, February 2004	
Ryukhtin, V.: **Microstrucutrue investigation og cavitation in ceramics using small-angle neutron scattering** Charles University in Prague, June 2004	V4

Publications 2004
BENSC Experiments and BENSC Authors

2002 (supplement)	
Baldelli Bombelli, F.; Berti, D.; Keiderling, U.; Baglioni, P.: **Giant polymerlike micelles formed by nucleoside-functionalized lipids** Journal of Physical Chemistry B **106** (2002) 11613 - 11621	V4 IHP I: 144
Janousova, B.; Svoboda, P.; Sechovsky, V.; Prokes, K.; Nakotte, H.; Chang, S.; Ouladdiaf, B.; Cisarova, I.: **Neutron diffraction study of CePtSn** Applied Physics A: Materials Science and Processing **74** (2002) 731	E4
Mergia, K.; Baczewski, L.T.; Messoloras, S.; Hamada, S.; Shinjo, T.; Gamari-Seale, H.; Hauschild, J.: **Polarized neutron reflectivity study of a Gd/Cr multilayer** Applied Physics A: Materials Science and Processing **74** (2002) 1520 - 1522	V6
2003 (supplement)	
Campbell, B.J.; Sinha, S.K.; Osborn, R.; Rosenkranz, S.; Mitchell, J.F.; Argyriou, D.N.; Vasiliu-Doloc, L.; Seeck, O.H.; Lynn, J.W.: **Polaronic orbital polarization in a layered colossal magnetoresistive manganite** Physical Review B **67** (2003) 020409(R)	---
Gokhman, A; Böhmert, J.; Ulbricht, A.: **Kinetic study of copper precipitates under VVER-type reactor conditions** Radiation Effects & Defects in Solids **158** (2003) 783 - 792	V4
Roennow, H.M.; Enderle, M.; McMorrow, D.F.; Regnault, L.-P.: **The field-induced soliton phase of $CuGeO_3$** Physica B **329-333** (2003) 675-678	V2 / E4 IHP I: 201 IHP II: 507
Wolter, A.U.B.; Rakoto, H.; Costes, M.; Honecker, A.; Brening, W.; Klümper, A.; Klauss, H.-H.; Litterst, F.J.; Feyerherm, R.; Jérome, D.; Süllow, S.: **High-field magnetization study of the $S=^1/_2$ antiferromagnetic Heisenberg chain $[PMCu(NO_3)_2(H_2O)_2]_n$ with a field-induced gap** Physical Review B **68** (2003) 220406	---
2004	
Ahrens, H.; Büscher, K; Eck, D.; Luap, C.; Papastavrou, G.; Schmitt. J.; Steitz, R.; Helm, C.A.: **Poly (styrene sulfonate) adsorption: electrostatic and secondary interactions** Macromolecular Symposia **211** (2004) 93 - 105	V6
Aksenov, V.; Nikitenko, Yu.; Progliado, V.; Fritzsche, H.; Gavrilov, V.; Raitman, E.: **Neutron Reflection by Ultrasonically Exited Glass Surface** Latvian Journal Phys. Tech. Sci. **6** (2004) 3 - 11	V6 IHP II: 463
Aldridge, L.P.; Bordallo, H.N.; Desmedt, A.: **Water dynamics in cement pastes** Physica B **350** (2004) e565 - e568	NIST
Andreev, A.V.; Mushnikov, N.V.; Goto, T.; Honda, F.; Sechovsky, V.; Prokes K.: **High-field magnetization of a UCuGe single crystal** Physica B **346-347** (2004) 132-136	15 T
Auffermann, G.; Müller, P.; Bronger, W.: **Neutron Scattering as a powerful tool in solid state chemistry. examples from the investigations in crystal structures and properties of metal hydrogen and metal chalcogen compounds** Z. Anorg. Allg. Chem. **630** (2004) 2113 - 2124	E6, E9

Publications 2004
BENSC Experiments and BENSC Authors

Baldelli Bombelli, F.; Berti, D.; Pini, F.; Keiderling, U.; Baglioni, P.: **Flexibility of dilauroyl-phosphatidyl-nucleoside wormlike micelles in aqueous solutions** Journal of Physical Chemistry B **108** (2004) 16427 - 16434	V4
Balog, E.; Becker, T.; Oettl, M.; Lechner, R.; Daniel, R.; Finney, J.; Smith, J.C.: **Direct determination of vibrational density of states change on ligand binding to a protein** Physical Review Letters **93** (2004) 028103 - 1/4	ILL
Barthes, M.; Bordallo, H.N.; Denoyer, F.; Lorenzo, J.-E.; Zaccaro, J.; Robert, A.; Zontone, F.: **Micro-transitions or breathers in L-alanine?** European Physical Journal **B 37** (2004) 375-382	ESRF
Bazela, W.; Penc, B.; Stüßer, N.; Szytula, A.; Wawrzynska, E.; Zygmunt, A.: **Neutron diffraction studies of R_2RhSi_3 (R=Dy, Ho, Er) compounds** Physica B **350** (2004) e167 - e170	E6 IHP I: 153
Birkholz, M.; Genzel, C.; Jung, T.: **X-ray diffraction study on residual stress and preferred orientation in thin titanium films subjected to a high ion flux during deposition** Journal of Applied Physics **96** (2004) 7202-7211	ETA (Xray)
Böhmert, J.; Viehrig, H.-W.; Ulbricht, A.: **Correlation between irradiation-induced changes of microstructural parameters and mechanical properties of RPV steels** Journal of Nuclear Materials **334** (2004) 71 - 78	V4
Bonini, M.; Wiedenmann, A.; Baglioni, P.: **Small angle polarized neutrons (SANSPOL) investigation of surfactant free magnetic fluid of uncoated and silica-coated cobalt-ferrite nanoparticles** Journal of Physical Chemistry B **108** (2004) 14901 - 14906	V4
Bonini, M.; Wiedenmann, A.; Baglioni, P.: **Synthesis and characterization of surfactant and silica-coated cobalt ferrite nanoparticles** Physica A **339** (2004) 86 - 91	V4
Bordallo, H.N.; Herwig, K.W.; Luther, B.M.; Levinger, N.E.: **Quasi-elastic neutron scattering study of dimethyl-sulfoxide-water mixtures: probing molecular mobility in a nonideal solution** Journal of Chemical Physics **121** (2004) 12457-12464	IPNS
Bordallo, H.N.; Chapon, L.C.; Manson, J.L.; Hernández-Velasco, J.; Ravot, D.; Reiff, W.M.; Argyriou, D.N.: **S =1/2 Ising behavior in the two-dimensional molecular magnet $Fe(NCS)_2(pyrazine)_2$** Physical Review B: Condensed Matter **69** (2004) 224405-1/8	E6, E9
Bordallo, H.N.; Zsigmond, G.; Champion, J.D.M.: **Benchmark simulation of a Fermi-chopper instrument** Physica B **350** (2004) e717 - e720	VITESS
Borisov, S.; Hansen, T.; Kumzerov, Yu.; Naberezhnov, A.; Simkin, V.; Smirnov, O.; Sotnikov, A.; Tovar, M.; Vakhrushev, S.: **Neutron diffraction study of NaNO2 ferroelectric nanowires.** Physica B **350** (2004) e1119 - e1121	E9
Bourdarot, F.; Fåk, B.; Habicht, K.; Prokes, K.: **Evidence for a hidden order parameter in URu_2Si_2** Journal of Magnetism and Magnetic Materials **272-276** (2004) e31 - e32	V2
Brakhman, E.; Danilyan, G.; Fedorov, A.; Karpikhin, I.; Krakhotin, V.; Pavlov, V.; Golub, R.; Korobkina, E.; Wilpert, T.: **Search for P-odd asymmetry of prompt neutrons emission in ^{235}U fission induced by cold polarized neutrons** Journal of Experimental and Theoretical Physics Letters **80** (2004) 803 - 805	V13

Publications 2004
BENSC Experiments and BENSC Authors

Branca, C.; Faraone, A.; Magazu, S.; Maisano, G.; Mangione, A.: **A quasi-elastic neutron scattering and neutron spin-echo study of hydrogen bonded system** Physica B **350** (2004) e355 – e358	V5
Bruno, G.; Ceretti, M.; Girardin, E.; Giuliani, A.; Manescu, A.: **Relaxation of residual stress in MMC after combined plastic deformation and heat treatment** Scripta Materialia **51** (2004) 999 – 1004	E3 IHP I: 023 IHP I: 071
Butter, K.; Hoell, A.; Wiedenmann, A.; Petukhov, A.V.; Vroege, G.-J.: **Small angle neutron and X-ray scattering of dispersions of oleic-acid-coated magnetic iron particles** Journal of Applied Crystallography **37** (2004) 847 – 856	V4 IHP I: 314
Calandrini, V.; Deriu, A.; Onori, G.; Lechner, R.E.; Pieper, J.: **Diffusive dynamics of water in tert-butyl alcohol/water mixtures** Journal of Chemical Physics **120** (2004) 4759 – 4767	V3 IHP II: 512
Chaboussant, G.; Basler, R.; Sieber, A.; Ochsenbein, S.T.; Güdel, H.-U.: **Neutron scattering studies of magnetic molecular spin clusters** Physica B **350** (2004) e51 – e54	V3
Charalambopoulou, G.Ch.; Steriotis, Th.A.; Hauss, Th.; Stubos, A.K.; Kanellopoulos, N.K.: **Structural alterations of fully hydrated human stratum corneum** Physica B **350** (2004) e603 – e606	V1 IHP I: 190 IHP II: 451
Cho, S.J.; Kang, H.Y.; Lee, C.H.; Kim, Y.J.; Krist, Th.: **Crystallization and magnetic properties of FeCo/Si multilayer** Nuclear Instruments and Methods in Physics Research A 529 (2004) 94 – 97	V14
Czeslik, C.: **Factors ruling protein adsorption** Zeitschrift für Physikalische Chemie **218** (2004) 771 – 801	V6
Czeslik, C.; Jackler, G.; Hazlett, T.; Gratton, E.; Steitz, R.; Wittemann, A.; Ballauff, M.: **Salt-induced protein resistance of polyelectrolyte brushes studied using fluorescence correlation spectroscopy and neutron reflectometry** Physical Chemistry Chemical Physics **6** (2004) 5557 – 5563	V6
Czeslik, C.; Jackler, G.; Steitz, R.; von Grünberg, H.-H.: **Protein binding to like-charged polyelectrolyte brushes by counterion evaporation** Journal of Physical Chemistry B **108** (2004) 13395 – 13402	V6
De Stefanis, A.; Tomlinson, A.A.G.; Steriotis, Th.A.; Stefanopoulos, K.L.; Keiderling, U.: **Nanostructural characterisation of catalysts by SANS** Physica B **350** (2004) e521 – e524	V4 IHP I: 055
Desmedt, A.; Stallmach, F.; Lechner, R.E.; Cavagnat, D.; Lassègues, J.-C.; Guillaume, F.; Grondin, J.; Gonzalez, M.A.: **Proton dynamics in the perchloric acid clathrate hydrate $HClO_4 \cdot 5.5H_2O$** Journal of Chemical Physics **121** (2004) 11916-11926	ILL
Efimov, V.V.; Khasanov, S.S.; Mavrin, B.N.; Novikova, N.N.; Shilnikov, A.V.; Burkhanov, A.I.; Sikolenko, V.V.; Sternberg, A.; Tiutiunnikov, S.I.; Többens, D.M.; Yakovlev, V.A.: **Structure and lattice dynamics in PLZT 8/65/35 ceramics irradiated by high-current pulsed electron beam** Ferroelectrics **302** (2004) 327 – 333	E9
Feyerherm, R.; Loose, A.; Landsgesell, S.; Manson, J.L.: **Magnetic ordering in iron tricyanomethanide** Inorganic Chemistry 43 (2004) 6633-6639	E9
Feyerherm, R.; Loose, A.; Nojiri, H.: **Low-temperature magnetization of the distorted triangular magnet manganese tricyanomethanide** Journal of Magnetism and Magnetic Materials **272-276** (2004) 1054-1055	Magnetisation

Publications 2004
BENSC Experiments and BENSC Authors

Feyerherm, R.; Loose, A.; Ishida, T.; Nogami, T.; Kreitlow, J.; Baabe, D.; Litterst, F.J.; Süllow, S.; Klauss, H.-H.; Doll, K.: **Weak ferromagnetism with very large canting in a chiral lattice: $Fe(pyrimidine)_2Cl_2$** Physical Review B: Condensed Matter **69** (2004) 134427 – 1/8	E6, E9
Fick, J.; Steitz, R.; Leiner, V.; Tokumitsu, S.; Himmelhaus, M.; Grunze, M.: **Swelling behavior of self-assembled monolayers of alkanethiol-terminated poly(ethylene glycol): a neutron reflectometry study** Langmuir **20** (2004) 3848-3853	ILL
Fitzsimmons, M.R.; Fritzsche, H.; Gierlings, M.; Major, J.; Pynn, R.: **Measuring Scattering Angles with Neutron Spin Echo** Nuclear Instruments and Methods in Physics Research Section A **529** (2004) 10 – 15	V6
Fritzsche, H.; Liu, Y.T.; Hauschild, J.; Maletta, H.: **Magnetization of uncovered and V-covered ultrathin Fe(100) films on V(100)** Physical Review B: Condensed Matter **70** (2004) 214406-1/6	V6
Frontzek, M.; Kreyssig, A.; Doerr, M.; Hoffman, J.-U.; Hohlwein, D.; Bitterlich, H.; Behr, G.; Loewenhaupt, M.: **Magnetic properties of Tb_2PdSi_3** Physica B **350** (2004) e187 – e189	E2
Gamari-Seale, H.; Troyanchuk, I.O.; Bushinsky, M.; Stefanopoulos, K.L.; Hernandez-Velasco, J.: **The effect on highly Cr-substituted manganite $Nd_{0.6}\,Ca_{0.4}(Mn_{0.5}\,Cr_{0.5})O_3$** Acta Physica Polonica A **105** (2004) 81 – 86	E6 IHP II: 405
Gamari-Seale, H.; Troyanchuk, I.O.; Khalyalin, D.; Szymczak, H.; Stefanopoulos, K.L.; Hernandez-Velasco, J.: **Magnetic structure of $Nd_{0.92}\,Ca_{0.08}\,MnO_3$** Journal of Magnetism and Magnetic Materials **272-276** (2004) e483 – e484	E6 IHP II: 406
Gamari-Seale, H.; Troyanchuk, I.O.; Khalyavin, D.; Stefanopoulos, K.L.; Hern!andez-Velasco, J.: **Neutron powder diffraction study of Nd0.92Ca0.08MnO3** Physica B **350** (2004) e19 – e21	E6 IHP II: 406
Garcia-Matres, E.; Wiedenmann, A.; Kumar, G.; Eckert, J.; Hermann, H.; Schultz, L.: **Hard magnetic properties of bulk amorphous $Nd_{60}Fe_{20}Co_{10}Al_{10}$ investigated by SANSPOL** Physica B **350** (2004) e315 – e318	V4
Gardiner, C.H.; Boothroyd, A.T.; McKelvy, M.J.; McIntyre, G.J.; Prokes, K.: **Field-induced magnetic and structural domain alignment in PrO_2** Physical Review B **70** (2004) 024416 – 1/11	E4 IHP I: 227
Genzel, C.: **Problems related to X-ray stress analysis in thin films in the presence of gradients and texture** In: Mittemeijer E.J. ; Scardi P. [Eds.] : Diffraction analysis of the microstructure of materials. Berlin: Springer, Springer series in materials science (ISBN 3-540-40519-4) **68** (2004) 473-503	X-ray
Gil, A.; Kaczorowski, D.; Hernández-Velasco, J.; Penc, B.; Wawrzynska, E.; Szytula, A.: **Magnetic structures of RCu_xGe_2 (R=Ho, Er) compounds** Journal of Alloys and Compounds **384** (2004) L4 – L6	E6 IHP I: 216
Gil, A.; Penc, B.; Hernandez-Velasco, J.; Szytula, A.; Zygmunt, A.: **Neutron diffraction studies of Rni_xSn_2 (R=Tb, Dy and Ho) compounds** Physica B **350** (2004), e119 – e122	E6 IHP I
Gil, A.; Penc, B.; Stüßer, N.; Szytula, A.: **Magnetic phase transitions in $Tb_{0.4}\,Nd_{0.6}\,NiGe_2$ compound** Physica B **350** (2004) e327 – e330	E6 IHP I: 216
Gil, A.; Penc, B.; Wawrzynska, E.; Hernandez-Velasco, J.; Szytula, A.; Zygmunt, A.: **Magnetic properties and magnetic structures of Rco_xSn_2 (R=Gd-Er) compounds** Journal of Alloys and Compounds **365** (2004) 31 – 34	E6 IHP I: 216

Publications 2004
BENSC Experiments and BENSC Authors

Giuliani, A.; Albertini, G.; Manescu, A.: **Residual stress analysis on tensile MMC specimens after loading/unloading tests in several conditions** Physica B **350** (2004) e499 - e502	E3 IHP I: 204
Glavatska, N.; Mogylnyy, G.; Danilkin, S.; Hohlwein, D.: **Temperature dependence of lattice parameters in Martensite and effect of the external magnetic field on Martensite structure in Ni2MnGa Studied In-Situ with neutron diffraction** Materials Science Forum **443-444** (2004) 397 - 400	E2
Gondek, L.; Szytula, A.; Baran, S.; Szajek, A.; Hernandez-Velasco, J.: **Neutron-diffraction studies of $R3Co_8Sn_4$ (R=Y, Tb, Ho, Er) compounds** Physica B **350** (2004) e123 - e126	E6 IHP I: 315 IHP II: 466
Gondek, L.; Szytula, A.; Baran, S.; Hernandez-Velasco, J.: **Neutron diffraction studies of the hexagonal RTIn (R=rare earth, T=Au or Ni) compounds** Journal of Magnetism and Magnetic Materials **272-276** (2004) E443 - E444	E6 IHP II: 465
Gondek, L.; Szytula, A.; Baran, S.; Rams, M.; Hernandez-Velasco, J.; Tyvanchuk, Yu.: **Magnetic structures of non-stoichiometric hexagonal $Rni_{1-x}In_{1+x}$ (R=Dy, Ho, Er) compounds** Journal of Magnetism and Magnetic Materials **278** (2004) 392 - 396	E6 IHP II: 577
Gratz, E.; Paul-Boncour, V.; Hense, K.; Hilscher, G.; Pieper, M.W.; Hoser, A.; Markosyan, A.S.; Niki, H.: **Magnetic instabilities in Er1 xYxCo3 pseudo-binary compounds (x=0.1, 0.3, and 0.5)** Physica B **350** (2004) e151 - e154	E6 IHP II: 442
Gutberlet, T.; Steitz, R.; Fragneto, G.; Klösgen, B.: **Phospholipid bilayer formation at a bare Si surface: a time-resolved neutron reflectivity study** Journal of Physics: Condensed Matter **16** (2004) S2469-S2476	ILL
Gutberlet, T.; Klösgen, B.; Krastev, R.; Steitz, R.: **Neutron reflectivity as a method to study in-situ adsorption of phospholipid layers to solid-liquid interfaces** Advanced Engineering Materials **6** (2004) 832-836	V6 IHP II: 553
Habicht, K.; Golub, R.; Mezei, F.; Keimer, B.; Keller, T.: **Temperature-dependent phonon lifetimes in lead investigated with neutron-resonance spin-echo spectroscopy** Physical Review B **69** (2004) 104301 - 1/8	V2
Habicht, K.; Keller, T.; Golub, R.: **The resolution matrix for neutron spin-echo three-axis spectroscopy** Physica B **350** (2004) e803 - e806	no n
Han, Y.S.; Seong, B.S.; Lee, C.H.; Lee, G.H.; Rhee, C.K.; Kim, W.W.; Wiedenmann, A.: **SANS study of microstructural inhomogeneities on Al nano-powder compacts** Physica B **350** (2004) e1015 - e1018	V4
Harjo, S.; Motohashi, Y.; Saroun, J.; Ryukhtin, V.; Strunz P.; Baron, M.; Loidl, R.: **Cavitation behaviours in a tetragonal zirconia polycrystal subjected to superplastic deformations measured by SANS method** Materials Science Forum **447-448** (2004) 67 - 72	
Harjo, S.; Saroun, J.; Motohashi, Y.; Kojima, N.; Ryukhtin, V.; Strunz, P.; Baron, M.; Loidl, R.: **Flat cavities formed in TZP caused by superplastic deformations at high strain-rates and their effect on elongation** Materials Transactions **45** (2004) 824 - 832	
Heinemann, A.; Wiedenmann, A.; Kammel, M.: **The full potential of small-angle scattering with polarised neutrons for structure parameter evaluation in magnetic liquids** Physica B **350** (2004) e207 - e210	V4

Publications 2004
BENSC Experiments and BENSC Authors

Heinemann, A.; Wiedenmann, A.; Kammel, M.; Boennemann, Matousevitch, H.N.: **High-quality structure parameter for magnetic liquids obtained by small-angle scattering of polarized neutrons** Applied Organomet. Chem. **118** (2004) 561 - 564	V4
Hense, K.; Gratz, E.; Novotny, H.; Hoser, A.: **Lattice dynamics and the interaction with the crystal electric field in $NdCu_2$** J. Phys. Condens. Matter **16** (2004) 5751-5768	E1 IHP I: 183
Hoell, A.; Wiedenmann, A.; Heyen, U.; Schüler, D.: **Nanostructures and field-induced arrangement of magnetosomes studied by SANSPOL** Physica B **350** (2004) e309 - e314	V4
Hoelzel, M.; Danilkin, S.A.; Ehrenberg, H.; Toebbens, D.M.; Udovic, T.J.; Fuess, H.; Wipf, H.: **Effects of high-pressure hydrogen charging on the structure of austenitic stainless steels** Materials Science and Engineering A **384** (2004) 255 - 261	E9
Hofmann, M.; Campbell, S.J.; Edge, A.V.J.: **Valence and magnetic transitions in $YbMn_2Si_{2-x}Ge_x$** Journal of Magnetism and Magnetic Materials **272-276** (2004) e489 - e490	E6 IHP I: 228
Hofmann, M.; Campbell, S.J.; Edge, A.V.J.: **EuMn2Ge2 and $EuMn_2Si_2$ - Magnetic Structures and Valence Transitions** Physical Review B: Condensed Matter **69** (2004) 1174432 - 174440	E6
Hofmann, M.; Campbell, S.J.; Ehrhardt, H.; Feyerherm, R.: **The magnetic behaviour of nanostructured zinc ferrite** Journal of Material Science **39** (2004) 5057 - 5065	E6
Hoinkis, E.: **Small-angle scattering studies of adsorption and of capillary condensation in porous solids** Part. Part. Syst. Charact. **21** (2004) 80 - 100	V4
Hoinkis, E.; Lima, E.B.F.; Schubert-Bischoff, P.: **A study of Carbon Corax N330 with small-angle scattering of neutrons and X-rays** Langmuir **20** (2004) 8823 - 8830	V4
Hutanu, V.; Habicht, A.; Rupp, A.: **Neutron spin filters (NSF) obtained by metastability- exchange optical pumping (MEOP) and mechanical compressing of ^3He gas** Proceedings of SPIE (SPIE, Bellingham, WA) **5581** (2004) 418 - 427	
Hutanu, V.; Rupp, A.: **Studies on optical pumping cells (OPC) to polarize ^3He** Physica B **350** (2004) e703 - e706	-
Iolin, E.; Rusevich, L.; Strobl, M.; Treimer, W.; Mikula, P.: **Application of ultrasound for the simultaneous improvement intensity and resolution of the Bonse-Hart diffractometer** Nuclear Instruments and Methods in Physics Research **A 529** (2004) 152-156	V12a IHP II: 570
Jauch, W.: **Electron densities in relation to magnetism: gamma-ray diffraction from transition-metal monoxides and difluorides** Acta Crystallographica A **60** (2004) 397-401	X-ray
Jauch, W.; Reehuis, M.: **Electron density distribution in paramagnetic and antiferromagnetic NiO: a γ-ray diffraction study** Physical Review **B 70** (2004) 195121 - 1/8	X-ray
Jauch, W.; Reehuis, M.; Schultz, A.J.: **Gamma-ray and neutron diffraction studies of CoF_2: magnetostriction, electron density and magnetic moments** Acta Crystallographica Section A: Foundations of Crystallography **60** (2004) 51 - 57	X-ray + IPNS

Publications 2004
BENSC Experiments and BENSC Authors

Jaworska-Golab, T.; Szytula, A.; Baran, S.; Penc, B.; Zygmunt, A.; Stüßer, N.: **Magnetic ordering of $TbRu_{2-x}Pd_xSi_2$ solid solutions investigated by magnetometric and powder neutron diffraction** Physica B **350** (2004) e183 - e186	E6 IHP I: 041
Jensen, A.; Norgaard Toft, K.; Abrahamsen, A.B.; Andersen, N.H.; Jensen, J.; Hedegard, P.; Klenke, J.; Prokes, K.; Smeibidl, P.; Danilkin, S.; Sikolenko, V.; Eskildsen, M.R.; Canfield, P.C.: **Magnetic phase diagram of $ErNi_2B_2C$** Physica C **408-410** (2004) 97 - 99	E1, E4 IHP II: 403 IHP II: 501
Jensen, A.; Norgaard Toft, K.; Abrahamsen, A.B.; McMorrow, D.F.; Eskildsen, M.R.; Andersen, N.H.; Jensen, J.; Hedegard, P.; Klenke, J.; Danilkin, S.; Prokes, K.; Sikolenko, V.; Smeibidl, P.; Bud'ko, S.L.; Canfield, P.C.: **Field-induced magnetic phases in the normal and superconducting states of $ErNi_2B_2C$** Physical Review B **69** (2004) 104527 - 1/11	E1, E4 IHP II: 403 IHP II: 501
Keller, T.; Habicht, K.; Golub, R.; Mezei, F.: **Roton and phonon linewidths in superfluid ^4He** Europhysics Letters **67** (2004) 773-778	V2
Kolenda, M.; Hofmann, M.; Penc, B.; Szytula, A.: **Magnetic structures of $ErPd_2X$ (X=Si, Ge) compounds** Physica B **350** (2004) e191 - e194	E6 IHP I: 041
Krist, Th.: **Solid state and conventional neutron optical elements** Nuclear Instruments and Methods in Physics Research Section A **529** (2004) 50 - 53	V14
Kumar, M.S.; Shah, V.R.; Schanzer, C.; Böni, P.; Krist, T.; Horisberger, M.: **Polarized neutron reflectivity of FeCoV/Ti multilayers** Physica B **350** (2004) e241 - e244	V14
Lake, B.; Aeppli, G.; Christensen, N.B.; Lefmann, K.; McMorrow, D.F.; Clausen, K.N.; Roennow, H.M.; Vorderwisch, P.; Smeibidl, P.; Mankorntong, M.; Sasagawa, T.; Nohara, M.; Takagi, H.; Hussey, N.E.: **Effects of magnetic field on the cuprate high-T_C superconductor $La_{2-x}Sr_xCuO_4$** Notiziario Neutroni e Luce di Sincrotrone **Vol. 9** No. 1 (2004) 4-9	
Lebedev, V.T.; Torok, Gy.; Vinogradova, L.V.; Orlova, D.N.; Melenevskaya, E.Yu.; Zgonnik, V.; Treimer, W.: **Superstructures of polymeric stars with fullerene core in solutions** Fullerenes, Nanotubes, and Carbon Nanostructures **12** (2004) 377-383	V12a
Lieutenant, K.; Zsigmond, G.; Manoshin, S.; Fromme, M.; Bordallo, H.N.; Champion, J.D.M.; Peters, J.; Mezei, F.: **Neutron instrument simulation and optimization using the software package VITESS** In: Sanchez del Rio M. [Ed.] : Avances in Computational Methods for X-ray and Neutron Optics : 3, 5 August 2004, Denver, Colorado, USA. Bellingham, Wash.: SPIE, 2004 (SPIE proceedings series ; 5536). - ISBN 0-8194-5474-5, p. 134-145	Simulation
Lieutenant, K.; Zsigmond, G.: **Optimisation of guide exits by combining MC simulations and optimising routines** Physica B **350** (2004) e687 - e690	Simulation
Ling, C.D.; Granado, E.; Neumeier, J.J.; Lynn, J.W.; Argyriou, D.: **Magnetic inhomogeneities in electron-doped $Ca_{1-x}La_xMnO_3$** Journal of Magnetism and Magnetic Materials **272-276** (2004) 246-248	NCNR
Liu, Y.T.; Fritzsche, H.; Hauschild, J.; Maletta, H.: **Polarized neutron refelctometry study of thin Fe films prepared on V(100)** Physica B **350** (2004) e225 - e227	V6
Llobet, A.; Bao, W.; Moreno, N.O.; Pagliuso, P.G.; Sarrao, J.L.; Thompson, J.D.; Prokes, K.; Mignot, J.M.: **Interplay between magnetism and superconductivity in $CeMIn_5$ heavy fermion** Journal of Magnetism and Magnetic Materials **272-276** (2004) 175 - 176	E4

Publications 2004
BENSC Experiments and BENSC Authors

Lonkai, Th.; Amann, U.; Tomuta, D.G.; Hohlwein, D.; Ihringer, J.: **Magnetostriction in hexagonal HoMnO3** Proceedings of the NATO Advanced Research Workshop "Magnetoelectric Interaction Phenomena in Crystals", Herausgeber: M. Fiebig, V. Eremenko und I. Chupis, Cluwer, Dordrecht (2004) 115 - 123	E2
Lonkai, Th.; Tomuta, D.G.; Amann, U.; Ihringer, J.; Többens, D.; Hendrikx, R.; Mydosh, J.: **Development of the high temperature phase of hexagonal manganites** Physical Review B: Condensed Matter **69** (2004) 134108 - 1/10	E9
Lottermoser, Th.; Lonkai, Th.; Amann, U.; Hohlwein, D.; Ihringer, J.; Fiebig, M.: **Magnetic phase control by an electric field** Nature **430** (2004) 541 - 544	E2
Mang, P.K.; Larochelle, S.; Mehta, A.; Vajk, O.P.; Erickson, A.S.; Lu, L.; Buyers, W.J.L.; Marshall, A.F.; Prokes, K.; Greven, M.: **Phase decomposition and chemical inhomogeneity in $Nd_{2-x}Ce_xCuO_{4\pm delta}$** Phys. Rev. B **70** (2004) 094507 - 1/10	E4
Matas, S.; Batko, I.; Flachbart, K.; Paderno, Y.; Shitsevalova, N.; Siemensmeyer, K.: **Neutron diffraction on HoB_{12}** Journal of Magnetism and Magnetic Materials **272-276** (2004) e435 - e437	E6
Matsuura, M.; Dai, P.; Kang, H.J.; Lynn, J.W.; Argyriou, D.N.; Onose, Y.; Tokura, Y.: **Magnetic-field effect on static antiferromagnetic order above hte upper critical field in $Nd_{1.85}Ce_{0.15}CuO_4$** Physical Review B: Condensed Matter **69** (2004) 104510-1/5	E4
McKinsey, D.N.; Brome, C.R.; Butterworth, J.S.; Dzhosyuk, S.N.; Golub, R.; Habicht, K.; Huffman, P.R.; Mattoni, C.E.H.; Yang, L.; Doyle, J.M.: **Detecting ionizing radiation in liquid helium using wavelength shifting light collection** Nuclear Instruments and Methods in Physics Research A 516 (2004) 475-485	
Milne, C.J.; Argyriou, D.N.; Chemseddine, A.; Aliouane, N.; Veira, J.; Landsgesell, S.; Alber, D.: **Revised superconducting phase diagram of hole-doped $Na_x(H_3O)_2CoO_2 * yH_2O$** Physical Review Letters **93** (2004) 247007 - 1/4	X-ray + NAA
Mitsuda, S.; Okano, H.; Kobayashi, S.; Prokes, K.: **Non-magnetic impurity effect on domain growth kinetics in an isosceles triangular Ising antiferromagnet $CoNb_2O_6$** Journal of Magnetism and Magnetic Materials **272-276** (2004) e993-e994	Jaeri
Mukherjee, C.J.; Coldea, R.; Tennant, D.A.; Koza, M.; Enderle, M.; Habicht, K.; Smeibidl, P.; Tylczynski, Z.: **Field-induced quantum phase transition in the quasi 1D XY-like antiferromagnet Cs_2CoCl_4** Journal of Magnetism and Magnetic Materials **272-276** (2004) 920 - 921	V2 IHP I: 230 IHP II: 476 IHP II: 522
Niewa, R.; Zherebtsov, D.A.: **New phases in the lithiumnitridovanadate system - the solid solution Li7-2xMgx[VN4] (0 <x < 1)** Z. Anorg. Allg. Chem. **630** (2004) 229 - 233	E9
Niewa, R.; Zherebtsov, D.A.; Schnelle, W.; Wagner, F.R.: **Metal-metal bonding in $ScTaN_2$. A new compound in the system ScN - TaN** Inorganische Chemie **43** (2004) 6188 - 6194	E9
Norgaard Toft, K.; Abrahamsen, A.B.; Eskildsen, M.R.; Lefmann, K.; Andersen, N.H.: **Neutron diffraction study of anomalous high-field magnetic phases in $TmNi_2B_2C$** Physical Review B **69** (2004) 214507	V2 TMR/IHP DK.07
Ohl, M.; Monkensbusch, M.; Richter, D.; Pappas, C.; Lieutenant, K.; Krist, Th.; Zsigmond, G.; Mezei, F.: **The high-resolution neutron spin-echo spectrometer for the SNS with t>=1µs** Physica B **350** (2004) 147 - 150	
Panckow, A.N.; Sladkov, D.; Singh, P.K.; Genzel, Ch.: **Low-temperature metal ion implantation assisted deposition of hard coatings** Surface and Coatings Technology **188-189** (2004) 214-219	ETA (X-ray)

Publications 2004
BENSC Experiments and BENSC Authors

Pebler, J.; Frommen, C.; Mangold, M.; Stief, R.; Krimmel, A.; van de Kamp, R.; Ohl, M.; Regnault, L.-P.: **Comparison of the non-linear spin dynamics in antiferromagnetic chain compounds Na_2MnF_5 and $(ND_4)_2MnF_5$** Z. Anorg. Allg. Chem. **630** (2004) 829 - 840	V2
Penc, B.; Wawrzynska, E.; Szytula, A.; Gil, A.; Hernández-Velasco, J.; Zygmunt, A.: **Magnetic structure of ErT_xSn_2 (T=Co, Ni) compounds** Journal of Alloys and Compounds **375** (2004) L1 - L3	E6 IHP I: 216
Penc, B.; Szytula, A.; Wawrzynska, E.; Hernández-Velasco, J.: **Magnetic structures and magnetic phase transitions in $TbCoSi_2$** Journal of Alloys and Compounds **366** (2004) 120 - 123	E6 IHP I: 216
Pieper, J.; Irrgang, K.-D.; Renger, G.; Lechner, R.E.: **Density of vibrational states in the light-harvesting complex II of green plants studied by inelastic neutron scattering** Journal of Physical Chemistry B **108** (2004) 10556 - 10565	V3
Pintschovius, L.; Reznik, D.; Pfleiderer, C.; v. Löhneysen, H.: **Partial order in the itinerant-electron magnet MnSi** PRAMANA-journal of physics **63** (2004) 117 - 123	V4
Pop, L.; Hilljegerdes, J.; Odenbach, S.; Wiedenmann, A.: **The microstructure of ferrofluids and their rheological properties** Applied Organometallic Chemistry **18** (2004) 523 - 528	V4
Prager, M.; Pieper, J.; Buchsteiner, A.; Desmedt, A.: **Methyl rotational potentials as a probe of the cage potential surface in methyl iodide clathrate** Physica B **350** (2004) e399 - e402	V3
Prager, M.; Pieper, J.; Buchsteiner, A.; Desmedt, A.: **Probing adsorption sites in a cubic II water clathrate cage by methyl rotational tunneling of CH_3I guest molecules** Journal of Physics: Condensed Matter **16** (2004) 7045 - 7061	V3
Pritula, O.; Smrcok, L.; Többens, D.M.; Langer, V.: **X-ray and neutron Rietveld quantitative phase analysis of industrial Portland cement clinkers** Powder Diffraction **19** (2004) 232 - 239	E9 IHP II: 580
Regulski, M.; Przenioslo, R.; Sosnowska, I.; Hohlwein, D.; Schneider, R.: **Neutron diffraction study of the magnetic structure of α-Mn_2O_3** Journal of Alloys and Compounds **362** (2004) 236 - 240	E2
Regulski, M.; Przenioslo, R.; Sosnowska, I.; Hoffmann, J.-U.: **Short and Long Range Magnetic Ordering in β-MnO_2 - A Temperature Study -** Journal of the Physical Society of Japan **73** (2004) 3444 - 3447	E9 IHP II: 576
Rogante, M.; Battistella, P.; Rustichelli, F.: **Residual stress measurement by neutron diffraction in AA6082 extruded samples submitted to different quenching rates** Journal of Alloys and Compounds **378** (2004) 335 - 338	E3
Rüegg, Ch.; Cavadini, N.; Furrer, A.; Güdel, H.U.; Krämer, K.; Mutka, H.; Habicht, K.; Vorderwisch, P.; Wildes, A.: **Spin dynamics in the BEC phase of the S=1/2 quantum spin system $TlCuCl_3$** Journal of Magnetism and Magnetic Materials **272-276** (2004) 195 - 196	V2
Rüegg, Ch.; Oettli, M.; Schefer, J.; Zaharko, O.; Furrer, A.; Tanaka, H.; Krämer, K.W.; Güdel, H.U.; Vorderwisch, P.; Habicht, K.; Polinski, T.; Meissner, M.: **Neutron scattering study of the field-dependent ground state and the spin dynamics in spin-one-half NH_4CuCl_3** Physical Review Letters **93** (2004) 37207-1 - 37207-4	V2 IHP II: 543 NMI3: 1006
Ryukhtin, V.; Saroun, J.; Harjo, S.; Motohashi, Y.; Wiedenmann, A.; Strunz, P.: **SANS investigations of pore anisotropy in superplastically deformed ceramics** Physica B **350** (2004) e1019 - e1020	V4 IHP II: 445

Publications 2004
BENSC Experiments and BENSC Authors

Saroun, J.; Kocik, J.; Strunz, P.: **Investigation of radiation damage in VVER-440 reactor vessel steels by SANS** Physica B **350** (2004) e755 - e758	V4 IHPI: 039
Schanzer, C.; Shah, V.R.; Böni, P.; Krist, T.: **Investigation of magnetization reversal in FeCoV/Ti multilayers** Physica B **350** (2004) e221 - e224	V14
Schmitz, D.; Hauschild, J.; Imperia, P.; Liu, Y.T ; Maletta, H.: **Element-specific investigation of the magnetization of ultrathin Fe on a V(110) single crystal** Journal of Magnetism and Magnetic Materials **269** (2004) 89 - 94	UE46-PGM
Schorr, S.; Tovar, M.; Stüßer, N.; Bente, K.: **Investigation of structural anomaly and metal ordering in the solid solution 2ZnS-CuInS$_2$ by neutron** Physica B **350** (2004) e411 - e414	E6
Schüpp, B.; Sekar, C.; Gruner, W.; Auffermann, G.; Bähtz, C.; Krabbes, G.: **Crystal structure investigations and thermal behaviour of the five-leg spin ladder compound La$_8$Cu$_7$O$_{19}$** Z. Anorg. Allg. Chem. **630** (2004) 663 - 668	E9
Shi, H.; Zhang, S.; Steitz, R.; Chen, J.; Uredat, S.; Findenegg, G.H.: **Surface coatings of PEO-PPO-PEO block copolymers on native and polystyrene-coated silicon wafers** Colloids and Surfaces A: Physiochemical and Engineering Aspects **246** (2004) 81-89	X-Ray Refl.
Sikolenko, V.V.; Sazonov, A.P.; Troyanchuk, I.O.; Többens, D.; Zimmermann, U.; Pomjakushina, E.V.; Szymczak, H.: **Magnetic properties of La$_{\{1-x\}}$Sr$_x$CoO$_3$ (x = 0.15 and 0.3)** Journal of Physics: Condensed Matter **16** (2004) 7313-7320	E9
Stefanopoulos, K.L.; Steriotis, T.A.; Mitropoulos, A.C.; Kanellopoulos, N.K.; Treimer, W.: **Characterisation of porous materials by combining mercury porosimetry and scattering techniques** Physica B **350** (2004) e525 - e528	V4, V12a IHP I: 056
Steitz, R.; Müller-Buschbaum, P.; Schemmel, S.; Cubitt, R.; Findenegg, G.H.: **Lateral structure of a surfactant layer adsorbed at a hydrophilic solid/liquid interface** Europhysics Letters **67** (2004) 962-968	ILL
Steriotis, Th.; Kikkinides, E.; Kainourgiakis, M.; Stubos, A.: **Monitoring adsoption by small angle neutron scattering in tandem with digital reconstruction-simulation techniques** Colloids and Surfaces A: Physicochem. and Eng. Aspects **241** (2004) 231 - 237	V4
Steriotis, Th.; Stefanopoulos, K.; Kanellopoulos, N.; Mitropoulos, A.; Hoser, A.: **The structure of adsorbed CO$_2$ in carbon nanopores: a neutron diffraction study** Colloids and Surfaces A: Physicochem. and Eng. Aspects **241** (2004) 239 - 244	E2 IHP I: 020
Stockert, O.; Faulhaber, E.; Zwicknagl, G.; Stüßer, N.; Jeevan, H.S.; Deppe, M.; Borth, R.; Küchler, R.; Loewenhaupt, M.; Geibel, C.; Steglich, F.: **Nature of the a phase in CeCu$_2$Si$_2$** Physical Review Letters **92** (2004) 136401 - 1/4	E6
Stockert, O.; Hossain, Z.; Deppe, M.; Hohlwein, D.; Geibel, C.: **Magnetic order of CePd$_5$Ge$_3$ and CePt$_5$Ge$_3$** Journal of Magnetism and Magnetic Materials **272-276** (2004) e479 - e480	E2
Strobl, M.; Treimer, W.; Hilger, A.: **Small angle scattering signals for (neutron) computerized tomography** Applied Physics Letters 85 (2004) 488 - 490	V12a
Strobl, M.; Treimer, W.; Hilger, A.: **First realisation of a three-dimensional refraction contrast computerised neutron tomography** Nuclear Instruments and Methods in Physics Research B **222** (2004) 653 - 658	V12a

Publications 2004
BENSC Experiments and BENSC Authors

Strobl, M.; Treimer, W.; Hilger, A.; Feye-Treimer, U.: **Neutron tomography in double crystal diffractometers** Physica B **350** (2004) 155 - 158	V12a
Strunz, P; Schumacher, G; Vassen, R.; Wiedenmann, A.: **In-situ SANS study of pore microstructure in YSZ thermal barrier coatings** Acta Materialia **52** (2004) 3305 - 3312	V4
Stüßer, N.; Schotte, U.; Hoser, A.; Meißner, M.: **Field-distorted magnetic spiral structure of $CsCuCl_3$** Physica B **350** (2004) e47 - e50	E1
Szytula, A.; Duraj, R.; Hernández-Velasco, J.; Penc, B.; Venturini, G.; Wawrzynska, E.: **Magnetic structure of $NdMn_{2-x}$ Fe_xGe_2 (x=0.1 and 0.15) compounds** Journal of Alloys and Compounds **377** (2004) 21 - 24	E6 IHP I: 315
Szytula, A.; Oles, A.; Penc, B.; Stüßer, N.: **Magnetic structure of the HoPdSn compound** Journal of Alloys and Compounds **370** (2004) L14 - L16	E6 IHP I: 217
Szytula, A.; Penc, B.; Wawrzynska, E.; Hernández-Velasco, J.; Zygmunt, A.: **Magnetic structure of $HoPd_2Ge_2$** Journal of Alloys and Compounds **365** (2004) 39 - 42	E6 IHP I: 153
Szytula, A.; Wawrzynska, E.; Penc, B.; Hernández-Velasco, J.; Zygmunt, A.: **Magnetic ordering and phase transitions in $R_3Cu_4X_4$** Journal of Magnetism and Magnetic Materials **272-276** (2004) 618 - 619	E6 IHP II: 466 IHP II: 519
Szytula, A.; Wawrzynska, E.; Penc, B.; Stüßer, N.; Tomkowicz, Z.; Zygmunt, A.: **Magnetic properties and electronic structure of $R_3T_4X_4$ (R: La-Nd, Gd-Er; T: Mn, Cu; X: Ge, Sn)** Journal of Alloys and Compounds **367** (2004) 224 - 229	E6 IHP II: 466
Tatchev, D.; Heinemann, A.; Wiedenmann, A.; Hoell, A.: **Determination of particle size distributions by small-angle scattering with polarized neutrons usnig maximum-entropy method** Journal of Applied Crystallography **37** (2004) 40 - 47	
Terada, N.; Mitsuda, S.; Prokes, K.; Suzuki, O.; Kitazawa, H.; Aruga Katori, H.: **Impact of small number of non-magnetic impurity on H-T magnetic phase diagram of $CuFeO_2$** Physical Review B: Condensed Matter **70** (2004) 174412 - 1/7	E4
Toda, M.; Fujii, Y.; Chiba, M.; Kawano, S.; Goto, T.; Klenke, J.; Graf, H.A.; Steiner, M.: **Neutron diffraction study of the field-induced order in singlet-ground state magnet $CsFeCl_3$** Journal of Magnetism and Magnetic Materials **272-276** (2004) 378 - 379	E1
Troyanchuk, I.O.; Khomchenko, V.A.; Tovar, M.; Szymczak, H.; Barner, K.: **Orbital correlations and magnetic phase transitions in lightly doped $La_{0.88}MnO_x$ and $LaMn_{0.94}O_y$ manganites.** Acta Physica Polonica A **105** (2004) 27 - 44	E9 IHP II: 520
Troyanchuk, I.O.; Khomchenko, V.A.; Tovar, M.; Szymczak, H.; Barner, K.: **Antiferromagnet-ferromagnet and structural phase transitions in $La_{0.88}MnO_x$ manganites** Physical Review B: Condensed Matter **69** (2004) 54432 - 1/12	E9 IHP II: 520
Ulbricht, A.; Böhmert, J.: **Small angle neutron scattering analysis of the radiation susceptibility of reactor pressure vessel steels** Physica B **350** (2004) e483 - e486	V4
v. Klitzing, R.; Wong, J.E.; Jaeger, W.; Steitz, R.: **Short range interaction in polyelectrolyte multilayers** Current Oppinion in Colloid and Interface Science **9** (2004) 158 - 162	V6
Vorderwisch, P.; Sobolev, O.; Desmedt, A.: **NH_3 quantum rotators in Hofmann clathrates: intensity and width of rotational transition lines** Physica B **350** (2004) e391 - e394	V3

Publications 2004
BENSC Experiments and BENSC Authors

Wagner, V.; Hesse, J.; Klenke. J.; Pappas, C.: **Dynamics of spin freezing in the re-entrant spin glass FeNiMn** Physica B **350** (2004) e1051 - e1054	V5
Wawrzynska, E.; Hernández-Velasco, J.; Penc, B.; Szytula, A.: **Magnetic structures of $R_3Cu_4Sn_4$ (R=Tb-Er)** Physica B **350** (2004) e127 - e130	E6 IHP II: 466
Wawrzynska, E.; Hernández-Velasco, J.; Penc, B.; Szytula, A.: **Magnetic structures of $R_3Cu_4Sn_4$ (R=Pr and Nd)** Journal of Physics: Condensed Matter **16** (2004) 45 - 52	E6 IHP II: 466
Wawrzynska, E.; Hernández-Velasco, J.; Penc, B.; Szytula, A.; Tomala, K.: **Magnetic structures of $R_3Ag_4Sn_4$ (R=Pr, Nd) and $Nd_3Cu_4Ge_4$** Journal of Physics: Condensed Matter **16** (2004) 7535 - 7544	E6 NMI3: 1027
Wawrzynska, E.; Hernández-Velasco, J.; Penc, B.; Szytula, A.: **Magnetic structures of R3Cu4Si4 (R=Dy, Ho and Er)** Journal of Magnetism and Magnetic Materials **280** (2004) 234 - 242	E6 IHP II: 519
Weissmuller, J.; Michels, A.; Michels, D.; Wiedenmann, A.; Krill, C.E.; Sauer, H.M.; Birringer, R.: **Spin structure of nanocrystalline terbium** Physical Review B: Condensed Matter **69** (2004) 54402-1/16	V4
Wiechert, H.; Kortmann, K.D.; Stüßer, N.: **Realization of a two-dimensional Ising system: Deuterium physisorbed on krypton-preplated graphite** Physical Review B: Condensed Matter **70** (2004) 125410-1/14	E6
Wiedenmann, A.; Kammel, M.; Hoell, A.: **Pseudo-crystalline ordering in ferrofluids induced by magnetic fields** Journal of Magnetism and Magnetic Materials **272-276** (2004) 1487 - 1489	V4
Wilmer, D.; Feldmann, H.; Lechner, R.E.: **Fast cation conduction and anion rotational disorder in the high-temperature phase of lithium sodium sulfate** Z. Phys. Chem. **218** (2004) 1439 - 1454	V3
Wilmer, D.; Feldmann, H.; Lechner, R.E.; Combet, J.: **Correlated motion of anions and cations in fast cation conducting rotor phases** Solid State Ionics **175** (2004) 463 - 466	V3
Wolter, A.U.B.; Wzietek, P.; Süllow, S.; Litterst, F.J.; Auban-Senzier, P.; Jérome, D.; Feyerherm, R.; Klauss, H.H.: **^{13}C-NMR study of the S=1/2 antiferromagnetic coupled spin chain compound [PM $Cu(NO_3)_2(H_2O)_2]_n$ under pressure** Journal de Physique IV **114** (2004) 147 - 148	no n
Wolter, A.U.B.; Wzietek, P.; Süllow, S.; Litterst, F.J.; Auban-Senzier, P.; Jérome, D.; Feyerherm, R.; Klauss, H.-H.: **^{13}C-NMR under pressure on [PM * $Cu(NO_3)$ * $(H_2O)_2]_n$** Journal of Magnetism and Magnetic Materials **272-276** (2004) 1056 - 1057	no n
Wosnitza, J.; Hagel, J.; Stockert, O.; Pfleiderer, C.; Schlueter, J.A.; Mohtasham, J.; Gard, G.L.: **Fermi surface reconstruction close to a pressure-induced metal-insulator transition** Journal de Physique IV **114** (2004) 277 - 281	E6
Young, S. H.; Baek, S. S.; Chang, H. L.; Geun, H. L ; Chang, K. R.; Whung Whoe, K.; Wiedenmann, A.: **SANS study of microstructural inhomogeneities on Al nano-powder compacts** Physica B **350** (2004) e1015 - e1018	V4
Zheludev, A.; Shapiro, S.M.; Honda, Z.; Katsumata, K.; Grenier, B.; Ressouche, E.; Regnault, L.-P.; Chen, Y.; Vorderwisch, P.; Mikeska, H.-J.; Kolezhuk, A.K.: **Dynamics of an anisotropic Haldane antiferromagnet in a strong magnetic field** Physical Review B: Condensed Matter **69** (2004) 054414 - 1/10	V2

Publications 2004
BENSC Experiments and BENSC Authors

Zrník, J.; Strunz, P.; Vrchovinský, V.; Muranský, O.; Hornak, P.; Wiedenmann, A.: **Creep deformation and microstructural examination of a prior thermally exposed nickel base superalloy** Key Engineering Materials **274-276** (2004) 925 - 930	V4 IHP I: 221
Zsigmond, G.; Lieutenant, K.; Manoshin, S.; Bordallo, H.N.; Champion, J.D.M.; Peters, J.; Carpenter, J.M.; Mezei, F.: **A survey of simulations of complex neutronic systems by VITESS** Nuclear Instruments and Methods in Physics Research Section A **529** (2004) 218 - 222	VITESS
Zvyagin, S.A.; Kolezhuk, A.K.; Krzystek, J.; Feyerherm, R.: **Excitation hierarchy of the quantum sine-Gordon spin chain in a strong magnetic field** Physical Review Letters **93** (2004) 027201 - 1/4	no n

Seminars and Conference Contributions 2004

Invited Talks

Argyriou, D.: **$Na_{0.35}CoO_2 \cdot 1.37D_2O$: implications for the superconducting phase diagram** BENSC Users' Meeting, HMI Berlin, May 14, 2004	
Argyriou, D.N.; Milne, C.J.; Chemseddine, A.; Aliouane, N.; Veira, J.; Landsgesell, S.; Alber, D.; Radaelli, P.G.; Chapon, L.C.; Cox, S.; Mathur, N.D.; Midgley, P.A.: **Structure and superconductivity in $Na_x(H_3O)_zCoO_2 \cdot yH_2O$** Deutsche Neutronenstreutagung 2004, TU Dresden, September 2004	E9
Bonini, M.: **Silica coated magnetic nanoparticles: synthesis and characterization** BENSC Users' Meeting, HMI Berlin, May 14, 2004	V4
Clemens, D.: **Progress report on neutron guide hall II and new instruments** BENSC Users' Meeting, HMI Berlin, May 14, 2004	
Dreiss, C.: **Investigation of alcohol ethoxylate surfactant in solution and adsorbed at interfaces** BENSC Users' Meeting, HMI Berlin, May 14, 2004	V4
Gamari-Seale, H.; Troyanchuk, I.O.; Sazonov, A.P.; Stefanopoulos, K.L.; Toebbens, D.M.: **Magnetic structure and magnetic behaviour of $La_{0.8}Sr_{0.2}Mn_{0.5}Co_{0.5}O_3$** 20th Hellenic Conference of Solid State Physics and Material Science, Ioannina, Greece, Sept. 2004	E9
Gamari-Seale, H.; Troyanchuk, I.O.; Sazonov, A.P.; Stefanopoulos, K.L.; Toebbens, D.M.: **The destruction of the magnetic order of La0.7Ca0.3MnO3 by 50% substitution of Mn by Co** 20th Hellenic Conference of Solid State Physics and Material Science, Ioannina, Greece, Sept. 2004	E9
Garcia-Matres, E.; Perroud O.; Kumar, G.; Wiedenmann A.: **Magnetic and crystalline nanostructure in Nd-Fe-Co-Al bulk amorphous alloys studied by SANSPOL** Sociedad española de técnicas neutrónicas and XV Symposium del grupo especializado de cristalografía, Tenerife 20-SEP-04 - 25-SEP-04	V4
Helm, C.A.: **Polyelectrolytes at interfaces** Gordon Conference on Polymer Physics, Connecticut, MS, USA, August 2004	
Ingersoll, M.: **Using neutron scattering to investigate the biological specificity of neutrophil elastase** BENSC Users' Meeting, HMI Berlin, May 14, 2004	V3, V4
Jauch, W.: **Electron densities in prototypic antiferromagnets from gamma-ray diffraction** 22nd European Crystallographic Meeting, Budapest (Ungarn) 26-AUG-04 - 31-AUG-04	
Jauch, W.: **Charge density studies of prototypic antiferromagnets by gamma-ray diffraction** XVI International School on Physics and Chemistry of Condensed Matter, Bialowieca (Polen) 01-JUL-04 - 10-JUL-04	
Kaiser-Bischoff, I.: **Diffuse scattering of cation and anion doped ZrO_2** BENSC Users' Meeting, HMI Berlin, May 14, 2004	E2
Kardjilov, N.: **Simulation of neutron radiography experiments** Int. Topical Meeting on Neutron Radiography - 5, München, Deutschland 26-JUL-04 - 26-JUL-04	V7

Seminars and Conference Contributions 2004

Krastev, R.: **Adsorption of natural polymers on modified solid surfaces studied by neutron reflectometry** BENSC Users' Meeting, HMI Berlin, May 14, 2004	V6
Krist, T.: **Neutronenoptische Bauelemente vom HMI Berlin** Vortrag, Institut für Gerätebau, Berlin Adlershof 05-NOV-04 - 05-NOV-04	
Lieutenant, K.; Zsigmond, G.; Fromme, M.; Manoshin, S.: **General features of the neutron instrument simulation package VITESS** New Opportunities for Better User Group Software (NOBUGS) 2004, PSI, Schweiz, 18-OCT-04 - 20-OCT-04	
Lieutenant, K.; Zsigmond, G.; Fromme, M.; Manoshin, S.: **New features in Vitess 2.5 and 2.5.1** MCNSI-Meeting, Villigen, Schweiz (PSI) 21-OCT-04 - 21-OCT-04	
Lieutenant, K.; Zsigmond, G.; Manoshin, S.; Fromme, M.; Bordallo, H.N.; Champion, J.D.M.; Peters, J.; Mezei, F.: **Neutron instrument simulation and optimization using the software package VITESS** SPIE International Symposium, Denver 02-AUG-04 - 06-AUG-04	
Lieutenant, K.: **Introduction to VITESS** VITESS at KAERI, Korean Atomic Energy Research Institute (KAERI), Daejon, Korea, 31-MAY-04 - 31-MAY-04	
Lieutenant, K.: **Simulation of guides using VITESS** VITESS at KAERI, Korean Atomic Energy Research Institute (KAERI), Daejon, Korea, 01-JUN-04 - 01-JUN-04	
Lieutenant, K.: **Simulation off reflectometers using VITESS** VITESS at KAERI, Korean Atomic Energy Research Institute (KAERI), Daejon, Korea, 04-JUN-04 - 04-JUN-04	
Lieutenant, K.; Zsygmond, G. **Simulation of SANS instruments using VITESS** VITES at KAERI, Korean Atomic Energy Research Institute (KAERI), Daejon, Korea JUN-04 - 30-JUN-04	
Lonkai, Th.; Amann, U.; Hohlwein, D.; Lottermoser, Th.; Fiebig, M.; Ihringer, J.: **The origin of the magnetoelectric phase control in hexagonal $HoMnO_3$** First International Workshop on Smart Materials and Structures, Kiel, 08.10.2004	E2
Manoshin, S.; Drabkin,G.; Mezei, F.: **Simulation of double Drabkin 2-PI resonators** Joint VITESS and McStas Training Course & Workshop, ISIS Facility, Abingdon, United Kingdom 05-FEB-04 - 05-FEB-04	
Mezei, F.: **Neutron scattering instruments for the study of magnetism** LANSCE Winter School on Neutron Scattering, Los Alamos, NM, USA 10-JAN-04 - 12-JAN-04	
Mezei, F.: **Time-of-flight diffraction at CW neutron sources** EXED Workshop, HMI Berlin, 09-MAY-04 - 11-MAY-04	
Mezei, F.: **Polarized neutron scattering research, the beginnings and a glimpse of the future** Conference on Polarized Neutron in Condensed Matter Investigations 2004, Washington, USA 01-JUN-04 - 04-JUN-04	
Mezei, F.: **The European spallation source project** Common meeting of the Hungarian and Austrian Physical Societies, Szombathely, Hungary, AUG-04	

Seminars and Conference Contributions 2004

Mezei, F.: **Less conventional approaches to optimize Time-of -Flight spectrometers** Workshop on Inelastic Neutron Spectroscopy 2004, Tokai, Japan 02-DEC-04 - 05-DEC-04	
Mezei, F. **Neuron scattering instruments for the study of magnetism** LANSCE Winter School on Neutron Scattering, Los Alamos, USA 10-MAY-04 - 10-MAY-04	
Perroud, O.; Garcia-Matres, E.; Eckert, J.; Wiedenmann, A.: **Magnetische und kristlline Nanostrukturen in Nd_Fe Co Al alloys** DFG SPP1120, Bad Honeff 25-MAR-04 - 25-MAR-04	V4
Pieper, J., Irrgang, K.-D., Weß, M., Hauß, Th., Dencher, N. A., Renger, G., Lechner, R.E.: **Light-induced protein dynamics in photosynthetic chromophor-protein complexes** 7th International Conference on Quasielastic Neutron Scattering (QENS 2004), Arcachon (France), 01.09.2004 - 04.09.2004	V3
Pieper, J., Irrgang, K.-D., Weß, M., Hauß, Th., Renger, G., Lechner, R.E. **Protein dynamics in photosynthetic pigment-protein complexes** 11th International Conference on Neutron Scattering Investigations in Condensed Matter, Poznan (Poland), 06.05.2004 - 08.05.2004	V3
Pintschovius, L.: **Partial magnetic order in the itinerant-elctron magnet MnSi** Conference on Neutron Scattering 2004, Bhabha Atomic Research Centre (BARC), Mumbai (India), 02.01.2004 - 04.01.2004	V4
Pop, L.M.; Odenbach, S., Wiedenmann, A.: **Untersuchung der Strukturbildung in Co-Ferrofluiden mittels Kleinwinkel-Neutronen-Streuung** Deutsche Neutronenstreutagung 2004, TU Dresden, September 2004	V4
Pynn, R.: **Probing distance and time correlations in surfaces layers** Neutron Inelastic Scattering from Surfaces, PSI, 2004	V6
Rack, A.; Eschricht, N.: **Charakterisierung von Metallschäumen mittels Synchrotron-Tomographie und 3D-Bildanalyse** Kooperation HMI-ITWM, ITWM Fraunhofer, Kaiserlautern, Germany 21-JUN-04 - 21-JUN-04	
Rüegg, Ch.: **Bose-Einstein condensation of the triplet states in the magnetic insulator $TlCuCl_3$** 20th Condensec Matter Division Conference of the European Physical Society Prague, Czech Republic, July 19-23, 2004	V2
Rupp, A.: **Polarised ^{3}He at HMI - status quo and plans** (PNT & NSF)-JRA Joint Meeting, Grenoble 18-MAR-04 - 19-MAR-04	
Schorr, S.; Tovar, M.; Stüßer, N.: **Electronic similar elements distinguished by neutron diffraction** BENSC Users' Meeting, HMI Berlin, May 14, 2004	E6, E9
Schorr, S.; Tovar, M.; Stüßer, N.; Kockelmann, W.: **Electronic similar elements distinguished by neutron diffraction** 11th International Seminar on Neutron Scattering Investigations in Condensed Matter, Poznan, Poland 6.- 8.5.2004	E9
Steitz, R.: **New aspects of water depletion and nanobubbles at extended solid/liquid interfaces** GemSem, Stranski-Laboratorium, TU Berlin, Berlin 30-JUN-04 - 30-JUN-04	V6
Steitz, R.; Schemmel, S.; Findenegg, G. H.: **New aspects of water depletion and nanobubbles at extended solid/liquid interfaces** French-German Network "Complex Fluids: from 3 to 2 Dimensions", Toulouse 12-MAY-04 - 15-MAY-04	V6
Steitz, R.; Shi, H.; Findenegg, G. H.: **Microstructured PEO-PPO-PEO block copolymer layers on silicon wafers** French-German Network Complex Fluids: from 3 to 2 Dimensions, Münster 18-NOV-04 - 20-NOV-04	V6

Seminars and Conference Contributions 2004

Steitz, R.; v. Klitzing, R.: **Internal Structure of polyelectrolyte multilayers at solid interfaces** Workshop on Exploring the nanostructures of soft materials with x-rays, Bad Honnef, 09.05.2004 - 12.05.2004	V6
Steriotis, Th.: **Investigations of stratum corneum: structural and dynamic properties based on neutron techniques** BENSC Users' Meeting, HMI Berlin, May 14, 2004	V1, V3, V4
Stockert, O.: **Nature of the A-Phase in $CeCu_2Si_2$** BENSC Users' Meeting, HMI Berlin, May 14, 2004	E4, E6
Strobl, M.: **Tomography at HMI: status and projects in progress** BENSC Users' Meeting, HMI Berlin, May 14, 2004	V 7 V12
Strunz, P.; Schumacher, G.; Vassen, R.: **Sintering process in ceramic thermal barrier coatings** 6th SINQ-Users' Meeting, PSI Villigen, 22.01.2004 - 22.01.2004	V4
Szytula, A.: **Magnetic phase transitions in the rare earth intermetallic** MAG-EL-MAT Members Meeting- New Materials for magnetoelectronics, Poznan, 13.04.2004 - 16.04.2004	E6
Szytula, A.; Gil, A.; Hernandez-Velasco, J.; Penc, B.; Wawrzynska, E.: **Magnetic properties of CeRxGe2 compounds** Int. Conf. on Strongly Correlated Electron Systems, SCES'04, Karlsruhe, Germany	(E6)
Szytula, A.; Wawrzynska, E.; Penc, B.; Hernandez-Velasco, J.: **Influence of the local symmetry on the magnetic ordering in R3Cu4Si4** 11^{th} Int. Seminar on Neutron Scattering Investigation in Condensed Matter, Poznan, 06.05.2004 - 08.05.2004	E6
Szytula, A.; Gondek, L.; Penc, B.; Hernandez-Velasco, J.: **Spin frustration in some magnetic compounds** School Superconductivity and Other Phenomena in Perovskites, Warszawa, 06.06.2004 - 10.06.2004	E6
Ulrich, C.; Lebon, A.; Maljuk, A.; Lin, C.T.; Keimer, B., Reehuis, M., Niedermayer, Ch.; Cavadini, N.; Altorfer, F., Reznyk, D.: **Helical spin arrangement and spin dynamics in metallic $SrFeO_{3-\delta}$** Deutsche Neutronenstreutagung 2004, TU Dresden, September 2004	E5
Vorderwisch, P.; Stuhr, U.; Shapiro, S.M.: **Phononendispersion in der ferromagnetischen Formgedächtnislegierung Ni_2MnGa** Deutsche Neutronenstreutagung 2004, TU Dresden, September 2004	V2
Vorderwisch, P.; Stuhr, U.; Shapiro, S.M.: **Phonon dispersion in the ferromagnetic shape memory alloy Ni_2MnGa studied by neutron spectroscopy** XIII International Materials Research Congress with Symposium on Magnetic Shape Memory Alloys, Cancun, Mexico 22-AUG-04 - 26-AUG-04	V2
Wiedenmann, A.: **Nanostructures probed by SANS** Wokshop on X-ray and Neutron Scattering, Daejeon, Korea 09-DEC-04 - 10-DEC-04	V4
Wiedenmann, A.: **Magnetic nanostructures as probed by SANSPOL** International Conference on Polarised Neutrons in Condensed Matter investigations (PNCMI 2004), Washington 02-JUN-04 - 05-JUN-04	V4
Wiedenmann, A.: **Nanostructures in liquids and amorphous materials** Int. Conference on Liquid and Amorphous materials LAM 12, Metz, France 09-JUL-04 - 14-JUL-04	V4

Seminars and Conference Contributions 2004

Wiedenmann, A.: **Nanostructures in liquids and amorphous materials as probed by SANS** Center for nanostructured Materials Technology, Seoul, Korea 08-DEC-04 - 09-DEC-04	V4
Wiedenmann, A.: **Magnetic nanostructures as probed by polarized small angle neutron scattering** Conference on Neutron Scattering, Mumbai 02-JAN-04 - 05-JAN-04	V4
Wiedenmann, A.; Heinemann, A.; Hoell, A.; Kammel, M.: **Ordering phenomena in ferrofluids observed by Small Angle Neutron Scattering** 10th International Conference on Magnetic Fluids ICMF10, Guarujá, Brasil 02-AUG-04 - 07-AUG-04	V4
Willumeit, R.: **Interaction of antibiotic peptides withmodel membranes: What can we learn from structure investigations** Einladung zum Kolloqium, Rutherford-Appleton Laboratories, ISIS, 15.06.2004	V1
Wong, J.E.; Voigt, U.; Steitz, R.; v. Klitzing, R.: **Short range interactions in polyelectrolyte multilayers** Symposium on Short range interactions in soft condensed matter, Regensburg, 26.02.2004 - 28.02.2004	V6
Zsigmond, G.; Lieutenant, K.; Manoshin, S.; Bordallo, H.N.; Champion, J. D. M.; Peters, J.; Carpenter, J. M.; Mezei, F.: **A survey of simulations of complex neutronic systems by VITESS** Joint Meeting on Neutron Optics and Detectors, Tokyo 12-JAN-04 - 16-JAN-04	

Talks

Bayrakci, S.P.; Keller, T.; Keimer, B., Habicht, K.: **Neutron resonance spin echo (NRSE) study of the magnon linewidth in MnF_2** Deutsche Neutronenstreutagung 2004, TU Dresden, September 2004	V2
Borisov, S.; Vakhrushev, S.; Golosovsky, I.; Kumzerov, Yu; Naberezhnov, A.; Simkin, V.; Smirnov, O.; Dorner, B.; Hansen, T.; Tovar, M.; Zalar, B.; Lebar, A.; Blinc, R.: **Phase transitions in nanostructured ferroelectrics** 18th Workshop on Applications of Neutron Scattering in Study of Condensed Matter, 12-16 October 2004, Zarechny, Russia	
Danilyan, G.; Fedorov, A.; Karpikhin, I.; Krakhotin, V.; Pavlov, V.; Golub, R.; Korobkina, E.: **Search for P-odd asymmetry of prompt neutrons emission in 235U fission induced by cold polarized neutrons** XII International Seminar on Interaction of Neutrons with Nuclei. Neutron Spectroscopy, Nuclear Structure, Related Topics, Dubna, 26.05.2004 - 29.05.2004	V13
Goll, G.; Stockert, O.; Bombardi, A.; Prager, M.; Stüßer, N.; Takabatake, T.: **Investigation of the low ordered moment in CeBiPT** Deutsche Neutronenstreutagung 2004, TU Dresden, September 2004	E6
Golosovsky, I.; Hansen, T.; Koroleva, E.; Korotkov, L.; Naberezhnov, A.; Kumzerov; Yu; Tovar, M.: **Peculiarities of phase transitions in nanostructured ferroelectrics** XXI International Conference on Relaxation Phenomena in Solids (RPS-21), October 5-8, Voronezh, Russia	
Haibel, A.: **Synchrotron-Tomographie zur Charakterisierung komplexer Materialsysteme** 3.Seminar zur Nutzung des Wellenlängen-schieber-Messplatzes bei BESSY, Berlin 29-NOV-04 - 30-NOV-04	BESSY
Haibel, A.: **Synchrotron-Tomographie und 3D-Bildanalyse an keramischen und metallischen Schäumen** Seminarveranstaltung der Arbeitsgruppe Prof. Schubert, Berlin 22-NOV-04 - 22-NOV-04	BESSY

Seminars and Conference Contributions 2004

Kainourgiakis, M.; Steriotis, Th.; Charalambopoulou, G.; Kikkinides, E.; Stubos, A.: **Combination of small angle neutron scattering data and mesoscopic simulation techniques as a tool for the structural characterization and prediction of properties of biphasic media** Neutrons and Numerical Methods II, Grenoble (France) September 14-18, 2004	
Krist, T.: **Neutron optics from Hahn-Meitner Institute Berlin** Seminar talk, Kyoto University, Research Reactor Insti 08-JAN-04 - 08-JAN-04	
Lieutenant, K.: **Protein dynamics investigated by EPR and neutron scattering experiments** Physik-Seminar, Universität Osnabrück, Osnabrück, Germany 04-MAY-04 - 04-MAY-04	
Lonkai, Th.; Hohlwein, D., Lottermoser, Th.; Fiebig, M., Amann, U.; Ihringer, J.: **Structural explanation of magnetoelectric phase transitions in hexagonal $HoMnO_3$** Deutsche Neutronenstreutagung 2004, TU Dresden, September 2004	E2
Lottermoser, Th.; Lonkai, Th.; Amann, U.; Ihringer, J.; Hohlwein, D.; Fiebig, M.: **Gigantischer magnetoelektrischer Effekt im ferroelektrischen Antiferromagneten $HoMnO_3$** Frühjahrstagung des Arbeitskreises Festkörperphysik der Deutschen Physikalischen Gesellschaft, Regensburg, 11.03.2004	
Mezei, F.: **Multi-MW Spallation Sources:A quantum leap in neutron research opportunities** Seminar, Universität Braunschweig 22-JUN-04 - 22-JUN-04	
Pieper, J.; Irrgang, K.-D.; Renger, G.; Lechner, R.E.: **Density of states of low-frequency protein vibrations in the light-harvesting cComplex II of green plants** International Workshop on Light-Harvesting Systems, St.Adele (Canada) August 2004	
Pop, L.; Odenbach, S.: **Untersuchung der Mikrostruktur von Ferrofluiden mittels Kleinwinkel-Neutronenstreuung** Deutsche Physikalische Gesellschaft (DPG), Regensburg, Germany, March 2004	V4
Pop, L.; Odenbach, S.; Wiedenmann, A.: **Investigation of the microstructure of ferrofluids using small angle neutron scattering** GAMM (Gesellschaft für Angewandte Mathematik und Mechanik), Dresden, Germany, March – April, 2004	V4
Pop, L.; Odenbach, S.; Wiedenmann, A.: **Investigation of the microstructure of ferrofluids using small angle neutron scattering** 5th Colloquium DFG-Priority Program "Kolloidale magnetische Flüssigkeiten: Grundlagen Entwicklung und Anwendungen neuartiger Ferrofluide", Benediktbeuern, Germany, September 2004	V4
Pop, L.; Odenbach, S.; Wiedenmann, A.: **Investigation of the microstructure of ferrofluids using small angle neutron scattering** 10th International conference on magnetic fluids, Guarujá, São Paulo, Brazil, August 2004	V4
Pop, L.; Odenbach, S.; Wiedenmann, A.: **Untersuchung der Mikrostruktur von Ferrofluiden mittels Kleinwinkel-Neutronenstreuung** Deutsche Neutronenstreutagung 2004, TU Dresden, September 2004	V4
Raasch, S.; Doerr, M.; Rotter, M.; Kreyssig, A.; Loewenhaupt, M.: **Change of the crystal structure of $Tb_{0.5}Dy_{0.5}Cu_2$ induced by an external magnetic field** Frühjahrstagung der Deutschen Physikalischen Gesellschaft, Regensburg, March 2004	E2
Rocha, A.; Hirsch, Th., IWT Bremen, *Schneider, R.:* **Vergleich unterschiedlicher Probekörper bzw. Pulver zur Bestimmung der spannungsfreien Gitterkonstante eines Einsatzstahls 20 MnCr 5** Deutsche Neutronenstreutagung 2004, TU Dresden, September 2004	E3
Schorr, S.; Tovar, M.; Stüßer, N.; Geandier, G.: **Struktur und Phasenbeziehungen im Mischkristallsystem 2(ZnX) - $CuInX_2$ (X=S, Se, Te)** Deutsche Mineralogische Gesellschaft, Sektionstreffen Physik, Chemie und Kristallographie der Minerale, Eisenach, Germany, 5. – 6.4.2004	E6

Seminars and Conference Contributions 2004

Schorr, S.; Tovar, M.; Stüßer, N.; Sheptyakov, D.: **Strukturuntersuchungen mit Neutronen** Sommerschule des Universitätsverbundes Halle-Jena-Leipzig, Jena, Germany, 9. – 10.7.2004	E6
Schorr, S.; Tovar, M.; Stüßer, N.; Shetyakov, D.; Geandier, G.: **Structure and phase relations of the solid solution series 2(ZnX) – $CuInX_2$ (X=S, Se, Te)** 14th International Conference on Ternary and Multinary Compounds, Denver, USA, 27.9. – 2.10.2004	E9
Schorr, S.; Tovar, M.; Stüßer, N.; Shetyakov, D.: **Structure and phase relations of the solid solution series 2(ZnX) – CuInX2 (X=S, Se, Te)** Seminar Talk, PSI Villigen, Switzerland, 21.6.2004	E9
Steitz, R.: **Neutron reflectivity and soft condensed matter** Institutsseminar, Lehrstuhl für Angewandte Physikalische Chemie: Prof. Dr. M. Grunze, Heidelberg 02-DEC-04 – 02-DEC-04	V6
Steitz, R., Schemmel, S.; Findenegg, G.H.; Müller-Buschbaum, P.; Cubitt, R.: **Water depletion and nanobubbles at a solid-liquid interface** Deutsche Neutronenstreutagung 2004, TU Dresden, September 2004	V6
Strobl, M.; Treimer, W.; Hilger, A.; Kardjilov, N.: **Tomography with monochromatic neutrons** Deutsche Neutronenstreutagung 2004, TU Dresden, September 2004	V12
Strunz, P.: **Microstructure of superalloys and ceramic coatings** LNS Research Themes 2004 and Beyond, Klosters, Switzerland, 24.03.2004 – 27.03.2004	V4
Treimer, W.: **Alte und neue bildgebende Signale in der Computertomography** Seminarvortrag, Universität Wien 09-MAY-04 – 09-MAY-04	
Treimer, W.; Strobl, M.; Hilger, A.; Kardjilov, N.: **Neue Wege in der Neutronentomography** Seminarvortrag, TUM Garching 10-FEB-04 – 10-FEB-04	V 7 V12
Ulbricht, A.; Böhmert, J.: **Characterization of radiation effects in reactor pressure vessel steels by means of small-angle neutron scattering** Jahrestagung Kerntechnik 2004, Düsseldorf, 25.05.2004 – 27.05.2004	V4
Vorderwisch, P.; Stuhr, U.; Shapiro, S.M.: **Phonondispersion in der ferromagnetischen Formgedächtnislegierung Ni_2MnGa** Deutsche Neutronenstreutagung 2004, TU Dresden, September 2004	V2
Wiedenmann, A.: **Magnetic nanostructures as probed by polarized small angle neutron scattering** General seminar at ILL (College 9), Grenoble, France 03-MAR-04 – 03-MAR-04	V4
Wiedenmann, A.; May, R.; Dewhurst, Ch. **Polarisation option on D22** ILL General seminar (College 1), Grenoble, France 13-SEP-04 – 13-SEP-04	
Wong, J.E.; Steitz, R.; v. Klitzing, R.: **Sensitivity of polyelectrolyte multilayers to outer parameters** ACS Meeting (American Chemical Society), Yale university (New Haven), 20.06.2004 – 23.06.2004	V6
Wong, J.E.; v. Klitzing, R.: **The Hofmeister series revisited: construction and destruction of polyelectrolyte multilayers** ECIS 2004, Almeria (Spain), 19.09.2004 – 24.09.2004	V6
Wong, J.E.; v. Klitzing, R.: **Interactions between polyelectrolytes and monovalent ions in adsorbed nanofilms** DPG-Tagung, TU Berlin, 04.03.2005 – 09.03.2005	V6

Seminars and Conference Contributions 2004

Poster Presentations

Aliouane, N.; Argyriou, D.N.; Landsgesell, S.; Milne, C.J.; Hoffmann, J.-U.: **Neutron diffraction study of $TbMnO_3$** Deutsche Neutronenstreutagung 2004, TU Dresden, September 2004	E2
Amann, U.; Ritter, C.; Hohlwein, D.; Pfrommer, A.; Ihringer, J.; Lonkai, Th.; Hoffmann, J.-U.: **Magnetic structure of $Y_{0.1}Ca_{0.9}MnO_3$ with manganese substituted by iron or gallium** Deutsche Neutronenstreutagung 2004, TU Dresden, September 2004	E2
Auffermann, G.; Prots, Y.; Chemnitzer, R.; Kniep, R., Többens, D.M.; Tovar, M., Parker, S.F.: **Neutronenbeugungsexperimente an Nitrid-Diazeniden** Deutsche Neutronenstreutagung 2004, TU Dresden, September 2004	E9
Charalambopoulou, G.; Steriotis, Th.; Stubos, A.; Kanellopoulos N.: **Investigating the effect of excess hydration on human stratum corneum morphology** 9th Intenational Perspectives in Percutaneous Penetration Conference, La Grande Motte – France, April 13–17, 2004	V1
Dennison, S.R.; Dante, S.; Hauß, T.; Harris, F.; Brandenburg, K.; Phoenix. D.A.: **Deuteration affects the conformational behaviour and membrane interactive potential of a bioactive protein segment** Congress on "Peptide-Membrane Interactions, Namur, Belgium, 9. – 12. 10. 2004	V1
Dennison, S.R.; Dante, S.; Hauß, T.; Harris, F.; Brandenburg, K.; Phoenix, D.A.: **Biophysical studies into the membrane interactions m-calpain** BioScience2004, from molecules to organisms, Glasgow, 18. – 22.7.2004	V1
Dennison, S.R.; Dante, S.; Hauß, T.; Harris, F.; Siligardi, G.; Phoenix. D.A.: **Neutron diffraction studies show the smaller subunit of m-calpain to contain a lipid interactive alpha-helical segment** Congress on "Peptide-Membrane Interactions, Namur, Belgium, 9. – 12.10.2004	V1
Dennison, S.R.; Dante, S.; Hauß, T.; Harris, F.; Siligardi, G.; Phoenix. D.A.: **CD analysis and Neutron Diffraction shows that deuteration** BioScience2004, from molecules to organisms, Glasgow, 18. –22.7.2004	V1
Faulhaber, E.; Loewenhaupt, M.; Stockert, O.; Jeevan, H.S.; Geibel, C.; Steglich, F.; Prokes, K.; Stüßer, N.: **Magnetic field dependence of the A-phase in $CeCu_2Si_2$** Deutsche Neutronenstreutagung 2004, TU Dresden, September 2004	E4, E6
Faulhaber, E.; Stockert, O.; Jeevan, H.S.; Prokes, K.; Deppe, M.; Geibel, C.; Steglich, F.; Loewenhaupt, M.: **Magnetic field dependence of the magnetic order in A-type $CeCu_2Si_2$** SCES'04, Karlsruhe, 26.07.2004 – 30.07.2004	
Frontzek, M.; Kreyssig, A.; Doerr, M.; Loewenhaupt, M.: Hoffmann, J.-U.: **Magnetic strucutre of Tb_2PdSi_3: Investigation of long- and shortrange magnetic order ni external magnetic fields** Deutsche Neutronenstreutagung 2004, TU Dresden, September 2004	E2
García-Matres, E.; Perroud, O.; Wiedenmann, A., Kumar, G.; Eckert, J.: **SANSPOL studies of hard magnetic $Nd_{60}Fe_xCo_{30-x}Al_{10}$ bulk amorphous alloys** Deutsche Neutronenstreutagung 2004, TU Dresden, September 2004	V4
Garvey, C.J.; Ferris, J.: **Fractal scaling and the assembly of biosilica into diatom frustules** 4th AINSE Symposium on Neutron Scattering, Sydney, December 2004	V4
Garvey, C.J.; Ferris, J.: **Small angle neutron scattering (SANS) and TEM studies of the internal porosity of three cultured diatom frustules** 5th International Conference on Biological Physics, Gothenburg, 23. – 27.8.2004	V12a

Seminars and Conference Contributions 2004

Garvey, C.J.;. Ferris, J.: **Fractal scaling and the assembley of biosilica into diatom frustules** Australian Society for Biophysics 28th Annual Scientific Meeting, Fremantle, October 2004	V4
Gierlings, M.; Riegel, D.; Prandolini, M.J., Fritzsche, H., Gruyters, M.: **Specular and off-specular PNR during the magnetization reversals in an exchange biased $[Co/CoO/Au]_{20}$ multilayer** Deutsche Neutronenstreutagung 2004, TU Dresden, September 2004	V6
Gilles, R.; Mukherji, D.; Hoelzel, M.; Strunz, P.; Barbier, B.; Toebbens, D.M.: **Scattering methods to investigate nano-sized precipitates extracted from Ni-base superalloys** 7th International Conference on Nanostructured Materials, Wiesbaden, 20.06.2004 - 24.06.2004	
Harker, S J; Pappas, C.; Mulders, A.; Hicks, T J. **Time of flight spectrometry with polarisation analysis study of the magnetic diffuse scattering in disorderedantiferromagnetic Mn90Cu10** 4th AINSE Symposium on Neutron Scattering, Lucas Heights, Sydney, Decemeber 14 – 15, 2004	V5
Heinemann, A.; Wiedenmann, A.; Kammel, M.: **SANSPOL for ordered magnetic nano-structure analysis** Deutsche Neutronenstreutagung 2004, TU Dresden, September 2004	V4
Hölzel, M.; Danilkin, S.A.; Toebbens, D.M.; Udovic, T.J.; Rameriz-Cuesta, T.; Rajevac, V.; Wipf, H.; Fuess, H.: **Elastic and inelastic neutron scattering on hydrogenated austenitic stainless steels** 22nd European Crystallographic Meeting, Budapest, 26.08.2004 - 31.08.2004	
Hölzel, M.; Gilles, R.; Mukherji, D.; del Genovese, D.; Strunz, P.; Rösler, J.; Toebbens, D.M.: **Misfit measurements on W-rich Ni-base superalloys and phase analysis of Ni-Fe-base superalloys** Deutsche Neutronenstreutagung 2004, Dresden, 01.09.2004 - 04.09.2004	E9
Hoffmann, J.-U.; Lonkai, Th., Ihringer, J.: **The next generation of Flat-Cone diffraction** Deutsche Neutronenstreutagung, TU Dresden, September 2004	E2
Kaiser-Bischoff, I.; Boysen, H.; Frey, F., Lerch, M., Hoffmann, J.-U., Scherf, C.: **Fehlordnung in anionen- und kationendotiertem ZrO_2** Deutsche Neutronenstreutagung 2004, TU Dresden, September 2004	E2
Kamarad, J.; Arnold, Z.; Prokhnenko, O.; Prokes, K.: **Invar and Invar-like materials under pressure - new experimental data** 42th European High Pressure Research Group Meeting, Lausanne, Swiss, 01.09.2004 - 04.09.2004	E4
Kamarad, J.; Prokes, K.; Prokhnenko, O.; Meissner, M.: **High pressure prague cells for neutron diffraction studies in Hahn-Meitner-Institut** Medium Pressure Advances for Neutron Scattering, Grenoble, France, 20.10.2004 - 23.10.2004	E4
Kamarad, J.; Prokhnenko, O.; Arnold, Z.; Prokes, K.: **Magnetization and neutron diffraction studies of Lu2Fe17 under high pressure** Medium Pressure Advances for Neutron Scattering, Grenoble, France, 20.10.2004 - 23.10.2004	E4
Köbler, U.; Hoser, A.; Schäfer, W.; Stüßer, N.: **Universal magnetic behaviour for $T \rightarrow 0$ and $T \rightarrow T_c$** Deutsche Neutronenstreutagung 2004, TU Dresden, September 2004	E6
Krastev, R.; Steitz, R.; Gutberlet, Th.; Klösgen, B.: **Lipid membranes on hydrophilic polymer cushions - A study by neutron reflectometry** Deutsche Neutronenstreutagung 2004, TU Dresden, September 2004	V6
Krist, Th.; Mezei, F.: **Neutronenoptische Bauelemente vom HMI Berlin** Deutsche Neutronenstreutagung 2004, TU Dresden, September 2004	
Lonkai, Th.; Lottermoser, Th.; Fiebig, M.; Amann, U.; Hohlwein, D.; Ihringer, J.: **Magnetoelectric phase transitions in hexagonal $HoMnO_3$** 3rd Berlin Workshop on Orbital Physics and Novel Phenomena in Transition Metal Oxides, Hahn-Meitner Institut, Berlin, 06.10.2004	

Seminars and Conference Contributions 2004

Lottermoser, Th.; Lonkai, Th.; Amann, U.; Ihringer, J.; Hohlwein, D.; Fiebig, M.: **Kontrolle der magnetischen Ordnung durch ein elektrisches Feld in $HoMnO_3$** Frühjahrstagung des Arbeitskreises Festkörperphysik der Deutschen Physikalischen Gesellschaft, Regensburg, 09.03.2004	
Prokes, K.; Brück, E.; Sechovsky, V.: **Competition of two AF structures in UNiAl single crystal** Deutsche Neutronenstreutagung 2004, TU Dresden, September 2004	E1, E4, V2
Prokes, K.; Brück, E.; Sechovsky, V.: **Melting of the AF structure in UNiAl near T_N** Deutsche Neutronenstreutagung 2004, TU Dresden, September 2004	E2
Psychogios, J.; Kainourgiakis, M.; Charalambopoulou, G.; Steriotis, Th.; Stubos, A.: **Prediction of porcine stratum corneum stratum corneum transport properties from USANS data and numerical simulations** 9th Intenational Perspectives in Percutaneous Penetration Conference, La Grande Motte (France) April 13-17, 2004	
Raasch, S.; Doerr, M.; Kreyssig, A.; Loewenhaupt, M.; Rotter, M.; Hoffmann, J.-U.: **New model for conversion process in Rcu_2 (R= rare earth)** Deutsche Neutronenstreutagung 2004, TU Dresden, September 2004	E2
Rößler, U.K.; Handstein, A.; Idzikowski, B; Kozlova, N.; Nenkov, K.; Müller, K.-H.;Kreyssig, A.; Loewenhaupt, M.;Stüßer, N.; Hoell, A.; Heinemann, A.: **Neutron diffraction study on the magnetic structure of $Mn_{1-x}Fe_xAu_2$** Deutsche Neutronenstreutagung 2004, TU Dresden, September 2004	E6
Schorr, S., Tovar, M.; Stüßer, N., Sheptyakov, D., Geandier, G.: **Structure and phase relations of the solid solution series 2(ZnX)-$CuInX_2$ (X=S, Se, Te)** Deutsche Neutronenstreutagung 2004, TU Dresden, September 2004	E9, E6
Schorr, S.; Tovar, M.; Stüßer, N.; Kockelmann, W.: **Eectronic similar elements distinguished by neutron diffraction** 12. Jahrestagung der Deutschen Gesellschaft für Kristallographie, Jena, Germany, 15. – 19.3.2004	E6
Schorr, S.; Tovar, M.; Stüßer, N.; Kockelmann, W.: **Electronic similar elements distinguished by neutron diffraction** International Materials Congress, London, GB, 1.4.2004	E9
Shin, T.; Findenegg, G.H., Keiderling, U.: **Surfactant aggregate structure in SBA-15 silica nanopores** Deutsche Neutronenstreutagung 2004, TU Dresden, September 2004	V4
Steriotis, Th.; Charalambopoulou, G.; Pieper, J.; Lechner, R.; Stubos, A.: **Hydration of stratum corneum: A QENS-NMR study to unravel the dynamics of different water phases** 7th International Conference on Quesielastic Neutron Scattering, Arcachon-France, 1 – 4.9. 2004	
Stüßer, N.; Schotte, U.; Klenke, J., Sadykov, R., Hoser, A.: **Study of the magnetic spirals in $CsCuCl_3$ and $RbCuCl_3$ under pressure and field by neutron diffraction** Deutsche Neutronenstreutagung 2004, TU Dresden, September 2004	E1, E6
Süllow, S.; Otop, A., Loose, A.; Klenke, J.; Feyerherm, R., Mydosh, J.A.: **Magnetic and structural disorder in single crystalline UPt_2Si_2** Deutsche Neutronenstreutagung 2004, TU Dresden, September 2004	E1 E5
Tovar, M.; Torabi, R., Fleischer, F.: **Strukturelle und magnetische Eigenschaften von Jahn-Teller-Cu-Ni-Cr-Spinellen** Deutsche Neutronenstreutagung 2004, TU Dresden, September 2004	E9
Ulbricht, A.; Brgner, F.: **Characterization of radiation defects in RPV-steels after irradiation and annealing by means of small-angle neutron scattering** Deutsche Neutronenstreutagung 2004, TU Dresden, September 2004	V4

Seminars and Conference Contributions 2004

v. Klitzing, R.; Wong, J.E.; Steitz, R.: **Response of polyelectrolyte multilayers to external stimuli** DPG-Tagung, Regensburg, 08.03.2004 - 12.03.2004	V6
Wawrzynska, E.: **Magnetic properties of R3T4X4 (R=Pr, Nd; T=Cu, Ag; X=Ge, Sn) compounds** Int. Conf. on Strongly Correlated Electron Systems, SCES'04, Karlsruhe, Germany	(E6)
Willumeit, R.; Kumpugdee, M.; Linser, S., Andrä, J., Hauß, Th.: **Structural evidence given by neutron diffraction for the membrane destabilisation mechanism of the peptide NK-2** Deutsche Neutronenstreutagung 2004, TU Dresden, September 2004	V1
Willumeit, R.; Kumpugdee, M.; Linser, S.; Hauß, T.; Funari, S.S.; Andrä, J. **The interaction of the peptide NK-2 with model Mmmbranes: Insights by neutron diffraction and X-ray scattering** Herbsttagung der Gesellschaft für Biochemie und Molekularbiologie, 19.-22.09.04, Münster, 18.09.2004 - 22.09.2004	V1
Willumeit, R.; Kumpugdee, M.; Linser, S.; Andrä, J.; Hauß, T.: **Structural evidence given by neutron diffraction for the membrane destabilisation mechanism of the peptide NK-2** Deutsche Neutronenstreutagung 2004, TU Dresden, September 2004	
Willumeit, R.; Kumpugdee, M.; Linser, S.; Funari, S.S.; Andrä, J.; Hauß, T.; Jelinek, R.: **The membrane destruction mechanism of the peptide antibiotic NK-2: A structural explanation** Structural Biology at Crossroads: From Biological Molecules to Biological Systems, EMBL, Hamburg, 15.09.2004 - 18.09.2004	
Willumeit, R.; Hauß,T.; Kumpugdee, M.; Linser, S.; Andrä, J.: **The peptide antibiotic NK-2: New insights in the membrane destruction mechanism** International Workshop on Biophysics of Cellular Communication: Networks and Molecular Interactions, Gomadingen, 22.03.2004 - 24.03.2004	
Witte, U.; Schedler, R.; Loewenhaupt, M.; Rotter, M.; Schmidt, W.: **Field dependence of the magnon dispersion $CeCu_2$** Deutsche Neutronenstreutagung 2004, TU Dresden, September 2004	
Wong, J.E.; Steitz, R. Hedicke, G.; v. Klitzing, R.: **Short range interactions in polyelectrolyte multilayers** Condensed Matter Divison (European Physical Society), Prag, 19.07.2004 - 23.07.2004	V6
Wong, J.E.; Steitz, R.; v.Klitzing, R.: **Ion specific effects in polyelectrolyte multilayers according to the Hofmeister series** 14th Ostwald Colloquium, Harnackhaus, Berlin, 22.11.2004 - 23.11.2004	V6
Wong, J.E.; v. Klitzing, R.: **Short-range interaction in adsorbed polyelectolyte films** Polyelectrolytes 2004, Amherst (USA), 15.06.2004 - 18.06.2004	V6
Zhang, L.; Moze, O.; Prokes, K.; Tegus, O.; Bruck, E.: **Neutron diffraction study of history dependence in $MnFeP_{0.6}Si_{0.4}$** Joint European Magnetic Symposia 2004, Dresden, Germany	E6

Contributions to the 12th BENSC Users' Meeting, May 2004

INVITED ORAL CONTRIBUTIONS

Daniel Clemens, BENSC:
"Progress Report on Neutron Guide Hall II and New Instruments"

Dimitri Argyriou
"$Na_{0.35}CoO_2 \cdot 1.37D_2O$: Implications for the Superconducting Phase Diagram"

Markus Strobl
"Tomography at HMI: Status and Projects in Progress"

Molly Ingersoll
"Using Neutron Scattering to Investigate the Biological Specificity of Neutrophil Elastase"

Rumen Krastev
"Adsorption of Natural Polymers on Modified Solid Surfaces Studied by Neutron Reflectometry"

Cécile Dreiss, Univ. of Bristol, UK
"Investigation of Alcohol Ethoxylate Surfactant in Solution and Adsorbed at Interfaces"

Theodore Steriotis, NCSR Demokritos, GR
„Investigations of Stratum Corneum: Structural and Dynamic Properties Based on Neutron Techniques"

Massimo Bonini, Univ. Firenze, I
"Silica Coated Magnetic Nanoparticles: Synthesis and Characterization"

Susan Schorr, Univ. Leipzig
„Electronic Similar Elements Distinguished by Neutron Diffraction"

Oliver Stockert, MPI Dresden
"Nature of the A-Phase in $CeCu_2Si_2$"

Ines Kaiser-Bischoff, LMU München
"Diffuse Scattering of Cation and Anion Doped ZrO_2"

POSTER PRESENTATIONS

TAS Instruments E1, V2 (FLEX)

Sobolev, O.; Vorderwisch, P.; HMI Berlin, *Desmedt, A.,* Univ. de Bordeaux I, France
Free quantum rotations of NH_3 groups in Hoffmann clathrates (V2, V3)

Idzikowski, B.; PAS, Poznan, PL, *Kudryavtsev, Y.V.,* NAS, Kiev, *Hyun, Y.H.; Pak-Lee, Y.,* Univ. Seoul, Korea, *Klenke, J.,* HMI Berlin
Neutron investigations of the stoichiometric and off-stoichiometric Ni_3Al itinerant ferromagnet (E1)

Stüßer, N.; Schotte, U.; Meißner, M., HMI Berlin, *Hoser, A.,* FZ Jülich
Field distorted magnetic spiral structure of $CsCuCl_3$ (E1)

Süllow, S.; Otop, A., TU Braunschweig, *Loose, A.; Klenke, J.; Feyerherm, R.,* HMI Berlin, *Mydosh, J.A.,* Leiden University, NL, MPI Dresden
Magnetic and structural disorder in single crystalline UPt_2Si_2 (E1, E5)

Diffraction, Instruments E2, E6, E9

Kaiser-Bischoff, I.; Boysen, H.; Frey, F.; Lerch, M., LMU München
Diffuse scattering of cation doped ZrO_2 (E2)

Hoffmann, J.-U.; Lonkai, Th., HMI Berlin, *Ihringer, J.,* Univ. Tübingen
The next generation of flat cone diffraction (E2)

Lonkai, Th.; Hoffmann, J.-U., HMI Berlin, *Pfrommer, A.; Amann, U.; Ihringer, J.,* Univ. Tübingen
Magnetism and structure in Ga-doped manganites $Y_{0.1}Ca_{0,9}Ga_xMn_{1-x}$x=0,005 ...0,16 (E2)

Lonkai, Th.; Ihringer, J., Univ. Tübingen, *Lottermoser, Th.; Fiebig, M.,* MBI Berlin, *Amann, U.,* Univ. Tübingen & ILL Grenoble, F, *Hohlwein, D.,* Univ. Tübingen & HMI Berlin
Structural explanations of magnetoelectric phase transitions in hexagonal $HoMnO_3$ (E2)

Gratz, E.; Hense, K., TU Wien, *Hoser, A.; Hilscher, G.; Pieper, M.,* FZ Jülich, *Paul-Boncour, V.,* CNRS LCMTR Thiais, *Markosyan, G.A.S.,* Moscow State Univ., RU
Unusual magnetic properties of $Er_xY_{1-x}Co_3$ (X=01, 03,05) (E6)

Köbler, U.; Hoser, A., FZ Jülich
Long range magnetic order in three-dimensions, a non-trivial and unsolved problem

Stockert, O., MPI-CPfS Dresden, *Goll, G.,* Univ. Karlsruhe, *Stüßer, N.,* HMI Berlin, *Bombardi, A.,* ILL Grenoble, *Prager, M.,* FZ Jülich, *Takabatake, T.,'* Univ. Hiroshima
Investigation of the low ordered moment in CeBiPt (E6)

Wawrzynska, E.; Penc, B.; Szytula, A.; Tomkowicz, Z., Jagiellonian Univ. Krakow, PL, *Hernandez-Velasco, J.,* HMI Berlin
Magnetic structures of $R_3Cu_4Si_4$ (R = Tb, Dy, Ho, Er) and $R_3Pd_4Ge_4$ (R = Tb and Er) compounds (E6)

Flachbart, K.; Batko, I.; Gabani, S.; Mat'as, S., SAS Kosice, *SK, Meissner, M.; Siemensmeyer, K.,* HMI Berlin; *Paderno, Y.; Czopnik, A.,* PAS ILTSR, Wroclaw; *N. Shitsevalova,* NAS Kiev
Intricate magnetic properties of HoB_{12} (E6)

Krimmel, A.; Loidl, A., MPI FKF-Stuttgart, *Reehuis, M.,* MPI FKF-Stuttgart & HMI Berlin, *Prokofiev, A.,* Univ. Frankfurt/Main
Crystal structure against orbital order in ZnV2O4 (E6, E9)

Franz, A.; Schorr, S., Univ. Leipzig; *Tovar, M.; Többens, D.,* HMI Berlin
Stoichiometric and non-stoichiometric perovskite $BaPbO_{3-x}$ (E9)

Contributions to the 12th BENSC Users' Meeting, May 2004

Schorr, S., Univ. Leipzig; *Tovar, M.; Stüßer, N.,* HMI Berlin, *Kockelmann, W.,* ISIS
Electronic similar elements distinguished by neutron diffraction (E9, E6)

Pritula, O.; Smrcok, L., SAS Bratislava, SL Institute of Inorganic Chemistry
Neutron and X-ray Rietveld quantitative phase analysis of industrial Portland cement clinkers (E9)

Bordallo, H.N.; Többens, D.; Argyriou, D.N., HMI Berlin, *Barthès, M.,* Univ. Montpellier, F
Re-investigation of the structure of the model peptide $CH_3NHCOCH_3$ (E9)

Naberezhnov, A.; Sotnikov, S.; Kumzerov, Yu.; Smirnov, O., RAS Ioffe PTI St. Petersburg, RU, *Tovar, M.; Toebbens, D.,* HMI Berlin
Sodium nitrite in a restricted geometry: properties and phase transitions (E9)

Sazonov, A.P.; Sikolenko, V.V., ISSSP NAS, Minsk, Belarus, *Többens, D.,* HMI Berlin
Magnetic properties of $La_{1-x}Sr_xCoO_3$ (x = 0.15 and 0.3) system (E9)

Efimov, V.V.; Tyutyunnikov, S.I.; Efimova, E.A.; Mavrin, B.N.; Sternberg, A.; Novikova, N.N.; Shilnikov, A.V.; Yakovlev, V.A.; Khasanov, S.S.; Burhanov, A.I., JINR, Dubna, RU, *Sikolenko, V.V.; Többens, D.,* HMI Berlin
Studies of the structural, optical and dielectrical charges in PLZT 8/65/35 ceramics induced by high-current pulsed electron beam (E9)

Hoelzel, M., TU Darmstadt & TU München, *Gilles, R.,* TU München, *Mukherji, D.,* ETH Zürich, *del Genovese, D.,* TU Braunschweig, *Strunz, P.,* PSI, Villigen, CH, *Toebbens, D.,* HMI Berlin
Misfit measurement on W-rich Ni-base super alloys and phase analysis of Ni-Fe base super alloys (E9)

Tovar, M., HMI Berlin, *Fleischer, F.,* MPI Halle
Re-investigation of the pollucite type compound $Cs_2CuSi_5O_{12}$ (E9)

Four Cycle Diffractometer E5

Reehuis, M., MPI FKF-Stuttgart & HMI Berlin, *Ulrich, C.; Keimer, B.,* MPI FKF-Stuttgart, *Hemberger, J.,* Univ. Augsburg, EKM
Structural and magnetic properties of $YTiO_3$ and $LaTiO_3$

Loose, A., HMI Berlin, *Wozniak, K.; Dominiak, P.M.,* Warsaw Univ., PL, *Smirnov, L.S.,* FSUE SSC RF, Moscow, RU, *Melnyk, G.; Berntsen, N.,* Joh. Gutenberg-Univ. Mainz, *Shuvalov, L.A.,* A.V. Shubnikov Inst. of Crystallography RAS, Moscow
The refinement of hydrogen positions in $(NH_4)_2SeO_4$

Membrane Spectrometer V1

Kiselev, M.A., FLNP JINR, Dubna, RU & MLU Halle, *Zbytovska, J.; Wartewig, S.; Neubert, R.,* MLU Halle, *Dante, S.,* HMI Berlin, *Hauß, Th.,* HMI Berlin & Univ. Düsseldorf
Investigation of model stratum corneum membrane structure and hydration via neutron diffraction (V1)

Feyerherm, R.; Loose, A.; Landsgesell, S., HMI Berlin
Magnetic ordering in iron tricyanomethanide $Fe[C(CN)_3]_2$ (V1, E9)

Kim, D.; Klösgen, B., MEMPHYS, SDU Odense, DK, *Dathe, M.,* FMP Berlin, *Bezrukow, S.,* NICHD, NIH, Bethesada, USA, *Gutberlet, T.,* PSI Villigen, CH, *Dante, S.,* TU Darmstadt, *Hauß, Th.,* Univ. Düsseldorf & HMI Berlin, *Krastev, R.,* HMI Berlin & MPI-KGF Golm & TU Berlin
Membrane pore formation by the lytic peptide KLA1 (V1)

Steriotis, Th.A.; Charalambopoulou, G.; Stefanopoulos, K.L.; Stubos, A.K., NCSR Demokritos, GR, *Pieper, J.; Lechner, R.,* HMI Berlin, *Hauß, Th.,* HMI Berlin & Univ. Düsseldorf
Investigation of stratum corneum structural and dynamic properties based on neutron techniques (V1, V3, V4, V12)

ToF Spectrometer V3 (NEAT)

Bordallo, H.N.; Fehr, C.; Argyriou, D.N., HMI Berlin, *Barthès, M.:* **L-alanine (E9, V3)**

Bordallo, H.N.; Hernández-Velasco, J.; Argyriou, D.N., HMI Berlin, *Chapon, L.,* ISIS Rutherford, Didcot, UK, *Manson, J.L.,* Eastern Washington University, Cheney, USA, *Ravot, D.,* Univ. Montpellier, F, *Reiff, W.M.,* Northeastern Univ. Boston, USA
S=1/2 Ising behavior in the 2D molecular magnet $Fe(NCS)_2(pyrazine)_2$ (V3, E9, E6)

Tripadus, V.;Serban, A., IFIN-HH Bucharest, RO, *Radulescu, A.,* FZ Jülich, *Pieper, J.; Buchsteiner, A.,* HMI Berlin
Quasi-elastic incoherent neutron scattering on triglycine sulphate (TGS) below and above the ferroelectric - paraelectric phase transition (V3)

Jalarvo, N.; Lechner, R.E., HMI Berlin, *Desmedt, A.,* Univ. de Bordeaux I, France, *Steiner, T.,* FU Berlin
The dynamical properties of an aromatic hydrogen *, M.; Rols, S.,* Univ. Montpellier, F
Dynamics and structural studies of the of model system bonds (V3)

Pieper, J.; Lechner, R.E., HMI Berlin; *Irrgang, K.D.; Weß, M.; Renger, G.,* TU Berlin; *Hauß, Th.,* HMI Berlin & Univ. Düsseldorf
Dynamic structure and function of photosynthetic pigment-protein complexes (V3)

Contributions to the 12th BENSC Users' Meeting, May 2004

Spin-Echo Spectrometer V5 (SPAN)

Triolo, A., CNR Messina, Italy, *Mezei, F.; Russina, O.; Pappas, C.; Többens, D.,* HMI Berlin, *Arrighi, V.,* Heriot-Watt Univ. Edinburgh, UK, *Triolo, R.,* Univ. Palermo, Italy
Neutron spin echo characterization of the fast to-slow-collective dynamcis in atactic polypropylene (E9, V5)

SANS Instrument V4

de Stefanis, A.; Tomlinson, A.A.G.; Stefanopoulos, K.L., CNR, Roma, I, *Steriotis, Th.A.; Charalambopoulou, G.,* NCSR Demokritos, GR, *Keiderling, U.,* HMI Berlin
Nanostructural characterisation of catalysts by SANS

Shukla, A.; Neubert, R.H.H., MLU Halle-Wittenberg, *Kiselev, M.A.,* JINR, Dubna, RU, *Hoell, A.,* HMI Berlin
Characterization of nanoparticles in w/o microemulsions using small angle neutron scattering and dynamic light scattering

Pop, L.; Odenbach, S., ZARM, Bremen, *Wiedenmann, A.,* HMI Berlin, *Bönnemann, H.,* MPI für Kohlenforschung, Mülheim an der Ruhr
Structure formation in ferrofluids studied by small angle neutron scattering (SANS)

Strunz, P., PSI Villigen, CH, *Schumacher, G.; Wiedenmann, A.,* HMI Berlin, *Vassen, R.,* FZ Jülich
In-situ SANS investigation of porosity in ceramic thermal barrier coatings

Garcia-Matres, E.; Perroud, O.; Kumar, G.; Wiedenmann, A., HMI Berlin
Small angle Neutron scattering studies of hard magnetic $Nd_{60}Fe_xCo_{30-x}Al_{10}$ (x=20, 7.5 and 0) bulk amorphous alloys (V4)

Haug, J.; Schiffmann, R.; Banhart, J., HMI Berlin
SANS investigation of precipitation in heat-treated AA6016 alloy (V4)

Heinemann, A.; Wiedenmann, A.; Kammel, M.; Bönnemann, H., HMI Berlin
SANSPOL experiments observing partially ordered structures in Co-ferrofluids (V4)

Reflectometer V6

Raitman, E.; Gavrilov, V., IPE, Riga, Latvia, *Fritzsche, H.,* Chalk River Lab. CA, *Gierlings, M.,* HMI Berlin, *Nikitenko, Yu.,* JINR, Dubna, RU
Neutron reflection by ultrasonically excited surfaces

Gierlings, M.; Prandolini, M.J.; Riegel, D., HMI Berlin; *Fritzsche, H.,* Chalk River Lab. CA; *Gruyters, M.,* HU Berlin
Specular and off-specular scattering from a $[Co/CoO/Au]_{20}$ multilayer in the exchange bias state at 10 K using PNR

Gopinadhan, M.; Ahrens, H.; Helm, C.A., Univ. Greifswald; *Steitz, R.,* HMI Berlin & MPI-KGF Golm & TU Berlin
Internal order of polyelectrolyte multilayers

Klösgen, B., MEMPHYS, SDU Odense, DK, *Gutberlet, T.,* PSI Villigen, CH, *Krastev, R.; Steitz, R.,* HMI Berlin & MPI-KGF Golm & TU Berlin
Model membranes on a soft hydrophilic support

Neutron Audioradiography of Paintings B8

Laurenze-Landsberg, C.; Schmidt, C., Gemäldegalerie Berlin, *Mertens, L.A.; Schröder-Smeibidl, B.,* HMI Berlin
Neutron autoradiography of the painting "Armida abducts the sleeping Rinaldo" (~1637) by Nicolas Poussin, 120 x 150 cm^2, Catalogue No. 486 - an experiment at the instrument B8

Laurenze-Landsberg, C.; Schmidt, C., Gemäldegalerie Berlin, *Mertens, L.A.; Schröder-Smeibidl, B.,* HMI Berlin
Neutron autoradiography of the painting "Valley with Diane and her nymphs" by Jan Tilens (1589-1630), 89 x 156 cm^2, Catalogue No. 732 - an experiment at the instrument B8

Instrumental Developments and Other

Schneider, R.; Poeste, T., HMI Berlin, *Hofmann, M.,* HMI Berlin & TU München, *Henkel, F.,* TU Berlin
Stress and strain analysis: The new material research diffractometer E3 at the HMI (E3, E7)

Peters, J.; Lieutenant, K.; Clemens, D.; Mezei, F., HMI Berlin
EXED – an instrument in progress (EXED)

Kardjilov, N.; Hilger, A.; Manke, I.; Strobl, M.; Treimer, W., HMI Berlin
First results from the cold neutron tomography facility (CONRAD) at HMI (V7)

Haibel, A.; Rack, A.; Banhart, J., HMI Berlin *Riesemeier, H.; Goebbels, J.; Wiedemann, G.,* BAM Berlin
Synchrotron tomography at BESSY (BESSY)

Hoell, A.; Zizak, I.; Bieder, H.; Krauser, H.-D.; Mokrani, L.; Plewka, K.; Winter, W.; Klaumünzer, S.; Banhart, J., HMI Berlin
The new SAXS facility at Hahn-Meitner-Institute (SAXS at BESSY)

Rusevich, L., Inst. of Phys. Energetic Riga, LV, *Strobl, M.; Treimer, W.,* HMI Berlin, *Mikula, P.,* ASCR NPI, Re near Prague, CZ
Inelastic neutron scattering by ultrasound. Research by bonse-hart and DC diffractometers (V12a)

Danilyan, G.V.; Fedorov, A.V.; Karpikhin, I.L.; Krakhotin, V.A.; Pavlov, V.S., RF SSC ITEP, Moscow, RU, *Golub, B.; Korobkina, E.,* HMI Berlin
Search of angular correlation for scission neutrons by measurement (V13)

AUTHOR INDEX

AUTHOR INDEX

author	page
A	
Abernathy, D.L.	91
Ahrens, H.	120
Aliouane, N.	39, 40, 41, 42, 43, 44
Allan, M.	48
Almeida, F.	65
Ando, Y.	1, 2, 18
Annighöfer, B.	132
Appavou, M.-S.	132
Argyriou, D.	1, 2, 39, 40, 41, 42, 43, 44, 124
Arndt, J.	7
Ashley, R.	129
Auffermann, G.	75, 76
B	
Baczewski, T.	68
Baglioni, P.	56, 126, 141
Balali-Mood, K.	128, 129
Baldelli Bombelli, F.	126, 141
Baran, S.	24, 26
Barthès, M.	124, 139
Bartolome, F.	58
Bastürk, M.	174
Bayrakci, S.	86
Bellido, N.	30
Bellissent-Funel, M.-C.	132
Berti, D.	141
Betti, F.	56, 141
Birgeneau, R.J.	45
Blumberg, G.	18
Bonini, M.	56
Bordallo, H.N.	124, 134, 139
Borowiec, M.T.	71
Boué, F.	99, 100, 101
Bouwstra, J.	127
Bowers, J.	115
Braden, M.	47
Bradshaw, J.	128, 129
Brakhman, E.	205
Brand, R.A.	88, 92
Brandt, A.	102
Brezesinski, G.	109, 110
Bronger, W.	75
Brûlet, A.	54
Brunke, O.	158
Brunner, J.	184
Buchsteiner, A.	83, 94, 95, 131, 132, 137, 138, 139, 196
Bull, M.	22
C	
Cable, T.	171
Calbucci, V.	175
Campo, J.	58
Carrot, G.	99, 100
Charalambopoulou, G.	90, 127, 130, 140
Clemens, D.	103
Coldea, R.	9
Condre, J.M.	154
Cosgrove, T.	103, 104
Cousin, F.	101
Czarnecki, P.	95
D	
da S. Rocha, A.	146
Dai, P.	1, 2
Danilyan, G.V.	205
Dante, S.	117
Darul, J.	32, 33
de Francesco, A.	135
de Stefanis, A.	90
del Genovese, D.	153
Delajon, C.	116
Dencher, N.	138
Denoyer, F.	124, 139
Desmedt, A.	89
Doster, W.	131
Dreiss, C.	103, 104
E	
Edwards, L.	148, 149
Ehlers, G.	91
El Harrak, A.	99
Enderle, M.	51
Engler, H.	158
F	
Falus, P.	189
Faulhaber, E.	8
Fedorov, A.V.	205
Fehr, C.	92, 106, 124, 139
Felcher, G.	189
Ferris, J.	142, 143
Feyerherm, R.	4, 21, 31
Findenegg, G.H.	84, 85, 111, 118, 123
Fiori, F.	170, 175
Fitzsimmons, M.	183
Förster, F.	125
Franz, A.	78, 79
Fritzsche, H.	183
Frontera, C.	30
Frontzek, M.	11, 12
Frost, C.	22
Fuertes-Marrón, D.	82
G	
Garcia, V.	58
Garcia-Matres, E.	59, 60, 62, 134
Garcia-Munoz, J.L.	30
Garvey, C.	142, 143
Georgiev, P.A.	152
Gierlings, M.	66, 67
Gil, A.	26
Gilardi, R.	50
Gilbert, E.P.	57
Gilles, R.	153, 156, 157
Gjoka, M.	37
Glavatska, N.	145
Glavatskyy, I.	145
Golub, R.	205
Gómez Sal, J.C.	28
Gondek, L.	24
Gooris, G.	127
Gopinadhan, M.	120
Granroth, G.E.	91
Griesche, A.	167
Gromelski, S.	108
Grunze, M.	113
Guenet, J.M.	102
Gummel, J.	101
Günther, J.-U.	120
Gyn, Y.	105
H	
Habicht, K.	47, 51, 86, 88, 180
Hagiwara, M.	46
Haibel, A.	186
Haouz, A.	133
Harker, S.	64
Haug, J.	101, 142, 161, 164, 181, 182
Hauß, Th.	117, 127, 128, 134, 137, 138, 140
Heil, W.	165
Heinemann, A.	61, 160, 162, 163, 198
Helm, C.A.	120
Hemberger, J.	19
Henkel, F.	148, 149
Hernandez-Velasco, J.	24, 25, 26, 29, 28, 30, 62, 82
Herrero-Albillos, J.	58
Hesse, J.	63
Hicks, T.	64
Hilger, A.	170, 171, 173, 174, 177, 184, 200, 201, 202, 203, 204
Hirsch, T.	146
Hoffmann, J.-U.	8, 9, 69, 93, 145, 193
Hofmann, M.	23, 150
Hohl, A.	70
Hölzel, M.	153
Hornák, P.	159
Hutanu, V.	178

AUTHOR INDEX

author	page
I	
Ingersoll, M.	134
Inomotoy, Y.	16
Iolin, E.	188
Irrgang, K.-D.	136
Izerrouken, M.	111
J	
Jalarvo, N.	89
Janousova, B.	13
Jansen, M.	27
Javorský, P.	14
Jericha, E.	203, 204
Jestin, J.	99, 100
K	
Kaczorowski, D.	26
Kaiser-Bischoff, I.	69
Kamarád, J.	15
Kammel, M.	158, 160, 198
Kang, H.J.	1, 2
Kardjilov, N.	166, 167, 168, 169, 170, 171, 172, 173, 174, 177, 184
Karpikhin, I.	205
Kastner, M.A.	45
Kausche, S.	16
Keiderling, U.	84, 85, 90, 105, 140, 154, 155, 159, 164, 181, 182
Keimer, B.	17, 18, 19, 20, 86
Keller, T.	86, 88
Keune, W.	195
Khalil-Allafi, J.	151
Khaykovich, B.	45
Klenke, J.	3, 4, 63, 178, 192
Klimko, S.	51
Kniep, R.	76
Korobkina, E.	205
Krakhotin, V.A.	205
Krastev, R.	108, 109, 110, 116, 119, 121, 122, 144
Kreitlow, J.	21
Kreyßig, A.	10, 11, 12
Krimmel, A.	38
Krist, Th.	189, 190
Kuncser, V.	195
L	
L'abbé, C.	65
Lake, B.	22
Lau, J.	105
Laurenze-Landsberg, C.	206, 207, 208
Lechner, R.E.	89, 136, 137, 138
Lee, Y.S.	45
Lehn, J.M.	102
Lerch, M.	77
Lerf, A.	94
Lewis, C.	171
Leynaud, O.	27, 191
Linser, S.	125
Lo Celso, F.	176
Longeville, S.	133
Lonkai, T.	12, 70, 93
Loose, A.	21, 73
Loosvelt, H.	66
Loewenhaupt,	10
Luis, M.	58
M	
Maccarini, M.	113
Magazù, S.	107
Major, J.	183
Manescu, A.	175
Mang, P.	49
Manke, I.	166, 168, 169, 173
Marcano, N.	28
Marczak, A.	95
Martin, C.	54
McLure, I.A.	115
Meersschaut, J.	65
Mergia, K.	37, 68
Mertens, L.A.	206, 207, 208
Mesot, J.	50
Messoloras, S.	37, 68
Mezei, F.	86, 89, 93, 96, 97, 106, 191
Mickiewicz, A.	83
Migliardo, F.	107
Mikula, P.	188
Milani, S.	126
Milne, C.	39, 40, 41, 42, 43, 44
Mishra, N.C.	119
Mitsuda, S.	16
Mook, H.A.	1, 2
Moze, O.	3
Mukherji, D.	153, 156, 157
N	
Naberezhnov, A.	81, 192, 193
Nagler, S.E.	91
Nakajima, T.	16
Novikov, A.	98
Nowicki, W.	32, 33
O	
Oberdisse, J.	99
Odenbach, S.	158
Oettli, M.	48
Ohl, M.	72
Ohms, C.	147
P	
Paciaroni, A.	135
Panagopoulos, C.	22
Pappas, C.	63, 92, 106
Pavlov, V.S.	205
Penc, B.	25, 26
Perroud, O.	59, 60, 197
Peters, J.	186, 191
Pfleiderer, C.	53
Pieper, J.	98, 130, 132, 133, 135, 136, 137, 138, 139, 195, 196
Pintschovius, L.	53
Pissas, M.	34
Piszora, P.	32
Poeste, T.	146, 148, 149, 150
Pop, L.	158
Popova, O.	66, 67
Pratihar, S.	148, 149
Prchal, J.	14
Prokes, K.	13, 14, 15, 16, 17, 71
Prokhnenko, O.	15
Pynn, R.	183
Q	
Qissabi, A.	200, 201, 202
R	
Raasch, S.	10, 11, 12
Rack, A.	186
Radulescu, A.	196
Ramsay, J.D.F.	154
Rätsep, M.	136
Rauch, H.	174
Reehuis, M.	18, 19, 20, 72
Regnault, L.-P.	46
Regulski, M.	35
Rehfeldt, F.	114
Renger, G.	137
Reznik, D.	53
Richardson, R.	105
Robinson, R.A.	57
Rocha, S.	109, 110
Roennow, H.M.	50
Ropers, M.H.	122
Rösler, J.	156, 157
Ross, D.L.	152
Roßmeier, Th.	74
Rotter, M.	10
Rüegg, Ch.	48
Ruffo, I.	176
Rupp, A.	165, 178
Rusevich, L.	188
Russina, M.	96, 97
Russina, O.	93, 96, 97, 106
Rustichelli, F.	170, 172

AUTHOR INDEX

author	page
S	
Sadykov, R.	5
Sahoo, B.	195
Sahoo, K.L.	161
Sarazin, D.	102
Saurel, D.	54
Sazonov, A.P.	36
Schemmel, S.	112, 117, 118, 123
Schilling, H.	77
Schmahl, W.	151
Schmidt, C.	206, 207, 208
Schneck, E.	114
Schneider, R.	146, 148, 149, 150
Scholta, J.	173
Schorr, S.	78, 79, 80
Schröder-Smeibidl, B.	206, 207, 208
Sedev, R.	111
Seidel, K.	114
Shapiro, S.M.	52, 87
Shin, T.	84, 85
Sikolenko, V.	13, 15, 16, 36, 71
Simon, Ch.	54
Slaboszewska, M.	83
Slawinski, W.	35
Smeibidl, P.	9, 51, 52
Smirnov, L.S.	73
Smirnova, E.	81
Sobolev, O.	98
Sofin, M.	27
Stamopoulos, D.	34
Steffens, P.	47
Steichele, E.	23
Steitz, R.	111, 112, 113, 114, 117, 118, 123
Steriotis, T.A.	90, 127, 130, 140, 154
Stockert, O.	7, 8
Strobl, M.	143, 171, 172, 173, 174, 175, 176, 177, 179, 185, 187, 188, 194, 199, 200, 201, 202, 203, 204
Strunz, P.	153, 156, 157, 159
Stüßer, N.	5, 26, 31, 75
Süllow, S.	4, 21
Svoboda, P.	6
Szymczak, H.	36
Szytula, A.	25, 26
T	
Tan, J.M.L.	148, 149
Tanaka, M.	114
Temst, K.	66
Tennant, D.A.	9
Theato, P.	121
Tiedemann, J.	169
Többens, D.	31, 35, 37, 38, 76, 153
Toca Herrera, J.L.	144
Tomala, K.	25
Tovar, M.	32, 33, 77, 78, 79, 80, 81, 152, 193
Treimer, W.	171, 177, 185, 187, 188, 199, 200, 201, 202, 203, 204
Trinker, M.	203, 204
Triolo, A.	96, 97, 106
Triolo, R.	166, 176
Tripadus, V.	196
Troyanchuk, I.O.	36
U	
Ulbricht, A.	155
Ulrich, C.	17, 18, 19, 20
V	
v. Klitzing, R.	112
Vakhrushev, S.	192
Vorderwisch, P.	46, 52, 87
Vorobiev, A.	189
W	
Wagner, V.	63
Wakimoto, S.	45
Walter, J.	194
Wawrzynska, E.	25, 26
Webster, J.R.P.	115
Weß, M.	137
Wiedenmann, A.	56, 59, 60, 61, 160, 162, 163, 164, 165, 181, 182, 197, 198
Willumeit, R.	125
Wilpert, Th.	205
Wimpory, R.C.	147
Wollgarten, M.	161
Wolska, E.	32, 33
Wong, J.E.	112
Woodward, R.	57
Y	
Yamada, K.	45
Yu, D.	57
Z	
Zarbakhsh, A.	115
Zheludev, A.	46
Zrnik, J.	159
Zychlinsky, A.	134
Zygmunt, A.	26